

# **Microbial Fuel Cell-based Biosensors for Estimation of Biochemical Oxygen Demand and Detection of Toxicity**

Martin William Armstrong Spurr

A thesis submitted for the degree of  
Doctor of Philosophy

School of Civil Engineering & Geosciences  
Faculty of Science, Agriculture and Engineering



February 2017





## Abstract

There is a global requirement to establish state-of-the-art monitoring techniques for analysis of water quality to ensure that standards are maintained with increasing domestic and industrial water usage. An important parameter used in water quality assessment is Biochemical Oxygen Demand (BOD), a measurement of the oxygen consumed by micro-organisms in the oxidation of biodegradable organic material. BOD measurements have been correlated with the output from Microbial Fuel Cells (MFCs), which are a potential solution for online monitoring of wastewaters. Previously studied MFC sensors have had a limited amperometric range of approximately 250 mg/l O<sub>2</sub> BOD<sub>5</sub>; which is often attributed to substrate saturation of the anode biofilm.

In this work, a proof-of-concept configuration of multi-stage MFCs connected hydraulically in series was tested extensively to eliminate the saturation effect and extend the sensing range. The summed current generated by a three-stage array was calibrated against BOD<sub>5</sub> for different glucose-glutamic acid concentrations in artificial wastewater. A linear response was obtained up to approximately 750 mg/l O<sub>2</sub> BOD<sub>5</sub> with  $R^2 > 99\%$  and average standard deviation  $< 9\%$ . The array range was three times greater than obtained with the first MFC operating individually. Batch-mode sensors were also operated to develop greater understanding of the long-term performance characteristics and establish how changes in operating parameters affect sensor calibration.

Additionally, the effect of toxicant presence (4-nitrophenol) on the multi-stage sensor response was studied. Toxic and low BOD events which both resulted in current decreases could be differentiated using the MFC-based sensor. The modular mode of operation permitted high-strength BOD wastewaters to be measured online without dilution and an explicit differentiation between toxic and low BOD events based on the ordered response of MFCs. The MFC-based sensors were tested with samples of real influent wastewater and recommendations have been made for 'best practice' operation and calibration of MFC sensors.



## **Acknowledgements**

I would like to thank all those that have helped me along the way during my PhD.

I have received a great amount of guidance, support and encouragement from my supervisor Professor Ian Head. Being given the opportunity to develop my project proposal, conduct independent work and discuss findings in detail has been invaluable. I am grateful that I have been allowed to pursue opportunities for further development of the sensor designed in this work, which will hopefully lead to exciting prospects for the future.

I have also received support and access to state-of-the-art electrochemistry facilities from my CEAM supervisors, Dr Eileen Yu and Professor Keith Scott. The knowledge of the academics involved in Bioelectrochemical Systems research at Newcastle has been extremely insightful to my studies. I would also like to thank Professor Tom Curtis for keeping me in mind when discussing sensing opportunities with potentially interested parties such as Northumbrian Water.

My thanks are given to the technical workshop team of the Chemical Engineering department. Simon Daley assisted me brilliantly with the wiring of dataloggers and the construction of heating platform and UV lamp enclosure. I must also thank Paul Sterling for constant support in the operation of the CEAM autoclave service. In the Civil Engineering department I received a thorough understanding of the various analytical techniques I employed from David Race and I also thank Sarah Jane Smith for assistance with the running of the Ion Torrent gene sequencing.

Special thanks go out to Ed Milner and Dorin Popescu, who gave me a crash-course of the MFC basics from day 1 and I think after countless lunch-time discussions we all came to improve each others ideas. I must also thank Swee Su Lim for his 'drip chamber' design which allowed me to conduct experiments safe in the knowledge that medium bottles would remain sterile.

I would also like to thank my wife, Helen, over the course of my PhD we have become engaged, married and gone on honeymoon and hopefully the PhD work didn't get in the way too much! Thank you for all your love and support.



## Table of Contents

<b>1</b>	<b>Introduction</b>	<b>1</b>
1.1	Background and Context . . . . .	1
1.2	Research Problem, Hypotheses and Aims . . . . .	2
<b>2</b>	<b>Literature Review of Wastewater Quality Assessment &amp; Bioelectrochemical System Sensors</b>	<b>7</b>
2.1	Introduction . . . . .	7
2.2	Oxygen Demand . . . . .	7
2.2.1	Overview, Context & Regulatory Requirements . . . . .	7
2.2.2	Biochemical Oxygen Demand . . . . .	9
2.2.3	BOD Sensors . . . . .	11
2.2.4	Alternatives to Oxygen Demand Measurement . . . . .	14
2.3	Toxicity . . . . .	15
2.3.1	Context & Regulations . . . . .	15
2.3.2	Measurement Methods . . . . .	16
2.4	Overview of Bioelectrochemical Systems . . . . .	17
2.4.1	Microbial Fuel Cells . . . . .	17
2.4.2	Other Types of BES Cells . . . . .	18
2.4.3	BES Modes of Operation & Cell Architecture . . . . .	19
2.4.4	Applications of BES . . . . .	20
2.5	BES-based BOD Sensor Characteristics . . . . .	21
2.5.1	Substrate . . . . .	22
2.5.2	Linear Detection Range & Response Time . . . . .	22
2.5.3	Mode of Operation . . . . .	27
2.5.4	Stability & Reproducibility . . . . .	28
2.5.5	Optimisation of Sensor and Configuration . . . . .	29
2.5.6	Control of Environmental Variables . . . . .	32
2.5.7	Application & Advancement . . . . .	34
2.6	Combined Biomonitoring & Non-BOD BES-based Sensors . . . . .	35
2.6.1	Microbial Activity . . . . .	35
2.6.2	Dissolved Oxygen . . . . .	35

2.6.3	Toxicity . . . . .	36
2.7	Conclusions . . . . .	39

### 3 Materials and Methods 41

3.1	Set-up of Microbial Fuel Cells . . . . .	41
3.1.1	Cell Architecture . . . . .	41
3.1.2	Electrodes . . . . .	43
3.1.3	Membranes . . . . .	45
3.2	Set-up and Methods for Modes of MFC Operation . . . . .	46
3.2.1	Temperature Regulation . . . . .	46
3.2.2	50 ml Batch-mode Cells Set-up & Operation . . . . .	46
3.2.3	Open Circuit Potential Electrodes Set-up & Operation . . . . .	46
3.2.4	10 ml Flow-mode Cells Set-up . . . . .	47
3.2.5	Single-Pass Flow-mode Operation . . . . .	47
3.2.6	Recirculation Flow-mode Operation . . . . .	47
3.2.7	In-line Prevention of Back-contamination with Flow-mode System . . . . .	47
3.2.8	Multi-stage SCMFC Set-up & Operation . . . . .	48
3.2.9	Peristaltic Pump Flow Rates & Hydraulic Retention Time . . . . .	49
3.2.10	Medium Replacement & Introduction of Test Analyte to Flow-mode System . . . . .	50
3.2.11	Sludge Removal from Flow-mode System . . . . .	50
3.3	Preparation of Anolyte Medium . . . . .	51
3.3.1	Inoculum . . . . .	51
3.3.2	Preparation of Phosphate Buffer Solution . . . . .	51
3.3.3	Composition of Anolyte Medium . . . . .	52
3.3.4	Sterilisation of Anolyte Medium . . . . .	52
3.3.5	Degassing Anolyte Medium . . . . .	53
3.3.6	Toxicant-doped Medium . . . . .	53
3.3.7	Raw Wastewater . . . . .	54
3.4	MFC Sensor Calibration Methods . . . . .	54
3.4.1	BOD Calibration Methods . . . . .	54
3.4.2	Current Decrease Calibration Methods . . . . .	55
3.5	Sampling Methods . . . . .	55
3.5.1	Batch-mode Anolyte Sampling . . . . .	55
3.5.2	Flow-mode Anolyte Sampling . . . . .	56
3.5.3	Flow-mode Sludge Sampling . . . . .	56
3.5.4	Electrode Biofilm Sampling . . . . .	56
3.6	Anolyte Analysis Methods . . . . .	57
3.6.1	Biochemical Oxygen Demand . . . . .	57
3.6.2	Chemical Oxygen Demand . . . . .	58

3.6.3	Dissolved Inorganic & Organic Carbon . . . . .	58
3.6.4	Volatile Fatty Acids . . . . .	59
3.6.5	Anions . . . . .	59
3.6.6	D-Glucose . . . . .	60
3.6.7	L-Glutamic Acid . . . . .	60
3.6.8	4-Nitrophenol . . . . .	61
3.6.9	pH . . . . .	62
3.6.10	Conductivity . . . . .	62
3.6.11	Temperature . . . . .	62
3.7	Microbial Community Analysis . . . . .	63
3.7.1	DNA Extraction . . . . .	63
3.7.2	PCR Amplification of 16S rRNA Gene Fragments . . . . .	63
3.7.3	Electrophoresis . . . . .	64
3.7.4	PCR Product Purification . . . . .	65
3.7.5	DNA Quantification . . . . .	65
3.7.6	Sample Pooling & Dilution . . . . .	65
3.7.7	Ion Torrent™ 16S rRNA Gene Sequencing . . . . .	66
3.7.8	QIIME . . . . .	66
3.7.9	Gene Copy Number Adjustment . . . . .	67
3.8	Microbial Imaging and Cell Counts . . . . .	67
3.8.1	Visualisation of Bacterial Cells on Electrodes Using Nucleic Acid Stain Fluorescence Microscopy . . . . .	67
3.8.2	Bacterial Cell Counts on Electrodes . . . . .	68
3.9	Electrochemical Methods . . . . .	69
3.9.1	Electrical Load . . . . .	70
3.9.2	Voltage Measurements . . . . .	70
3.9.3	Polarisation and Power Density Curve Measurement . . . . .	70
3.9.4	Electrochemical Impedance Spectroscopy . . . . .	72
3.9.5	Linear Sweep Voltammetry . . . . .	72
3.9.6	Cyclic Voltammetry . . . . .	72
3.10	Data Handling Methods . . . . .	73
3.10.1	Raw Data . . . . .	73
3.10.2	Current . . . . .	73
3.10.3	Charge . . . . .	73
3.10.4	Power . . . . .	74
3.10.5	Theoretical Oxygen Demand . . . . .	74
3.10.6	Coulombic Efficiency . . . . .	74
3.10.7	Partial Mass Balance . . . . .	75
3.10.8	BOD Sensor Calibration Data . . . . .	75
3.10.9	Sensor Response Normalisation . . . . .	76

3.10.10	Toxicity, Inhibition and Starvation Calibration Data . . . . .	77
3.11	Statistical Techniques . . . . .	77
3.11.1	Replicate Measurements . . . . .	77
3.11.2	Calibration Modelling . . . . .	78
3.11.3	Calibration Performance Characteristics . . . . .	82

#### **4 Batch-mode MFCs for Optimisation and Exploration of Sensing**

	<b>Characteristics using GGA Medium</b>	<b>83</b>
4.1	Introduction . . . . .	83
4.2	Experimental . . . . .	84
4.3	Results & Discussion . . . . .	88
4.3.1	Microbial Fuel Cell Enrichment & Operation . . . . .	88
4.3.2	Biochemical Oxygen Demand Sensing & Calibration . . . . .	89
4.3.3	Long-term Calibration Drift & Sensor Reproducibility . . . . .	97
4.3.4	Effect of External Resistance on Calibration . . . . .	100
4.3.5	MFC Performance Measurement by Electrochemical Analysis . . .	104
4.3.6	Bacterial Cell Density & Community Analysis . . . . .	111
4.4	Conclusions . . . . .	114

#### **5 Development and Application of Multi-stage, Flow-mode MFCs as Sensors for Enhanced BOD Detection**

		<b>117</b>
5.1	Introduction . . . . .	117
5.2	Experimental . . . . .	118
5.3	Results & Discussion . . . . .	124
5.3.1	Microbial Fuel Cell Enrichment & Operation . . . . .	124
5.3.2	Development of a Working Protocol for Staging Multiple MFCs in a Single-pass, Continuous Flow-mode System . . . . .	126
5.3.3	Biochemical Oxygen Demand Sensing & Calibration . . . . .	133
5.3.4	Effect of Flow Rate on BOD Sensor Calibration . . . . .	140
5.3.5	MFC Performance Measurement by Electrochemical Analysis . . .	145
5.3.6	Substrate Utilisation Across the Hydraulic Array of MFCs . . . . .	148
5.3.7	Bacterial Cell Density & Community Analysis . . . . .	154
5.4	Conclusions . . . . .	165

#### **6 Using Multi-stage MFC-based Sensors to Differentiate Current Decrease Events Due to Substrate Excess, BOD Decreases & Toxicity**

		<b>167</b>
6.1	Introduction . . . . .	167
6.2	Experimental . . . . .	169



6.3	Results & Discussion . . . . .	170
6.3.1	Multi-stage Microbial Fuel Cell Operation & Response to Substrate Excess . . . . .	170
6.3.2	Response of Multi-stage MFCs to Decreases in BOD . . . . .	174
6.3.3	Response of Multi-stage MFCs to Toxicant Presence . . . . .	176
6.4	Conclusions . . . . .	181
<b>7</b>	<b>Recommendations for BOD Sensor Validation from Estimation of BOD with Different Substrates and Real Wastewater</b>	<b>183</b>
7.1	Introduction . . . . .	183
7.2	Experimental . . . . .	183
7.3	Results & Discussion . . . . .	185
7.3.1	Comparison of Validation Techniques for Glucose, Glutamic acid and GGA-based Medium . . . . .	185
7.3.2	Effect of Artificial Wastewater Composition on Calibration . . . . .	188
7.3.3	Response of MFC-based BOD Sensors to Raw Wastewater . . . . .	193
7.3.4	Critical Appraisal of Sensor Validation Methods Reported in the Literature for BES-based BOD Sensors . . . . .	196
7.4	Conclusions & Recommendations for Standardised Validation of BES-based BOD Sensors . . . . .	201
<b>8</b>	<b>Conclusions &amp; Future Work</b>	<b>205</b>
8.1	Conclusions . . . . .	205
8.1.1	Defining the Research Problem . . . . .	205
8.1.2	Optimisation & Characterisation of MFCs . . . . .	206
8.1.3	Calibration of MFC-based BOD Sensors . . . . .	207
8.1.4	Overcoming Limitations of MFC-based BOD Sensors and Toxicity Detection . . . . .	208
8.2	Recommendations for Future Work . . . . .	210
8.2.1	Development of a Optimised Cell & System Architecture . . . . .	210
8.2.2	Determination of Working Range & Correction Factors for Non-Target Variables . . . . .	211
8.2.3	Application to Real-world Wastewater Treatment Plants and Beyond	212
	<b>Appendix A Literature Survey Data</b>	<b>213</b>
	<b>Appendix B Method Data</b>	<b>223</b>
	<b>Appendix C Batch Calibration Data</b>	<b>231</b>

<b>Appendix D</b>	<b>Flow Calibration Data</b>	<b>243</b>
<b>Appendix E</b>	<b>Electrochemical Analysis Data</b>	<b>253</b>
<b>Appendix F</b>	<b>Microbiological Analysis Data</b>	<b>261</b>
<b>References</b>		<b>267</b>

## List of Figures

1.1	Schematic diagram of scenarios regarding BOD sensing and inhibition leading to current loss to be addressed with multi-stage, flow-mode MFCs. . . . .	4
2.1	Schematic diagram of a typical MFC. . . . .	18
3.1	Schematic exploded diagrams of (a) 50 ml SCMFC and (b) 10 ml SCMFC. . .	42
3.2	Reference electrode photograph. . . . .	45
3.3	Schematic diagrams of a single flow channel with MFC 1A in (a) Single-pass flow-mode and (b) Recirculation flow-mode. . . . .	48
3.4	Schematic cut-away diagram of (a) UV enclosure for flow-past medium sterilisation and (b) drip chamber for in-line bubble trap. . . . .	49
3.5	Schematic diagram of set-up for triplicate channels of three-stage SCMFCs and position of three-way (3-W M, 3-W L, 3-W 1, 3-W 2 and 3-W 3) valves. . . . .	49
3.6	Skeletal formula of 4-nitrophenol. . . . .	54
3.7	Calibration of measured BOD <sub>5</sub> values against substrate concentration of glucose (G), glutamic acid (GA) and GGA in anolyte medium. . . . .	57
3.8	Annotated current response charts with peak and maximum average stable current densities. . . . .	76
3.9	Typical calibration of MFC BOD biosensor response against substrate concentration fitted with (a) linear, (b) Michaelis-Menten and (c) Hill model lines. . . .	81
4.1	Timeline of events summarising the operation of batch-mode MFCs (A and B) and OCP electrodes. . . . .	85
4.2	Timeline of events summarising the operation of batch-mode MFCs (C and D). . . . .	86
4.3	Start-up of batch-mode cells A & B with average measured current density and anode potential, temperatures, estimated BOD <sub>5</sub> and events. . . . .	89
4.4	Start-up of batch-mode cells C & D with average measured current density, anode and cathode potentials, temperatures, estimated BOD <sub>5</sub> and events. . . . .	90
4.5	The average response of batch-mode MFCs A and B current density and anode potential to changes in BOD <sub>5</sub> during Calibration 4. . . . .	91
4.6	Average peak current density calibration curves fitted with linear, Michaelis-Menten and Hill models for Calibration 4 of batch-mode MFCs A and B. . . . .	92
4.7	Plots of average current density during each medium cycle in (a) Calibration 3 and (b) Calibration 4 for batch-mode MFCs A and B. . . . .	94

4.8	Average total charge density calibration curve for the complete medium cycle fitted with a linear model for Calibration 4 of batch-mode MFCs A and B. . . . .	95
4.9	Lag time in current density response of batch-mode cell A followed by cell B during a medium replacement recorded using high-resolution data-logging. . .	96
4.10	Charts showing response in 1 <sup>st</sup> hour since medium replacement and the resulting coulometric calibration for batch-mode MFCs A and B. . . . .	96
4.11	Normalised, average peak current density calibration data obtained during calibrations of batch-mode MFCs A, B, C and D with $R_{Ext} = 43.2 \Omega$ . . . . .	99
4.12	Plots of (a) typical average current density for $R_{Ext} = 43.2, 305, 953$ and $5100 \Omega$ and (b) average current density for batch-mode MFCs A and B. . . . .	100
4.13	Average peak current density calibration curves from batch-mode MFCs A and B at (a) $305 \Omega$ , (b) $953 \Omega$ and (c) $5100 \Omega$ resistances. . . . .	102
4.14	'Normalised' peak current density Hill models and sensor parameters at $R_{Ext} = 43.2, 305, 953$ and $5100 \Omega$ for batch-mode MFCs A and B. . . . .	103
4.15	Cyclic voltammograms at $240 \text{ mg/l O}_2$ and $1199 \text{ mg/l O}_2$ for batch-mode cells A and B. . . . .	104
4.16	1 <sup>st</sup> derivative cyclic voltammogram on day 842 of operation with $1199 \text{ mg/l O}_2$ BOD <sub>5</sub> medium for batch-mode cells A and B. . . . .	105
4.17	Charts showing average electrochemical performance parameters measured over time determined from polarisation curves for MFCs A and B. . . . .	108
4.18	Average polarisation and power density curves and, anode and cathode potentials recorded on cells A and B. . . . .	110
4.19	SYBR® Gold-stained cells from $5000\times$ diluted anode samples of anodes from batch-mode cells (a) A and (b) B. . . . .	112
4.20	Relative abundance and cell density weighted abundance of bacterial genera identified on batch-mode MFC anodes A and B and electrodes incubated at OCP.	113
4.21	Unweighted Unifrac principal coordinate analysis of communities analysed for batch-mode cells A & B and OCP electrodes A, B & C. . . . .	113
5.1	Schematic diagram of scenarios regarding BOD sensing to be addressed with multi-stage, flow-mode MFCs. . . . .	118
5.2	Schematic diagram of set-up for triplicate channels of three-stage SCMFCs and position of three-way (3-W M, 3-W L, 3-W 1, 3-W 2 & 3-W 3) valves. . . . .	119
5.3	Timeline of events summarising the operation of flow-mode MFCs (1A, 1B, 1C, 2A, 2B, 2C, 3A, 3B and 3C). . . . .	120
5.4	Timeline of events summarising the operation of flow-mode MFCs (1D, 1E, 1F, 2D, 2E, 2F, 3D, 3E and 3F). . . . .	121
5.5	Start-up of Stage 1 flow-mode cells (1A, 1B & 1C) and Stage 2 flow-mode cells (2A, 2B & 2C) and Stage 3 cells (3A, 3B, 3C). . . . .	125
5.6	Start-up of three stages of flow-mode cells in flow channels D, E and F (1D, 1E, 1F, 2D, 2E, 2F, 3D, 3E & 3F). . . . .	126

5.7	Photographs of various sludge-related operational issues. . . . .	127
5.8	Average current density and anode potential response to an increase in BOD <sub>5</sub> followed by return to baseline current. . . . .	132
5.9	Cumulative HRT profile for the flow-mode system path at 0.52 and 1.24 ml/min and the unit volume of each component. . . . .	132
5.10	(a) Photograph and (b) microscope image of SYBR®Gold-stained, degraded GDE showing biofouling upon membrane-covered surface. . . . .	133
5.11	Average current density and anode potential response of three stages of 'ABC' flow-mode MFCs to changes in BOD <sub>5</sub> during Calibration 1 (ABC). . . . .	134
5.12	Average current density and anode potential response of three stages of 'ABC' flow-mode MFCs to changes in BOD <sub>5</sub> during Calibration 6 (ABC). . . . .	136
5.13	Average current density calibration curves fitted with linear, Michaelis-Menten and Hill models for data obtained during Calibration 6 (ABC). . . . .	137
5.14	Predicted BOD <sub>5</sub> plotted against estimated BOD <sub>5</sub> for values predicted by the linear and Hill models from Calibration 6 conducted with the 'ABC' cells. . . . .	139
5.15	Current density and anode potential response of three stages of 'ABC' flow-mode MFCs to changes in estimated BOD <sub>5</sub> during Calibration 7 (ABC) at 1.24 ml/min. . . . .	141
5.16	Average current density calibration curves fitted with the Hill equation for data obtained during Calibration 7 (ABC) of the flow-mode MFCs. . . . .	142
5.17	Normalised average current density calibration curves fitted with the Hill equation for data obtained during Calibration 7 (ABC) and Calibration 1 (DEF). . . . .	143
5.18	Predicted BOD <sub>5</sub> plotted against estimated BOD <sub>5</sub> for values predicted by the linear and Hill models from Calibrations 7 (ABC) and 1 (DEF). . . . .	144
5.19	Hill-modelled, amperometric calibration curves of the three-stage, flow-mode MFCs at 0.52 ml/min and 1.24 ml/min. . . . .	145
5.20	Cyclic voltammograms on the flow-mode MFCs in the 'ABC' and 'DEF' series. . . . .	146
5.21	Polarisation and power density curves and, anode and cathode potentials recorded on 'ABC' flow-mode cells using 480 mg/l O <sub>2</sub> BOD <sub>5</sub> medium. . . . .	147
5.22	Average measured chemical parameters of samples obtained during Calibration 7 (ABC) of the flow-mode MFCs. . . . .	149
5.23	Average measured dissolved carbon determined using a TOC analyser compared to calculated organic carbon from chemical analyses in a partial mass balance. . . . .	152
5.24	Photographs of sludge samples, before and after centrifugation and supernatant removal, taken from first stage MFC (1A). . . . .	156
5.25	Relative abundance of bacterial phyla, classes and orders obtained from MFC anodes, non-polarised electrodes and sludge. . . . .	157
5.26	Relative abundance of bacterial families and genera obtained from MFC anodes, non-polarised electrodes and sludge. . . . .	158
5.27	Unweighted and weighted Unifrac principal coordinate analysis of communities analysed with polarised and non-polarised samples highlighted. . . . .	160

5.28	Average relative abundance of bacterial genera obtained from MFC anodes, non-polarised electrodes and sludge. . . . .	161
5.29	Phylogenetic tree of 16S rRNA gene sequences extracted from electrode and sludge samples and high-similarity database sequences. . . . .	164
6.1	Schematic diagram of scenarios regarding BOD sensing and inhibition leading to current decrease to be addressed with multi-stage, flow-mode MFCs. . . . .	168
6.2	Normalised average current density calibration curves for each stage of flow-mode MFCs fitted with the Hill and Haldane equations. . . . .	171
6.3	Average 'normalised' current density response of the flow-mode MFCs to a BOD increase from 300 to 360 mg/l O <sub>2</sub> BOD <sub>5</sub> . . . . .	172
6.4	Average 'normalised' current density response of the flow-mode MFCs to a BOD increase from 150 to 1199 mg/l O <sub>2</sub> BOD <sub>5</sub> . . . . .	173
6.5	Normalised average current density response of three stages of MFCs to decreases in BOD <sub>5</sub> from 360 to 60 mg/l O <sub>2</sub> . . . . .	174
6.6	Normalised, current density loss calibration curve fitted with Hill model for response of the flow-mode MFCs to 90-minute decreases in BOD. . . . .	175
6.7	COD measured at each sampling point after 90 minutes of BOD decrease from 360 mg/l O <sub>2</sub> BOD <sub>5</sub> . . . . .	176
6.8	Normalised average current density response of three stages of MFCs to increasing concentrations of 4-nitrophenol (4-NP) from 0 to 150 mg/l. . . . .	177
6.9	Normalised average current density response of the first stage of MFCs to 150 mg/l 4-NP, followed by the recovery to 100%. . . . .	178
6.10	Normalised, average current density loss calibration curve fitted with Hill model for response of the flow-mode MFCs to 90-minute decreases in BOD. . . . .	179
6.11	4-Nitrophenol (4-NP) concentrations measured at each sampling point after 90 minutes of toxicant exposure. . . . .	180
7.1	Average current density response for batch cycles in which 300 mg/l (a) glucose, (b) glutamic acid and (c) GGA was fed to batch-mode MFCs C and D. . . . .	187
7.2	Average peak anode and cathode potential plotted against time showing cathode degradation for batch-mode cells C and D. . . . .	188
7.3	The average response of batch-mode MFCs A and B current density, anode and cathode potential to changes in BOD <sub>5</sub> during Calibration 10. . . . .	189
7.4	The average response of batch-mode MFCs C and D current density, anode and cathode potential to changes in BOD <sub>5</sub> during Calibration 1. . . . .	190
7.5	Calibration of batch-mode cells A, B, C and D with different concentrations of glucose (G), glutamic acid (GA) and GGA. . . . .	191
7.6	Average current density response for batch cycles in which 1000 mg/l glucose, glutamic acid and GGA was fed to batch-mode MFCs C and D. . . . .	192

7.7	Positioning of wastewater samples on Hill-modelled calibrations of batch-mode cells A, B, C and D and summed current density from multi-stage 'DEF' MFCs.	194
7.8	Evaluation of predicted BOD <sub>5</sub> values using G, GA and GGA calibrated batch-mode MFCs and GGA calibrated flow-mode MFCs.	195
7.9	Comparison of linear ranges of amperometric and coulometric BES-based sensors reported in the literature.	198
7.10	Comparison of typical BOD and COD values (on a logarithmic scale) for a selection of municipal wastewaters and industrial wastewaters.	200
8.1	Representative examples of the limitations present with single-stage, flow-mode MFCs.	205
8.2	Representative examples of the average current densities obtained from multi-stage MFCs to scenarios not distinguishable with single-stage MFCs.	209
8.3	Optimised tubular, multi-staged MFC design with inner anodic flow chamber surrounded by membrane/gas diffusion electrode-lined walls.	211
B.1	Schematic diagram of detailed set-up for triplicate channels of three-stage SCM-FCs and position of three-way valves including tubing sizing and type.	224
B.2	Chart showing removal of dissolved oxygen from 250 ml solution of GGA medium whilst sparging with N <sub>2</sub> .	224
B.3	Calibration of absorbances measured from (a) 10 to 150 mg/l O <sub>2</sub> and (b) 25 to 1500 mg/l O <sub>2</sub> photometric COD test kits with known solutions of GGA medium.	225
B.4	Charts showing ion chromatogram recorded for VFA standard solution and calibration of peak areas for known VFA concentrations.	225
B.5	Charts showing ion chromatogram and single-point calibration of peak areas for known anion concentrations.	226
B.6	Calibration of absorbances measured from D-glucose UV spectrophotometric assay with known solutions of GGA medium.	226
B.7	Calibration of absorbances measured from L-glutamic acid UV spectrophotometric assay with known solutions of GGA medium.	227
B.8	Calibration of absorbances measured from known solutions of toxicant-doped GGA medium containing 4-nitrophenol at 320 nm.	227
B.9	Microscope images of stage micrometer at 100× and 400× magnification.	227
B.10	Typical images of (a) micrograph of SYBR® Gold-stained bacteria and (b) CellC automated counting result.	228
B.11	Calculation of the theoretical oxygen demand (ThOD) of (a) 150 mg/l glucose and (b) 150 mg/l glutamic acid.	229
C.1	Peak current density calibration curves fitted with Hill models for data obtained during calibrations of batch-mode MFCs.	232
C.2	Cycle charge density calibration curves fitted with Hill models for data obtained during calibrations of batch-mode MFCs.	235

C.3	Plots of average current density in Calibrations 1, 2, 5, 7, 8 and 9 for batch-mode MFCs A and B. . . . .	239
C.4	Plots of average current density in Calibration 10 for batch-mode MFCs A and B and Calibration 1a for cells C and D. . . . .	240
D.1	Average current density calibration curves fitted with the Hill equation for the 'ABC' series of flow-mode MFCs. . . . .	245
D.2	Average current density calibration curves fitted with the linear model for Calibration 7 of the 'ABC' flow-mode MFCs. . . . .	247
D.3	Normalised average current density calibration curves fitted with the linear model for Calibration 7 (ABC) and 1 (DEF). . . . .	247
D.4	Average measured chemical parameters of samples obtained during Calibration 7 (ABC) of the flow-mode MFCs. . . . .	251
E.1	Linear sweep voltammetry measured over time at 1 mV/s under two different BOD <sub>5</sub> concentrations for batch-mode cells A and B. . . . .	254
E.2	Polarisation curves recorded on cells A & B over time. . . . .	255
E.3	Average ohmic resistance as measured by EIS and internal resistance estimated by PC gradient over time for cells A & B. . . . .	257
E.4	Charts showing effect of operational $R_{Ext}$ on average electrochemical performance parameters for batch-mode cells A and B. . . . .	258
E.5	Linear sweep voltammetry measured over time for flow-mode MFCs. . . . .	258
E.6	1st derivative cyclic voltammograms measured over time at 5 mV/s for flow-mode MFCs in the (a) 'ABC' series and (b) 'DEF' series. . . . .	259
F.1	Photograph showing biofouled membranes and GDEs extracted from the 'ABC' series of flow-mode MFCs. . . . .	263
F.2	Representative micrographs of SYBR® Gold-stained electrodes from 5000× diluted anode samples from flow-mode cells in the 'ABC' series. . . . .	265
F.3	Electrophoresis gel plate images taken (a) after PCR and (b) after AMPure® purification showing a band between 400 and 500 base pairs (no band in controls)	266



## List of Tables

2.1	Comparison of BOD <sub>5</sub> measurement methods, previously developed 'BOD' sensors and alternative methods for measurement of carbonaceous organic matter. . .	16
2.2	Literature survey of BES-based BOD sensor characteristics including amperometric and coulometric detection ranges, validation method and response time.	23
3.1	Comparison of characteristics of 50 ml & 10 ml SCMFCs. . . . .	43
3.2	Composition of anolyte medium stock solutions. . . . .	53
3.3	Automated thermocycler program for PCR amplification. . . . .	64
4.1	Details of calibrations performed using batch-mode cells A and B. . . . .	87
4.2	Details of calibrations performed using batch-mode cells C and D. . . . .	87
4.3	Model parameters determined from calibrations over time performed using batch-mode cells A, B, C and D with $R_{Ext} = 43.2 \Omega$ . . . . .	98
4.4	Average response time to reach 95% peak current density at different $R_{Ext}$ from batch-mode cells A, B, C & D. . . . .	101
4.5	Electrochemical performance parameters determined from CV and LSV analysis of batch-mode cells A and B . . . . .	106
4.6	MPL and Pt catalyst loadings on GDEs used for operation of MFCs A, B, C & D.	107
4.7	Logarithm of cell densities for batch-mode cells A and B and OCP electrodes A, B and C (and cell count of sterile PBS control). . . . .	112
5.1	Details of calibrations performed using the 'ABC' (1A, 1B, 1C, 2A, 2B, 2C, 3A, 3B & 3C) and 'DEF' (1D, 1E, 1F, 2D, 2E, 2F, 3D, 3E & 3F) flow-mode cells. . .	123
5.2	Photographs showing the contents removed from each of flow-mode cells in comparison to liquid samples taken from the medium bottle and inline feed. . .	128
5.3	Average current response of each stage of MFCs in the 'ABC' flow-mode series to GGA concentrations of 100, 400, 900 and 2000 mg/l during sludge accumulation.	129
5.4	Average stable current densities ( $\pm$ SD) measured before and after the sludge removal procedure for each stage of triplicate MFCs in the 'ABC' flow-mode series.	130
5.5	Logarithm of cell densities flow-mode anodes from the 'ABC' series (and cell count for sterile PBS control). . . . .	155
6.1	Recovery times of three-stage MFCs to toxic media containing 4-NP. . . . .	178

7.1	Details of calibrations involving different substrates; glucose (G), glutamic acid (GA) and GGA, performed using batch-mode cells A & B and C & D. . . . .	184
7.2	Comparison of values measured by validation methods and MFC response outputs for a medium containing 300 mg/l glucose, glutamic acid and GGA. . .	186
7.3	Comparison of water quality parameters for a 300 mg/l GGA artificial wastewater medium and two samples of real raw influent wastewater. . . . .	193
7.4	Characteristics of MFC-based BOD sensors developed in the present study. . .	203
A.1	Literature survey of BES-based BOD sensor materials & operating parameters.	214
A.2	Comparison of typical BOD and COD values for a selection of municipal wastewaters and industrial wastewaters taken from the literature. . . . .	219
B.1	Hydraulic retention time of each component and total path of the flow-mode system at 0.52 & 1.24 ml/min. . . . .	230
C.1	Evaluation of predicted BOD <sub>5</sub> values using the calibrated linear and Hill models from the batch-mode MFCs for samples of real wastewater. . . . .	241
D.1	Pt catalyst loadings on replacement GDEs used for operation of 'ABC' and 'DEF' flow-mode MFCs. . . . .	244
D.2	Evaluation of predicted BOD <sub>5</sub> values using the calibrated linear and Hill models from the flow-mode MFCs for 300 mg/l GGA. . . . .	248
D.3	Evaluation of predicted BOD <sub>5</sub> values using the GGA calibrated linear and Hill models from the flow-mode MFCs for real wastewater. . . . .	249
F.1	Barcoded V4 forward (5'-adapter-barcode-primer-3') and V5 reverse (5'-adapter-primer-3') primers used in PCR amplification of 16S rRNA. . . . .	262
F.2	DNA extraction quantification and quality scores. . . . .	264

## List of Terms, Abbreviations & Acronyms

$\alpha$	Temperature Correction Coefficient	ANOVA	Analysis of Variance
$\gamma$	Activity Coefficient	AnS	Anaerobic Sludge
$\Delta$	Difference Operator	APHA	American Public Health Association
$\varnothing$	Diameter	AS	Activated Sludge
$\eta$	Overpotential	As	Arsenic
$\theta$	Temperature (°C)	ATC	Automatic Temperature Compensation
$\kappa$	Conductivity	ATP	Adenosine triphosphate
$\mu$	Ionic Strength	ATU	Allylthiourea
$\rho$	Mass Concentration	Au	Gold
$\sum$	Summation	Ave	Average
$\tau$	Hydraulic Retention Time	AWW	'Artificial' Wastewater
$\bar{x}$	Mean	BES	Bioelectrochemical System
$y'$	Fitted value	BLAST	Basic Local Alignment Search Tool
3-W	3-Way Valve	BOD	Biochemical Oxygen Demand
4-NP	4-Nitrophenol	BOD <sub>5</sub>	5-Day BOD Test
$A$	Absorbance	BOM	Biodegradable Organic Matter
$a_X$	Activity	C	Carbon
$A_{Eff}$	Effective Electrode Area	$c$	Intercept
$A_r$	Relative Atomic Mass	$C_E$	Coulombic Efficiency
$A_{Tot}$	Total Electrode Area	$Cat$	Cathode
AC	Alternating Current	CBOD	Carbonaceous Biochemical Oxygen Demand
ADP	Adenosine diphosphate	Cd	Cadmium
ADS	Anaerobic Digester Sludge	CEM	Cation Exchange Membrane
Ag	Silver		
Ag/AgCl	Silver / Silver chloride		
$An$	Anode		

Cl	Chlorine	$F$	Faraday Constant
Co	Cobalt	$f$	Final
COD	Chemical Oxygen Demand	FAS	Ferrous Ammonium Sulphate
Cr	Chromium	Fe	Iron
Cu	Copper	$FoV$	Field of View
CV	Cyclic Voltammetry	G	Glucose
Cyc	Cycle	$g$	Gravitational Acceleration
d	Depth	G-6-PDH	Glucose-6-phosphate dehydrogenase
DAQ	Data Acquisition	GA	Glutamic acid
DCMFC	Dual Chamber Microbial Fuel Cell	GDE	Gas Diffusion Electrode
DEFRA	Department for Environment Food and Rural Affairs	GDL	Gas Diffusion Layer
$DF$	Dilution Factor	GGA	Glucose-Glutamic acid
DI	Deionised	GIDH	Glutamate dehydrogenase
DNA	Deoxyribonucleic acid	H	Hydrogen
dNTP	Deoxyribose nucleoside triphosphate	$h$	Hill Coefficient
DO	Dissolved Oxygen	H	Height
DOC	Dissolved Organic Carbon	Hg	Mercury
dsDNA	Double-stranded DNA	HK	Hexokinase
$E$	Potential	HRT	Hydraulic Retention Time
$E^\ominus$	Standard Reduction Potential	$I$	Current
$e_y$	Error	$i$	Initial
EA	Environment Agency	$\bar{I}$	Mean Current Density
EC <sub>50</sub>	Half Maximal Effective Concentration	$\hat{I}$	Peak Current Density
EDTA	Ethylenediaminetetraacetic acid	IC	Inorganic Carbon
EIS	Electrochemical Impedance Spectroscopy	ID	Inner Diameter
$emf$	Electromotive Force	INT	Iodonitrotetrazolium chloride
EPS	Extracellular Polymeric Substances	K	Potassium
EU	European Union	$k$	Rate Constant
		$K_a$	Acid Dissociation Constant
		$K_I$	Inhibition Constant
		$K_M$	Michaelis Constant
		ktoe	Kilotonnes of Oil Equivalent

LOD	Limit of Detection	OD	Oxygen Demand
LOQ	Limit of Quantification	OECD	Organization for Economic Cooperation and Development
LSV	Linear Sweep Voltammetry	ORR	Oxygen Reduction Reaction
$M$	Molar Mass	OSA	Octanesulfonic acid
$m$	Slope	OTU	Operational Taxonomic Unit
$M_r$	Relative Molecular Mass	OUR	Oxygen Uptake Rate
$m_X$	Mass	P	Phosphorous
M-M	Michaelis-Menten	$P$	Power
$Max$	Maximum	Pb	Lead
MDC	Microbial Desalination Cell	PBS	Phosphate-buffered Saline
MEA	Membrane-Electrode Assembly	PCoA	Principal Coordinate Analysis
MEC	Microbial Electrolysis Cell	PCR	Polymerase Chain Reaction
MFC	Microbial Fuel Cell	pe	Population Equivalent
MPL	Microporous Layer	PEMFC	Proton Exchange Membrane Fuel Cell
N	Nitrogen	PES	Polyethersulfone
$N$	Number	PHB	Poly- $\beta$ -hydroxybutyrate
$n$	Moles	Pt	Platinum
$N_{Eq}$	Normality	Pt/C	Platinum on Carbon Black
$N_2$	Number	PTFE	Polytetrafluoroethylene
Na	Sodium	PyNAST	Python Nearest Alignment Space Termination
$NAD^+$	Nicotinamide adenine dinucleotide	$Q$	Charge
$NADP^+$	Nicotinamide adenine dinucleotide phosphate	$q$	Flow Rate
NCBI	National Center for Biotechnology Information	$Q_R$	Reaction Quotient
ND	Not Detected	QIIME	Quantitative insights into microbial ecology
NGS	Next-Generation Sequencing	$R$	Universal Gas Constant
Ni	Nickel	$R^2$	Coefficient of Determination
$Norm$	Normalised	$R_{Ext}$	External Resistance
NPT	National Pipe Thread Taper	$R_{Int}$	Internal Resistance
O	Oxygen	$R_{\Omega}$	Ohmic Resistance
OC	Organic Carbon	RDP	Ribosomal Database Project
OCP	Open Circuit Potential		

RE	Reference Electrode	ThOD	Theoretical Oxygen Demand
RNA	Ribonucleic acid	Ti	Titanium
rRNA	Ribosomal RNA	TOC	Total Organic Carbon
rrnDB	Ribosomal RNA Operon Database	<i>Tox</i>	Toxicant
SCMFC	Single Chamber Microbial Fuel Cell	U	Uranium
SCMFC	Submersible Microbial Fuel Cell	UK	United Kingdom
<i>SD</i>	Standard Deviation	UV	Ultraviolet
<i>SD<sub>Res</sub></i>	Residual Standard Deviation	UWWTD	Urban Waste Water Treatment Directive
SE	Standard Error	V	Vanadium
Se	Selenium	<i>V</i>	Potential Difference
SHE	Standard Hydrogen Electrode	<i>v</i>	Reaction Rate
<i>Sp</i>	Electrode Spacing	<i>v<sub>Max</sub></i>	Maximum Reaction Rate
<i>SS<sub>Res</sub></i>	Residual Sum of Squares	<i>V<sub>S</sub></i>	Volume of Seed
<i>SS<sub>Tot</sub></i>	Total Sum of Squares	VFA	Volatile Fatty Acid
ssDNA	Single-stranded DNA	<i>Vol</i>	Volume
Sub	Substrate	vol%	Percent by Volume
<i>T</i>	Temperature (K)	VP	Viewpoint
<i>t</i>	Time	w	Width
<i>tv</i>	Titre Volume	WFD	Water Framework Directive
TAE	Tris, Acetic acid & EDTA	wt%	Percent by Weight
TC	Total Carbon	WW	Wastewater
TE	Tris & EDTA	WWTP	Wastewater Treatment Plant
ThOC	Theoretical Organic Carbon	<i>z</i>	Number of Electrons

# Chapter 1. Introduction

## 1.1 Background and Context

Access to clean, safe water is a vital provision for all ecosystems. With ever-growing, worldwide consumption of water through domestic and industrial activities, effective wastewater treatment remains a highly important challenge. Determination of a water's quality is therefore also a significant consideration which must be addressed in order to establish the amount of treatment that is required and confirm that treatment has been successful.

Biochemical oxygen demand (BOD) is a significant constituent of wastewater which is required to be removed prior to discharge of treated waters. BOD is a measure of the dissolved oxygen consumed by micro-organisms in the oxidation of biodegradable organic material. Determination of BOD is the primary method used by the wastewater industry for quantifying biodegradable organic carbon pollution. The conventional Five-Day BOD test (BOD<sub>5</sub>) was developed over a 100 years ago by the Royal Commission on Sewage Disposal in the UK (published in 1912; Mara and Horan (2003)) and standardised by the American Public Health Association (APHA, 1999a). The test has changed very little since the method was introduced, except for the addition of nitrification inhibitors and the use of more advanced dissolved oxygen (DO) measurement probes. Today, with increasingly stringent water quality standards, imposed by legislation such as the European Union Water Framework Directive (WFD; Directive 2000/60/EC), the measurement of BOD<sub>5</sub> has become a burden on organisations dealing with wastewater treatment (Parliamentary Office of Science and Technology, 2014).

Identification and detection of toxic compounds in wastewater is of great importance for ensuring continued health and environmental safety. Existing methods identify toxic exposure by measurement of indirectly associated parameters (such as oxygen uptake or methane production) or by offline analysis of samples with known species of micro-organisms.

There is therefore a clear need for the development of a sensor capable of addressing the issues found with existing BOD and toxicity detection methods. The requirements for excessive manual labour, sample preparation, prolonged incubation, frequent recalibration and maintenance must be eliminated to ensure success. Ideally, a BOD–toxicity sensor will be able to be operated online, providing real-time estimation of the BOD and detection of

toxicant presence. Only by technological advancement of the BOD and toxicity measurement and provision of more timely readings can policy change be effected. Use of online monitoring devices would provide real-time data that would allow remedial actions to be implemented responsively rather than retro-actively. Such a development could result in more practical monitoring for treatment companies, improved quality of information for regulatory bodies, reduced treatment costs and ultimately increased water quality (by capturing more pollution incidents).

Microbial fuel cells (MFCs), a type of bioelectrochemical system (BES), are a technology which have the potential to revolutionise the field of water quality sensing. Two principles of measurement are available to MFC-based sensors; namely current generation and current inhibition. Electrical current generation by MFCs begins with oxidation of labile organic carbon present in solution and donation of electrons to an anode electrode on which an electrogenic biofilm is grown. The electrochemical circuit is completed by reduction of (typically) oxygen to water at a cathode electrode. Current inhibition occurs when a substance (*e.g.* toxicant), which is capable of inhibiting electrogenic bacteria present in the anodic biofilm, enters the anode chamber.

It has been established in the literature that a linear correlation can be determined with the concentration of labile organic carbon (*i.e.* the biochemical oxygen demand) and the electrical current (or charge) generated by the MFC (Kim *et al.*, 2003a, 2006a; Abrevaya *et al.*, 2015a). It is this feature which allows the output from an MFC to be used for sensing, as calibrations can be conducted with medium solutions containing known quantities of BOD. By contrast, toxicants including heavy metals, pesticides, pharmaceuticals and industrial chemicals have been demonstrated to inhibit the current generation by MFCs (Kim *et al.*, 2006b; Patil *et al.*, 2010; Xu *et al.*, 2016). As biosensors, MFCs uniquely act as both the bioreceptor and transducer meaning that the electricity generated or inhibited is due to a direct interaction of the analyte with the bacterial biofilm which interacts with the electrode. MFC devices can therefore be simply constructed without requiring installation of expensive measurement transducers (such as DO or manometric probes); a key advantage of the proposed technology.

## **1.2 Research Problem, Hypotheses and Aims**

There are limitations with microbial fuel cell-based sensors which have prevented their commercialisation and wide spread use to date. The upper amperometric detection limit of previously reported sensors has been constrained up to approximately 250 mg/l O<sub>2</sub> BOD<sub>5</sub> (Zhang and Angelidaki, 2011). Significant improvements to this range have not yet been achieved in subsequent studies (Abrevaya *et al.*, 2015a). The range upper limitation arises from a plateau in current density which is observed at high BOD concentrations, above which the current density no longer correlates linearly. This effect has been attributed to 'saturation' of the



anodic biofilm (Chang *et al.*, 2004). If BOD increases when the MFC has saturated there is no observed increase in current density and thus pollution incidents could pass undetected. With the existing dynamic range of MFC sensors they can be used to determine BOD levels of low-strength wastewaters, such as some municipal wastewaters, but are unsuitable for high-strength wastewaters including those from industrial and urban-municipal sources.

Another limitation of MFC-based sensors is that there is no existing method for distinguishing current decreases which occur due to decreases in BOD from those due to inhibition by toxicants. It is for this reason that most BES-based toxicity sensor studies have been conducted with an artificially fixed BOD concentration to ensure that changes in current density can be attributed to toxicity (Patil *et al.*, 2010; Stein *et al.*, 2010; Jiang *et al.*, 2015b). However, in real-world samples the BOD would be expected to vary independent from the potential toxicity and therefore practical solutions are required for application of the technology.

The aim of the present thesis is to enhance the dynamic range of BOD detection with MFC-based sensors and establish methods which can be employed to overcome the associated sensor limitations. The main limitation is the range-limiting effect of anode saturation at high levels of BOD, which prevents increases in BOD above these levels from being detected. The second limitation is the inability to explicitly distinguish between toxicant presence and decreases in BOD using MFC sensors.

The main focus of this thesis will be the development of a novel, flow-mode sensing system comprised of three microbial fuel cells staged hydraulically in series. It is expected that this proof-of-concept configuration will possess unique attributes which enable enhanced BOD sensing and potentially allow explicit differentiation between BOD decrease and toxicant exposure incidents (Figure 1.1).

Multi-stage MFCs have been successfully operated for electricity generation applications in the literature (Ieropoulos *et al.*, 2008; Chung and Okabe, 2009; Kim *et al.*, 2011c). In the present thesis, it is hypothesised that by staging MFCs hydraulically in series the additional information provided by each MFC will together allow estimation of greater ranges of BOD. At low concentrations of BOD, as medium passes through the first stage MFCs, substrate will be consumed and electricity generated (*i.e.* Figure 1.1a, 'Low' BOD). The resultant effluent will contain less substrate available for the downstream MFCs and therefore it is hypothesised that current generation will be of the order Stage 1 > 2 > 3. If the BOD concentration increases enough the first stage MFCs will saturate and substrate will be passed in the effluent into the downstream MFCs which can subsequently generate more electricity (*i.e.* Figure 1.1b, 'Mid-level' BOD). Therefore, it is expected that an enhanced BOD detection range can be established by this modular mode of operation as further increases in BOD can be detected by the output of the downstream MFCs (*i.e.* Figure 1.1c, 'High' BOD).

By contrast, toxicants which may be present in the feed will enter the first stage MFCs

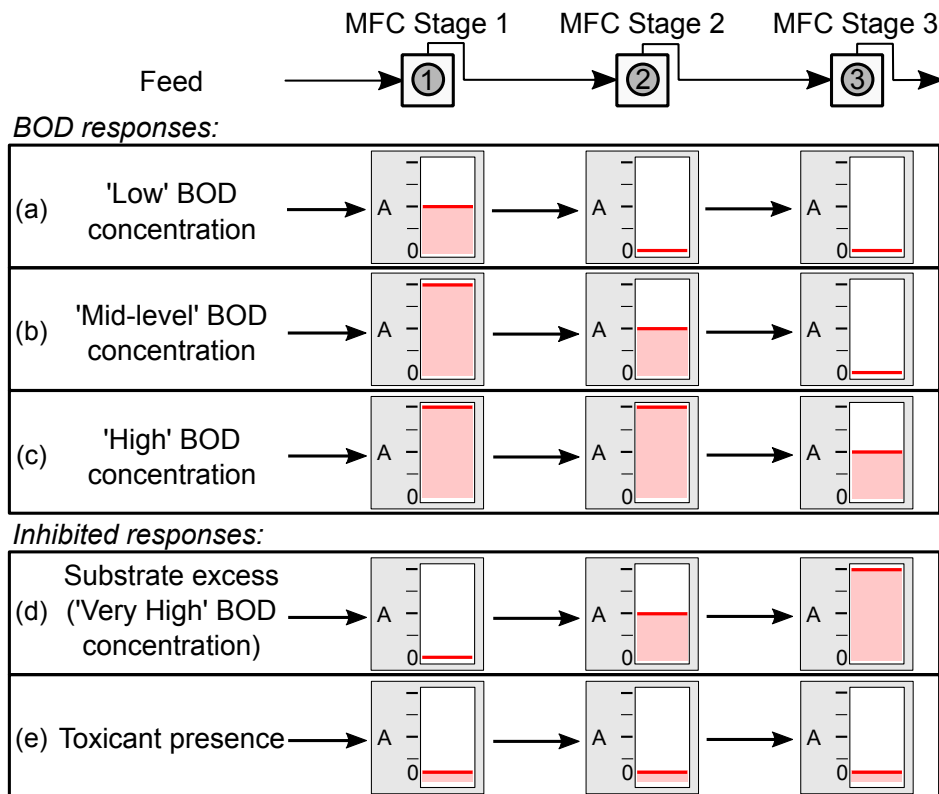


Figure 1.1: Schematic diagram of scenarios regarding BOD sensing and inhibition leading to decreases in current to be addressed with multi-stage, continuous flow-mode MFCs. Examples are given for (a) 'low', (b) 'mid-level' and (c) 'high' BOD concentrations and inhibition events of (d) substrate excess and (e) toxicant presence. The relative, hypothesised electrical current (— in amperes (A)) response is indicated for each MFC in a three-stage hydraulic array.

and inhibition will be observed with those cells first. Non-biodegradable toxicants (*e.g.* heavy metals) would not be consumed (oxidised), therefore the toxicant would pass on to downstream MFCs causing the same amount of inhibition (*i.e.* Figure 1.1e, Toxicant presence). The multi-stage system additionally provides a mechanism for identifying inhibition due to substrate excess or presence of degradable toxicants. As these compounds enter the first stage MFC, the greatest degree of inhibition would be observed, and the subsequent responses of the downstream MFCs would be expected to be inhibited less as the toxicant was degraded (or excess substrate consumed); with current decreases in the order Stage 1 > 2 > 3 (*i.e.* Figure 1.1d, Substrate excess).

Batch-mode microbial fuel cells will also be set up in order to establish greater understanding of the operation of MFC-based BOD sensors and to optimise parameters for best sensing performance. Specifically, experiments will be conducted with batch-mode MFCs to:

- Determine the detection range of the MFC sensor by calibration with medium containing different concentrations of BOD.
- Assess the effect of external resistance on BOD<sub>5</sub> calibration.

- Evaluate the effect of long term operation in regard to calibration drift and effect on MFC performance.
- Assess BOD calibration selectivity with different artificial medium compositions containing carbon sources of only glucose, only glutamic acid and a glucose-glutamic acid mixture (GGA; the standard used in BOD<sub>5</sub> tests (APHA, 1999b)).

The experimentally-derived, optimised parameters from batch-mode operation will be applied to the continuous flow-mode MFCs for improved operation and further experimentation. The aim of the experiments conducted with the three-stage array of MFCs was to provide data which validated the hypotheses made above (and illustrated in Figure 1.1). Specifically, the flow-mode, three-stage MFCs will be used to:

- Determine if an enhanced detection range could be achieved by considering the output from each stage of MFCs in a multi-stage array.
- Assess the effect of flow rate on BOD<sub>5</sub> calibration.
- Determine the response of multi-stage MFCs to toxicant presence with short-term exposure to 4-nitrophenol.

Additional objectives common to experiments conducted with both batch- and continuous flow-mode MFCs were to:

- Evaluate BOD<sub>5</sub> calibrations with non-linear kinetic models (such as Michaelis-Menten and Hill) to determine if the detection range can be extended.
- Determine the sensor calibration reproducibility across identical MFC configurations.
- Characterise the MFCs by electrochemical and microbiological analytical techniques.
- Determine the accuracy of the artificial BOD<sub>5</sub> calibrations with samples of real municipal wastewater.



## **Chapter 2. Literature Review of Wastewater Quality Assessment & Bioelectrochemical System Sensors**

### **2.1 Introduction**

Wastewater can be produced from many processes and must be treated to remove contaminants before it can be safely discharged. In addition to domestic wastewater, industrial processes generate wastewaters which require specialised treatment. According to Bitton (2005), there are 5 major constituents of wastewater which must be addressed during treatment. These comprise pathogens and parasites, biochemical oxygen demand (BOD), suspended solids, nutrients (such as nitrogen and phosphorous) and toxic chemicals. Different processes are used to reduce and eliminate certain contaminants employing physical, chemical and biological treatments.

The main focus of this review is on BOD; one of the major wastewater components highlighted above. The problems associated with its measurement and the technological solutions which have been investigated to improve its characterisation (including bioelectrochemical systems; the approach employed in this work) will be discussed. Brief mention will also be made regarding identification and measurement of toxic chemicals in wastewater.

### **2.2 Oxygen Demand**

#### **2.2.1 Overview, Context & Regulatory Requirements**

Measurement of oxygen demand (OD) is principally a broad method for estimating the total quantity of organic compounds present in a water sample, critically without requiring any knowledge of the identity of those compounds. If certain inorganic compounds are present (such as iron (II) and sulfides) they will also exert an oxygen demand. Instead of measuring each individual organic compound which could be present in a sample, which would be costly, complex and require multiple analyses, the measure simply represents how much dissolved oxygen will be lost from solution. This approach is effective because maintaining a high dissolved oxygen content is the primary environmental concern for which OD is measured. If wastewater with a high demand is discharged and a downstream water body becomes

anaerobic (depleted of oxygen) it can lead to aquatic organism death, eutrophication and algal blooms (Penn *et al.*, 2009).

Oxygen Demand is regulated by two experimentally-determined measurements; namely biochemical oxygen demand (BOD) and chemical oxygen demand (COD). BOD is determined by a standardised measurement of the dissolved oxygen (DO) depleted in a water sample during a specified incubation period by the biological oxidation of organic matter by micro-organisms (as will be discussed in detail in Section 2.2.2 below). Most commonly the sealed incubation lasts 5 days in a test known as the 5-Day BOD test ( $BOD_5$ ; APHA (1999a, 2005)). COD is a standardised measurement by which almost all of the carbonaceous (carbon-containing) organic constituents of a sample are acidified and oxidised by reaction with a strong chemical oxidising agent (usually potassium dichromate; APHA (1999b)). The Urban Waste Water Treatment Directive 1994 (UWWTD) states that samples from discharges should have  $BOD_5$  values less than 25 mg/l  $O_2$  with nitrification inhibited (carbonaceous demand) and a minimum of 70 to 90 % reduction during treatment in relation to the wastewater influent. Samples should also have less than 125 mg/l  $O_2$  COD and be reduced by 75% during treatment.

Population equivalents (pe) are values used to categorise the size of a catchment area (agglomeration) served by a wastewater treatment plant (WWTP). 1 pe represents a wastewater loading containing biodegradable organic matter which corresponds to a  $BOD_5$  value of 60 g  $O_2$  per day (based on the average weekly WWTP load; DEFRA (2012)). In the United Kingdom there are over 9000 municipal treatment plants treating 69m pe annually; of which 1900 plants treat agglomerations greater than 2000 pe (DEFRA, 2012). According to the UWWTD (1994), it is mandatory to take at least four samples per year for monitoring purposes for plants serving 2000 to 9999 pe, this requirement rises to monthly samples (12/year) between 10 000 and 49 999 pe and bimonthly samples (24/year) must be taken for plants treating more than 50 000 pe.

In the European Union (EU), the Water Framework Directive (WFD; Directive 2000/60/EC) is legislation encompassing water quality standards, emission limits and prioritised lists of contaminant substances. The WFD required all water bodies in the EU to attain 'good' or 'high' status by 2015 (excepting exemptions). In 2014, the UK Environment Agency (EA) estimated that only 25% of England's waters currently complied with the required standards set (Parliamentary Office of Science and Technology, 2014). The introduction of more stringent WFD legislation, which replaced previous EA standards, resulted in the percentage of rivers with a quality status of 'good' decreasing from 79% to only 21% which met the required standard. Failing to meet WFD requirements can lead to infractions and penalties; causing or knowingly permitting a pollution event in the UK carries a penalty of up to £50,000 and/or imprisonment for individuals, and greater fines for companies (The Environmental Permitting (England and Wales) Regulations (2010)). Now that the 2015 deadline has passed it is expected that there will be increased urgency to improve water quality monitoring and

subsequently treatment on an international scale.

The UK Parliamentary Office of Science and Technology wrote in 2014 that there were major gaps in water quality monitoring data in England which hinders classification and setting of priorities for treatment. It has been shown with increased monitoring in England and Wales that single 'snapshot' assessments are not necessarily representative of water quality and thus a need for continuous online monitoring is implied. Scotland is in the process of phasing in 'General Binding Rules' which allow companies which pose significant pollution risks to be prosecuted. This increases the liability for companies dealing with wastewater as they previously could only be prosecuted after pollution incidents had occurred. The Indian Central Pollution Control Board (2014) has recently required that all 'highly polluting' industries must install real-time online monitoring systems for a variety of water quality parameters (including flow rate, pH, COD, BOD and total suspended solids). Based on developing policy changes on top of the existing regulatory requirements there is growing evidence of a global market need for oxygen demand (organic matter) online monitoring technologies.

The Water Environment Federation (2008) emphasised that in addition to the compliance aspect there are additional benefits associated with online OD measurements. With infrequent 'snapshot' sampling routines, treatment is performed without prior knowledge of influent and effluent water qualities and therefore the risk of accidental discharge is high. With online monitoring there is possibilities for process control and collection of historical data to ensure that risks are reduced. Companies can be more responsive to incidents which could ultimately result in costly fines. Operational factors such as aeration rate could be varied in response to online measurements, which in turn could bring additional cost benefits to end-users.

### **2.2.2 Biochemical Oxygen Demand**

BOD is perhaps the most valuable measurement of oxygen demand because it quantifies the biodegradable portion of organic matter. The COD value includes an undetermined amount of non-biodegradable organic carbon which will not cause negative environmental effects once discharged (Bourgeois *et al.*, 2001).

The steps involved in the preparation of a sample for BOD<sub>5</sub> measurement are substantial and include pH adjustment, removal of DO super saturation and toxic and interfering substances. To confirm the BOD value several dilutions are needed and samples may be seeded with a micro-organism population (usually raw or primary settled wastewater) in order to ensure biochemical degradation of organic matter is successful. Furthermore, checks are done to assess the quality of seeded dilution water and the background oxygen demand from the seed sample (Delzer and McKenzie, 2003; APHA, 2005).

A glucose-glutamic acid standard solution (GGA) is prepared by dissolving 150 mg glucose and 150 mg glutamic acid in distilled water made up to 1 litre (APHA, 2005). This 'artificial'

wastewater (AWW), which also contains other nutrients, is chosen because it is said to exhibit a similar oxidation rate to that of municipal wastewater and allows the accuracy, precision, seed quality and experimental setup to be evaluated (APHA, 1999a). GGA check solutions must achieve a BOD<sub>5</sub> of  $198 \pm 30.5$  mg/l O<sub>2</sub> ( $\pm$  standard deviation), it has been generally acknowledged that this equates to a broad  $\pm 15\%$  acceptable precision in the BOD<sub>5</sub> test.

During the BOD<sub>5</sub> test conditions for the measurement must also be controlled. An incubation temperature of  $20 \pm 1$  °C is required and light must be excluded to prevent photosynthesis. The dissolved oxygen concentration is normally measured with a DO probe and the BOD<sub>5</sub> value is calculated after dilution and seeding has been taken into account (equation given in Equation 3.8 in Chapter 3). The value is representative of the quantity of dissolved oxygen (mg) per litre of prepared sample which is depleted during biochemical oxidation of organic matter. There are several criteria which must be met in order for a BOD measurement to be valid; the 5-day DO depletion must be  $> 2$  mg/l and the remaining DO level must be  $> 1$  mg/l. This gives the BOD<sub>5</sub> test a limited detection range of only 1.00 to 7.09 mg/l O<sub>2</sub> for undiluted samples at 20 °C (DO saturation is 9.09 mg/l O<sub>2</sub>; YSI (2013)). There are also time constraints on when a sample should be measured; ideally within 2 hours of collection (6 hours if cold storage is used and not if more than 24 hours has elapsed). The initial DO measurement should also be taken within 30 minutes of sample preparation and then the incubation time must be 5 days  $\pm 6$  hours.

BOD analysis of a water sample is a time dependent measurement and not all substrate is depleted during this time. In the first five days of incubation, if nitrification inhibitors are present, it is expected that the BOD value will approach the maximum oxygen depletion for a given substrate concentration, strictly the CBOD<sub>5</sub> (carbonaceous BOD) value (Delzer and McKenzie, 2003; APHA, 2005). If no inhibitors are present, nitrifying bacteria can also increase the oxygen demand by nitrification of ammonia to nitrite and nitrate. This process occurs at slower rates than oxidation of carbonaceous materials and may not occur during 5 days of incubation, this value is referred to as total BOD (Hammer Sr. and Hammer Jr., 2008).

The theoretical oxygen demand (ThOD) can be calculated from the stoichiometric amount of oxygen required to fully oxidise a known organic substrate to end products of water and carbon dioxide (Penn *et al.*, 2009). In the carbonaceous oxygen demand, where nitrification is inhibited, nitrogen-containing compounds remain unoxidised as ammonia. For the nitrogenous oxygen demand full oxidation of ammonia to nitrate must be accounted for. For a solution of 150 mg/l glucose and 150 mg/l glutamic acid the carbonaceous ThOD value is 306.67 mg/l O<sub>2</sub> ( $159.86 + 146.81$  mg/l O<sub>2</sub>). During the five day incubation period in the BOD<sub>5</sub> test it is clear from the accepted  $198 \pm 30.5$  mg/l value for the GGA calibration that not all the carbonaceous oxygen demand is consumed during the test period (only 65%). For complete consumption of all the carbonaceous oxygen demand it is estimated by Delzer



and McKenzie (2003) that the test would need to be at least 20 days for some wastewaters and this is evidently only useful for historical data and not suitable for any process control or plant operation diagnostics.

### 2.2.3 BOD Sensors

Sensors which measure BOD fall under two main categories; absolute and predictive determination methods (Jouanneau *et al.*, 2013). Absolute determinations stay true to the five-day incubation as in the standardised test but modify the dissolved oxygen detection transducer or improve upon automation.

Typically in the standard BOD<sub>5</sub> test a Clark-type dissolved oxygen probe is used; comprised of a gold or platinum working electrode and Ag/AgCl reference electrode held in a chamber separated from the analyte sample by a membrane. Clark-type DO probes are capable of measuring the electrocatalytic reduction of oxygen which passes through the membrane, however they cannot be used continuously, require stirring, require re-calibration and are subject to membrane fouling.

One example of an alternative absolute determination method includes the use of an optical DO probe (*e.g.* IDS Pro optical BOD Probe (YSI, USA)) where oxygen diffuses into a painted diffusion layer on to an immobilised luminescent dye layer (excited by a blue light). Oxygen impedes the emission intensity and lifetime of the luminescence measured by a built-in photo-diode detector (YSI, 2009). Optical DO probes do not require re-calibration or stirring but the immobilised dye cap must be replaced annually.

Photometric BOD<sub>5</sub> assays have also been developed (*e.g.* LCK555 BOD<sub>5</sub> cuvette test (Hach, USA)) in which the sample volume is greatly reduced from 4× 300 ml diluted to approximately 4 ml per cuvette. The concentration of dissolved oxygen is determined by addition of Fe<sup>2+</sup>/pyrocatechol reagents to the sample after five days which forms a red dye compound which can be read using a photometer at 620 nm (HACH, 2013). The limitations are that photometric tests can be biased with high chloride levels and interferences from strongly oxidising compounds react with the reagents to absorb at the same frequency.

The final absolute method which is a modification to the standard five-day test is carried out using a manometric pressure sensor head which can be fitted to a BOD bottle (*e.g.* BOD-System OxiDirect® (Lovibond, Germany)). Unlike the previous tests mentioned, the bottles used in manometric determinations are not completely filled and have a defined head space of air at the start of the test. As dissolved oxygen is consumed in solution, oxygen from the head space dissolves and carbon dioxide is evolved. A hydroxide-containing pellet or solution (in a raised container fitted to the bottle sensor head) is employed to absorb released CO<sub>2</sub>, resulting in a pressure drop. By using small sample volumes (a large head space) the range of the BOD<sub>5</sub> test can be considerably extended without dilution (*e.g.* up to 4000 mg/l O<sub>2</sub>) as

the quantity of oxygen is considerably increased (Lovibond, 2008). Manometric detection is the most expensive absolute method as a pressure transducer is required to be fitted to each bottle for the duration of the BOD<sub>5</sub> test and additional CO<sub>2</sub> absorption reagents are required.

As is evident, from the lengthy procedure required in order to take BOD<sub>5</sub> measurements, there is scope for a faster, less labour intensive and more accurate test. Predictive BOD measurements do not take five days to complete and therefore are not true determinations of BOD<sub>5</sub>. In the wastewater industry, BOD can be subdivided into either 'soft BOD' (which is readily biodegradable and typically is consumed within hours) and 'hard BOD' (including carbon-containing suspended solids which are not readily degraded and can take multiple days to break down); to some extent this is also reflected in the calculated wastewater BOD<sub>5</sub>/COD ratio (Davies, 2005). In predictive BOD sensors, typically only the labile organic matter ('soft BOD') is consumed and a correlation is established between the sensor value and the true BOD<sub>5</sub> test value. Often an assumption with predictive methods is made that the constituent make-up of the wastewater does not change over time (potentially resulting in the fraction of 'soft' BOD changing). Most predictive BOD sensors measure indirectly associated parameters instead of oxygen which enables them to overcome the range-limiting effect of dissolved oxygen saturation and estimate higher concentration BOD levels without dilution and in some cases without aeration.

Jouanneau *et al.* (2013) extensively reviewed the different methods which have been used for BOD detection. Methods have included use of redox mediators, immobilised bacteria, bioluminescent bacteria, bioreactors and bioelectrochemical systems (BES). The use of BES will be discussed in detail in Section 2.5. Previously developed detection systems have had some major limitations including poor stability, poor substrate range and frequent maintenance requirements, which has prevented their widespread use (Rabaey *et al.*, 2010).

Redox-mediated BOD sensors require the addition of sample to a culture of bacteria known to metabolise in the presence of a mediator. The mediator replaces oxygen as the terminal electron acceptor and therefore allows the test to be run without prior aeration of samples and without nitrification inhibitor addition. BOD<sub>5</sub> values can be estimated within 15 minutes up to approximately 300 mg/l O<sub>2</sub> undiluted and detected based on electrochemical potential, luminescence, fluorescence or photometric absorption. The substrate range for which this type of sensor can be used has been reduced by selectivity due to the limited number of bacteria which can utilise the specific redox mediator employed.

Immobilised strains of bacteria have been enclosed within systems including Clark-type dissolved oxygen electrodes. This allows the specialised probe to be used with less sample preparation and BOD<sub>5</sub> values have been correlated with DO consumption after hours rather than days. Immobilised bioluminescent bacteria have also been utilised as BOD sensors as the intensity of emission has been correlated with BOD<sub>5</sub> (Sakaguchi *et al.*, 2007). Less

accurate BOD<sub>5</sub> correlations have been reported with single strains of bacteria (for example  $R^2 < 0.6$  for some immobilised bacteria methods) as they have a higher substrate selectivity and therefore a limited substrate range. Single strains do not necessarily possess all the enzymes required for certain metabolic pathways to degrade the labile organic carbon present in a complex wastewater sample compared to the mixed culture employed in the BOD<sub>5</sub> test (Jouanneau *et al.*, 2013).

Bioreactor-type BOD sensors have shown the most promising potential for commercialisation to date. The principle involves a chemostat bioreactor in which a mixed culture of bacteria is maintained by continuously feeding with aerated wastewater and monitoring the changes in DO over time (normally using a Clark-type electrode). Changes have been correlated with BOD<sub>5</sub> measurements taken from the feed. The Ra-BOD (Applitek, Belgium) and MB-DBO (Biosensores, Spain) sensors have been used to monitor BOD levels based on the continuous output of Clark-type DO electrodes. Additionally, the Ra-COMBI (Applitek) and RODTOX NG (Kelma, Belgium) are sold with combined BOD and toxicity detection capabilities using the same technology principle (toxicity results in a loss of micro-organism activity, increase in BOD and DO). The BioMonitor (LAR, USA) is an innovative online sensor which uses multi-stage bioreactors hydraulically linked in series and the DO is measured in the final vessel of the cascade. In general, the upper limit of the measurement ranges claimed are in the order of 100 000 mg/l O<sub>2</sub> BOD<sub>5</sub> and response time of less than 30 minutes (Jouanneau *et al.*, 2013). There are detailed reports available of trials completed with these commercialised systems which highlight the benefits of online, faster BOD tests and also the limitations exhibited by the need for regular calibration and frequent maintenance (Kong *et al.*, 1996; Iranpour and Zermeno, 2008).

The Shepherd activated sludge monitoring system (Bactest, UK) utilises the principle of manometric BOD sensing in a commercial sensor which sells for £39 900. Online measurements are made by extracting a 2 litre sample once per hour from the aerated activated sludge lane of a WWTP. Instead of using consumable hydroxide pellets a small decrease in pressure is still observed without CO<sub>2</sub> absorption as oxygen is displaced over one hour (Bactest, 2015; IWA, 2016). In a recent review on the subject of BOD detection, Reshetilov *et al.* (2013) described a Japanese commercial BOD sensor which has a range of 0 - 500 mg/l, a response time of 30 - 60 minutes and costs \$80 000. The above sensors indicate the large capital costs these systems currently require. If an improved BOD sensor was developed there could be a lucrative potential market, especially in countries where discharge consents are strictly imposed.

Because GGA standards are used for calibration in the standardised BOD<sub>5</sub> test they have been widely adopted for calibration of BOD sensors and allow comparisons to be made between different systems. However, the equivalency of GGA solutions to 'real' wastewater (WW) is questionable and better estimations of synthetic wastewaters have since been developed, such as OECD synthetic wastewater (Organization for Economic Cooperation

and Development). The standard preparation features a complex mixture of substances (the main BOD-containing components are peptone, meat extract and urea) compared to the two-substrate GGA solution (OECD, 2010). Reshetilov *et al.* (2013) mentioned that the OECD wastewater may be more suitable for calibrating BOD sensors because, by necessity, analysis takes place over a significantly shorter time period than the BOD<sub>5</sub> test, therefore GGA oxidation rates will be different and correlation less agreeable.

There are eight properties which must be considered before using a sensor in wastewater monitoring applications according to Lynggaard-Jensen (1999). The properties of the sensors comprise; placement, principles of sampling, filtration, sample treatment and measurement, number of measurands, need of supplies and service intervals. Obviously, a sensor which can be operated on- or at-line, with no external sampling or filtration and in a continuous mode will be most desirable, especially if multiple parameters can be measured simultaneously. The consumables required and service intervals for calibration and cleaning are also important cost aspects to be considered. It is by these parameters that new biosensors for wastewater treatment applications should be evaluated. For online sensors, Lynggaard-Jensen (1999) offered the following characteristic performance indicators; linearity (range), lowest detectable change, limit of detection and quantification, selectivity, response, lag, rise and fall times, ruggedness, bias, repeatability, reproducibility, up time, drift and memory effects. These many characteristics must be determined, in some cases during field trials, before viability of a sensor for application can be assessed.

#### **2.2.4 Alternatives to Oxygen Demand Measurement**

The BOD<sub>5</sub> test is still carried out today because of the somewhat arbitrary, time-dependent nature, which makes BOD such a difficult parameter to develop novel sensors for that correlate and satisfy regulations for wastewater treatment. Other analytical techniques are also used in the water treatment industry for monitoring of organic compounds as a faster way to assess water quality.

Organic carbon (OC) can be quantified by a Total Organic Carbon (TOC) analyser which is an instrument which is used to calculate TOC from the difference between the amount of total carbon (TC) measured by the CO<sub>2</sub> given off from combustion and the amount of inorganic carbon (IC) given by carbonate acidification. In addition, for samples which have been passed through a 0.45 µm filter the dissolved organic carbon (DOC) fraction of the TOC can be determined. Akin to COD there is no distinction made regarding the biodegradability of the organic carbon present.

Assays of AOC (assimilable organic carbon) and BDOC (biodegradable dissolved organic carbon) are standardised tests frequently used for water quality assessment in drinking water treatment. AOC and BDOC are used to provide an estimate of the biodegradable organic matter (BOM) present in a sample (Escobar and Randall, 2001). The AOC method

incorporates incubation of a sterile sample with a known bacterial culture. The measured cell density after a period of time (e.g. 3 – 5 days) is used to calculate growth rates from growth yield coefficients derived from calibration with acetate. BDOC measurement is performed by determining the initial DOC concentration of a sterile sample and then incubating with micro-organisms over a period of time (e.g. 10 – 30 days) with repeated DOC measurements until no further consumption is observed (Page and Dillon, 2007). Both methods are highly sensitive and have low detection limits in the order of 10 to 100 µg/l C, however they are susceptible to organic contamination and, in the case of AOC, have a limited substrate spectrum set by the known micro-organisms employed. They also, like the BOD<sub>5</sub> test, take several days to complete and therefore cannot be used for online process control.

Peaks have been identified with UV absorbance measurements at 254 nm and fluorescence measurements in the range 270 to 530 nm which have been modelled and found to correlate with BOD<sub>5</sub> with  $R^2$  coefficients up to 0.71 (Kwak *et al.*, 2013). Online sensors based on this sensing technique have been developed where a correlation between the tryptophan-like fluorescence peaks and BOD<sub>5</sub> was established (Hudson *et al.*, 2008). To date, there have been issues in regard to turbidity of samples and assignment of spectra in highly contaminated samples; which indicates that the technology is most suited to effluent and drinking water applications (Page and Dillon, 2007). Non-biological methods may over- or under-estimate the true BOD value and provide no information about potential toxicity of samples; there is a 'market need' for an efficient, online sensing method for BOD (or related BOM parameter) determination. The previously developed BOD sensors and alternative methods are listed in Table 2.1.

## **2.3 Toxicity**

### **2.3.1 Context & Regulations**

Prevention of toxic compounds being released from wastewater treatment facilities is a highly important objective which must be met for ensuring health and environmental security of downstream ecosystems. Within a WWTP the secondary biological treatment process (*i.e.* activated sludge) hosts a population of micro-organisms required to consume organic matter. According to Quevauviller *et al.* (2007), it can take weeks to recover from the most serious toxic shock events (resulting in loss of the entire viable population of micro-organisms). The protection of the biomass present in the secondary biological treatment process is therefore a critical objective as the potential consequences are not only exposure of water users to toxic chemicals but also loss of treatment.

As mentioned previously, the EU WFD regulations stipulate priorities regarding contaminant compounds which must not exceed consent levels in WWTP treated effluent discharges (Directive 2000/60/EC). At present there are 33 regulated chemicals, which include heavy

Table 2.1: Comparison of BOD<sub>5</sub> measurement methods, previously developed 'BOD' sensors and alternative methods for measurement of carbonaceous organic matter.

Method	Parameter	Measurement Principle
<i>'Absolute' 5-day BOD sensing methods</i>		
Clark-type DO probe	BOD <sub>5</sub>	Electrical potential (DO)
Optical DO probe	BOD <sub>5</sub>	Luminescence
Photometric assay	BOD <sub>5</sub>	Absorbance
Manometric probe	BOD <sub>5</sub>	Pressure
<i>'Predictive' BOD sensing methods</i>		
Redox-mediated sensor	'BOD'	Electrical potential (mediator)
Immobilised bacteria + Clark-type DO probe	'BOD'	Electrical potential (DO)
Immobilised bioluminescent bacteria	'BOD'	Luminescence
Chemostat bioreactor + Clark-type DO probe	'BOD'	Electrical potential (DO)
Manometric sensor	'BOD'	Pressure
Microbial Fuel Cell sensor	'BOD'	Electrical potential (bacteria)
<i>Alternative sensing methods</i>		
Chemical Oxygen Demand	COD	Chemical titration / Absorbance
Total Organic Carbon	TOC / DOC	Infra-red (combusted to CO <sub>2</sub> )
Assimilable Organic Carbon	AOC	Colony counts
Biodegradable Dissolved Organic Carbon	BDOC	Δ DOC

metals, pesticides and industrial chemicals, listed either due to their toxicity, persistence or bioaccumulation properties.

### 2.3.2 Measurement Methods

Xiao *et al.* (2014) reviewed toxicity measurement methods which have been used for biological wastewater treatment processes and found three main categories; inhibition of reactant consumption, inhibition of product generation and indicators derived from known micro-organisms. Following identification of a toxic event, samples are normally taken for offline, laboratory analysis to determine toxicant identity and concentration so that potency and source of toxic compound can be determined.

The most common indicator of toxicity used in aerobic processes is determination of oxygen uptake rate (OUR) inhibition by respirometers (Quevauviller *et al.*, 2007). The standardised protocol is an offline, assay-based determination which requires samples to be taken and measured in comparison to a synthetic wastewater (OECD composition) and a standard toxicant dosing (3,5-dichlorophenol). The test takes 3 hours following which the change in dissolved oxygen is measured to calculate the OUR. In addition to OUR, other aerobic

toxicity indicators include CO<sub>2</sub> production and nitrification inhibition (Xiao *et al.*, 2014).

In anaerobic processes there is a limited number of toxicity assays. Commonly, the effect on methane production is a key indicator of methanogenesis toxicity derived from batch-mode assays and biogas volume accumulations. Malina (1992) noted that the tolerance of anaerobic processes to toxic compounds was observed to be higher than that of aerobic processes and in some cases reversible.

Online biosensors for toxicity have been developed based on bioluminescent reactors, chemostat bioreactors (measuring constant OUR) and bioelectrochemical systems (BES; Xiao *et al.* (2014)). Kong *et al.* (1996) reported that the response time and frequency of measurement intervals of a toxicity sensor had to be sufficiently short (< 1 hour) in order to accurately alert to shock loadings. Quevauviller *et al.* (2007) stated that tests designed for influent and effluent testing require different sensitivities to reflect the tolerance thresholds of downstream processes. As has been discussed for BOD sensors there can be significant issues regarding online measurement of luminescence and use of Clark-type DO probes which has also limited the application of these technologies. BES-based sensors are still an emerging technology and despite good correlations being achieved with electrical current decreases due to toxicants there is little comparison with the standardised OUR-based and CH<sub>4</sub>-based toxicity indication methods.

## **2.4 Overview of Bioelectrochemical Systems**

Bioelectrochemical systems (BESs) are a type of electrochemical cell in which micro-organisms or enzymes are involved in either oxidation reactions at the anode or reduction reactions at the cathode or both (Hamelers *et al.*, 2010). Microbial BESs can be operated passively as microbial fuel cells (MFCs) or actively as in microbial electrolysis cells (MECs) with an applied potential (Sharma *et al.*, 2014).

### **2.4.1 Microbial Fuel Cells**

Mediator-less microbial fuel cells (MFCs) are a developing technology in which micro-organisms oxidise organic materials and convert biochemical energy directly into electrical energy. MFCs are operated passively with no energetic inputs other than the calorific organic matter present in the medium. MFCs have an established research background in academic institutions for use in wastewater treatment and electricity generation but are yet to be realised commercially (Logan, 2008).

In a typical MFC setup (Figure 2.1), an anaerobic chamber is constructed containing an anode (of biocompatible material; *e.g.* carbon) and filled with medium (such as wastewater) containing substrate (an organic carbon source), nutrients and minerals to promote cell

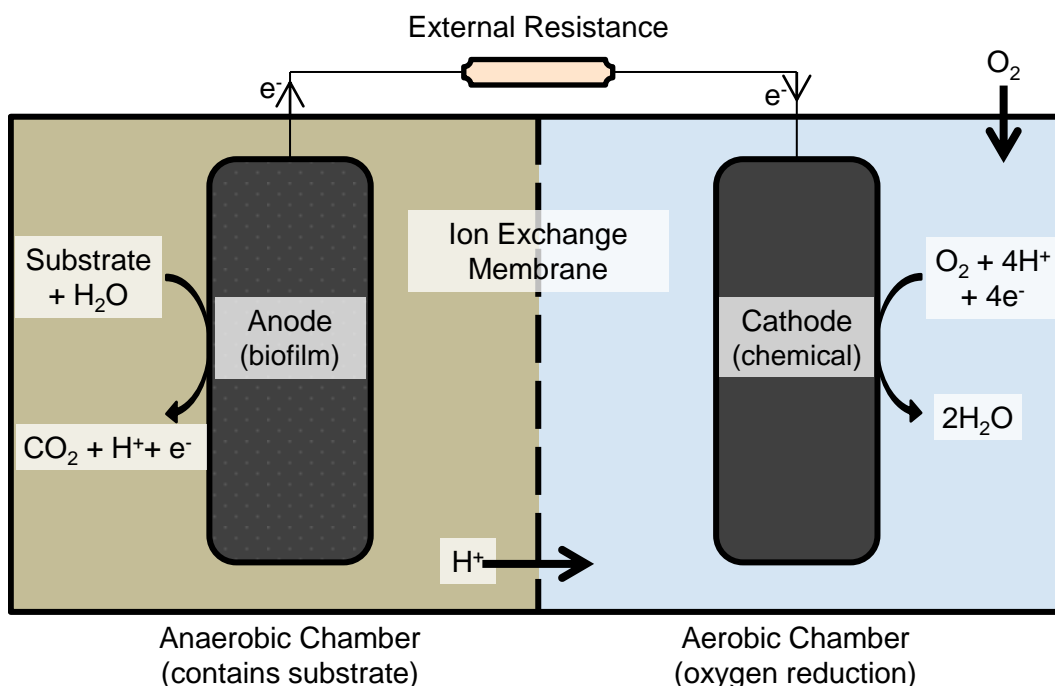


Figure 2.1: Schematic diagram of a typical MFC.

growth. To this chamber a microbial inoculum (*e.g.* activated sludge or a pure culture) is added. The anaerobic chamber is connected through an ion exchange membrane to an aerobic chamber, containing a cathode (typically a chemical catalyst (*e.g.* Platinum) or a biocathode). For clarity, this setup will be referred to as a Dual Chamber MFC (DCMFC). The circuit is completed by joining the two electrodes with an external resistor; as the bacterial biofilm grows, and oxidises the substrate present in the anolyte medium, electrons are accepted by the anode and the passage of electrons generates electrical current. At the cathode, electrons are donated to the oxygen reduction reaction (ORR) which occurs on a catalyst surface to produce water.

#### 2.4.2 Other Types of BES Cells

BESs run with an external potential applied instead of a resistor connected are classified as microbial electrolysis cells (MECs). MECs exhibit lowered overpotentials for redox reactions as there is more energy available in the circuit; reducing limitations from the working electrode. A special type of MEC is a poised potential half cell in which the external potential applied to the working electrode is actively controlled by a potentiostat device instead of a power supply. Poised potential half cells allow the reaction at the working electrode to be exclusively assessed without limitations from the corresponding counter electrode. A fixed potential can be set on the working electrode and the effect on biocatalytic performance can be determined through electrochemical analysis techniques.

Based on the same anode and cathode chamber as an MFC, microbial desalination cells (MDCs) have also been developed. MDCs have an additional third chamber sandwiched



between the anode and cathode chambers separated by an anion and cation exchange membrane respectively. As saline water is passed through the middle chamber, and the fuel cell generates electrical current, ions pass through the respective ion exchange membranes and the resulting effluent is desalinated (Cao *et al.*, 2009). Additionally, BES can be operated as microbial solar cells (MSCs) with applied solar energy to the micro-organisms to promote photo-catalytic reactions. Enzyme fuel cells are also classified as BES in which enzymes are immobilised on electrodes instead of micro-organisms (Wang *et al.*, 2015).

### **2.4.3 BES Modes of Operation & Cell Architecture**

Bioelectrochemical systems can be operated in two different modes; either batch or flow. Batch-mode cells operate in cycles from the point at which organic substrate-containing medium is added (and electrical current can be generated) until the substrate becomes depleted or can no longer be oxidised by the biofilm and the electrical current falls to zero. In flow-mode cells there are several types of operation; specifically fed-batch, single-pass and recirculation. Fed-batch is an extension of the batch-mode except medium replacement is achieved by pumping fresh medium in through an inlet port, whilst simultaneously displacing spent medium through an outlet port; performed each time the medium depletes. Single-pass flow-mode maintains a constant flow of substrate from a fresh medium source (*e.g.* a medium bottle in the laboratory or directly from a wastewater stream) and medium passes through the cell at a specific flow-rate (and therefore specific residence time) onwards into a waste vessel. Recirculation flow-mode is similar to single-pass with the differentiating feature being that instead of spent medium passing to waste it is returned to the medium source and continuously recirculated through the BES. In the laboratory, for obvious operational reasons batch-mode and recirculation are the most common modes used; whereas in field tests single-pass is the most applicable method where a continuous supply of wastewater is readily available.

With a continued drive towards sustainable energy generation from microbial fuel cells (and bio-electrochemical systems (BESs) in general) there have been several developments in MFC operational design in order to optimise efficiency and subsequently wastewater treatment.

Single Chamber MFCs (SCMFCs) remove the requirement for a cathode chamber and utilise a gas diffusion electrode (GDE) which is part of a membrane-electrode assembly (MEA); this interfaces between the solution-side (anode chamber) and external air-side of the cell. On the air-side oxygen is passively channelled through a hydrophobic, gas diffusion layer (GDL) to the catalyst layer (at which oxygen is reduced). As well as simplifying the cell construction there is also no longer a requirement for active aeration to the cathode chamber which reduces operational costs (Liu and Logan, 2004; Di Lorenzo *et al.*, 2009b).

Recently, instead of manufacturing a single, large-scale MFC to produce higher power

output and increase treatment capacity there has been heightened interest in multiple MFC configurations. By connecting many smaller MFCs, both electrically and hydraulically, there is evidence of much higher power density and treatment efficiency per anodic volume (Rabaey *et al.*, 2005; Ieropoulos *et al.*, 2008; Kim *et al.*, 2011c; Zhuang *et al.*, 2012). There are several types of multi-MFC setups which include; *serpentine* (in which multiple electrodes are placed in a common tank and medium is flowed from one end past each electrode), *tubular* (where MEAs are placed along the walls of a tube and a flow-through anode material (*e.g.* graphite granules) is used), *multi-stage* (where discrete cells are hydraulically connected in series) and *stacked* (in which inter-cell anode-cathode electrical connections are made through a bipolar plate). There is an emergent trend in which novel MFC architectures are developed using design ideas adapted from existing PEMFC (Proton Exchange Membrane Fuel Cell) configurations, which is a much larger and more established research area.

#### **2.4.4 Applications of BES**

Researchers have established several areas of application to which BES are well suited. Wang *et al.* (2015) reviewed the articles published on BES. In 2014 over 420 articles concerned electricity generation, additional research regarded wastewater treatment (> 180), hydrogen production (> 110), biosensing (> 30) and denitrification (> 10).

The primary research field has historically been electricity generation by MFCs. Water treatment is an energy intensive process, however, the wastewater itself contains a considerable amount of calorific energy (as much as 1760 kJ/pe/d (Wett *et al.*, 2007)). Utilising a fraction of this potential energy would reduce treatment costs in addition to generation of renewable energy. Current limitations with MFC technology, including problems with scale-up and operating with real wastewaters under real-world conditions, have prevented commercialisation to date (Logan and Rabaey, 2012; Oliveira *et al.*, 2013).

Following on from efforts to generate electricity, attention has been directed towards achieving more sustainable wastewater treatment without necessarily having a net energy gain. BES technology is capable of oxidising carbonaceous organic compounds without aeration, which is a key benefit. Aeration of activated sludge is responsible for 55.6% of the energy consumption in wastewater treatment according to Caffoo (2008).

BESs which utilise microbial electrodes and perform useful/valuable reactions are also an emerging use-case. Two categories of these types of BES include those used for synthesis of valuable chemicals and others used for recovery of resources from wastewater. Electrochemical hydrogen production at the cathode of a MEC is the most established research field using a microbial anode fed with wastewater. With application of a voltage in the range  $-0.13$  to  $-1.00$  V splitting of water can occur in an MEC which is a lower energy input requirement than the corresponding non-BES system (1.2 V; Logan and Rabaey (2012)). Similar to the electricity generation the application is limited by scale-up, economic and practical constraints.

Microbial electrochemical synthesis has also been used for production of; ethanol at the bioanode and methane, hydrogen peroxide and acetate (from CO<sub>2</sub>) at the cathode (Hamelers *et al.*, 2010; Mathuriya and Yakhmi, 2014). Additionally, recovery of resources contained within wastewaters has been achieved using BES for extraction of phosphorous, N<sub>2</sub> from denitrification and electroplating of various metals (V, Cr, Fe, Co, Cu, As, Se, Ag, Au, Hg, & U) onto cathodes (Mathuriya and Yakhmi, 2014; Wang and Ren, 2014).

It has been shown that the faradaic current or charge generated from a BES (most commonly MFCs) can be correlated to the concentration of substrate which is consumed. This attribute has led to an increasing push to develop BES-based sensors which can be used for detection of several environmental factors including BOD, specific substrates, dissolved oxygen and microbial activity (Kim *et al.*, 2003a; Liu *et al.*, 2011; Zhang and Angelidaki, 2012; Tront *et al.*, 2008). Conversely, inhibition leading to loss of current generation in BESs has led to development of sensors for toxicity and specific heavy metals (Patil *et al.*, 2010; Shen *et al.*, 2013).

BES-based sensors represent a rare situation where the anodic biofilm on a carbon electrode simultaneously acts as both the bioreceptor; which facilitates analyte interaction, and the transducer; which generates a measurable electrical signal (Stein *et al.*, 2011; Di Lorenzo, 2015). Typically with most biosensors, transducer probes (which measure a specific parameter) must be installed in close proximity to bioreceptors to enable sensing applications. BES-based sensors therefore have a significant advantage for biosensing in regard to cost and complexity of devices. It is much simpler and cost-effective to have multiple pieces of carbon cloth with grown anodic biofilms (BES transducers) than it is to have multiple probe devices (*e.g.* DO probes).

## **2.5 BES-based BOD Sensor Characteristics**

In previous reviews focus has been placed on monitoring wastewater quality (Lynggaard-Jensen, 1999; Bourgeois *et al.*, 2001), various methods of determining BOD (Namour and Jaffrezic-Renault, 2010; Ponomareva *et al.*, 2011; Górski *et al.*, 2012; Reshetilov *et al.*, 2010, 2013) and different types of microbial sensors (Nakamura *et al.*, 2008; Su *et al.*, 2011; Kimmel *et al.*, 2012). Of course there are many reviews which cover BESs (Du *et al.*, 2007; Pant *et al.*, 2010a; Zhou *et al.*, 2013) but only a few are specific to MFC-based BOD sensors; an excellent review is available by Kim *et al.* (2006a) and the subject is also covered in the books by Rabaey *et al.* (2010) and Scott and Yu (2015). Abrevaya *et al.* (2015a,b) conducted a thorough review of the various analytical applications of MFCs including as BOD sensors. Schneider *et al.* (2016) presented a state-of-the-art review in which the potential of BES devices for sensing applications was described. The electron transfer principles which permit the direct interaction between bacteria and electrode were assessed, as well as the advances which have been taken towards miniaturisation of the technology. In the

present literature review, a systematic approach has been taken for assessing the results and methods used for development of BES-based BOD sensors to date. Specifically, the sensors which utilised labile organic carbon correlated with “BOD” were reviewed (dissolved oxygen-sensing BES-based BOD sensors are discussed in Section 2.6).

The characteristics of BES-based BOD sensors reported in the literature are presented in Table 2.2 which summarises the performance of each sensor by the key indicators of linear detection range and response time. The substrate used and operation mode are also listed for comparative reasons.

### **2.5.1 Substrate**

As can be seen in Table 2.2, there is a variety of different substrates which have been used ranging from simple non-fermentable substrate (acetate) to real wastewater (starch processing and municipal WW) which is significantly more complex and is harder to calibrate due to not all the substrate being readily usable. Another aspect is the variety of validation methods employed by previous authors, of which a detailed discussion is conducted in Section 7.3.4 in Chapter 7.

The largest linear ranges have been determined using artificial wastewater (AWW) substrates and, of the real wastewater sensors reported, there is obviously further work which could be done to improve performance. In some of the studies where AWW was used for calibration and then tested with real wastewaters to determine applicability it is noted that the linear correlation is not quite as accurate and this is attributed to acclimation of the biofilm. Therefore it is proposed that development of a MFC-based BOD sensor would have to be completed with a medium composition similar to that which it will be used to measure. It is evident that a commercial BES-based BOD sensor could not be a standard product and each sensor would require bespoke start-up and calibration procedures for acclimation of the biofilm to the wastewater to be tested (Kang *et al.*, 2003). You *et al.* (2015) performed experiments in which MFCs were enriched with one substrate and switched to a different substrate after acclimatisation (using acetate and casein). The MFCs generated a stable current with each substrate, however the results indicated that the anodic biofilms had higher affinities for the original substrate and therefore the need for enrichment to be performed with the substrate of interest was demonstrated.

### **2.5.2 Linear Detection Range & Response Time**

The upper limits of linear detection achieved by previous authors are subdivided into amperometric (current-based) and coulometric (charge-based) sensors in Table 2.2 because the principle of measurement is quite different. For amperometric sensors the peak (or average

Table 2.2: Literature survey of BES-based BOD sensor characteristics including amperometric and coulometric detection ranges with validation method given in square brackets and response time.

Reference	Cell type <sup>c</sup>	Mode	Substrate <sup>c</sup>	Amperometric linear upper limit	Coulometric linear upper limit	Response time
Gil <i>et al.</i> (2003)	DCMFC	Batch	Starch WW	50 mg/l [COD]	400 mg/l [COD]	< 1 h <sup>a</sup>
Kim <i>et al.</i> (2003a)	DCMFC	Batch	Starch WW	25 mg/l [BOD <sub>5</sub> ]	206 mg/l [BOD <sub>5</sub> ]	10 h
Kang <i>et al.</i> (2003)	DCMFC	Flow	GGA	6 mg/l [COD]	-	30 m
Kim <i>et al.</i> (2003b)	DCMFC	Flow	GGA	-	150 mg/l [BOD <sub>5</sub> ]	45 m
			Municipal WW	-	122.8 mg/l [BOD <sub>5</sub> ]	45 m
Chang <i>et al.</i> (2004)	DCMFC	Flow	GGA	100 mg/l [COD]	-	1 h
Moon <i>et al.</i> (2004)	DCMFC	Flow	GGA	200 mg/l [COD]	-	36 m
Chang <i>et al.</i> (2005)	DCMFC	Flow	GGA	113.5 mg/l [COD]	-	< 1 h <sup>a</sup>
Moon <i>et al.</i> (2005)	DCMFC	Flow	GGA	20 mg/l [BOD <sub>5</sub> ]	-	15 h
Kim <i>et al.</i> (2006b)	DCMFC	Flow	AWW	-	200 mg/l [BOD <sub>5</sub> ]	< 1 h <sup>a</sup>
Kumlanghan <i>et al.</i> (2007)	DCMFC	Flow	Glucose	25000 mg/l [Sub] <sup>b</sup>	-	1 h
Di Lorenzo <i>et al.</i> (2009a)	SCMFC	Flow	Glucose	350 mg/l [COD]	500 mg/l [COD]	4 h
Di Lorenzo <i>et al.</i> (2009b)	SCMFC	Flow	Glucose	250 mg/l [COD]	-	3.5 h
Kim <i>et al.</i> (2009)	SCMFC	Batch		-	500 mg/l [COD]	4 h
Peixoto <i>et al.</i> (2010)	SBMFC	Batch	Municipal WW	78 mg/l [BOD <sub>5</sub> ]	-	10 h

<sup>a</sup> Estimated value. <sup>b</sup> Range claimed (not accounting for sample dilution). <sup>c</sup> AOC = Assimilable Organic Carbon; BOD<sub>5</sub> = 5-Day Biochemical Oxygen Demand; COD = Chemical Oxygen Demand; DC = Dual Chamber; MEC = Microbial Electrolysis Cell; MFC = Microbial Fuel Cell; OECD = Organization for Economic Cooperation and Development (synthetic wastewater); SB = Submersible; SC = Single Chamber; WW = Wastewater; Sub = Substrate Concentration.

Table 2.2: continued...

Reference	Cell type <sup>c</sup>	Mode	Substrate <sup>c</sup>	Amperometric linear upper limit	Coulometric linear upper limit	Response time
Liu <i>et al.</i> (2011)	DCMFC	Flow	AD WW	200 mg/l [COD]	-	12 h
Peixoto <i>et al.</i> (2011)	SBMFC	Batch	Municipal WW	78 mg/l [BOD <sub>5</sub> ]/ 118 mg/l [COD]	-	10 h
Zhang and Angelidaki (2011)	SBMFC	Batch	Acetate	250 mg/l [BOD <sub>5</sub> ]	-	10 h
			Glucose	250 mg/l [BOD <sub>5</sub> ]	-	10 h
			Municipal WW	250 mg/l [BOD <sub>5</sub> ]	-	10 h
Modin and Wilén (2012)	SCMEC	Batch	Acetate	-	1280 mg/l [Sub]	20 h
			Propionate	-	640 mg/l [BOD <sub>5</sub> ]	20 h
			Glucose	-	640 mg/l [BOD <sub>5</sub> ]	20 h
			Ethanol	-	640 mg/l [BOD <sub>5</sub> ]	20 h
Feng <i>et al.</i> (2013b)	SCMFC	Batch	Acetate	150 mg/l [COD]	200 mg/l [COD]	3 h
Yang <i>et al.</i> (2013)	SCMFC	Flow	GGA	120 mg/l [BOD <sub>5</sub> ]	-	2.2 h
Di Lorenzo <i>et al.</i> (2014)	SCMFC	Flow	Acetate	164 mg/l [COD]	-	< 10 m
Ghangrekar (2014)	DCMFC	Batch	Acetate	212 mg/l [COD]	-	2 h
Hsieh and Chung (2014)	DCMFC	Batch	Municipal WW	240 gm/l [BOD <sub>5</sub> ]	-	12 h
Quek <i>et al.</i> (2014)	DCMEC	Flow	Acetate	3 mg/l [Sub]	-	20 m <sup>a</sup>

<sup>a</sup> Estimated value. <sup>b</sup> Range claimed (not accounting for sample dilution). <sup>c</sup> AOC = Assimilable Organic Carbon; BOD<sub>5</sub> = 5-Day Biochemical Oxygen Demand; COD = Chemical Oxygen Demand; DC = Dual Chamber; MEC = Microbial Electrolysis Cell; MFC = Microbial Fuel Cell; OECD = Organization for Economic Cooperation and Development (synthetic wastewater); SB = Submersible; SC = Single Chamber; WW = Wastewater; Sub = Substrate Concentration.

Table 2.2: continued...

Reference	Cell type <sup>c</sup>	Mode	Substrate <sup>c</sup>	Amperometric linear upper limit	Coulometric linear upper limit	Response time
Ayyaru and Dharmalingam (2014)	SCMFC	Flow	Glucose	750 mg/l [Sub]	-	80 m
Tian <i>et al.</i> (2014)	DCMFC	Batch	Wastewater	50 mg/l [BOD <sub>5</sub> ]	100 mg/l [BOD <sub>5</sub> ]	3 - 10 h
Liu <i>et al.</i> (2014)	DCMFC	Flow	OECD WW + Glucose	100 mg/l [COD]	-	10 h <sup>a</sup>
Quek <i>et al.</i> (2015a)	DCMEC	Flow	Yeast Extract	100 mg/l [Sub]/ 64 mg/l [COD]	-	3.3 m <sup>a</sup>
Wu <i>et al.</i> (2015a)	DCMFC	Flow	Acetate	275 mg/l [Sub]/ 200 mg/l [COD]	-	2h
Quek <i>et al.</i> (2015b)	DCMFC	Flow	Acetate	12 mg/l [Sub]/ 4 mg/l [AOC]	36.9 mg/l [Sub]/ 10.8 mg/l [AOC]	1.6 h
Hsieh <i>et al.</i> (2015)	DCMFC	Flow	Glucose	235 mg/l [BOD <sub>5</sub> ]	-	10 m
			Methionine	235 mg/l [BOD <sub>5</sub> ]	-	10 m
			Acetate	235 mg/l [BOD <sub>5</sub> ]	-	10 m
			Glycerol	235 mg/l [BOD <sub>5</sub> ]	-	15 m
Jia <i>et al.</i> (2016)	SBMFC	Flow	Starch	3000 mg/l [COD] <sup>b</sup>	-	2.5 h
Commault <i>et al.</i> (2016)	SBMEC	Flow	OECD WW	-	1200 mg/l [BOD <sub>5</sub> ]	17.5 h

<sup>a</sup> Estimated value. <sup>b</sup> Range claimed (not accounting for sample dilution). <sup>c</sup> AOC = Assimilable Organic Carbon; BOD<sub>5</sub> = 5-Day Biochemical Oxygen Demand; COD = Chemical Oxygen Demand; DC = Dual Chamber; MEC = Microbial Electrolysis Cell; MFC = Microbial Fuel Cell; OECD = Organization for Economic Cooperation and Development (synthetic wastewater); SB = Submersible; SC = Single Chamber; WW = Wastewater; Sub = Substrate Concentration.

stable) current achieved in the period where the BES is fed with a sample of known concentration is recorded and used to produce a calibration curve. At first glance it appears that the largest amperometric linear detection ranges are reported by Kumlanghan *et al.* (2007) and Jia *et al.* (2016), however the set-up of their experiments brings into question the validity of the claimed range. In the articles, a linear range of up to 25 g/l glucose and 3 g/l COD were stated by the respective authors, however the methods describe injection of a sample into a large reactor vessel (2.5 and 10 litres respectively) which would have significantly lowered the actual concentration received by the biofilm. In the case of Kumlanghan *et al.* (2007), 10 ml of 25 g/l stock solution was injected into a cell joined to a recirculating 2.5 litre anaerobic reactor which, when considered together, the diluted concentration would have been only be approximately 135 mg/l glucose. This inconsistency goes some way to explaining why the reported range is significantly higher than other previously reported BES-based BOD sensors.

The next highest reported amperometric ranges are by Di Lorenzo *et al.* (2009a), Zhang and Angelidaki (2011) and Ayyaru and Dharmalingam (2014). In the Di Lorenzo *et al.* (2009a) study a single chamber MFC was used for the first time as a sensor, which calibrated up to 350 mg/l COD. SCMFCs have been shown in the literature to have higher coulombic efficiencies because the air-cathode has an improved oxygen supply (compared to aerated solutions used in DCMFCs). Zhang and Angelidaki (2011) showed that by utilising a novel submersible MFC (SBMFC), which also used an air-cathode, further range improvements could be made by optimising operating conditions up to 250 mg/l BOD<sub>5</sub>. Ayyaru and Dharmalingam (2014) employed a double air-cathode to obtain a linear range up to 750 mg/l glucose.

For coulometric sensors, at present the work by Modin and Wilén (2012) has by far the highest linear range; this can mainly be attributed to the fact that the cell was operated as a microbial electrolysis cell (MEC) by applying a voltage of +200 mV instead of using a fixed resistor. By using this mode of operation the cell was able to overcome the limiting factors of internal resistance and cathodic oxygen reduction reaction (ORR) catalysis and generate current at maximum capacity. The upper limit of the detection range was 1280 mg/l acetate, however it is noted that the range was only limited by the batch cycle time, which was chosen to be 20 hours. This long measurement time is a feature of all coulometric BES-based sensors because the charge is calculated by the cumulative current over a set period of time and therefore the longer the incubation time the higher the linear range will be. This is not necessarily the best approach because for process control applications these sensors would have a significant lag time which would impact their value.

It could be argued that a sensor which takes 20 hours to respond is not a significant improvement over the traditional 5 day BOD test. Amperometric sensors on the other hand have been observed to respond in as little as 5 minutes (Moon *et al.*, 2004; Kumlanghan *et al.*, 2007) at low concentrations of BOD and it is only at the higher concentrations where current generation becomes more prolonged due to substrate diffusion limitations or biofilm retention



of substrate (Zhang and Angelidaki, 2011). Nonetheless, the amperometric sensors still perform at faster rates than the coulometric sensors at higher concentrations. Moon *et al.* (2004), Di Lorenzo *et al.* (2009a,b, 2014) and Tian *et al.* (2014) were the only groups to establish rise and fall response times for their sensors, Di Lorenzo *et al.* (2009b) observed that for a 50 ml reactor with a 5 hour up-shift response it took 8.8 hours to stabilise a down-shift response (where the concentration of BOD decreased). This is an important aspect which has been often overlooked, it is clear that a BOD sensor must be able to monitor concentration decreases as well as increases. The reason a down-shift response can take longer is due to the fact that when the concentration is lowered residual substrate may still be retained in the cell/biofilm for a longer period.

There have been sensors designated as oligotrophic MFCs; in these studies the inoculum used was a source of oligotrophic microbes which were readily adapted to low substrate concentrations. Moon *et al.* (2005) assessed the limit of detection and found it to be 5 mg/l BOD<sub>5</sub> for an oligotrophic DCMFC, upon selective addition of the growth medium it was determined that a component of a trace mineral solution was contributing to the current generation by being oxidised. With lower concentrations of this component the limit of detection was reduced to 2 mg/l BOD<sub>5</sub>. Cheng *et al.* (2014) adapted a mediator-less MFC to hexacyanoferrate in order to prevent non-electrogenic processes occurring and obtained a lower detection limit of 320 µg/l assimilable organic carbon (AOC). More recently, several authors have attempted to use MFCs to measure low levels of AOC in marine waters without mediator addition (Quek *et al.*, 2014, 2015a,b). The advantage of these sensors is that they can be used to measure low concentrations; this is an important feature for effluent streams and surface waters in environmentally sensitive areas where even low levels of BOD<sub>5</sub> (< 25 mg/l O<sub>2</sub>) can be regulated (UWWTD, 1994).

### **2.5.3 Mode of Operation**

There are various options available for BES mode of operation and cell architecture design as discussed in Section 2.4.3. Traditionally, BESs have used the dual chamber configuration which is experimentally simple to set up and is the basis for much of the MFC sensor work to date. However, the sensors which have shown the highest detection ranges have been SCMFC-based (including SBMFCs and SCMECs) and this could be attributed to the air-cathode used which is easier to operate (because no aeration is needed) and the concentration of oxygen in the air is significantly higher than that which can be dissolved in a solution.

For coulometric sensors the batch mode of operation is mostly required as a fixed time period for detection must be set, however Kim *et al.* (2003b) showed that by using an interval-based flow system a coulometric sensor could be developed. Conversely, amperometric sensors are most suited to flow-based operation because a real-time, continuous signal is generated

which can be used for measurement of BOD concentrations. Batch-mode amperometric sensors have also been developed by calibrating with the peak current obtained from each measured sample. The submersible MFCs (SBMFCs) were listed as batch-mode sensors in Table 2.2, however this was not a requirement as this configuration requires no fixed anode chamber and therefore could equally be used in flow systems without any change to the cell architecture.

In the literature, following the successful use of MFCs for power generation and wastewater treatment, often further experiments have been completed which utilised the unique features offered by certain configurations for benefit of alternative applications. A common theme in follow-up studies has been demonstrating capabilities for sensing. Hydraulically connected MFCs (serpentine-, tubular- or multi-stage-type) have unique attributes because there is a continuous flow of unused substrate from primary cells which is then consumed by subsequent cells/electrodes. At the time of writing, these BES configurations have not been used as sensors but there are clear implications for the improvement BES sensor performance which could be realised.

#### **2.5.4 Stability & Reproducibility**

One of the key advantages of BESs and the reasons they are being explored for sensor applications is their long-term stability. One of the most widely cited articles in this field is by Kim *et al.* (2003a) because a 'starch processing wastewater'-consuming MFC biosensor was reported which operated for five years without requiring component replacement. The MFC was operated continuously; with the only requirement that substrate did not become a limitation (*i.e.* that wastewater always contained BOD). This was a significant and valuable assessment of the BES technology and proved that if other operational limitations could be overcome, BES-based BOD sensors have a major advantage over conventional probe-based sensors. In the Kumlanghan *et al.* (2007) and Di Lorenzo *et al.* (2009a) papers the variation in cell voltage across extended periods was assessed and found to only be 6 % and 15 % respectively, showing the reliability of such a sensor. In addition, Kim *et al.* (2003a) and Kumlanghan *et al.* (2007) observed standard deviations of 12 % and 9 % respectively for repeated calibrations over the period of operation. Reproducibility of determinations without re-calibration is a vital characteristic for assessing BOD sensors because it is a major limitation of the existing DO probe-based sensors (Tan *et al.*, 1992; Riordan, 2003).

Chang *et al.* (2004) determined that the longer a MFC-based BOD sensor was starved of substrate the longer the recovery time was. They found a 30 minute interruption could be regained in three hours, whereas 270 hours recovery was needed following an 80 hour starvation. By inhibiting protein synthesis (with chloramphenicol) they observed that the current could still be recovered and therefore the recovery period did not involve regeneration of new protein. Di Lorenzo *et al.* (2009a) used starvation of the biofilm prior to calibration

with different concentrations of substrate to ensure known concentrations were used. In the Namour and Jaffrezic-Renault (2010) review it was reported that starvation of the biofilm could lead to population drift within MFCs which could alter the calibrated current response, therefore it is most practical that BES-based BOD sensors are used continuously for wastewaters where non-limiting BOD levels have a constant presence (e.g. influent monitoring).

### **2.5.5 Optimisation of Sensor and Configuration**

The materials used and operating parameters of all the sensor studies detailed in Table 2.2 are summarised in Table A.1 in Appendix A. The studies relating to optimisation of operating parameters undertaken in the literature to improve sensor performance are discussed below.

Virtually all anode materials used in BES are carbon-based because they are biocompatible, conductive materials which act as a support for biofilm development. Moon *et al.* (2004) evaluated the effect of changing the anodic volume of a BOD biosensor by using cells of 25 ml and 5 ml capacity. They observed that by optimising and scaling down the MFC design the non-ideal flow of the system was reduced and this led to much improved up- and down-shift response times as low as 5 minutes and 11 minutes respectively. Di Lorenzo *et al.* (2009a) also observed this same outcome comparing a 50 ml cell to a 12.5 ml cell in which up-shift responses decreased from 4 hours to 40 minutes. This was attributed to having a closer anode-cathode spacing which is known to improve performance of MFCs.

The cathode materials used in the BES sensor literature use graphite- and carbon-based supports. With the addition of platinum or carbon nano-particle catalyst coatings the cathode materials were made significantly more active for the oxygen reduction reaction, this in turn meant that anode materials were less limited by cathode activity and biofilms developed and metabolised at maximum capacity. Kang *et al.* (2003) reported that, in a dual chamber setup, use of a highly active cathode enabled the oxygen requirement to be lowered and therefore this was beneficial for oligotrophic MFCs where diffusion of oxygen into the anodic chamber is especially detrimental. Kim *et al.* (2009) optimised the hot-pressing conditions for producing an membrane-electrode assembly (MEA) for a biosensor and found coulombic efficiency and sensor sensitivity could be improved. Gas diffusion electrodes utilised in single chamber and submersible BES configurations have been shown to have much increased performance compared to dual chamber MFCs. In fact the cells utilising air-cathodes all give the highest detection ranges which is a notable finding for these sensors (Table 2.2).

Wu *et al.* (2015a) and Quek *et al.* (2015b) made use of a mediated cathode using potassium ferricyanide which enables operation without aeration. Its usage is increasingly avoided in microbial fuel cells because it requires replenishment and more importantly is toxic to micro-organisms if it permeates through the ion exchange membrane (Verstraete and Rabaey, 2006).

The membrane between the anodic and cathodic chambers of a BES cell is required in order to prevent oxygen influx into the anode chamber, prevent biofouling of the cathode and allow protons to transfer from the oxidised substrate at the anode to the cathodic side for ORR. Cation exchange membranes (CEMs) have been used frequently in the literature as well as proton exchange membranes (PEMs), which are a more specific and expensive type of CEM. Ghangrekar (2014) used a ceramic separator as a low-cost alternative membrane for BES sensing. Kang *et al.* (2003) improved the coulombic efficiency and stability of an oligotrophic MFC by using the minimum area of membrane to reduce diffusion of oxygen into the anodic chamber; this approach could be used in other MFCs to improve anode efficiency although a compromise must be struck in regard to increases in cell internal resistance. Ayyaru and Dharmalingam (2014) employed a double-MEA configuration and observed sensor detection range improvements of 114%, higher current and coulombic efficiencies and lower response times.

Modin and Wilén (2012) argued that the use of a membrane leads to the build-up of protons in the anodic chamber and this decreases the pH and damages the biofilm, there is also the problem of biofouling which reduces performance significantly and requires maintenance in the long-term (Kim *et al.*, 2003b). In the Modin and Wilén (2012) article, filter paper was used instead of a membrane to prevent biofouling of the cathode surface and the influx oxygen was deemed negligible for measuring high concentrations of BOD. However, this approach seems counter-intuitive because there would constantly be a lower coulombic efficiency as electrons are accepted by oxygen preferentially than the anode electrode. The membrane-less approach is also being investigated for BES scale-up where the use of expensive membranes and replacement due to fouling is not desirable. However, where precious metal catalysts are used at the cathode a sacrificial membrane is perhaps a necessary barrier for biofouling to occur upon.

Kim *et al.* (2006a) states six factors which must be optimised to increase current generation from MFCs including; fuel oxidation by microbial activity, electron transfer to the electrode, resistance, proton transfer to cathode, oxygen supply / reduction at the cathode and oxygen diffusion into the anode chamber. In terms of BOD sensors, oxygen diffusion poses the greatest issue because oxygen can be used as an alternative electron acceptor by the microbes and therefore coulombic efficiency is decreased and BOD could be under-estimated.

One of the earliest reported mediator-less MFC-based sensors was a lactate sensor using a pure culture of *Shewanella putrefaciens* IR-1 at the anode (Kim *et al.*, 1999). The bacteria was chosen because it selectively used lactate as an electron donor. When the sensor was tested with acetate and glucose there was no response, however the sensor was found to give false-positive readings for pyruvate and formate which the bacterium could also use as electron donors. Consequently, BES sensor research has focused less on sensors for specific substrates and more on broader parameters (such as BOD). For this application it is broadly stated that a mixed community inoculum will give the best and most accurate

response because there are fewer electron donors which cannot be used or degraded. It is for this reason that many of the references listed in Table A.1 use aerobic and anaerobic sludges from WWTPs as an inoculum because they are diverse sources of bacteria used for degradation of a multitude of substrates (Erable *et al.*, 2010). After inoculation it can take a significant amount of time (in some cases months) to enrich BES biofilms before a stable current is reached with repeated batch cycles. Another approach which has been used in some papers is to use pre-enriched bacteria sourced from existing MFCs with biofilms acclimated to the growth medium to be used; this has led to improved start-up times in the region of days (Moon *et al.*, 2005; Di Lorenzo *et al.*, 2014; Liu *et al.*, 2014; Wu *et al.*, 2015b).

The external load of a MFC is an important variable which must be optimised in order to get the best performing sensor. In MFCs the current is calculated from the recorded cell voltage divided by the external resistance, therefore the lower the resistance the higher the current. This is optimal for MFC-based BOD sensors because the higher the current the greater the accuracy (signal to noise ratio) can be in determining concentration from a calibration curve, it is for this reason that many of the papers shown in Table A.1 use a 10  $\Omega$  resistor. Additionally, Wu *et al.* (2015a) found an extension to the detection range by decreasing the external resistance from 100 to 20  $\Omega$ .

Various approaches have been taken to investigate effect of the external resistance ( $R_{Ext}$ ) on the sensor performance. Gil *et al.* (2003) and Kang *et al.* (2003) found by changing the resistor after enrichment that at low  $R_{Ext}$  ( $\leq 200 \Omega$ ) the current reached peak values immediately after substrate replenishment and was followed by rapidly decreasing shoulder peaks due to limited cathode ORR. Whereas at  $R_{Ext}$  greater than 200  $\Omega$  the resistance became rate-limiting and the current profile was stable over the course of substrate cycle. Moon *et al.* (2004) found that increasing  $R_{Ext}$  from 10 to 100  $\Omega$  decreased slightly the up-shift response time, however the down-shift response was significantly longer and sensitivity was less, again showing that resistance limited the current generation.

Di Lorenzo *et al.* (2009a) conversely found that lowering the resistance lowered the up-shift response time (from 13.75 to 4.5 hours) but noted that below 50  $\Omega$  the current was not stable enough to record accurately. Zhang and Angelidaki (2012) operated a MFC as a combined BOD/DO sensor and observed a linear relationship between DO and current density for  $R_{Ext}$  between 10 - 2000  $\Omega$ . The linear regression coefficient ( $R^2$ ) increased with increasing  $R_{Ext}$ ; this is most likely due to more stable currents being recorded at higher values. They found that response time was up to five times longer with higher resistance. In summary, for BOD determination it appears for amperometric sensors where a peak current is used a lower resistance is beneficial as both current density and response times have been found to improve, whereas for coulometric sensors a higher resistance ( $> 500 \Omega$ ) would be required to have a stable current profile over a substrate cycle.

For continuous flow systems the flow rate is an important parameter which must be optimised to achieve best sensor performance; if the rate is too slow the biofilm may become mass transfer limited and if the rate is too high the biofilm may be sheared from the electrode. Additionally, a high flow rate may exceed the rate of conversion and the substrate will not be fully utilised because oxidant supply at the cathode side becomes limiting. Chang *et al.* (2004) observed increases in current up to 1.07 ml/min at which point the current plateaued with further increases in flow rate. Decreased coulombic efficiencies were obtained at higher rates due to incomplete substrate utilisation. This behaviour was also reported by Moon *et al.* (2004, 2005), Di Lorenzo *et al.* (2009a) and Hsieh *et al.* (2015), however the optimal flow rates differed as can be seen in Table A.1. One way of normalising the flow rates to allow comparisons to be made is to calculate the hydraulic retention time (HRT; Equation 3.3 in Chapter 3); the volume of the anodic chamber divided by the influent flow rate.

HRT represents the time substrate spends within the BES before being discharged in a continuous flow setup. The HRTs in the studies mentioned here ranged from 38 to 240 minutes which indicated that differences in the cell architectures led to differing rates at which point anode saturation occurred. Liu *et al.* (2011) operated a MFC with a volume of 1.6 ml in a wall-jet flow regime which involved a fast influent flow of 7.76 ml/min (HRT = 12 seconds) and the medium was recirculated over a period of two days to monitor an anaerobic digester process in near real-time. In general it has been found that the shorter the HRT the shorter the up-shift and down-shift response times will be, which is logical due to the rate at which residual substrate is replaced.

### **2.5.6 Control of Environmental Variables**

MFC current response profiles have been seen to exhibit fluctuations proportional to changes in temperature which could be falsely attributed to BOD in a sensor, therefore temperature regulation is necessary. It is for this reason that almost all the BES sensors listed in Table A.1 have some form of temperature control or for those operated at room temperature the variation was minimal (*e.g.*  $\pm 2^{\circ}\text{C}$ ). In tests completed at different temperatures with MFC sensors in the literature, positive linear correlations were established between current and temperature. The best coulombic efficiencies due to improved bacterial metabolism have been reported between 30 and 37 °C (Kumlanghan *et al.*, 2007; Di Lorenzo *et al.*, 2009a; Peixoto *et al.*, 2010, 2011; Zhang and Angelidaki, 2011, 2012). Another approach put forward by Peixoto *et al.* (2010) is that a correction factor could be modelled for various environmental factors which cause variations in a MFC sensor output to enable operation of the sensor without requiring control of every possible environmental variable.

The pH of the medium is another variable which alters the microbial activity of the anodic biofilm if not controlled, in most cases where AWW is used a buffer is added to prevent wide pH changes occurring during the operation of the BOD sensor. Even in cases where real

wastewater is used the medium is sometimes amended with buffer to provide controlled conditions. Studies have shown that the optimal pH for MFC-based BOD sensors is 7 with a tolerance between approximately pH 6 and 8 (Gil *et al.*, 2003; Wu *et al.*, 2009; Peixoto *et al.*, 2011; Zhang and Angelidaki, 2011, 2012; Yang *et al.*, 2013). The correction modelling approach could potentially be used to allow non-amended wastewaters to be monitored online.

The medium conductivity is a major factor to be considered during BES-based BOD sensing operations, this is because as the conductivity of the medium increases so will the current generated. Conductivity therefore is a factor which must be controlled or accounted for with modelling (Peixoto *et al.*, 2010, 2011; Zhang and Angelidaki, 2012). When calibrations were undertaken with real wastewater and dilutions Zhang and Angelidaki (2011) observed that the error in BOD estimation due to differing environmental factors was within normal accepted limits ( $\pm 15\%$ ) and therefore it may be possible to correct or allow for these depending on the expected variations in a wastewater treatment facility.

DO is another environmental variable which can have a linear response with current generated by a BES, Zhang and Angelidaki (2012) proved this by operating a BES as a combined BOD-DO sensor. Therefore, for accurate BOD detection the DO levels must be controlled. In most cases this is done by initially purging the medium feed vessel with nitrogen (Kang *et al.*, 2003; Di Lorenzo *et al.*, 2009a), continuously sparging (Kim *et al.*, 2003a) or connecting a nitrogen-filled gas bag to the influent head space (Kang *et al.*, 2003). Conversely, Modin and Wilén (2012) chose to aerate the nutrient medium with oxygen to control at a high level of DO (because no membrane was used), and as previously discussed this seems like a counter-intuitive practice for development of a BES-based BOD sensor where oxygen acts as an alternative electron acceptor to the anode.

Chang *et al.* (2005) presented an interesting paper in which respiratory inhibitors were used in a MFC-based BOD sensor. Nitrate and dissolved oxygen are both electron acceptors which can be present in wastewaters and in MFCs will decrease coulombic efficiency by being preferentially reduced over electron donation to the electrode. It was demonstrated that by using cyanide the nitrate reductase enzyme can be inhibited and therefore higher currents can be obtained. When azide was used as the inhibitor, cytochrome oxidase (responsible for aerobic respiration) was also inhibited and further coulombic efficiency improvements were made. Hsieh *et al.* (2015) conducted similar experiments and additionally used rotenone (a NADH dehydrogenase inhibitor) and observed improvements to the MFC performance when DO, nitrate, nitrite and sulphate were present. It was evident that the MFC performance was not negatively affected by these metabolic inhibitors, however the injection of additional reagents in order to achieve these gains brings into question the applicability of this approach long-term and at full scale. In the BOD<sub>5</sub> test there are several reagents which must be added in order to complete the test and it is this labour intensive type of analysis that novel sensors are attempting to reduce requirements for as it adds additional operational cost.

Nonetheless, for applications in which wastewaters contain high levels of nitrate, being able to use inhibitors to measure the BOD more accurately is surely an acceptable compromise for BES-based BOD sensors.

### 2.5.7 Application & Advancement

Application of developed BES-based BOD sensors to real-world treatment facilities is an under exploited area but one which requires a significant amount of attention as there are likely to be further challenges which have not been anticipated in laboratory experiments to date. Kim *et al.* (2003b) tested a coulometric MFC-based BOD sensor which was installed at a sewage treatment plant, and operated for over a year following calibration with artificial wastewater. During this time it was observed that the signal decreased over approximately six months, and this was attributed to clogging / biofouling of the membrane, thus decreasing coulombic efficiency. Kim *et al.* (2007) also presented data collected from a sensor applied to a wastewater treatment plant and showed that a diurnal BOD variation was observed due to increased BOD-inputs from human activity during the day leading to higher BOD concentrations in the influent. Liu *et al.* (2011) installed a sensor onto an anaerobic digester to monitor acetate-based intermediates. The findings were that at high concentrations there was an inhibition effect and this was possibly due to excessive substrate overloading or the presence of H<sub>2</sub>S in the feed. The observations made during field testing is already prompting further laboratory research into areas such as long term stability enhancements and prevention of biofouling which warrants more online, real wastewater trials to be completed.

Linear regression models used to assess correlations between BOD and BES response outputs (current and charge) are not capable of modelling the non-linear asymptotes of the calibration curve occurring at low and high concentrations. The Michaelis-Menten (M-M) equation (Equation 2.1) has conventionally been employed for modelling dose-response relationships in enzyme reactions and is mathematically identical to the Monod equation used to model bacterial growth curves over time (Kompala, 2011).

$$v = \frac{v_{Max} [S]}{K_M + [S]} \quad (2.1)$$

where  $v$  is the reaction rate (MFC current),  $v_{Max}$  is the maximum reaction rate,  $[S]$  is the substrate concentration (BOD<sub>5</sub>) and  $K_M$  is the Michaelis constant (Kompala, 2011). In the BES sensing literature, the M-M equation has been used for modelling the full concentration range in BES calibrations (Chang *et al.*, 2004; Liu *et al.*, 2014; Wu *et al.*, 2015a). Wu *et al.* (2015a) used the M-M-derived Michaelis constant ( $K_M$ ), the concentration at half saturation, to compare sensor calibrations with sodium acetate and substrate adsorption affinities obtained using granular activated carbon and graphite anodes.

Although many efforts have been made to optimise and enhance the detection range of BES-



based BOD sensors, research studies have also been driven to model the behaviour of MFCs under different conditions. Feng *et al.* (2013a) suggested a model which was successfully used to distinguish between four different substrates used in a microbial fuel cell based on the peak height and peak area of the current response. Artificial neural network kinetic models were used to establish features of the responses from the four substrates and allowed explicit identification of these substances. Another study used the same kinetic models to derive the COD concentration from the current response and the calibration with measured COD was linear with a regression coefficient of 0.99 (Feng *et al.*, 2013b). There is evidently a large scope for data processing methods to bring significant advances to prediction of MFC sensor behaviour under defined conditions. It is becoming apparent that modelling may be the key to making corrections for some of the environmental variables which are likely to be present in real wastewater applications where MFC-based BOD sensors will be used.

## **2.6 Combined Biomonitoring & Non-BOD BES-based Sensors**

### **2.6.1 *Microbial Activity***

A microbial activity sensor was produced by Zhang and Angelidaki (2011) which utilised a fresh anode (no biofilm) and demonstrated a linear response with different ATP concentrations in artificial groundwater, which were deemed to be an indicator of microbial activity. The sensor gave no linear response with a range of different BOD concentrations. The problem with this proposed sensor was there appeared to be nothing to prevent the formation of a biofilm on the fresh anode surface, which would result in a BOD-current response arising. However, the sensor did show evidence that a combined biomonitoring system was feasible and could be used with contaminated groundwaters to monitor microbial activity (ATP concentration) with no biofilm and BOD concentration when a biofilm is grown.

### **2.6.2 *Dissolved Oxygen***

Zhang and Angelidaki (2012) developed a MFC-based sensor and demonstrated how the current response could be calibrated to the DO concentration and the BOD concentration. It was notable however that in order to measure one variable linearly the other was required to be constant. This detection method is not likely to be a possible solution for monitoring DO in real wastewaters; as previously mentioned diurnal variations of BOD occur which would mean the DO could not be measured without application of a correction factor. At high levels of BOD concentration where the cell voltage plateaus the sensor could successfully be used providing that the wastewater remained at these levels continuously. Equally, if the DO concentration is not controlled or constant the BOD determination can be under or over estimated.

Recent research by Schievano *et al.* (2016) employed a novel, low-cost floating MFC configuration comprised of an EMEA (electrode-membrane-electrode assembly) in which the anode and cathode were pressed to both sides of the membrane held in a buoyant support. Two modes of operation were devised for MFC sensing; the first with the anode pointing downwards into the liquid analyte and the air-cathode facing upwards to the air. The second mode of operation was reversed with the cathode pointing downwards and the anode upwards into BOD-containing anoxic sediment. The principle of the second sensing approach utilises an aerobic biocathode for which the current response has been demonstrated to correlate with dissolved oxygen concentration (Milner, 2015). Sensing DO at the cathode negates the requirement for constant BOD as the anodic feed was controlled separately.

### **2.6.3 Toxicity**

The major combined biomonitoring system which has received the most interest in the literature is the combination of a BOD sensor and toxicity sensor. The combined sensor could be used in wastewater treatment plants which periodically receive toxic compounds in their influent streams. Unlike the previous two biomonitoring systems, this monitoring technique has two principles of measurement; the generation of current by BOD and the loss of current due to toxic inhibition. The application in this case requires a fast, early warning system enabling plant operators to take action to prevent damage to treatment facilities and prevent discharge of harmful effluents.

Kim *et al.* (2006b) detailed the first BOD/toxicity sensor in which BOD was monitored continuously and a signal change was observed when certain toxic substances were present. The toxic substances included heavy metals, biocides, organic compounds and surfactants and each induced a rapid decrease in cell voltage following introduction from inhibited microbial metabolism. The profile of the response showed an increase in current for increases in BOD and decreases in current with presence of toxic substances (from 'normal' operating conditions). Kim *et al.* (2007) also reported on a configuration comprised of two MFCs with one acting as a replacement following the inhibition of the first. When typical loadings of cadmium and lead were added (0.01 to 0.1 mg/l) the recovery of the sensor was fast, in the order of one hour, however when higher concentrations were added (1 mg/l) the recovery time of the sensor became prolonged up to 8 hours. Thus showing that although the MFC can be used for detection of toxic compounds it risks destroying the acclimated community at the anode and re-calibration would likely be required following toxic events. It is worth noting that, during the period of a year, no toxic events were observed by Kim *et al.* (2007) at the plant where the sensor was installed meaning that artificial toxic events had to be created; therefore showing the rarity of such occurrences at particular wastewater plants.

In more recent articles, BES devices have been employed exclusively as toxicity sensors, usually under saturated BOD conditions so that the non-toxic signal remained constant. Patil

*et al.* (2010) operated a MEC half cell inoculated with primary wastewater inoculum in comparison to a MEC half cell with anthraquinone-2-sulfonate mediator and planktonic bacteria. Response to toxicants including antibiotics (sulfamethaxazole and sulfadiazin), disinfectants (chloramine B) and  $\text{Cu}^{2+}$ ,  $\text{Ag}^+$ ,  $\text{Pb}^{2+}$  and  $\text{Hg}^{2+}$  were evaluated. No response (sensitivity) was observed with the mediator-less MEC half cell at  $10\times$  concentrations ordinarily found in wastewaters (*e.g.*  $< 15 \text{ mg/l}$  for the metal ions). Whilst this is not a good feature for toxicity sensing, this result can be used as a demonstration of the robustness of the anodic biofilm and resistance to antimicrobial compounds.

Stein *et al.* have published many articles relating to toxicity sensing using BES. They found that, in order to obtain a stable baseline current under non-toxic conditions for  $\text{Cu}^{2+}$  sensing, changes in pH and anode potential (of an MEC half cell) were required to be constant (Stein *et al.*, 2010). Using different membrane types (including anion exchange and bipolar) did not affect the sensitivity to positively-charged toxicants despite the fact that cation exchange membranes could permit passage through to the cathode chamber (Stein *et al.*, 2012a). In addition, a linear response between the current density and up to  $200 \text{ mg/l}$   $\text{Ni}^{2+}$  was established. The effect of external resistance was assessed with surfactant (sodium dodecyl sulfate) toxicant (Stein *et al.*, 2012b). At low resistance ( $100 \Omega$ ) the BES was more sensitive to toxic events but the recovery time was also longer (3.1 hours compared to 2.5 hours at  $1000 \Omega$ ). Kinetic models were developed for four modes of toxicity which affect BESs; (i) noncompetitive inhibition, (ii) toxicant acting as an alternative electron acceptor, (iii) toxicant inducing a change in reactant/product ratio (*e.g.* low pH reduces forward anodic reaction) and (iv) competitive inhibition between substrate and toxicant (Stein *et al.*, 2011). The overpotential set in a MEC half cell can alter the sensitivity to toxicity but depends on the mode of action (*e.g.* high overpotential is best for detection of toxicants which affect the biofilm affinity for substrate). In the Stein *et al.* (2012c) article, a kinetic model was used for estimation of substrate ("BOD") concentration with  $\text{Ni}^{2+}$  toxicant present by measuring polarisation curves in non-toxic and toxic conditions.

BES-based toxicity sensors have been used to measure toxic responses from toxicants including; heavy metals such as  $\text{Cd}^{2+}$  (Kim *et al.*, 2006b, 2007; Wu *et al.*, 2010; Di Lorenzo *et al.*, 2014; Jiang *et al.*, 2015a),  $\text{Cr}^{6+}$  (Kim *et al.*, 2006b; Xu *et al.*, 2015, 2016),  $\text{Cu}^{2+}$  (Patil *et al.*, 2010; Wu *et al.*, 2010; Stein *et al.*, 2010; Shen *et al.*, 2013; Jiang *et al.*, 2015b),  $\text{Ni}^{2+}$  (Stein *et al.*, 2012a,c; Xu *et al.*, 2015),  $\text{Pb}^{2+}$  (Kim *et al.*, 2006b, 2007; Patil *et al.*, 2010),  $\text{Hg}^{2+}$  (Kim *et al.*, 2006b; Patil *et al.*, 2010),  $\text{Ag}^+$  (Patil *et al.*, 2010), biocides (cyanide and arsenic) (Kim *et al.*, 2006b) and surfactants including sodium dodecyl sulfate (Kim *et al.*, 2006b; Stein *et al.*, 2012b). The list further includes petroleum (Showalter, 2013), pesticides such as aldicarb (King, 2014) and organophosphorus (Kim *et al.*, 2006b), industrial chemicals such as formaldehyde (Davila *et al.*, 2011; Wang *et al.*, 2012; Lee *et al.*, 2015), PCB (Kim *et al.*, 2006b), dimethyl-methylphosphonate and bisphenol-A; (King, 2014), antibiotics such as tobramycin (Wu *et al.*, 2014), sulfamethaxazole and sulfadiazin (Patil *et al.*, 2010), disinfectants such as

chloramine B (Patil *et al.*, 2010) and NaClO (Xu *et al.*, 2016), and acidity (HCl; Shen *et al.* (2012)).

Many of the authors have utilised microlitre-sized BES devices in order to improve sensitivities (Davila *et al.*, 2011; Showalter, 2013; Di Lorenzo *et al.*, 2014; Lee *et al.*, 2015; Xu *et al.*, 2015, 2016). A large number of studies also used the MEC half cell mode of operation with a fixed anode potential to amplify the effect of toxicity presence by controlling the overpotential on the working electrode (Stein *et al.*, 2010, 2012a,c; Shen *et al.*, 2012; Lee *et al.*, 2015; Jiang *et al.*, 2015b). Single strains of electroactive species such as *Geobacter sulfurreducens* and *Shewanella oneidensis* have been used to produce a defined toxic response, the disadvantages of this with regard to substrate range (or in this case toxicity mode of action range) have been discussed previously (Davila *et al.*, 2011; Wang *et al.*, 2012; Showalter, 2013; Wu *et al.*, 2014; Lee *et al.*, 2015).

Mono-nitrophenols are toxic chemicals used as precursors in the manufacture of various industrial chemicals (including pharmaceuticals, dyes and pesticides; US PHS (1992)) and are regulated by the United States Environmental Protection Agency (US EPA, 2014). 4-nitrophenol (4-NP) has been identified as the most toxic of the mono-nitrophenols. There have been reports of BES being acclimatised to utilise 4-NP as a substrate to achieve partial and complete degradation using biocathodes and bioanodes (Jiang *et al.*, 2016b). Liu *et al.* (2013) used 4-NP as a substrate in MFCs and, although a toxic effect was observed, electricity was generated in correlation with the concentration of 4-NP. Small coulombic efficiencies were calculated (< 1.1%) and complete degradation was observed after 142 hours of operation. Chen *et al.* (2016) operated MFCs as a 4-NP biosensor with a pure strain of *Pseudomonas monteilii* LZU-3 in an unusual aerobic anode configuration. Despite obvious coulombic losses due to the presence of oxygen, 4-NP was degraded to CO<sub>2</sub> and nitrite via non-toxic intermediates and the small amount of electricity generated (approximately 5  $\mu\text{A}/\text{cm}^2$ ) correlated with 4-NP concentration. Jiang *et al.* (2016b) analysed the communities of MFC bioanode and biocathode biofilms acclimatised to mono-nitrophenol degradation and found the smallest diversity with 4-NP. In addition to *Geobacter* and *Desulfovibrio* different syntrophic genera were found depending on the treatment.

The problem with attempting to quantify the amount of toxic substance present using the anode of a BES is that there are many variables which would be required to be controlled, including BOD; this is impractical just to quantify the amount of toxicant. Also, the inhibited response is not selective because if other toxic substances are present there is likely to be varying levels of inhibition. Therefore, a BES-based sensor for a specific toxicant would be difficult to calibrate, for similar reasons that development of BES sensors for specific substrates has been largely stopped in favour of developing broader monitoring systems for BOD/BOM. The monitoring application gains most value from providing an early warning system capable of alerting process control operators rather than attempting to quantify an unknown toxic substance.

## 2.7 Conclusions

As has been detailed in this systematic review, there has been a vast body of research completed on the development of BES-based BOD sensors to date. Many different configurations and operating parameters have been tested, and optimisations have been demonstrated which can improve the overall sensing capability of these systems. Many papers have covered only individual parameters, and often neglect to use improvements which have been proven in past research by other groups. There is definitely an opportunity for a sensor to be produced which takes into account all the optimisations listed in this review.

New approaches into cell design, combined biomonitoring and modelling are the leading themes of the state-of-the-art research in this area. There is also an opportunity to use existing methods from other fields to advance the MFC-based sensor technology. It is clear that in order to replace the BOD<sub>5</sub> test, and provide a suitable alternative, there are still some key performance issues which must be addressed regarding range and response time of BES sensors. MFCs have proven at least that the stability of such systems is considerably greater than other BOD sensors currently in use today.

Another area which could benefit the technology is the undertaking of more field tests with sensors being tested with real wastewaters; instead of so-called 'artificial' wastewaters often made up of only simple, readily degradable substrates. In order for these sensors to be commercially viable there will need to be numerous tests which prove they can actually operate on real-world wastewater treatment plants, and not only correlate accurately, but also offer benefits to plant operators who will use them by demonstrating improved process control and increased productivity.



## Chapter 3. Materials and Methods

### 3.1 Set-up of Microbial Fuel Cells

#### 3.1.1 Cell Architecture

Fifty millilitre single chamber microbial fuel cells (SCMFCs) were constructed from two  $85 \times 85 \times 12$  mm ( $w \times h \times d$ ) acrylic end plates compressed against a  $62.5 \times 40$  mm ( $\varnothing \times d$ ) acrylic cylindrical spacer (Figure 3.1a). Both the anode and gas diffusion end plates had four M5 bolt holes in the corners and a central recess of  $62.5 \times 5$  mm ( $\varnothing \times d$ ) with a 0.75 mm  $\varnothing$  top hole for wire connection. The gas diffusion end plate additionally had a central void of  $40 \times 7$  mm ( $\varnothing \times d$ ) to allow air to reach the gas diffusion electrode. The cylindrical spacer had a central void of  $40 \times 40$  mm ( $\varnothing \times d$ ) in addition to two top ports and a single bottom port of size 1/8" NPT. The bottom port was plugged and the top port closest to the anode electrode was used for a reference electrode. The second top port was sealed with a removable polyethylene seal for sampling and medium replacement. Each 50 ml cell was assembled with the anode electrode and 0.75 mm  $\varnothing$  titanium wire (Goodfellow, UK) enclosed in silicone gaskets (RS Components, UK) and compressed between the anode end plate and one side of the spacer. On the other side of the spacer, the gas diffusion electrode, titanium wire and membrane enclosed in silicone gaskets were compressed against the gas diffusion end plate. The complete cell was secured and compressed by M5 nuts and bolts (RS Components, UK) in each corner.

Ten millilitre SCMFCs were constructed from two  $50 \times 50 \times 9$  mm ( $w \times h \times d$ ) acrylic end plates compressed against a  $50 \times 50 \times 20$  mm ( $w \times h \times d$ ) acrylic spacer (Figure 3.1b). Both the anode and gas diffusion end plates had four M4 bolt holes in the corners and a central recess of  $37.5 \times 4$  mm ( $\varnothing \times d$ ), with a  $2 \times 4$  mm ( $w \times d$ ) top cut-out for wire connection. The gas diffusion end plate also had a central void of  $25 \times 5$  mm ( $\varnothing \times d$ ). The spacer had a central void of  $25 \times 20$  mm ( $\varnothing \times d$ ), two top ports and a side port of size 1/8" NPT. The side port was used for medium inlet, one top port used for medium outlet on a pumped system and the second top port used for a reference electrode. Each 10 ml cell was assembled in a similar manner to the 50 ml cells except, instead of titanium wire, a titanium disc current collector (62.5 mm  $\varnothing$  Ti disc spot-welded to 0.75 mm  $\varnothing$  Ti wire) was used at the anode side and a titanium ring current collector (37.5 mm outer  $\varnothing$  Ti ring with 25 mm inner  $\varnothing$  spot-welded

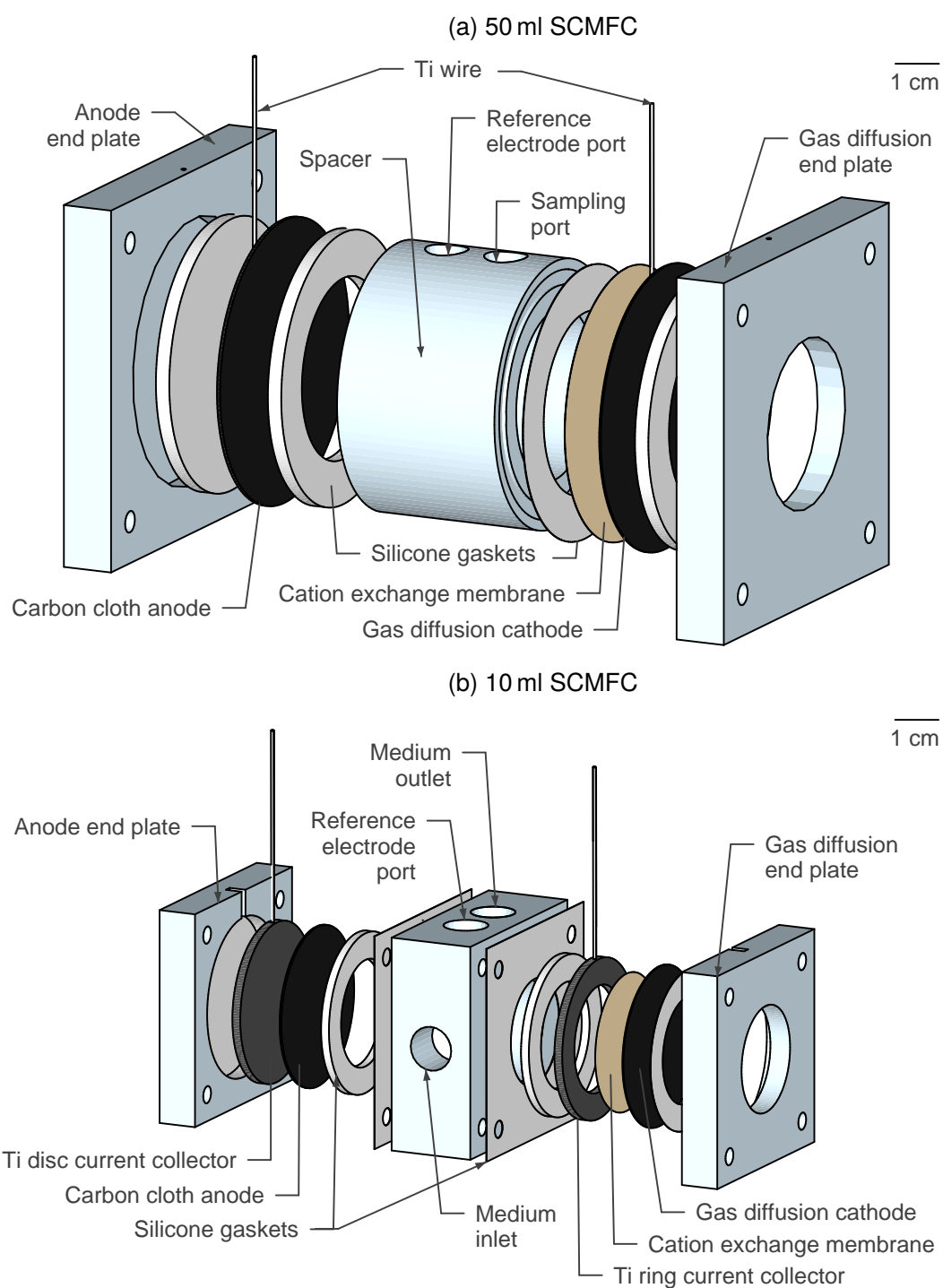


Figure 3.1: Schematic exploded diagrams of (a) 50 ml SCMFC and (b) 10 ml SCMFC.



to 0.75 mm Ø Ti wire) at the cathode side to improve electrical contact.

The 50 ml cells were used for batch-mode operation experiments and the 10 ml cells were used for flow-mode operation experiments. The characteristics of each cell are listed in Table 3.1. The 50 ml cell has a greater effective electrode area ( $A_{Eff}$ ; area not covered by the gasket and exposed to the cell contents) than the 10 ml cell but due to decreased electrode spacing the smaller cell has a two-times greater effective electrode area to cell volume ratio of 0.50 and therefore exhibits smaller internal resistance ( $R_{Int}$ ).

Table 3.1: Comparison of characteristics of 50 ml & 10 ml SCMFCs.

Term	Characteristic	SCMFC	
		50 ml	10 ml
$Sp$	Electrode spacing <sup>a</sup> (cm)	4.0	2.0
$A_{Tot}$	Total electrode area <sup>b</sup> (cm <sup>2</sup> )	19.6	11.0
$A_{Eff}$	Effective electrode area <sup>c</sup> (cm <sup>2</sup> )	12.6	4.9
$Vol$	Cell void volume <sup>d</sup> (cm <sup>3</sup> )	50.3	9.8
$\frac{A_{Eff}}{Vol}$	Effective electrode area to Cell volume ratio (cm <sup>-1</sup> )	0.25	0.50

<sup>a</sup> Distance between anode and cathode electrodes. <sup>b</sup> Area of electrode material as-cut.

<sup>c</sup> Area of electrode exposed to cell (not covered by gasket). <sup>d</sup> Cell volume (not including ports) =  $A_{Eff} \times Sp$ .

### 3.1.2 Electrodes

All microbial fuel cell anode biofilms were grown upon activated carbon cloth electrodes (Chemviron, Belgium). 19.6 cm<sup>2</sup> (2.5 cm Ø) circular electrodes were cut out for 50 ml SCMFCs and 11.0 cm<sup>2</sup> (1.9 cm Ø) circular electrodes were used for 10 ml SCMFCs. Carbon cloth electrodes were soaked in acetone (Sigma-Aldrich, UK) for 16 hours to remove organic contaminants before being rinsed thoroughly with deionised water (DI water) to remove the solvent.

For the cathode, gas diffusion electrodes (GDEs) were initially prepared using untreated carbon paper (Alfa Aesar, UK) according to Cheng *et al.* (2006a,b). The air-side of the untreated carbon paper was wet-proofed to prevent cell leakage by coating four hydrophobic layers of a polytetrafluoroethylene dispersion (60 wt% PTFE in water; Sigma-Aldrich, UK). In between each coating the electrode was dried at 100 °C. After the final application the layers were sintered at 370 °C for 30 minutes in a furnace. A microporous layer (MPL) of carbon was added to the cell-side of the carbon paper to increase gas diffusion to the catalyst layer and to provide a substrate for greater adhesion of the catalyst layer to the carbon paper. For the MPL an ink was prepared constituted of 2 mg carbon black (Ketjenblack® EC-300J; Azko Nobel, The Netherlands), 0.19 µl PTFE dispersion and 0.1 ml acetone per cm<sup>2</sup> of electrode. In later experiments, carbon paper which had been pre-coated with PTFE

and a MPL (H23C6; Freudenberg FCCT, Germany) was used for GDE preparation which resulted in greater PTFE/MPL loading reproducibility and reduced preparation time.

Catalyst ink was prepared to give a final platinum loading of 0.5 mg/cm<sup>2</sup> by using 2.5 mg Pt/C (platinum, nominally 20% on carbon black; Alfa Aesar, UK), 5.43 µl Nafion® perfluorinated resin solution (5 wt% in mixture of lower aliphatic alcohols and 45 wt% water; Sigma-Aldrich, UK) as a binder and 0.1 ml ethanol (Sigma-Aldrich, UK) per cm<sup>2</sup> of electrode. MPL and catalyst inks were both prepared and applied to the electrode using the same method. To homogenise the ink 3–5 glass beads were added to the ink vial and vortexed for 30 minutes then ultrasonicated for 20 minutes. The homogenised ink was applied to an electrode by pipetting 0.5 ml onto the cell-side surface, forming a meniscus and allowing the solvent to evaporate; ink was applied in this manner until full loading was achieved. The GDE was allowed to dry at room temperature over 16 hours before the final mass was recorded so that the percentage loading (%<sub>loading</sub>) of ink deposited could be calculated;

$$\%_{\text{loading}} = \frac{\Delta m_{\text{GDE}}}{m_{\text{Pt/C}}^i + m_{\text{Nafion}}^i} \times 100\% \quad (3.1)$$

where  $\Delta m_{\text{GDE}}$  is the difference in mass (mg) between the initial and final mass of the GDE,  $m_{\text{Pt/C}}^i$  is the mass (mg) of Pt/C added to the ink and  $m_{\text{Nafion}}^i$  is the mass (mg) of Nafion (from 5 wt% solution) added to the ink. The final mass of platinum ( $m_{\text{Pt}}^f$  in mg) loaded was calculated (assuming that the dry loading was a homogeneous mixture of Pt, C and Nafion) using the initial ratio of Pt in the ink composition;

$$m_{\text{Pt}}^f = \Delta m_{\text{GDE}} \times \frac{m_{\text{Pt}}^i}{m_{\text{Pt/C}}^i + m_{\text{Nafion}}^i} \quad (3.2)$$

where  $m_{\text{Pt}}^i$  is the initial mass (mg) of platinum (based upon 20 wt% Pt in Pt/C powder). The anode to cathode area ratio was kept at 1:1 for both 50 ml and 10 ml SCMFCs. Gas diffusion electrodes were placed into the gas diffusion end plate and 0.5 ml of 2 mol/dm<sup>3</sup> potassium phosphate buffer solution was added to the surface to remove air gaps and increase conductivity between the cathode and the membrane.

Silver / Silver chloride (Ag/AgCl) reference electrodes (RE-5B; BASi, USA) were used to enable anode and cathode potentials to be measured. The relative potential recorded using Ag/AgCl (3 mol/dm<sup>3</sup> NaCl) reference electrodes was +0.209 V vs. SHE (BASi, 2016; Bard and Faulkner, 2001). Throughout this thesis potentials will be quoted against the Ag/AgCl reference electrode potential. 3 mol/dm<sup>3</sup> NaCl agar salt bridges were constructed within 2 ml polypropylene syringes to protect the junction tip of the reference electrode from contamination by bacteria. Salt bridge solution was prepared by adding 2.000 g agar, 8.766 g sodium chloride (Sigma-Aldrich, UK) and 50 ml DI water to a beaker and heating (Figure 3.2).

The viscous gel was drawn into the syringe and the reference electrode was inserted into the gel, then allowed to cool and set. Assembled salt bridges were stored in 3 mol/dm<sup>3</sup> sodium chloride solution until cell installation (push-fitting into the cell port).



Figure 3.2: Photograph showing Ag/AgCl reference electrode salt bridge assembly push-fitted into a 10 ml MFC with a resistor wire connected between anode and cathode wires.

### 3.1.3 Membranes

Fumapem® F-930 cation exchange membranes (CEM; FuMA-Tech, Germany) were pre-treated by heating in 10 wt% HNO<sub>3</sub> for three hours at 60 °C and one hour in DI water at 60 °C in a water bath. Pre-treated membranes were rinsed with DI water until run-off was approximately pH 7 and then stored in DI water. 19.6 cm<sup>2</sup> (2.5 cm Ø) CEMs were installed in the 50 ml SCMFCs on top of the titanium wire and GDE surface covered with 0.5 ml of 2 mol/dm<sup>3</sup> potassium phosphate buffer solution. The membrane-electrode assemblies (MEA) were compressed against the gas diffusion end plate and spacer. For the 10 ml cells, 8.2 cm<sup>2</sup> (1.6 cm Ø) CEMs were placed on the center of 11.0 cm<sup>2</sup> GDEs covered with 0.5 ml of 2 mol/dm<sup>3</sup> potassium phosphate buffer solution. The titanium ring current collector was placed over the MEA contacting the GDE around the edges of the electrode not covered by the membrane. This enabled the membrane-electrode spacing and air gaps to be reduced.

MEAs constructed from membranes and gas diffusion electrodes were replaced when necessary *e.g.* when biofouling, degradation of cathode performance or leakage occurred. The anolyte (anodic chamber contents) was removed from the MFC, the gas diffusion end plate was unbolted and the MEA was replaced. Reassembly was achieved by rebolting the gas diffusion end plate to the MFC and resealing the wire holes with silicone sealant.

## **3.2 Set-up and Methods for Modes of MFC Operation**

### **3.2.1 *Temperature Regulation***

An aluminium heating platform was constructed with silicone heater mats (RS Components, UK) fitted on the underside. A set point controller enabled temperatures to be controlled thermostatically at a fixed platform temperature of 35 °C (approximately 28 °C liquid temperature inside vessels on the surface; Figure 4.3). The operating temperature of SCMFCs was regulated by placing cells on the heating platform within a polystyrene box (JB Packaging, UK). Additionally, this opaque enclosure prevented SCMFCs from exposure to light.

### **3.2.2 *50 ml Batch-mode Cells Set-up & Operation***

50 ml SCMFCs were set up by assembling the cell with electrodes, membrane and titanium wire current collectors. Cells were filled with inoculated anolyte medium using a needle and 60 ml syringe. The cells were sealed, a reference electrode was fitted to the top port and an external resistor was connected. Cells were placed onto a heating platform to maintain temperatures. Batch medium replacement was achieved by removing the complete liquid contents of the anodic chamber (anolyte) by needle and syringe, followed by refilling with fresh anolyte medium.

### **3.2.3 *Open Circuit Potential Electrodes Set-up & Operation***

11.0 cm<sup>2</sup> carbon cloth electrodes were placed into vessels containing inoculated anolyte medium. The vessels were sealed and placed on to a heating platform to maintain temperature. No electrical connection was made between anode and cathode so that the electrodes remained at open circuit potential (OCP; non-polarised). Batch medium replacement was achieved by removing the anolyte by needle and syringe, followed by refilling with fresh anolyte medium.

### **3.2.4 10 ml Flow-mode Cells Set-up**

10 ml SCMFCs were set up by assembling the cell with electrodes, membrane and titanium current collectors. Silicone sealant (Marine Silicone Rubber Sealant; Dow Corning Geocel) was applied to the wire slots to prevent leakage under flow-mode operation. Cells were completely filled with inoculum using a needle and syringe. A reference electrode was fitted to the top port and an external resistor was connected. Cells were placed onto a heating platform to maintain temperature.

### **3.2.5 Single-Pass Flow-mode Operation**

A single-pass flow-mode system was constructed in triplicate. For each replicate flow-through channel a 5 litre medium bottle, fitted with a 4-port cap (Duran, Germany), was used (Figure 3.3a). Through one port, nitrogen gas from a N<sub>2</sub> cylinder (BOC, UK) could be sparged through an in-line 0.2 µm PTFE filter into up to 5632 ml anolyte medium. Pressure equalisation was achieved through the second port into a 0.2 µm polyethersulfone (PES) filter. The third port was fitted with a silicone septum to allow injections of solutions into the vessel. From the fourth port anolyte medium was drawn through 1/16" ID C-Flex® tubing by a three-channel peristaltic pump (120S/DM3; Watson-Marlow, UK). Medium was pumped through 1.52 or 2.79 mm ID autoclavable Marprene® pump manifold tubing into 1/8" ID C-Flex® or Dow Corning® Pharma-50 tubing and into the medium inlet port of a 10 ml SCMFC placed on a heating platform inside a polystyrene box. Effluent from the SCMFC was pumped from the outlet port to a 15 l waste bottle. All tubing and fittings were supplied by Cole Parmer (USA). In Appendix B there is a more detailed schematic showing tubing and fitting connections (Figure B.1).

### **3.2.6 Recirculation Flow-mode Operation**

Recirculation flow-mode was not used for experiments and only used to keep the MFCs fed in a standby mode. To convert the flow-mode system from single-pass to recirculation mode the outlet line from the final MFC was removed from the 15 l waste bottle and connected to the second port of the 5 l medium bottle (Figure 3.3b). Pressure equalisation was then achieved by loosening the medium bottle cap when sparging with N<sub>2</sub>.

### **3.2.7 In-line Prevention of Back-contamination with Flow-mode System**

Building upon the core flow-mode system described in Section 3.2.5 and Figure 3.3, a modification was required in order to reduce and prevent medium bottle contamination by bacteria growing in the tubing against the direction of flow towards the source of substrate.

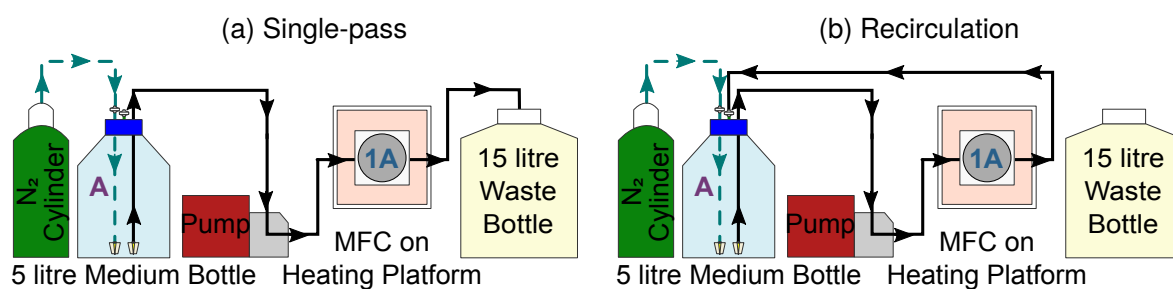


Figure 3.3: Schematic diagrams of a single flow channel with MFC 1A in (a) Single-pass flow-mode and (b) Recirculation flow-mode.

As in-line filtration was not possible at these flow regimes, alternative sterilisation methods were pursued (Figure 3.4).

An ultraviolet (UV) enclosure was designed which enabled real-time, flow-past sterilisation of medium within tubing pumped from the peristaltic pump. A wooden box (not susceptible to UV degradation) was constructed in which a shortwave UV lamp (254 nm, 4 W; Cole Parmer, USA) was installed. Slots were fitted with brushes (to prevent UV light exposure to user) to allow tubing to be fed past the 76 × 51 mm lamp window (Figure 3.4a). ChemFluor® 367 tubing was selected for its 89% transmission of UV light (Saint-Gobain, 2007) and proven application for inactivating bacteria (Geveke, 2005).

Additionally, a glass drip chamber was used which acted as a bubble trap and allowed for physical separation between the sterile medium bottle and SCMFCs (Figure 3.4b). Medium was drawn into the drip chamber by the action of the peristaltic pump. Medium dropped from the glass dropper to the base of the chamber and was subsequently drawn out as the pumping action proceeded. Bacteria growing in the tubing towards the medium bottle, against the direction of flow, were unable to traverse the air gap within the drip chamber. The UV enclosure was installed after the peristaltic pump whereas the drip chamber was installed upstream between the C-Flex® tubing from the medium bottle and the peristaltic pump.

### 3.2.8 Multi-stage SCMFC Set-up & Operation

Three stages of 10 ml SCMFCs were set up in triplicate channels (replicates A, B and C). The first stage MFC was connected to the tubing from the peristaltic pump at the inlet port, the outlet port was connected to the inlet of the second stage MFC. The outlet of the second stage MFC was connected to the inlet of the third stage MFC. The outlet of the third stage MFC was connected to the 15 l waste bottle in single-pass flow-mode. This hydraulic series channel allowed effluent from stage one cells to be passed to stage two and subsequently stage three cells. Three-way valves were installed before the peristaltic pump (Figure 3.5, 3-W M) to enable introduction of test analyte solutions, after the pump for feed line sampling (Figure 3.5, 3-W L) and at the outlet of each MFC to allow effluent sampling (Figure 3.5,

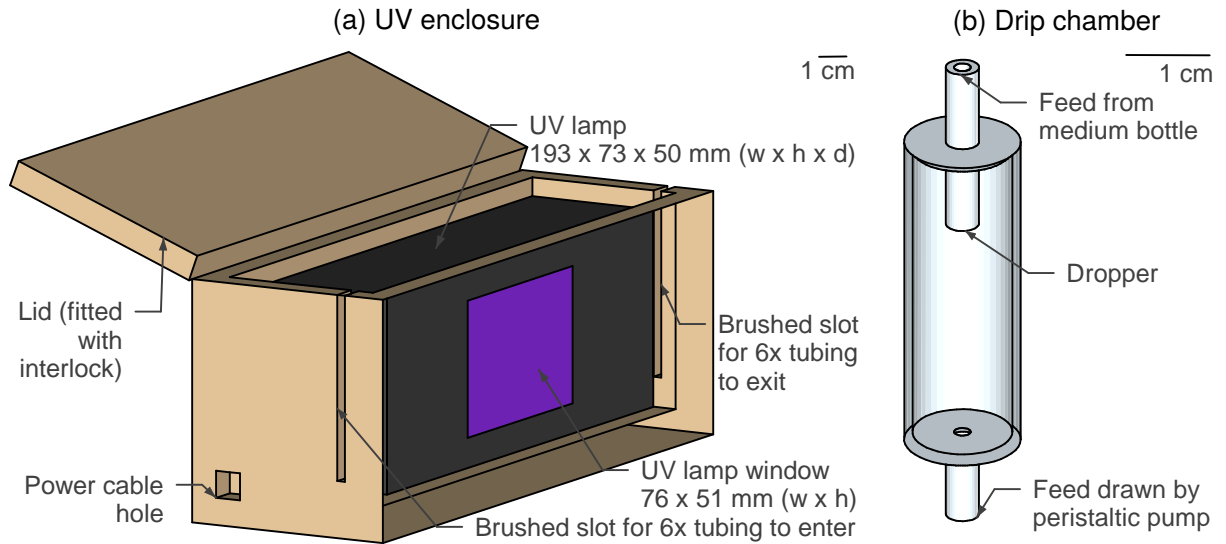


Figure 3.4: Schematic cut-away diagram of (a) UV enclosure for flow-past medium sterilisation and (b) drip chamber for in-line bubble trap.

3-W 1, 2 and 3). The closed port of each 3-way valve was capped when not in use. 3-way sampling valves were positioned so that inlet ports were in the horizontal position, sampling ports were in the upwards position and outlet ports were in the downwards position to prevent sludge build-up. The SCMFCs, which were hydraulically connected in series, were electrically isolated so that individual potentials at each stage could be measured.

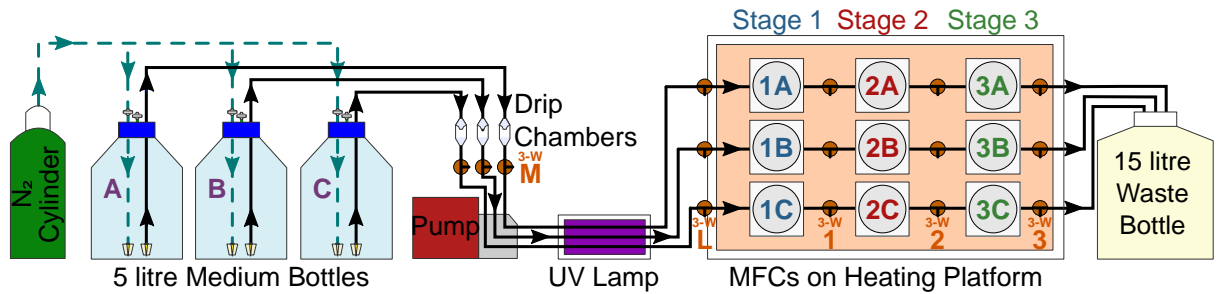


Figure 3.5: Schematic diagram of set-up for triplicate channels of three-stage SCMFCs and position of three-way (3-W M, 3-W L, 3-W 1, 3-W 2 and 3-W 3) valves (see Section 3.2.8).

### 3.2.9 Peristaltic Pump Flow Rates & Hydraulic Retention Time

Medium in the flow-mode system was pumped at pump speeds between 1 and 20 rpm corresponding to average flow rates of 0.09 to 4.51 ml/min. The hydraulic retention time (HRT or  $\tau$ ) defined by Metcalf & Eddy Inc (2002) as the average residence time of soluble compounds within a vessel of specified volume ( $Vol$ , ml) at a specified flow rate ( $q$ , ml/min) is given as;

$$\tau, \text{ min} = \frac{Vol}{q} \quad (3.3)$$

### **3.2.10 *Medium Replacement & Introduction of Test Analyte to Flow-mode System***

When medium was exhausted from the 5 l medium bottles it was necessary to replace with freshly prepared medium bottles. After briefly pausing the peristaltic pump, the feed lines up to the peristaltic pump tubing were also replaced with clean feed lines. The air present in the new feed lines was displaced with fresh medium by diverting the 3-way valves placed after the peristaltic pump (3-W L) away from the MFC inlet feed and into separate tubing to a waste collection beaker and operating the peristaltic pump at 25 ml/min. 3-W L valves were switched back to their original position and medium was flowed into the MFCs by resuming the peristaltic pump.

Using the 3-way valves installed upstream of the peristaltic pump (3-W M), analyte test solutions (e.g. toxicant solutions, wastewater) could be introduced into the flow-mode system without disconnecting the 5 l medium bottles. The peristaltic pump was paused and the 3-W M valves were diverted away from the medium bottle line to a separate line feeding from a sample bottle containing analyte solution. The same procedure as for medium replacement, using 3-W L valves, was used to fill feed lines with test analyte solution before introduction to the MFCs.

### **3.2.11 *Sludge Removal from Flow-mode System***

To prevent blockages occurring, it was necessary to remove sludge which built-up inside feed tubing, MFCs and valves. In order to remove sludge the peristaltic pump was stopped and all 3-way valves downstream of the pump were closed to prevent egress of medium when tubing was disconnected. The outlet tube from each MFC was disconnected from the corresponding 3-way valve and placed into a waste collection beaker; each cell in turn was then inverted, the inlet tube was removed and the entire cell and outlet tube contents (approximately 14 ml) were evacuated by gravity into the beaker. The outlet tubing was then reconnected to the valve and the inlet and outlet tubing from each cell was joined together using a 1/8" straight coupling fitting. The downstream 3-way valves were reopened and medium was pumped at 25 ml/min to flush out the tubing. In addition, the tubing was squeezed along its length to remove biofilms residing on tubing walls. One side-effect of the flushing step was that non-degraded medium was introduced into all of the tubing in the flow channel.

For reassembly, 3-way valves were closed to prevent medium egress. Inlet and outlet tubing was reconnected to corresponding ports on the MFC. The upward-facing sampling ports were uncapped and separate tubing was fitted to allow air and medium to flow into a waste collection beaker. The peristaltic pump was operated at 1.24 ml/min to purge air from the emptied MFC out of the succeeding 3-way valve to waste and to refill the system with medium. The 3-way sampling valve was then switched back to direct flow to the next stage MFC and



the sampling port was capped. This procedure was repeated for each MFC stage until the whole system had been purged. Due to the side-effect from the flushing step, upon restarting the peristaltic pump with MFCs attached, the second and third stage MFCs immediately experienced (for one HRT) higher concentration, non-degraded medium from the tubing until it was replaced with effluent from stage 1 MFCs.

### 3.3 Preparation of Anolyte Medium

#### 3.3.1 Inoculum

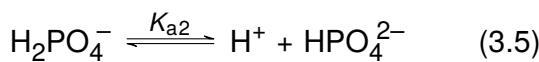
Activated sludge was collected from Tudhoe Mill sewage treatment works (Northumbrian Water, UK) and initially used to inoculate 50 ml SCMFCs. For subsequent inoculations the enriched anolyte effluent from 50 ml batch-mode SCMFCs grown with glucose-glutamic acid (GGA) medium was used. The inoculation procedure for batch cells was to make up the anolyte medium with 10% inoculum. For the flow-mode system each cell was filled with 100% inoculum and attached to the system at the inlet and outlet ports. Operating the peristaltic pump delivered medium containing substrate into the cells, beginning enrichment.

#### 3.3.2 Preparation of Phosphate Buffer Solution

It was necessary to calculate the required amounts of dibasic potassium hydrogen phosphate ( $K_2HPO_4$ ) and monobasic potassium dihydrogen phosphate ( $KH_2PO_4$ ) to prepare a 50 mmol/dm<sup>3</sup> phosphate buffer solution at pH 7. pH is defined as;

$$pH = -\log a_{H^+} = -\log \gamma_{H^+} [H^+] \xrightarrow{(\gamma_{H^+}=1)} -\log[H^+] \quad (3.4)$$

where  $a_{H^+}$  is the hydrogen ion (proton) activity,  $\gamma_{H^+}$  is the proton activity coefficient and  $[H^+]$  is the proton concentration (mol/dm<sup>3</sup>; Segel (1976)). pH 7 is close to the second logarithmic acid dissociation constant ( $pK_{a2}$ ) for phosphoric acid ( $H_3PO_4$ ), defined as 7.21 by Haynes (2010). Therefore,  $H_2PO_4^-$  will be the conjugate acid (HA) and  $HPO_4^{2-}$  will be the conjugate base ( $A^-$ ) present in the buffer;



$$K_{a2} = \frac{[H^+][HPO_4^{2-}]}{[H_2PO_4^-]} \quad (3.6)$$

However, the literature  $pK_a$  values are standardised at zero ionic strength ( $\mu$ ), yet for 50 mmol/dm<sup>3</sup> solution  $\mu = 0.10$  mol/dm<sup>3</sup> and the activity coefficients of  $H_2PO_4^-$  and  $HPO_4^{2-}$  are not equal to 1. The effect was corrected for using an 'apparent'  $pK_{a2}'$  value, given as 6.86

by CSH Protocols (2006). The molar ratio was then determined using the Henderson-Hasselbalch equation;

$$\frac{[A^-]}{[HA]} = 10^{(pH - pK_a)} \quad (3.7)$$

The molar ratio of  $K_2HPO_4$  to  $KH_2PO_4$  to produce a 50 mmol/dm<sup>3</sup> pH 7 buffer solution was calculated as 1.36 using  $pK_{a2}$  in Equation 3.7.

### 3.3.3 Composition of Anolyte Medium

Anolyte medium was prepared to establish the response of MFCs to different concentrations of carbon source under controlled conditions where environmental variables (*e.g.* pH, conductivity) were kept constant. A 1:1 wt% mixture of D-glucose and L-glutamic acid (GGA) was the carbon source primarily utilised for the medium. Additionally, D-glucose-only and L-glutamic acid-only media were prepared. Substrate concentrations were varied between 25 to 4000 mg/l in order to generate data for BOD sensor calibration. All medium solutions were prepared using the same in-house protocol, originally derived from Ter Heijne *et al.* (2008). 25 ml/l phosphate buffer (pH 7), 2 ml/l macro-nutrients, 2 ml/l micro-nutrients and 1 ml/l vitamins stock solutions (Table 3.2) were made up to the appropriate volume with DI water. Stock solutions were initially prepared by dissolving appropriate amounts of compounds in DI water. Substrate-free medium ('zero medium') was prepared in the same way without any additions of glucose or glutamic acid.

### 3.3.4 Sterilisation of Anolyte Medium

For the flow-mode system it was necessary to prepare anolyte medium aseptically in order to prevent contamination occurring inside the medium bottle. 92% of the total DI water and all the phosphate buffer solution were placed inside each 5 l bottle. The associated tubing and fittings of the feed line up to and including the drip chamber, the N<sub>2</sub> inlet and pressure equalisation gas filters were attached to each bottle and capped. The assembled bottles (with only water and phosphate buffer) were autoclaved at 121 °C for 30 minutes.

Glucose and glutamic acid stock solutions were freshly prepared in 0.36% and 3.6% of the total DI water respectively (concentration depending on mass of each substrate required). It was necessary to heat the glutamic acid stock solution in a water bath to 50 °C to complete dissolution. The 1 ml/l vitamins stock solution was diluted 11× in order to aid solubilisation. After sterilisation of the medium bottles, the remaining medium constituents were filter-sterilised through the septum using a 0.22 µm Sterivex™ GP PES filter unit (Millipore®, Germany) and flame-sterilised needle.

Table 3.2: Composition of anolyte medium stock solutions.

Stock solution	Chemical	Concentration in stock (g/l)	Concentration in medium (mg/l)
2 mol/dm <sup>3</sup> Phosphate buffer (pH 7; 25 ml/l)	KH <sub>2</sub> PO <sub>4</sub>	115.104	2878.00
	K <sub>2</sub> HPO <sub>4</sub>	201.031	5026.00
Macro-nutrients solution (2 ml/l)	NH <sub>4</sub> Cl	140.000	280.00
	MgSO <sub>4</sub> · 7 H <sub>2</sub> O	50.000	100.00
	CaCl <sub>2</sub>	2.150	4.30
Micro-nutrients solution (2 ml/l)	FeCl <sub>2</sub> · 4 H <sub>2</sub> O	2.000	4.00
	CoCl <sub>2</sub> · 6 H <sub>2</sub> O	1.000	2.00
	NiCl <sub>2</sub> · 6 H <sub>2</sub> O	1.000	2.00
	HCl	0.826	1.65
	MnCl <sub>2</sub> · 4 H <sub>2</sub> O	0.500	1.00
	Na <sub>2</sub> SeO <sub>3</sub>	0.105	0.21
	(NH <sub>4</sub> ) <sub>6</sub> Mo <sub>7</sub> O <sub>24</sub> · 4 H <sub>2</sub> O	0.070	0.14
	ZnCl <sub>2</sub>	0.050	0.10
	H <sub>3</sub> BO <sub>3</sub>	0.050	0.10
	CuCl <sub>2</sub> · 2 H <sub>2</sub> O	0.040	0.08
Vitamins solution (1 ml/l)	Pyridoxine hydrochloride	1.000	1.00
	Nicotinic acid	0.500	0.50
	Riboflavin	0.250	0.25
	Thiamine hydrochloride	0.250	0.25
	Biotin	0.200	0.20
	Folic acid	0.200	0.20
	Vitamin B12	0.010	0.01

### 3.3.5 Degassing Anolyte Medium

Medium solutions were made anaerobic prior to feeding of MFCs by sparging with nitrogen gas. For batch-mode preparations, the medium was sparged before being added to the cells. Medium for flow-mode operation was sparged whilst the pump was stopped when changing bottles of medium. The sparging process also acted to mix the filter-sterilised constituents into the bulk solution in the 5 l medium bottles. It was determined that 10 minutes of sparging was sufficient to deplete a solution of medium to less than 0.15 mg/l dissolved oxygen (DO) measured with a 9500 DO<sub>2</sub> meter and DO<sub>2</sub>/ATC probe (Bibby Scientific, UK; Figure B.2 in Appendix B).

### 3.3.6 Toxicant-doped Medium

4-nitrophenol (4-NP, *para*-nitrophenol; Figure 3.6) was the toxicant used in this study. Toxicant-doped medium was prepared by adding the appropriate volume from a 3 g/l stock solution of 4-nitrophenol to other medium constituents. All toxicity tests were conducted using medium

containing 600 mg/l GGA in order to establish the toxicity effect without varying BOD levels. The concentrations of 4-NP used ranged from 10 to 150 mg/l as 4-NP was known to have an  $EC_{50}$  value of 56 mg/l (at which concentration the growth rate is 50% of the rate in the absence of 4-NP) and caused 100% inhibition at concentrations greater than 120 mg/l in *Escherichia coli* K12-MG1655 (Brown, 2005).

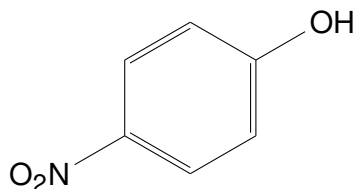


Figure 3.6: Skeletal formula of 4-nitrophenol.

### 3.3.7 Raw Wastewater

Raw influent wastewater was collected from Tudhoe Mill sewage treatment works (Northumbrian Water, UK). The only amendment to the wastewater was to increase the conductivity by titrating an appropriate amount of  $2 \text{ mol/dm}^3$  phosphate buffer solution until the conductivity was equal to that of artificial GGA medium (approximately 8 mS/cm).

## 3.4 MFC Sensor Calibration Methods

### 3.4.1 BOD Calibration Methods

To calibrate the batch-mode MFC sensors, the medium was first replaced with 'zero medium' (containing no organic substrate) to establish a minimum operating current density. Following this, medium was replaced sequentially with solutions containing different substrate concentrations. Generally the medium was replaced once a medium cycle had come to completion and the current density approached  $0 \mu\text{A/cm}^2$ . However, in some cases as soon as the peak current density ( $\hat{i}$ ) was observed and the current had begun to decline, the medium was replaced with the next test analyte (unless charge density or coulombic efficiency measurements were also made). Commonly the substrate concentration was increased with each replacement (step-up) until a maximum limiting current density was reached. The step-down response was checked periodically with lower substrate concentrations to confirm reproducibility and check sensor behaviour.

For the three-stage, flow-mode MFCs, medium bottles with fixed concentrations of substrate were attached to the peristaltic pump and generally ran for 1 to 3 days. Medium was replaced when the bottles were almost empty. During calibration the substrate concentration was varied during bottle preparation and, as with the batch-mode replacements, concentrations were

generally increased over the course of the calibration until a maximum limiting current density was reached. Periodic step-down checks were made with lower concentration medium.

### **3.4.2 Current Decrease Calibration Methods**

Only short (90 minute) “shock” tests leading to a decrease in current density were conducted in this study (*e.g.* with BOD decrease, substrate excess or toxicant presence). The 5 l medium bottles were kept constantly at 600 mg/l GGA concentration and ‘current-decreasing’ test analytes were introduced in small volumes (< 500 ml) by switching the influent feed from the 3-W M valve. In each case, the cells in Channel B (Figure 3.5) were retained on the 5 l “non-toxic” medium feed as a control and cells in Channels A and C were fed the test analyte. For toxicity tests, 4-nitrophenol concentrations were increased from low to high to maximise data collection in the event of total biofilm poisoning. For substrate excess inhibition tests and those involving medium with decreased BOD, the magnitude of changes in BOD ( $\Delta$ BOD) were increased from low to high concentration difference. After 90 minutes had passed the influent feed was returned back to the 5 l medium bottles (using the method discussed in Section 3.2.10) and the recovery in current density (from inhibition or starvation) was monitored.

Recovery times were calculated between the time at which the non-toxic medium feed was restored at the 3-W M valve and the time that the normalised current density in Channels A and C recovered to levels equal to that of the control (Channel B). HRT-adjusted recovery times were also calculated for each MFC stage, to subtract the time taken between the non-toxic feed being restored at the 3-W M valve and the medium passing through upstream MFCs (and associated tubing) to reach the analyte chamber of each respective cell (Table B.1). For example, at 1.24 ml/min, from medium entering the feed line at the 3-W M valve it took 17 minutes to reach MFC Stage 1, 33 minutes to reach MFC Stage 2 and 49 minutes to reach MFC Stage 3.

## **3.5 Sampling Methods**

### **3.5.1 Batch-mode Analyte Sampling**

Samples of analyte (approximately 5 ml) from batch-mode MFCs were taken during medium replacement operations and samples of freshly prepared analyte medium were taken before medium was injected into the cell. Samples were filtered through a 0.2  $\mu$ m PES filter before being frozen at  $-18^{\circ}\text{C}$ .

### **3.5.2 Flow-mode Analyte Sampling**

Three-way valves placed along the flow-mode system downstream of the peristaltic pump enabled the medium to be sampled at specific positions (Figure 3.5). From valve 3-W L medium was sampled immediately before entering the MFCs to enable the amount of in-line medium degradation in the upstream tubing to be determined. After each stage of MFCs (1, 2 and 3) a three-way valve enabled MFC effluent to be sampled. The procedure involved pausing the peristaltic pump, switching the three-way valve away from the downstream flow path and towards the sampling port. The peristaltic pump was restarted and, after discarding the initial effluent (from inside the port), samples were pumped into collection vessels. Following sampling; the pump was paused, valves were re-opened to the flow path through the MFCs, sample ports were capped and the pumping was resumed. Samples were filtered through 0.2 µm PES filters and frozen at -18 °C. When the whole flow-mode system was to be sampled, the sampling was performed from the last stage to the first (3-W 3 to 3-W L; Figure 3.5) so that upstream effluents were unaffected by diversion of the flow path during sampling (due to extra residence time).

### **3.5.3 Flow-mode Sludge Sampling**

During sludge removal (Section 3.2.11), samples were kept following evacuation of each cell and outlet tube. Approximately 7.5 ml of 0.2 µm filter-sterile ethanol was added to the 7.5 ml sample to give a 50 vol% ethanol/water ratio and fix the bacteria to prevent sample degradation. Before analysis samples were centrifuged for 8 minutes at relative centrifugal force of  $3220 \times g$  and then the supernatant was removed. The precipitate was used for downstream microbiological analyses.

### **3.5.4 Electrode Biofilm Sampling**

To sample biofilms from anodes and electrodes operated at OCP required the SCMFCs to be disassembled. The anode end plate was unbolted and each electrode was lifted into a collection tube. 2 ml of filter-sterile 50 vol% ethanol/water solution was added to this. The entire anodic electrode was homogenised with a sterile spatula and centrifuged as with the sludge sampling. After removing the supernatant, precipitated samples were used to obtain cell counts and to extract DNA for microbial community analysis.

### 3.6 Analyte Analysis Methods

#### 3.6.1 Biochemical Oxygen Demand

The BOD<sub>5</sub> test was carried out according to APHA (1999a). 1 ml/l each of phosphate buffer (pH 7.2, containing 8.5 g/l KH<sub>2</sub>PO<sub>4</sub>, 21.75 g/l K<sub>2</sub>HPO<sub>4</sub>, 33.4 g/l Na<sub>2</sub>HPO<sub>4</sub> and 1.7 g/l NH<sub>4</sub>Cl), MgSO<sub>4</sub> (22.5 g/l), CaCl<sub>2</sub> (27.5 g/l), FeCl<sub>3</sub> (0.25 g/l) and allylthiourea (2 g/l ATU, a nitrification inhibitor) was added to oxygen saturated distilled water and inoculated with settled sewage to prepare dilution water for the test. Four 1/250 diluted replicates of each sample and four blanks were prepared in BOD bottles; the first of each series was opened immediately for initial DO measurement, the remaining three replicates were incubated for 5 days at 20 °C. Dissolved oxygen was measured using a LBOD101 luminescent/optical dissolved oxygen probe and HQ40d meter (Hach, USA). BOD<sub>5</sub> was calculated as;

$$\text{BOD}_5, \text{ mg/l} = \left( \Delta \text{DO}_{\text{Sample}} - \left( \Delta \text{DO}_{\text{Blank}} \times \frac{V_{\text{Sample}}}{V_{\text{Blank}}} \right) \right) \times DF \quad (3.8)$$

where  $\Delta \text{DO}_{\text{Sample}}$  and  $\Delta \text{DO}_{\text{Blank}}$  are the change in DO measured over 5 days in the sample and blank respectively (mg/l),  $V_{\text{Sample}}$  and  $V_{\text{Blank}}$  are the volume of inoculation seed added to the sample and blank respectively (ml),  $DF$  is the dilution factor (APHA, 1999a). BOD<sub>5</sub> values were determined from the average of triplicate measurements.

For artificial wastewater solutions (containing either glucose, glutamic acid or a 1:1 GGA mixture as the BOD-containing substrates), a linear calibration achieved with known concentrations of substrate in the anolyte medium was used to confirm linearity between mg/l substrate and mg/l O<sub>2</sub> BOD<sub>5</sub> (Figure 3.7). In this thesis, the fitted linear regression models were used to estimate BOD<sub>5</sub> values from known medium preparations; except where explicitly stated that BOD<sub>5</sub> was measured (*e.g.* real wastewater in Chapter 7).

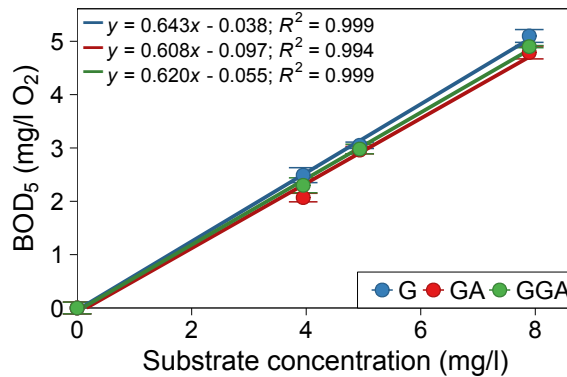


Figure 3.7: Linear calibration of measured BOD<sub>5</sub> values against substrate concentration of glucose (G), glutamic acid (GA) and GGA in anolyte medium. Calibrations were used to estimate BOD<sub>5</sub> values from known artificial wastewater compositions. Error bars represent  $\pm$ SD from triplicate BOD<sub>5</sub> measurements for each concentration.

### 3.6.2 Chemical Oxygen Demand

COD was determined by two different methods. Initially, the closed reflux method (APHA, 1999b) was used to determine COD values of fresh medium samples (Chapter 7). Duplicate 2 ml 1/4 diluted samples were digested with 2 ml 0.075 N potassium dichromate containing mercuric sulphate and 3.5 ml sulphuric acid/silver sulphate solution (5.5 g Ag<sub>2</sub>SO<sub>4</sub>/kg H<sub>2</sub>SO<sub>4</sub>) at 150 °C for 2 hours. Once cooled, the samples were titrated with 0.025 N ferrous ammonium sulphate (FAS) against ferroin indicator. The average COD values were calculated as;

$$\text{COD, mg/l} = \frac{(tv_{\text{Blank}} - tv_{\text{Sample}}) \times N_{\text{Eq}} \times 8000}{Vol_{\text{Sample}}} \times DF \quad (3.9)$$

where  $tv_{\text{Blank}}$  and  $tv_{\text{Sample}}$  are the titration volume (ml) for blank and sample respectively and  $N_{\text{Eq}}$  is the normality ( $\text{mol}_{\text{Eq}}/\text{dm}^3$ ) of FAS, 8000 is the conversion factor from mol to mg/l derived from the stoichiometric molar ratio of K<sub>2</sub>Cr<sub>2</sub>O<sub>7</sub> to FAS divided by the moles of K<sub>2</sub>Cr<sub>2</sub>O<sub>7</sub> added,  $Vol_{\text{Sample}}$  is the volume of sample and  $DF$  is the dilution factor.

COD photometric cell tests were used to determine COD values of samples (Chapters 4, 5 and 6) in the range 10–150 mg/l and 25–1500 mg/l COD (Merck Millipore, Germany). Samples were diluted with appropriate amounts of DI water in order to satisfy the range limitations of the assay kits (based on the known COD present in the fresh medium). 3 ml diluted samples were digested in vials containing potassium dichromate, mercuric sulfate and silver sulfate catalyst at 148 °C for 2 hours. Once cooled, samples were swirled and the absorbances were read using a Spectroquant® Pharo 300 spectrophotometer (Merck Millipore, Germany). For both closed reflux and photometric methods a linear calibration achieved with known concentrations of GGA analyte medium was used to confirm linearity and correspond absorbance to mg/l COD respectively (Figure B.3 in Appendix B). COD values for samples from each stage were calculated from the average of COD measurements of each cell in that stage.

### 3.6.3 Dissolved Inorganic & Organic Carbon

Samples which had been passed through a 0.2 µm filter were tested using a TOC 5050A Total Organic Carbon analyser (Shimadzu, Japan) to determine dissolved organic carbon (DOC) concentrations. 7 ml 1/5 diluted samples were added to a vial in an ASI-5000A autosampler and portions were measured simultaneously for total carbon (TC, mg/l; combusted at 800 °C to CO<sub>2</sub> which is measured with an infrared detector) and inorganic carbon (IC, mg/l; acidified to convert inorganic carbonate into CO<sub>2</sub>). Total (dissolved) organic carbon was calculated using;



$$\text{TOC, mg/l} = \text{TC} - \text{IC} \quad (3.10)$$

DOC and IC values for samples from each stage were calculated from the average of DOC and IC measurements of each cell in that stage.

#### **3.6.4 Volatile Fatty Acids**

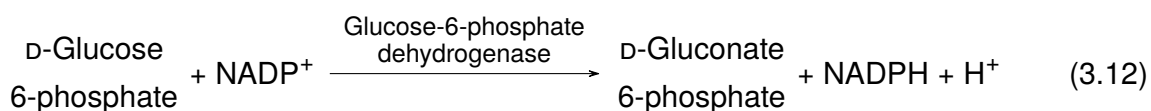
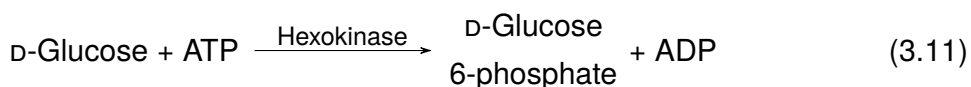
An ICS-1000 ion chromatography system fitted with a  $9 \times 250$  mm ( $\varnothing \times \text{D}$ ) Dionex™ IonPac™ ICE-AS1 column (for aliphatic organic acids and alcohols; Thermo Fisher Scientific, USA) was used to determine volatile fatty acid (VFA) concentrations from anolyte samples. A  $1 \text{ mmol/dm}^3$  octanesulfonic acid (OSA; pH 0 - 7) eluent was used at 0.8 ml/min and detection was made using a suppressed conductivity detector. 0.4 ml of  $0.1 \text{ mol/dm}^3$  OSA was added to 0.4 ml diluted sample to acidify and remove carbonate (Dionex, 2012; Manning and Bewsher, 1997). Prepared samples were ultra-sonicated for 40 minutes to drive off  $\text{CO}_2$  from acidified solutions. Samples were added to polypropylene vials fitted with filter caps and loaded into an AS40 automated sampler. A standard solution containing formic-, acetic-, propionic-, isobutyric-, butyric-, isovaleric- & valeric acid, each at 5 to 500 mg/l was used to calibrate the instrument and identify VFAs in the sample based on their retention time and quantify based on the peak areas ( $\mu\text{S min}$ ; Figure B.4 in Appendix B). VFA concentrations for each stage were calculated using the average concentration of samples from each cell in that stage.

#### **3.6.5 Anions**

An ICS-1000 ion chromatography system fitted with a  $3 \times 150$  mm ( $\varnothing \times \text{D}$ ) Dionex™ IonPac™ AS14A column (for inorganic anions; Thermo Fisher Scientific, USA) was used for measurement of anion concentrations. A  $8 \text{ mmol/dm}^3$  sodium carbonate and  $1 \text{ mmol/dm}^3$  sodium bicarbonate (pH 0 - 14) eluent was used at 0.5 ml/min and detection was made using a suppressed conductivity detector. 5 ml 1/10 diluted anolyte samples were added to polypropylene vials fitted with filter caps and added to an AS40 automated sampler. A single point calibration was carried out using a standards solution containing 5 mg/l fluoride, 10 mg/l chloride, 15 mg/l nitrite, 20 mg/l bromide, 25 mg/l nitrate, 40 mg/l phosphate & 30 mg/l sulphate ions (Figure B.5 in Appendix B). Anions were identified based on their retention times and peak areas ( $\mu\text{S min}$ ) were used for quantification. Anion concentrations for each stage were calculated using the average concentration of samples from each cell in that stage.

### 3.6.6 D-Glucose

The concentration of D-glucose, present as a carbon source in the anolyte medium, was determined using a UV spectrophotometric assay (K-GLUHK; Megazyme, Ireland). To each well in a 96-well microplate 10  $\mu$ l buffer and 10  $\mu$ l NADP<sup>+</sup>/ATP solutions were added to 210  $\mu$ l diluted samples and mixed on a microplate shaker for 30 seconds. After 3 minutes the blank absorbance at 340 nm ( $A_1$ ) was read using a SPECTROstar® Nano microplate reader (BMG Labtech, Germany). Following this, 2  $\mu$ l hexokinase (HK) and glucose-6-phosphate dehydrogenase (G-6-PDH) solution was added to wells and the enzymatic phosphorylation of glucose was initiated (Equation 3.11);



where ATP and ADP are tri- and di-phosphorylated forms of adenosine and NADP<sup>+</sup> and NADPH are the oxidised and reduced forms of nicotinamide adenine dinucleotide phosphate respectively. The G-6-PDH enzyme converts D-glucose 6-phosphate into D-gluconate 6-phosphate with reduction of NADP<sup>+</sup> to NADPH (Equation 3.12). The NADPH generated was measured by its absorbance at 340 nm ( $A_2$ ) using the microplate reader after 5 and 7 minutes to confirm the reaction had reached an end-point. The assay gave a linear response with 10  $\mu$ l sample per well in the range 10 to 800 mg/l D-glucose and appropriate sample dilutions with DI water were chosen based on the original glucose concentration in the fresh medium (Figure B.6 in Appendix B). The change in absorbance ( $\Delta A_{\text{Standard}}$ ) between  $A_1$  and  $A_2$  for a standard 400 mg/l D-glucose solution was determined in order to correlate change in sample absorbances ( $\Delta A_{\text{Sample}}$ ) with concentration;

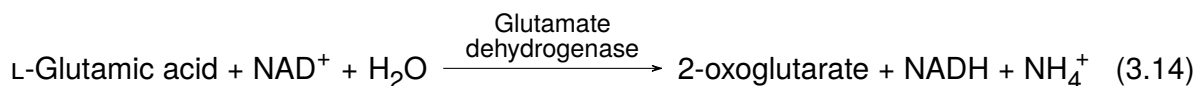
$$\text{D-Glucose, mg/l} = \frac{\Delta A_{\text{Sample}}}{\Delta A_{\text{Standard}}} \times \rho_{\text{Standard}} \times DF \quad (3.13)$$

where  $\rho_{\text{Standard}}$  is the mass concentration (mg/l) of the standard solution and  $DF$  is the dilution factor. Glucose concentrations for samples from each cell were calculated using the average of duplicate measurements and for each stage from the average concentration determined for each cell in that stage.

### 3.6.7 L-Glutamic Acid

The concentration of L-glutamic acid, a carbon source present in the anolyte medium, was determined using a UV spectrophotometric assay (K-GLUT; Megazyme, Ireland). To each

well in a 96-well microplate 50 µl buffer, 20 µl NAD<sup>+</sup>/INT and 5 µl diaphorase solutions were added to 210 µl diluted samples and mixed on a microplate shaker for 30 seconds. After 2 minutes the blank absorbance at 492 nm ( $A_1$ ) was read using a SPECTROstar® Nano microplate reader (BMG Labtech, Germany). Following this, 5 µl glutamate dehydrogenase (GIDH) solution was added to wells to initiate the enzymatic oxidation of glutamic acid to 2-oxoglutarate with reduction of NAD<sup>+</sup> to NADH (Equation 3.14);



where NAD<sup>+</sup> and NADH are the oxidised and reduced forms of nicotinamide adenine dinucleotide respectively and INT is idonitrotetrazolium chloride. The diaphorase enzyme converts INT into INT-formazan with regeneration of NAD<sup>+</sup> (Equation 3.15). The INT-formazan generated was measured by its absorbance at 492 nm ( $A_2$ ) using the microplate reader after 10 and 12 minutes to confirm the reaction had reached an end-point. The assay gave a linear response with 10 µl sample per well in the range 10 to 200 mg/l L-glutamic acid (Figure B.7 in Appendix B). Appropriate sample dilutions were chosen based on the original medium concentration. The change in absorbance ( $\Delta A_{\text{Standard}}$ ) between  $A_1$  and  $A_2$  for a standard 100 mg/l L-glutamic acid solution was determined in order to correlate change in sample absorbances ( $\Delta A_{\text{Sample}}$ ) with concentration;

$$\text{L-Glutamic acid, mg/l} = \frac{\Delta A_{\text{Sample}}}{\Delta A_{\text{Standard}}} \times \rho_{\text{Standard}} \times DF \quad (3.16)$$

where  $\rho_{\text{Standard}}$  is the mass concentration (mg/l) of the standard solution and  $DF$  is the dilution factor. Glutamic acid concentrations for samples from each cell were calculated from the average of duplicate measurements and for each stage using the average concentration determined for each cell in that stage.

### 3.6.8 4-Nitrophenol

The concentration of 4-nitrophenol (4-NP), a toxic chemical used in the toxicant-doped anolyte medium, was determined by measuring its absorbance with a UV spectrophotometer. Samples were acidified to pH 3–4 by addition of approximately 4 µl HCl (35%) to 1 ml sample (colour change from yellow to colourless). Between pH 5 and 9 the 4-nitrophenol and deprotonated form of 4-nitrophenolate are present in solution resulting in bimodal absorbance peaks at 320 and 405 nm respectively (Biggs, 1954). To each well in a 96-well microplate 250 µl anolyte samples were added and mixed with a microplate shaker for 15 seconds.

The absorbance at 320 nm was read using a SPECTROstar® Nano microplate reader (BMG Labtech, Germany). The 4-NP absorbance was linear in the range 0 to 30 mg/l 4-NP (Figure B.8 in Appendix B). Appropriate sample dilutions were chosen based on the original toxicant-doped medium concentration. 4-nitrophenol concentrations for samples from each cell were calculated from the average of duplicate measurements and for each stage using the average concentration determined from each cell in that stage.

### 3.6.9 pH

The pH of anolyte medium samples was measured using a HI 9025 pH meter (Hanna Instruments, USA) fitted with a slim-line pH electrode (11542543; Fisher-Scientific, UK) calibrated between pH 4.01 and 7.01. Average pH for each stage were calculated using the average pH measured from each cell in that stage.

### 3.6.10 Conductivity

Conductivity was measured using a FE30 conductivity meter fitted with 0.01–200 mS/cm automatic-temperature-compensation (ATC) conductivity probe (Mettler Toledo, Switzerland) calibrated at 12.88 mS/cm. The temperature correction coefficient was given as  $\alpha_{25} = 1.88\% / ^\circ\text{C}$  for 10 wt% KCl at 25 °C (Mettler Toledo, 2012) and linear temperature compensation was performed automatically using;

$$\kappa_{25} = \frac{\kappa_{\theta}}{1 + (\alpha_{25}/100) (\theta - 25)} \quad (3.17)$$

where  $\kappa_{25}$  is the calculated conductivity at 25 °C,  $\kappa_{\theta}$  is the measured conductivity and  $\theta$  is the measured temperature in degrees Celsius (Barron and Ashton, 2007). Average conductivity for each stage was calculated using the measured conductivity of each cell in that stage and reported as the conductivity at 25 °C.

### 3.6.11 Temperature

Temperatures inside the polystyrene box housing the SCMFCs were measured periodically using a temperature logger with an external probe (EBI 20-TE1; Ebro, Germany). For operational reasons the probe was not used inside MFC chambers but inserted into a 10 ml volumetric flask filled with DI water and temperatures were monitored to observe improvements with temperature regulation (Section 3.2.1). Data was retrieved from the data logger using Winlog.basic analysis software (Ebro).

### 3.7 Microbial Community Analysis

#### 3.7.1 DNA Extraction

Deoxyribonucleic acid (DNA) was extracted from samples of biofilms and sludge using a PowerSoil® DNA isolation kit (Mo Bio Laboratories, USA). 0.25 g samples were taken from precipitates of centrifuged biofilm samples (electrode samples still contained the carbon cloth material) and represented approximately 11 wt% 19.6 cm<sup>2</sup> electrode, 15 wt% 11.0 cm<sup>2</sup> electrode and 100 wt% sludge sample (Section 3.5.4). The 'Experienced User' protocol (Mo Bio Laboratories, 2013) was followed. Samples were added to PowerBead tubes and, after briefly vortexing, 60 µl SDS cell lysis reagent was added. Tubes were vortexed at 6 m/s for 40 seconds using a FastPrep®-24 homogeniser (MP Biomedicals, USA) and then centrifuged at 10 000 ×g for 30 seconds using a Mikro 200 centrifuge (Hettich, Germany). 500 µl supernatant was transferred to a collection tube, 250 µl inhibitor removal reagent was added to precipitate non-DNA from solution and tubes were briefly vortexed and incubated for 5 minutes at 4 °C. After centrifuging at 10 000 ×g for 1 minute 600 µl supernatant was transferred to a new collection tube and a second inhibitor removal reagent was added and the vortex, incubate, centrifuge and transfer process was repeated. 1.2 ml high-concentration salt solution was added to 750 µl supernatant and briefly vortexed. 675 µl aliquots of sample were loaded onto a spin filter to bind DNA and then centrifuged with the flow through discarded. Once all sample had been added to the spin filter and centrifuged, 500 µl ethanol-based wash solution was added to the spin filter and centrifuged twice to further remove contaminants and wash solution. This was followed by addition of 100 µl sterile, DNA-free water to the spin filter over a new collection tube and centrifugation to elute DNA. Extracted DNA samples were stored at -18 °C.

#### 3.7.2 PCR Amplification of 16S rRNA Gene Fragments

Sterile, polymerase chain reaction (PCR) grade, DNA-free water was prepared by passing ultra-pure water (18.2 MΩ cm Milli-Q®; Merck Millipore, Germany) through a sterile 0.2 µm PES filter and using a UV crosslinker device.

For amplification of the V4-V5 region of 16S rRNA genes thin-walled PCR tubes were used and to each tube 0.5 µl DNA template (sample from DNA extraction), 0.5 µl barcoded V4 forward primer, 0.5 µl non-barcoded V5 reverse primer and 23.5 µl PCR master mix containing *Taq* polymerase, PCR reagents and blue agarose loading dye (MegaMix-Blue; Cambio, UK) was added. Forward primers included the Ion Torrent™ A adapter, unique 12 base pair (bp) Golay error-correcting barcode and V4 forward primer sequences in the order 5'-adapter-barcode-GTGNCAGCMGCCGCGGTAA-3'. Reverse primers included the Ion Torrent™ trP1 adapter and V5 reverse primer sequences in the order 5'-adapter-CCGYCAATTYMTTTRAGTTT-3'

(Life Technologies, 2011). Details of the individual barcode sequences are given in Table F.1 in Appendix F. For the V4f - V5r primer set, a 481 bp partial gene fragment (including barcodes and adaptors) was targeted in the highly conserved region between the V4 and V5 hypervariable regions of the 16S ribosomal RNA (rRNA) gene.

PCR tubes were loaded into a Techne TC-512 gradient thermocycler (Bibby Scientific, UK) and the polymerase chain reaction was conducted according to the program in Table 3.3.

Table 3.3: Automated thermocycler program for PCR amplification.

Step	Set Temp. <sup>a</sup> (°C)	Hold Time (min)
Pre-heated lid	105	-
Initial denaturation	95	4:00
<i>30 cycles:</i>		
Denaturation	95	1:00
Annealing	55	0:45
Elongation	72	1:00
Final elongation	72	10:00
Final hold	4	∞

<sup>a</sup> Temperature ramp gradient = 3 °C/s

### 3.7.3 Electrophoresis

Gel electrophoresis was used to confirm that PCR amplification was successful. A gel was prepared by dissolving 1.5 g agarose in 150 ml 1× TAE buffer (pH 8.5; containing 40 mmol/dm<sup>3</sup> Tris, 20 mmol/dm<sup>3</sup> acetic acid, and 1 mmol/dm<sup>3</sup> pH 8.0 EDTA) and heating until completely dissolved. 15 µl DNA gel stain (SYBR® Safe; Thermo Fisher Scientific, USA) was added to the gel solution and dissolved. The gel was poured into a gel cast and well combs were added. Once set, the combs were removed and the cast was placed into a electrophoresis tank containing 1× TAE buffer. 4 µl molecular weight marker (Hyperladder™ 50bp; Bioline, UK) was added to the first and final wells and amplicon samples were added to the remaining wells (for purified PCR products 7 µl was used plus 1 µl 8× loading dye). 100 V constant voltage was applied for 40 minutes using a PowerPac™ 300 power supply (Bio-Rad, UK). After completion gels were transferred to a UV transilluminator and gel images were recorded with a gel documentation system (BioSpectrum® Imaging System; UVP, USA). Using VisionWorks LS software, gels were imaged with a Biochemi HR camera at *f*1.8 aperture, 45.9% focus and 0.405 second exposure. Samples were assessed for the presence of a band appearing between 400 and 500 bp bands in the molecular weight ladder track (sample fragment size was 481 bp).

### 3.7.4 PCR Product Purification

20 µl amplicon samples from PCR were purified using 22 µl Agencourt® AMPure® XP beads (Beckman Coulter, USA). A 1.1 to 1 beads to sample ratio was used to select for fragments in the 300 to 2000 bp range (target of 481 bp) so that primer dimers, excess reagents and unspecific amplification products could be removed. The PCR purification protocol (Beckman Coulter, 2013) was followed. 22 µl AMPure® XP reagent was added to 20 µl PCR product samples in thin-walled PCR tubes and mixed by pipette aspiration. Tubes were added to a DynaMag™ (Thermo Fisher Scientific, USA) magnetic sample rack on its side for 2 minutes. Supernatant was removed from the tube and replaced with 60 µl sterile, 70 vol% ethanol wash solution and this step was repeated twice. The remaining pellet was air dried for 10 minutes (to allow ethanol to evaporate). Tubes were removed from the magnet and 20 µl PCR water was added to each tube and aspirated. The tube was then returned to the magnet and the resulting supernatant was removed and transferred to a new PCR tube. Two rounds of this procedure were performed in order to obtain a purified sample. Gel electrophoresis (Section 3.7.3) was repeated to verify that the DNA present in the sample remained and that purification was successful.

### 3.7.5 DNA Quantification

DNA which had been extracted was quantified using a Nanodrop® ND-1000 spectrophotometer (Thermo Fisher Scientific, USA) in ng/ml of sample. The ratio of absorbances at 260 and 280 nm were used to assess sample quality (with 1.8 being the value for 'pure' DNA) and the 260/230 nm ratio for nucleic acid purity (2.0 to 2.2; Thermo Scientific (2008)).

Purified amplicons were quantified using a Qubit® dsDNA HS assay (Thermo Fisher Scientific, USA). The assay protocol (Life Technologies, 2015) was followed involving addition of  $Vol = 4 \mu\text{l}$  sample to 196 µl working solution and vortexing to mix. Solutions were measured using a calibrated Qubit® 2.0 Fluorometer and DNA mass concentrations ( $\rho_{\text{DNA}}$ ) in samples were calculated using;

$$\rho_{\text{DNA}}, \text{ ng/ml} = \rho_{\text{DNA}}^{\text{Fl}} \times \frac{200 \mu\text{l}}{Vol} \quad (3.18)$$

where  $\rho_{\text{DNA}}^{\text{Fl}}$  is the mass concentration (ng/ml) of DNA measured by the fluorometer.

### 3.7.6 Sample Pooling & Dilution

The quantity of DNA in  $\text{pmol/dm}^3$  of purified amplicon samples was calculated from the quantity in ng/ml;

$$\text{DNA, pmol/dm}^3 = \frac{\text{ng/mlDNA}}{N_N \times 660 \text{ pg/pmol}} \times \frac{10^3 \text{ pg}}{1 \text{ ng}} \times \frac{10^3 \text{ ml}}{1 \text{ dm}^3} \quad (3.19)$$

where  $N_N$  is the number of nucleotides (481 bp) and 660 g/mol is the average molecular weight of a nucleotide base pair (Promega, 2010). Each sample was diluted with the appropriate amount of ultra-pure, DNA-free water to give a final DNA concentration of 100 pmol/dm<sup>3</sup>. A pooled amplicon library was created by adding 5 µl eqimolar amounts of each sample to a single vial. Before sequencing, 100 pmol/dm<sup>3</sup> pooled libraries were diluted to 26 pmol/dm<sup>3</sup> with TE buffer (pH 8.0; 10 mmol/dm<sup>3</sup> Tris, 1 mmol/dm<sup>3</sup> EDTA).

### 3.7.7 Ion Torrent™ 16S rRNA Gene Sequencing

Clonal amplification of pooled amplicon libraries was achieved by emulsion PCR which was performed to immobilise multiple copies of a single amplicon fragment onto a micro-bead (Ion Sphere™ particle). The micro-beads coated with amplicon template were added to a Ion 316™ microchip and centrifuged to deposit beads into micro-wells (Life Technologies, 2014). The microchip was loaded into an Ion Torrent™ Ion Personal Genome Machine™ (PGM; Thermo Fisher Scientific, USA) and partial 16S rRNA genes from each amplicon sample were sequenced using a Hi-Q™ sequencing kit. Ion Torrent™ technology is a next-generation sequencing (NGS) method which utilises a semi-conductor sensor array to sense changes in H<sup>+</sup> concentrations in each micro-well. Gene sequencing was achieved by sequentially flowing deoxyribose nucleoside triphosphate (dNTP) solutions of A (dATP), C (dCTP), G (dGTP) and T (dTTP). If a complementary dNTP became incorporated by the polymerase, a release of H<sup>+</sup> occurred which was detected as a voltage increase on the detector transistor and recorded by the PGM™ system (Merriman *et al.*, 2012). The sequence data was downloaded in FASTQ format from the Torrent Suite™ server following successful sequencing runs.

### 3.7.8 QIIME

Microbial community 16S rRNA gene sequence data were analysed using the 'Quantitative insights into microbial ecology' pipeline (QIIME; Caporaso *et al.* (2010)). First, FASTQ files were separated into sequence files (FASTA format) and quality score files (QUAL format) using the script `convert_fastaqual_fastq.py`. A mapping file which described sample identification, grouping and identifying primer barcode was used to label sequences according to each sample and remove those which did not match a barcode, meet a minimum quality score of 20 or minimum read length of 200 bp (using `split_libraries.py` script). Operational taxonomic units (OTUs) were selected using the uclust OTU picking method (Edgar, 2010) according to a closed reference database (Greengenes 16S rRNA database at 97% identity), followed by de novo picking for unmatched sequences. Taxonomic as-



signment was performed on a representative set of sequences using the RDP classification algorithm (Wang *et al.* (2007); `pick_open_reference_otus.py`). Sequences were then aligned to a PyNAST (Python Nearest Alignment Space Termination) template, filtered to remove universal gaps from sequences and OTUs which failed to align (`parallel_align_seqs_pynast.py`, `filter_alignment.py` and `filter_otus_from_otu_table.py`). Chimeric sequences (formed from multiple parent sequences) were identified and removed from the aligned sequences and OTU table (`parallel_identify_chimeric_seqs.py`, `filter_fasta.py` and `filter_otus_from_otu_table.py`). Following this, the phylogenetic connections and core diversity analyses were generated from the resulting sequences (`make_phylogeny.py` and `core_diversity_analyses.py`).

### **3.7.9 Gene Copy Number Adjustment**

The relative taxon abundance data obtained from QIIME microbial community analysis represented the abundance of sequences per taxon but did not take into account the number of 16S rRNA gene copies each taxon has. It was necessary to adjust the abundance data to correct for the number of gene copies to more accurately reflect the relative abundance of different organisms in the microbial population. The ribosomal RNA operon database (rrnDB) was used to determine gene copy numbers from the representative set of sequences (based on the lowest determined hierarchical taxa of at least 80% confidence; Stoddard *et al.* (2015)). Each sequence was weighted by the reciprocal mean gene copy number so that total abundance remained as 100% using the 'rrnDB Estimate' classifier tool.

## **3.8 Microbial Imaging and Cell Counts**

### **3.8.1 Visualisation of Bacterial Cells on Electrodes Using Nucleic Acid Stain Fluorescence Microscopy**

Sampled electrodes were stained with a fluorescent nucleic acid stain in order for bacteria present on the surface to be imaged. SYBR® Gold nucleic acid gel stain (Thermo Fisher Scientific, USA) is membrane-permeable and binds to double- and single-stranded DNA (dsDNA and ssDNA) and RNA of both dead and live cells. The dye-nucleic acid complex has fluorescence excitation peaks at 300 and 495 nm and a fluorescence emission peak at 537 nm (Tuma *et al.*, 1999).

A 1 × SYBR® Gold solution was prepared by diluting 10 000× concentrate with 50 mmol/dm<sup>3</sup> phosphate buffer solution. Small (15 × 5 mm) portions of electrode were cut out and placed into a vial to which 200 µl 1 × SYBR® Gold solution was added and incubated for 30 minutes at room temperature in the dark. The electrode was removed from the vial with sterile forceps and rinsed in a stream of sterile 50 mmol/dm<sup>3</sup> phosphate buffer solution to remove excess

stain. The electrode was placed onto a glass microscope slide and covered with a cover slip.

Microscope slides were imaged using a BX40 epifluorescence microscope fitted with an E-400 digital camera (Olympus, Japan) at 100× and 400× magnification. Field of view dimensions were calculated using a 1 mm stage micrometer with 10 µm graduations (Figure B.9 in Appendix B).

### **3.8.2 Bacterial Cell Counts on Electrodes**

Cell counts were performed on sampled electrodes taken for community analysis. A 1× phosphate-buffered saline (PBS) solution was prepared containing 8.00 g/l NaCl, 0.20 g/l KCl, 1.44 g/l Na<sub>2</sub>HPO<sub>4</sub>, 0.24 g/l KH<sub>2</sub>PO<sub>4</sub>, adjusted to pH 7.4 with HCl and made up to volume with DI water (Sigma Aldrich, UK; Sambrook *et al.* (1989)). PBS and DI water were sterilised by autoclaving and passing through a 0.2 µm PES filter. 100 mg electrode samples (taken from ethanol-fixed, precipitates from centrifuged electrodes; Section 3.5.4) were added to a vial. The electrode sample represented approximately 3 wt% of 19.6 cm<sup>2</sup> electrodes and 5 wt% of 11.0 cm<sup>2</sup> electrodes and still contained carbon cloth material. 5 ml filter-sterile PBS was added to give a 1/50 dilution, from this 10 µl aliquots were further diluted with 990 µl PBS to give a dilution factor of  $DF_{\text{Sample}} = 5000$ . 50 µl 100× SYBR® Gold solution was added to each diluted sample and a 1 ml filter-sterile PBS control and incubated for 30 minutes at room temperature in the dark.

For each sample, a 13 mm diameter, 0.22 µm pore size, hydrophilic polycarbonate membrane filter (Merck Millipore, Germany) was aseptically fitted using sterile forceps to a stainless steel analytical filter holder in a Büchner flask. The membrane was drawn onto the filter holder and rinsed by attaching a vacuum pump to the flask and addition of 1 ml filter-sterile DI H<sub>2</sub>O. After addition to the filter holder the liquid was allowed to pass through by vacuum suction before proceeding. Once the initial water had been drawn through, the 1.05 ml SYBR® Gold-stained sample was added, followed by three additions of 1 ml filter-sterile DI H<sub>2</sub>O to wash excess stain from the filter surface. Finally, the vacuum was run for an extra 3 minutes to dry the filter.

A drop of Citifluor™ CFM-1 antifadent (Citifluor, UK) was added to a clean microscope slide, to this the 13 mm filter was aseptically transferred using forceps and a second drop of antifadent was added on top and enclosed by a microscope slide cover-slip. Filters were imaged as per Section 3.8.1 from at least 14 viewpoints per sample at 400× magnification for electrode samples and 100× for the control.

The number of SYBR® Gold-labelled bacteria present in each imaged field of view was counted using CellC automated image analysis software (Figure B.10 in Appendix B; Selin-ummi *et al.* (2005)). The counting software was set to discount areas smaller than 0.5 µm<sup>2</sup>,

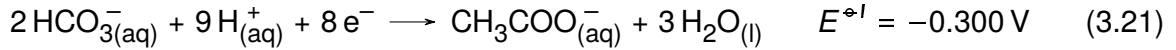
have maximum cell clustering division and automatic correction for background and intensity thresholds. The average number of cells per field of view ( $N_{Ave}$ ) was calculated per sample. The number of cells per  $\text{cm}^2$  effective electrode area was calculated as;

$$\text{Cells per cm}^2 = \frac{N_{Ave} \times N_{FoV} \times DF_{\text{Sample}} \times DF_{\text{Electrode}} \times m_{\text{Electrode}}}{A_{\text{Eff}}} \quad (3.20)$$

where  $N_{FoV}$  is the number of fields of view per membrane,  $DF_{\text{Electrode}}$  is the dilution factor of the electrode equal to the mass of electrode precipitate divided by the original electrode mass,  $m_{\text{Electrode}}$  is the original mass of the electrode (mg),  $A_{\text{Eff}}$  is the effective electrode area ( $\text{cm}^2$ ); it was assumed there were no bacteria present on the gasket-covered electrode surface.

### 3.9 Electrochemical Methods

A MFC is defined by the half-cell reactions occurring at the anode (e.g. acetate oxidation) and cathode (oxygen reduction) written by convention as reduction reactions;



where  $E^{\circ I}$  is the pH 7-adjusted value for the standard reduction potential ( $E^{\circ}$ , V) vs. SHE (Logan, 2008). The adjusted values were calculated using the Nernst equation which allows the theoretical reduction potential to be calculated under specified conditions;

$$E^{\circ I} = E^{\circ} - \frac{RT}{zF} \ln Q_R \quad (3.23)$$

where  $R$  is the universal gas constant ( $8.314 \text{ J K}^{-1} \text{ mol}^{-1}$ ),  $T$  is the temperature (K),  $z$  is the number of moles of electrons transferred and  $F$  is the Faraday constant ( $9.648 \times 10^4 \text{ C mol}^{-1}$ ).  $Q_R$  is the reaction quotient given as the ratio of concentrations of products to reagents to the power of their stoichiometric coefficients, given here for the anode (Equation 3.24) and cathode (Equation 3.25) reactions;

$$Q_R^{\text{An}} = \frac{[\text{CH}_3\text{COO}^-]}{[\text{HCO}_3^-]^2 [\text{H}^+]^9} \quad (3.24)$$

$$Q_R^{\text{Cat}} = \frac{1}{p\text{O}_2 [\text{H}^+]^4} \quad (3.25)$$

where  $p\text{O}_2$  is the partial pressure of  $\text{O}_2$  (0.2 atm). The maximum theoretical cell voltage

( $E_{Cell}^{\circ}$ ) for a 1 g/l acetate-oxidising anode with oxygen-reducing GDE is  $E_{Cat}^{\circ} - E_{An}^{\circ} = +0.805 \text{ V} - (-0.300 \text{ V}) = +1.105 \text{ V}$  (Logan, 2008). However, the maximum cell electromotive force potential ( $E_{emf}$ ) which can be measured between the anode and cathode at OCP is always less than  $E_{Cell}^{\circ}$ . The value is less because the overpotential losses (V) from the anode ( $\sum \eta_{An}$ ) and cathode ( $\sum \eta_{Cat}$ ) and ohmic losses must be taken into account;

$$E_{emf} = E_{Cell}^{\circ} - (\sum \eta_{An} + |\sum \eta_{Cat}| + I R_{\Omega}) \quad (3.26)$$

where  $I$  is the current (A) and  $R_{\Omega}$  is the ohmic resistance ( $\Omega$ ; part of internal resistance ( $R_{Int}$ )).

### 3.9.1 Electrical Load

The constructed 50 ml and 10 ml cells were operated as microbial fuel cells with an external resistor ( $R_{Ext}$ ) connected between the anode wire and the cathode wire. Resistor leads were constructed by cutting 5 cm leads in half, soldering a resistor between the exposed ends and electrically insulating the resistor and connection using heat-shrink sleeves (RS Components, UK). This enabled MFCs to be wired without possibility of short-circuiting from proximity to other cells' wiring. Over the course of experiments SCMFCs were operated using  $R_{Ext} = 44, 305, 953, 2390$  and  $5100 \Omega$  resistors.

### 3.9.2 Voltage Measurements

2 m shielded leads attached to a NI USB-6225 data acquisition device (DAQ; National Instruments, USA) were connected to measure cell voltage between anode and cathode electrodes, and anode potential between reference and anode electrodes over time. LabVIEW™ Signal-Express software was programmed to acquire data at 1 kHz from differential voltage channels with a Butterworth low pass signal processing filter applied at 10 Hz (0.1 s) to reduce noise. A data sampling period of 5 minutes was chosen for monitoring of MFCs. For high-resolution data logging an additional data sampling step was added to the logging routine to record data every 1 second, allowing the initial current response of MFCs to medium replacements to be determined. The open circuit potential (OCP) of cells and anodes was measured with the external resistor disconnected using a voltage measurement device (data logger, potentiostat or digital multimeter).

### 3.9.3 Polarisation and Power Density Curve Measurement

To determine peak power performance of MFCs polarisation curves were recorded. Cells were put into open circuit by disconnecting the external resistor and time was allowed for

a steady-state open circuit potential to be reached (up to 3 hours or when voltage change was less than +10  $\mu\text{V/s}$ ) before the cell and anode potentials were monitored. To each cell an external resistor was connected in the sequence; 52 300, 12 700, 5100, 1820, 953, 503, 305, 200, 100, 44 and 10.6  $\Omega$ . Approximately 20 minutes was allowed between each resistor change in order for the voltages to stabilise and be recorded. Following the final measurement the original resistor used for MFC operation was connected and normal operation was resumed.

Polarisation and power density curves were constructed by plotting cell voltage and power respectively against current recorded from the MFCs. The power density curve exhibited a maximum point from which the external resistance ( $R_{Ext}$ ) at which peak power performance is achieved could be determined.

Three regions of the voltage-current polarisation curve were present; as  $R_{Ext}$  was initially decreased from OCP the reaction was limited by catalyst and bacterial enzyme kinetic rates and a voltage drop was observed (activation polarisation region), as  $R_{Ext}$  was decreased further and bacterial metabolism of substrate occurred a linear correlation was observed (ohmic polarisation region) and at low  $R_{Ext}$  values a further loss was seen as the reactions became mass transfer limited (concentration polarisation region). The linear correlation in the ohmic polarisation region is given by the equation;

$$V = OCP^* - I R_{Int} \quad (3.27)$$

where  $V$  is the measured cell voltage (V),  $OCP^*$  (V) is the y-intercept of the linear ohmic polarisation region (not the measured OCP),  $I$  is the measured current (A) and  $R_{Int}$  is the internal resistance ( $\Omega$ ). Equation 3.27 was used to calculate an estimate of the total internal resistance of the cell ( $R_{Int}$ ) from the measured polarisation curve (Logan, 2008). The MFC cell voltage ( $V$  or  $E_{Cell}$  in V) is given as;

$$V = E_{Cell} = E_{Cat} - E_{An} \quad (3.28)$$

The measured anode potential ( $E_{An}$ , V) and the cathode potential ( $E_{Cat}$ , V; calculated from the measured cell voltage) were adjusted to compensate for ohmic drop between the non-polarisable Ag/AgCl reference electrode and working electrode using;

$$E_{An}^* = E_{An} - I R_{\Omega} \quad (3.29)$$

$$E_{Cat}^* = E_{Cat} + I R_{\Omega} \quad (3.30)$$

where  $E_{An}^*$  and  $E_{Cat}^*$  are the ohmic drop compensated values (V),  $I$  is the current (A) and  $R_{\Omega}$  is the ohmic resistance ( $\Omega$ ; Bard and Faulkner (2001)).

### **3.9.4 Electrochemical Impedance Spectroscopy**

Electrochemical Impedance Spectroscopy (EIS) performed on cells, anode and cathode electrodes allowed the ohmic resistance ( $R_{\Omega}$ ) to be determined. A potentiostat passed a small alternating current (AC) (10 mV amplitude was used in this study) across a wide range of frequencies, enabling current response to be recorded without interfering with the performance of the MFC. Two potentiostats were used for EIS determinations namely an Ivium CompactStat.e with IviumSoft electrochemistry software (Ivium Technologies, The Netherlands) and Autolab PGSTAT203 with NOVA software (Metrohm, Switzerland). 50 frequencies were measured over the frequency range 10 000 to 0.1 Hz. All EIS spectra were recorded at the OCP of the studied electrode or cell. EIS was used in a two-electrode set-up for cell measurements (with the cathode as the working electrode and the anode acting as the counter and reference electrode) and three-electrode set-up for electrode measurements (using a separate Ag/AgCl reference electrode).

Nyquist charts were constructed plotting the real impedance against the imaginary impedance. The intercept point where the real impedance intersects the x-axis is defined as the ohmic resistance ( $R_{\Omega}$ ). EIS spectra can be interpreted by fitting equivalent circuits to determine the other polarisation and charge transfer resistances which together make up the total internal resistance ( $R_{Int}$ ). However, for MFCs there is no simple equivalent circuit which can resemble the bacterial biofilm (Logan, 2008; He and Mansfeld, 2009); therefore no further analysis or parameters were extracted from EIS data in this study.

### **3.9.5 Linear Sweep Voltammetry**

Linear Sweep Voltammetry (LSV) was performed to assess the performance of MFC anodes using an Autolab PGSTAT203 potentiostat and NOVA electrochemistry software (Metrohm, Switzerland). With the anode acting as the working electrode, cathode as counter electrode and Ag/AgCl reference electrode, an applied potential was swept from the OCP up to +0.2 V vs. Ag/AgCl. A scan rate of 1 mV/s was chosen to minimise capacitive effects on the electrode.

### **3.9.6 Cyclic Voltammetry**

Cyclic Voltammetry (CV) was used for kinetic analysis of MFC anode biofilms using an Autolab PGSTAT203 potentiostat and NOVA electrochemistry software (Metrohm, Switzerland). With the anode acting as the working electrode, cathode as counter electrode and Ag/AgCl reference electrode an applied potential was swept from the OCP up to +0.2 V vs. Ag/AgCl, down to -0.5 V vs. Ag/AgCl and returned to the OCP. Three cycles were performed until

a stable voltammogram was obtained and the initial scans were discarded. A scan rate of 5 mV/s was chosen with potential steps of 0.5 mV.

### 3.10 Data Handling Methods

#### 3.10.1 Raw Data

Data logging data was recorded to plain text files. A Microsoft® Excel® macro was developed which collated multiple logging files, converted timestamps to date-time format and plotted current-response charts for each MFC. An additional worksheet was developed for the recording of 'event' data such as medium changes, pump operations, sampling and set-up changes with precise timestamps. Analytical data were recorded either by hand directly from the instrument or saved in plain text files.

#### 3.10.2 Current

Current ( $I$ , A) was calculated using Ohm's law from recorded voltage data ( $V$ , V) and the known external resistor ( $R_{Ext}$ ,  $\Omega$ ) connected to MFCs;

$$I, A = \frac{V}{R_{Ext}} \quad (3.31)$$

Current density ( $\mu A/cm^2$ ;  $I/A_{Eff}$ ) was calculated by normalising the current (in  $\mu A$ ) by anode effective area (in  $cm^2$ ).

#### 3.10.3 Charge

The approximate electrical charge ( $Q$ ), in coulombs ( $C = A s$ ), passed between two time points was calculated using the trapezoidal rule. The charge passed between each data logging interval ( $\Delta t$  in seconds) was first calculated from the current recorded at each point ( $I_i$  and  $I_f$  in A);

$$Q, C = \int_{t_i}^{t_f} I dt \approx \frac{(I_i + I_f) \Delta t}{2} \quad (3.32)$$

The sum of charge from each interval was calculated for reporting the total charge passed over a specified time period. Charge density ( $C/cm^2$ ;  $Q/A_{Eff}$ ) was calculated by normalising the charge (in C) by anode effective area (in  $cm^2$ ).

### 3.10.4 Power

Power ( $P$ , W) was calculated from recorded voltage data ( $V$ , V) and the known external resistor ( $R_{Ext}$ ,  $\Omega$ ) connected to the MFCs;

$$P, W = \frac{V^2}{R_{Ext}} \quad (3.33)$$

Power density ( $\mu\text{W}/\text{cm}^2$ ;  $P/A_{Eff}$ ) was calculated by normalising the power (in  $\mu\text{W}$ ) by anode effective surface area (in  $\text{cm}^2$ ).

### 3.10.5 Theoretical Oxygen Demand

Carbonaceous Theoretical Oxygen Demand (ThOD,  $\text{mg/l O}_2$ ) was calculated using the molar ratio of  $\text{O}_2$  required to completely oxidise each substrate to  $\text{CO}_2$  and  $\text{H}_2\text{O}$  with nitrification inhibited (Equation 3.34).

$$\text{ThOD, mg/l} = \frac{n_{\text{O}_2}}{n_{\text{Sub}}} \times \frac{M_{\text{O}_2}}{M_{\text{Sub}}} \times \rho_{\text{Sub}} \quad (3.34)$$

where  $n_{\text{O}_2}$  is the number of moles of oxygen required to oxidise  $n_{\text{Sub}}$  moles of substrate,  $M_{\text{O}_2}$  and  $M_{\text{Sub}}$  are the molar masses of oxygen and substrate respectively and  $\rho_{\text{Sub}}$  is the substrate mass concentration. Equation 3.34 was used to calculate the ThOD values for solutions of 150  $\text{mg/l}$  glucose and 150  $\text{mg/l}$  glutamic acid (Figure B.11 in Appendix B). 1.07 g of oxygen was required to oxidise 1 g of glucose giving a ThOD of 160  $\text{mg/l O}_2$ . Whereas, 0.98 g was the required amount to oxidise 1 g glutamic acid with nitrification inhibited giving a carbonaceous ThOD value of 147  $\text{mg/l O}_2$ . The carbonaceous ThOD of a 300  $\text{mg/l}$  1:1 glucose-glutamic acid (GGA) solution was therefore  $160 + 147 = 307 \text{ mg/l}$  (MFC anode chambers are anaerobic therefore nitrification does not occur readily).

### 3.10.6 Coulombic Efficiency

Coulombic efficiency ( $C_E$ , %) was calculated from the known concentration of substrate present in the medium and the number of electrons transferred per mole.  $C_E$  was calculated for batch-mode MFCs (Equation 3.35);

$$C_E = \frac{M_{r \text{ Sub}} Q}{z F \text{Vol}_{An} \Delta[\text{Sub}]} \approx \frac{M_{r \text{ O}_2} Q}{z F \text{Vol}_{An} \Delta\text{COD}} \quad (3.35)$$

where  $M_{r \text{ Sub}}$  and  $M_{r \text{ O}_2}$  are the substrate and oxygen relative molecular mass respectively,



$Q$  is the charge passed between sampling points (C),  $z$  is the number of electrons transferred per mole,  $F$  is the Faraday constant ( $9.648 \times 10^4 \text{ C mol}^{-1}$ ),  $Vol_{An}$  is the anodic chamber volume (l) and  $\Delta[\text{Sub}]$  and  $\Delta\text{COD}$  are the change in substrate concentration ( $\text{mol/dm}^3$ ) and COD ( $\text{mg/l O}_2$ ) respectively (Logan, 2008). In this study  $\Delta\text{COD}$  concentration was used because COD was more conveniently measured than substrate concentration for complex substrates. For flow-mode MFCs the coulombic efficiency was calculated using;

$$C_E = \frac{M_{r \text{ Sub}} I}{z F q \Delta[\text{Sub}]} \approx \frac{M_{r \text{ O}_2} I}{z F q \Delta\text{COD}} \quad (3.36)$$

where  $I$  is the current (A) and  $q$  is the pump flow rate (l/s).

### 3.10.7 Partial Mass Balance

Using the known starting concentrations of substrate and results from DOC, IC and VFA analyses and D-glucose and L-glutamic acid assays a mass balance was constructed. Only a partial mass balance could be created as the identity and concentration of some substrate degradation products were unknown or unmeasured. The concentrations from known compounds (VFAs, glucose and glutamic acid) were normalised to mass concentration of carbon ( $\rho_C$ , mg/l C) so the values from each method were comparable to the results from DOC analysis;

$$\rho_C = \rho_X \times \frac{n_C A_{rC}}{M_{rX}} \quad (3.37)$$

where  $\rho_X$  and  $M_{rX}$  are the mass concentration (mg/l) and relative molecular mass of the known compound (X) respectively and  $n_C$  and  $A_{rC}$  are the number and relative atomic mass of carbon respectively.

### 3.10.8 BOD Sensor Calibration Data

Calibration plots were constructed by plotting output from the MFC sensor against known  $\text{BOD}_5$  concentrations (estimated from the substrate concentration; Figure 3.7). The output from the sensor was either peak/average current density (amperometric detection) or charge density (coulometric detection). Peak current density ( $\hat{I}$ ) was recorded from batch-mode MFCs; with each medium cycle a peak was observed in the current-time plot (Figure 3.8a). Average current density ( $\bar{I}$ ) was determined for flow-mode MFCs over the period of stable current resulting from constant flow of medium (Figure 3.8b). The period of stable current ( $I_{\text{Stable}}$ ) was defined as the point at which the 1st derivative of the current ( $dI/dt$ ) fell below a threshold set at 3% of the peak current ( $\hat{I}$ ). As the current density stabilised the 1st derivative

(slope) approached zero as the response plateaued (Figure 3.8a, Deriv. threshold). Charge density ( $Q$ ) was determined for batch- and flow-mode operation for time periods of the first hour and complete medium cycles.

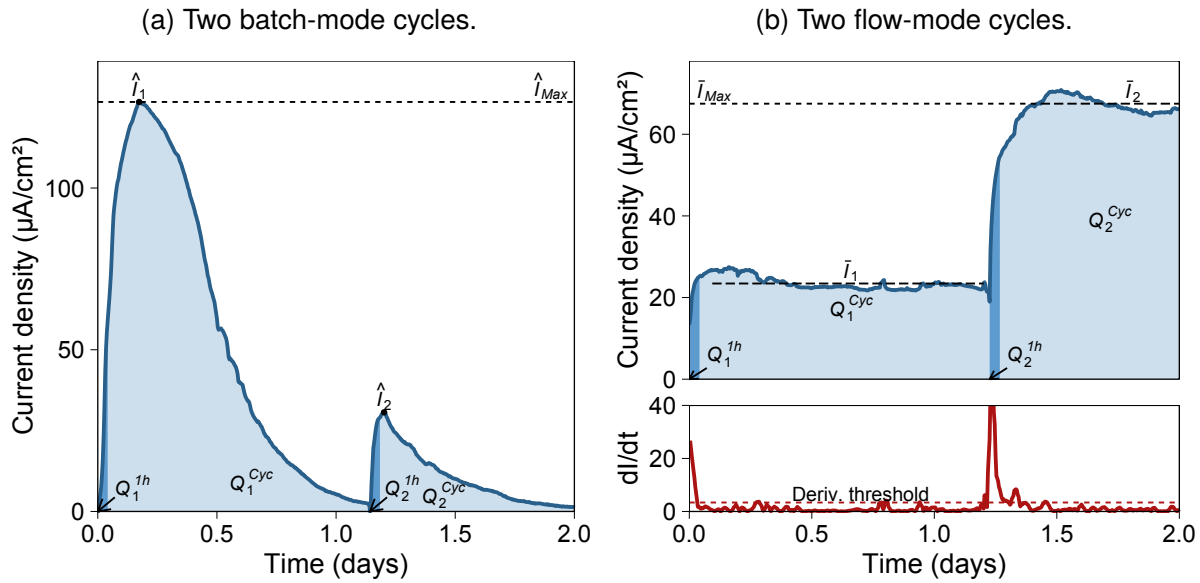


Figure 3.8: Current response charts annotated with (a) peak ( $\hat{I}$ ), and maximum peak ( $\hat{I}_{Max}$ ) current densities and (b) average stable ( $\bar{I}$ ) and maximum average stable ( $\bar{I}_{Max}$ ) current densities (stable period was when 1<sup>st</sup> derivative of the current was below threshold). Shaded areas represent charge densities for the first hour ( $Q^{1h}$ ) and complete medium cycle ( $Q^{Cyc}$ ).

With the three-stage flow-mode channels the sum of the current densities ( $\sum I$ ,  $\mu A/cm^2$ ) and sum of the charge densities ( $\sum Q$ ,  $C/cm^2$ ) was calculated from each stage of MFCs;

$$\sum I = I_{MFC1} + I_{MFC2} + I_{MFC3} \quad (3.38)$$

$$\sum Q = Q_{MFC1} + Q_{MFC2} + Q_{MFC3} \quad (3.39)$$

where  $I_{MFC\#}$  and  $Q_{MFC\#}$  are the mean current density and charge density respectively from each MFC stage ( $\# = 1, 2$  and  $3$ ) in the three-stage channel. The average sum current and charge density values ( $\sum I$  and  $\sum Q$ ) were calculated by first adding the values from each stage within a flow channel and then determining the average of the sum across flow channels (to avoid under-estimation of the average value where, for example, peak currents across replicate cells do not coincide).

### 3.10.9 Sensor Response Normalisation

The sensor response was normalised to a percentage-based scale so that calibrations across different operating conditions could be compared. The normalised ‘anode saturation’ parameters were defined relative to the maximum limiting peak current density ( $\hat{I}_{Max}$ ), average current density ( $\bar{I}_{Max}$ ) or charge density ( $Q_{Max}$ ) achieved during calibration;

$$\hat{I}_{Norm} = \frac{\hat{I}}{\hat{I}_{Max}} \times 100\% \quad (3.40)$$

$$\bar{I}_{Norm} = \frac{\bar{I}}{\bar{I}_{Max}} \times 100\% \quad (3.41)$$

$$Q_{Norm} = \frac{Q}{Q_{Max}} \times 100\% \quad (3.42)$$

where  $\hat{I}$ ,  $\bar{I}$  and  $Q$  are a given peak current density, mean current density or charge density respectively. The multi-stage flow-mode parameters ( $\sum \bar{I}$  and  $\sum Q$ ) were also normalised using the same equations (Equation 3.41 and Equation 3.42) with the maximum limiting, summation mean current density ( $\sum \bar{I}_{Max}$ ) and charge density ( $\sum Q_{Max}$ ). The resulting data were not dependent on the magnitude of the current, which was subject to variation due to declining cathode/membrane performances with age (perhaps due to catalyst poisoning or biofouling). Normalisation allowed calibrations to be compared from experiments with different external resistances ( $R_{Ext}$ ) as the current/charge was normalised to the same scale.

#### 3.10.10 Toxicity, Inhibition and Starvation Calibration Data

The calibration plots for current decreases were constructed with the sensor outputs from the multi-stage flow-mode system ( $\bar{I}$  and  $\sum \bar{I}$ ) against known 4-nitrophenol toxicant concentrations ([4-NP]; toxic inhibition) and BOD changes ( $\Delta BOD$ ) for excess inhibition and starvation. Sensor response was also normalised to show a positive correlation with increasing toxicant concentration or decreasing BOD by calculating percentage 'current loss' ( $\%I_{Loss}$ );

$$\%I_{Loss} = \frac{\bar{I}_{Max} - \bar{I}_{Tox}}{\bar{I}_{Max}} \times 100\% \quad (3.43)$$

where  $\bar{I}_{Max}$  is the maximum limiting mean current density and  $\bar{I}_{Tox}$  is the given current density with toxicant/inhibitor/starvation presence.

### 3.11 Statistical Techniques

#### 3.11.1 Replicate Measurements

Batch-mode MFC experiments were conducted in duplicate and flow-mode MFC experiments were conducted in triplicate channels of three-stage MFCs. For all data from each replicated experiment mean values ( $\bar{x}$ ) were calculated and reported as given in Equation 3.44. The

weighted grand mean ( $\bar{x}_{GM}$ ) of averaged values from cells (e.g. mean of mean current ( $\bar{i}$ ) from replicate cells) was calculated as given in Equation 3.45;

$$\bar{x} = \frac{\sum x}{N} \quad (3.44) \quad \bar{x}_{GM} = \frac{\sum \bar{x} N_d}{\sum N_d} \quad (3.45)$$

where  $x$  is the individual value from each MFC,  $N$  is the number of values (e.g. replicates) and  $N_d$  is the number of data points in the dataset from each replicate cell. For duplicate measurements ( $N = 2$ ) the range ( $Rng$ ) was calculated from the difference between the two values;

$$Rng = |x_i - x_{ij}| \quad (3.46)$$

where  $x_i$  and  $x_{ij}$  are the measurements from the two replicate cells. Mean values from duplicated experiments were reported as  $\bar{x} \pm 1/2 Rng$  and the range was used for error bars in plots. For experiments where  $N > 2$  the standard deviation ( $SD$ ), representing the variance from the mean from each set of replicated values, was calculated as in Equation 3.47. The grand standard deviation ( $SD_{GM}$ ) was calculated for replicated datasets (of  $N_d$  values) from the sum of squares within groups and between groups as in Equation 3.48;

$$SD_{\bar{x}} = \sqrt{\frac{\sum (x - \bar{x})^2}{N - 1}} \quad (3.47)$$

$$SD_{GM} = \sqrt{\frac{\sum (x - \bar{x})^2 + \sum N_d (\bar{x} - \bar{x}_{GM})^2}{\sum N_d - 1}} \quad (3.48)$$

Mean values (from  $N > 2$  values) were reported as  $\bar{x} \pm SD$  and the standard deviation was used for error bars in plots from these experiments (Cumming *et al.*, 2007; Field, 2008).

### 3.11.2 Calibration Modelling

Calibration models were used to determine unknown quantities of target analyte (e.g. BOD<sub>5</sub> or toxic compound concentration) from outputs of the MFC sensor (e.g. current or charge density). Statistical models and related parameters were calculated using the R programming language inside RStudio integrated development environment (R Core Team, 2015; RStudio Team, 2015). Linear regression analysis, the simplest calibration model, was performed by fitting an explanatory variable ( $x$ ; e.g. known quantities of target analyte) and response variable ( $y$ ; e.g. measured MFC outputs) to the linear regression formula;

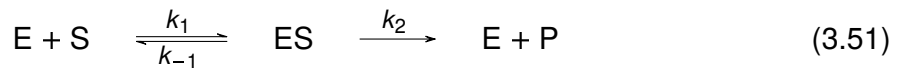
$$y' = mx + c + (e_y) \quad (3.49)$$

where  $y'$  is the fitted value predicted by the model,  $m$  is the slope of the line,  $c$  is the intercept and  $e_y$  is the error in determining  $y'$ . According to IUPAC (1997) the following parameters must also be reported alongside linear calibrations; number of observations, relational equation, fitted parameters, standard deviations of the parameters and about the line ( $SD_{Res}$ ), and the independent variable with confidence limits. Data were fitted to a line of best fit (Figure 3.9a) using least squares regression which minimised the residual sum of squares ( $SS_{Res}$ ; the sum of the difference between observed and fitted values squared);

$$SS_{Res} = \sum (y - y')^2 \quad (3.50)$$

where  $y$  is the measured value and  $y'$  is the fitted value. In addition, using an analysis of variance (ANOVA) linear regression model, it was possible to establish  $p$ -values for calibration fits, with a value less than 0.05 deemed as significant correlation.

The problem with linear calibration is that the model does not describe the plateau reached at high analyte concentration. Alternatively, biosensor calibrations can be modelled using non-linear equations formulated for enzyme kinetics simulations. The Michaelis-Menten (M-M) kinetic model (equivalent to the empirically-derived Monod model for microbial growth kinetics) is commonly used by those aiming to model dose-response relationships (Ketep *et al.*, 2013; Cheng *et al.*, 2008; Wang *et al.*, 2014).



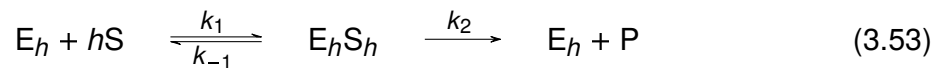
where E is the enzyme, S is the substrate, ES is an enzyme-substrate complex and P is the product formed.  $k_1$  and  $k_{-1}$  are the forward and reverse rate constants for formation of ES and  $k_2$  is the rate constant for formation of P (Sauro, 2012). The M-M model assumes that the enzyme-substrate complex rapidly reaches steady-state (rate of formation = rate of dissociation) and therefore the Michaelis-Menten equation can be derived to relate substrate concentration ( $[S]$ ) to reaction rate ( $v$ );

$$v = \frac{v_{Max} [S]}{K_M + [S]} \quad (3.52)$$

where  $v_{Max}$  is the maximum reaction rate and  $K_M$  is the Michaelis constant (Kompala, 2011). In MFC biosensing  $v$  is equivalent to the sensor output ( $\hat{I}$ ,  $\bar{I}$  or  $Q$ ) and  $[S]$  is the substrate concentration or related parameter (e.g. BOD<sub>5</sub>).  $K_M$  is equal to the substrate concentration that results in half maximal rate (equivalent to EC<sub>50</sub>). The M-M equation models the exponential growth, decelerating growth and stationary phases typically observed

in bacterial growth profiles (Kompala, 2011).

The initial lag and accelerating growth phases are not simulated by the M-M model which can result in fitted curves which do not represent the calibration data accurately (Figure 3.9b). An extension of this model is the Hill equation (Equation 3.54; Goutelle *et al.* (2008); Weiss (1997));



$$v = \frac{v_{Max} [S]^h}{K_M^h + [S]^h} \quad (3.54)$$

where the additional term,  $h$ , is the Hill coefficient. Theoretically, the Hill coefficient should represent the number of binding sites on a multi-site enzyme. The Hill equation was developed by Hill (1910) to model the sigmoidal dose-response curves exhibited by the binding of oxygen to haemoglobin and originally predicted that there was likely an aggregate of multiple enzyme molecules (or haemoglobin) hence  $h$  was non-integral (Hill, 1913). The aggregation theory was later disproven and it is now known that haemoglobin has four haem groups which can bind four  $O_2$  molecules. With each successive binding the affinity increases until saturation, known as co-operative binding (Bindslev, 2008). Sauro (2012) states that the model is too simplistic to result in true integer values and thus can provide no mechanistic information, however  $h$  does provide a solution to quantify the deviation from standard dose-response curves (*i.e.* Michaelis-Menten). The Hill coefficient ( $h$ ) defines the co-operativity of the binding reaction, with values greater than 1 representing positive co-operation and less than 1 negative co-operation. In this study the three-parameter Hill equation (Equation 3.54) was used (as the fourth parameter ( $v_{Min}$ ) was constrained to zero) because the expected MFC response with 0 mg/l  $O_2$  BOD present is 0  $\mu A/cm^2$  (Figure 3.9c).

Both the Michaelis-Menten and Hill models are irreversible models which predict that once the stationary phase has been reached the rate will continue to approach  $v_{Max}$  and are not capable of simulating the inhibition of response (or death phase) observed at excess substrate concentrations. Therefore, 'normal' calibrations in this study were only modelled up to maximum non-inhibiting substrate concentrations.

Reversible equations which are able to model the substrate excess inhibition phase (such as the reversible forms of the M-M and Hill models) incorporate extra parameters (such as inhibitor and/or 'product' concentration) which are not easily measured with the MFC sensor (Imperial and Centelles, 2014). Adding additional terms to be modelled based on solely a single response variable (*e.g.* current density) increases the magnitude of the confidence and prediction intervals significantly. The Haldane equation (Equation 3.55) is commonly used for simulating substrate-inhibited responses in enzyme kinetics (Sonnad and Goudar, 2004).

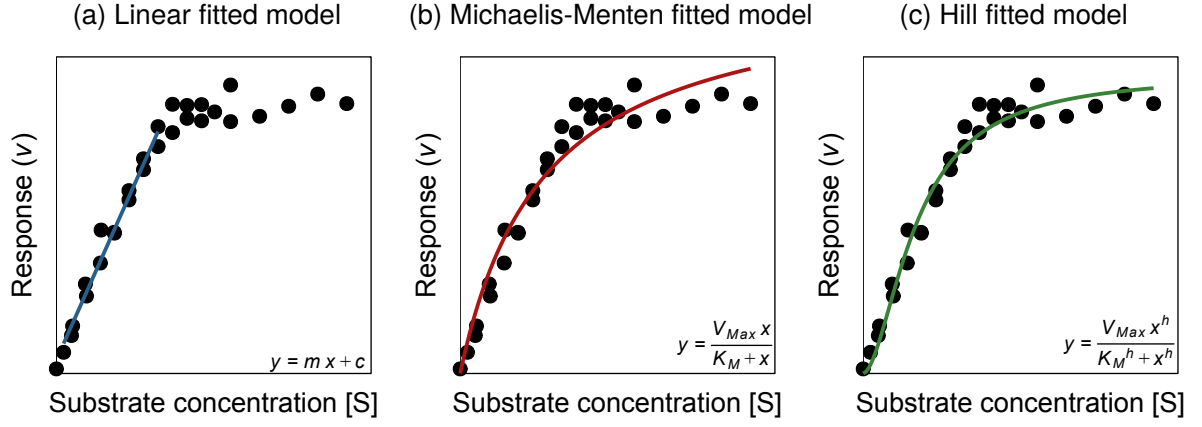


Figure 3.9: Typical calibration of MFC BOD biosensor response against substrate concentration fitted with (a) linear, (b) Michaelis-Menten and (c) Hill model lines.

$$v = \frac{v_{Max} [S]}{K_M + [S] + \frac{[S]^2}{K_I}} \quad (3.55)$$

where  $K_I$  is the inhibition constant (mg/l). With the addition of the  $[S]^2/K_I$  term to the Michaelis-Menten equation, the Haldane model predicts a decrease in response when the substrate concentration ( $[S]$ ) becomes greater than the inhibition constant.

The coefficient of determination ( $R^2$ ) was calculated using Equation 3.56 to measure the degree of correlation and goodness of fit of the data to the modelled line (at  $R^2 = 1$ ; Prichard and Barwick (2003)).  $R^2$  was also calculated for non-linear fits of Michaelis-Menten and Hill models as was done previously by Kurganov *et al.* (2001) for fitting biosensor calibration curves to the Hill equation.

$$R^2 = 1 - \frac{SS_{Res}}{SS_{Tot}} = 1 - \frac{\sum (y - y')^2}{\sum (y - \bar{y})^2} \quad (3.56)$$

where  $SS_{Res}$  and  $SS_{Tot}$  are the residual and total sum of squares respectively,  $y$  is the observed value of biosensor output,  $\bar{y}$  is the average of all observed  $y$  values and  $y'$  is the fitted value predicted by the model. The residual standard deviation ( $SD_{Res}$ ) about the fitted lines was also calculated in the units of the response variable.

Prediction bands were used to show where 95% of the measurements were likely to position on the calibration curves (Motulsky and Christopoulos, 2004; Gadagkar and Call, 2015). The prediction bands were calculated using the 95% confidence intervals of the fitted coefficients (slope, intercept or  $K_M$ ,  $v_{Max}$  and  $h$ ).

### 3.11.3 Calibration Performance Characteristics

For each calibration the detection range by both linear and non-linear regression was assessed (as described in Section 3.11.2). The lower limits of the linear detection range, namely limit of detection (LOD) and quantification (LOQ), were determined using the following equations:

$$\text{LOD} = 3.3 \times \frac{SD_{Res}}{m} \quad (3.57)$$

$$\text{LOQ} = 10 \times \frac{SD_{Res}}{m} \quad (3.58)$$

where  $SD_{Res}$  is the residual standard deviation about the fitted calibration line and  $m$  is the slope of the linear regression analysis (Shrivastava and Gupta, 2011). LOD represents the lowest concentration which can be detected and LOQ is the lowest amount which can be quantified with a signal to noise ratio greater than 10 (Hui, 2006). The upper limit was defined as the point at which the slope tends to zero (plateaus). The sensitivity was calculated by the following equation originally defined by Di Lorenzo *et al.* (2014) for toxicity sensors:

$$\text{Sensitivity} = \frac{\Delta I}{\Delta[S] A_{Eff}} = m \quad (3.59)$$

where  $\Delta I$  is the change in current,  $\Delta[S]$  is the change in analyte concentration (*e.g.* BOD<sub>5</sub> or toxicant concentration),  $A_{Eff}$  is the effective anode area and the sensitivity is equal to  $m$  the slope of linear regression of current density against  $[S]$ .

The response time for changes in analyte concentration (BOD<sub>5</sub> or toxicant) was determined as the time to reach 95% steady state current. Lag time was measured as the time between fresh analyte entering the MFC and a measurable change in response being recorded by the data-logger. Rise and fall response times, defined as step changes between concentrations, were recorded as the time between fresh analyte entering the MFC to the response reaching 95% steady state current. Recovery time (from toxic, excess substrate or starvation exposures) was recorded as the time between the original medium feed being restored and the current reaching the original baseline current.

Accuracy was assessed by the percentage difference between replicated sensor measurements and known values of analyte. Precision was assessed as the standard deviation between replicated measurements. As Biochemical Oxygen Demand is a broad measurement intended to be non-selective and indicate biodegradability of organic matter, the selectivity was only assessed by measuring different medium compositions, namely glucose, glutamic acid, GGA and wastewater. Equally, toxicity is a broad term meant to be non-selective for specific toxicants. It is a feature of MFC sensors that the response is non-selective and therefore able to correlate well with these measurands. Robustness was not assessed in this study as the environmental parameters which could affect analysis were kept constant.



## Chapter 4. Batch-mode MFCs for Optimisation and Exploration of Sensing Characteristics using GGA Medium

### 4.1 Introduction

Batch-mode microbial fuel cells (MFCs) can be used as BOD sensors which provide a convenient platform for offline, laboratory-based testing of wastewater samples. MFC sensor response can be evaluated in static systems without the need to consider mass-transfer related conditions such as hydraulic retention time which is necessary when using flow-mode systems. Establishment of optimum operating parameters for MFCs have been exhaustively determined for electricity generation and wastewater treatment applications (Du *et al.*, 2007; Pant *et al.*, 2010b; Zhou *et al.*, 2013) however this has not been as extensive for MFCs as BOD sensors (Kim *et al.*, 2006a; Hsieh *et al.*, 2015).

Previous MFC sensor studies have explored methods to optimise operating parameters for improving sensor performance (Section 2.5 of Chapter 2). As current density is the primary sensing output, most researchers opt for a low external resistance (*e.g.*  $R_{Ext} = 10\ \Omega$ ) in order to achieve high values, however a measurable voltage with an acceptable signal:noise ratio must also be considered. Additionally, Gil *et al.* (2003) demonstrated how the response profile changes from a plateau to a peak with lower  $R_{Ext}$ , which is beneficial for peak current calibrations. Comparisons between up-shift and down-shift response times have been established at different  $R_{Ext}$  by several authors (Moon *et al.*, 2004; Di Lorenzo *et al.*, 2009a; Zhang and Angelidaki, 2012).

The aim of this chapter was to determine optimised performance of batch-mode MFCs, specifically for BOD sensing. It was considered how the electrochemical parameters (*i.e.* external resistance) and microbiology of the MFCs related to the observed sensing behaviour and the long-term performance of batch-mode MFCs as BOD sensors was assessed. Using glucose and glutamic acid-based, 'artificial' wastewater medium (the standard used in BOD<sub>5</sub> tests), the outputs from the MFC were calibrated.

## 4.2 Experimental

To determine optimal operating conditions for the batch-mode BOD sensor, MFCs enriched and acclimatised to GGA-based medium were used. The sensors were calibrated independently on multiple occasions using different GGA concentrations and the effect of external resistance was determined. In addition, the electrochemical performance was characterised by polarisation curves, CV, LSV and EIS and the anodic biofilm community composition was determined for polarised MFC anodes and control electrodes maintained at OCP.

Duplicate 50 ml batch-mode SCMFCs (referred to as A and B) were assembled with carbon cloth anodes, Pt/C-coated gas diffusion cathodes and cation exchange membranes (as detailed in the Section 3.1 of Chapter 3). Cells were inoculated with 10% activated sludge and operated using glucose-glutamic acid (GGA) medium containing 50 mmol/dm<sup>3</sup> phosphate buffer, nutrients and vitamins. Figure 4.1 provides a comprehensive visual overview of the operation of cells A and B over 848 days. From day 847 combined effluent taken from cells A and B was used to inoculate two new replicate batch-cells (C and D) which were operated for 183 days (Figure 4.2).

At start-up of MFCs A and B, a 953  $\Omega$  external resistor was connected between the anode and cathode of each cell. At specific times, 43.2, 305, 2400 and 5100  $\Omega$  resistors were substituted as the operational external resistance ( $R_{Ext}$ ) (Figure 4.1a). Cell voltage and anode potentials were recorded using a voltage data-logger and from day 428 cathode potentials were also logged using the same reference electrode present in the anode chamber. For MFCs C and D 43.2  $\Omega$  was used at start-up and 5100  $\Omega$  was also substituted briefly as the external load (Figure 4.2a).

During enrichment it became apparent that changes in ambient temperature were influencing the current generated by the MFCs, consequently a heating platform was designed and installed from day 42 of operating cells A and B. At the same time cells were re-inoculated with activated sludge to recover the anodic biofilms. The initial implementation had the heating platform placed below the enclosure at a set point of 40 °C. On day 46 the MFCs were placed directly on the heating platform surface and the entire setup was housed within a polystyrene enclosure. From day 50 onwards the temperature control set-up was finalised with the set point decreased to 35 °C (ambient temperature of 28–29 °C). The heating platform was used for cells C and D from the 2<sup>nd</sup> day of operation.

BOD calibration was achieved by altering the GGA concentration in the medium before feeding the cells. Batch-mode cycles typically lasted 1–3 days (dependent on substrate concentration). 10 independent calibrations were carried out with cells A and B (Figure 4.1f and Table 4.1) and an additional calibration was performed with cells C and D (Figure 4.2f and Table 4.2).

After 812 days of operation of MFCs A and B, three replicate non-polarised electrodes (termed

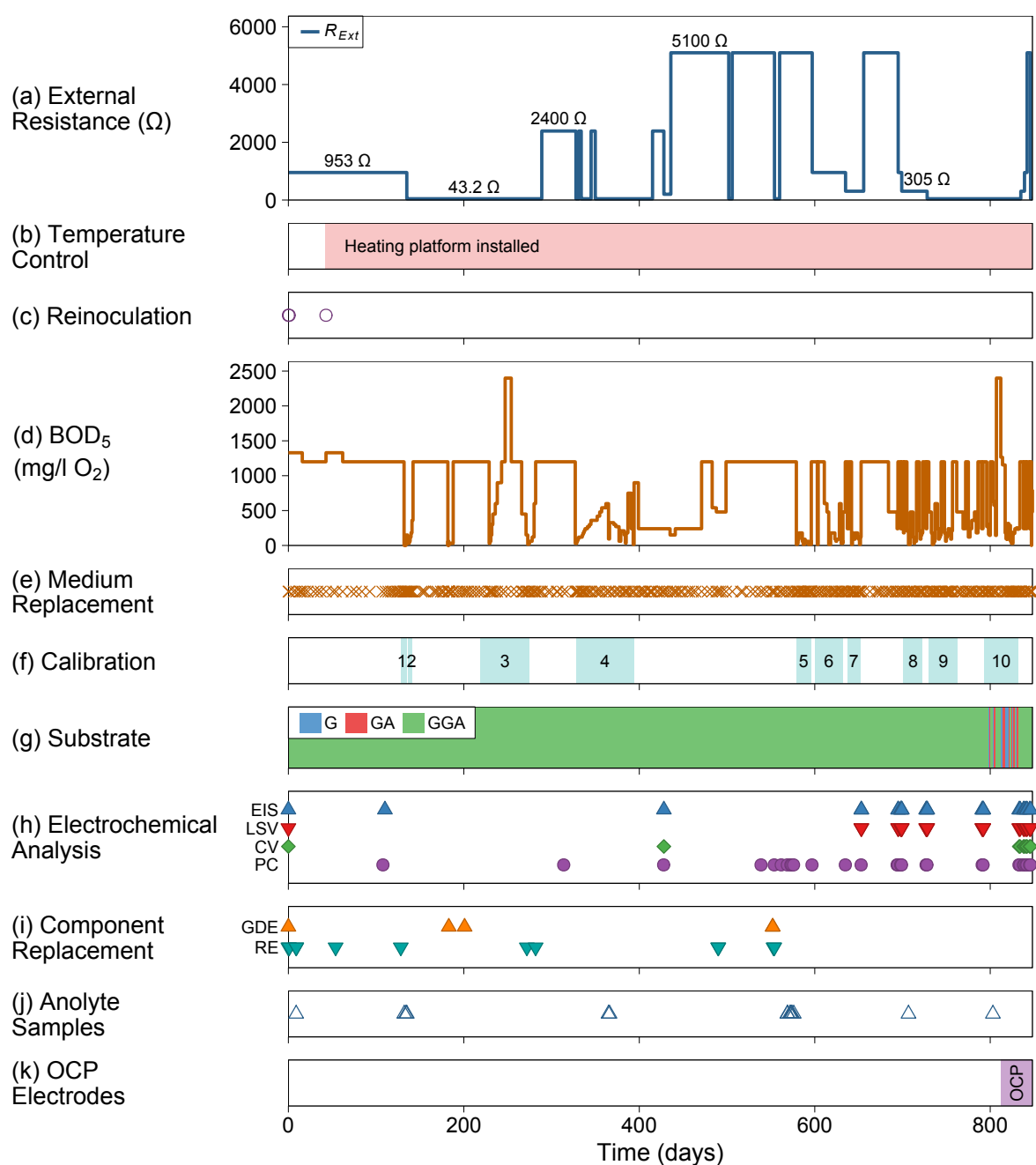


Figure 4.1: Timeline of events summarising the operation of batch-mode MFCs (A and B) and OCP electrodes including (a) external resistance used for MFC operation, (b) temperature control installation, (c) reinoculation events, (d) known BOD<sub>5</sub> medium concentrations, (e) medium replacement events, (f) labelled calibration bands representing range of included batch cycles, (g) medium substrate type, (h) electrochemical analysis, (i) component replacement, (j) analyte sample events and (k) band representing length of OCP electrode operation.

G = Glucose; GA = Glutamic acid; GGA = Glucose-Glutamic acid; EIS = Electrochemical Impedance Spectroscopy; LSV = Linear Sweep Voltammetry; CV = Cyclic Voltammetry; PC = Polarisation Curve; GDE = Gas Diffusion Electrode; RE = Reference Electrode. Non-GGA calibrations discussed in Chapter 7.

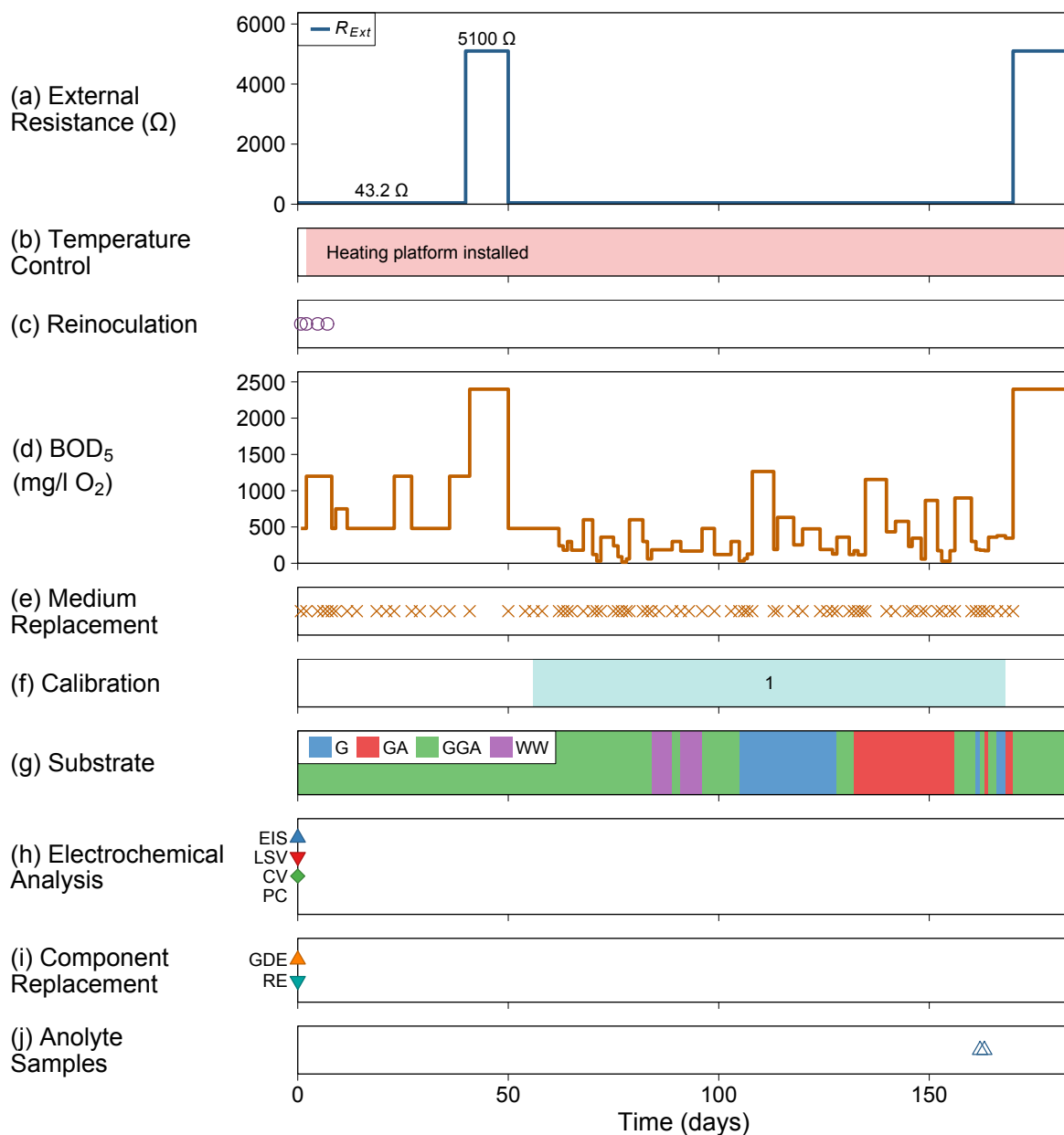


Figure 4.2: Timeline of events summarising the operation of batch-mode MFCs (C and D) including (a) external resistance used for MFC operation, (b) temperature control installation, (c) reinoculation events, (d) known BOD<sub>5</sub> medium concentrations, (e) medium replacement events, (f) labelled calibration bands representing range of included batch cycles, (g) medium substrate type, (h) electrochemical analysis, (i) component replacement and (j) analyte sample events.

G = Glucose; GA = Glutamic acid; GGA = Glucose-Glutamic acid; WW = Wastewater; EIS = Electrochemical Impedance Spectroscopy; LSV = Linear Sweep Voltammetry; CV = Cyclic Voltammetry; PC = Polarisation Curve; GDE = Gas Diffusion Electrode; RE = Reference Electrode. Non-GGA calibrations discussed in Chapter 7.

Table 4.1: Details of calibrations performed using batch-mode cells A and B.

ID	Start time (day) <sup>a</sup>	No cycles <sup>b</sup>	Substrate	BOD <sub>5</sub> range (mg/l O <sub>2</sub> )	$R_{Ext}$ ( $\Omega$ )
1	128	7	GGA	0–2399	953
2	136	6	GGA	30–2399	43.2
3	219	18	GGA	16–2399	43.2
4	328	28	GGA	15–900	43.2
5	579	15	GGA	15–1199	5100
6	600	18	GGA	15–1199	953
7	637	12	GGA	15–1199	305
8	701	15	GGA	15–1199	305
9	730	22	GGA	15–1199	43.2
10a	792	8	GGA	32–1199	43.2
10b	792	8	G <sup>c</sup>	29–1264	43.2
10c	792	10	GA <sup>c</sup>	60–1155	43.2

<sup>a</sup> Start time of first medium cycle included in calibration.<sup>b</sup> Number of cycles included in the calibration.<sup>c</sup> Non-GGA calibrations discussed in Chapter 7.

Table 4.2: Details of calibrations performed using batch-mode cells C and D.

ID	Start time (day) <sup>a</sup>	No cycles <sup>b</sup>	Substrate	BOD <sub>5</sub> range (mg/l O <sub>2</sub> )	$R_{Ext}$ ( $\Omega$ )
1a	56	27	GGA	15–900	43.2
1b	56	13	G <sup>c</sup>	32–1264	43.2
1c	56	15	GA <sup>c</sup>	29–1155	43.2

<sup>a</sup> Start time of first medium cycle included in calibration.<sup>b</sup> Number of cycles included in the calibration.<sup>c</sup> Non-GGA calibrations discussed in Chapter 7.

OCP electrodes A, B and C) were placed into closed vessels and fed medium according to the same regime as polarised, batch-mode cells A and B. These electrodes were removed after 36 days and used to provide data on community composition and cell density for an electrode maintained at open circuit, for comparison with the microbial communities on the polarised MFC anodes.

Periodically, as indicated in Figure 4.1h, the electrochemical performance of the cells A and B was analysed using a potentiostat and two-electrode cell EIS, anode LSV and/or CV measurements were recorded. Polarisation curves were measured by recording the cell voltage at OCP and then attaching sequentially lower resistors from 536 k $\Omega$  down to 10  $\Omega$ . Measurements were taken when a steady-state cell voltage was achieved with each resistor. Except for initial measurements taken before inoculation to confirm set-up replication (*i.e.* that cells C and D were identical to cells A and B), no electrochemical analyses were performed

on cells C and D.

When cathode performance decreased significantly (as measured by its potential) or an air gap developed in the reference electrode salt bridge, gas diffusion electrode (GDE) and reference electrode (RE) components were replaced as necessary. Anolyte samples were taken at the end of batch cycles during medium replacement and COD was analysed to determine the coulombic efficiency of the cells.

At the termination of batch-mode cells A and B and the OCP electrodes (after 848 and 36 days of operation respectively) electrode samples were taken for community analysis and cell counts (see Section 3.7 and 3.8 in Chapter 3 respectively).

## 4.3 Results & Discussion

### 4.3.1 Microbial Fuel Cell Enrichment & Operation

After 77 days of operation, an average stable current density of  $22.5 \pm 10.3 \mu\text{A}/\text{cm}^2$  was achieved with batch-mode MFCs A and B over a  $953 \Omega$  load (Figure 4.3).

During start-up, significant temperature variations were observed in the range  $8.5$  to  $20.7^\circ\text{C}$  with an average temperature of  $14.0^\circ\text{C}$  ( $\pm 2.7^\circ\text{C}$  SD). Diurnal variation in current density from the MFCs was observed and this correlated with diurnal changes in temperature (higher temperatures resulted in higher current densities; Figure 4.3, top panel inset). A heating platform was installed in order to maintain a constant temperature and raise overall temperatures (as only minimal current development was seen with the lowest temperatures  $<10^\circ\text{C}$ ). A drop in temperature of approximately  $2^\circ\text{C}$  occurred each time the enclosure lid was removed (*e.g.* for medium replacement). Using the final implementation of temperature regulation (set point =  $35^\circ\text{C}$ ) the range of vessel temperatures observed was  $26.8$  to  $29.8^\circ\text{C}$  with an average temperature of  $28.0^\circ\text{C}$  ( $\pm 0.7^\circ\text{C}$  SD) from day 50.

The start-up current development of batch-mode cells C and D is shown in Figure 4.4. For the first 7 days effluent from cells A and B was included in the medium fed to cells C and D as inoculum. The medium concentration was initially increased to  $1199 \text{ mg/l O}_2 \text{ BOD}_5$ , however it was returned to  $480 \text{ mg/l O}_2$  as inhibition appeared to be occurring due to substrate excess (apparent from the high variability of current density and anode potential between day 2–8; Figure 4.4). A stable peak current density of  $233.9 \pm 11.7 \mu\text{A}/\text{cm}^2$  was achieved over a  $43.2 \Omega$  load after 18 days of operation (Figure 4.4). The range of temperatures observed during operation of cells C and D was  $26.3$  to  $30.5^\circ\text{C}$  with an average temperature of  $29.1^\circ\text{C}$  ( $\pm 0.8^\circ\text{C}$ ) from day 2.

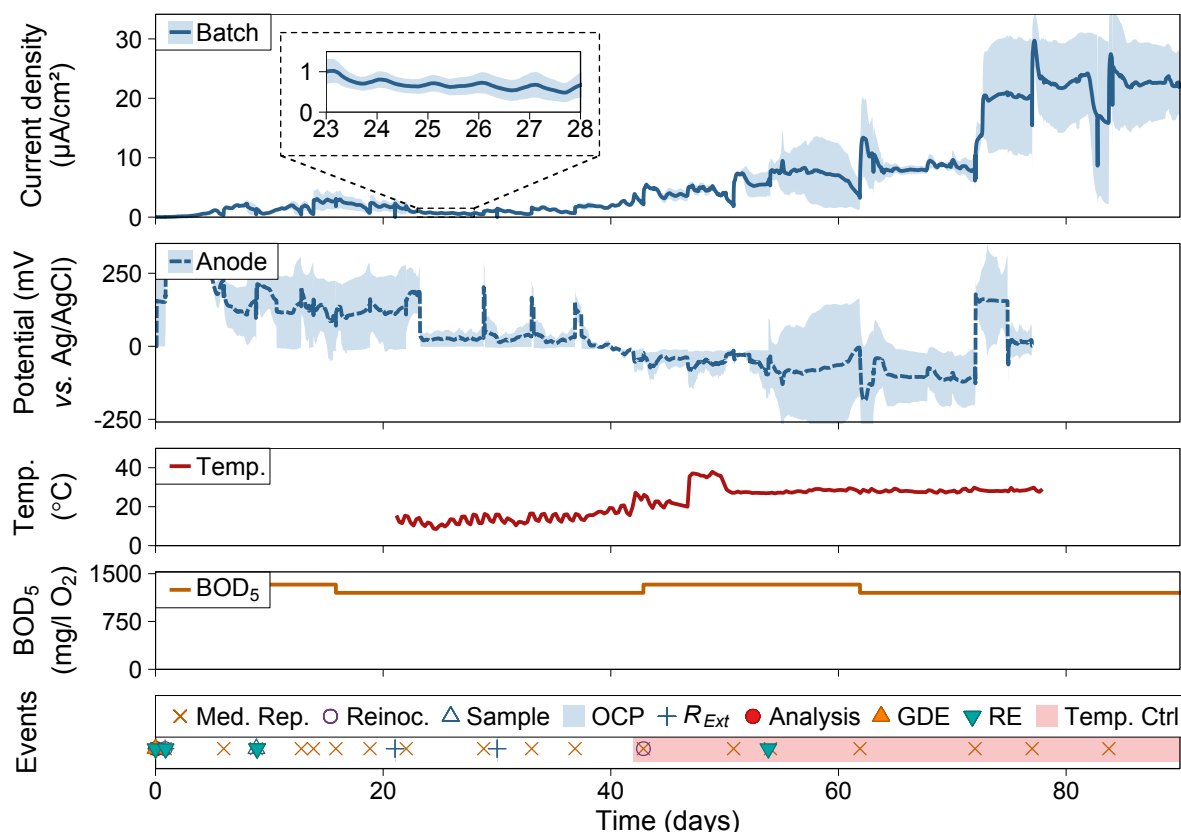


Figure 4.3: Start-up of batch-mode cells A & B with average measured current density and anode potential (shaded region is range), temperatures, BOD<sub>5</sub> (estimated from GGA concentration) and events (including medium replacements, reinoculations, samples, periods at OCP,  $R_{Ext}$  changes, electrochemical analyses, GDE/RE replacements and temperature control installation). Inset shows fluctuations in current density related to ambient temperature changes.

Med. Rep. = Medium replacements; Reinoc. = Reinoculations; OCP = Open Circuit Potential; GDE = Gas Diffusion Electrode; RE = Reference Electrode; Temp. Ctrl. = Temperature Control.

#### 4.3.2 Biochemical Oxygen Demand Sensing & Calibration

Batch-mode cells A and B were calibrated using different concentrations of GGA medium ten times over the course of operation and an additional calibration was performed using cells C and D to determine reproducibility (Table 4.1 & 4.2). Amperometric detection is the most common calibration method employed in the literature (see Table 2.2 in Chapter 2). It relies on the MFC-generated electrical current correlating with the substrate concentration (BOD<sub>5</sub>). As a typical example of calibrations performed in this study, Calibration 4 (Figure 4.1f and Table 4.1) will be discussed in detail here (other calibrations can be found in Appendix C).

Between days 328 and 399 (71 days) the medium for cells A and B was replaced 30 times with GGA concentrations ranging from 25 to 1500 mg/l (equivalent to 15 to 900 mg/l O<sub>2</sub> BOD<sub>5</sub>; Figure 4.5). Two medium changes were discarded from the calibration due to the external resistance being changed mid-cycle (as indicated by gaps in the calibration band in Figure 4.5,

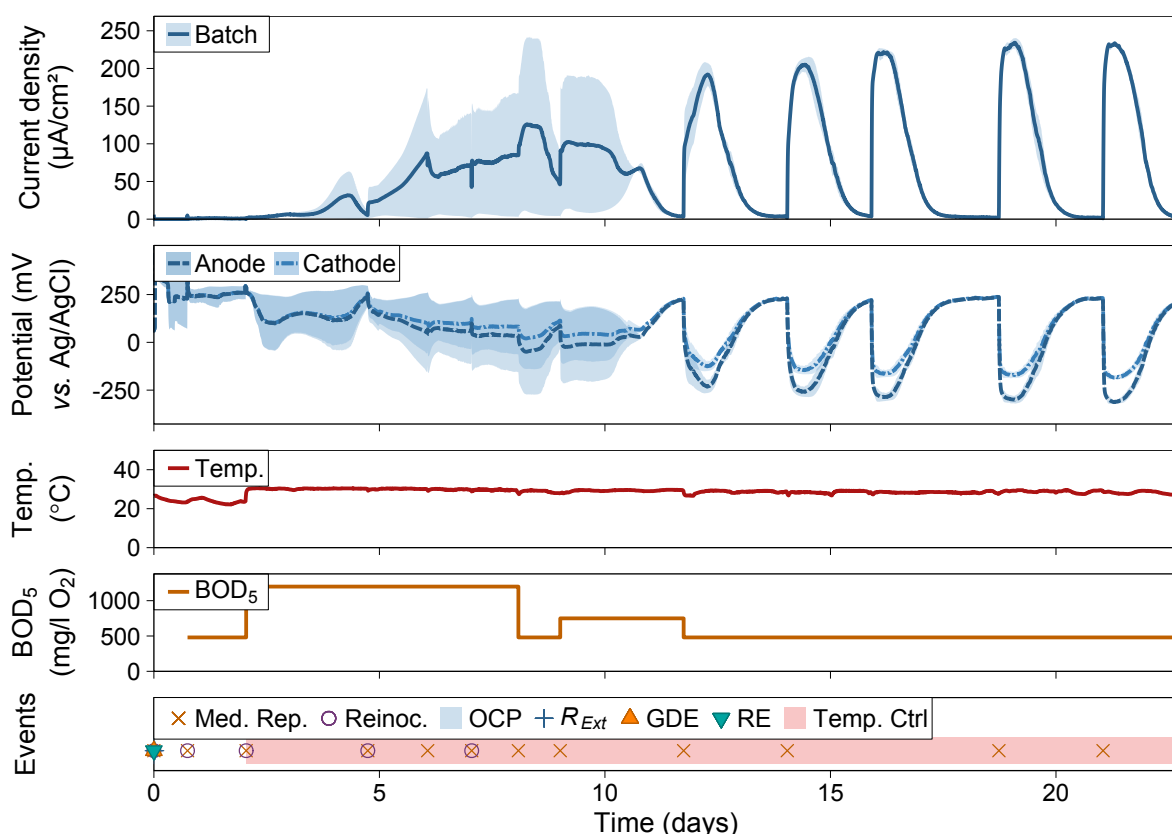


Figure 4.4: Start-up of batch-mode cells C & D with average measured current density, anode and cathode potentials (shaded region is range), temperatures, BOD<sub>5</sub> (estimated from GGA concentration) and events (including medium replacements, reinoculations, periods at OCP,  $R_{Ext}$  changes, GDE/RE replacements and temperature control installation).

Med. Rep. = Medium replacements; Reinoc. = Reinoculations; OCP = Open Circuit Potential; GDE = Gas Diffusion Electrode; RE = Reference Electrode; Temp. Ctrl. = Temperature Control.

bottom panel). With each batch cycle, over an external resistance of  $43.2\ \Omega$ , an initial current increase up to a peak was observed after fresh medium was added, followed by a fall in current as the substrate became depleted. The general trend was for the peak current density to increase with increases in BOD<sub>5</sub> up to a limiting value of approximately  $130 \pm 12\ \mu\text{A}/\text{cm}^2$  and  $116 \pm 10\ \mu\text{A}/\text{cm}^2$  for cells A and B respectively. This corresponded to a decrease in anode potential down to a limiting potential of  $-255 \pm 27\ \text{mV}$  and  $-393 \pm 11\ \text{mV}$  vs. Ag/AgCl for cells A and B respectively. It should be noted that measured potentials were subject to systematic shifts due to the reference electrode potential drifting from the  $+0.209\ \text{V}$  vs. SHE reference point. Over the course of continuous operation, RE potential shifts on the order of tens of mV were observed if the electrode was allowed to dry out for extended periods due to air gaps which developed in the salt bridge. Periodically (every 3–6 months), reference electrodes were checked externally in a 3M NaCl solution against a clean, stable Ag/AgCl reference electrode ( $< \pm 10\ \text{mV}$  indicated stability; Section 3.1.2 in Chapter 3).

Amperometric calibration curves were created by plotting peak current densities from each batch cycle against the prepared medium BOD<sub>5</sub> value (Figure 4.6). The linear model ( $y = mx + c$ ) was fitted to points which correlated with changes in BOD<sub>5</sub> until a plateau was ob-



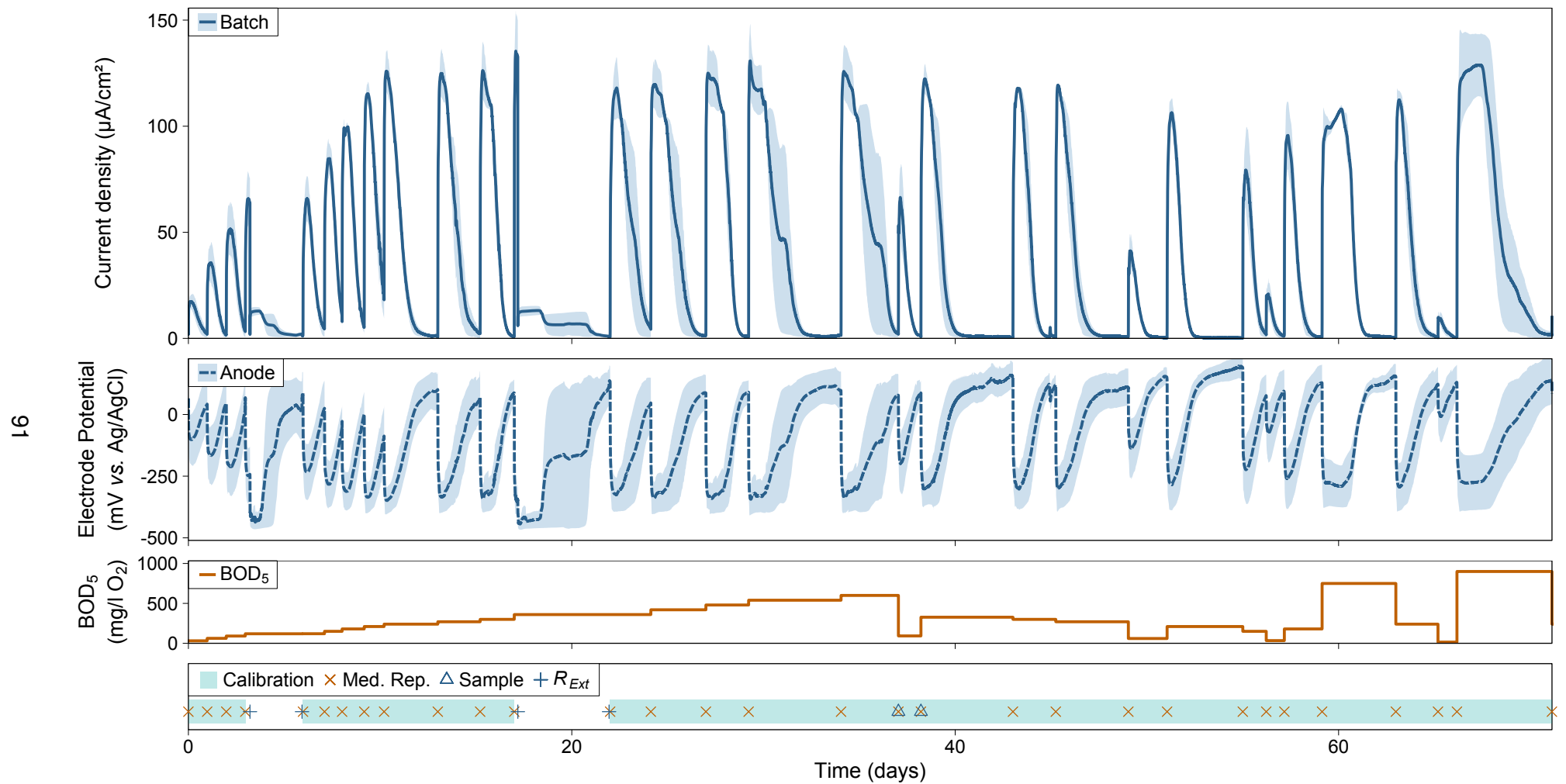


Figure 4.5: The average response of batch-mode MFCs A and B current density and anode potential to changes in BOD<sub>5</sub> (estimated from GGA concentration) with each medium replacement during Calibration 4 (shaded region is range).

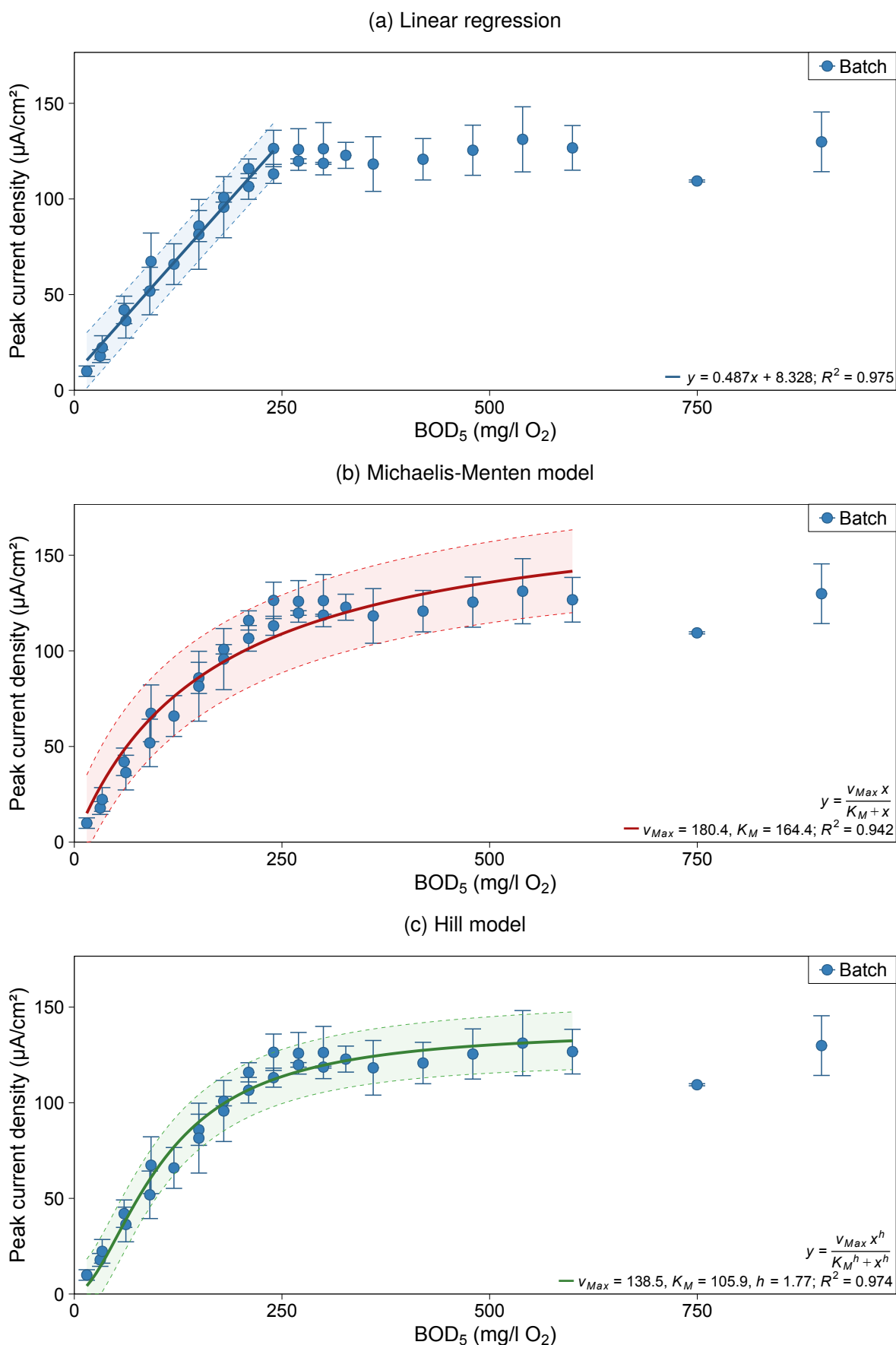


Figure 4.6: Average peak current density calibration curves fitted with (a) linear, (b) Michaelis-Menten and (c) Hill models against BOD<sub>5</sub> (estimated from GGA concentration) for data obtained during Calibration 4 of batch-mode MFCs A & B. Shaded bands represent the 95% prediction interval from model lines and error bars are the range from duplicate cells.

served (Figure 4.6a). For Calibration 4, a fitted line through the average current densities in the range 15 to 240 mg/l O<sub>2</sub> BOD<sub>5</sub> ( $n = 16$ ) had a slope of  $m = 0.487 \pm 0.021 \mu\text{A}/\text{cm}^2$  per mg/l O<sub>2</sub> BOD<sub>5</sub> and intercept of  $c = 8.33 \pm 3.09 \mu\text{A}/\text{cm}^2$ . The  $R^2$  was 0.975 indicating a high degree of correlation, the residual standard deviation was  $6.15 \mu\text{A}/\text{cm}^2$  (5% of  $\hat{I}_{Max}$ ) and the regression  $p$ -value was  $1.22 \times 10^{-12}$  indicating a statistically significant correlation. The limits of detection and quantification were determined as LOD = 41.6 mg/l O<sub>2</sub> and LOQ = 126.1 mg/l O<sub>2</sub>. The response time to reach peak current did not correlate with substrate concentration and on average 95% of the peak current density was reached after  $2.05 \pm 1.01$  hours.

Michaelis-Menten (M-M) and Hill models were also applied to the amperometric data by fitting the data within the range 15 to 600 mg/l O<sub>2</sub> BOD<sub>5</sub> ( $n = 26$ ; up to the point where substrate inhibition occurred in cell A). Both models successfully simulated the saturation plateau observed; thus increased the sensor range to include the non-linear asymptotes. The M-M model line was fitted with the parameters  $v_{Max} = 180.4 \pm 51.5 \mu\text{A}/\text{cm}^2$  and  $K_M = 164.4 \pm 117.0 \text{ mg/l O}_2$  (Figure 4.6b). Regression statistics were determined as  $R^2 = 0.942$  and  $SD_{Res} = 9.63 \mu\text{A}/\text{cm}^2$ . For non-linear models a lack-of-fit test was performed (with a null hypothesis that the non-linear model fits no better than the intercept model), where a  $p$ -value greater than 0.05 indicated that there is no evidence the model does not fit the data. For the M-M model the  $p$ -value was 0.071 which is close to 0.05 indicating a poor fit; from the line plotted on Figure 4.6b it was evident that the  $V_{Max}$  parameter was an over-estimate of the true value. The fitted Hill model parameters were  $v_{Max} = 138.5 \pm 25.6 \mu\text{A}/\text{cm}^2$ ,  $K_M = 105.9 \pm 33.4 \text{ mg/l O}_2$  and a positive Hill coefficient of  $h = 1.77 \pm 0.89$  indicating positive co-operativity with increased BOD<sub>5</sub>. The Hill equation modelled the response with a higher degree of confidence and based on the prediction band shown in Figure 4.6c was able to resolve values more accurately than the M-M model. This was reflected in the regression statistics of  $R^2 = 0.974$ ,  $SD_{Res} = 6.63 \mu\text{A}/\text{cm}^2$  and high lack-of-fit  $p$ -value = 0.352.

A medium concentration of 300 mg/l GGA was known to have a BOD<sub>5</sub> of  $179.9 \pm 9.4 \text{ mg/l O}_2$  ( $\pm$  SD) measured by the five day test and in Calibration 4 from two medium cycles a peak current density of  $98.3 \pm 13.5 \mu\text{A}/\text{cm}^2$  ( $\pm$  14% SD) was recorded from cells A and B. Using the calibrated linear, M-M and Hill models the estimated BOD<sub>5</sub> values were  $184.5 \pm 28.7 \text{ mg/l O}_2$ ,  $196.5 \pm 56.6 \text{ mg/l O}_2$  and  $175.2 \pm 34.4 \text{ mg/l O}_2$  respectively ( $\pm$  95% prediction interval). Both the linear and Hill models were capable of simulating BOD<sub>5</sub> values for a given current density, with approximately the same precision, within the error of the true value measured by the BOD<sub>5</sub> test. In the BOD<sub>5</sub> test a standard deviation of  $\pm$  15% (30 mg/l O<sub>2</sub>) is generally accepted; in this case the linear model achieves better accuracy and the Hill model was close to the required level. As the Michaelis-Menten model failed to correlate with a high enough degree of accuracy (and the Hill model indicated there was a co-operativity effect) the model was no longer used in this study for batch-mode calibrations. The Hill equation provides a convenient method for comparing complete calibrations with just three parameters ( $v_{Max}$ ,  $K_M$  and  $h$ ).

Coulometric calibration is an alternative method for evaluating MFC-based BOD biosensors (see Table 2.2 in Chapter 2). For Calibration 3 (in which a greater BOD<sub>5</sub> range was calibrated) and Calibration 4 it was observed that as BOD<sub>5</sub> increased (Figure 4.7, red to green coloured lines), in addition to the peak current density increasing, so did the length of cycle before substrate depletion occurred (indicated by a decrease in current density).

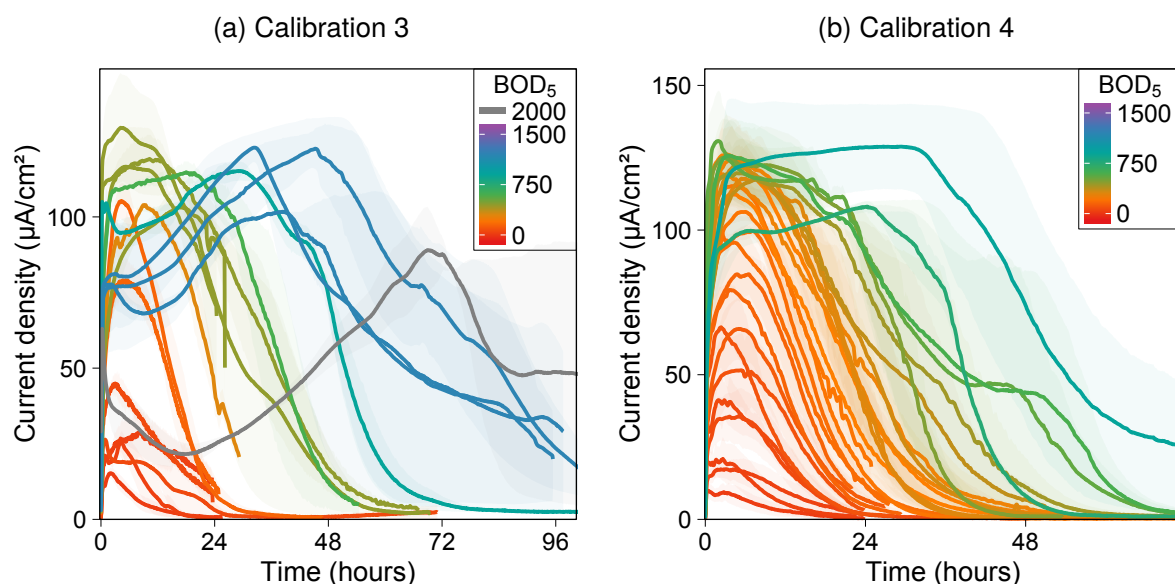


Figure 4.7: Plots of average current density during each medium cycle in (a) Calibration 3 and (b) Calibration 4 for batch-mode MFCs A and B. Each average response line is coloured by the estimated medium BOD<sub>5</sub> (from GGA concentration) (in mg/l O<sub>2</sub>) and shaded by the range between cell A and B. Substrate-inhibited response was observed with BOD<sub>5</sub> concentrations > 750 mg/l O<sub>2</sub> (dark green - blue - grey).

Additionally, the rate at which substrate rapidly depletes appears to decrease as the BOD<sub>5</sub> was increased. The prolonged depletion could be due to the bacteria storing excess substrate in biopolymer compounds such as poly-β-hydroxybutyrate (PHB), which was then consumed when substrate in the bulk medium was depleted (as previously suggested by Kim *et al.* (2011c); Pant *et al.* (2010b)). There is evidence of the response behaviour changing at the two highest concentrations in Calibration 4 (Figure 4.7b, dark green/blue coloured lines; which were omitted from the non-linear models due to apparent substrate inhibition) and more clearly shown by the five highest concentration medium cycles in Calibration 3 (Figure 4.7a, dark green/blue/grey coloured lines). A single, immediate peak was observed at low BOD<sub>5</sub> concentrations (Figure 4.7, red to green lines). At high BOD<sub>5</sub> concentrations the response shifts to a bimodal response with a sharp peak followed by a steady increase to a higher peak then a slow decline due to substrate depletion (Figure 4.7). The response observed indicated that at very high substrate concentrations (> 750 mg/l O<sub>2</sub> BOD<sub>5</sub>) the anode biofilm current generation was inhibited. The peak current density was not reached until much later in the cycle (after 24-72 hours), perhaps when the substrate had depleted to non-inhibiting levels.

By calculating the amount of charge passed over a specified time period, such as the com-

plete cycle time, coulometric calibration curves were plotted (Figure 4.8 and in Appendix C). A linear correlation was observed with increases in BOD<sub>5</sub> resulting in increases in charge

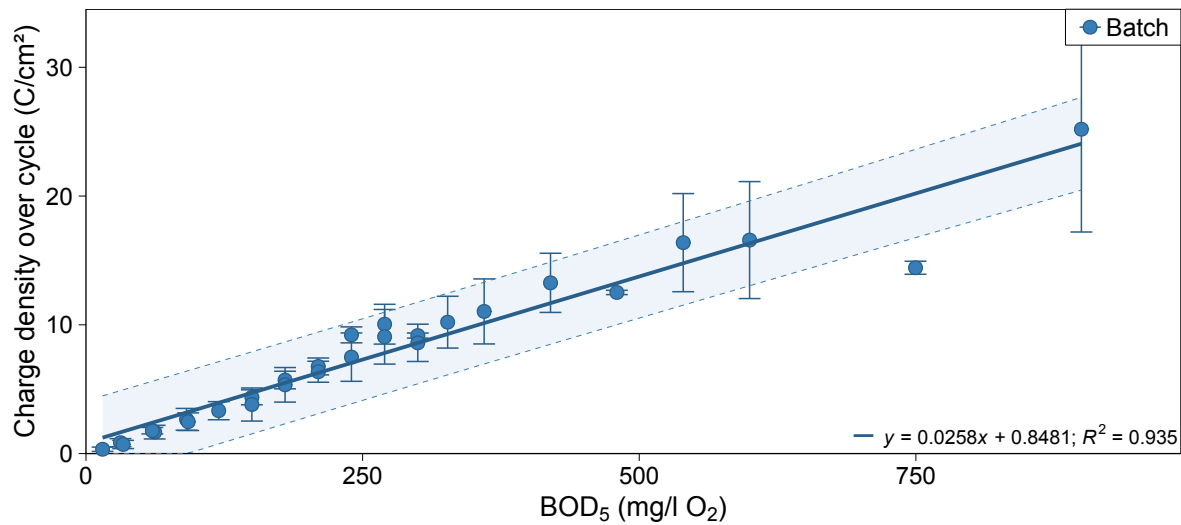


Figure 4.8: Average total charge density calibration curve for the complete medium cycle fitted with a linear model against BOD<sub>5</sub> (estimated from GGA concentration) for data obtained during Calibration 4 of batch-mode MFCs A and B. Shaded bands represent the 95% prediction interval from model lines and error bars are the range of values from duplicate cells.

density, greatly exceeding the detection range established using amperometric detection. For the BOD<sub>5</sub> range 15 to 900 mg/l O<sub>2</sub>, linear regression analysis fitted a slope of  $m = 0.026 \pm 0.001$  C/cm<sup>2</sup> per mg/l O<sub>2</sub> and intercept of  $c = 0.848 \pm 0.460$  C/cm<sup>2</sup>. The regression statistics  $R^2 = 0.935$ ,  $SD_{Res} = 1.51$  C/cm<sup>2</sup> and a  $p$ -value of  $2.2 \times 10^{-16}$  indicated a significant correlation. The fit was improved significantly without the result at 750 mg/l O<sub>2</sub> ( $R^2 > 0.99$ ), however it is undetermined why this result was anomalous (shown at  $t = 59$  days in Figure 4.5).

The practical drawback with this type of coulometric detection is that the entire cycle must be completed before the BOD can be estimated. Depending on the BOD<sub>5</sub> concentration the cycle time increased from approximately 18 hours to over 110 hours (4.6 days) with BOD<sub>5</sub> of 15 and 900 mg/l O<sub>2</sub> respectively; in comparison with the standard five-day BOD test this shows little improvement in response time. By contrast, the amperometric method yielded a value after two hours. The MFC does have the benefit of not requiring sample dilution (which is required by the standard BOD<sub>5</sub> test), but alternative competing technologies for BOD prediction can give a response in the order of minutes to hours rather than days.

Using high-resolution data-logging with an interval rate of 1 Hz, the initial response following medium replacement was recorded. With this level of resolution it was possible to estimate the lag time between fresh medium being added to the cell and a current response being observed. As can be seen in Figure 4.9 the response was almost instantaneous and within 15 seconds, faster than the time taken to syringe fresh medium into the cell, the current density was observed to increase rapidly in each cell as soon as the medium was replaced.

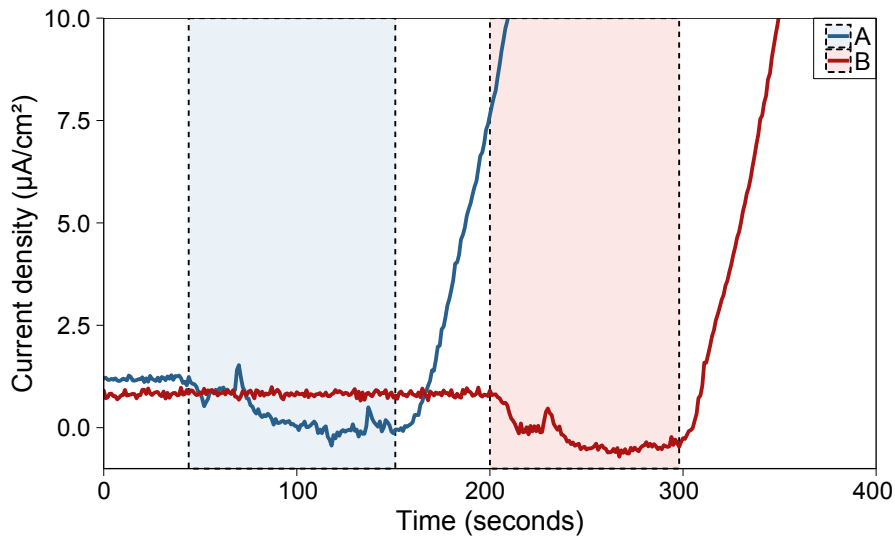


Figure 4.9: Lag time in current density response of batch-mode cells during a medium replacement of cell A (50–150 secs) followed by cell B (200–300 secs) recorded using high-resolution data-logging. The time period during which medium was being removed and replaced (cell was empty) is represented by the shaded area for each cell.

The initial current response following medium replacement was observed to increase in rate with increasing BOD<sub>5</sub> until substrate-inhibiting concentrations (> 750 mg/l O<sub>2</sub>) where the current generation rate was reduced (Figure 4.10a). Given that the response to medium

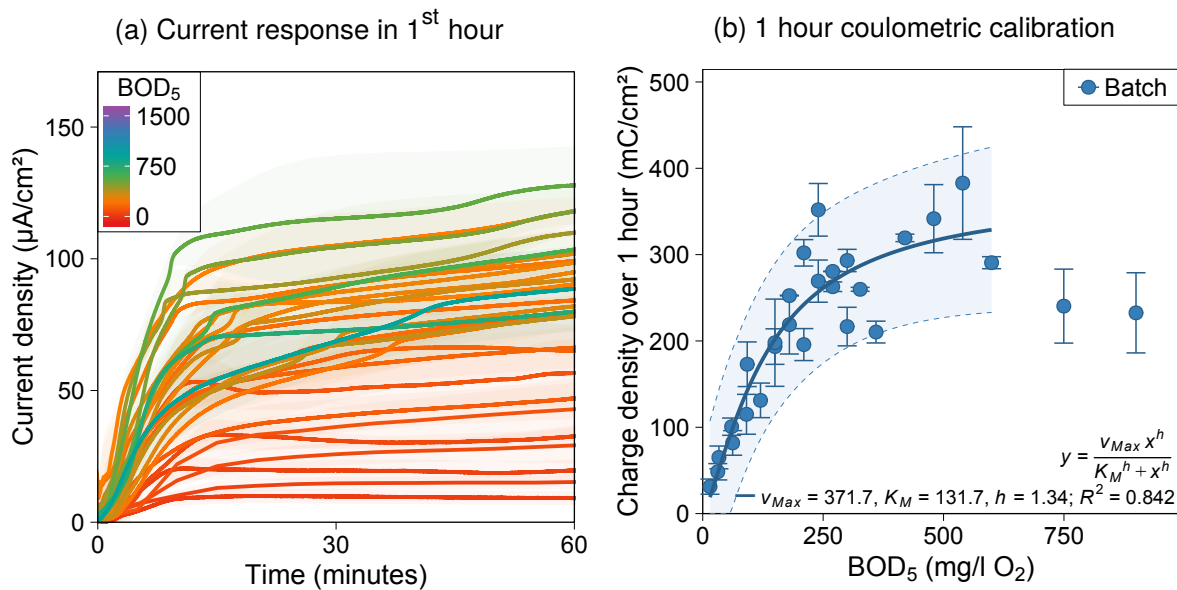


Figure 4.10: Charts showing (a) average current density response in the 1<sup>st</sup> hour since medium replacement during Calibration 4 (coloured by estimated BOD<sub>5</sub> (in mg/l O<sub>2</sub>) and shaded by range) and (b) the resulting coulometric calibration with the average response modelled by the Hill equation for batch-mode MFCs A and B (shaded bands are 95% prediction interval and error bars are the range).

replacement was very rapid and that full cycle coulometric calibration could take many hours, short time-frame calibration was tested as an alternative approach to calibrating the MFC sensor. Coulometric calibration curves were created using only the charge passed over

the first hour following medium replacement (instead of the entire cycle) against BOD<sub>5</sub> (Figure 4.10b). The correlation observed was not of the same linear form seen for total cycle charge but instead mirrored the peak current density calibration, albeit with a much lower prediction confidence ( $R^2 = 0.842$ ,  $SD_{Res} = 40.65 \text{ mC/cm}^2$ , lack-of-fit  $p$ -value = 0.74).

The 1 hour coulometric calibration was therefore less accurate but able to resolve an estimated BOD<sub>5</sub> value within 60 minutes in comparison to more than 2 hours (amperometric method) or longer (total charge calibration). Using a 300 mg/l solution ( $179.9 \pm 9.4 \text{ mg/l O}_2$  BOD<sub>5</sub>) an average of  $235.7 \pm 33.9 \text{ mC/cm}^2$  of charge was passed in the 1st hour following medium replacement which was estimated to have a BOD<sub>5</sub> of  $184.7 \pm 40.2 \text{ mg/l O}_2$  and  $198.2 \pm 165.2 \text{ mg/l O}_2$  by the linear and Hill models respectively. This demonstrates how the 1 hour calibration could be used to predict BOD<sub>5</sub> values accurate to 100-200 mg/l O<sub>2</sub> which could be used in an early-warning monitoring system where trends rather than exact values are sufficient, before the true values can be estimated more precisely (e.g. by the time peak current or total cycle has completed).

#### 4.3.3 Long-term Calibration Drift & Sensor Reproducibility

Data from Calibrations 2, 3, 4, 9 and 10a from cells A and B and Calibration 1a from cells C and D were collated to determine the effect of long-term calibration drift and reproducibility across identical cells under the same conditions (*i.e.* external resistance of  $43.2 \Omega$ ). Long-term, the cathode potentials were observed to decrease over time (this will be discussed in detail in Section 4.3.5), therefore it was necessary to normalise the current densities in order for valid comparisons between calibrations performed at different time periods to be made (Table 4.3). Normalisation was performed by dividing the observed current density by the maximum limiting current density recorded in each calibration (so maximum response should be 100%).

It was observed that the modelled parameters for each calibration (once normalised) were all approximately the same value within one standard deviation. With repeated calibrations of cells A & B and in both paired replicate cells A & B and C & D the same linear calibration range of 15 to 240 mg/l O<sub>2</sub> BOD<sub>5</sub> was obtained. Figure 4.11 shows the complete dataset of calibrations performed with cells A, B, C and D and  $R_{Ext} = 43.2 \Omega$ . It was evident that most points fall within the 95% prediction band of the Hill-modelled line of the combined dataset. There was no appearance of bias through time, with the variation between repeated concentrations arising as much within calibrations as between them. Additionally, the calibration performed using separate, replicate cells C and D fell on the line showing that they had a response to GGA medium that was no different from cells A and B. The Hill equation was fitted with the parameters;  $v_{Max} = 106 \pm 22 \%$ ,  $K_M = 99.7 \pm 44.0 \text{ mg/l O}_2$  and  $h = 1.92 \pm 1.55$  and regression statistics of  $R^2 = 0.918$ ,  $SD_{Res} = 9\%$  and lack-of-fit  $p$ -value = 0.400 indicating a good fit.

Table 4.3: Model parameters determined from calibrations over time performed using batch-mode cells A, B, C and D with  $R_{Ext} = 43.2 \Omega$ . Parameter values are given with precision  $\pm$  SD.

ID	Time (days)	Linear BOD <sub>5</sub> range <sup>a</sup> (mg/l O <sub>2</sub> )	Linear model $y = mx + c$			Hill model $v = \frac{v_{Max} [S]^h}{K_M^h + [S]^h}$		
			No cycles <sup>b</sup>	$m$ (%/(mg/l O <sub>2</sub> ))	$c$ (mg/l O <sub>2</sub> )	$v_{Max}$ (%)	$K_M$ (mg/l O <sub>2</sub> )	$h$
2 (AB)	136	30–180	5	$0.434 \pm 0.026$	$1.43 \pm 2.67$	$133 \pm 73$	$151.0 \pm 146.0$	$1.37 \pm 0.84$
3 (AB)	219	16–150	7	$0.485 \pm 0.068$	$5.94 \pm 5.95$	$105 \pm 19$	$82.9 \pm 46.0$	$1.60 \pm 1.29$
4 (AB)	328	15–240	16	$0.397 \pm 0.017$	$7.28 \pm 2.55$	$112 \pm 20$	$103.6 \pm 31.9$	$1.77 \pm 0.88$
9 (AB)	730	15–240	16	$0.345 \pm 0.036$	$9.69 \pm 5.41$	$106 \pm 28$	$107.9 \pm 50.6$	$1.67 \pm 1.40$
10a (AB)	792	60–300	7	$0.400 \pm 0.028$	$0.31 \pm 5.11$	$104 \pm 14$	$115.5 \pm 39.6$	$2.61 \pm 1.57$
1a (CD)	56	15–240	13	$0.442 \pm 0.044$	$3.34 \pm 6.38$	$109 \pm 38$	$103.3 \pm 58.0$	$2.08 \pm 2.83$
Combined	-	15–240	64	$0.391 \pm 0.016$	$7.05 \pm 2.24$	$106 \pm 22$	$99.7 \pm 44.0$	$1.92 \pm 1.55$

<sup>a</sup> Estimated BOD<sub>5</sub> (from GGA concentration).

<sup>b</sup> Number of medium replacement cycles (from which peak current densities were determined) included in the linear model.



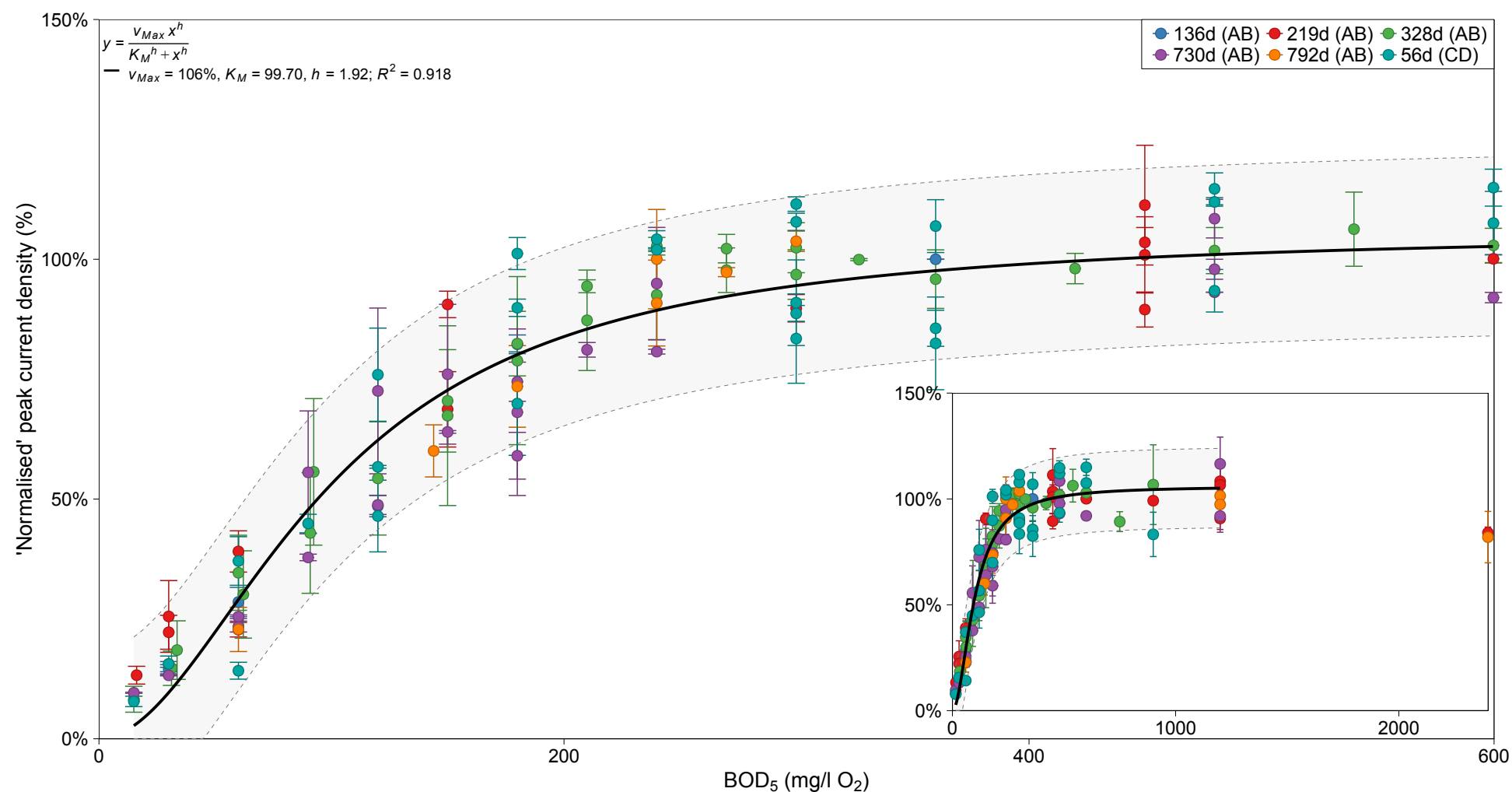


Figure 4.11: Average peak current density calibration data (normalised by maximum current density) against  $BOD_5$  (estimated from GGA concentration) obtained during calibrations at different time points during operation of batch-mode MFCs A, B, C and D with  $R_{Ext} = 43.2 \Omega$  fitted with the Hill equation. The shaded band represents the 95% prediction interval from the Hill model line and error bars are the range of values from duplicate cells.

The results demonstrated that the calibration range was not significantly affected by changing conditions in the MFC such as cathode degradation (or MEA replacement) or anodic biofilm age and therefore, effectively, the MFC required no re-calibration as long as the maximum current density could be determined regularly and used for subsequent normalisation of recorded values. The correlation also showed that identical cells of the same cell architecture could be constructed which, once fully enriched, would display the same sensing characteristics and calibration range. This is an important finding as it indicates there is a highly reduced maintenance requirement, which has significant implications for the future commercial viability of MFC-based BOD sensors. Kim *et al.* (2003a) also reported that an MFC-based biosensor was operated for over 5 years with minimal maintenance indicating the longevity and robustness of the technology. It remains to be determined which environmental (e.g. pH, conductivity, wastewater composition and temperature) and operational conditions, known to affect the *performance* of a MFC, will affect the actual calibration *range* of a MFC. The normalised calibration will correct for factors which only affect performance (*i.e.* maximum current density) and not calibration range.

#### 4.3.4 Effect of External Resistance on Calibration

Over the course of operation of cells A and B the external resistor ( $R_{Ext}$ ) used for operation was changed periodically (Figure 4.1a). With increasing  $R_{Ext}$  a reduction in current density was observed (Figure 4.12a; as explained by the MFC polarisation curves in Section 4.3.5). Additionally, the shape of the batch cycle response changed from a peak to a plateau. This

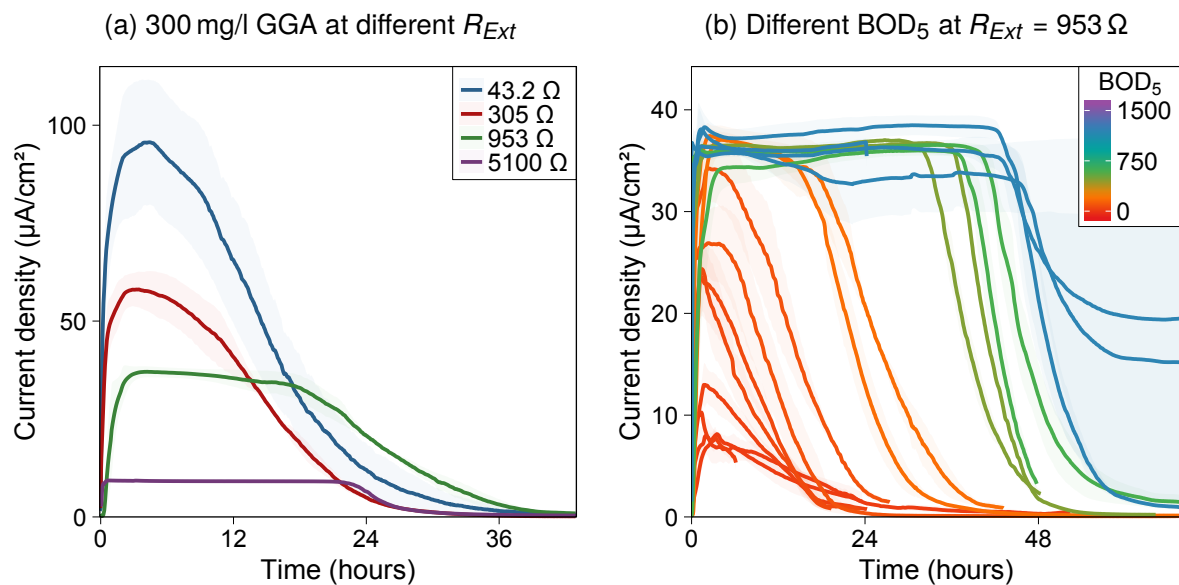


Figure 4.12: Plots of (a) typical average current density during a 300 mg/l GGA medium cycle for  $R_{Ext} = 43.2, 305, 953$  and  $5100 \Omega$  and (b) average current density in Calibration 6 (coloured by estimated  $BOD_5$  (in mg/l  $O_2$ ) at  $953 \Omega$  showing no substrate inhibition for batch-mode MFCs A and B. Inset shows full calibration range. Shaded bands are the range between cell A and B.

behaviour has been described previously by Gil *et al.* (2003) and attributed to the external resistance becoming the rate-limiting factor. Figure 4.12b shows that, for an operational  $R_{Ext}$  of 953  $\Omega$ , little or no substrate inhibition was observed at high BOD<sub>5</sub> concentrations indicating a greater resilience of the anodic biofilm. The response at 953  $\Omega$  reaches a saturation plateau at very low concentration and subsequent increases in BOD<sub>5</sub> result in an extension of the cycle length and thus increase in charge passed. Previous studies have discussed the effect of external resistance on the MFC sensor response time (Moon *et al.*, 2004; Di Lorenzo *et al.*, 2009b). In the present study the response time was found to decrease from  $2.3 \pm 1.6$  hours to  $1.4 \pm 1.4$  hours with increasing  $R_{Ext}$  of 43.2 to 5100  $\Omega$  (Table 4.4), in agreement with the findings of Moon *et al.* (2004).

Table 4.4: Average response time to reach 95% peak current density at different  $R_{Ext}$  using calibration data (for medium cycles < 750 mg/l O<sub>2</sub> BOD<sub>5</sub> for response times and cycles which had run to completion for %CE) from batch-mode cells A, B, C & D.

$R_{Ext}$	No cycles <sup>a</sup> (< 750 mg/l O <sub>2</sub> )	95% response time ( $\pm$ SD)	Coulombic efficiency ( $\pm$ SD)
43.2 $\Omega$	86	$2.3 \pm 1.6$ hours	$37 \pm 17$ %
305 $\Omega$	22	$1.9 \pm 1.4$ hours	$25 \pm 15$ %
953 $\Omega$	15	$1.5 \pm 0.8$ hours	$21 \pm 14$ %
5100 $\Omega$	14	$1.4 \pm 1.4$ hours	$9 \pm 6$ %

<sup>a</sup> Number of cycles included in the response time calculation.

Anolyte samples taken from batch-mode cells at the end of a feed cycle, prior to medium replacement were analysed for COD so that the coulombic efficiency at various points over the operation could be determined. In all samples the measured COD was below the lower detection limit of the photometric assay kit (30 mg/l O<sub>2</sub> COD at 1:3 dilution). Based on this, coulombic efficiency calculations assumed that, for cycles which were allowed to run to completion (*i.e.* reach approximately 0  $\mu\text{A}/\text{cm}^2$ ), the entirety of the substrate was consumed and therefore the  $\Delta\text{COD}$  value was equal to the fresh medium initial COD value. As can be seen in Table 4.4, the coulombic efficiency decreased as the  $R_{Ext}$  increased. This could be attributed to the biofilm oxidation rate becoming limited by the  $R_{Ext}$ , which results in less substrate being consumed and therefore more substrate available for non-electrogenic, competitive processes (such as fermentation).

The effect of different operating resistances of 305, 953 and 5100  $\Omega$  was investigated in comparison to the calibrations performed at 43.2  $\Omega$  (Figure 4.11). Data from Calibrations 7 and 8 conducted at 305  $\Omega$ , and Calibrations 1 and 6 at 953  $\Omega$  were collated, (Calibration 5 was the sole calibration performed at 5100  $\Omega$ . Figure 4.13).

Using an  $R_{Ext}$  of 305  $\Omega$  a similar sigmoidal-shaped calibration to the one obtained at 43.2  $\Omega$  was recorded (Figure 4.14a). The main difference between the two calibrations was the  $K_M$  value of  $80.1 \pm 56.4$  mg/l O<sub>2</sub> BOD<sub>5</sub> compared to  $99.7 \pm 44.0$  mg/l for 43.2  $\Omega$ . This cor-

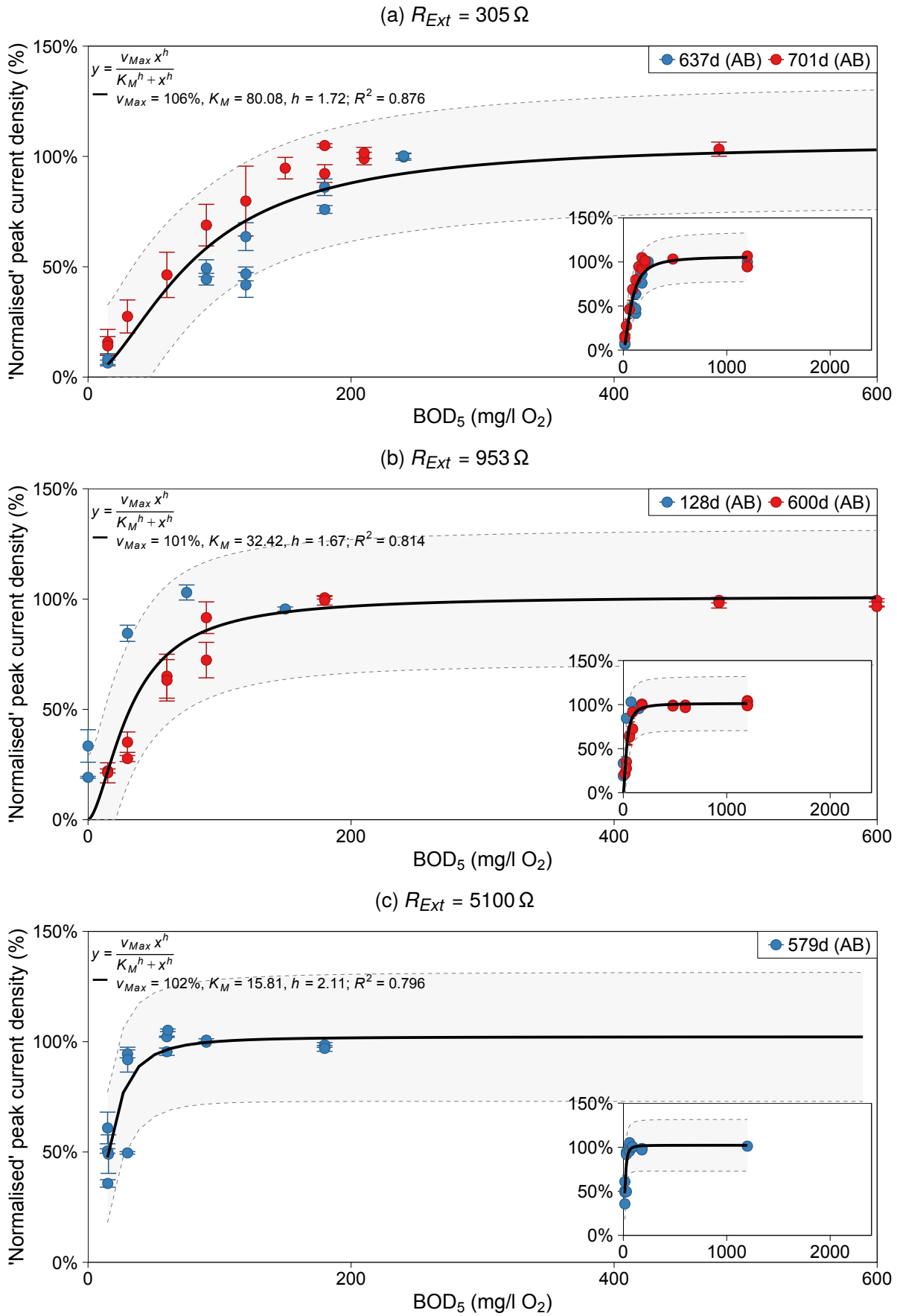


Figure 4.13: Average peak current density calibration curves against  $BOD_5$  (estimated from GGA concentration) fitted with data obtained during calibrations of batch-mode MFCs A and B at (a)  $305 \Omega$ , (b)  $953 \Omega$  and (c)  $5100 \Omega$  resistances. Insets show full calibration range. Shaded bands represent the 95% prediction interval from model lines and error bars are the range of values from duplicate cells.

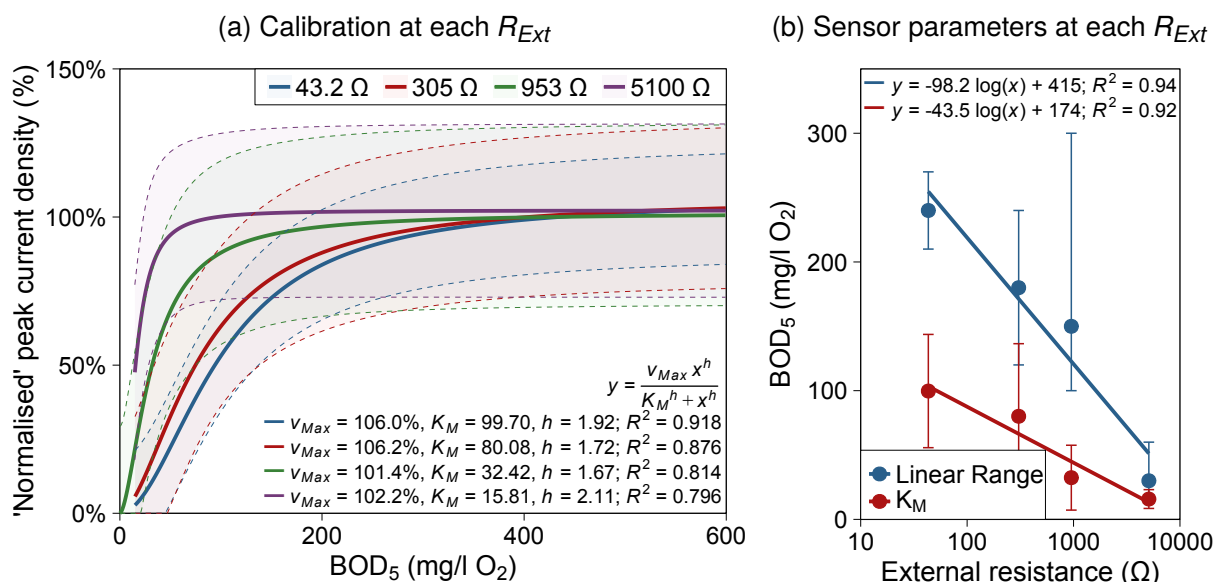


Figure 4.14: (a) 'Normalised' peak current density Hill model lines (where  $v_{Max}$  should equal 100%) against BOD<sub>5</sub> (estimated from GGA concentration) obtained from combined calibrations at  $R_{Ext} = 43.2, 305, 953$  and  $5100 \Omega$  for batch-mode MFCs A and B. Shaded bands represent the 95% prediction interval from model lines. (b) shows the sensor parameters (linear range and  $K_M$ ) plotted against the logarithm of  $R_{Ext}$  (error bars are uneven as they are the next nearest calibrated BOD<sub>5</sub> values within each calibration).

responded to a linear calibration range of 15–180 mg/l O<sub>2</sub> BOD<sub>5</sub>; a reduction of 60 mg/l. A similar observation was made with the calibrations performed with 953 and 5100 Ω  $R_{Ext}$  with  $K_M$  values of  $32.4 \pm 25.2$  and  $15.8 \pm 7.3$  mg/l O<sub>2</sub> and calibration ranges of 15–150 mg/l and 15–30 mg/l respectively (Figure 4.14b). A clear reduction in the calibration detection range (and therefore  $K_M$ ) was observed with increasing  $R_{Ext}$  (Figure 4.14). A logarithmic regression line was fitted to the upper limit of the linear calibration range and  $K_M$  values for each  $R_{Ext}$  employed (Figure 4.14b). Based on the intercept of the log-linear regression lines, the theoretical maximum linear range (at short-circuit  $R_{Ext} = 0 \Omega$ ) was up to  $415.3 \pm 50.7$  mg/l and a maximum  $K_M$  value of  $174.5 \pm 25.1$  mg/l O<sub>2</sub> BOD<sub>5</sub>.

In previous studies the use of low external resistance has been rationalised from a response time perspective (as discussed in Section 2.5 of Chapter 2) and in terms of configuring a fuel cell which does not limit electron donation by the biofilm anode to the electrode (the rate of oxidation in the biofilm therefore becomes the limiting factor). The data from the present study demonstrates the effect this operational parameter has on the MFC sensor calibration detection range. As the  $R_{Ext}$  was increased the BOD concentration at which the anodic biofilm saturated with substrate decreased resulting in a decreased calibration range. This result was recently validated by Wu *et al.* (2015a) for acetate-fed MFCs with a limited  $R_{Ext}$  range of 20, 30, 50 and 100 Ω. In that study the Michaelis-Menten  $K_M$  value was found to decrease from 141 to 41 mg/l O<sub>2</sub> COD with increasing  $R_{Ext}$ .

### 4.3.5 MFC Performance Measurement by Electrochemical Analysis

Electrochemical analytical techniques were employed to evaluate the microbial fuel cell performance. Before inoculation ( $t = 0$  days) the anode carbon cloth was assessed in the presence of GGA medium at 1199 mg/l  $O_2$  BOD<sub>5</sub>. Periodically, over the operation of cells A and B, cyclic voltammetry was performed on the anode (Figure 4.15); voltammograms were recorded at 5 mV/s using two different medium BOD<sub>5</sub> concentrations of 240 mg/l  $O_2$  and 1199 mg/l  $O_2$ .

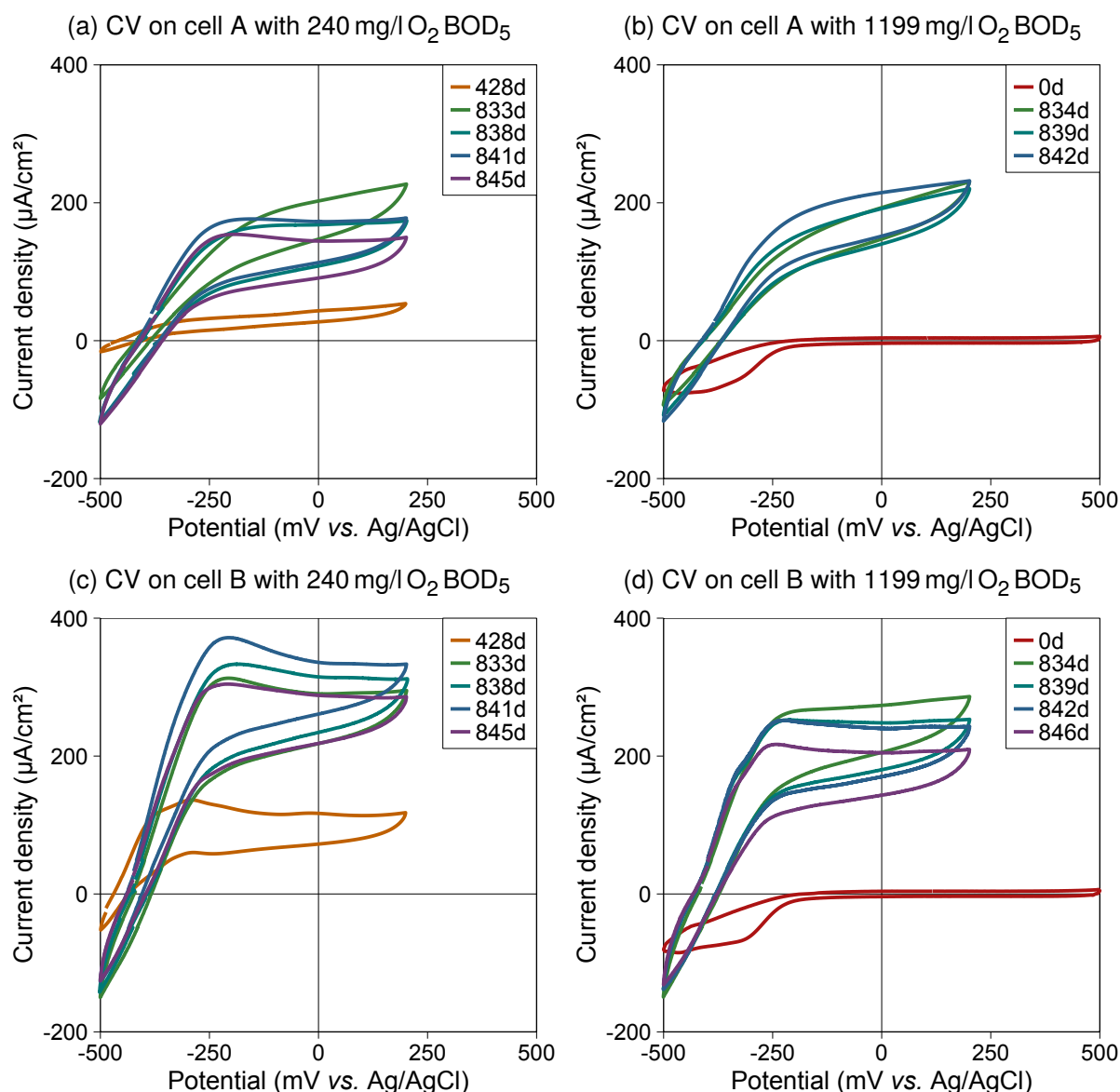


Figure 4.15: Cyclic voltammograms measured at 5 mV/s over days of operation under two different BOD<sub>5</sub> concentrations; (a) & (c) at 240 mg/l  $O_2$  and (b) & (d) at 1199 mg/l  $O_2$  for batch-mode cells A and B respectively. The decreased performance in cell A is attributed to lower GDE Pt loading (Table 4.6).

Figures 4.15b and 4.15d show the difference between the anode electrode before inoculation (carbon cloth) and after full enrichment ( $> 830$  days) of an anodic biofilm. For the voltammograms taken at 0 days, no significant oxidation current was observed with an onset

potential of 129 and 120 mV vs. Ag/AgCl measured for cells A and B respectively at the lowest point positive current was recorded. Figures 4.15a and 4.15c show that an oxidation current density of 75.4 and 155.1  $\mu\text{A}/\text{cm}^2$  had been established for cells A and B respectively by day 428 displaying the typical bioelectrocatalytic s-shape (Lohner, 2014). An increase in electrode capacitance was observed for both cells, indicated by the increase in current density difference between the anodic and cathodic sweeps in regions where no reaction was occurring (e.g.  $> 0$  mV vs. Ag/AgCl). In most cases a limiting current density was reached at approximately  $-250$  mV vs. Ag/AgCl indicating that the static solution predicated by the batch-mode of operation was resulting in mass-transfer limitations between the electrode and electron donor (GGA substrate).

The CVs on cell B show an oxidation peak was also more pronounced than cell A at this potential. By looking at the first derivative voltammogram (Figure 4.16) it was possible to see that cell B exhibited two oxidation redox couples with formal potentials of approximately  $-392$  mV and  $-326$  mV vs. Ag/AgCl whereas cell A only had one redox couple with a formal potential of  $-372$  mV vs. Ag/AgCl. The peaks observed for cell B corresponded to the 2<sup>nd</sup>

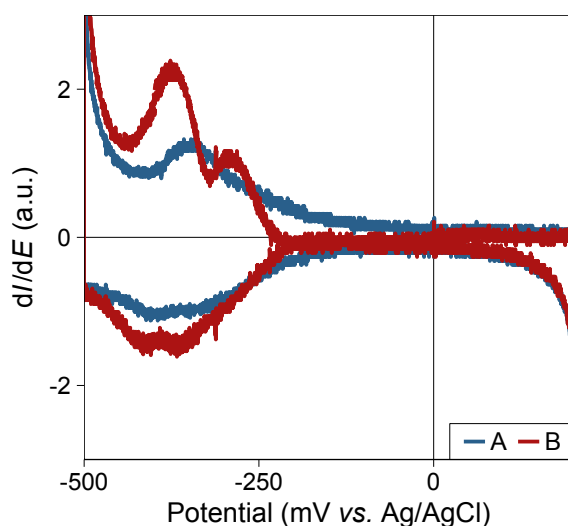


Figure 4.16: 1<sup>st</sup> derivative cyclic voltammogram measured at 5 mV/s on day 842 of operation with 1199 mg/ $\text{IO}_2$  BOD<sub>5</sub> medium for batch-mode cells A and B.

and 3<sup>rd</sup> formal potentials of cytochromes (OmcB and OmcZ) from CV of pure cultures of *Geobacter sulfurreducens* reported previously in the literature (Lohner, 2014; Richter *et al.*, 2009). Fricke *et al.* (2008) observed a similar voltammogram to those recorded for cell A in this study and they noted that the single peak was approximately the average of the two formal potentials and in non-turnover CVs were able to observe the presence of both peaks. The less resolved turnover CV features were attributed to a higher performing biofilm having an increasing cell density and/or membrane-bound cytochromes; in this study the converse was true (cell A had lower current density than cell B) but could potentially still be attributed to the bacterial cell density of non-*Geobacter* species as the anodic biofilm comprised a complex, mixed microbial community rather than a pure culture (see Section 4.3.6).

The oxidation onset potentials and maximum limiting currents are presented in Table 4.5 for cyclic and linear sweep voltammograms recorded between 833 and 846 days. The linear sweep voltammograms are shown in Figure E.1 in Appendix E. No trends relating

Table 4.5: Electrochemical performance parameters determined from CV and LSV analysis of batch-mode cells A and B with (a) 240 mg/l O<sub>2</sub> BOD<sub>5</sub> and (b) 1199 mg/l O<sub>2</sub> BOD<sub>5</sub> GGA medium between 833 and 846 days of operation.

(a) 240 mg/l O<sub>2</sub> BOD<sub>5</sub>

Time (days)	$R_{Ext}$ ( $\Omega$ )	CV				LSV			
		$E_{Onset}$ (mV) <sup>a</sup>		$I_{Max}$ ( $\mu$ A/cm <sup>2</sup> )		$E_{Onset}$ (mV) <sup>a</sup>		$I_{Max}$ ( $\mu$ A/cm <sup>2</sup> )	
		A	B	A	B	A	B	A	B
833	43.2	-416	-418	248	327	-432	-457	211	332
838	305	-381	-418	178	359	-430	-435	200	364
841	953	-384	-423	184	397	-431	-435	214	384
845	5100	-371	-424	154	340	-434	-435	177	330
$\bar{x} \pm SD$		-388 $\pm 20$	-421 $\pm 3$	191 $\pm 40$	356 $\pm 30$	-432 $\pm 2$	-440 $\pm 11$	200 $\pm 17$	353 $\pm 26$

(b) 1199 mg/l O<sub>2</sub> BOD<sub>5</sub>

Time (days)	$R_{Ext}$ ( $\Omega$ )	CV				LSV			
		$E_{Onset}$ (mV) <sup>a</sup>		$I_{Max}$ ( $\mu$ A/cm <sup>2</sup> )		$E_{Onset}$ (mV) <sup>a</sup>		$I_{Max}$ ( $\mu$ A/cm <sup>2</sup> )	
		A	B	A	B	A	B	A	B
834	43.2	-400	-411	243	307	-435	-435	211	275
839	305	-384	-411	228	277	-433	-434	210	296
842	953	-383	-397	242	263	-435	-435	241	275
846	5100		-399		232		-435		246
$\bar{x} \pm SD$		-389 $\pm 10$	-405 $\pm 7$	238 $\pm 9$	269 $\pm 31$	-434 $\pm 1$	-435 $\pm 0$	221 $\pm 17$	273 $\pm 21$

<sup>a</sup> All onset potentials recorded vs. Ag/AgCl.

to onset potential or limiting current were observed with a difference in operating external resistance ( $R_{Ext}$ ). The oxidation onset potentials measured by LSV, using a 1 mV/s scan rate, were approximately the same for all cells at all conditions with an average of -435  $\pm$  6 mV vs. Ag/AgCl. This indicated that the mechanism for substrate oxidation was not changing and was likely to be the same across all electrical loads, using the same bacterial cytochromes and potentially the same species. There was a clear difference between voltammograms recorded at 240 and 1199 mg/l O<sub>2</sub> BOD<sub>5</sub> concentrations; the maximum current density recorded by both CV and LSV was found to increase for cell A (by 47



and  $21 \mu\text{A}/\text{cm}^2$  respectively), whereas for cell B the current actually decreased by 87 and  $80 \mu\text{A}/\text{cm}^2$  respectively (Table 4.5). The reasons for this decrease are unclear and require further investigation across a range of substrate concentrations. One explanation could be inhibition due to substrate excess which occurred at high substrate concentrations for cell B, which resulted in lower current density as part of the biofilm was reduced in capacity to oxidise substrate.

Polarisation curves were measured at various points over the course of operation of cells A and B (Figure E.2 in Appendix E). Data from multiple polarisation curves were collated to enable observations to be made about the performance of cells A and B over time in relation to experimental conditions (Figure 4.17).

There was a general trend of increasing current density over the time that cells A and B were operated ( $+0.18 \pm 0.02 \mu\text{A}/\text{cm}^2$  per day,  $p\text{-value} = 8.19 \times 10^{-8}$ ; Figure 4.17a). Power density showed a decreasing trend (from day 552;  $-0.04 \pm 0.01 \mu\text{W}/\text{cm}^2$  per day,  $p\text{-value} = 2.09 \times 10^{-6}$ ; Figure 4.17b) until each GDE replacement event where the power density increased significantly. The maximum peak power density was achieved on day 569, soon after a GDE replacement (Table 4.6), of  $23.3 \mu\text{W}/\text{cm}^2$  and  $37.2 \mu\text{W}/\text{cm}^2$  for cells A and B respectively corresponding to a  $R_{Ext}$  of  $305 \Omega$  (Figure 4.17b).

Table 4.6: MPL and Pt catalyst loadings on GDEs used for operation of MFCs A, B, C & D.

Time (days)	GDE base	MPL loading		Pt loading	
		A	B	A	B
0	PTFE-treated carbon paper	$1.34 \text{ mg}/\text{cm}^2$ (96%)	$1.21 \text{ mg}/\text{cm}^2$ (86%)	$0.19 \text{ mg}/\text{cm}^2$ (37%)	$0.38 \text{ mg}/\text{cm}^2$ (75%)
182	PTFE & MPL carbon paper	-	-	-	$0.45 \text{ mg}/\text{cm}^2$ (89%)
200	PTFE & MPL carbon paper	-	-	$0.51 \text{ mg}/\text{cm}^2$ (101%)	-
552	PTFE & MPL carbon paper	-	-	$0.54 \text{ mg}/\text{cm}^2$ (105%)	$0.46 \text{ mg}/\text{cm}^2$ (91%)
		C	D	C	D
0	PTFE & MPL carbon paper	-	-	$0.42 \text{ mg}/\text{cm}^2$ (83%)	$0.48 \text{ mg}/\text{cm}^2$ (94%)

<sup>a</sup> MPL = Microporous layer

The decrease in power density was strongly correlated with decrease in cathode OCP. The OCP determined when polarisation curves were recorded appears to provide a measure of cathode performance degradation over time (Figure 4.17c). The original GDEs in cells A and B were replaced with GDEs prepared using Freudenberg GDE carbon paper (pre-treated with PTFE and MPL layers), whereas they were used from start-up in cells C and D.

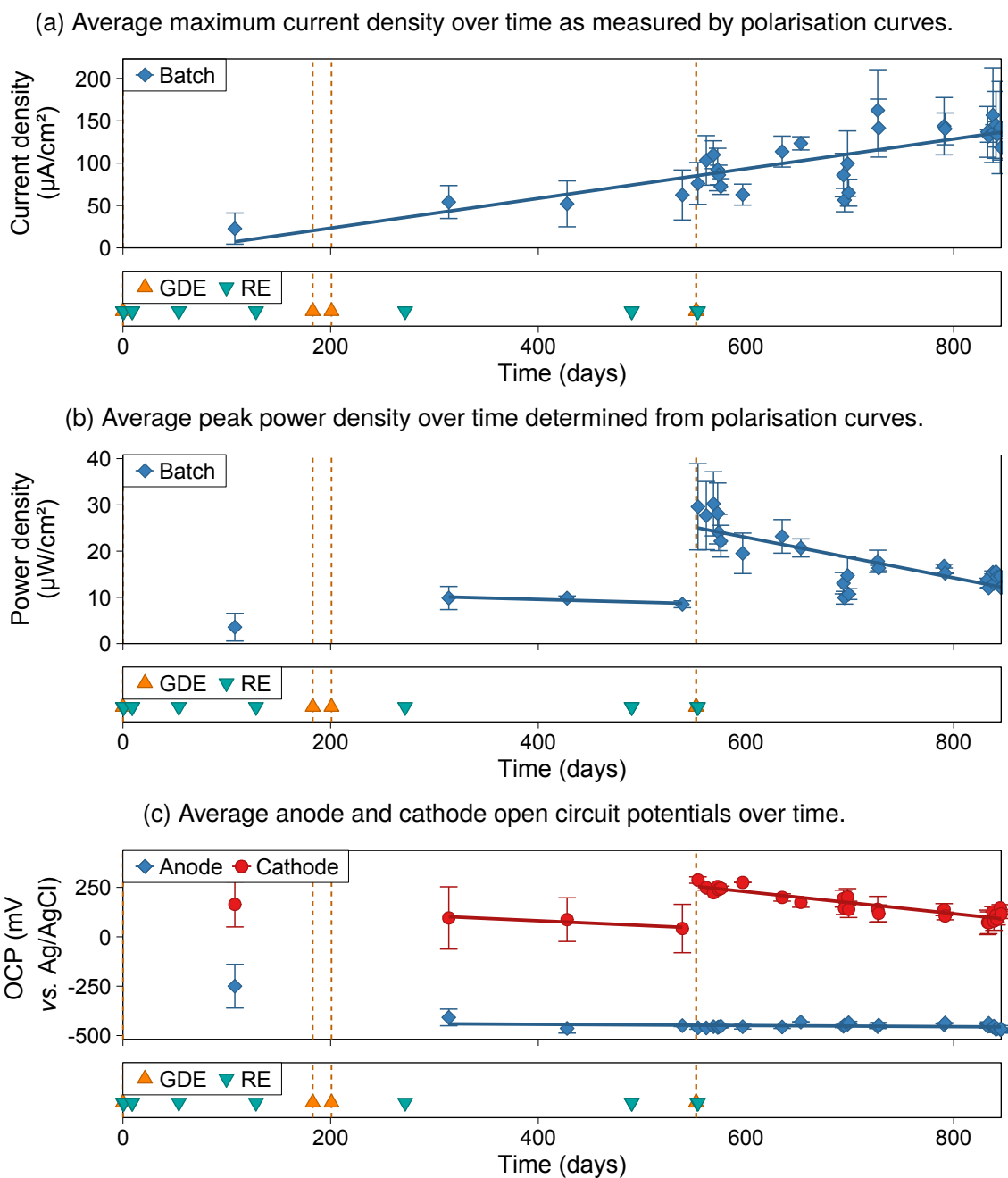


Figure 4.17: Charts showing average electrochemical performance parameters (a) maximum current density, (b) peak power density and (c) OCP measured over time determined from polarisation curves for MFCs A and B. GDE replacements are indicated by orange dashed lines and RE replacements by cyan symbols.

Platinum loading and reproducibility (a range of 83 to 105 %) was greater using carbon paper with manufacturer-applied MPL than with PTFE-treated carbon paper used for the initially prepared electrodes (Table 4.6). The initial GDE prepared for cell A only had a platinum loading of 37%. However, as fresh inoculum had been collected and all other experimental apparatus was set up, the operation of cell A was still proceeded to prevent further delays and loss of inoculum viability by repeating the three-day GDE preparation procedure. The higher Pt loading on cell B (75%) at start-up likely contributed to the development of a more active biofilm on the anode (less cathode limited) than with cell A; resulting in greater current and power densities being recorded with cell B. Subsequent GDE replacements (where cell A had similar or higher Pt loadings) resulted in approximately equal power densities, but cell B continued to generate higher current densities than cell A (Table 4.5,  $I_{Max}$ ; Figure E.2 in Appendix E).

In contrast to the cathode OCP, the anode potential exhibited an initial decrease to a value of  $-452 \pm 18$  mV vs. Ag/AgCl and remained relatively constant over the whole course of the experiment (Figure 4.17c). This open circuit anode potential was close to the  $-435 \pm 6$  mV vs. Ag/AgCl onset potential determined in LSV analysis (Table 4.5).

The estimated internal resistance ( $R_{Int}$ ) was observed to decrease to approximately  $264 \pm 37 \Omega$  over time, whereas the ohmic resistance ( $R_{\Omega}$ ; measured by EIS) was found to be constant over time with a value of  $44 \pm 4 \Omega$  (Figure E.3 in Appendix E). No significant correlation was observed with change in  $R_{Ext}$  other than a slight peak in current and power density when operating over  $305 \Omega$  load. This was the resistor at which peak power was observed in most power density curves; Figure E.4 in Appendix E). The observed experimental results conform to Jacobi's Law; peak power was achieved when external and internal resistances are equal (Ieropoulos *et al.*, 2010).

There was a reduction in average peak power density from  $14.82 \pm 0.79 \mu\text{W}/\text{cm}^2$  to  $12.88 \pm 1.02 \mu\text{W}/\text{cm}^2$  comparing power density curves recorded on cells A and B with 240 mg/l  $\text{O}_2$  and 1199 mg/l  $\text{O}_2$  BOD<sub>5</sub> but the difference was not statistically significant ( $p$ -value = 0.101; Figures 4.18a and 4.18c).

As was observed with CV and LSV a slight increase in current density was observed in cell A with increased BOD<sub>5</sub>, however Figure 4.18b shows that this was due to an 'overshoot' in the anode potential at high current densities at low BOD<sub>5</sub> (observed at the point cell voltage sharply decreases with decreasing power density). No 'overshoot' was observed with cell B and consequently the current density was  $48.7 \mu\text{A}/\text{cm}^2$  larger at lower BOD<sub>5</sub>. Other authors have reported overshoots occurring in MFC polarisation curves; Ieropoulos *et al.* (2010) explain this as a 'temporary overload' where the electron demand overtakes the rate at which electrons are donated by the microbial biofilm, however the actual cause of power overshoot is not well understood (Ahn and Logan, 2013). Hong *et al.* (2011) claimed the effect could be overcome by acclimatisation to lower external resistances and Ieropoulos *et al.* (2010)

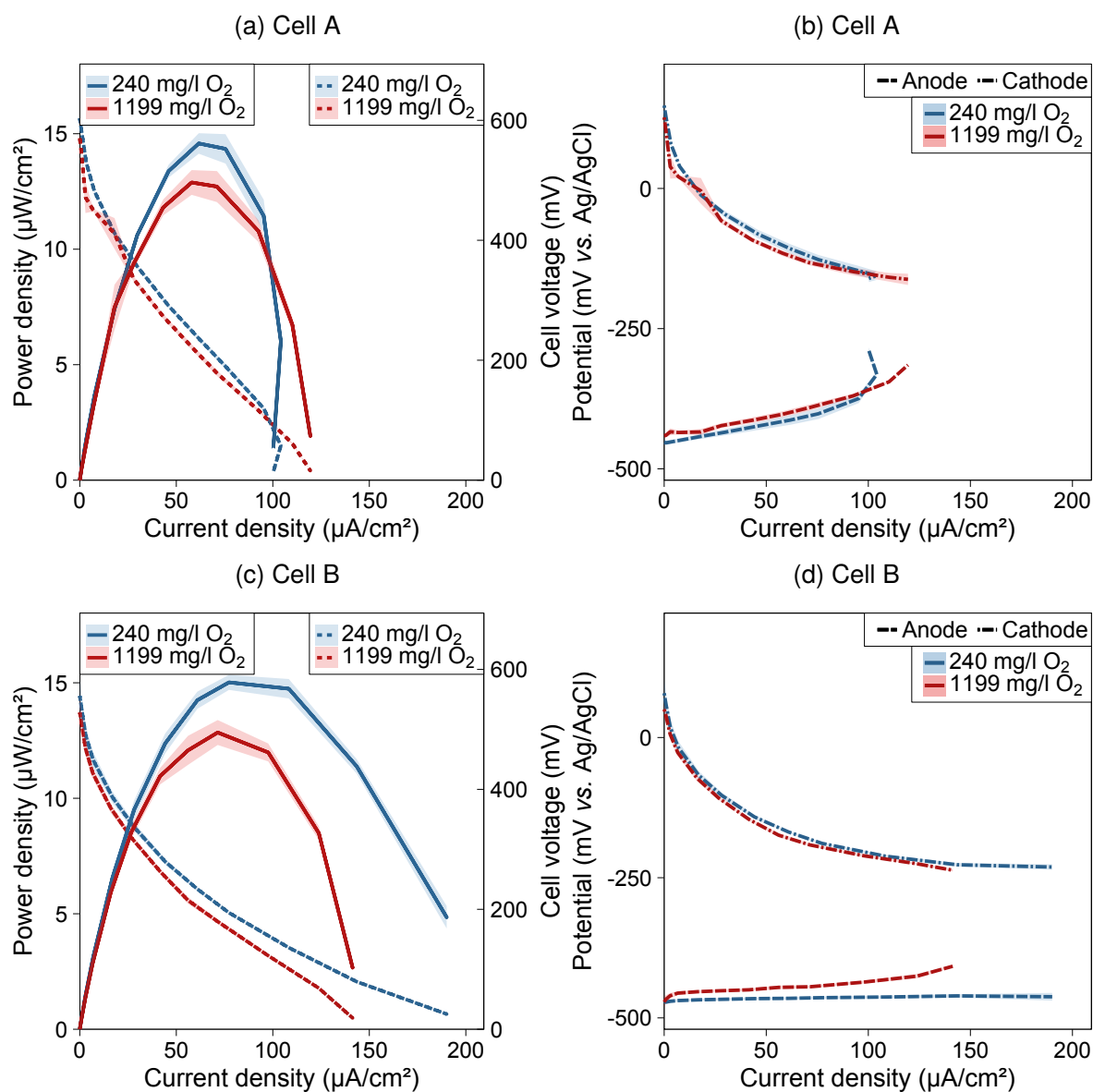


Figure 4.18: Charts showing (a) and (c) Average polarisation and power density curves and (b) and (d) anode and cathode potentials recorded on cells A and B between day 833 and 846 using 240 mg/l  $\text{O}_2$  and 1199 mg/l  $\text{O}_2$  BOD<sub>5</sub> GGA medium. Shaded bands are the standard deviation from four polarisation curves.

suggested overshoot in developed biofilms could be due to increased non-conductive cellular biomass on the electrode surface and substrate depletion at the biofilm surface.

In the present study it was clearly shown that the  $R_{Ext}$  had no effect on 830-day-old MFCs which had been operated at low  $R_{Ext}$  ( $43.2\ \Omega$  for over 100 days prior to recording curves (in Figure 4.18; each power curve was an average of four measured under the same  $BOD_5$  conditions at different  $R_{Ext}$ ). Additionally, the  $BOD_5$  was alternated between low and high concentration and the overshoot was only observed with low  $BOD_5$  in cell A; this indicates biomass build-up was not the cause of overshoot as the  $R_{Int}$  (gradient of cell voltage in Figures 4.18a) was not different for each  $BOD_5$  treatment. The experimental data collected in the present study suggest that the medium composition can affect power overshoot and may be an effect of temporary substrate depletion occurring at the biofilm surface which causes current density to decrease until it is replenished from the bulk solution.

At higher  $BOD_5$ , the anode OCP increased from  $-461.8 \pm 12.7\text{ mV}$  to  $-456.3 \pm 21.4\text{ mV}$  vs. Ag/AgCl and cathode OCP decreased from  $113.5 \pm 50.2\text{ mV}$  to  $88.6 \pm 46.7\text{ mV}$  vs. Ag/AgCl (resulting in overall cell OCP reduction but again the  $p$ -values of 0.795 and 0.676 indicated the effect was not statistically significant; Figures 4.18b and 4.18d). In both cells the gradient of the electrode potential with increasing current density was steeper with the cathode indicating that the fuel cells were cathode-limited. Based on the decline in cathode potential observed over time (Figure 4.17c), this is perhaps to be expected given that the cathode had been in operation for more than 280 days. No trend was observed in ohmic and internal resistance through time or with change in  $BOD_5$ .

#### **4.3.6 Bacterial Cell Density & Community Analysis**

After 848 days of operation of batch-mode MFCs A and B the cells were dismantled and the anode electrodes were stored in 50% aqueous ethanol solution. At the same time OCP electrodes A, B and C were extracted after 36 days of incubation at open circuit condition. Following centrifugation and removal of supernatant, 100 mg of precipitated electrode containing biomass and carbon cloth was sampled for cell counting to determine bacterial cell density present on each electrode. Representative micrographs of anodes from MFCs A and B which were used for counting are shown in Figure 4.19 and the cell densities calculated are presented in Table 4.7.

All cell counts were 3 orders of magnitude higher (approximately  $10^6$  per membrane) for sampled electrodes than the sterile PBS control. The calculated cell densities were of the order  $10^9$  cells per  $\text{cm}^2$  of electrode. For the  $12.5\text{ cm}^2$  effective anode area MFC electrodes higher cell densities were observed than for  $11.0\text{ cm}^2$  OCP electrodes, however this cannot solely be attributed as an effect of polarisation, as the size and operational lifetime of the electrodes also differed.

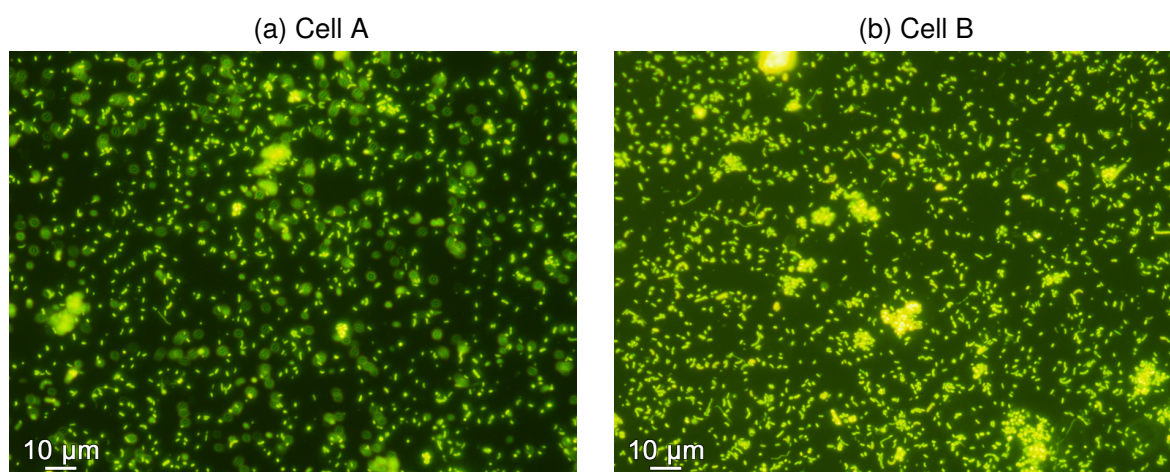


Figure 4.19: SYBR® Gold-stained cells from 5000 $\times$  diluted anode samples of anodes from batch-mode cells (a) A and (b) B.

Table 4.7: Logarithm of cell densities for batch-mode cells A and B and OCP electrodes A, B and C (and cell count of sterile PBS control).

Electrode	No images	$DF_{\text{Sample}}$	Cell count $\pm$ SE (per membrane) <sup>a</sup>	Log(Cell density) (per cm <sup>2</sup> )	Log(SE) (per cm <sup>2</sup> ) <sup>a</sup>
Control	16	1	$(2.938 \pm 0.101) \times 10^3$	-	
Batch A	15	5313	$(3.492 \pm 0.001) \times 10^6$	9.672	5.510
Batch B	15	4916	$(5.053 \pm 0.001) \times 10^6$	9.776	5.423
OCP A	16	5107	$(3.280 \pm 0.001) \times 10^6$	9.538	5.398
OCP B	17	5144	$(1.957 \pm 0.001) \times 10^6$	9.443	5.498
OCP C	16	5214	$(1.826 \pm 0.001) \times 10^6$	9.309	5.440

<sup>a</sup> Standard error (SE) =  $SD/\sqrt{N_0}$

Ion Torrent™ 16S rRNA gene sequencing was performed using electrode samples from batch-mode cells (A and B) and OCP electrodes (A, B and C). The relative abundance and abundance weighted by cell density were determined (Figures 4.20 and 4.21). Bacteria from the genus *Geobacter* and *Porphyromonadaceae* family were found to be selectively enriched by 2-3 orders of magnitude (cell densities of  $10^8$  to  $10^9$  per cm<sup>2</sup>) on polarised electrodes. Unclassified *Cryomorphaceae* were exclusively enriched on polarised electrodes. The relative abundance of the potential electrogenic bacteria were 26%, 39% and 4% for *Geobacter* spp., unclassified *Porphyromonadaceae* and *Cryomorphaceae* respectively. The *Anaeromusa* genus was found in 3% relative abundance on polarised electrodes (and also on OCP electrodes); in the literature members of this genus have been associated with amino acid fermentation including glutamate (Ouattara *et al.*, 1992).

*Anaeromusa* was found at much higher relative abundance on OCP electrodes (30%) indicating the bacteria were more enriched when the anode was not present as an electron acceptor. Members of the *Enterobacteriaceae* family (including the genera *Trabulsiella* and

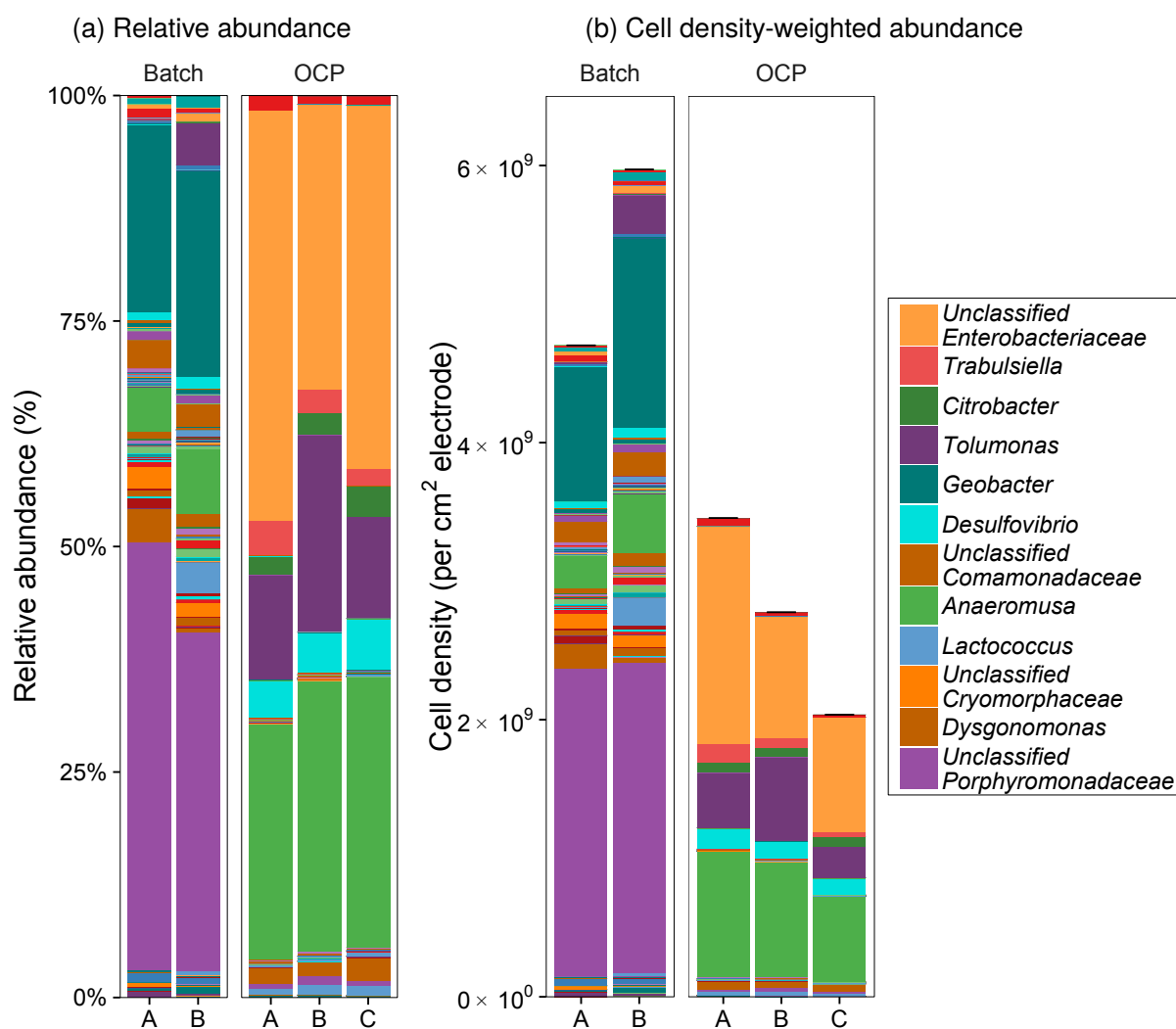


Figure 4.20: (a) Relative abundance and (b) cell density weighted abundance of bacterial genera obtained from Ion Torrent sequencing of 16S rRNA genes from identified on batch-mode MFC anodes A and B and electrodes incubated at open circuit potential (OCP A, B and C). Error bars are the standard error from cell count procedure.

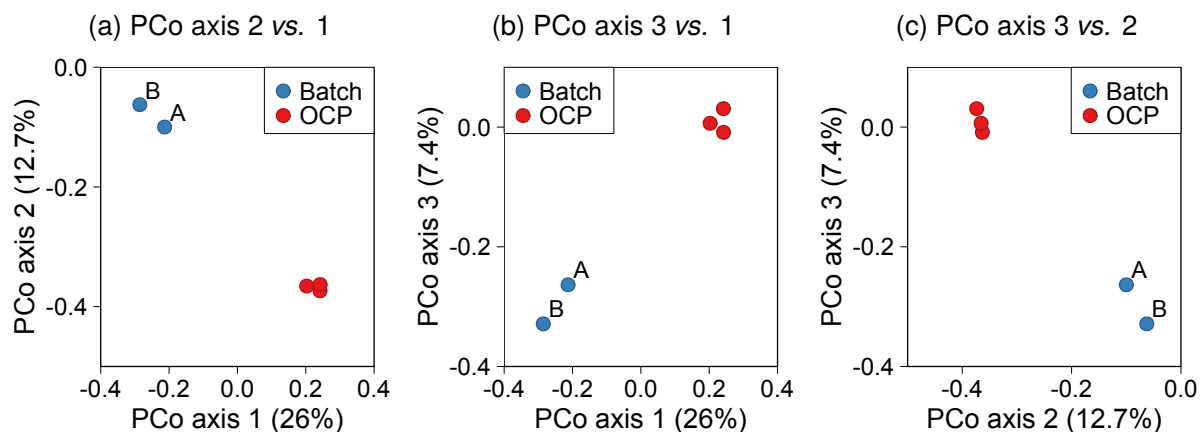


Figure 4.21: Unweighted Unifrac principal coordinate analysis of communities analysed for batch-mode cells A & B and OCP electrodes A, B & C.

*Citrobacter*) were primarily found on OCP electrodes at 39% relative abundance compared to less than 1% on polarised electrodes. The genera *Tolumonas*, *Desulfovibrio* and *Dysgonomonas* were common to both polarised and non-polarised electrodes but at higher relative abundance (2–8%) on OCP electrodes. The common bacteria are likely to have performed non-electrogenic, auxiliary functions such as glucose-fermentation (e.g. *Tolumonas* spp. (Tindall, 1996) and *Dysgonomonas* spp. (Kodama *et al.*, 2012)) and glutamate-fermentation (*Desulfovibrio* spp. (Stams and Hansen, 1984)).

The 1<sup>st</sup> unweighted Unifrac PCo axis accounts for 26% of the difference between samples and there was clear evidence of separate clustering of polarised and non-polarised electrodes (Figure 4.21). The polarised MFC electrodes clustered close together with the electrode from cell A positioned closer to the OCP electrodes, indicating that the communities were marginally more similar in composition than the cell B electrode. This was consistent with other findings in this study which showed that cell B had a higher relative abundance of *Geobacter* spp. (a genus which includes well known electrogens, is frequently found on anodes from MFCs and is known to be dominate in highly performing MFCs; Rotaru *et al.* (2015)), in addition to achieving greater electrochemical performance as a fuel cell.

#### 4.4 Conclusions

The following conclusions were drawn from experiments involving batch-mode MFCs fed with GGA-based artificial wastewater medium:

- The calibrated response from batch-mode MFCs to changes in BOD could be modelled by the Hill equation up to the point at which substrate inhibition (due to excess) occurred.
- The MFC-based biosensor did not require re-calibration. Once fully enriched, the linear detection range and minimum limiting anode potential of an MFC sensor appear to have been fixed by the operating conditions (e.g. cell architecture, external resistance). Therefore if the response is normalised by the maximum operating current density, the same calibration could be used over multiple years, and even with exact replica cells.
- The detection range of a MFC-based BOD sensor was altered with changes in external resistance ( $R_{Ext}$ ). At high external resistances the anodic biofilm saturated with substrate at lower BOD<sub>5</sub> concentrations, whereas with a low resistance the range was extended. The theoretical maximum linear detection range with this specific MFC configuration at the minimum external resistance was calculated as 415 mg/l O<sub>2</sub> BOD<sub>5</sub>.
- At low external resistances and high BOD<sub>5</sub> concentrations (i.e. > 750 mg/l O<sub>2</sub>) substrate inhibition of the anodic biofilm created a bimodal response and caused peak current density to be reduced. No substrate inhibition was observed at higher external resistances ( $\geq 953 \Omega$ ).



- From duplicate MFCs, the best-performing fuel cell (with highest current density, peak power and lowest ohmic resistance) did not have the best BOD detection range. Increased mass transfer limitations caused the concentration (BOD<sub>5</sub>), at which the anodic biofilm became saturated, to shift to higher values resulting in an increased linear detection range as a sensor.
- The GGA-fed, anodic biofilm community was dominated by species from the genus *Geobacter* (26%; bacteria likely to be involved in electrogenic processes), *Porphyromonadaceae* (39%) and *Cryomorphaceae* (4%) families in addition to glucose- and amino acid-fermenting genera.



## Chapter 5. Development and Application of Multi-stage, Flow-mode MFCs as Sensors for Enhanced BOD Detection

### 5.1 Introduction

Microbial fuel cells are poised to become a significant technology in the field of BOD sensing, as the current generated (which is readily measured) can be correlated with labile organic carbon parameters such as BOD<sub>5</sub> values. One limitation of MFC-based BOD sensors has been the upper limit of the current density which is reached at high substrate concentrations (approximately 250 mg/l O<sub>2</sub> BOD<sub>5</sub>; Figure 7.9). The current plateau has been attributed to saturation of the anodic biofilm (Chang *et al.*, 2004). The consequence of this saturation for BOD sensors is that increases in BOD<sub>5</sub> above the point at which current saturates will be undetected by the sensor. This necessitates that samples are diluted within a set range which increases the cost and complexity of analysis. The upper range limit prevents the sensors from being applied to higher concentration wastewater streams such as those from industrial sources and urban municipalities.

Operating MFCs in continuous flow-mode is essential for scale-up, optimisation and application to real-world scenarios. Batch-mode MFCs are viable in a laboratory setting but the level of maintenance required (*i.e.* constant feeding with substrate) is not practical for field testing of sensors. With the flow mode of operation there are additional parameters to consider such as the flow rate which influences the hydraulic retention time (HRT), mass transfer to and from the anode and potentially the development of the biofilm itself under flowing conditions. Ledezma *et al.* (2012) identified that at low flow rates specific growth rate was affected in MFCs. It was determined that as flow rate was increased up to 0.83 ml/min the rate increased linearly until a maximum plateau was reached; at which point maximum electrical power was also produced. For sensing applications the optimum electrochemical performance is not the main priority as changes in flow rate may lead to changes in the BOD detection range.

In the literature for non-sensing MFCs, multiple cells have been connected in various hydraulic configurations and improvements have been observed in terms of power generation and substrate utilisation (treatment) (Ieropoulos *et al.*, 2008; Chung and Okabe, 2009; Kim *et al.*, 2011c). At the time of writing, none of these configurations have been operated as sensors. The potential benefits to sensing applications by having multi-stage MFCs hydraulically linked in series are hypothesised in Figure 5.1.

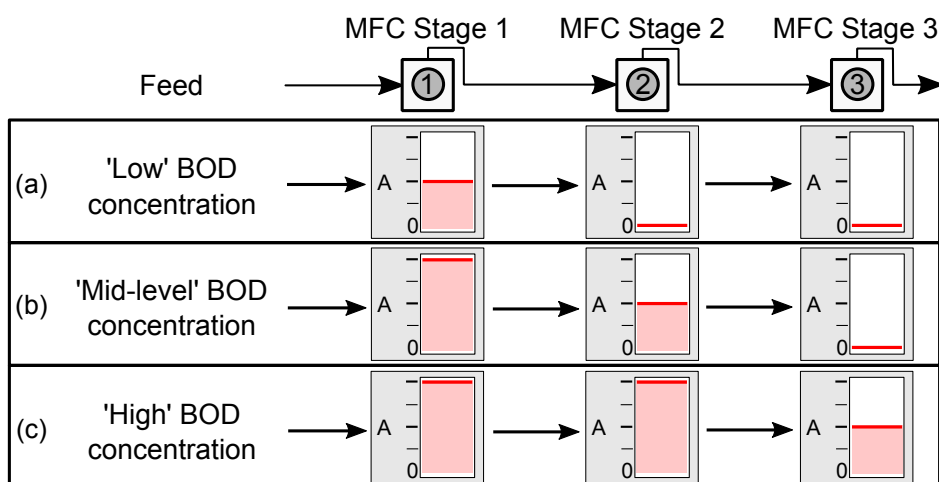


Figure 5.1: Schematic diagram of scenarios regarding BOD sensing to be addressed with multi-stage, flow-mode MFCs. Examples are given for (a) 'low', (b) 'mid-level' and (c) 'high' BOD concentrations. The relative, hypothesised current response (— in amperes (A)) is indicated for each MFC in a three-stage hydraulic array.

It was the aim of this study to enhance the BOD detection range of a flow-mode MFC sensor by exploiting the operational features of staging three MFCs connected hydraulically in series (as shown in Figure 5.1). It was expected that the first stage MFCs (in position 1) would receive the highest concentration of BOD resulting in saturating current above  $\approx 250 \text{ mg/l O}_2 \text{ BOD}_5$ . The downstream MFCs (in positions 2 and 3) were expected to generate electricity based on the remaining substrate present in effluents from the first stage MFCs. This modular mode of operation lends itself to industrialisation of the technology because different numbers of MFCs could be staged to enable different strength wastewaters to be analysed without requiring dilution or pre-treatment.

Multiple strategies were undertaken to evaluate the multi-staged approach to BOD sensing with MFCs. The first objective was to establish a working protocol which would allow multi-stage MFCs to be operated hydraulically in series with a constant stream of medium fed in a single-pass flow-mode. To determine the response of MFCs to changes in BOD a calibration protocol was established and used to assess the detection ranges of each stage. The effect of flow rate on BOD calibration was determined in addition to monitoring of electrochemical performance, substrate utilisation and microbial community composition to gain a greater understanding of the processes occurring through the hydraulic array of MFCs.

## 5.2 Experimental

### MFC Set-up

Ten millilitre SCMFCs were assembled with carbon cloth anodes, Pt/C-coated gas diffusion cathodes and cation exchange membranes (as detailed in Section 3.1 of Chapter 3). Initially,

three cells were constructed in triplicate (referred to as cells 1A, 1B and 1C) and inoculated with 100% combined effluent from batch-mode MFCs enriched with glucose-glutamic acid (GGA) medium (cells A & B in Chapter 4). Each new flow-mode cell was fed from one of three bottles of sterile GGA medium (A, B and C respectively) containing 50 mmol/dm<sup>3</sup> phosphate buffer, nutrients and vitamins. Medium was continuously fed to the cells using the single-pass flow system described in Section 3.2 of Chapter 3 (Figure 5.2).

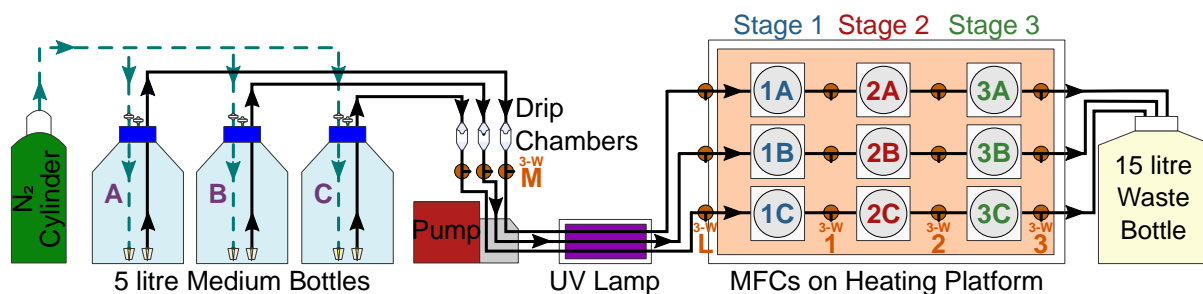


Figure 5.2: Schematic diagram of set-up for triplicate channels of three-stage SCMFCs and position of three-way (3-W M, 3-W L, 3-W 1, 3-W 2 & 3-W 3) valves.

From start-up, cells were operated on a heating platform programmed with a set point of 35 °C inside a polystyrene enclosure with an ambient temperature of approximately  $28.2 \pm 2.0$  °C. Peripheral apparatus (including medium bottles and peristaltic pump) was at room temperature ( $14.0 \pm 2.7$  °C; unregulated). From day 155 and day 212 (of operation of the first stage cells), second and third stages of three identical SCMFCs were hydraulically connected to the flow channels downstream of the MFC outlets and operated for 603 and 546 days respectively (cells referred to as a 2A, 2B, 2C, 3A, 3B and 3C; Figure 5.2). The second and third stage MFCs were started without any external source of micro-organisms and inoculated only by receiving the effluent pumped from the first stage MFCs. Figure 5.3 provides a comprehensive visual overview of the operation of flow-mode cells in channels A, B and C over 757 days.

Following the completion of the first series of flow-mode experiments (referred to as the 'ABC' series) a new set of MFCs was assembled in the same three stage by three channel configuration (flow channels referred to as D, E and F or together as the 'DEF' series). The new cells (referred to as 1D, 1E, 1F, 2D, 2E, 2F, 3D, 3E and 3F) were inoculated all on the same day ( $t = 0$  days) using 100% combined effluent from the still-operating batch-mode MFCs A and B (767 days after the original inoculation of the first stage 'ABC' MFCs). The 'DEF' series of cells were started-up in batch-mode and reinoculated several times with the combined batch-mode cells effluent (A & B; Chapter 4) until a appreciable cell voltage was obtained. The second series ('DEF' series) of flow-mode MFCs was operated for 148 days and the relevant operational parameters are shown visually in Figure 5.4.

With each stage of flow-mode MFCs in the first experimental series (cells in flow channels A, B and C) a 953  $\Omega$  external resistor was connected between the anode and cathode at start-up. Over the period of operation 43.2, 305 and 1823  $\Omega$  resistors were used as the

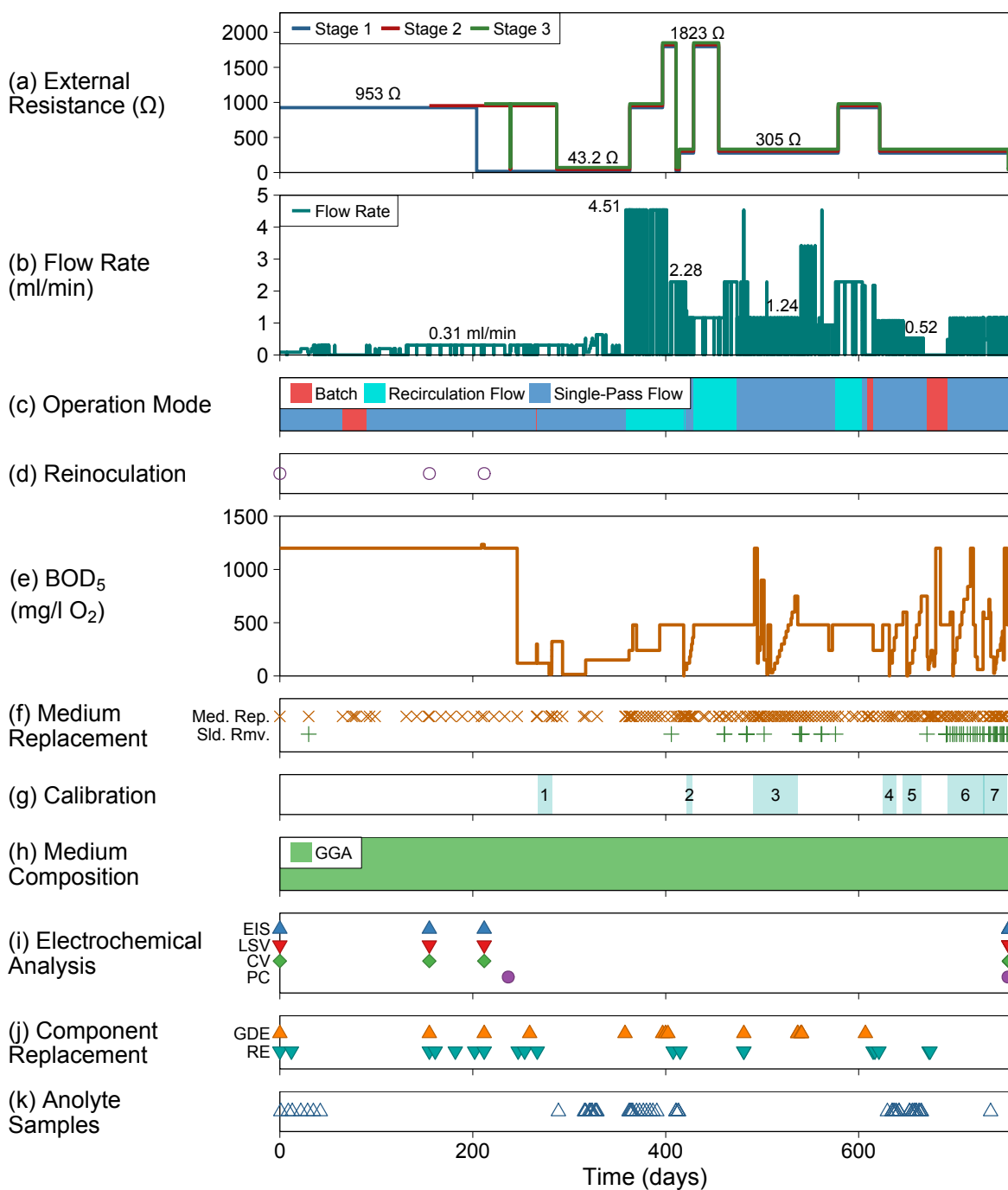


Figure 5.3: Timeline of events summarising the operation of flow-mode MFCs (1A, 1B, 1C, 2A, 2B, 2C, 3A, 3B and 3C) including (a) external resistance used for MFC operation, (b) medium flow rate, (c) mode of operation, (d) reinoculation events, (e) BOD<sub>5</sub> (estimated from known GGA concentrations), (f) medium replacement events, (g) labelled calibration bands representing range of included medium replacements, (h) medium composition, (i) electrochemical analysis, (j) component replacement, (k) analyte sample events.

Med. Rep. = Medium Replacement, Sld. Rmv. = Sludge Removal, GGA = Glucose-Glutamic acid; EIS = Electrochemical Impedance Spectroscopy; LSV = Linear Sweep Voltammetry; CV = Cyclic Voltammetry; PC = Polarisation Curve; GDE = Gas Diffusion Electrode; RE = Reference Electrode.



Figure 5.4: Timeline of events summarising the operation of flow-mode MFCs (1D, 1E, 1F, 2D, 2E, 2F, 3D, 3E and 3F) including (a) external resistance used for MFC operation, (b) medium flow rate, (c) mode of operation, (d) reinoculation events, (e) BOD<sub>5</sub> (estimated from known GGA concentrations), (f) medium replacement events, (g) labelled calibration bands representing range of included medium replacements, (h) medium composition, (i) electrochemical analysis, (j) component replacement, (k) analyte sample events.

Med. Rep. = Medium Replacement, Sld. Rmv. = Sludge Removal, GGA = Glucose-Glutamic acid; 4-NP = 4-Nitrophenol; WW = Wastewater; EIS = Electrochemical Impedance Spectroscopy; LSV = Linear Sweep Voltammetry; CV = Cyclic Voltammetry; PC = Polarisation Curve; GDE = Gas Diffusion Electrode; RE = Reference Electrode.

4-NP was included in the medium when testing for toxicity in Chapter 6 and experiments conducted with WW are discussed in Chapter 7.

external resistance ( $R_{Ext}$ ; Figure 5.3a). Cell voltage and anode potentials were recorded using a voltage data-logger. With the second series of flow-mode MFCs (in flow channels D, E and F) 43.2  $\Omega$  resistors were mainly used as the external load, except for a non-calibrated period between days 42 and 65 when a 953  $\Omega$  resistor was used (Figure 5.4a).

Equipment was installed to prevent bacteria growing against the direction of flow (*i.e.* towards the medium bottles) after inoculation. On day 98 of the 'ABC' series of flow-mode MFCs, a UV lamp enclosure was fitted around the tubing between the peristaltic pump and the first stage of MFCs. An improvement to the experimental setup was made on day 564 with installation of an in-line drip chamber upstream of the peristaltic pump in which a trapped air bubble caused a physical separation between the feed bottle and downstream feed tubing (detailed setup described in Section 3.2.7 of Chapter 3).

## Calibration

BOD calibration was performed in single-pass flow-mode by two different methods. The 'bottle amendment' method involved sequentially injecting concentrated GGA solution into a medium bottle and mixing by sparging with  $N_2$ . The 'bottle replacement' method involved altering the GGA concentration in the preparation of the medium bottle before feeding to the cells. 7 independent calibrations were carried out with the 'ABC' series of flow-mode cells (Figure 5.3g and Table 5.1) and an additional calibration was performed with the 'DEF' series of flow-mode cells (Figure 5.4g). For Calibration 1 (ABC), the 'bottle amendment' method was used and the first stage MFCs were operated with  $R_{Ext} = 43.2 \Omega$  and for the second and third stage cells  $R_{Ext}$  was 953  $\Omega$  (Table 5.1). For all subsequent calibrations (Calibrations 2–7 (ABC) & 1 (DEF), Table 5.1), all cells had  $R_{Ext} = 305 \Omega$  and BOD calibration was achieved using the 'bottle replacement' method.

Over the course of experiments the flow rate was varied for experimental purposes and for ongoing development of a working protocol for operation of the flow-mode cells (*i.e.* to minimise in-line biomass growth; Figure 5.3b and 5.4b). At start-up of the 'ABC' series a flow rate of 0.31 ml/min was selected as the slowest rate achievable with the peristaltic pump and associated pump tubing to prolong the operating period with each 5 litre medium bottle. After identifying improvements to the working protocol (Section 5.3.2) a flow rate of 0.52 to 1.24 ml/min was used for start-up of the 'DEF' series of MFCs.

A constant flow rate was used for each of the calibrations; flow rates ranging from 0.52 to 1.24 ml/min were used for the 'bottle replacement' method calibrations. Calibrations 6 and 7 (ABC) were performed back-to-back to assess the effect of flow rate (hydraulic retention time) on calibration and three-stage MFC performance.

Under certain circumstances (*e.g.* between calibrations) the flow-mode was switched from single-pass to recirculation mode. This enabled a continuous flow to be maintained through



Table 5.1: Details of calibrations performed using the ‘ABC’ (1A, 1B, 1C, 2A, 2B, 2C, 3A, 3B & 3C) and ‘DEF’ (1D, 1E, 1F, 2D, 2E, 2F, 3D, 3E & 3F) flow-mode cells. Calibrations 1–5 (ABC) were only briefly analysed due to methodological and operational issues detailed in footnotes c–e.

Calibration ID	Start time (day) <sup>a</sup>	No cycles <sup>b</sup>	BOD <sub>5</sub> range (mg/l O <sub>2</sub> )	$R_{Ext}$ ( $\Omega$ ) (Stage 1/2/3)	Flow rate (ml/min)	†
1 (ABC)	266	9	0–2399	43.2 / 953 / 953	0.31	<sup>c</sup>
2 (ABC)	421	5	200–600	305 / 305 / 305	1.24	<sup>d</sup>
3 (ABC)	491	23	15–1199	305 / 305 / 305	1.24	<sup>e</sup>
4 (ABC)	624	7	0–480	305 / 305 / 305	1.09	<sup>d</sup>
5 (ABC)	645	9	0–750	305 / 305 / 305	0.53	<sup>d</sup>
6 (ABC)	691	15	60–1199	305 / 305 / 305	0.52	
7 (ABC)	728	15	25–1199	305 / 305 / 305	1.24	
1 (DEF)	67	9	60–480	305 / 305 / 305	1.24	

<sup>a</sup> Start time of first medium cycle included in calibration. <sup>b</sup> Number of cycles included in the calibration.

<sup>c</sup> Calibration was performed using the ‘bottle amendment’ method. <sup>d</sup> Calibration was interrupted due to leaking cells. <sup>e</sup> Calibration was conducted with sludge present inside MFCs.

the MFCs without the requirement for frequent medium bottle replacements due to the limitation of a finite medium volume. Additionally, during periods where significant leaks had developed, the MFCs were switched to batch-mode (static operation) to allow seals to set completely and/or modifications to be made to the peripheral tubing and experimental apparatus (Figure 5.3b and 5.4b).

## Analysis

As indicated in Figure 5.3i and 5.4i, the electrochemical performance of the flow-mode cells was analysed using a potentiostat and measurements of two-electrode cell EIS, anode LSV and/or CV were taken. Polarisation curves were measured by recording the cell voltage at OCP and attaching sequentially lower resistors from 536 k $\Omega$  down to 10  $\Omega$ . Measurements were recorded and resistors were exchanged once a steady-state cell voltage was achieved with each polarisation.

When cathode performance decreased significantly (as measured by its potential), or leaks developed to the extent that flow operation could not viably proceed, the gas diffusion electrode (GDE) and membrane assembly was replaced and resealed as required. When an air gap developed in the reference electrode (RE) salt bridge the component was replaced as necessary.

Three-way valves (indicated by ‘3-W’ in Figure 5.2) were installed before the peristaltic pump (3-W M), before the first stage MFC (3-W L) and after the outlets of each MFC (3-W 1, 2

and 3). Medium samples were taken directly from the remaining medium present in the feed bottle after a cycle. In addition, anolyte samples were taken at various points along the continuous flow path (specifically from the 3-W L, 1, 2 and 3 positions). Samples were analysed for pH, conductivity, COD, VFAs, anions and GGA concentrations to allow a profile of the degradation processes occurring to be constructed and the coulombic efficiency to be determined.

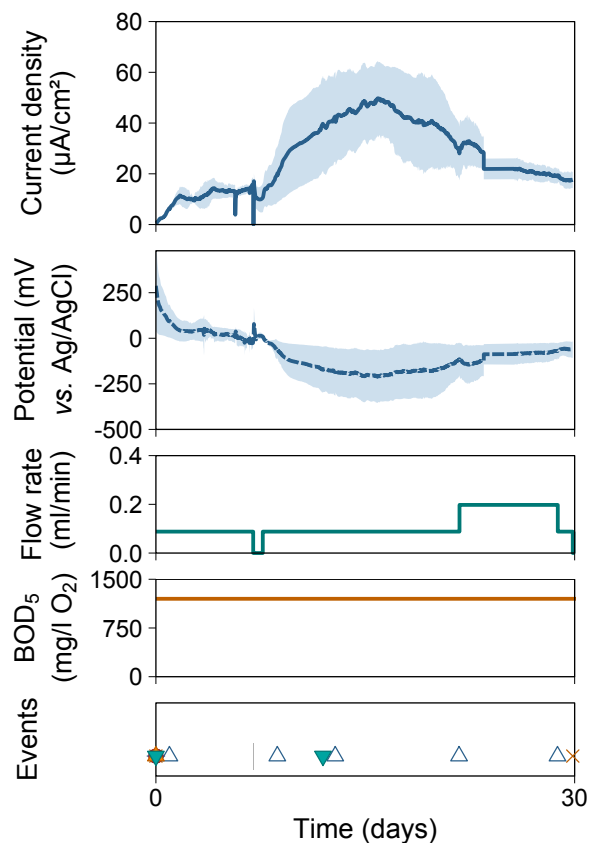
At the termination of the 'ABC' series of flow-mode cells, electrode samples were taken from the first (1A, 1B & 1C), second (2A, 2B & 2C) and third (3A, 3B & 3C) stages of MFCs after 756, 601 and 545 days of operation respectively (termination date was the same). Biomass sludge samples were taken from the first stage 'ABC' MFCs after the sludge removal procedure (Section 3.2.11 in Chapter 3). Electrode and sludge samples were taken for community analysis and cell counts according to the methods described in Chapter 3, Sections 3.7 and 3.8.

## 5.3 Results & Discussion

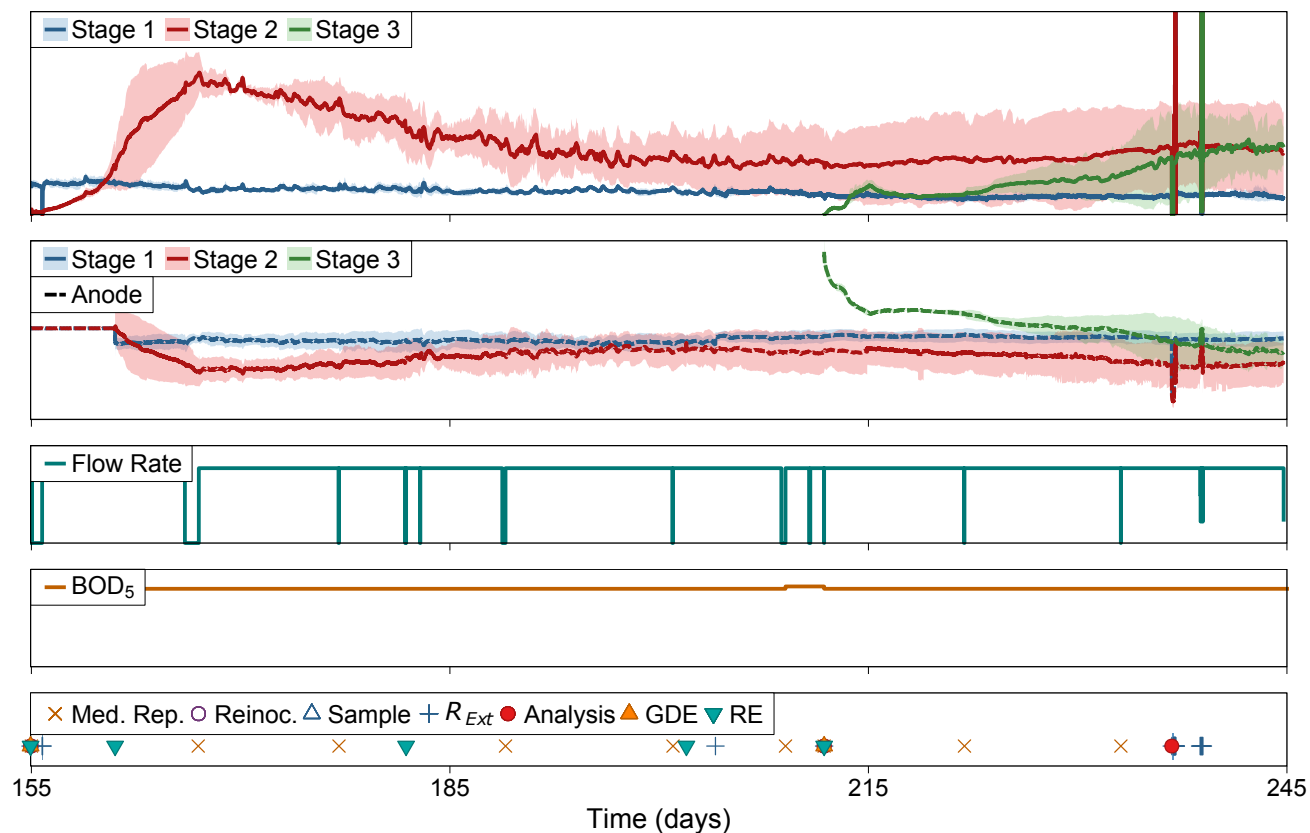
### 5.3.1 Microbial Fuel Cell Enrichment & Operation

The first stage of MFCs in the 'ABC' flow channels (cells 1A, 1B and 1C) achieved a peak current density of  $49.8 \pm 14.7 \mu\text{A}/\text{cm}^2$  over a  $R_{Ext}$  of  $953 \Omega$  in single-pass mode at a flow rate of 0.09 ml/min (Figure 5.5a). The second and third stage 'ABC' MFCs (cells 2A, 2B, 2C, 3A, 3B and 3C), installed on day 155 and day 212 respectively, achieved peak current densities of  $56.0 \pm 7.9$  and  $27.9 \pm 9.4 \mu\text{A}/\text{cm}^2$  with  $R_{Ext} = 953 \Omega$  at 0.31 ml/min (Figure 5.5b). The peak values were obtained 16, 12 and 32 days after inoculation for the first, second and third stage MFCs respectively.

The MFCs in the 'DEF' flow channels (cells 1D, 1E, 1F, 2D, 2E, 2F, 3D, 3E and 3F), which were all inoculated on the same day, achieved peak current densities of  $246.7 \pm 12.3$ ,  $245.4 \pm 21.6$  and  $265.7 \pm 11.1 \mu\text{A}/\text{cm}^2$  in the first, second and third stages respectively (Figure 5.6). Following the 11-day enrichment to reach peak values in batch-mode over a  $R_{Ext}$  of  $43.2 \Omega$ , it was observed that the batch cycle length was only approximately 6 hours and with extended periods of starvation (48 hours) the maximum current density could not be achieved without frequent medium replacements. The single-pass mode of operation was initiated on day 14 and similar maximum current densities were observed for each cell in the flow-mode when the  $\text{BOD}_5$  concentration was high enough;  $> 600 \text{ mg/l O}_2 \text{ BOD}_5$  for the first and second stages and  $> 720 \text{ mg/l O}_2 \text{ BOD}_5$  for the third stage (Figure 5.6).



(a) Start-up of Stage 1 'ABC' flow-mode cells.



(b) Start-up of Stage 2 & 3 'ABC' flow-mode cells.

Figure 5.5: Start-up of (a) Stage 1 flow-mode cells (1A, 1B & 1C; inoculated at  $t = 0$ ) and (b) Stage 2 flow-mode cells (2A, 2B & 2C; inoculated at  $t = 155$  days) and Stage 3 cells (3A, 3B, 3C; inoculated at  $t = 212$  days) with average measured current density and anode potential (shaded region is  $\pm$ SD), flow rate, estimated  $BOD_5$  and events (including medium replacements, reinoculations, samples, periods where cells were offline,  $R_{Ext}$  changes, electrochemical analyses and GDE/RE replacements).

Med. Rep = Medium replacements; Reinoc. = Reinoculations; GDE = Gas Diffusion Electrode; RE = Reference Electrode.

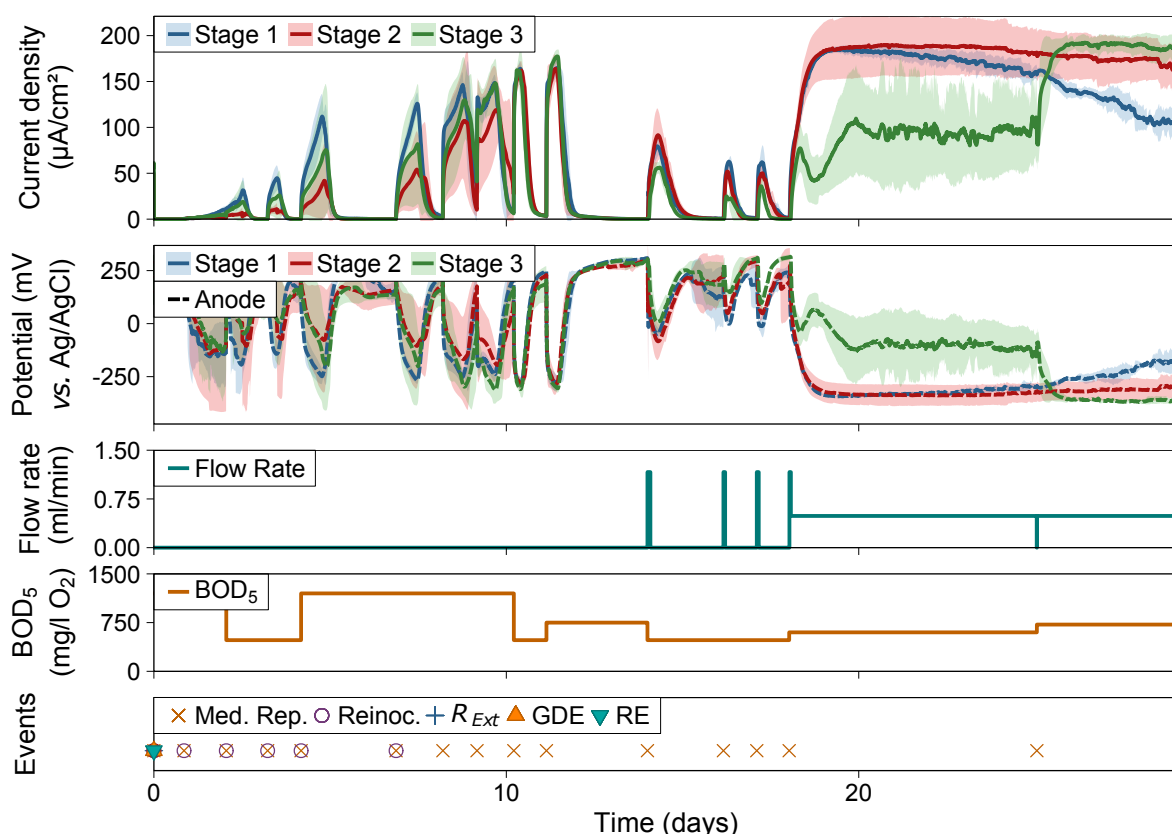


Figure 5.6: Start-up of three stages of flow-mode cells in flow channels D, E and F (1D, 1E, 1F, 2D, 2E, 2F, 3D, 3E & 3F; inoculated at  $t = 0$ ) with average measured current density and anode potential (shaded region is  $\pm$ SD), flow rate, estimated  $BOD_5$  and events (including medium replacements, reinoculations, periods where cells were offline,  $R_{Ext}$  changes, electrochemical analyses and GDE/RE replacements).

Med. Rep = Medium replacements; Reinoc. = Reinoculations; GDE = Gas Diffusion Electrode; RE = Reference Electrode.

### 5.3.2 Development of a Working Protocol for Staging Multiple MFCs in a Single-pass, Continuous Flow-mode System

#### Operational Issues Arising from Sludge Accumulation

Various operational issues arose during the course of experiments conducted with the 'ABC' series of flow-mode MFCs which were not apparent with the batch-mode MFCs. Issues stemmed from non-electrogenic biomass growth which became prevalent at high concentrations of GGA as a consequence of operating a single-pass, continuous flow system with constant delivery of fresh substrate-containing medium. Inline growth of bacteria against the direction of flow towards the medium bottle (source of substrate) was reduced by installation of a UV lamp enclosure around the inlet feed and eventually (on day 564) halted altogether by fitting a sterilised drip chamber between the medium bottle and feed lines (Section 3.2.7).

The design of the MFC reactors (outlet at the top of the cell; Figure 3.1b in Chapter 3) and other positions in the peripheral flow system, including downward pointing ports in the

three-way valves and narrow orifices in tubing fittings, enabled biomass sludge to accumulate and cause blockages. In addition to preventing flow of anolyte medium, blockages led to a multitude of issues arising from a build-up of pressure (Figure 5.7). Swollen tubing, ruptured GDEs and even cracked acrylic end plates were the result of blockages not being cleared in time. Overcoming these operational problems could not be solved by installation of new equipment as the growth was occurring inside the cells themselves. In order to combat the biomass growth, from day 690, a vigorous sludge removal procedure was employed with every medium bottle change (every 1-5 days; Figure 5.3f) which involved complete removal of the MFCs contents and clearing of the peripheral feed tubing (Section 3.2.11 of Chapter 3).

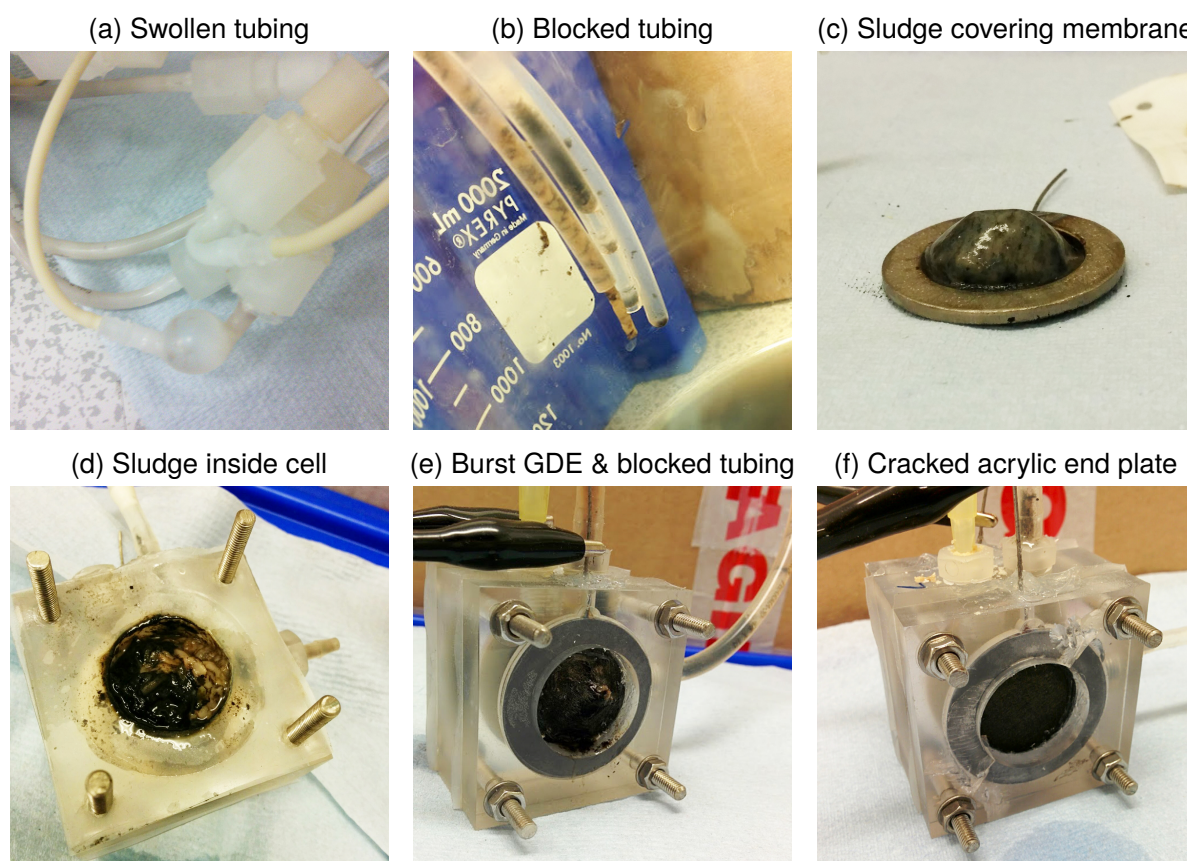


Figure 5.7: Photographs of various sludge-related operational issues; (a) swollen tubing arising from a blocked connector, (b) blocked tubing being cleared, (c) a removed membrane-electrode-current collector assembly covered in sludge, (d) sludge visible inside a cell with the MEA and cathode end plate removed, (e) a ruptured GDE and blocked tubing and (f) a cracked end plate.

During the seventh BOD calibration of the 'ABC' series of flow-mode MFCs, samples of the cell contents from the sludge removal procedure were taken. The amount of sludge accumulated in each MFC over 3-5 days of continuous flow at 1.24 ml/min for GGA concentrations of 100, 400, 900 and 2000 mg/l (equating to 100, 240, 540 and 1199 mg/l  $O_2$  BOD<sub>5</sub>) is shown in Table 5.2.

No sludge was obtained from samples of the spent medium (taken directly from the medium



Table 5.2: Photographs showing the contents removed from each of the cells in the ‘ABC’ flow-mode series in comparison to liquid samples taken from the medium bottle and inline feed (at 3-W L valve). The development of biomass sludge was observed in the MFCs as GGA concentration was increased from 100 to 2000 mg/l. Photos were taken after allowing the sludge to settle for > 30 minutes after sampling.





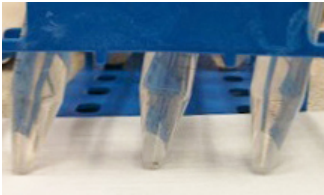
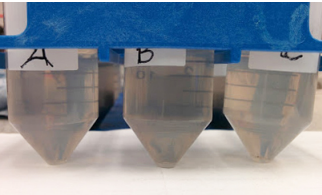
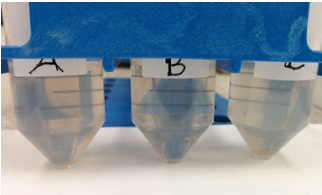
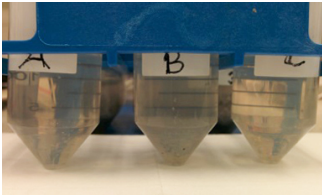
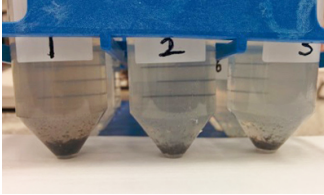
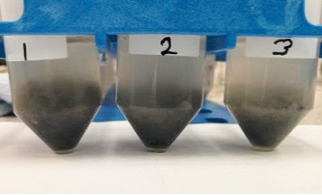
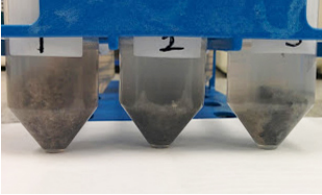
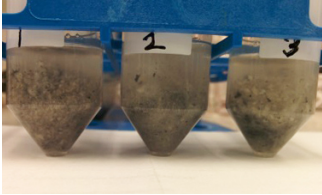
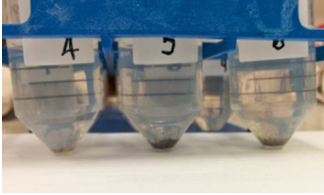
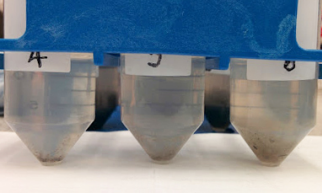
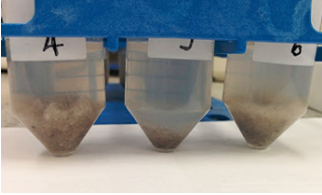
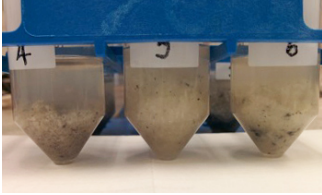
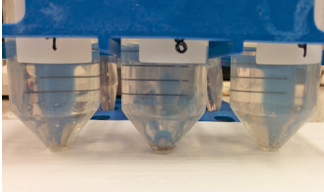
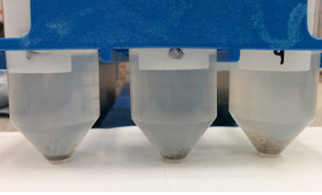
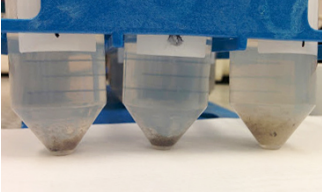
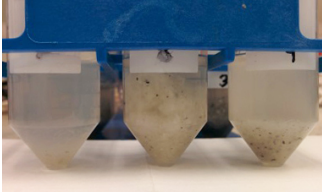
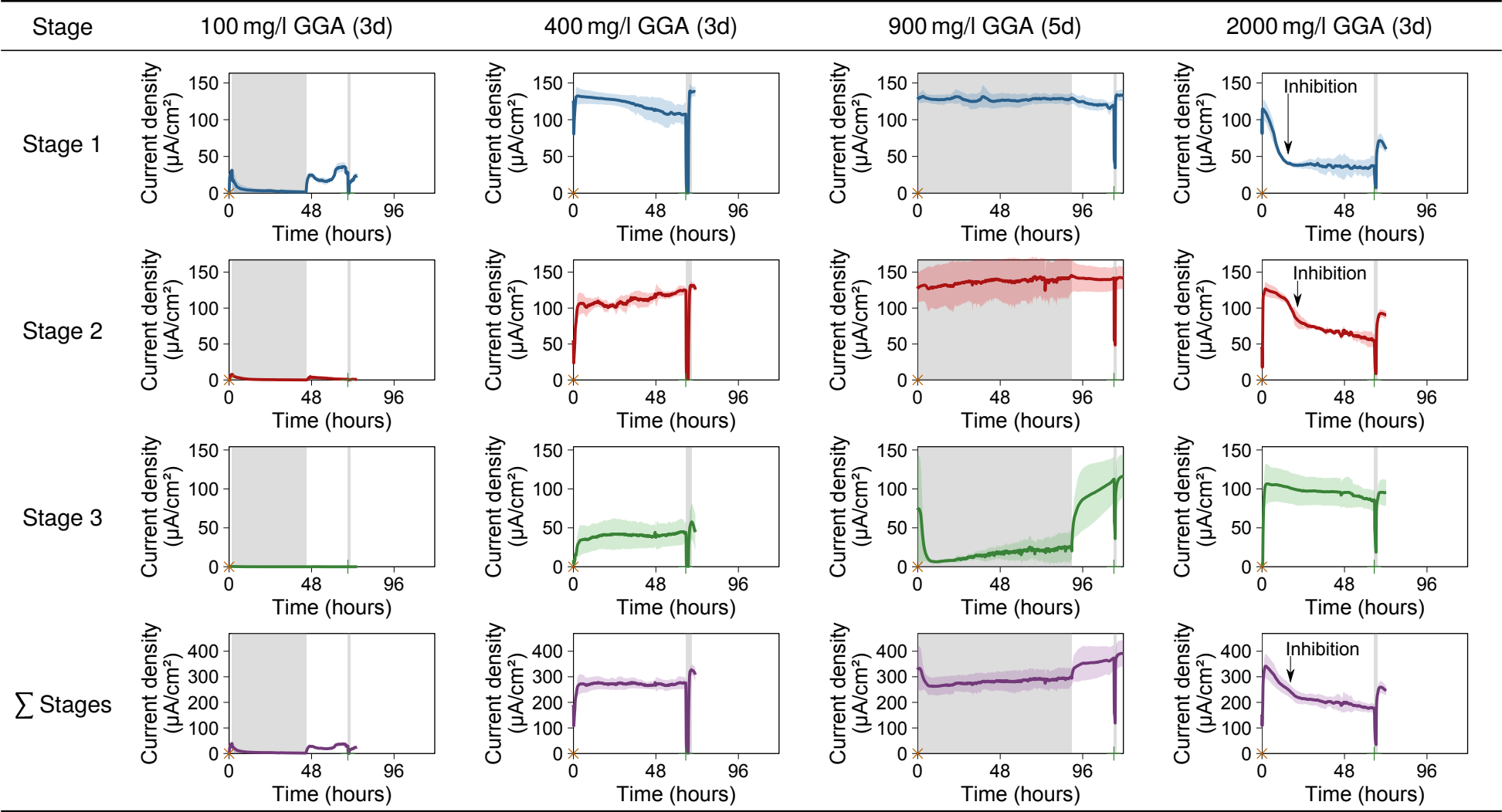
Sampling location	100 mg/l GGA (3d)	400 mg/l GGA (3d)	900 mg/l GGA (5d)	2000 mg/l GGA (3d)
Medium bottle				
Feed line (3-W L)				
Stage 1 (3-W 1)				
Stage 2 (3-W 2)				
Stage 3 (3-W 3)				

Table 5.3: Average current response of each stage of MFCs in the ‘ABC’ flow-mode series to GGA concentrations of 100, 400, 900 and 2000 mg/l during sludge accumulation over 3-5 days. Medium replacements (✕) and sludge removals (+) are indicated along the x-axis of each chart. Grey bands indicate occasions when the MFCs were either offline or at a different flow rate and should be disregarded for comparisons.



bottle at the end of the flow cycle) nor the sample taken from the feed line upstream of the MFCs (at 3-W L valve; Table 5.2). As the GGA concentration increased from 100 to 2000 mg/l the amount of sludge accumulating inside the first stage MFCs increased from approximately 10 vol% to almost 100 vol% and the appearance changed from a dark brown sediment to a mixed brown and white coloured sludge (Table 5.2). In the second stage MFCs the amount of sludge below 400 mg/l was minimal (< 10 vol%) but at 900 and 2000 mg/l GGA a mixed sludge was produced (at approximately 50 and 80 vol% respectively). With the third stage of MFCs there was minimal sludge generation until 2000 mg/l GGA when a considerable amount (10-70 vol%) of white coloured sludge was generated (Table 5.2). Figure 5.7d is a photograph taken of sludge inside a MFC during a GDE replacement; it was evident that the white coloured biomass was present closest to the MFC inlet and the dark coloured sludge was in the hydraulic dead space of the anode chamber.

### Effect of Sludge Presence on MFC Current Density

The average stable current densities before and after sludge removal were recorded for medium compositions of 100, 400, 900 and 2000 mg/l GGA (Table 5.3 and Table 5.4). The sludge removal procedure was carried out close to the end of medium cycles (in advance of the next medium bottle replacement), consequently the period recorded *before* sludge removal was approximately 24-72 hours, whereas the period *after* removal was typically only 5 hours (Table 5.3).

Table 5.4: Average stable current densities ( $\pm$ SD) measured before and after the sludge removal procedure for each stage of triplicate MFCs in the 'ABC' flow-mode series with GGA concentrations of 100, 400, 900 and 2000 mg/l.

Stage	Average stable current density ( $\mu$ A/cm <sup>2</sup> )							
	100 mg/l GGA		400 mg/l GGA		900 mg/l GGA		2000 mg/l GGA	
	<i>Before</i>	<i>After</i>	<i>Before</i>	<i>After</i>	<i>Before</i>	<i>After</i>	<i>Before</i>	<i>After</i>
1	22 $\pm$ 4	23 $\pm$ 3	120 $\pm$ 13	138 $\pm$ 5	122 $\pm$ 7	133 $\pm$ 6	46 $\pm$ 22	67 $\pm$ 8
2	4 $\pm$ 2	1 $\pm$ 1	110 $\pm$ 12	131 $\pm$ 4	141 $\pm$ 15	142 $\pm$ 13	81 $\pm$ 23	92 $\pm$ 5
3	0	0	40 $\pm$ 15	52 $\pm$ 19	93 $\pm$ 32	115 $\pm$ 23	97 $\pm$ 16	95 $\pm$ 14
$\Sigma$	26 $\pm$ 4	24 $\pm$ 4	270 $\pm$ 23	323 $\pm$ 18	355 $\pm$ 50	389 $\pm$ 42	223 $\pm$ 50	254 $\pm$ 19

With each stage of MFCs the average stable current density increased as the GGA concentration increased up to 900 mg/l (540 mg/l O<sub>2</sub> BOD<sub>5</sub>). At 2000 mg/l GGA the current density was observed to decline in the first and second stage MFCs at the same time that > 80 vol% sludge was observed in the cell contents. On average, stable current densities were 21% higher immediately after sludge removal indicating that sludge presence was having an inhibitory effect on the anodic biofilm current generation (Table 5.4). The current loss could have been a result of decreased mass transfer to the biofilm (increased internal resistance)



due to sludge occupying the void volume of the anode chamber and thus reducing the residence time of the medium considerably.

The presence of sludge in the cell appeared to affect the baseline current of the MFC when the BOD<sub>5</sub> level was low (*i.e.* < 30 mg/l O<sub>2</sub>). For example, Figure 5.8 shows the response of the 'ABC' flow-mode MFCs from baseline current to an increase in BOD<sub>5</sub> (to a current-saturating concentration of 480 mg/l O<sub>2</sub>) and then returned to 30 mg/l O<sub>2</sub> (conducted before the sludge removal regime had begun). The response showed that the first and second stage MFCs (from which the most biomass was collected; Table 5.2) had relatively high baseline current densities of  $58 \pm 13$  and  $39 \pm 12 \mu\text{A}/\text{cm}^2$  compared to the third stage MFCs for which the baseline current density was  $11 \pm 1 \mu\text{A}/\text{cm}^2$ . The theoretical current density when no substrate is present is  $0 \mu\text{A}/\text{cm}^2$ ; therefore indicating that the sludge itself was retaining substrate which was consumed by the electrogenic biofilm when the feed was depleted. Extracellular polymeric substances (EPS) which are typically employed by bacteria for the assembly of a biofilm are known to also synthesise substrate storage compounds which are secreted from the bacterial cells (compounds such as polysaccharides; (de Souza and Sutherland, 1994; Nogaj *et al.*, 2015)). Alternatively, the sludge may prevent flushing of the anode chamber resulting in a 'reservoir' of medium providing substrate to the biofilm. The effect of the increased baseline current resulted in a decrease in the magnitude of the saturation current to baseline current ratio, which negatively impacted the ability to use the current generated by the MFC for sensing (especially with the first stage MFCs; Figure 5.8, arrows).

It was interesting to note that during the sludge removal procedure the anodic biofilm was resilient enough to withstand removal of the cells contents and exposure to air, and was still able to recover and reliably generate current when the feed was restored. In addition, despite a considerable amount of biomass covering the membrane between the anode and cathode (Figure 5.7c), the MFCs still generated electricity.

## Optimisation of Working Protocol

Fewer operational issues were experienced when the flow rate was increased as biomass accumulation in tubing fittings was reduced and thus blockages less likely. The hydraulic retention time (HRT) of the flow-system decreased as the flow rate increased (Figure 5.9), the unit HRT for each component and cumulative flow path HRT are listed in Table B.1 in Appendix B alongside component identification names. For each individual MFC, the unit HRT at 0.52 ml/min was 18.9 minutes and 7.6 minutes at 1.24 ml/min. The HRT from the medium bottle to the first, second and third stage MFCs was 53, 93 and 134 minutes respectively at 0.52 ml/min and 21, 37 and 53 minutes respectively at 1.24 ml/min.

Over the course operation, both due to cathodic performance degradation (Chapter 4, Section 4.3.5) and also leaks which developed, it was necessary to replace the membrane-

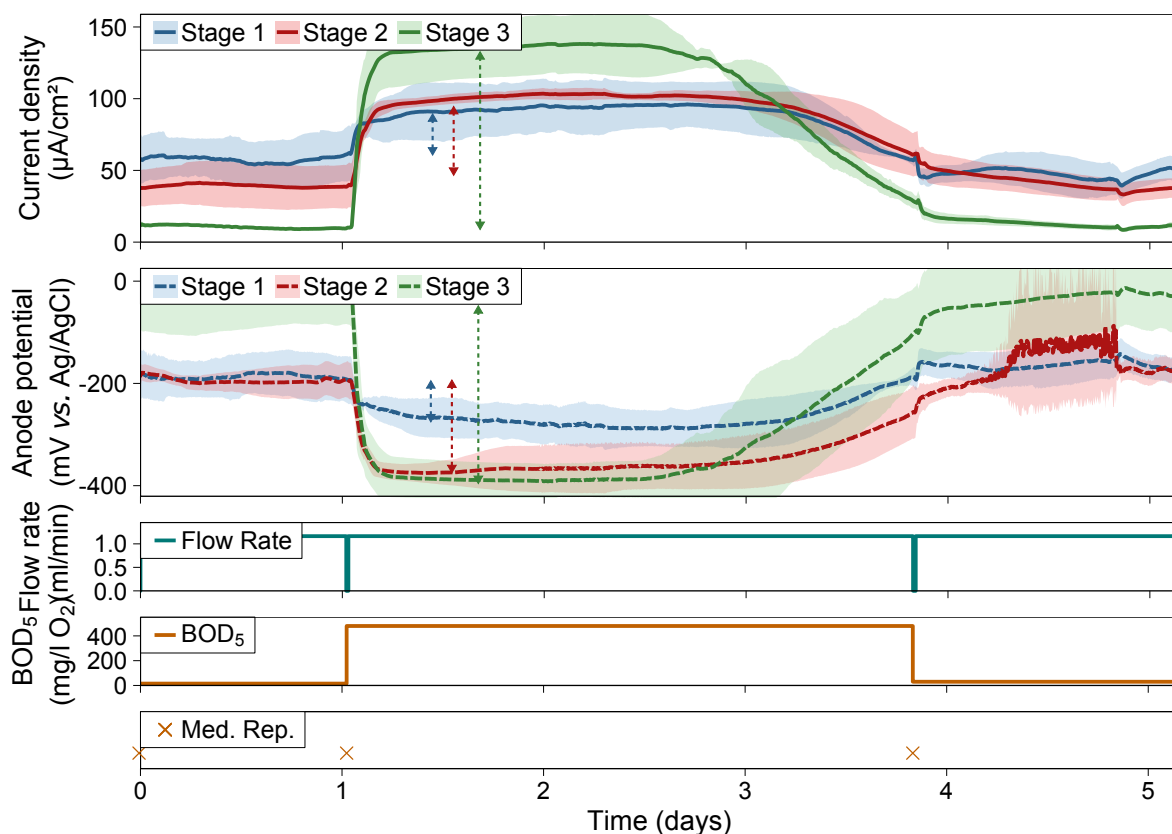


Figure 5.8: Average current density and anode potential response to an increase in  $BOD_5$  (estimated from GGA concentration) followed by return to baseline current of each stage of the 'ABC' flow-mode MFCs with biomass sludge present inside the MFCs. Shaded bands indicate  $\pm SD$  for the triplicate MFCs in each stage. Dashed arrows indicate the magnitude of change from baseline current/anode potential to saturation current/anode potential.

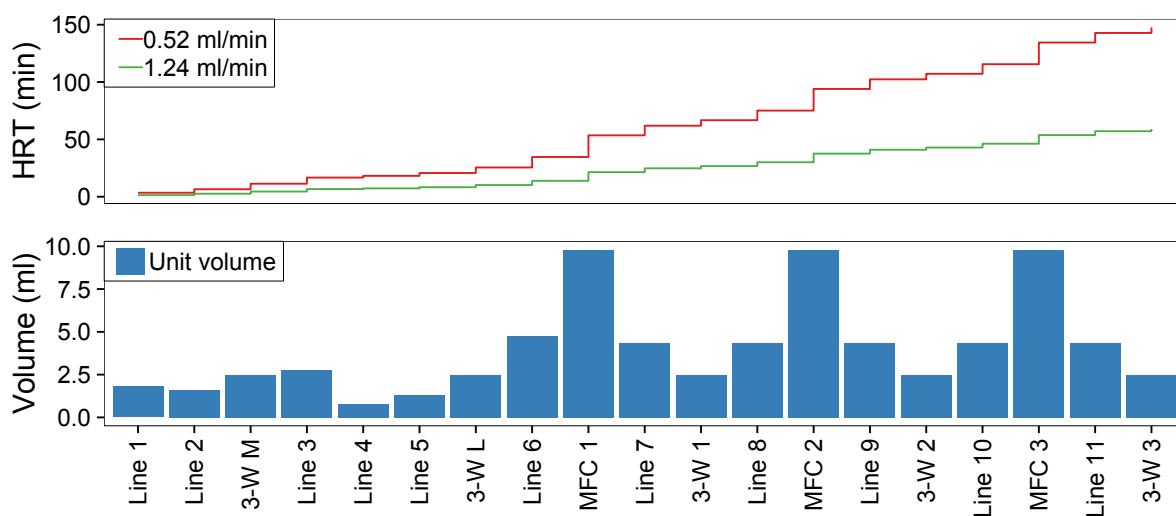


Figure 5.9: Cumulative HRT profile for the flow-mode system path at 0.52 and 1.24 ml/min and the unit volume of each component (corresponding data table is Table B.1 in Appendix B).

electrode assembly (MEA; replacements detailed in Table D.1 in Appendix D). On day 607 of the 'ABC' series of MFCs all nine of the MEAs were replaced (photograph in Figure F.1 in Appendix F) with freshly prepared membranes and electrodes to ensure the performance of each cell was not negatively affected by degraded cathodic performance (low cell voltage). For the 'DEF' series of flow-mode MFCs, the original GDEs were used for the entire 148 day experimental period.

It was observed that, when degraded GDEs were replaced, a deposit had accumulated on the membrane-covered surface (Figure 5.10a). Initially, the deposit was assumed to be a chemical compound precipitated by evaporation of the 2 mol/dm<sup>3</sup> phosphate buffer solution which was added to the GDE surface during assembly. To test for presence of bacterial cells, a cut-out section of a degraded GDE was stained with SYBR® Gold nucleic acid gel stain and imaged at 400× magnification (Figure 5.10b). The portion of electrode which was covered and compressed by the gasket fluoresced significantly less than the membrane-covered central portion. This indicated that there was fouling by microbial cells on the surface of the electrode and that the membrane had been breached. Thus it could be concluded that one reason for the degradation of the GDEs could be biofouling and/or membrane failure.

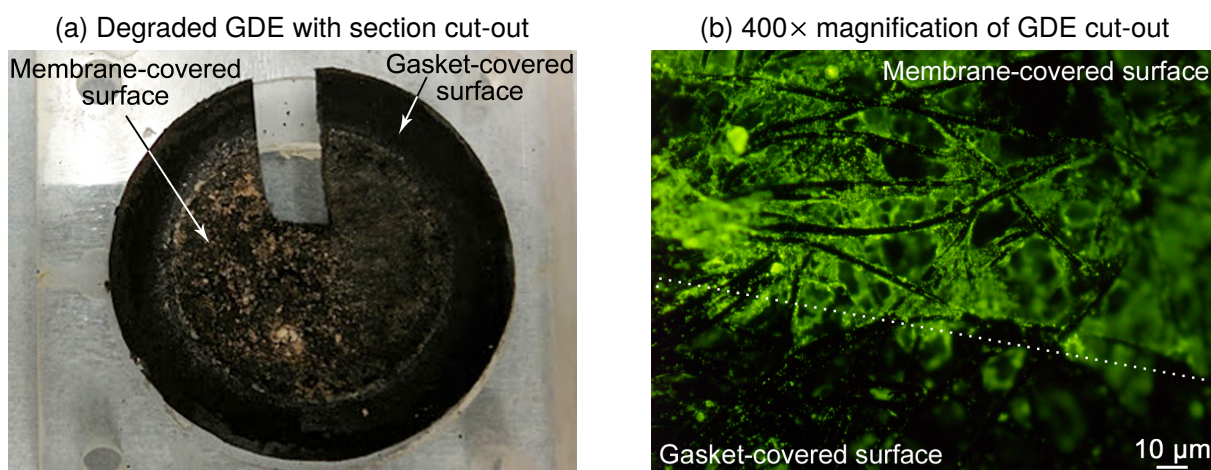


Figure 5.10: (a) Photograph and (b) microscope image of SYBR®Gold-stained, degraded GDE showing biofouling upon membrane-covered surface.

### 5.3.3 Biochemical Oxygen Demand Sensing & Calibration

In Calibration 1 (ABC) (Table 5.1), the 'bottle amendment' method was employed involving sequential injection of GGA into a bulk volume of medium to increase the BOD concentration. The response over 50 minutes for 8 concentrations in the range 15 to 324 mg/l O<sub>2</sub> BOD<sub>5</sub> was assessed (Figure 5.11). The response of the MFCs did not resemble the step-wise changes in BOD<sub>5</sub>, however an increase in current density was observed in the first stage followed by the second stage. The result indicated that, at 0.31 ml/min flow rate, 50 minutes was not sufficient to establish a stable current density. Subsequently, the remaining calibrations

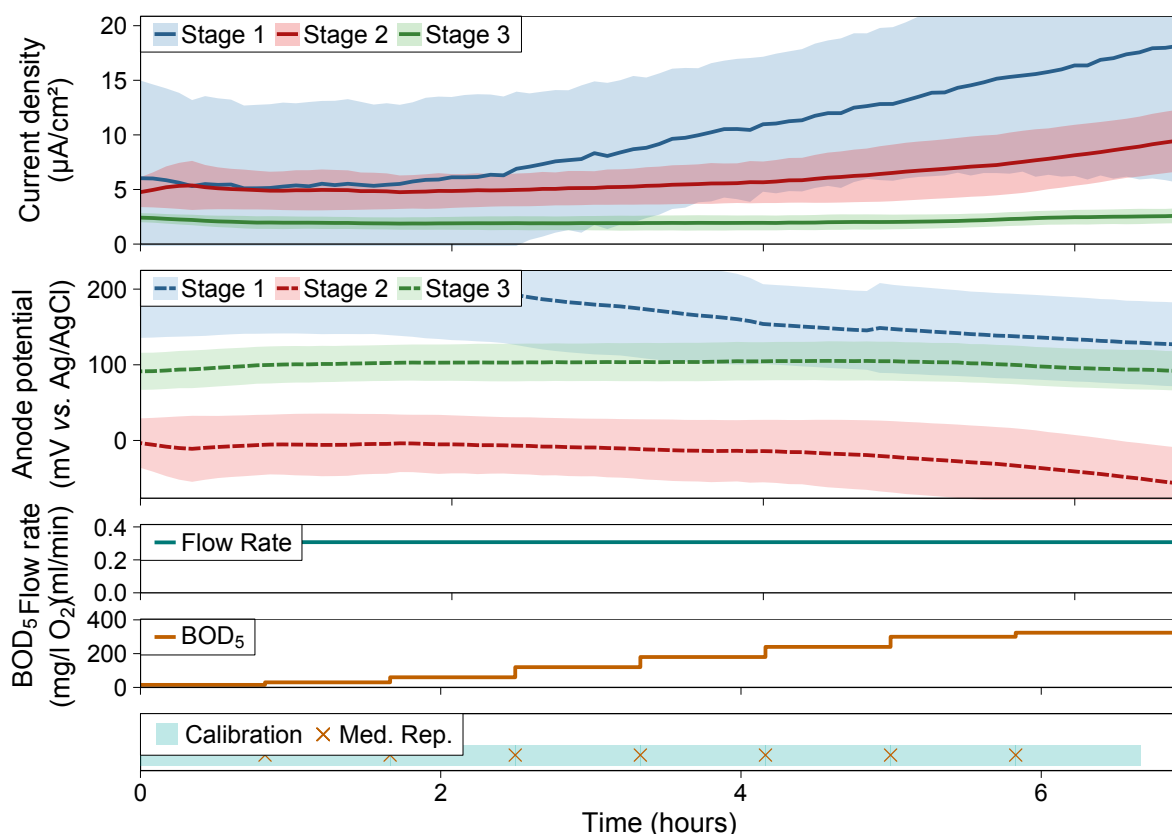


Figure 5.11: Average current density and anode potential response of three stages of 'ABC' flow-mode MFCs to changes in estimated BOD<sub>5</sub> with GGA substrate injections with the 'bottle amendment' method during Calibration 1 (ABC) at a fixed flow rate of 0.31 ml/min.

(Calibrations 2–7 (ABC) and 1 (DEF)) employed the 'bottle replacement' method over at least 5 hours per concentration (usually 1-3 days).

Of the seven BOD calibrations performed using the 'ABC' series of flow-mode MFCs, three (Calibrations 2, 4 & 5 (ABC); Table 5.1) had to be terminated mid-calibration due to GDE leakage problems from at least one MFC. The interruption prevented determination of the maximum current density of each cell at saturating concentrations and thus calibrations could not be normalised for comparison. Another calibration (Calibration 3 (ABC)) was performed with cathodes which had been operated for up to 336 days (and consequently performance was significantly decreased) and with biomass sludge present inside the reactor (increasing the baseline current). The operational issues led to a high degree of variability in the MFC response meaning that the linear regression coefficient was only  $R^2 = 0.803$ . The corresponding calibration curves resulting from Calibrations 2–5 (ABC) can be found in Appendix D. The final 'ABC' series calibrations (Calibrations 6 & 7 (ABC)) and the only 'DEF' series calibration (Calibration 1 (DEF)) were performed with sludge removal in between every medium bottle replacement in order to counteract the development of biomass over the course of the calibration period.

Calibration 6 (ABC) was carried out at a fixed flow rate of 0.52 ml/min with medium of between 1830 to 2745 ml volume fed to MFCs over the course of 1-3 days each (Figure 5.12). The

GGA range calibrated was 100 to 2000 mg/l (60 to 1199 mg/l O<sub>2</sub> BOD<sub>5</sub>). With each medium bottle cycle a steady current density was achieved after a period of stabilisation as the biofilms responded to changes in BOD<sub>5</sub>. When biofilms became saturated with substrate, maximum current densities ( $\bar{I}_{Max}$ ) of  $135 \pm 11 \mu\text{A}/\text{cm}^2$  for the first stage MFCs (1A, 1B & 1C),  $149 \pm 20 \mu\text{A}/\text{cm}^2$  for second stage MFCs (2A, 2B & 2C) and  $139 \pm 20 \mu\text{A}/\text{cm}^2$  for third stage MFCs (3A, 3B & 3C) were reached. This corresponded to an average limiting anode potential of  $-381 \pm 20$ ,  $-384 \pm 13$  and  $-345 \pm 36$  mV vs. Ag/AgCl for the first, second and third stage cells respectively.

Amperometric calibration curves of average stable current densities from each medium cycle were plotted against the known medium BOD<sub>5</sub> values (Figure 5.13). The linear model ( $y = mx + c$ ) was fitted to points from each stage which correlated with changes in BOD<sub>5</sub> until the current plateaued (Figure 5.13a). A linear response was observed for the average stable current densities in the range 60 to 360 mg/l O<sub>2</sub> BOD<sub>5</sub> ( $n = 5$ ) for the first stage MFCs with a slope of  $m = 0.445 \pm 0.047 \mu\text{A}/\text{cm}^2$  per mg/l O<sub>2</sub> BOD<sub>5</sub> and intercept of  $c = -7.57 \pm 10.30 \mu\text{A}/\text{cm}^2$ . The limits of detection and quantification were determined as LOD = 81 mg/l O<sub>2</sub> and LOQ = 245 mg/l O<sub>2</sub>. Substrate consumption by the first stage of MFCs led to a smaller current response from the second and third stages of MFCs (current remained below  $10 \mu\text{A}/\text{cm}^2$ ) until the BOD<sub>5</sub> in the feed was increased. Above 180 mg/l O<sub>2</sub>, current was generated by the second stage MFCs when the first stage biofilms became saturated with substrate and the current plateaued. The third stage MFCs generated current with medium containing over 480 mg/l O<sub>2</sub> BOD<sub>5</sub>. The linear response of the second and third stages was shifted to higher BOD<sub>5</sub> concentrations as a consequence of receiving depleted effluent from the upstream MFCs. The linear correlations obtained were in the range 240 to 540 mg/l ( $n = 6$ ) and 480 to 840 mg/l O<sub>2</sub> BOD<sub>5</sub> ( $n = 8$ ) respectively. The corresponding slopes were  $m = 0.445 \pm 0.091$  and  $0.304 \pm 0.042 \mu\text{A}/\text{cm}^2$  per mg/l O<sub>2</sub> BOD<sub>5</sub> and intercepts were  $c = -110.03 \pm 40.06$  and  $-140.49 \pm 25.41 \mu\text{A}/\text{cm}^2$  respectively.

The  $R^2$  for the individual stages was 0.967, 0.857 and 0.898 respectively indicating a positive correlation, the residual standard deviations were 10.91, 22.33 and  $14.45 \mu\text{A}/\text{cm}^2$  (8-15% of  $\bar{I}_{Max}$ ) and the regression  $p$ -values were all less than 0.05 indicating a statistically significant correlation.

The output from each stage of MFCs demonstrated the effect of hydraulically linking MFCs in series. With most BES applications, focused on generating electricity for energy or treatment purposes, multi-staged MFCs are stacked electrically in series or parallel because increased current and power densities have been observed (Ledezma *et al.*, 2013). For biosensing applications, achieving the highest electrochemical performance is not a priority and electrically isolated, hydraulically linked in series MFCs have been shown here for the first time to significantly enhance the BOD sensing range. The output from each MFC provides valuable information about how substrate is consumed through the hydraulic array which would not be accessible if the electrical signal was combined in a MFC stack.

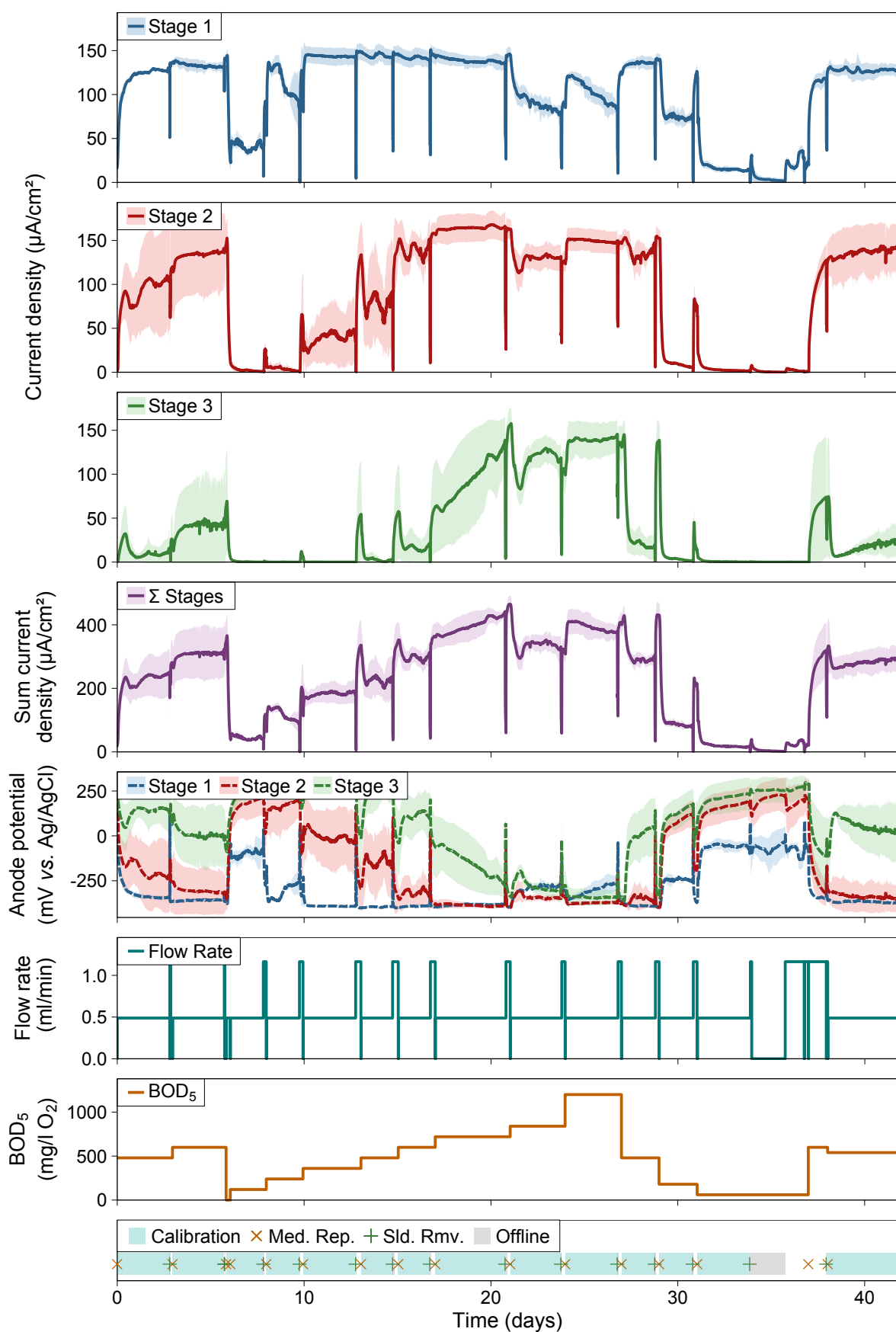


Figure 5.12: Average current density and anode potential response of three stages of 'ABC' flow-mode MFCs to changes in  $BOD_5$  (estimated from GGA concentration) during Calibration 6 (ABC) at a flow rate of 0.52 ml/min.

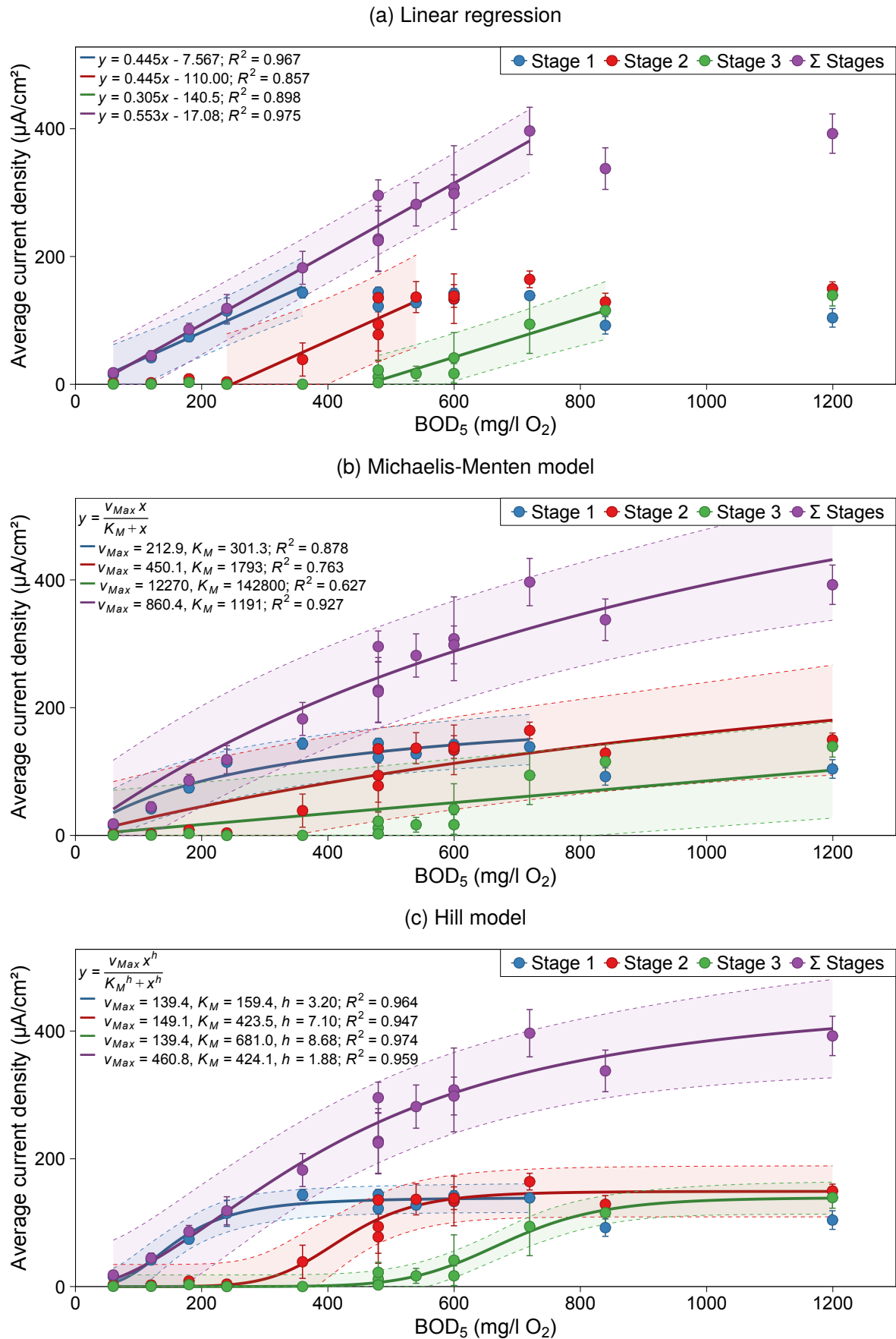


Figure 5.13: Average current density calibration curves fitted with (a) linear, (b) Michaelis-Menten and (c) Hill models against  $\text{BOD}_5$  (estimated from GGA concentration) for data obtained during Calibration 6 (ABC) of the flow-mode MFCs. Shaded bands represent the 95% prediction intervals from model lines and error bars are  $\pm\text{SD}$  from triplicate cells.

The sum of the current densities from each stage of MFCs was calculated for each logged data-point. A calibration curve was produced by plotting the average stable summed current density against BOD<sub>5</sub> (Figure 5.13,  $\Sigma$  Stages). The linear model fitted to the summed data exhibited an extended range (compared to the individual MFCs) of 60 to 720 mg/l O<sub>2</sub> BOD<sub>5</sub> ( $n = 12$ ). The fitted slope was  $m = 0.553 \pm 0.028 \mu\text{A}/\text{cm}^2$  per mg/l O<sub>2</sub> BOD<sub>5</sub> and intercept was  $-17.08 \pm 12.66 \mu\text{A}/\text{cm}^2$ . The regression statistics were  $R^2 = 0.975$ , residual standard deviation =  $19.59 \mu\text{A}/\text{cm}^2$  and the  $p$ -value was  $2.41 \times 10^{-9}$  indicating a high degree of linearity and statistically significant correlation. The average step-up response time to reach stable current was  $1.2 \pm 0.7$  hours and the step-down response time was  $7.4 \pm 3.5$  hours.

Michaelis-Menten (M-M) and Hill models were also fitted to the amperometric data up to the point at which inhibition was observed (a decrease in maximum current density due to substrate excess). The non-linear, fitted range for the first stage MFCs was 60 to 720 mg/l O<sub>2</sub> BOD<sub>5</sub> ( $n = 12$ ); whereas no inhibition was observed with the second and third stages so the entire calibration range was fitted (60 to 1199 mg/l O<sub>2</sub> BOD<sub>5</sub>,  $n = 14$ ). Similar to the batch-mode MFCs (discussed in Section 4.3.2 of Chapter 4), the Michaelis-Menten model did not correlate well with the observed measurements ( $R^2 = 0.627\text{--}0.927$ ,  $SD_{Res} = 15.89\text{--}34.68 \mu\text{A}/\text{cm}^2$  & lack-of-fit  $p$ -value =  $0.17\text{--}0.51$  (poor fit)). Consequently, M-M models were not used for simulating additional calibrations with flow-mode MFCs.

The Hill model increased the sensor range by successfully simulating the non-linear asymptotes of both the lag phase and saturation plateau in each stage of MFCs (Figure 5.13c). The fitted  $v_{Max}$  values of  $139.4 \pm 16.0$ ,  $149.0 \pm 34.2$ ,  $139.4 \pm 31.8$  and  $460.8 \pm 205.5 \mu\text{A}/\text{cm}^2$  were close to the experimentally determined values for the first, second, third and summed stages respectively ( $134.9$ ,  $149.4$ ,  $138.8$  and  $356.5 \mu\text{A}/\text{cm}^2$ ). The half maximal BOD<sub>5</sub> concentrations ( $K_M$ ) were  $159$ ,  $423$  and  $681$  mg/l O<sub>2</sub> for the first, second and third stages of MFCs respectively. The  $K_M$  values were concurrent with the trend observed in current generation by each stage of MFCs. Downstream MFCs did not generate current until higher concentrations were reached and substrate (present in the upstream MFCs effluent) entered the cells. Positive Hill coefficients were calculated for each stage's calibration with  $h = 3.20$ ,  $7.10$  and  $8.68$ . The increasing  $h$  values indicated an increasingly positive co-operativity in downstream MFCs; this was logical as the third stage MFCs were feeding from effluent of the first and second stage MFCs. The Hill-modelled calibrations had smaller prediction bands (Figure 5.13c) and therefore were able to resolve values more accurately than the M-M model (Figure 5.13b). The greater degree of correlation was quantified by the regression statistics of  $R^2 = 0.947\text{--}0.974$ ,  $SD_{Res} = 8.27\text{--}27.09 \mu\text{A}/\text{cm}^2$  and greater lack-of-fit  $p$ -values =  $0.61\text{--}0.97$ .

300 mg/l GGA medium (with BOD<sub>5</sub> =  $179.9 \pm 9.4$  mg/l O<sub>2</sub>) was measured by the multi-staged MFCs; the stable current densities and predicted BOD<sub>5</sub> values by the calibrated linear and Hill models are given in Table D.2 in Appendix D. For 300 mg/l GGA the recorded current



densities were 74.2, 8.5 and 3.0  $\mu\text{A}/\text{cm}^2$  for the sequential stages of MFCs and 85.9  $\mu\text{A}/\text{cm}^2$  for the summed current density. Thus, the second and third stages were inaccurate at predicting the  $\text{BOD}_5$  value as the current was so low. The linear and Hill models calibrated to the first stage MFCs and summed current density predicted the  $\text{BOD}_5$  values with mean percentage error of +2–3% (+4–6 mg/l  $\text{O}_2$ ) and  $\pm 8\%$  ( $\pm 14$  mg/l  $\text{O}_2$ ) respectively. Therefore, the calibrated flow-mode MFC response achieved better accuracy than the accepted standard deviation of  $\pm 15\%$  (30 mg/l  $\text{O}_2$ ) in the  $\text{BOD}_5$  test.

Figure 5.14 shows the predicted  $\text{BOD}_5$  values by the linear and Hill calibration models. The linear models for the second and third stage MFCs were incapable of predicting  $\text{BOD}_5$  values below 240 and 480 mg/l  $\text{O}_2$  respectively. The Hill models however predicted lower concentration values closer to (but still over-estimates of) the true  $\text{BOD}_5$  values.

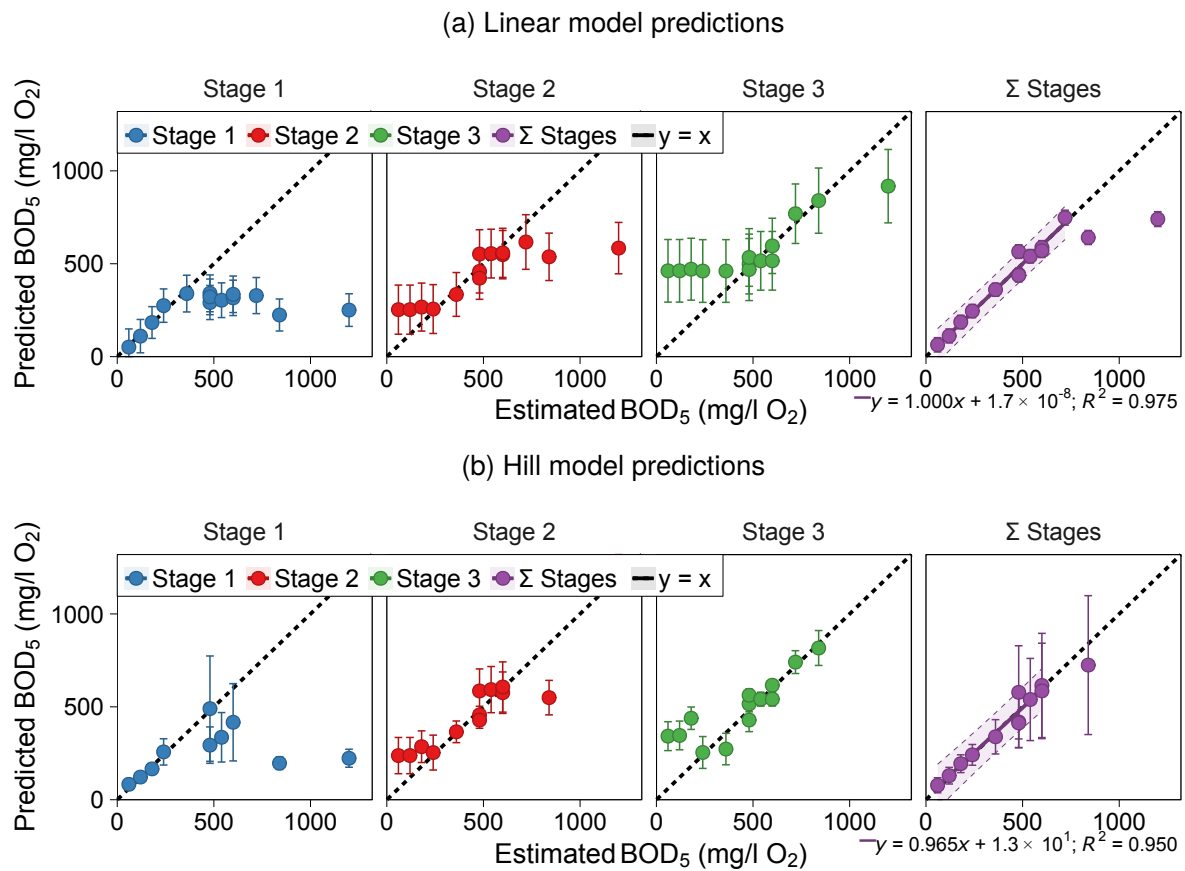


Figure 5.14: Predicted  $\text{BOD}_5$  plotted against estimated  $\text{BOD}_5$  (from GGA concentration) for values predicted by the (a) linear and (b) Hill calibration models using current densities obtained during Calibration 6 conducted with the 'ABC' cells. A linear regression line and 95% prediction band is shown for the ' $\Sigma$  Stages' predicted values.  $y = x$  is shown as the 'ideal' prediction. Outliers with a Predicted  $\text{BOD}_5$  above 1000 mg/l  $\text{O}_2$  were removed from the Hill plot as the error bars were outside the limits of the model.

Above the concentration at which the current densities plateaued, the prediction models were incapable of estimating  $\text{BOD}_5$  values accurately. Linear regression lines were calculated for the ' $\Sigma$  Stages' predicted values (Figure 5.14a and 5.14b, purple lines). It is evident by the size of the 95% prediction bands and  $R^2$  values that the linear model was capable of

resolving BOD<sub>5</sub> values more accurately than the Hill model (within its range limits). The linear prediction model is close to ideal ( $y = x$ ) with a regression equation of  $y = x + 1.7 \times 10^{-8}$ . The Hill prediction model could theoretically be used for the full calibration range, however it only exhibited linearity below 600 mg/l O<sub>2</sub> (when current densities were below  $v_{Max}$ ). Above the concentration of  $K_M$ , as summed current densities approached  $v_{Max}$ , error bars became very large and prediction resolving power was lost. The Hill equation was convenient for description of a calibration using  $v_{Max}$ ,  $K_M$  and  $h$  but did not have the prediction power of the linear models.

#### 5.3.4 Effect of Flow Rate on BOD Sensor Calibration

Calibration 7 (ABC) of the flow-mode MFCs was carried out at 1.24 ml/min to assess the effect of flow rate in comparison to Calibration 6 (ABC) at 0.52 ml/min. Medium bottles of 2745 to 5632 ml volume (1-3 days feed) were used to calibrate a GGA range of 42.5 to 2000 mg/l (25 to 1199 mg/l O<sub>2</sub> BOD<sub>5</sub>; Figure 5.15). As with the previous calibrations a steady current density was achieved after a period of stabilisation, at this flow rate the step-up response time was  $2.6 \pm 2.4$  hours and step-down response was  $2.3 \pm 2.0$  hours (falling between the response times at 0.52 ml/min). The response time appeared to be lengthened by previous starvation of downstream (third stage) MFCs (Figure 5.15, Stage 3 current density). Maximum current densities ( $\bar{I}_{Max}$ ) were determined as  $121 \pm 13 \mu\text{A}/\text{cm}^2$  for the first stage MFCs (1A, 1B & 1C),  $140 \pm 14 \mu\text{A}/\text{cm}^2$  for second stage MFCs (2A, 2B & 2C) and  $118 \pm 32 \mu\text{A}/\text{cm}^2$  for third stage MFCs (3A, 3B & 3C). The maximum current densities were 9–21  $\mu\text{A}/\text{cm}^2$  less than those observed during Calibration 6 (ABC) (this could be attributed to GDE degradation or decreased HRT). The saturation of the anode biofilm resulted in average limiting anode potentials of  $-378 \pm 22$ ,  $-366 \pm 35$  and  $-312 \pm 35$  mV vs. Ag/AgCl for the first, second and third stage cells respectively (up to 33 mV more positive than those observed at 0.52 ml/min).

The average stable current densities were plotted against medium BOD<sub>5</sub> concentrations to produce amperometric calibration curves (Figure 5.16). The linear models (Figure D.2 in Appendix D) correlated well with measured BOD<sub>5</sub> values indicated by the regression statistics of  $R^2 = 0.912\text{--}0.952$ ,  $SD_{Res} = 8.3\text{--}25.8 \mu\text{A}/\text{cm}^2$  and regression  $p$ -values =  $1.15 \times 10^{-7}\text{--}1.22 \times 10^{-11}$  (significant). The Hill equation also fitted the calibration data ( $n = 29$ ; Figure 5.16) with regression statistics of  $R^2 = 0.930\text{--}0.970$ ,  $SD_{Res} = 10.1\text{--}25.7 \mu\text{A}/\text{cm}^2$  and lack-of-fit  $p$ -values of 0.14–0.84 (model fitted data).

The linear BOD<sub>5</sub> detection ranges were 25–180 mg/l, 60–240 mg/l and 120–420 mg/l O<sub>2</sub> for the first, second and third stages of MFCs respectively. The linear detection range of the summed current density was 60–300 mg/l O<sub>2</sub> BOD<sub>5</sub>. The corresponding Hill-modelled  $K_M$  values were  $102 \pm 33$ ,  $171 \pm 22$ ,  $268 \pm 80$  and  $167 \pm 30$  mg/l O<sub>2</sub>. The correlations indicated that the effect of increasing the flow rate (reducing the HRT) had decreased the linear

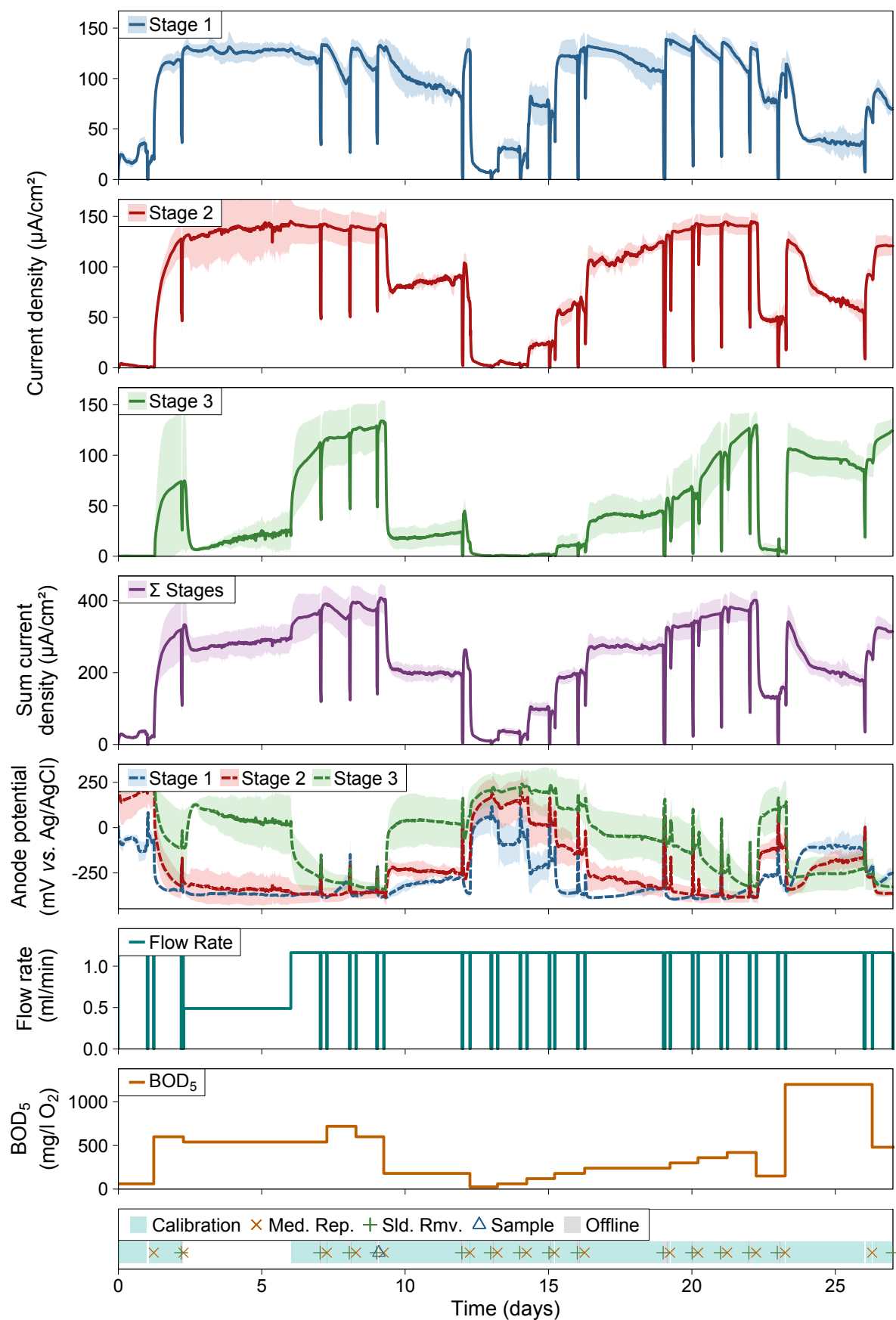


Figure 5.15: Average current density and anode potential response of three stages of 'ABC' flow-mode MFCs to changes in BOD<sub>5</sub> (estimated from GGA concentration) during Calibration 7 (ABC) at a flow rate of 1.24 ml/min.

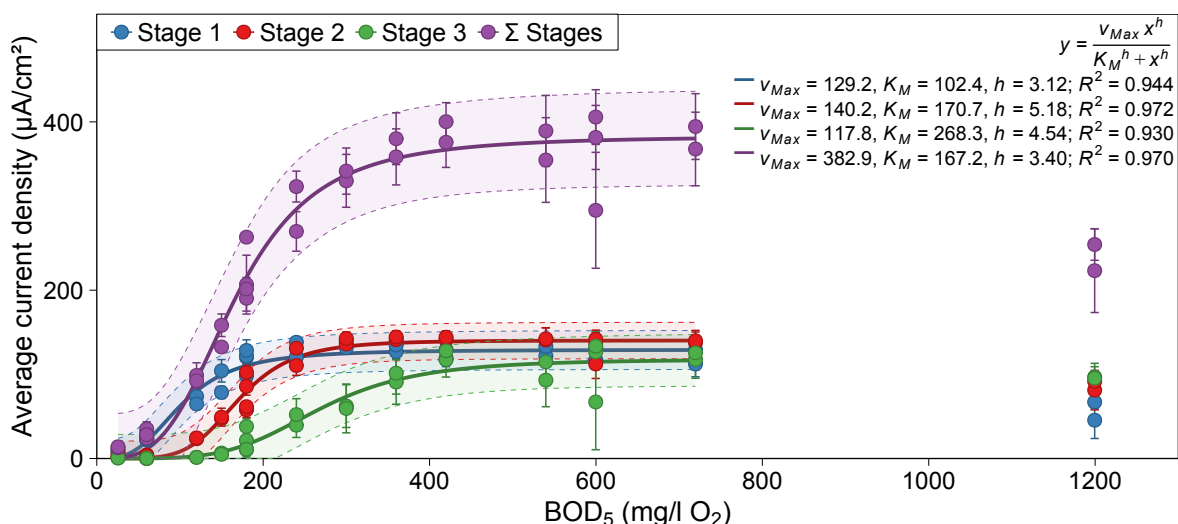


Figure 5.16: Average current density calibration curves fitted with the Hill equation against  $\text{BOD}_5$  (estimated from GGA concentration) for data obtained during Calibration 7 (ABC) of the flow-mode MFCs. Shaded bands represent the 95% prediction intervals from model lines and error bars are  $\pm\text{SD}$  from triplicate cells.

detection range of the MFC sensor array. Alternatively, it could be said that the increased flow rate decreased the concentration at which point the biofilm became saturated with substrate (due to increased mass transfer). The fitted Hill coefficients were  $h = 3.12$ , 5.18 and 4.54 for the first, second and third stage respectively. The  $h$  values were less than the corresponding values in the 0.52 ml/min calibration; thus the co-operativity or dependence of the downstream MFCs on upstream MFCs was reduced.

At 1.24 ml/min and  $\text{BOD}_5$  concentration of 1199 mg/l  $\text{O}_2$  (2000 mg/l GGA), current decrease due to substrate excess inhibition was observed in all stages of cells (Figure 5.16). As was shown in Table 5.2 above, at this concentration, sludge was observed in all MFCs. With the same concentration at 0.52 ml/min, substrate excess current loss was only observed in the first stage MFCs (Figure 5.13c). This result therefore indicated that the reduced residence time at higher flow rates caused downstream MFCs to become exposed to excessive amounts of substrate.

The first calibration of the 'DEF' series of MFCs (Calibration 1 (DEF); Table 5.1) was carried out using the same configuration and under the same conditions as Calibration 7 (ABC) (at 1.24 ml/min). The resulting current densities were normalised by dividing by the maximum achieved current density in each calibration to allow comparisons to be made without the influence of GDE degradation. Figure 5.17 shows the Hill-modelled response for the combined data from the 'ABC' seventh calibration and 'DEF' first calibration (Figure D.3 in Appendix D shows the linear modelled response).

It is evident that the same behaviour was observed with the flow-mode cells that was previously observed with the batch-mode cells (Section 4.3.3 of Chapter 4). The two calibrations overlaid each other and the between-calibration variation was not more than the within-calibration

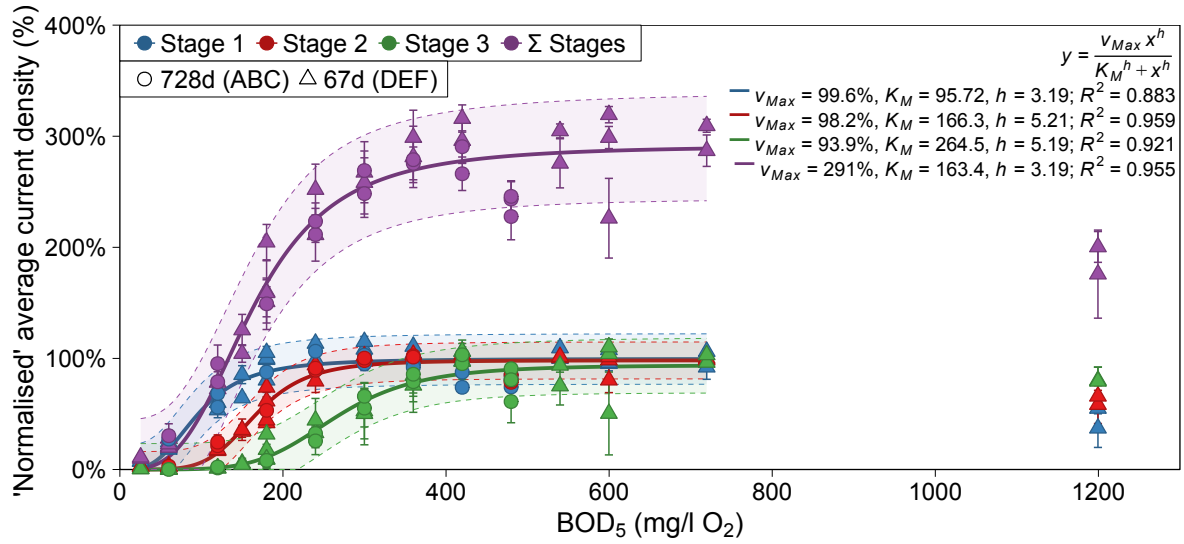


Figure 5.17: Normalised average current density calibration curves fitted with the Hill equation against BOD<sub>5</sub> (estimated from GGA concentration) for data obtained during Calibration 7 of the 'ABC' series (●) and Calibration 1 of the 'DEF' series (▲) of flow-mode MFCs. The  $\Sigma$  Stages data is normalised to 300% (sum of three MFC stages) to permit comparisons to non-normalised data for convenience. Shaded bands represent the 95% prediction intervals from model lines and error bars are  $\pm$ SD from triplicate cells.

variation. The combined calibration with normalised data had  $K_M$  values of 96, 166 and 265 mg/l O<sub>2</sub> BOD<sub>5</sub> for the first, second and third stages of MFCs respectively (within  $\pm$  8 mg/l O<sub>2</sub> of the values determined for the 'ABC' calibration in isolation). The corresponding  $h$  values were also approximately the same. The linear regression statistics were;  $R^2 = 0.937$ – $0.968$ ,  $SD_{Res} = 7$ – $17$  % of  $v_{Max}$  and  $p$ -values were less than  $3.14 \times 10^{-12}$ .

For the Hill models the statistics were  $R^2 = 0.883$ – $0.959$  and  $SD_{Res} = 8$ – $22$  %. The Hill-modelled, lack-of-fit  $p$ -values were less than the significance level of 0.05, indicating that the model did not fit accurately. Because the linear regression was statistically significant it is thought that the lack-of-fit is due to fitting of data in the high concentration, non-linear asymptote. Wide variations in saturation current densities resulted in some normalised data values exceeding 100% (e.g. at 300 mg/l O<sub>2</sub> BOD<sub>5</sub>) and others which were much less than 100% (e.g. at 480 and 600 mg/l O<sub>2</sub> BOD<sub>5</sub> in Figure 5.17). The over-normalised values were because an average, maximum current density was used for normalisation. The under-normalised values appeared to be associated with medium cycles following periods of starvation (e.g. day 6 in Figure 5.15). GDE degradation over the calibration period could have also contributed to under-normalisation.

Figure 5.18 shows the predicted BOD<sub>5</sub> values from the combined linear and Hill models for the 1.24 ml/min calibrations. As was observed previously at 0.52 ml/min, the linear model had a higher prediction power and for measurements outside of the range limits the prediction was a fixed maximum or minimum value. The Hill-predicted values show that, above the  $K_M$  value in each stage of cells, there is a large amount of uncertainty in predicted values where the current density was close to  $v_{Max}$ . It is for this reason the model does not statistically fit

the whole calibration range but below 300 mg/l O<sub>2</sub> BOD<sub>5</sub> there is a linear correlation with equation  $y = 0.987x + 12$  and correlation coefficient of  $R^2 = 0.939$ .

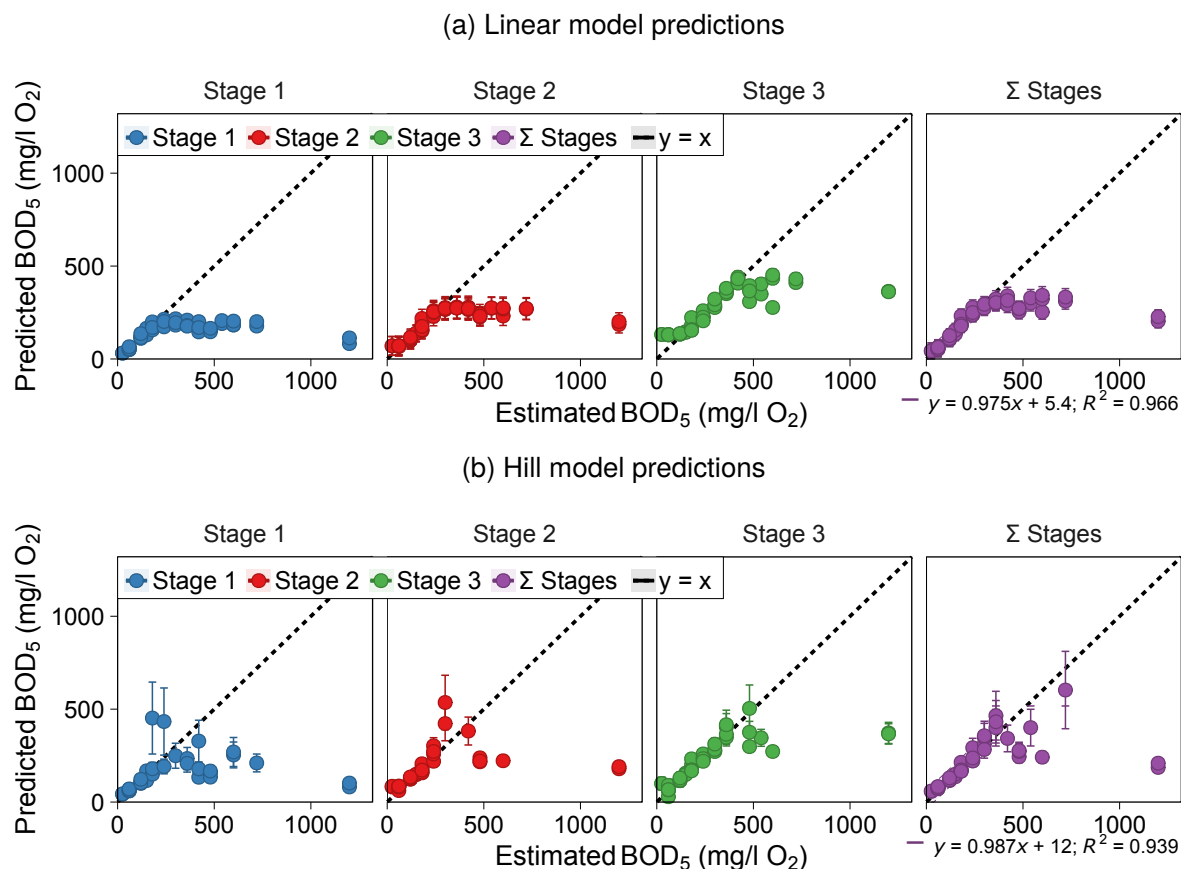


Figure 5.18: Predicted BOD<sub>5</sub> plotted against BOD<sub>5</sub> (estimated from GGA concentration) for values predicted by the (a) linear and (b) Hill calibration models shown in Figure 5.17 using current densities obtained during both Calibrations 7 (ABC) and 1 (DEF). A linear regression line and 95% prediction band is shown for the 'Σ Stages' values.  $y = x$  is shown as the 'ideal' prediction. Outliers with a Predicted BOD<sub>5</sub> above 1000 mg/l O<sub>2</sub> were removed from the Hill plot as the error bars were outside the limits of the model.

The Hill models fitted using data from experiments conducted at 0.52 and 1.24 ml/min were compared (Figure 5.19). The extension of the detection range is illustrated at lower flow rates. In all stages the higher flow rate achieved maximum current density at lower concentrations (indicated by half-maximal concentration,  $K_M$ ). The Hill equations of the first stage MFCs were quite similar owing to the fact that the cells receive relatively non-degraded medium at the inlet port. As was discussed in Section 5.3.2 above, the increased hydraulic retention time at 0.52 ml/min means that medium takes an extra 56 minutes to reach the second stage MFCs and 81 minutes extra to reach the third stage MFCs (in comparison to 1.24 ml/min; Figure 5.9). This is reflected in Figure 5.19 by the 'lag' observed before current is generated by the second and third stages. The increased residence time at lower flow rates means that greater BOD consumption occurs within the upstream MFC chambers which causes the resulting feed which enters the downstream MFCs to be more depleted. Thus, no current was observed with the downstream MFCs until the BOD<sub>5</sub> concentration increased sufficiently

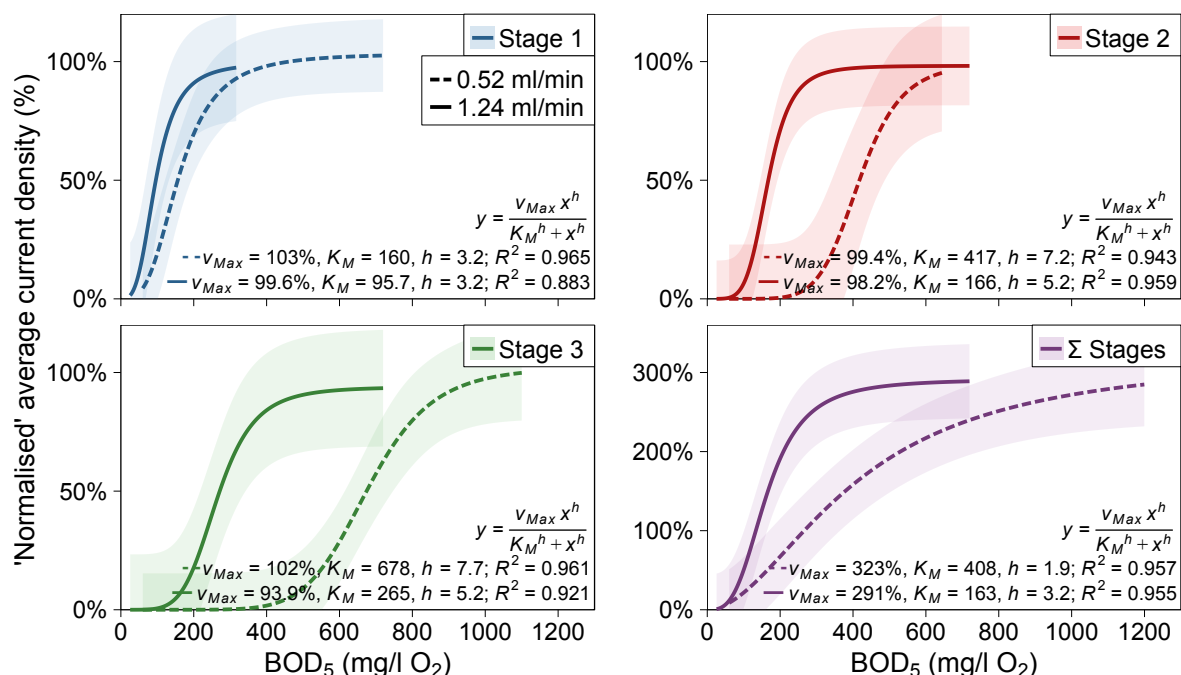


Figure 5.19: Hill-modelled, amperometric calibration curves using average data obtained from estimated BOD<sub>5</sub> calibrations of the three-stage, flow-mode MFCs at 0.52 ml/min (dashed lines) and 1.24 ml/min (solid lines). The Σ Stages data is normalised to 300% (sum of three MFC stages) to permit comparisons to non-normalised data for convenience. Shaded bands represent the 95% prediction intervals from model lines.

to saturate the upstream MFC biofilms.

The results of this study demonstrate that the flow rate could be used to fine-tune operating conditions for establishing a working range for a desired wastewater application of BES-based BOD sensing. It has been shown that the response of the flow-mode MFCs was the same on day 728 of operating the 'ABC' series of cells compared to a new calibration with separately inoculated MFCs on day 67 of the 'DEF' series. It appears that, for the same medium composition, the calibration was fixed by the architecture and operating conditions (*i.e.* flow rate and  $R_{Ext}$ ) and did not drift over time. This is an important finding in terms of implications for long term operational stability and recalibration requirements of commercial, BES-based BOD sensors.

### 5.3.5 MFC Performance Measurement by Electrochemical Analysis

The electrochemical performance of the three-stage MFCs was recorded prior to inoculation and at the end of the experimental period (after 756 and 144 days for 'ABC' and 'DEF' cells respectively). Cyclic voltammograms (Figure 5.20) and corresponding linear sweep voltammograms (Figure E.5 in Appendix E) were measured on each cell in the hydraulic arrays under a constant flow rate of 1.24 ml/min to ensure a constant supply of substrate to the cells.



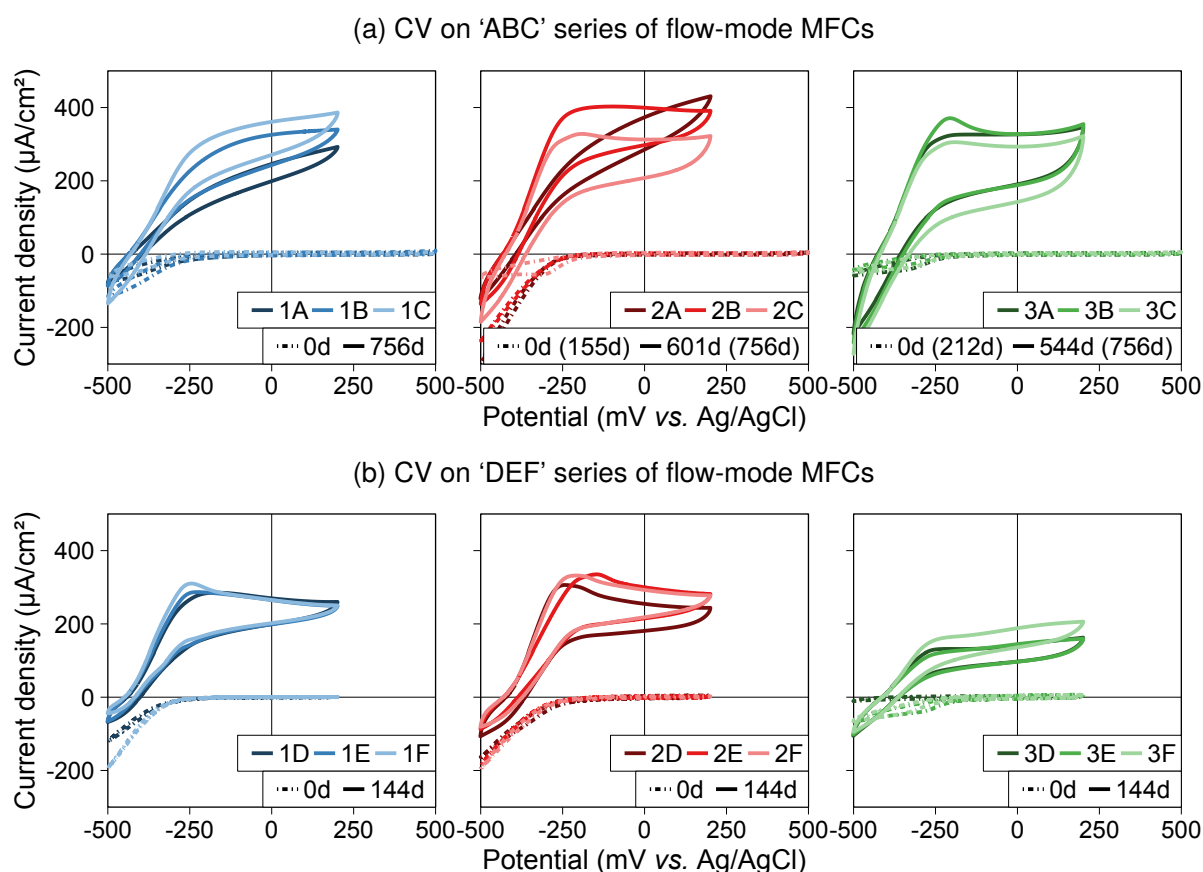


Figure 5.20: Cyclic voltammograms measured at 5 mV/s on the flow-mode MFCs in the (a) 'ABC' and (b) 'DEF' series. The days after inoculation the CV was measured is given in the legend (with days of series operation in brackets).

In all cases an oxidation wave was present in the enriched biofilm voltammograms. The onset potentials (at which point positive current was observed) became more negative down the hydraulic array with an average potential of  $-377.4 \pm 11.5$ ,  $-403.5 \pm 16.4$  and  $-416.0 \pm 10.9$  mV vs. Ag/AgCl for the first, second and third stage 'ABC' MFCs respectively. The same trend was observed with the 'DEF' MFCs with average values of  $-384.6 \pm 1.2$ ,  $-390.7 \pm 5.8$  and  $-421.5 \pm 10.7$  mV vs. Ag/AgCl. This observation implied that the third stage MFC biofilms were a better biocatalyst for substrate oxidation (lowered overpotential), possibly due to the presence of less biomass sludge or the result of receiving more-readily oxidised, degraded substrates from the effluent of the upstream MFCs.

The first derivative cyclic voltammograms (Figure E.6 in Appendix E) exhibited a single redox couple at a formal potential of approximately  $-357$  mV vs. Ag/AgCl (similar to the observation for a batch-mode MFC in Section 4.3.5 of Chapter 4). The redox peak in this position potentially confirmed the presence of cytochromes consistent with *Geobacter sulfurreducens*, a commonly found bacteria associated with electricity generation in MFCs (Fricke *et al.*, 2008).

Analysis by electrochemical impedance spectroscopy (EIS) enabled the ohmic resistance ( $R_{\Omega}$ ) to be calculated for each MFC. With the 'ABC' series of flow-mode cells  $R_{\Omega} = 72.0 \pm 3.7$ ,



$70.8 \pm 2.5$  and  $70.8 \pm 3.2 \Omega$  for the first, second and third stage MFCs respectively. The 'DEF' series exhibited the same trend with decreasing ohmic resistance down the hydraulic series ( $R_{\Omega} = 74.6 \pm 2.8$ ,  $69.9 \pm 1.8$  and  $66.9 \pm 1.7 \Omega$ ). The increased ohmic resistance ( $R_{\Omega}$ ) in the EIS spectra of the upstream MFCs indicated electron transport to the biofilm or ion transport within the bulk solution was more limited in those cells (potentially a decrease in the ionic conductivity of the anodic chamber).

Polarisation and power density curves were measured on day 754 of the 'ABC' series of flow-mode MFCs (Figure 5.21). The average peak power densities were observed to increase

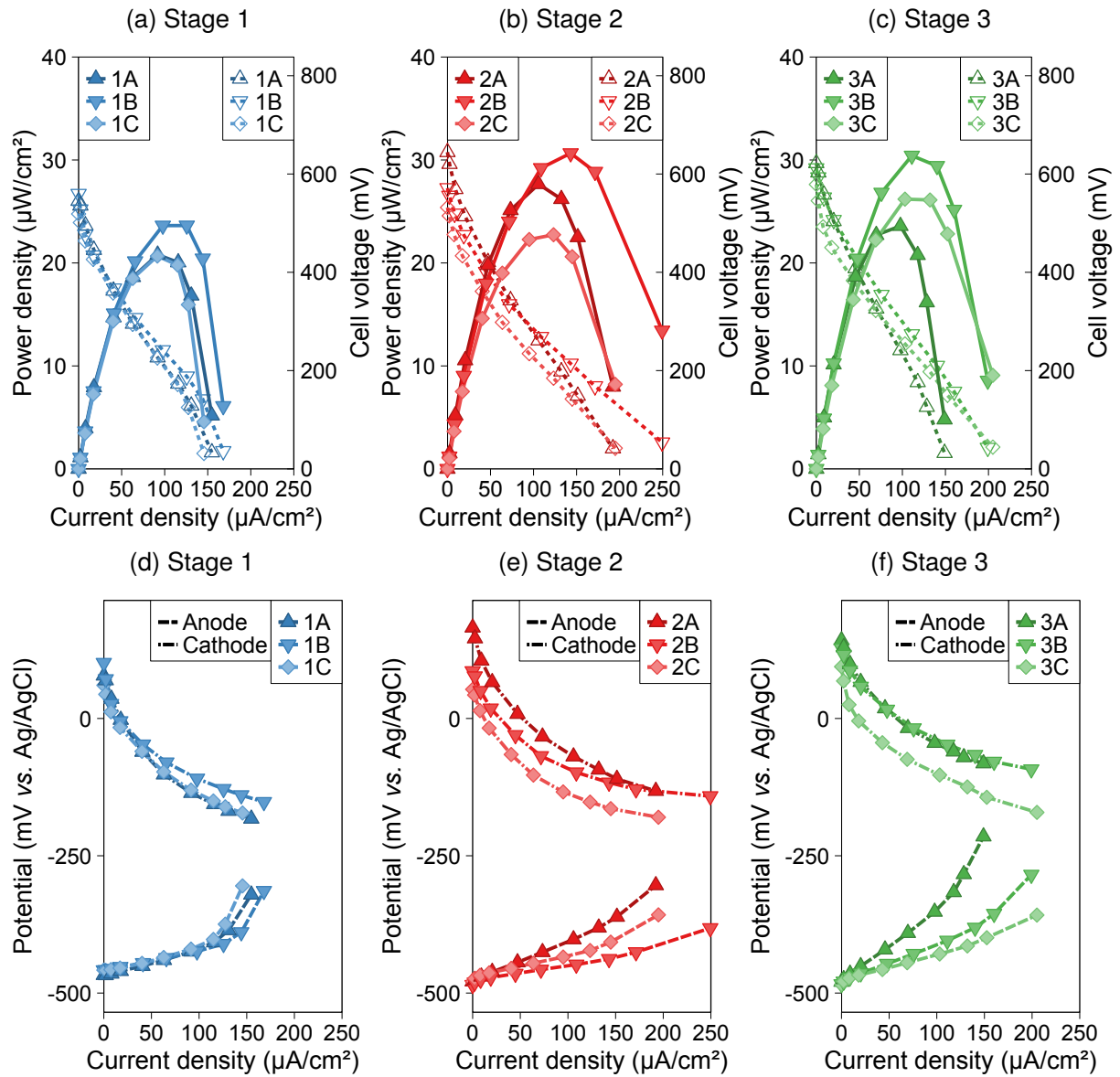


Figure 5.21: (a–c) Polarisation and power density curves and (d–f) anode and cathode potentials recorded on 'ABC' flow-mode cells on day 754 of operation using 480 mg/l  $O_2$  BOD<sub>5</sub> medium.

down the hydraulic series; calculated as  $21.7 \pm 3.6$ ,  $26.5 \pm 6.4$  and  $26.7 \pm 9.0 \mu W/cm^2$  for the first, second and third stages of MFCs. The corresponding external resistor at peak power was between 305 and 503  $\Omega$  (the operational  $R_{Ext}$  was 305  $\Omega$ ). The average maximum current

densities were  $156.1 \pm 13.3$ ,  $212.2 \pm 57.1$  and  $184.4 \pm 50.2 \mu\text{A}/\text{cm}^2$  for the first, second and third stages respectively.

The cell OCP increased down the hydraulic array from 541 to 582 to 604 mV. Figure 5.21d–f shows that the first stage MFCs were more cathode-limited than the other stages (cathode curves steeper relative to the gradient of anode curves), whereas the third stage MFCs was more anode-limited (steeper anode curves) but had higher variability. The corresponding first, second and third stage electrode average OCPs were –461, –481 and –482 mV vs. Ag/AgCl for the anodes and 80, 102 and 122 mV vs. Ag/AgCl for the cathodes. The first stage MFCs had less positive cathode potentials and more positive anode potentials; indicating a more degraded cathode and potentially a less electrogenic anodic biofilm community.

The range of electrochemical techniques have pointed to an improvement in electrochemical performance down the hydraulic series (from first stage to third stage). Sludge build-up is known to have been an issue most prevalent inside the first stage MFCs and this may have caused a reduction (and inhibition at very high concentration) of performance. The electrochemical performance was reduced by the presence of sludge causing the ionic conductivity to decrease in the bulk solution (increasing  $R_{\Omega}$ ) and/or MEA biofouling resulting in degradation of cathodic performance. Ionic conductivity could be reduced by the sludge preventing the medium replenishment to the anodic chamber (feed bypassed directly from cell inlet to outlet), resulting in depletion of conductive nutrient ions within the sludge/chamber.

### **5.3.6 Substrate Utilisation Across the Hydraulic Array of MFCs**

During Calibration 7 (ABC) of the flow-mode MFCs, samples were taken from the spent medium bottles and three-way sampling valves along the hydraulic array (using valves 3-W L, 1, 2 and 3; Figure 5.2). Various measurements were made to determine substrate utilisation and processes occurring across the array of MFCs. For the majority of samples ( $n = 16$  sets) the pH and conductivity was measured immediately after sampling. Seven sets of samples (from positions M, L, 1, 2 and 3) were measured using a photometric COD assay kit; specifically, samples from medium cycles where the initial concentration was 120, 150, 240, 300, 360, 600 and 1199 mg/l  $\text{O}_2$  BOD<sub>5</sub>. Furthermore, the samples from the 120, 240, 360 and 1199 mg/l  $\text{O}_2$  BOD<sub>5</sub> medium cycles were additionally analysed using enzymatic assays for glucose and glutamic acid. DOC, IC, VFAs and anions were also analysed in these samples to give a more detailed overview of substrate degradation (Figure 5.22 & Figure D.4 in Appendix D).

#### **pH**

The medium pH was found to decrease with increased BOD<sub>5</sub> values (Figure 5.22, pH). The acidity was likely caused by increased concentration of glutamic acid (a 11.25 g/l concentrated

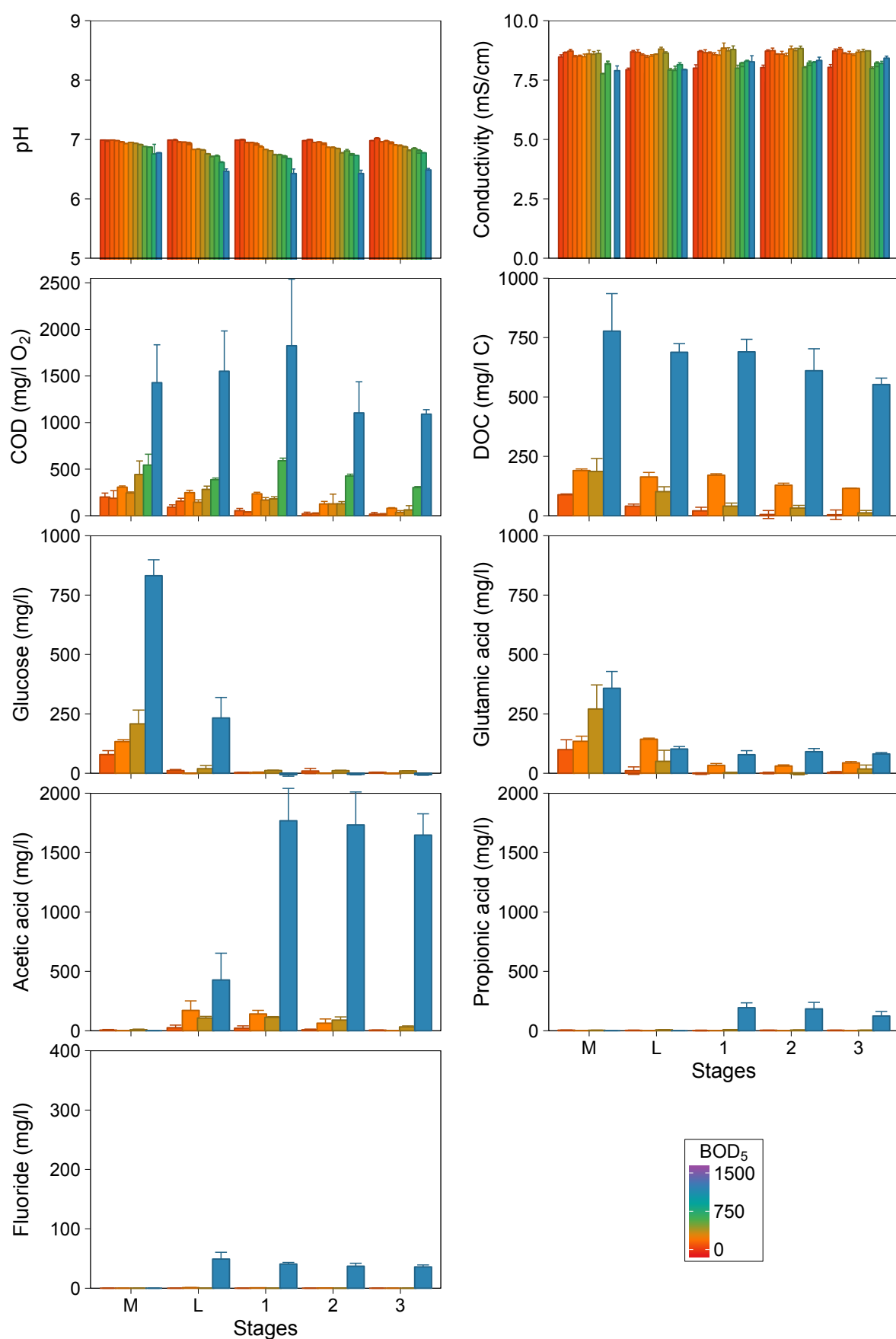


Figure 5.22: Average measured chemical parameters of samples obtained during Calibration 7 (ABC) of the flow-mode MFCs. Bars are coloured according to the estimated  $BOD_5$  of the as-prepared GGA medium. Number of bars indicates number of samples measured for each technique. Sampling was performed at the 3-W valves at medium bottle (M), feed line (L) and after each MFC (1, 2, 3). Error bars are  $\pm$ SD from triplicate cells. Supplementary data is Figure D.4 in Appendix D.

stock solution had a pH of 3.25). The pH was 6.99 and 6.77 for GGA medium containing 25 and 1199 mg/l O<sub>2</sub> BOD<sub>5</sub> respectively. As medium passed through the hydraulic system, the sharpest decrease in pH was observed between medium bottle and the feed line after the UV lamp and peristaltic pump (3-W L), for example at 1199 mg/l O<sub>2</sub> BOD<sub>5</sub> (2000 mg/l GGA) the decrease was 0.31 units to pH 6.46. The reason for the decline could be due to in-line fermentation to produce VFAs. The UV lamp was not expected to cause oxidation of glucose or glutamic acid at 254 nm (Wang *et al.*, 2001). In all cases after this initial decrease, the pH increased as the medium passed through each MFC; this was attributed to the consumption of glutamic acid and fermentation products including VFAs (as measured by the chemical analyses).

## Conductivity

Conductivity remained approximately constant with an average of  $8.34 \pm 0.37$  mS/cm and no trends were observed with changes in BOD<sub>5</sub> or as medium passed through the flow system (Figure 5.22, Conductivity). The conductivity remaining constant is an important requirement for the BES sensor being able to reliably detect changes in BOD as conductivity affects the electrical current. The medium employed in this study was artificially buffered at pH 7.0 with 50 mmol/dm<sup>3</sup> phosphate buffer solution and therefore changes in conductivity would have been resisted between pH 5.8 and 8.0.

## COD & DOC

The measured COD and DOC values indicated that, below 150 mg/l O<sub>2</sub> BOD<sub>5</sub> medium concentration, organic compounds were fully assimilated by the time the feed had reached the valve downstream of the third stage cells (3-W 3) down to a limiting concentration of 1–37 mg/l O<sub>2</sub> COD. The effluent of the third stage MFCs contained  $14.8 \pm 3.8$  mg/l inorganic carbon for a 120 mg/l O<sub>2</sub> BOD<sub>5</sub> medium cycle. At these lower medium concentrations, only the first stage MFCs received appreciable concentrations of COD for oxidation and thus the data reflects the amperometric calibration curve (Figure 5.16).

The average coulombic efficiency was calculated for each stage of MFCs at a flow rate of 1.24 ml/min and found to be only 2%, 4% and 2% for the first, second and third stages respectively. This was lower than the average coulombic efficiency of 25% determined for the batch-mode cells over the same  $R_{Ext}$  (Table 4.4 in Chapter 4); thus indicating that the reduced HRT (only 7.6 minutes per cell) decreased the electrogenic consumption of substrate by the anodic biofilm. The production of sludge inside the reactor will also have significantly lowered the coulombic efficiency by competing for substrate. With 600 mg/l O<sub>2</sub> BOD<sub>5</sub> medium cycles and higher concentrations, the COD was observed to increase after the first stage MFCs higher than the level observed in the feed line (3-W L). These were concentrations at which

sludge was observed inside the reactors and therefore could be contributing to the COD level. However, the error for the replicate COD samples was quite large and the observed trend of increasing COD in the first stage of MFCs was not statistically significant.

The dissolved organic carbon (DOC) values, which would be expected to mirror the COD values, showed the carbon level decreasing steadily through the hydraulic array as medium passed through the system. It was possible that metabolites could be completely mineralised to CO<sub>2</sub>, however a full mass balance was not possible as the reactor design did not allow for headspace analysis under continuous flow operation. The total inorganic carbon (comprised of dissolved CO<sub>2</sub>, carbonate and bicarbonate) present in solution mirrored the response of the VFAs (formic, acetic, propionic and isobutyric acids) which increased from approximately zero in the medium through the feed line to the first stage MFC and then remained approximately constant through to the second and third stages (Figure D.4, IC). The average inorganic carbon concentration in the MFCs was  $30.0 \pm 10.3$  mg/l C. Further investigation would be required in order to more reliably determine the changes in COD, DOC and substrate utilisation across a broader range of samples in a multi-stage hydraulic array of MFCs.

### **Glucose, Glutamic acid & VFAs**

The glucose assay results showed that in all cases the effluents from the first, second and third stage MFCs contained no detectable glucose (Figure 5.22, Glucose). With all feed concentrations, except the 1199 mg/l O<sub>2</sub> BOD<sub>5</sub> cycle, glucose had been depleted in the feed lines through the UV lamp enclosure and peristaltic pump before reaching the MFCs. With glutamic acid, the same in-line consumption was observed. However, glutamic acid was still present in the effluent of the third stage MFCs at medium concentrations of 360 mg/l O<sub>2</sub> BOD<sub>5</sub> and above (Figure 5.22, Glutamic acid).

Acetic acid was the most abundant VFA produced through the hydraulic array of MFCs; up to  $1767.8 \pm 272.5$  mg/l was produced with the 1199 mg/l O<sub>2</sub> BOD<sub>5</sub> medium ((Figure 5.22, Acetic acid). Propionic acid followed the same trend as the acetic acid up to maximum concentrations of 194 mg/l (Figure 5.22, Propionic acid). Formic acid was primarily measured in samples from the feed line at concentrations up to 25 mg/l and then observed to decrease as medium passed through the MFCs (Figure D.4). Isobutyric acid was only found in concentrations up to 5 mg/l and mainly in the samples from the lowest-concentration medium cycle (120 mg/l O<sub>2</sub> BOD<sub>5</sub>). Butyric, isovaleric and valeric acids were not detectable in any of the samples.

Figure 5.23 shows the partial mass balance achieved with stoichiometric quantities of organic carbon derived from values determined from glucose and glutamic acid assays and VFA analysis compared to the DOC (and IC) measured by TOC analyser. The sample sets from 240 and 1199 mg/l O<sub>2</sub> BOD<sub>5</sub> medium cycles were analysed at the same time and the sample sets from 120 and 360 mg/l O<sub>2</sub> medium cycles were analysed at a different occasion after a

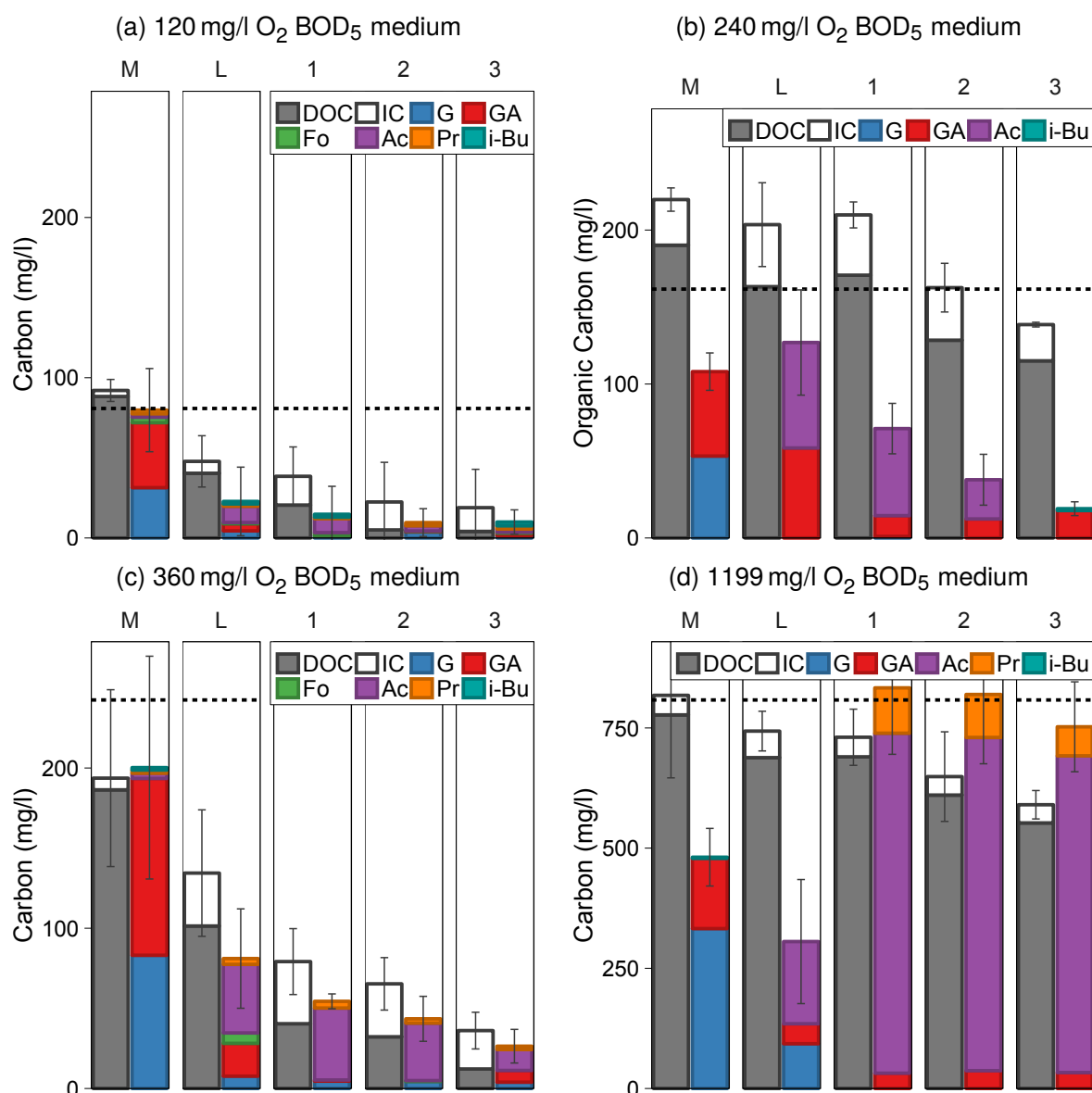


Figure 5.23: Average measured quantities of dissolved carbon (DOC and IC) determined using a TOC analyser compared to the calculated organic carbon from various chemical analyses in a partial mass balance. Dashed lines are the theoretical initial quantity of organic carbon present in the prepared medium bottle.

M = Spent medium sample; L = Feed line sample; 1,2&3 = MFC stage effluents; DOC = Dissolved Organic Carbon; IC = Inorganic Carbon; G = Glucose; GA = Glutamic acid; Fo = Formic acid; Ac = Acetic acid; Pr = Propionic acid; i-Bu = Isobutyric acid.

longer period of storage at  $-18\text{ }^{\circ}\text{C}$ . Despite storing samples after filter-sterilisation it appeared that there had been some degradation, or insufficient mixing of samples after defrosting, as the  $240\text{ mg/l O}_2$  samples had higher concentrations than the  $360\text{ mg/l O}_2$  samples. Nonetheless, trends within sample sets can be considered as analysis was performed all at the same time. Inherently because several analysis techniques had been used the resultant errors meant that in some cases the sum of the calculated mass balance was greater than the measured DOC value. From the spent medium the DOC values were approximately equal to the theoretical DOC values indicating that the upstream sterilisation equipment was successful (UV enclosure and drip chambers). The medium samples contained approximately equal concentrations of glucose and glutamic acid, although the accuracy of the assay kits in microplate wells led to quite large standard deviations of up to  $80\text{ mg/l}$ .

At each concentration a decrease in DOC, glucose and glutamic acid was observed as medium passed through the hydraulic array. At the feed line sampling location (3-W L), acetic acid was the primary degradation product measured and formic and propionic acid were found in some samples. With the MFCs, acetic acid accounted for a large proportion of the DOC (20–120% estimated) and at medium concentrations of  $360\text{ mg/l O}_2$  and above propionic acid was also measured. Small quantities of isobutyric acid were measured in samples at medium concentrations of  $240\text{ mg/l O}_2$  and below. In certain samples (Figure 5.23), the summed estimation of organic carbon was less than the measured DOC indicating that there was potentially additional fermentation metabolites present (such as lactate or ethanol) which were not measured in the present study.

The fermentation and oxidation of glucose in MFCs was modelled by de los Ángeles Fernandez *et al.* (2016). Electrogenic fermentation could be achieved through three pathways to organic products of acetic, propionic and isobutyric acids (the VFAs identified in the present study). In addition, direct electrogenic oxidation of glucose and its fermentation products to  $\text{CO}_2$  were incorporated into the model. The non-electrogenic products possible from glucose fermentation were acetic, propionic, isobutyric and lactic acids and ethanol. It is notable that the MFCs in this study actually received relatively low concentrations of glucose as the inline, non-electrogenic fermentation was responsible for much of the consumption. The electricity generation was therefore, mainly fuelled by the degradation products of the two substrates; glucose and glutamic acid. Of the VFAs identified in samples from this study it is clear that the primary fermentation pathways were producing acetic acid.

Five pathways have been identified for glutamic acid fermentation in the literature (Buckel, 2001). All pathways generate ammonia, acetate and  $\text{CO}_2$  as end-products, three of the five produce butyrate. Of the remaining two pathways one produces propionate and valerate and the other solely produces propionate as the additional fermentation product (Buckel, 2001). As no butyrate or valerate was detected in the samples from the flow-mode MFCs it is anticipated that the fifth-listed pathway was employed by bacteria in this system. The fifth pathway proceeds via a enzyme-catalysed rearrangement of a pyruvate intermediate

to methylaspartate, followed by disproportionation to propionate, acetate and CO<sub>2</sub> (Buckel, 2001). Bacteria from the order of *Clostridiales* have been associated with the methylaspartate-based pathways (Baena *et al.*, 1998; Buckel, 2001).

## Anions

The anion measurements showed one unexpected result in that the concentration of fluoride (Figure 5.22, Fluoride) was observed to increase as medium passed through the hydraulic array, especially for the 1199 mg/l O<sub>2</sub> BOD<sub>5</sub> cycle where concentrations increased up to 50 mg/l F<sup>-</sup>. In no medium samples was fluoride found indicating that the ion was being introduced within the flow-mode system. It is thought that the UV-transparent tubing used within the UV lamp enclosure, ChemFluor® 367, must be the inline source of F<sup>-</sup> as the highest concentrations were measured just after the UV lamp at valve 3-W L. It is unknown why the highest BOD<sub>5</sub> concentration resulted in the greatest F<sup>-</sup>-stripping but the lower pH caused by the higher glutamic acid concentration and presence of acidic fermentation products (VFAs) could be a factor.

Chloride and phosphate (present in the macro-/micro-nutrients and phosphate buffer solutions respectively) remained approximately constant over the course of medium passage (Figure D.4). Sulphate ions were observed to decrease with increases in BOD<sub>5</sub>. For medium concentrations above 120 mg/l O<sub>2</sub> BOD<sub>5</sub>, the sulphate concentration in the medium bottle decreased to almost zero in the first stage MFC samples, followed by an increase in the second and third stage samples. Nitrate was measured almost exclusively in the lowest-concentration medium cycle (120 mg/l O<sub>2</sub> BOD<sub>5</sub>) up to concentrations of only 3 mg/l NO<sub>3</sub><sup>-</sup>. Bromide was only observed in one of the samples (7 mg/l) which could have been an anomaly with the ion chromatography instrument as no bromide was present in the medium. Additionally, no nitrite was observed in any of the samples.

### 5.3.7 Bacterial Cell Density & Community Analysis

At the end of the experimental period of the 'ABC' series of flow-mode MFCs (day 757), cells were disassembled and the anode biofilms on carbon cloth were stored in 50% aqueous ethanol solution. After centrifugation and supernatant removal, 100 mg of pelleted electrode sample containing biomass and carbon cloth was filtered onto a membrane for cell counting to determine bacterial cell density. The cell densities were calculated with the assumption that no bacteria were present under the area covered by the gasket (in accordance with observations made in Figure 5.10). The calculated cell densities are presented in Table 5.5 (representative micrographs of electrodes which were used for counting are shown in Figure F.2 in Appendix F).

The electrode cell counts were 3 orders of magnitude higher (10<sup>6</sup> per membrane) than the



Table 5.5: Logarithm of cell densities flow-mode anodes from the 'ABC' series (and cell count for sterile PBS control).

Electrode	No images	$DF_{\text{Sample}}$	Cell count $\pm$ SE (per membrane) <sup>a</sup>	Log(Cell density) (per cm <sup>2</sup> )	Log(SE) (per cm <sup>2</sup> ) <sup>a</sup>
Control	16	1	$(2.938 \pm 0.101) \times 10^3$	-	-
Flow 1A	18	5015	$(5.854 \pm 0.001) \times 10^6$	9.777	5.288
Flow 1B	16	4762	$(2.762 \pm 0.001) \times 10^6$	9.784	5.646
Flow 1C	16	4708	$(3.102 \pm 0.001) \times 10^6$	9.844	5.719
Flow 2A	16	4789	$(3.132 \pm 0.001) \times 10^6$	9.799	5.634
Flow 2B	18	4854	$(2.899 \pm 0.001) \times 10^6$	9.692	5.548
Flow 2C	18	5128	$(2.668 \pm 0.001) \times 10^6$	9.738	5.628
Flow 3A	16	5482	$(2.470 \pm 0.001) \times 10^6$	9.713	5.680
Flow 3B	16	4673	$(2.260 \pm 0.001) \times 10^6$	9.443	5.596
Flow 3C	16	4708	$(2.683 \pm 0.001) \times 10^6$	9.309	5.745

<sup>a</sup> Standard error (SE) =  $SD/\sqrt{N_0}$

sterile PBS control (Table 5.5). Similar to the batch-mode and OCP electrodes (Table 4.7 in Chapter 4), the calculated cell densities were of the order  $10^9$  cells per cm<sup>2</sup> of electrode. The cell densities increased with age of anode biofilm with average log-transformed values of 9.802, 9.743 and 9.700 per cm<sup>2</sup> of electrode for the first, second and third stages respectively (*p*-values from pair-wise *t*-tests were all less than 0.05 indicating significance).

DNA was extracted from samples of the centrifuge-pelleted 'ABC' flow-mode anode electrodes, sludge obtained from the first stage MFCs during medium cycles of 400 and 2000 mg/l GGA and a sample of the supernatant from the centrifuged cell 1A sample (to confirm that pelleted material contained majority of sample DNA). The two sets of precipitated sludge samples were different in appearance with the 400 mg/l sludge a uniform brown colour and the 2000 mg/l sludge a mixed brown-white colour (Figure 5.24).

The community analysis results will be discussed here in comparison to the duplicate 19.6 cm<sup>2</sup> batch-mode anodes (Batch A and B) and triplicate 11.0 cm<sup>2</sup> electrodes incubated at OCP (OCP A, B and C) from Chapter 4. The extracted DNA from all samples was quantified with a spectrophotometer and the 260/280 nm and 260/230 nm quality score ratios were calculated (Table F.2 in Appendix F). On average for 0.25 g community analysis samples, 14.45 ng DNA was extracted for the batch-mode MFCs and 25.01 ng DNA for the flow-mode MFCs (it is expected that the 19.6 cm<sup>2</sup> electrodes had lower extraction quantities due to the higher proportion of the gasket-covered electrode in the homogenised sample). The DNA extracted from OCP electrodes, sludge at 400 mg/l GGA and sludge at 2000 mg/l GGA was 33.02, 67.30 and 35.52 ng respectively. With the supernatant sample only 12.99 ng DNA was extracted (compared with 5.11 ng for the sterile DI water control), however the absorbances at 260 and 280 nm were less than 0.01 for these samples making the determination from the

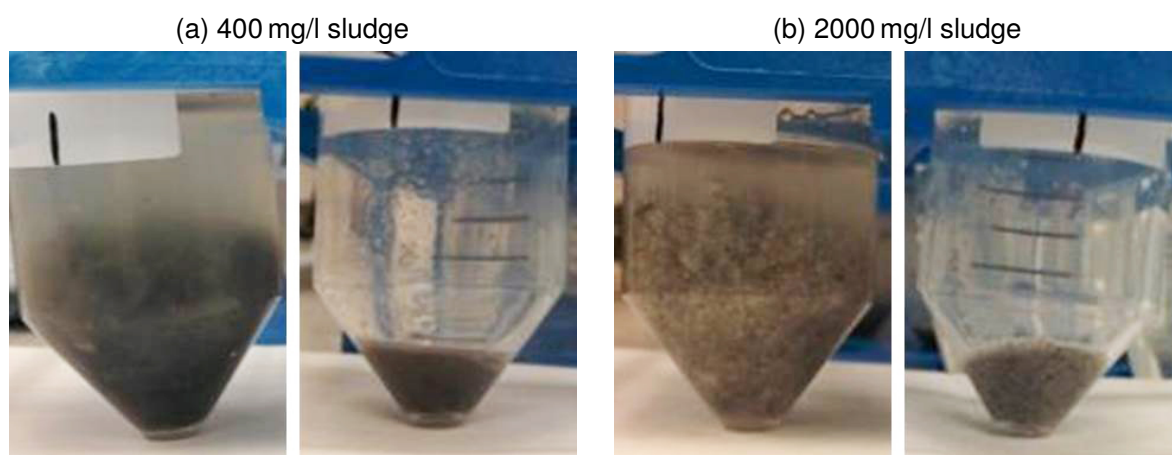


Figure 5.24: Photographs of sludge samples, before (left) and after (right) centrifugation and supernatant removal, taken from first stage MFC (1A) during medium cycles of (a) 400 mg/l and (b) 2000 mg/l GGA concentration.

ratio inaccurate.

The polarised electrode samples (from batch- and flow-mode cells) had 260/280 nm ratios between 1.73–1.96 (1.8 is ‘pure’ DNA) and 260/230 nm ratios between 1.15–1.79 (2.0–2.2 is ‘pure’ nucleic acid). The OCP and sludge samples had similar DNA quality (1.81–1.91) but higher nucleic acid quality scores were measured (2.42–4.11) which could be related to the biomass accumulating planktonically and co-extraction of contaminants which absorb at 260 nm (Thermo Scientific, 2008). The supernatant sample had much lower quality scores of 260/280 nm = 1.45 and 260/230 nm = 1.14; therefore further analysis of this sample was not progressed as the corresponding pelleted sample appeared to contain the highest quantity and purest DNA extract. The extracted DNA was amplified and purified with analysis by agarose gel electrophoresis to confirm procedural success after each step (Figure F.3 in Appendix F).

16S rRNA genes were amplified from the extracted DNA and Ion Torrent sequencing was performed on samples from the batch-mode and flow-mode anodes, OCP electrodes and sludge samples taken during 400 and 2000 mg/l GGA medium cycles. The relative abundance of bacteria at each taxonomic rank from phylum to genus was determined (Figures 5.25 and 5.26). Additionally, the calculated cell densities were used to weight the abundances determined at the genus level (Figure 5.26c). The cell density-weighted abundances were corrected for the different number of 16S rRNA gene copies of each identified genus using the ‘rrnDB Estimate’ classifier tool (Stoddard *et al.*, 2015).

It should be noted that the age of the biofilms grown upon the electrodes was considerably different (Batch = 848 days, Flow Stage 1 = 757 days, Flow Stage 2 = 602 days, Flow Stage 3 = 545 days, OCP = 36 days). This discrepancy potentially negates some of the comparisons which can be made between sets of electrodes but the general trends and identities of bacteria involved were expected to be apparent after this length of incubation.

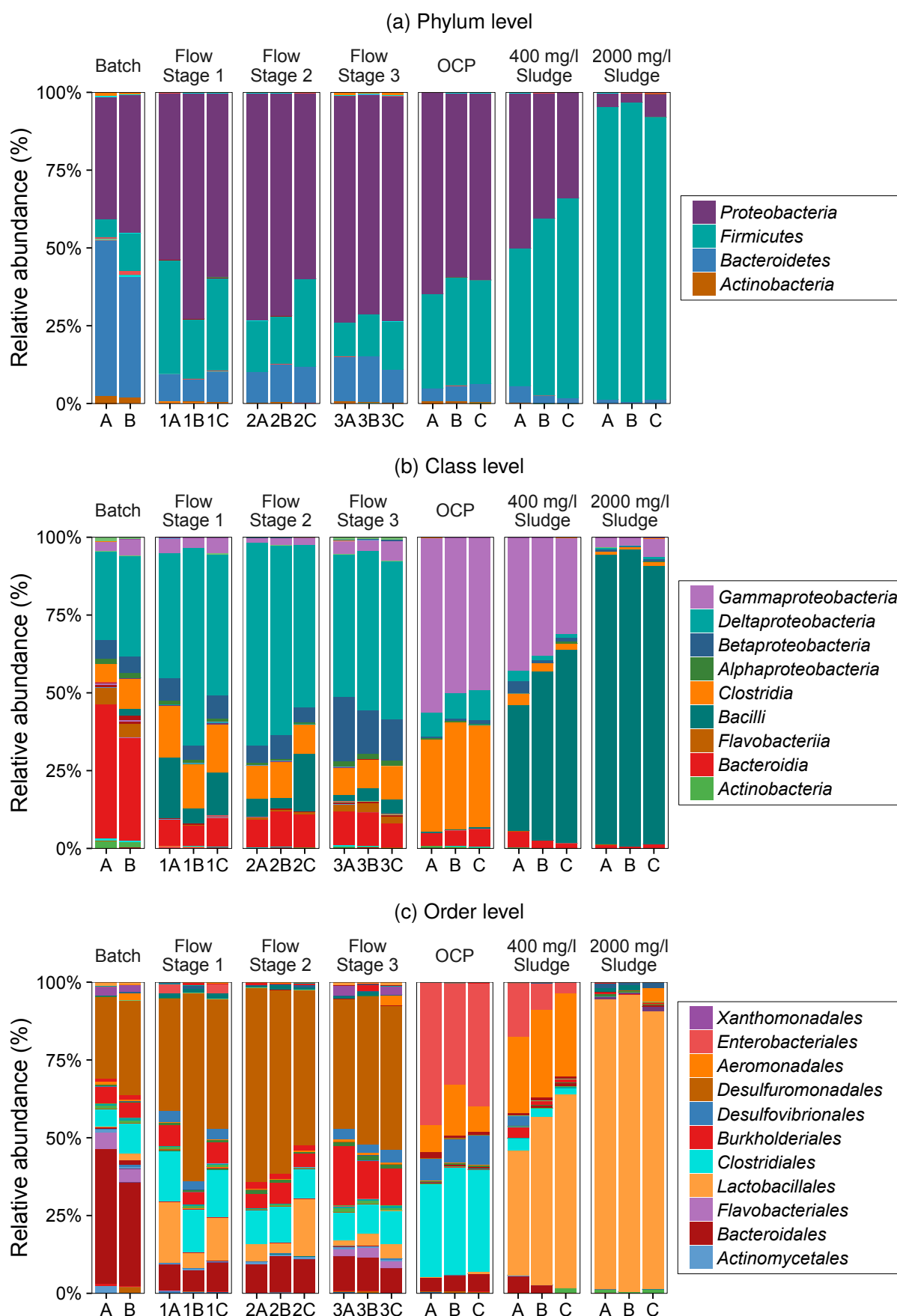


Figure 5.25: Relative abundance of bacterial (a) phyla, (b) classes and (c) orders obtained from Ion Torrent sequencing of 16S rRNA genes from MFC anodes, non-polarised electrodes (OCP) and sludge.

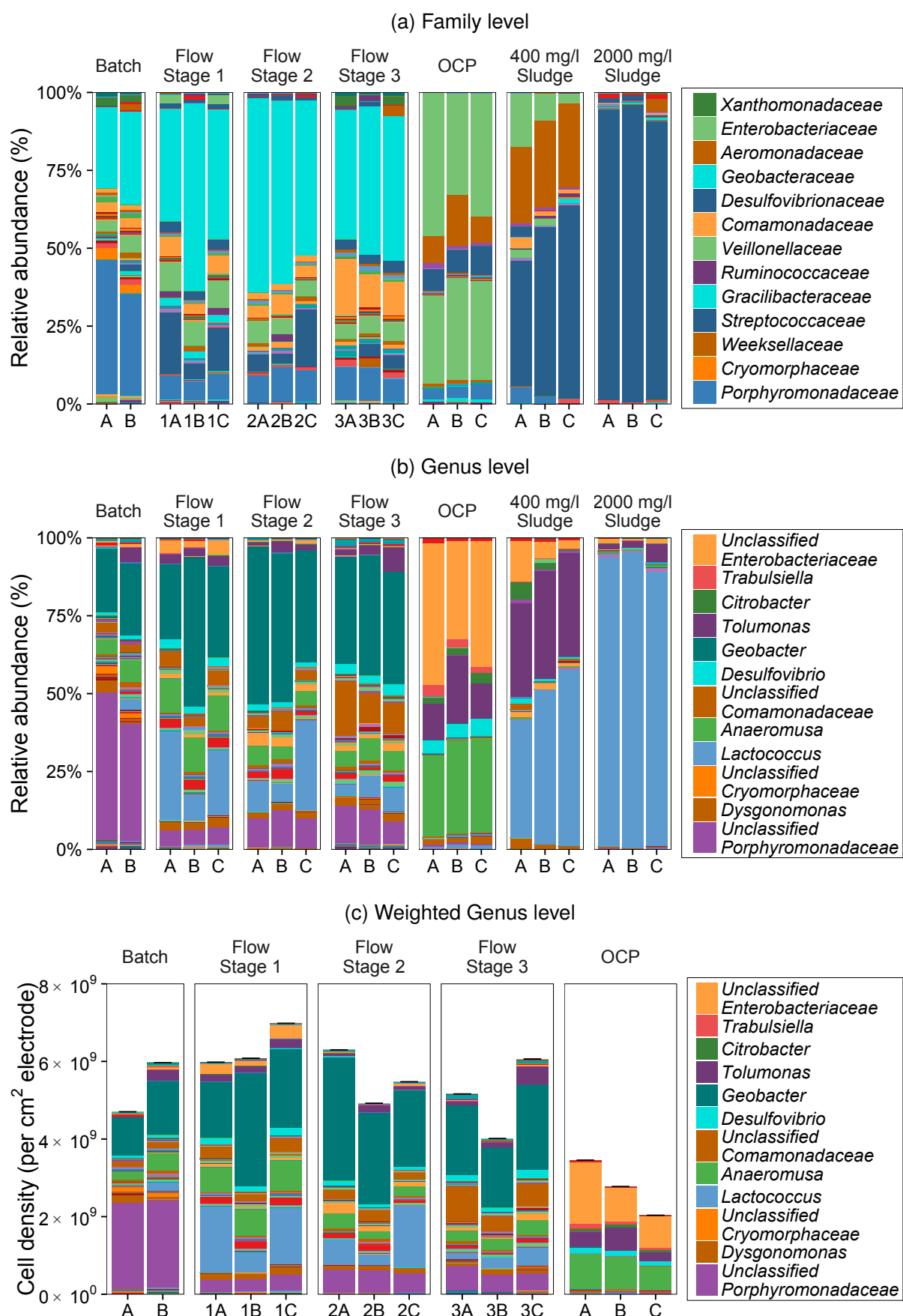


Figure 5.26: Relative abundance of bacterial (a) families and (b) genera and (c) cell density-weighted abundance of bacterial genera obtained from Ion Torrent sequencing of 16S rRNA genes from MFC anodes, non-polarised electrodes (OCP) and sludge.

MFCs generated electricity within hours of inoculation and enrichment was achieved within 16 days for most electrodes in the present study, so electrogenic bacteria would be expected to have established after this time.

Differences between the microbial communities from the different samples was evaluated by principal coordinate analysis (PCoA; Figure 5.27). By constructing a Unifrac distance matrix based on community composition the similarity of sample communities could be established. In the unweighted principle co-ordinate charts (Figure 5.27a–c), the first and second axis (PCo axis 1 and 2) explained 25.9% and 12.6% of the total variance between samples. There was clear clustering of replicate samples as well as two broad clusters (highlighted) of the polarised and non-polarised samples. This indicated that there were compositional differences between treatments. Sludge samples and electrodes incubated at OCP clustered separately from each other. The third principle co-ordinate axis (PCo axis 3) accounted for a further 7.7% of the variance (46.2% for the first three axes together) and in Figure 5.27b the clustering of the flow-mode MFCs was observed to be in order of first, second and third stage MFCs. The abundance-weighted PCoA plots (Figure 5.27d–f) exhibited the same clustering with greater percentages of 53.2%, 33.9% and 6.2% for the first, second and third PCo axes respectively (total of 93.3%).

Figure 5.28 shows each genus which was present at greater than 2% relative abundance on any of the community analysis samples. BLAST (Basic Local Alignment Search Tool) searches of the NCBI (National Center for Biotechnology Information) Nucleotide database collection (containing GenBank, EMBL, DDBJ, PDB & RefSeq sequences) were conducted using sequences of abundant operational taxonomic units (OTUs) found in samples from this study. Abundant sequences were chosen if they were present at greater than 2% relative abundance in any sample. The search results allowed information to be retrieved regarding identity and isolation conditions of similarly sequenced bacteria. For sequence-matched species below the accession numbers are given in brackets and for samples from the present study the OTU identification number is given.

The batch-mode MFC anodes were dominated by phyla of *Proteobacteria* and *Bacteroidetes*, which mainly corresponded to bacteria from the genera *Geobacter* (21%) and unclassified *Porphyromonadaceae* (47%) respectively. The flow-mode anodes also contained 24–50% *Geobacter* spp. and it was observed that unclassified *Porphyromonadaceae* increased down the hydraulic array (from first to third stage) from 5 to 12% relative abundance. Almost no *Geobacter* spp. or unclassified *Porphyromonadaceae* (< 0.2 and 1% respectively) were obtained from non-polarised samples (OCP electrodes and sludge), indicating that the two genera were likely involved in electrogenic processes which interact with the anode.

Three OTUs of *Geobacter* spp. (OTU1725261, OTU19 & OTU1102952) were on average present at 1%, 1% and 39% relative abundance respectively in the batch- and flow-mode electrode samples analysed in the present study. *Geobacter* is a genus often identified in

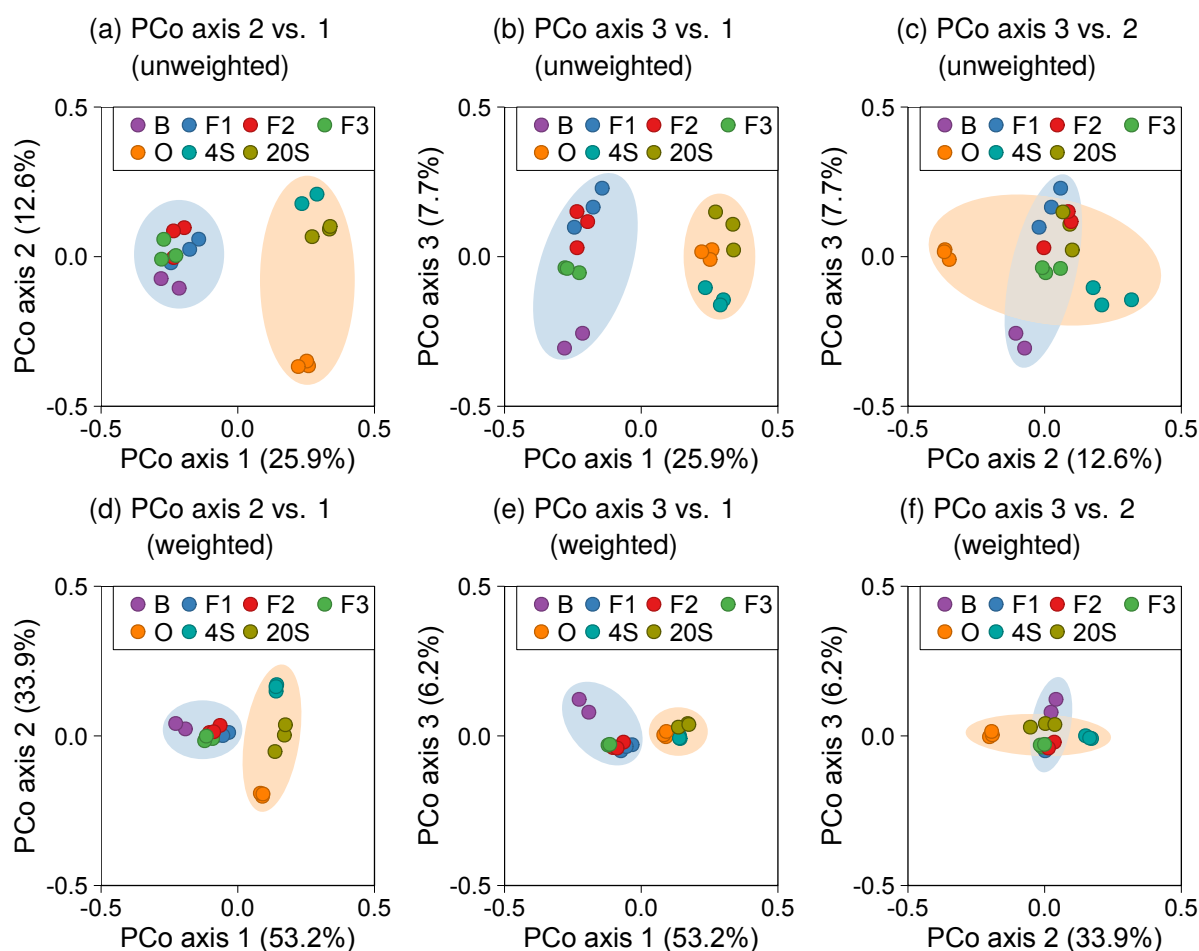


Figure 5.27: (a–c) Unweighted and (d–f) weighted Unifrac principal coordinate analysis of communities analysed with polarised (■) and non-polarised (■) samples highlighted.

B = Batch; F1 = Flow Stage 1; F2 = Flow Stage 2; F3 = Flow Stage 3; O = OCP; 4S = 400 mg/l Sludge; 20S = 2000 mg/l Sludge.

acetate-fed MFCs and has been associated with direct electron donation to the electrode via conductive nanowires (Reguera *et al.*, 2006; Logan, 2008; Richter *et al.*, 2009). The three identified *Geobacter* spp. OTUs were almost identical (> 99% 16S rRNA gene sequence identity) to an uncultured bacterium from iron (III) reducing, anoxic rice paddy soil (JQ640215.1) and a bacterial strain of *Geobacter lovleyi* iso10-09 isolated from a eutrophic brackish lake sediment (AB795545.1). *G. lovleyi* has been described as an interesting strain of *Geobacter* for its ability to bioremediate various contaminants (including iron (III) and uranium) coupled to acetate oxidation (Wagner *et al.*, 2012). In addition to acetate; hydrogen and pyruvate were also identified as viable electron donors but the bacterium was unable to oxidise a range of other substrates including glucose, lactate and ethanol (Sung *et al.*, 2006).

The unclassified *Porphyromonadaceae* OTU from the present study (OTU4466138) was present at 27% relative abundance on batch-mode anode samples and only 5% relative abundance on flow-mode anodes. The OTU had 99% 16S rRNA gene sequence identity to an uncultured bacterium found in a MEC study with an acetate-fed bioanode and methanogenic biocathode (JX462549.1; Van Eerten-Jansen *et al.* (2013)); indicating it may have a role

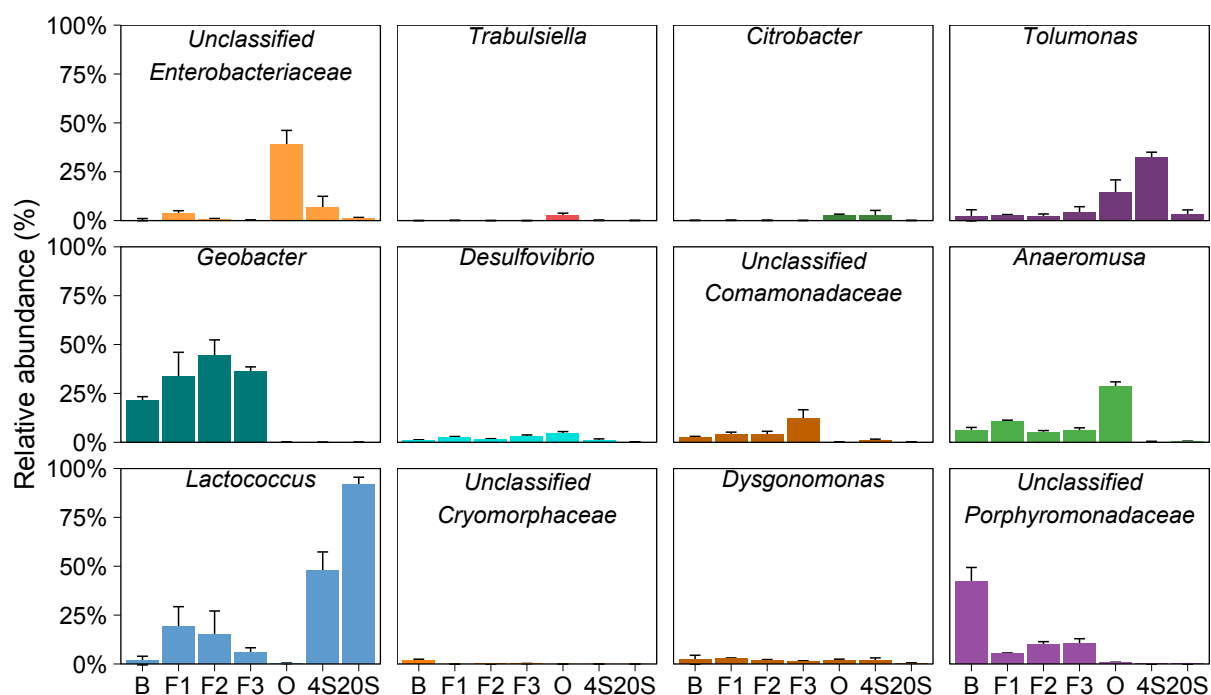


Figure 5.28: Average relative abundance of bacterial genera obtained from Ion Torrent sequencing of 16S rRNA genes from MFC anodes, non-polarised electrodes (OCP) and sludge in individual plots to allow comparisons between samples.

B = Batch; F1 = Flow Stage 1; F2 = Flow Stage 2; F3 = Flow Stage 3; O = OCP; 4S = 400 mg/l Sludge; 20S = 2000 mg/l Sludge.

in electrogenesis. Additionally, the unclassified *Porphyromonadaceae* OTU had 98% 16S rRNA gene sequence identity to a bacterial strain of *Petrimonas sulfuriphila* Marseille-P1901 (LT558828.1). *P. sulfuriphila* has been reported to perform fermentation of glucose and lactate to acetate, CO<sub>2</sub> and H<sub>2</sub> using sulfur and nitrate as terminal electron acceptors (Grabowski *et al.*, 2005). *Dysgonomonas* spp. is also a member of the *Porphyromonadaceae* family but was observed mainly on first stage flow-mode anodes, OCP electrodes and 400 mg/l sludge. The *Dysgonomonas* sp. OTU had 99% 16S rRNA gene sequence identity to *Dysgonomonas oryzae* Dy73, which was isolated from a peptone/starch/fish extract-fed MFC bioanode (Kodama *et al.*, 2012). *D. oryzae* was not able to reduce Fe(III) and has been observed to produce lactate and acetate as major products from glucose fermentation. The ability of bacteria to reduce Fe(III) was previously thought to relate to involvement with electrogenic processes, however recent research by Rotaru *et al.* (2015) has linked direct interspecies electron transfer between *Geobacter* spp. and methanogens with high performing current-generating electrogenic bacteria.

Less dominant genera found almost exclusively on the polarised electrodes were unclassified *Comamonadaceae* (3–17%) which also increased down the flow series. The abundant *Comamonadaceae* OTUs (OTU4297171 and OTU366977) were found to be 99–100% similar to an uncultured bacterium found in a fermentation reactor fed with glycerol (KT287261.1; Moscoviz *et al.* (2016)), a SCMFC fed organic waste digestate (99%; LC070492.1; Suzuki *et al.* (2016)) and *Acidovorax caeni* T-X2D from a garden pond (99% KU355878.1). *A. caeni*

is a denitrifying bacterium which has been observed to assimilate glutamic acid and VFAs to products including formic and propionic acids (and tested negative for glucose utilisation; Heylen *et al.* (2008)).

*Anaeromusa* spp. was found on polarised electrodes at relative abundance of 4–11% but also found in higher abundance (26–30%) on the electrodes incubated at OCP. *Anaerovibrio burkinabensis* DSM 6283 was a highly similar strain (99%; NR\_025298.1) which has been associated with fermenting glutamate and lactate to acetate and propionate (Ouattara *et al.*, 1992); indicative of the methylaspartate-based pathway. *Anaeromusa* spp. is a member of the *Clostridiales* order which have previously been associated with that pathway (Buckel, 2001).

*Desulfovibrio* spp. were common to both polarised and non-polarised electrodes. The most abundant OTU (OTU513307) was similar to an uncultured bacterium from a bioreactor fed glucose (KC179078.1) and *Desulfovibrio simplex* DSM4141 (NR\_117110.1); a sulfate-reducing bacterium isolated from anaerobic sour whey digester grown on formate and lactate. Electron acceptors for *D. simplex* included sulfate, thiosulfate and nitrate; lactate was incompletely oxidized to acetate and CO<sub>2</sub> during sulfate reduction (Zellner *et al.*, 1989). Stams and Hansen (1984) described how *Desulfovibrio* spp. were able to consume hydrogen present at low concentrations to enhance the rate of glutamate fermentation by *Acidaminobacter hydrogeniformans* (a member of the *Clostridiales* order) to produce acetate and propionate via a methylaspartate intermediate.

*Tolomonas* spp. was also found in low relative abundance (1%) on polarised electrodes but at 15, 33 and 3% relative abundance on the OCP electrodes, 400 mg/l sludge and 2000 mg/l sludge samples respectively. *Tolomonas auensis* DSM 9187 (NR\_074805.1) had 99% 16S rRNA gene sequence identity with the OTUs identified in samples from the present study and has been observed to produce toluene. When *T. auensis* was fed with glucose the major fermentation products were acetate, ethanol and formate (Tindall, 1996). This indicated that the genera (*Anaeromusa* and *Tolomonas*) were most likely involved in fermentation of glutamic acid and glucose respectively. The bacteria were present in highest relative abundances in OCP electrodes indicating that they did not compete well with other fermentative bacteria which acted in co-ordination with the electrogenic bacteria when the anode was available as an electron acceptor.

An unclassified member of the family *Cryomorphaceae* was exclusively identified on batch-mode anode samples. The most abundant OTU (OTU809916) had 99% 16S rRNA gene sequence identity to an uncultured bacterium from a denitrification bioreactor (HQ232447.1) and 92% similarity to *Crocinitomix* sp. (FM175783.1) from a Tufa rock core. *Crocinitomix* sp. was determined to be cold-adapted and require organic forms of nitrogen for metabolism (however was not able to utilise glutamate; Bowman *et al.* (2003)).

Of the non-polarised samples (OCP electrodes and sludge), members of the *Enterobacteri-*



aceae family were prevalent. Seven *Enterobacteriaceae* OTUs were present at more than 2% relative abundance in any sample; one OTU was identified from the genus *Trabulsiella*, another from the genus *Citrobacter* and the remaining five were unclassified. *Citrobacter* sp. (OTU814442) and unclassified *Enterobacteriaceae* (OTU676211) were found in the OCP and 400 mg/l sludge samples, similar (100% and 99% 16S rRNA gene sequence identity respectively) to *Citrobacter freundii* K6 (KX156769.1) and *Citrobacter amalonaticus* 4BeCh (KX355663.1). *Trabulsiella* sp. (OTU4406193) and four unclassified *Enterobacteriaceae* OTUs (OTU691423, OTU4328189, OTU4418165 & OTU228556) were found almost exclusively on the electrodes incubated at OCP. Those OTUs were similar to *Klebsiella oxytoca* IG28 (KU851817.1; Govindasamy *et al.* (2008)), *Raoultella planticola* KK 8a (KP858918.1) and an uncultured bacterium from a fermentation reactor (KX032256.1). *Citrobacter* and *Klebsiella* have been associated with fermentation of glycerol to produce 1,3-propanediol, acetate and lactate, fermentation of glucose and amino acids, nitrate assimilation and production of  $\beta$ -lactamases (which provide resistance to  $\beta$ -lactam antibiotics, e.g. penicillin) (Underwood and Avison, 2004; Obst *et al.*, 2005; Morozkina and Zvyagilskaya, 2007; Homann *et al.*, 1990). *Raoultella planticola* was separated from the *Klebsiella* genus and is known to use glucose as a sole carbon source to produce VFAs and H<sub>2</sub> (Drancourt *et al.*, 2001).

*Lactococcus* spp. completely dominated the 2000 mg/l sludge samples, with relative abundances as high as 95% and was also found at 48% relative abundance in the 400 mg/l sludge, which was more diverse and contained similar genera to those found at OCP. In the flow-mode anodes, *Lactococcus* spp. were observed to decrease in abundance from 19% to 6% down the hydraulic series (consistent with the trends observed in sludge accumulation). *Lactococcus raffinolactis* JCM 5706 was identified with 100% 16S rRNA gene sequence identity to the *Lactococcus* sp. OTU (LC071827.1) from the present study. *L. raffinolactis* has previously been isolated from raw cow's milk and wastewater tanks and is able to convert glucose and other sugars (including lactose and maltose) to lactic acid (Dworkin *et al.*, 2006).

In summary, bacteria likely involved with electrogenic processes were found solely on the polarised electrodes (*Geobacter* sp., unclassified *Porphyromonadaceae* & potentially unclassified *Cryomorphaceae*). The composition of the bacterial community on polarised electrodes additionally contained sugar fermenters (*Dysgonomonas* spp., *Lactococcus* spp. and members of *Enterobacteriaceae*) and amino acid fermenters (*Anaeromusa* spp., unclassified *Comamonadaceae* & *Tolomonas* spp.) which degraded the medium constituents glucose and glutamic acid. The fermentation products (including lactate, acetate, propionate and ethanol) were further degraded (by *Anaeromusa* spp. & *Desulfovibrio* spp.) to produce additional acetate which was consumed by the electrogenic bacteria.

The non-polarised electrodes incubated at OCP contained a high relative abundance of members of the family *Enterobacteriaceae* (glucose fermentation) and *Anaeromusa* spp., *Desulfovibrio* spp. and *Tolomonas* spp. (glutamate fermentation). The sludge obtained from 400 mg/l GGA cycles had a high relative abundance of *Lactococcus* spp. and *Tolomonas*

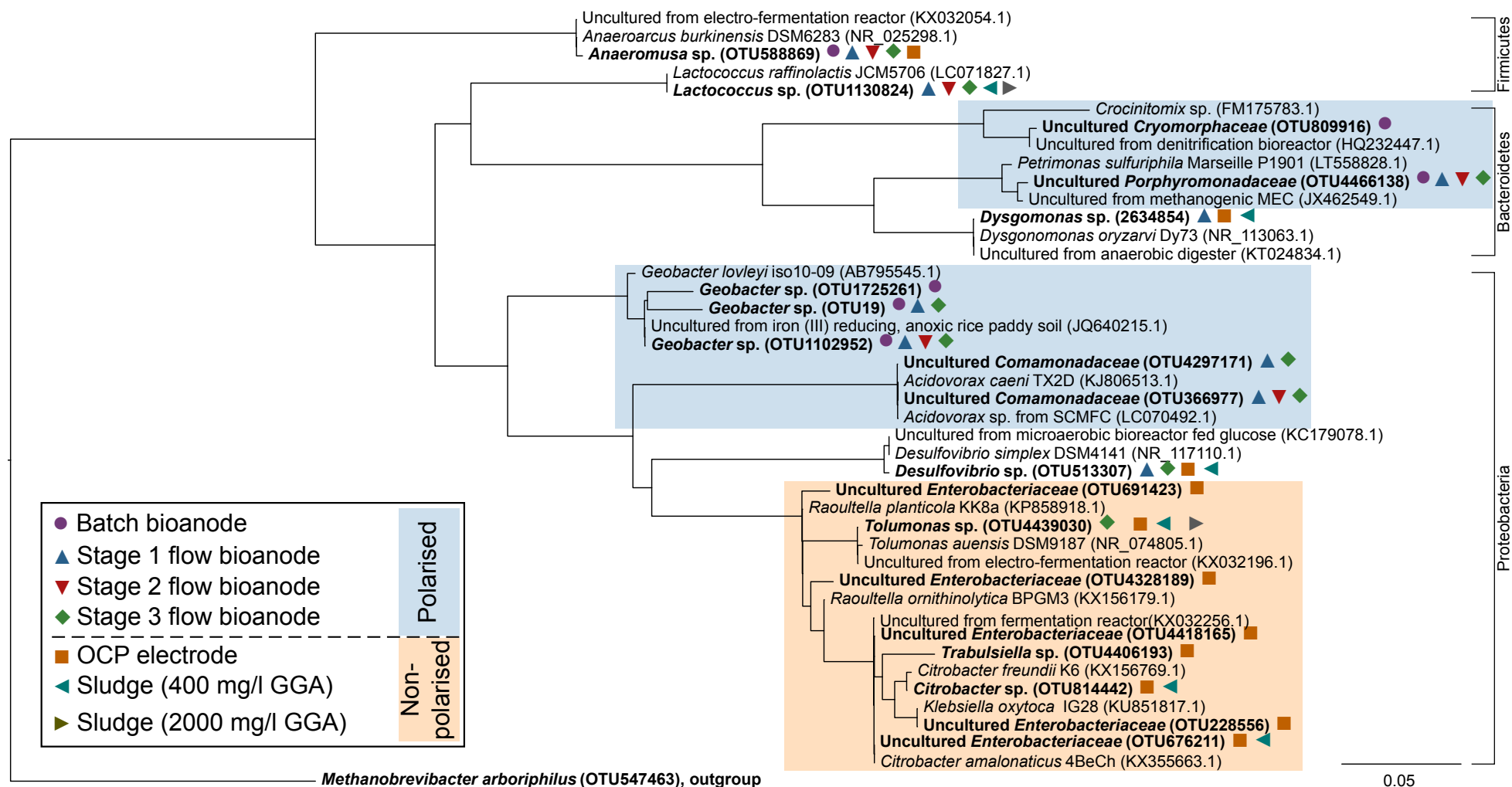


Figure 5.29: Phylogenetic tree of 16S rRNA gene sequences extracted from this study (**bold**) for electrode and sludge samples from batch-mode and multi-stage, flow-mode SCMFCs (symbols). Only sample OTUs which represented at least 2% of the total relative abundance are shown. Additional high-similarity sequences are from the NCBI Nucleotide database collection (Accession number in brackets). Sequences exclusively (>2%) from polarised (blue) and non-polarised (orange) samples are highlighted. *M. arboriphilus* was used as an archeal outgroup. The scale bar indicates the number of nucleotide position changes.

spp. for fermentation of glucose and glutamic acid respectively. The sludge obtained from 2000 mg/l GGA cycles was completely dominated by *Lactococcus* spp. indicating that there was a high degree of glucose to lactate conversion occurring. In the batch-mode electrodes *Lactococcus* spp. was less present, perhaps indicative that the glucose was rapidly fermented and thus most of the medium cycle was with glucose not present, whereas the flow-mode MFCs received a constant stream of fresh substrate from the medium bottles.

A phylogenetic tree was produced from 16S rRNA gene sequences recovered in the present study and highly similar sequences retrieved from the NCBI BLAST search (Figure 5.29). The phylogenetic tree clearly shows bacterial clades which were solely found on polarised electrodes (above 2%) or only on non-polarised electrodes.

Fung *et al.* (2006) determined the bacterial community down to class level from glucose and glutamic acid-fed MFC bioanodes which had been grown under oligotrophic conditions (10 mg/l GGA) and copiotrophic conditions (200 mg/l GGA). They observed that with low GGA concentration, 64.4%  $\alpha$ -*Proteobacteria*, 21.1%  $\beta$ -*Proteobacteria* and 3.3%  $\gamma$ -*Proteobacteria* were enriched. Whereas, with 200 mg/l GGA the enriched community contained only 1.4%  $\alpha$ -*Proteobacteria* and 6.8%  $\beta$ -*Proteobacteria* with the relative abundance of  $\gamma$ -*Proteobacteria*,  $\delta$ -*Proteobacteria* and Firmicutes being 36.5%, 14.9% and 13.4% respectively. The data from copiotrophic MFCs in the present study, which analysed communities down to the genus and family level, identified  $\gamma$ -*Proteobacteria* of the *Enterobacteriaceae* family and *Tolumonas* spp.,  $\delta$ -*Proteobacteria* of mainly *Geobacter* spp., and Firmicutes including *Anaeromusa* spp. and *Lactococcus* spp. The lack of  $\delta$ -*Proteobacteria* in the oligotrophic conditions suggested that the electrogenic processes were mediated by bacteria other than *Geobacter* spp.

## 5.4 Conclusions

A comprehensive, multi-faceted evaluation of using multi-stage MFCs as BOD sensors has been completed. Despite initial operational issues a working protocol was established to enable experiments to be conducted in a controlled, repeatable manner. The following conclusions were drawn from the completed study:

- MFCs hydraulically connected downstream of an enriched MFC could be inoculated entirely from the effluent of upstream MFCs (without external addition of micro-organisms).
- For the first time the summed current density from each MFC in a multi-staged hydraulic array was correlated to BOD<sub>5</sub> and used for biosensing.
- At 0.52 ml/min a BOD<sub>5</sub> calibration of the summed current densities from three-stage, flow-mode MFCs achieved a linear detection range of 60 to 720 mg/l O<sub>2</sub> ( $R^2 = 0.975$ ). This range was three-fold greater than the range of the first-stage cell in isolation.
- The Hill equation could be used to model dose-response relationships in each stage

of MFCs up to non-inhibiting concentrations including the 'lag'-phase exhibited by downstream MFCs which did not generate current until upstream MFCs had saturated with substrate.

- The detection range of multi-stage MFC BOD sensors could be increased by increasing the HRT (decreasing the flow rate) and therefore the resulting effluent which was fed to downstream MFCs in the hydraulic array was more degraded.
- The reproducibility of the BOD calibration was excellent across different series of multi-stage MFCs and demonstrated that re-calibration would not be required (providing that the feed composition remained relatively constant).
- In-line feed contamination by bacteria against the direction of peristaltic pump flow could be reduced by UV light exposure at 254 nm and physically prevented from reaching the medium bottle by installation of a sterile drip chamber.
- With high concentrations of GGA medium *Lactococcus*-dominated sludge accumulated in dead zones inside the MFCs with the highest sludge biomass in the first stage cells and lowest in the third stage cells.
- Sludge present inside MFCs inhibited the current generation reversibly (on average by 21%). The sludge occupied the void volume of the anode chamber; reducing the residence time of the medium and exposure to the anode biofilm.
- Degraded gas diffusion electrodes were observed to be fouled by bacterial cells, indicating that membrane failure and subsequent biofouling could have contributed to the decline in performance.
- *Geobacter* spp. and unclassified *Porphyromonadaceae* were highly enriched in MFC anode biofilms and likely responsible for electricity generation from acetate and glucose/acetate respectively.
- Glucose was rapidly fermented in the flow-mode system; primarily in the feed lines leading up to the MFCs. *Dysgonomonas* spp., *Lactococcus* spp. and members of *Enterobacteriaceae* were key bacteria identified in the MFCs associated with sugar fermentation. Despite the consumption of the substrate, the MFC calibrations correlated to medium BOD<sub>5</sub> remained reproducible for given flow rates.
- Glutamic acid was oxidised in the feed lines and through the hydraulic array of MFCs. Glutamate fermenters such as *Anaeromusa* spp. were highly enriched and likely to have employed the methylaspartate pathway to produce acetic and propionic acids.
- Acetic acid and propionic acid were identified as fermentation products accumulated in the flow-mode MFCs. There was a strong indication that lactic acid was probably also produced (unmeasured) based on the community analysis composition.

## **Chapter 6. Using Multi-stage MFC-based Sensors to Differentiate Current Decrease Events Due to Substrate Excess, BOD Decreases & Toxicity**

### **6.1 Introduction**

Two principles of sensing are available to microbial fuel cell-based devices. The primary principle involves electrical current generation by consumption of labile organic carbon ("BOD" or related parameter) by the anodic biofilm. The secondary principle conversely relies upon inhibition of the electrical current by external influences ("toxicity").

Decreases in BOD are the only events leading to loss of current which are desired with sensors solely focused on determination of BOD. Other events which decrease the current due to inhibition cause the calibration models to under-estimate BOD<sub>5</sub> values; therefore reducing the viability and reliability of such a sensor. With combined biomonitoring systems for BOD and toxicity, clear differentiation is required between changes in BOD and presence of toxicants. When used for online process control, the outcomes of the sensor misreporting values are severe. Low BOD indicates that treatment processes (*e.g.* aeration rate) can be reduced, whereas high BOD containing toxicants requires prompt notification to operators that higher levels of treatment are required or possibly diversion of the wastewater feed to protect the micro-organisms in the biological treatment processes.

Combined biomonitoring MFC-based sensors for BOD and toxicity have been the focus of a number of articles in the literature (Kim *et al.*, 2006b; Stein *et al.*, 2010; Di Lorenzo *et al.*, 2014; Xu *et al.*, 2016). The problem many sensors face is that in order to sense toxicity changes the BOD is required to be fixed or *vice versa*. Jiang *et al.* (2016a) recently outlined the issue of detecting combined 'shock' events of BOD and toxicity. They proposed a solution involving maintenance of an additional MFC, fed with artificial feed, to provide a background signal for when toxic events occur. However, the expectation that BOD is constant or the approach involving artificially fixing the substrate concentration is unlikely to be cost-effective, maintainable or transferable to real-world applications.

With single-stage MFCs (the sole subject of the published literature on MFC-based sensing to date), if the BOD is not fixed there is no reliable method for determination of the cause of current decrease events. Because calibration models quantify BOD based on the value of

the electrical current, a decrease can be falsely attributed to a decrease in BOD in certain scenarios. The multi-stage MFCs employed in the present study were hypothesised to possess unique capabilities, permitting three different types of current decrease event to be explicitly differentiated using only the measured current density (Figure 6.1). The three-stage hydraulic array receives the highest concentration of compounds in the first stage MFC, where those which can be degraded are consumed. The second and third stages of MFCs receive the degraded effluent from the upstream MFCs.

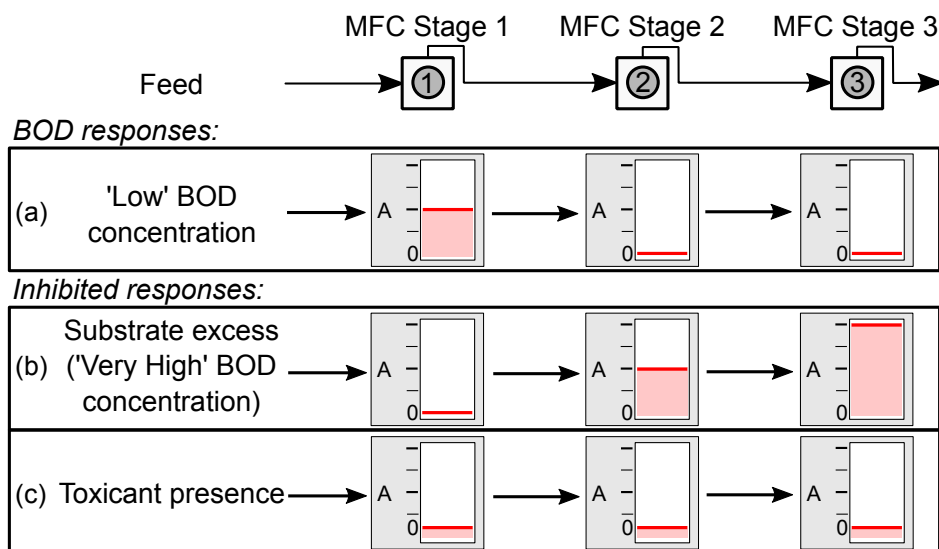


Figure 6.1: Schematic diagram of scenarios regarding BOD sensing and inhibition leading to current loss to be addressed with multi-stage, flow-mode MFCs. Examples are given for (a) 'low' BOD concentrations and inhibition events of (b) substrate excess and (c) toxicant presence. The relative, hypothesised current response (— in amperes (A)) is indicated for each MFC in a three-stage hydraulic array.

Under typical operation of a three-stage BOD sensor (as discussed in Section 5.3.3 of Chapter 5), decreases in BOD result in the greatest current decrease in the third stage MFC. Essentially, the third cell 'starves first' as it receives the degraded effluent of the upstream MFCs. Once BOD is lowered below the saturation concentration of the second and first stage MFCs, the current would be observed to decrease in those cells as well. The current decrease during the course of BOD decrease events could thus be characterised by a  $3 > 2 > 1$  order.

When the BOD concentration is increased significantly beyond levels which the anodic biofilm can withstand, current decrease can be observed due to substrate excess inhibition. In this case, the substrate acts as a biodegradable toxicant and inhibits electrogenic activity by anodic bacteria. As the first stage MFCs receive the highest dose of medium they would be expected to respond (inhibit) the most. As substrate is consumed non-electrogenically in the upstream MFCs, the BOD level decreases to non-inhibiting levels and thus less inhibition is expected to be observed in downstream MFCs. If the downstream MFCs were not saturated they will exhibit a current increase due to increased levels of BOD in the feed that they receive. The current decrease during substrate excess events could therefore be characterised by a

1 > 2 > 3 order of inhibition.

When a toxic compound (toxicant) is present in the feed, similar to the previous case the first staged MFCs will receive the highest dose. However, for non-biodegradable toxicants no consumption will occur and the toxicant concentration would not decrease between the first and third MFC. Consequently the downstream MFCs would be expected to be inhibited the same amount resulting in a lowered current response being observed with each MFC in the hydraulic array. Non-biodegradable toxicant inhibition could be characterised by an approximately equal inhibition in each MFC.

In this chapter, the aim was to demonstrate the capabilities of a multi-stage MFC-based sensor for combined detection of BOD and toxicity 'shock' events. The MFC current was evaluated in response to changes in BOD<sub>5</sub> and presence of 4-nitrophenol (as a model toxicant which is conveniently measured by its UV absorbance with a spectrophotometer) to test the three hypotheses outlined above (Figure 6.1).

## 6.2 Experimental

Flow-mode MFCs (1D, 1E, 1F, 2D, 2E, 2F, 3D, 3E & 3F) which were previously employed for BOD<sub>5</sub> measurement were used in this study (the 'DEF' series of MFCs). The assembly, enrichment, performance and calibration with GGA-based medium were detailed in Chapter 5. For 90-minute tests resulting in current decreases the UV lamp was not operated.

The standard (non-toxic) medium was prepared from phosphate buffer solution, macro-, micro-nutrients, vitamins and a 1:1 mixture of glucose and glutamic acid (GGA; Section 3.3.3). BOD was altered by varying the quantity of GGA in the standard medium. Toxicant-doped medium was prepared by an appropriate addition from a 3 g/l stock solution of 4-nitrophenol (4-NP) to the medium components before the volume was made up with DI water. Toxicity was varied by altering the quantity of 4-NP used in the medium preparation (up to 150 mg/l 4-NP).

For 'shock' testing of inhibition events the BOD<sub>5</sub> was fixed at 360 mg/l O<sub>2</sub> (600 mg/l GGA) in the 5 litre medium bottle and events were simulated by switching the peristaltic pump inlet feed at 1.24 ml/min from the 5 litre bottle to a 500 ml bottle of analyte to be tested (Section 3.3.6 of Chapter 3). The inlet was diverted using the three-way valve (3-W M in Figure 3.5, Chapter 3) installed upstream of the pump. Samples of the effluent from the three-stage MFCs were taken from the final three-way valves (3-W 3). Only short exposure tests were conducted with 'current-decreasing' media pumped for 90 minutes before reconnecting to the non-inhibitory medium feed via valve 3-W M and monitoring the recovery of the current generation. Experiments were conducted starting with the lowest concentration of toxicant (or smallest  $\Delta$  BOD<sub>5</sub>) to ensure that the maximum data could be amassed in the case of total biofilm death due to toxic exposure (Section 3.4.2).

BOD<sub>5</sub> and COD measurements were taken in accordance with the protocols outlined in Section 3.6 of Chapter 3. 4-NP concentrations in acidified anolyte samples were measured directly by the absorbance at 320 nm with a UV spectrophotometer (Section 3.6.8).

The percentage loss (of current) was calculated using Equation 6.1;

$$\%I_{Loss} = \frac{\bar{I}_{Max} - \bar{I}_{Tox}}{\bar{I}_{Max}} \times 100\% \quad (6.1)$$

where  $\bar{I}_{Max}$  is the maximum limiting mean current density and  $\bar{I}_{Tox}$  is the current density with toxicant/inhibitor/starvation presence. The normalised current density (%) was equal to  $\bar{I}/\bar{I}_{Max}$ .

## 6.3 Results & Discussion

### 6.3.1 Multi-stage Microbial Fuel Cell Operation & Response to Substrate Excess

Current decrease due to inhibition by substrate excess was observed during operation of batch-mode MFCs resulting in a lowered current density (Figure 4.7 in Chapter 4). With the single-stage MFC there was no explicit method for determining whether current was decreased due to low BOD or some form of inhibition; consequently the fitted BOD<sub>5</sub> value predicted by the calibration model was less reliable.

During the calibration of the three-stage MFCs as a BOD sensor the linear detection ranges of each stage was determined (Section 5.3.4 of Chapter 5). The range of the first, second and third stages was 25–180 mg/l O<sub>2</sub>, 60–240 mg/l O<sub>2</sub> and 120–420 mg/l O<sub>2</sub> respectively (Figure 6.2a).

The Haldane equation was fitted to the data obtained from BOD calibration up to substrate-excess conditions (1199 mg/l O<sub>2</sub> BOD<sub>5</sub>; Figure 6.2b). The Haldane equation did not simulate the current density response accurately. This was quantified by the regression statistics of  $R^2 = 0.770$ – $0.872$  and  $SD_{Res} = 14$ – $40\%$  indicating a poor fitting model to the data. The estimated  $v_{Max}$  values were highly over-estimated (289–314% for the MFC stages) and there was no difference between the dissociation constants for the concentration at half-maximal current density ( $K_M$ ) and concentration at inhibited current density ( $K_I$ ). Additionally, unlike the Hill equation, the Haldane equation was not able to simulate the ‘lag’ observed with second and third stage MFC calibrations. Jafary *et al.* (2013) previously used the Haldane equation to model inhibited MFC responses to glucose and date syrup concentrations of 2000–30 000 mg/l with  $R^2 = 0.98$ , however did not consider the how well the model fitted the non-inhibited response at low BOD concentrations (*i.e.* < 2000 mg/l).



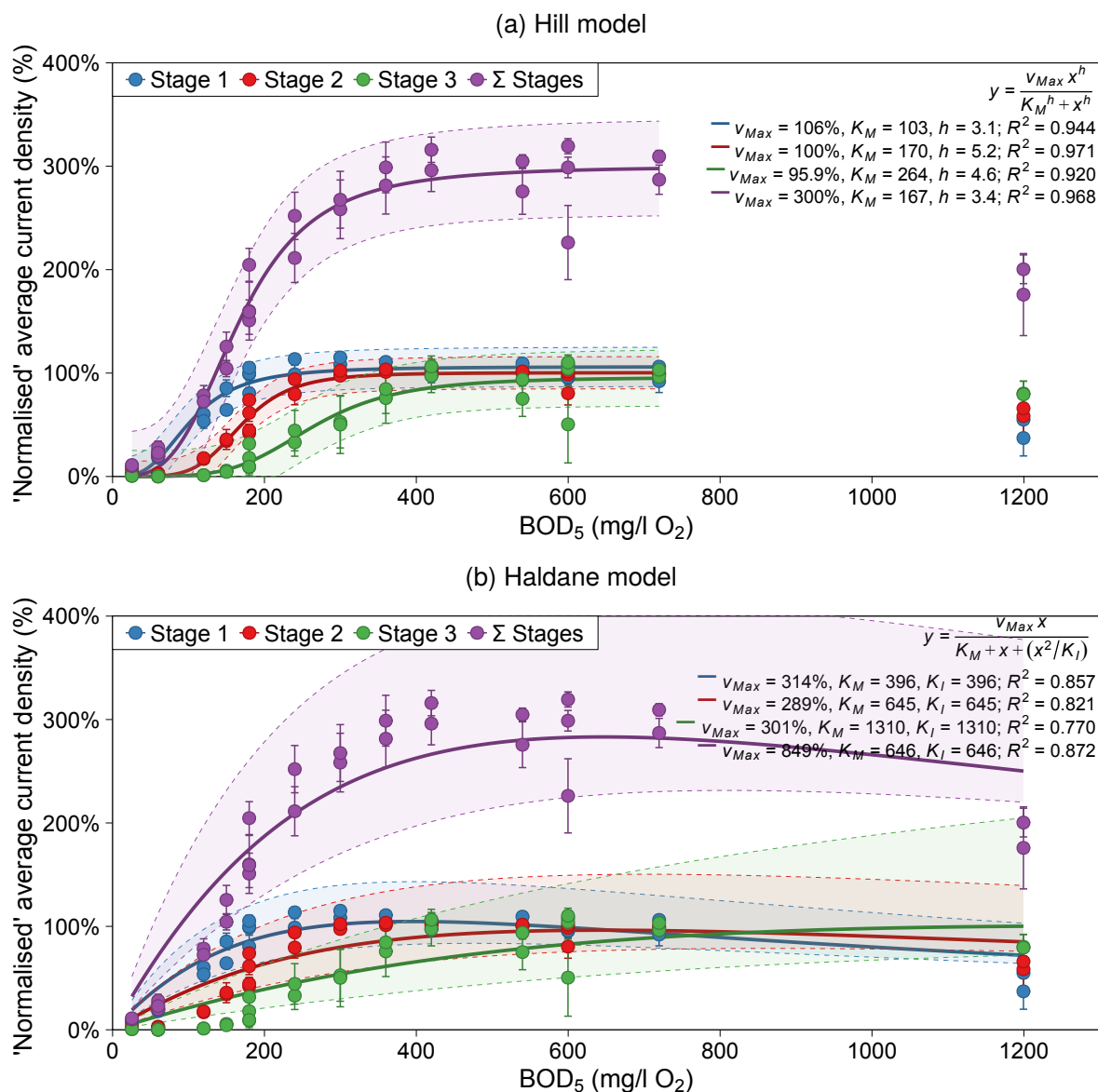


Figure 6.2: Normalised average current density calibration curves for each stage of flow-mode MFCs fitted with the (a) Hill equation up to non-inhibiting concentrations of BOD<sub>5</sub> (estimated from GGA concentration) and (b) Haldane equation for the full calibration range. Data from Calibration 7 (ABC) of the 'ABC' series of flow-mode MFCs (Figure 5.16). The Σ Stages data is normalised to 300% (sum of three MFC stages) to permit comparisons to non-normalised data for convenience. Shaded bands represent the 95% prediction intervals from model lines and error bars are  $\pm$ SD from triplicate cells.

Similar to the observations made with the Michaelis-Menten-fitted calibration curves previously (Section 5.3.3 of Chapter 5), the low and high concentration response was inaccurately modelled by the Haldane equation resulting in an over-estimate of current density. The  $h$  coefficients from the Hill models (Figure 6.2a) indicated a positive co-operativity with increasing concentrations of BOD<sub>5</sub> (GGA) meaning that the affinity for current generation was increased as the concentration was increased (potentially related to the co-community of fermentative bacteria present on the anodes). For this reason (and because adding additional terms to the Haldane model was likely to result in over-fitting errors) use of the Haldane equation was not continued.

The fixed feed concentration of 360 mg/l O<sub>2</sub> BOD<sub>5</sub> was chosen for current decrease tests, as preliminary tests determined that it was sufficient to saturate the first and second stage MFCs and give capacity in the third stage MFCs to increase or decrease current output based on inhibition and starvation treatments (Figure 6.3).

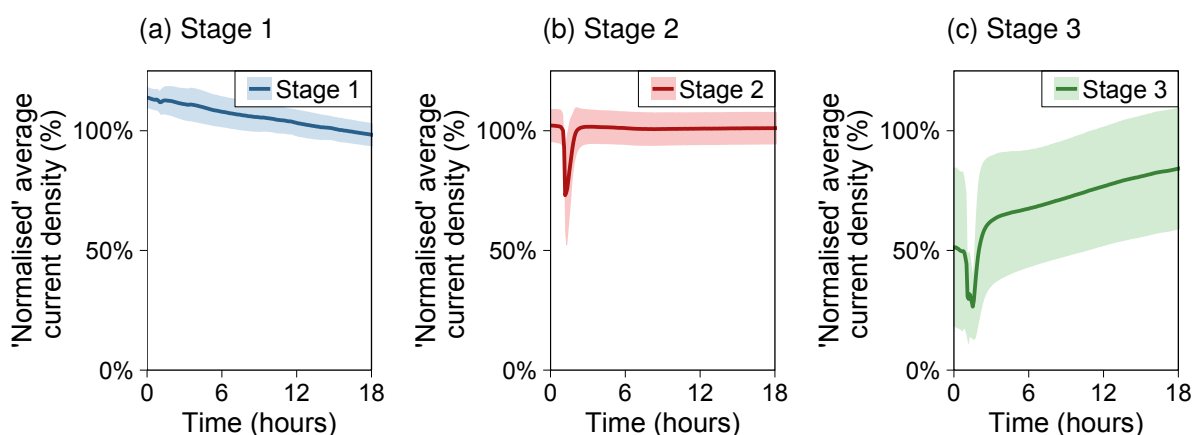


Figure 6.3: Average 'normalised' current density response of the (a) first, (b) second and (c) third stages of flow-mode MFCs to a BOD increase (medium bottle replacement) from 300 to 360 mg/l O<sub>2</sub> BOD<sub>5</sub> (estimated from GGA concentration; showing an increase in third stage response). The inflection point at approximately 1 hour was when the medium replacement procedure occurred (Section 3.2.10). Shaded bands are  $\pm$ SD from triplicate cells.

With a step-up change in BOD<sub>5</sub> from 300 to 360 mg/l the average first and second stage MFCs were observed to remain at 100% of the normalised current density. The average response of the third stage MFCs was to increase up to 76% ( $\pm$  24%) normalised current density (Figure 6.3).

The current density of the three-stage MFCs was assessed in response to a medium concentration step-up change from 150 to 1199 mg/l O<sub>2</sub> BOD<sub>5</sub> (250 to 2000 mg/l GGA; Figure 6.4). At the starting concentration of 150 mg/l O<sub>2</sub>, the first stage MFCs had reached the upper limit of linearity and were almost saturated with an average normalised current density of 85% ( $\pm$  8%). The second and third MFC stages were not saturated at this concentration and had average normalised current densities of 36% ( $\pm$  10%) and 4% ( $\pm$  4%) respectively.

With the 1199 mg/l O<sub>2</sub> medium, as the upper limits of linearity for each stage had been

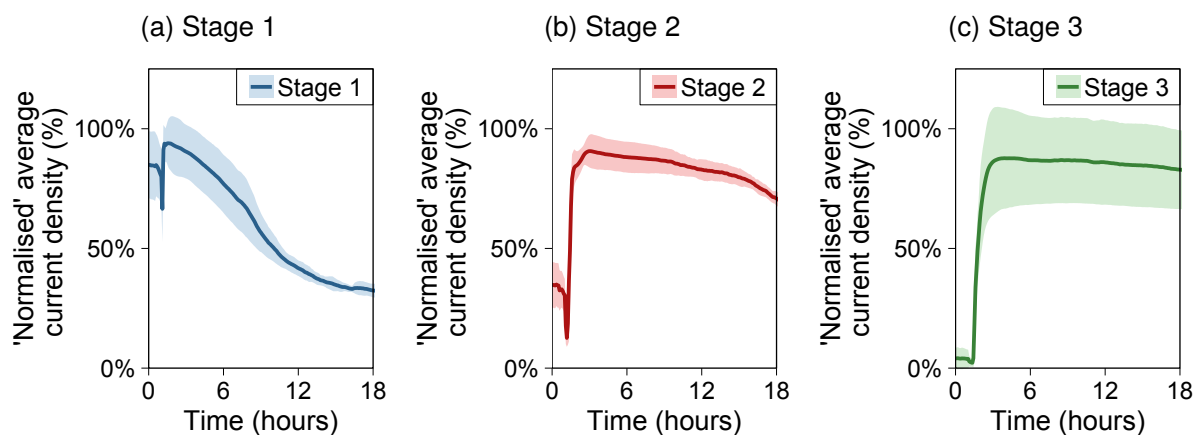


Figure 6.4: Average 'normalised' current density response of the (a) first, (b) second and (c) third stages of flow-mode MFCs to a BOD increase (medium bottle replacement) from 150 to 1199 mg/l O<sub>2</sub> BOD<sub>5</sub> (estimated from GGA concentration; showing greatest current decrease in first stage response). The inflection point at approximately 1 hour was when the medium replacement procedure occurred (Section 3.2.10). Shaded bands are  $\pm$ SD from triplicate cells.

previously determined (as 180, 240 and 420 mg/l O<sub>2</sub> BOD<sub>5</sub> respectively), each MFC was expected to output the maximum current density at this concentration (100%). Immediately after medium replacement the normalised current densities in each stage were observed to increase close to 100% (Figure 6.4). However, despite the increase in concentration, a steady decrease in normalised current density was observed in the first stage MFCs to 37% ( $\pm$  17%). The normalised current density in the second stage of MFCs fell to 58% ( $\pm$  17%) and the third stage MFCs remained at a normalised current density of 80% ( $\pm$  12%).

The trend in normalised current densities (37% < 58% < 80%) showed an increase down the hydraulic series which was concurrent with the predicted order hypothesised earlier (3 > 2 > 1; Figure 6.1). This behaviour of the three-stage MFCs suggested an inhibiting substance was present in the upstream MFCs which was not passed on to the downstream MFCs (*i.e.* a biodegradable inhibitor/toxicant). In this case, because the medium feed is an artificial, known solution and has not changed composition (only concentration) it can be asserted that this effect is the result of substrate excess inhibition.

In Chapter 5, observations were made regarding the MFCs operating with this inhibiting level of substrate. It was found that almost 100 vol% *Lactococcus* spp.-dominated biomass sludge was generated in the first stage MFCs. In the second and third stage MFCs 70 and 35 vol% was found respectively. The sludge reduced the void volume of the anodic chamber, thus resulting in medium spending a reduced residence time inside the cell and a reduced rate of mass transfer to the electrogenic biofilm. Additionally, current decreases were observed at this concentration in the batch-mode cells (Chapter 4) but no sludge was found in the removed anolyte indicating the effect could be more to do with bacterial community composition changes (*i.e.* rapid growth of *Lactococcus* spp.) than physical constraints of the sludge.

### 6.3.2 Response of Multi-stage MFCs to Decreases in BOD

The response of the multi-stage MFCs was assessed in regard to decreases in BOD by diverting the medium feed using the 3-W M three-way valve from a 360 mg/l O<sub>2</sub> BOD<sub>5</sub> medium bottle to a solution of lowered BOD<sub>5</sub> concentration. Five decreased BOD<sub>5</sub> solutions were tested, each over a 90 minute period, before switching back to the 360 mg/l O<sub>2</sub> feed (Figure 6.5).

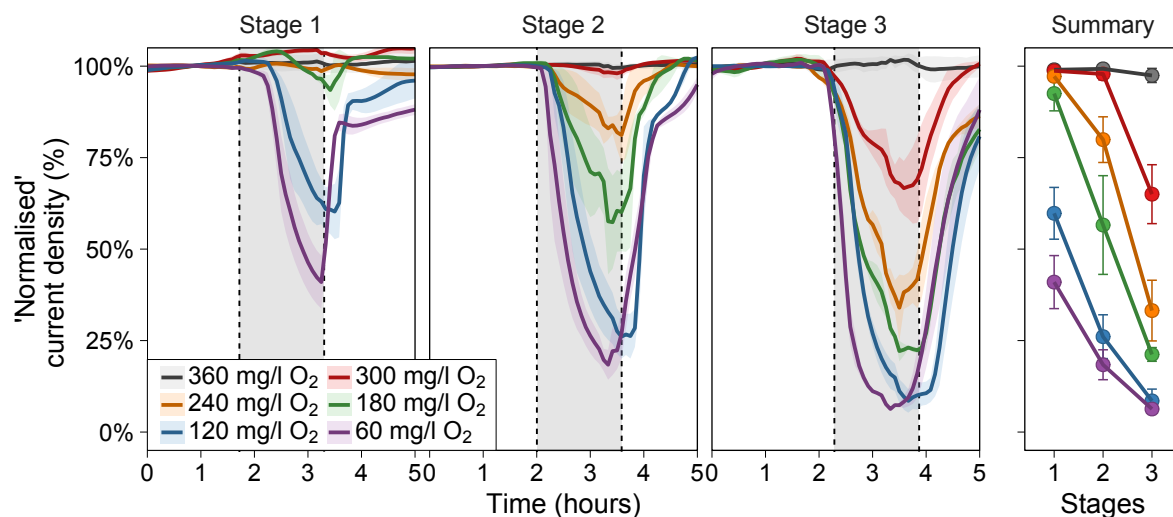


Figure 6.5: Normalised average current density response of three stages of MFCs to decreases in BOD<sub>5</sub> from 360 to 60 mg/l O<sub>2</sub> (estimated from GGA concentration). The dashed line-enclosed region is the period during which the low-BOD medium was fed to MFCs and current decreases were observed. Coloured, shaded bands and error bars are the range of values from duplicate MFCs in flow channels A and C (channel B is black control fed 360 mg/l O<sub>2</sub> BOD<sub>5</sub>). Summary plot shows minima values from each current decrease test cycle at each MFC stage.

With a 300 mg/l O<sub>2</sub> ( $\Delta$  60 mg/l O<sub>2</sub>) BOD<sub>5</sub> medium concentration, no loss of response was observed in the first and second stages of MFCs (*i.e.* remained at 100% ( $\pm$  2%)). The third stage MFCs normalised current density decreased to 65% ( $\pm$  8%). As the BOD<sub>5</sub> concentration was lowered further in subsequent cycles, greater decreases in current density were observed with the third followed by the second and first stages of MFCs. When a 60 mg/l O<sub>2</sub> ( $\Delta$  300 mg/l O<sub>2</sub>) BOD<sub>5</sub> medium was passed through the cells the first, second and third stage MFCs were reduced to 41% ( $\pm$  7%), 18% ( $\pm$  4%) and 6% ( $\pm$  0%) normalised current density respectively.

The trend observed (clearly shown by the Summary plot in Figure 6.5), followed the same order as step-up BOD increases due to the first stage MFCs receiving the highest concentration of substrate, followed by the second and then third stages of MFCs. Thus the third stages responded first ('starved first') as they were fed last. The trend in normalised current densities (*e.g.* 41% < 18% < 6%) showed a decrease down the hydraulic series which was concurrent with the predicted order hypothesised earlier (1 > 2 > 3; Figure 6.1). A calibration

curve fitted to the Hill equation was produced by transforming the current density to current density loss (%) and the medium BOD<sub>5</sub> to the change in BOD<sub>5</sub> ( $\Delta$  BOD<sub>5</sub>; Figure 6.6).

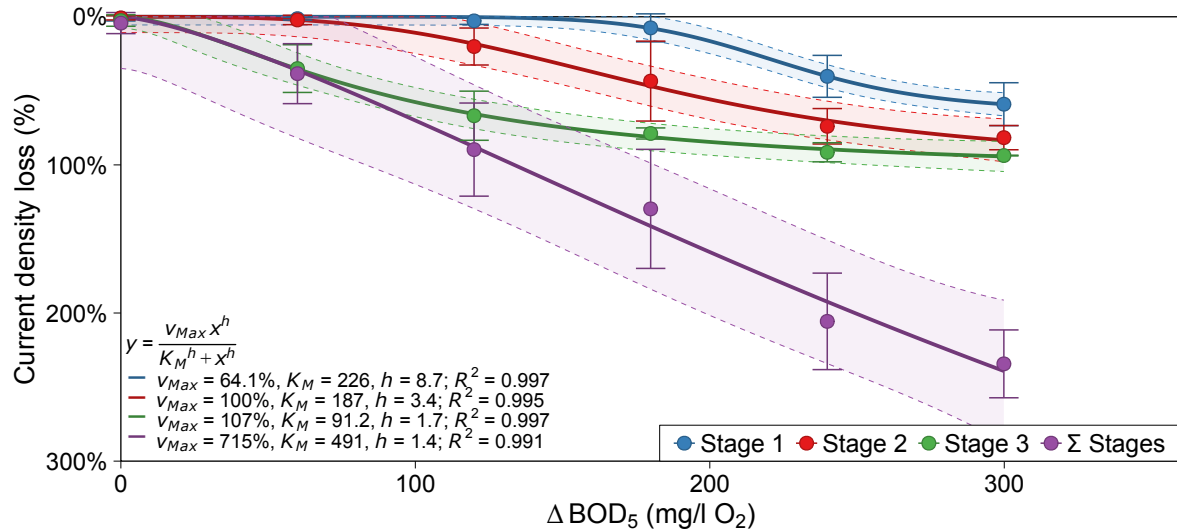


Figure 6.6: Normalised, current density loss calibration curve fitted with Hill model for response of the flow-mode MFCs to 90-minute decreases in BOD ( $\Delta$  BOD<sub>5</sub>; estimated from GGA concentration). Analysis uses 360 mg/l O<sub>2</sub> BOD<sub>5</sub> as the reference point (0% current loss). The  $\Sigma$  Stages data is normalised to 300% (sum of three MFC stages) to permit comparisons to non-normalised data for convenience. Shaded bands represent the 95% prediction intervals from model lines and error bars are range from duplicate cells in flow channels A and C.

The BOD decrease current loss calibration was a reflection of the response observed with current generation (Figure 6.2a). With current generation, the first stage MFCs responded first to the smallest increases in BOD and once they became saturated the second and third MFCs responded. With current loss (due to BOD decrease), the third stage MFCs responded first as the smallest decreases resulted in those cells receiving the least substrate.

The Hill models fitted to the 90-minute BOD decrease calibrations of the first, second, third and sum of stages were highly correlated; with  $R^2$  greater than 0.991 and  $SD_{Res}$  less than 11% of the current density.  $K_M$  values were calculated for decreases in BOD as  $-226 \pm 11$ ,  $-187 \pm 43$  and  $-91 \pm 24$  mg/l O<sub>2</sub> BOD<sub>5</sub> for the first, second and third stage MFCs respectively. A decrease in  $h$  values was observed down the hydraulic array from 8.7 to 3.4 to 1.7. This trend indicated the dependence on the third and second stage MFCs to deplete before the first stage would become depleted.

### Analysis of Effluent from MFCs During BOD Decrease Events

Immediately following the restoration of the 360 mg/l O<sub>2</sub> BOD<sub>5</sub> feed samples were taken from each flow channel at the 3-W 3 three-way sampling valve. The flow path took 59 minutes at 1.24 ml/min to reach the 3-W 3 valves (passing through the first, second and third MFC stages), therefore after 90 minutes of testing low BOD solutions the effluent would have been

flowing past this sampling point for 45 minutes already (Table B.1 in Appendix B). Samples were also taken of the fresh low BOD medium prior to feeding to the MFCs (Figure 6.7).

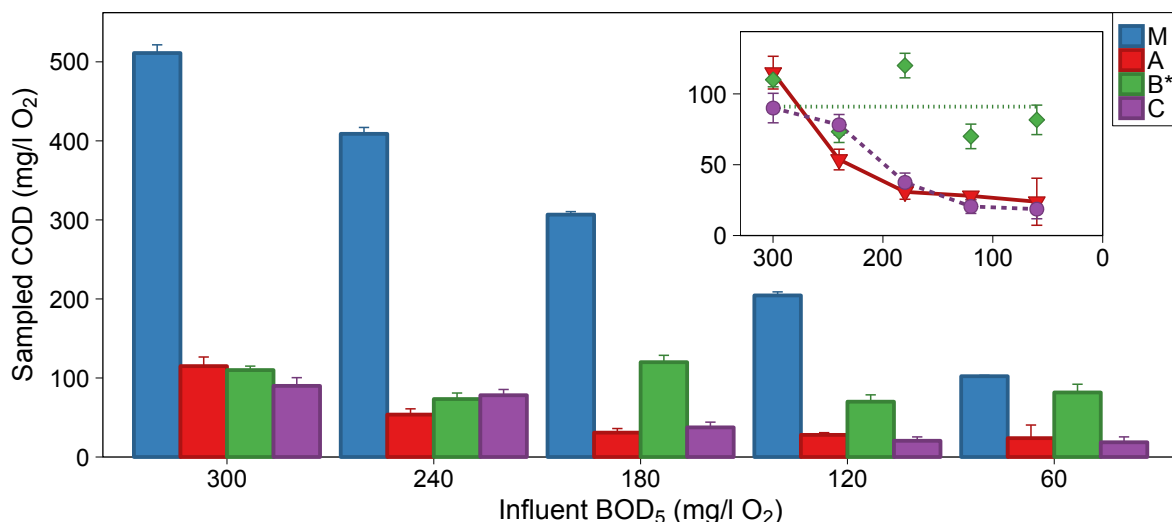


Figure 6.7: COD measured at each sampling point after 90 minutes of BOD decrease from 360 mg/l O<sub>2</sub> BOD<sub>5</sub> (estimated from GGA concentration; M = Fresh medium sample; A, B & C = Final effluents from 3-W 3 valve in each flow channel). Inset shows effluents from each channel in a line graph. Error bars are the range from duplicate measurements. \*Channel B was maintained at 360 mg/l O<sub>2</sub> BOD<sub>5</sub> as a control.

With each decrease down to 60 mg/l O<sub>2</sub> BOD<sub>5</sub> (102 mg/l O<sub>2</sub> COD), the effluent COD of the flow channels A and C was observed to decrease by  $84 \pm 5\%$ . The effluent reduced from  $115 \pm 12$  mg/l O<sub>2</sub> COD and  $90 \pm 10$  mg/l O<sub>2</sub> COD down to  $24 \pm 1$  mg/l O<sub>2</sub> COD and  $19 \pm 7$  mg/l O<sub>2</sub> COD in channels A and C respectively. The effluent from flow channel B, which was maintained as a control at a constant BOD<sub>5</sub> of 360 mg/l O<sub>2</sub> (613 mg/l O<sub>2</sub> COD), was quite variable between samples but remained approximately constant at  $91 \pm 23$  mg/l O<sub>2</sub> COD averaged over all treatments (Figure 6.7, inset).

The samples analysis confirmed the theory that with decreases in BOD the concentration of substrate received at the third stage of MFCs decreased. This led to the observed order in current decreases as the third stages of MFCs became depleted of substrate (starved) first and thus generated the least current.

### 6.3.3 Response of Multi-stage MFCs to Toxicant Presence

The response of the multi-stage MFCs to toxicant exposure was assessed with 4-nitrophenol (4-NP) present in the anolyte feed. A similar method to Section 6.3.2 for testing BOD decreases was employed, which involved diversion of the medium feed using the 3-W M three-way valves from a 360 mg/l O<sub>2</sub> BOD<sub>5</sub> medium bottle to a solution of toxicant-doped medium at the same BOD<sub>5</sub> concentration as the control. Five toxicant-doped medium solutions were tested over a 90 minute period each before switching back to the 360 mg/l O<sub>2</sub> feed to enable biofilm recovery (Figure 6.8).



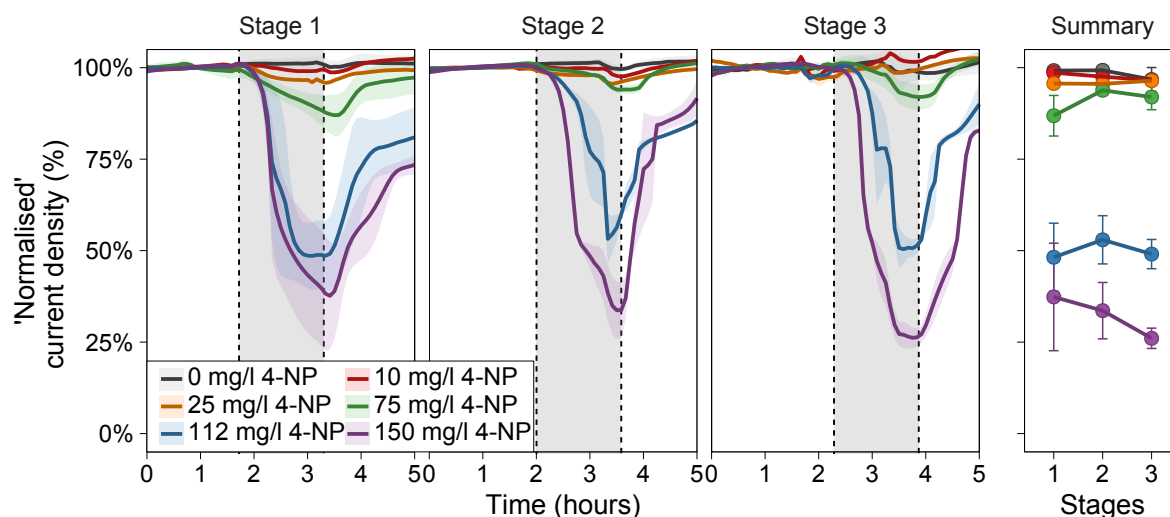


Figure 6.8: Normalised average current density response of three stages of MFCs to increasing concentrations of 4-nitrophenol (4-NP) from 0 to 150 mg/l. The dashed line-enclosed region is the period during which the toxicant-doped medium was fed to MFCs and current decreases were observed. Coloured, shaded bands and error bars are the range of values from duplicate MFCs in flow channels A and C (channel B is black control fed 0 mg/l 4-NP). Summary plot shows minima values from each current decrease test cycle at each MFC stage.

No loss in current response was detectable with 4-NP concentrations of 10 and 25 mg/l in the three-stage MFCs. As the 4-NP concentration was increased to 75 mg/l and above in subsequent cycles, decreases in current density were observed in each MFC stage. When a 150 mg/l 4-NP-doped medium was passed through the cells the first, second and third stage MFCs were reduced to 37% ( $\pm 29\%$ ), 34% ( $\pm 15\%$ ) and 26% ( $\pm 6\%$ ) normalised current density respectively. There was no ordered trend observed along the hydraulic series (shown by approximately equal current decreases (inhibition) in each MFC stage in the Summary plot in Figure 6.8). Thus the decrease in current density response was distinct from BOD-related current decreases (both substrate excess inhibition and BOD decreases). This observation suggested that the toxicant was not consumed within the MFCs and each stage received approximately the same dose of toxicant, resulting in the same degree of inhibition (as hypothesised for non-biodegradable toxicants in Figure 6.1).

After the non-toxic medium had been restored, the current density recovery following the 150 mg/l 4-NP toxic exposure was monitored (Figure 6.9). 11.5 hours after the 360 mg/l BOD<sub>5</sub> medium feed had been restored, the inhibited MFCs recovered to the same normalised current density as the control MFC (in flow channel B). This recovery period was much greater than the recoveries up to four hours observed for the exposure tests with 4-NP concentrations below 112.5 mg/l (Table 6.1). Kim *et al.* (2007) also observed increased recovery times following increased levels of toxicity (up to 8 hours following a 1 mg/l cadmium dosing). The fact the biofilm completely recovered to pre-toxic current density showed the resilience of a MFC-based sensor.

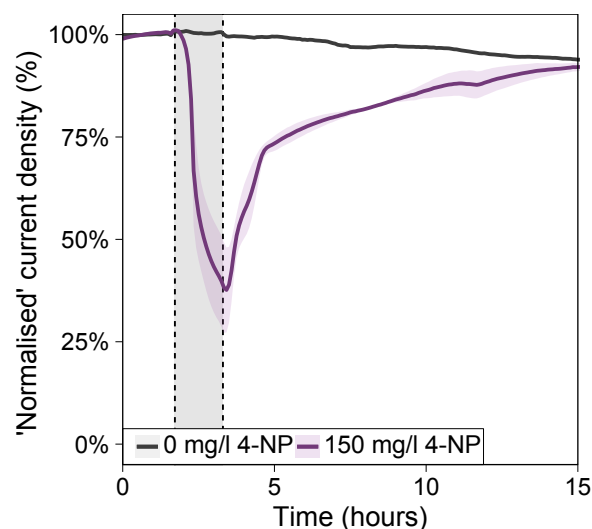


Figure 6.9: Normalised average current density response of the first stage of MFCs to 150 mg/l 4-NP, followed by the recovery to 100% normalised current density over 11.5 hours. The dashed line-enclosed region is the period during which the toxicant-doped medium was fed to MFCs and decreases in current density were observed. The coloured, shaded band is the range of values from duplicate MFCs in position 1A and 1C (the 1B response is the control fed 0 mg/l 4-NP in black).

Table 6.1: Recovery times of three-stage MFCs to toxic media containing 4-NP. Recovery times calculated between time that non-toxic feeding was restored from valve 3-W M and the point at which the normalised current density in Channels A and C was equal to that of Channel B (control fed with no 4-NP). The HRT-adjusted recovery times (time between non-toxic feed reaching the MFC and the normalised current density recovering) are given in brackets for each MFC stage (as detailed in Section 3.4.2).

4-NP (mg/l)	Recovery time (hours)						$\Sigma$ Stages
	Stage 1		Stage 2		Stage 3		
10.0	1.2	(0.9)	2.0	(1.5)	2.0	(1.2)	2.0
25.0	1.5	(1.2)	2.0	(1.5)	2.0	(1.1)	2.0
75.0	2.7	(2.4)	2.7	(2.1)	2.8	(1.9)	2.8
112.5	3.8	(3.5)	2.8	(2.2)	3.1	(2.2)	3.8
150.0	11.5	(11.2)	2.8	(2.2)	3.5	(2.6)	11.5



A calibration curve fitted to the Hill equation was produced by transforming the current density to current density loss (%; Figure 6.10). The 4-nitrophenol calibration was distinct from the BOD-varying calibrations (Figures 6.2a and 6.6). The response from each stage of MFCs was approximately the same and there was no statistical difference between the Hill model of each stage.

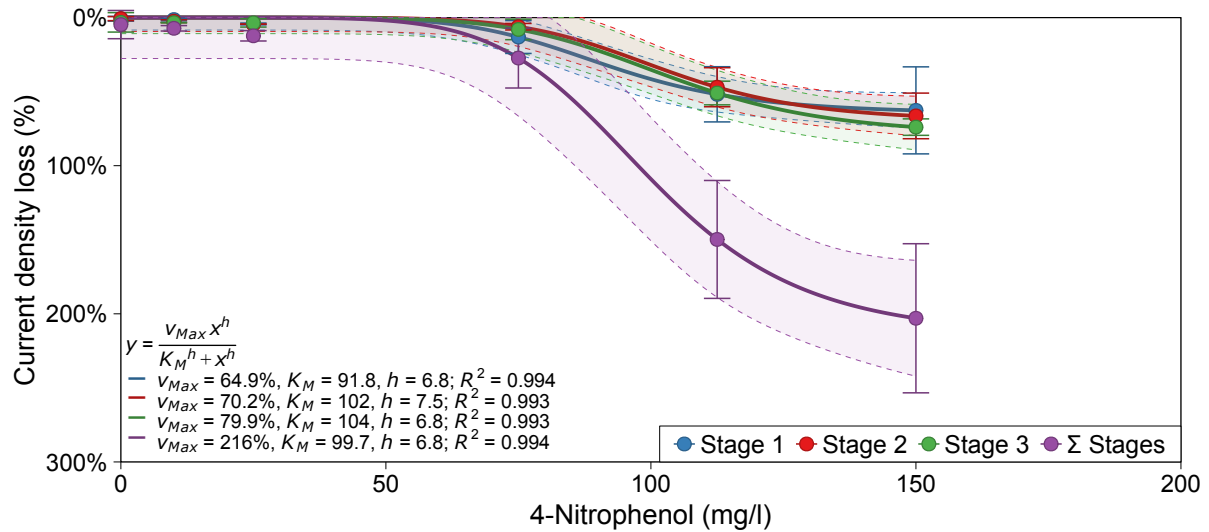


Figure 6.10: Normalised, average current density loss calibration curve fitted with Hill model for response of the flow-mode MFCs to 90-minute exposures to 4-NP. The  $\Sigma$  Stages data is normalised to 300% (sum of three MFC stages) to permit comparisons to non-normalised data for convenience. Shaded bands represent the 95% prediction intervals from model lines and error bars are range from duplicate cells in flow channels A and C.

The Hill models fitted to the 90-minute 4-NP exposure calibrations of the first, second, third and sum of stages were highly correlated; with  $R^2$  greater than 0.993 and  $SD_{Res}$  less than 9% of the current density. However only three data points were non-zero (current decreases occurred only at concentrations of 75 mg/l 4-NP and above) which is not sufficient for creating an accurate calibration model. The  $K_M$  values were calculated for inhibition due to exposure to 4-NP as  $92 \pm 9$ ,  $102 \pm 9$  and  $104 \pm 10$  mg/l 4-NP for the first, second and third stage MFCs respectively. Approximately equal  $h$  values were observed of  $6.8 \pm 2.9$ ,  $7.5 \pm 3.8$  and  $6.8 \pm 3.6$  respectively. These parameters quantified how similar each response and resulting calibration was from each MFC stage. With increasing concentrations of 4-NP, each MFC stage approached 100% loss of current at the same rate.

### Analysis of Effluent from MFCs Exposed to 4-Nitrophenol

As with the low BOD experiments, samples were taken from the 3-W 3 valve in each channel immediately following the restoration of the non-inhibitory GGA feed (360 mg/l  $O_2$  BOD<sub>5</sub>). Samples were also taken of the fresh 4-NP-doped medium prior to feeding to the MFCs (Figure 6.11).

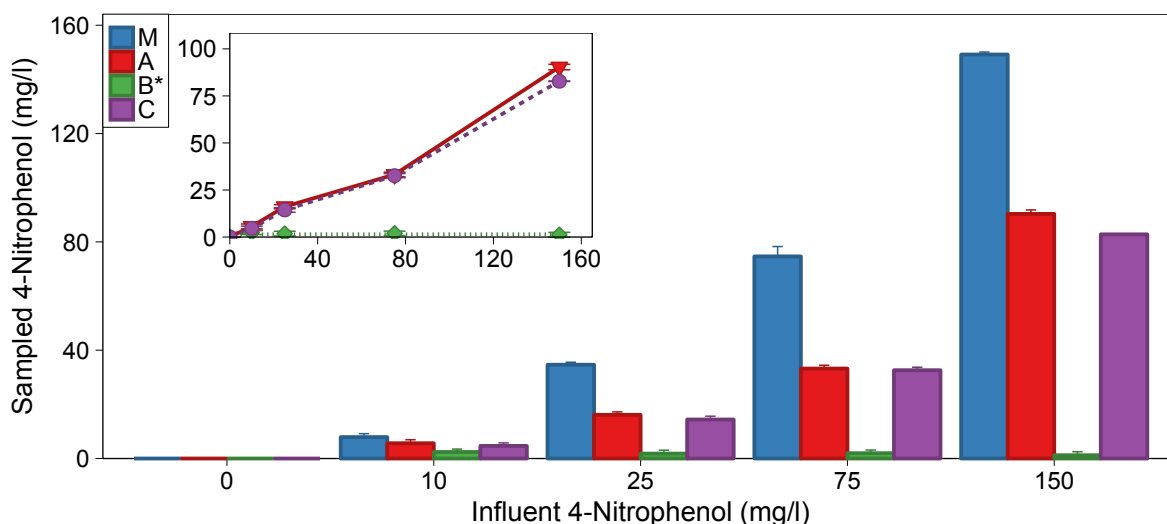


Figure 6.11: 4-Nitrophenol (4-NP) concentrations measured at each sampling point after 90 minutes of toxicant exposure (M = Fresh medium sample; A, B & C = Final effluents from 3-W 3 valve in each flow channel). Inset shows effluents from each channel in a line graph. Error bars are the range from duplicate measurements. \*Channel B was maintained with no 4-NP as a control.

The effluent 4-NP concentration of the flow channels A and C was observed to decrease compared to the initial 4-NP-doped medium concentrations of up to 150 mg/l 4-NP. The 4-NP concentrations in effluents from channels A and C decreased on average by  $47 \pm 10\%$  (Figure 6.7). The effluent from flow channel B, which was maintained as a control at a constant  $\text{BOD}_5$  of 360 mg/l  $\text{O}_2$  showed no absorption in the UV-vis spectra indicating that the values obtained for channels A and C could be attributed to 4-NP presence.

The samples analysis showed that there had been a decrease in 4-NP concentration through the hydraulic array of MFCs. 4-nitrophenol is biodegradable in aerobic environments by specially adapted bacteria which are able to convert 4-NP to non-toxic nitrite and then utilise the carbon- and nitrogen-containing degradation products (Samuel *et al.*, 2014). Bacteria in anaerobic methanogenesis bioreactors have previously been acclimatised to 4-NP degradation up to 100 mg/l after weeks of exposure (O'Connor and Young, 1989). However, the tests in the present study were conducted over the course of 90 minutes which was not expected to be enough time to acclimatise 4-NP-degrading bacteria (by the time the feed had reached the 3-W 3 valve and sampling was performed after only 45 minutes of exposure had elapsed).

It is therefore thought that the decrease in 4-NP occurred due to non-biological processes such as dilution due to the HRT or adsorption within the hydraulic array. When the 4-NP reached each 10 ml MFC chamber it is possible that the toxicant may have become mixed with non-toxic medium and thus diluted. With the HRT to reach the 3-W 3 valve approximately 45 minutes, and only 90 minute toxicity tests being conducted (for operational and biofilm recovery reasons), it is likely that steady-state mixing and equilibration of the toxic medium across the hydraulic array had not occurred at the time of sampling (at least  $3 \times \text{HRT} = 135$

minutes would be required). By 4-NP persisting for longer within the hydraulic array it would explain the prolonged recovery time of the MFCs with high concentrations of 4-NP. The observed current response of the MFCs did not appear to show that the 4-NP was being consumed/degraded, as an equal degree of inhibition was observed in each stage. For toxicants which are degraded as medium passed through the hydraulic array the response would be expected to be similar to the substrate excess where the first stage MFCs receive the greatest dose. Further investigations, including lengthier exposure periods and sampling after each stage of MFCs would be required to confirm degradation pathways of 4-NP.

## 6.4 Conclusions

Three operating scenarios were hypothesised to be distinctly identifiable with a multi-stage MFC sensor. The results from this chapter successfully provided examples which were in agreement with the outlined hypotheses. The following conclusions were drawn:

- Multi-stage MFC-based sensors provide valuable, additional information which is unavailable with single-stage sensors. By comparing Figures 6.4a, 6.6 (Stage 1) and 6.10 (Stage 1), there is no way to differentiate between substrate excess, BOD decrease or toxicant presence leading to decreased current density. The multi-stage MFCs exhibited an ordered response which could be used to explicitly differentiate 'shock' event types.
- Under 'normal' (non-inhibited) operation of a three-stage MFC sensor; increases in BOD<sub>5</sub> generated current in the first stage MFCs until saturation occurred, followed by the second and third stages of MFCs at higher concentrations (indicated by fitted  $K_M$  values of 96, 166 and 265 mg/l O<sub>2</sub>). The current *increases* followed the order 1 > 2 > 3.
- Increases in BOD<sub>5</sub> to excessive levels of substrate (e.g. 1199 mg/l O<sub>2</sub>) resulted in the loss of current in the upstream MFCs first as the 'strongest dose' was received there. Current decreases due to substrate excess inhibition were observed to have an ordered inhibited response of 1 > 2 > 3.
- Decreases in BOD<sub>5</sub> led to a decrease in current density (as would be expected for a BOD sensor). The decrease in current densities due to BOD decreases were observed to have an ordered inhibited response of 3 > 2 > 1. The reason the order was the reverse of the order observed with current increases is that the third stage MFCs received the lowest concentration of substrate and therefore 'starved first' (confirmed by a lower level of COD obtained from effluent samples during low BOD tests).
- The effect of toxicant presence was assessed using 4-NP, and current decreases were observed with increasing concentrations of toxicant. No ordered response was observed, with each stage of MFC being equally inhibited by the toxicant (non-competitive

inhibition) as the medium passed through the hydraulic array.

- 4-NP concentrations taken from the effluent of the hydraulic array were lower than the fresh toxicant-doped medium concentrations. Further investigation would be required to determine whether the reduction was due to (a) biodegradation, (b) adsorption or (c) simply a HRT dilution effect due to the short incubation (90 minutes incubation vs. 45 minutes HRT) following operation with non-toxic medium.
- MFC-based toxicity sensors were shown to be capable of full recovery to pre-toxic current densities, however recovery from highly toxic 'shock' events could take considerable time (*e.g.* 11.5 hours following a 150 mg/l 4-NP dosing) to recover to 100% normalised cell density.

## **Chapter 7. Recommendations for BOD Sensor Validation from Estimation of BOD with Different Substrates and Real Wastewater**

### **7.1 Introduction**

Performance criteria for assessment of BES-based BOD sensors are required to enable valid comparisons between different studies. A sensor is defined by its calibrated response and it is therefore essential that standardised protocols are used. Previous investigators have performed calibrations using artificial wastewater and then tested sensors using real wastewater. Many authors have noted an under-estimate of BOD by the sensor when compared by a standard validation method (Kang *et al.*, 2003; Kim *et al.*, 2003b; Moon *et al.*, 2005; Di Lorenzo *et al.*, 2009a). Feng *et al.* (2013b) proposed an innovative model in which four different substrates (acetate, butyrate, glucose and corn starch) of the same concentration could be identified by the peak height and area of their current response profile. Additionally, Kaur *et al.* (2013) reported different responses observed for MFCs acclimated with different VFAs (acetate, propionate and butyrate). Hsieh *et al.* (2015) tested various carbohydrates, amino acids, organic acids and alcohols with MFCs acclimated to GGA medium and established that different current densities were obtained with each, under a fixed concentration of 100 mg/l O<sub>2</sub> BOD<sub>5</sub>. By contrast, Zhang and Angelidaki (2011) and Yang *et al.* (2013) stated that their artificial calibrations (with acetate/glucose and GGA respectively) could successfully predict real wastewater BOD<sub>5</sub> values with high accuracy and highly similar current density values. The limited number of reports in the literature, especially with regard to field tests with real wastewaters, indicate the need for further investigation.

In this chapter the aim was to demonstrate the difference between calibrations (rather than just current density) obtained using media of different composition and outline the need for standard validation techniques for predictive BOD sensors.

### **7.2 Experimental**

Validation techniques were compared using 'artificial' wastewater standards comprising either only glucose, only glutamic acid or GGA as the carbon source. The effect on BOD

calibration of batch-mode MFC sensors enriched with GGA-based medium was determined. The response of batch-mode and multi-stage, flow-mode sensors to real raw wastewater was also evaluated. To underline the need for standardised validation, a systematic comparison of the data from the present study and data obtained from BES-based sensors reported in the literature was used.

Medium was prepared from phosphate buffer solution, macro-, micro-nutrients and vitamins in addition to various concentrations of carbon source of either D-glucose (G), L-glutamic acid (GA) or a 1:1 mixture of each (GGA). Raw influent wastewater was collected from Tudoe Mill sewage treatment works (Northumbrian Water, UK). The conductivity of the wastewater was adjusted to approximately 8 mS/cm in order to match the ionic conductivity of the artificial (G, GA and GGA-based) media employed to ensure calibration validity.

BOD<sub>5</sub> and COD measurements were taken in accordance with the protocols outlined in Section 3.6. ThOD was calculated from the stoichiometric amount of oxygen required to oxidise each substrate (Figure B.11 in Appendix B). Substrate concentrations were calculated as the weighed out masses divided by the as-prepared medium volume. In addition, the pH, conductivity, dissolved organic carbon (DOC), inorganic carbon (IC) and anion concentrations were determined (as detailed in Section 3.6).

Batch-mode MFCs (replicates A & B and C & D) and flow-mode MFCs (1D, 1E, 1F, 2D, 2E, 2F, 3D, 3E & 3F) were the same cells as used in Chapter 4 and 5 respectively, where the assembly, enrichment, performance and long-term calibrations with GGA-based medium were detailed. The multi-substrate calibrations of batch-mode MFCs of concern in this chapter were Calibration 10 from cells A and B and Calibration 1 from cells C and D, repeated in Table 7.1 below for clarity.

Table 7.1: Details of calibrations involving different substrates; glucose (G), glutamic acid (GA) and GGA, performed using batch-mode cells A & B and C & D.

ID	Start time (day) <sup>a</sup>	No cycles <sup>b</sup>	Substrate	BOD <sub>5</sub> range (mg/l O <sub>2</sub> ) <sup>c</sup>	<i>R</i> <sub>Ext</sub> (Ω)
10a (AB)	792	8	GGA	32–1199	43.2
10b (AB)	792	8	G	29–1264	43.2
10c (AB)	792	10	GA	60–1155	43.2
1a (CD)	56	27	GGA	15–900	43.2
1b (CD)	56	13	G	32–1264	43.2
1c (CD)	56	15	GA	29–1155	43.2

<sup>a</sup> Start time of first batch medium cycle included in calibration.

<sup>b</sup> Number of cycles included in the calibration.

<sup>c</sup> BOD<sub>5</sub> estimated from substrate concentration.

## 7.3 Results & Discussion

### 7.3.1 Comparison of Validation Techniques for Glucose, Glutamic acid and GGA-based Medium

Solutions of glucose (G), glutamic acid (GA) and GGA medium of 300 mg/l substrate concentration were analysed using the BOD<sub>5</sub> test and COD photometric assay. The theoretical oxygen demand (ThOD) and theoretical organic carbon (ThOC) were also calculated. The average current density, charge density and coulombic efficiency over a 300 mg/l medium cycle (until depletion at approximately 24 hours) was calculated from batch-mode cells A, B, C and D (Table 7.2).

It was evident from the results that the aerobic oxygen demand determinations each exhibited the same correlation; which was to be expected for completely assimilable substrates. The ThOD values indicated that, for complete oxidation at equal mass concentrations (300 mg/l), glucose had a 5% higher carbonaceous oxygen demand and glutamic acid demanded 5% less than the equivalent GGA value (Table 7.2). The COD test oxidises all carbonaceous organic matter and therefore COD values were expected to be close to the ThOD values; according to Ramalho (1977) the values should not be equal due to inefficiencies and interferences which occur with chemical oxidation and the dichromate reflux method.

The BOD<sub>5</sub> values for glucose and glutamic acid as a percentage of the GGA values (105% and 96% respectively) were approximately equal to the ThOD percentages (104% and 96%; Table 7.2). This indicated that glucose and glutamic acid had similar net biological oxidation rates over five days; the carbonaceous organic matter present in a sample is only partially consumed over five days in the BOD<sub>5</sub> test. This was reflected in the similar BOD<sub>5</sub>/COD ratios for glucose and glutamic acid of 0.640 and 0.584 respectively (significant with a  $p$ -value of  $7.27 \times 10^{-7}$  from Welch's unequal variances t-test with a null hypothesis that glucose and glutamic acid BOD<sub>5</sub>/COD ratios were equal; Table 7.2). With all validation methods and MFC response outputs the GGA values determined from medium with a 1:1 ratio of each substrate were approximately the mean of the glucose-only and glutamic acid-only values.

The average response outputs ( $\hat{I}$ ,  $Q_{Cyc}$  and  $C_E$ ) from the batch-mode MFC sensors exhibited the opposite trend compared to the oxygen demand determination methods (BOD<sub>5</sub>, COD and ThOD). The values for glucose were approximately 25% *less* than the corresponding GGA values and glutamic acid values were approximately 25% *higher*. For medium containing glutamic acid only higher peak current densities, larger charge densities and higher coulombic efficiencies ( $C_E$ ) than for glucose medium cycles were observed (Figure 7.1).

This is an important finding which demonstrates that although the MFC response can be correlated with oxygen demand for specific substrates, the same calibration cannot be applied for different individual compounds or mixtures without recalibration. In previous studies, this

Table 7.2: Comparison of values measured by validation methods and MFC response outputs (peak current ( $\hat{I}$ ), charge over cycle ( $Q_{Cyc}$ ) and coulombic efficiency ( $C_E$ )) for a medium containing 300 mg/l glucose, glutamic acid and GGA. The MFC data are the average ( $\pm$ SD) from batch-mode cells A, B, C & D.

Validation Method	GGA Value	Glucose		Glutamic acid		<i>t</i> -test ( <i>p</i> -value) <sup>a</sup>
		Value	% of GGA	Value	% of GGA	
Mass conc. (mg/l)	300.0	300.0	(100%)	300.0	(100%)	-
Molar conc. (mmol/dm <sup>3</sup> )	1.833	1.665	(91%)	2.039	(111%)	-
ThOC (mg/l C)	121.2	120.0	(99%)	122.5	(101%)	-
ThOD (mg/l O <sub>2</sub> )	306.7	319.7	(104%)	293.6	(96%)	-
BOD <sub>5</sub> (mg/l O <sub>2</sub> )	179.9 $\pm$ 9.4	189.7 $\pm$ 8.0	(105 $\pm$ 4%)	173.2 $\pm$ 13.0	(96 $\pm$ 7%)	6.33 $\times 10^{-3}$
COD (mg/l O <sub>2</sub> )	282.0 $\pm$ 4.1	296.3 $\pm$ 2.7	(105 $\pm$ 1%)	266.0 $\pm$ 3.3	(94 $\pm$ 1%)	2.90 $\times 10^{-4}$
BOD <sub>5</sub> /COD ratio	0.607 $\pm$ 0.031	0.640 $\pm$ 0.026	(105 $\pm$ 4%)	0.584 $\pm$ 0.042	(96 $\pm$ 7%)	7.27 $\times 10^{-7}$
$\hat{I}$ ( $\mu$ A/cm <sup>2</sup> )	96.5 $\pm$ 22.0	71.4 $\pm$ 19.8	(74 $\pm$ 21%)	109.9 $\pm$ 17.3	(114 $\pm$ 18%)	2.69 $\times 10^{-2}$
$Q_{Cyc}$ (C/cm <sup>2</sup> )	53.0 $\pm$ 11.6	40.3 $\pm$ 11.1	(76 $\pm$ 21%)	66.7 $\pm$ 10.5	(126 $\pm$ 20%)	1.37 $\times 10^{-2}$
$C_E$ (%)	34 $\pm$ 7%	25 $\pm$ 7%	(73 $\pm$ 20%)	43 $\pm$ 7%	(128 $\pm$ 21%)	8.87 $\times 10^{-3}$

<sup>a</sup> *p*-value from Welch's unequal variances *t*-test with a null hypothesis that the values from glucose and glutamic acid measurements have equal means. In all cases the null hypothesis was rejected at the 95% confidence level (*p*-value < 0.05); indicating that the difference between glucose and glutamic acid measurements were statistically significant.



phenomenon has been attributed to biofilm acclimatisation and recommendations have suggested starting up MFCs with feed of a similar composition to samples that will be measured (Kang *et al.*, 2003).

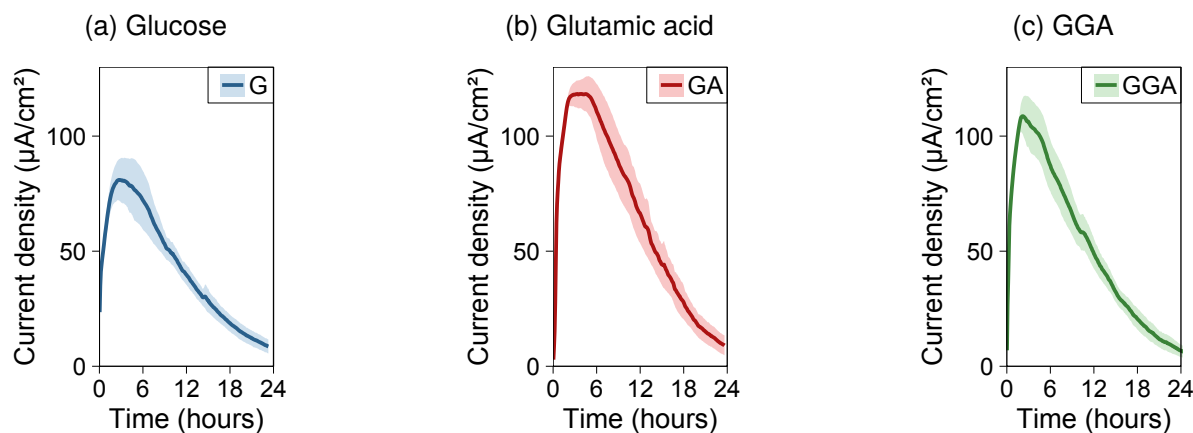


Figure 7.1: Average current density response for batch cycles in which 300 mg/l (a) glucose, (b) glutamic acid and (c) GGA was fed to batch-mode MFCs C and D. Cycles were recorded between 161 and 164 days of operation where cathode degradation was negligible and thus current densities can be compared. Shaded bands are the range between cell C & D.

In the present work, the biofilms were enriched and operated using a 1:1 mixture of glucose and glutamic acid, therefore the biofilm will have developed with bacteria selected for their ability to oxidise both these two substrates and generate electricity. This is believed to be the first study where the difference between different substrate responses cannot be attributed solely to biofilm acclimatisation. There is an increasing body of evidence showing that, because the MFC-based sensing is performed anaerobically, there are fundamental differences between oxidation rates in MFCs when compared to aerobic oxygen demand validation methods (Feng *et al.*, 2013b; Kaur *et al.*, 2013; Commault *et al.*, 2015; Hsieh *et al.*, 2015).

The coulombic efficiencies ( $C_E$ ) showed that less than half the substrate consumption resulted in electricity generation; only 25% with glucose, 43% with glutamic acid and 33% in GGA-fed cycles (Table 7.2). This indicated that other significant processes which consumed substrate were occurring in competition to the electrogenic anode biofilm. MFCs are not expected to achieve 100% coulombic efficiency as some substrate is consumed for biomass production and, with SCMFCs especially, an influx of oxygen through the MEA allows bacteria to metabolise without interacting with the electrode. Nonetheless, Logan (2008) estimated that the highest coulombic efficiencies in MFCs have been approximately 85% with 15% used for creation of biomass, thus indicating in the present study there were additional processes occurring.

Microbial fermentation and methanogenesis are key anaerobic processes which do not occur aerobically (Torres *et al.*, 2007; Kim *et al.*, 2011b); coulombic losses are due to metabolite generation and gas production ( $H_2$  and  $CH_4$  respectively). In the present study (Section 4.3.6),

fermentative bacteria which have been reported to assimilate glucose; unclassified *Porphyromonadaceae*, *Tolumonas* sp. and *Lactococcus* sp. (Tindall, 1996; Grabowski *et al.*, 2005; Dworkin *et al.*, 2006) were present at average relative abundances of 27%, 1% and 1% respectively on batch-mode cell A and B anodes. Whereas, *Anaeromusa* sp. and unclassified *Comamonadaceae*, which have been associated with amino acid fermentation (including glutamate; Ouattara *et al.* (1992); Heylen *et al.* (2008)), were present at only 3% and 1% relative abundance respectively. The archaeon *M. arboriphilus* was found in only 0.06% average abundance in the batch-cells A and B indicating that methanogenesis was probably minimal. Further discussion regarding the role of these bacteria is in Section 5.3.7 of Chapter 5.

### 7.3.2 Effect of Artificial Wastewater Composition on Calibration

Paired, batch-mode MFCs A & B and C & D were calibrated as BOD sensors using a range of different concentrations of glucose, glutamic acid and GGA medium over a 40 and 114 day period respectively (Table 7.1; Figure 7.3 and 7.4).

In the calibration of cells A and B, substrate was alternated with each medium cycle, whereas with cells C and D, calibrations were mostly performed for each substrate in sequence in the order GGA, glucose and glutamic acid (denoted by green, blue and red coloured lines in Figure 7.3 and 7.4). During the lengthy period of calibration of cells C and D, the peak cathode potential was observed to decrease over time by approximately 0.4 mV per day attributed to biofouling/degradation as discussed in Section 4.3.5. The anode potential minima at saturated conditions remained approximately constant at  $-337 \pm 26$  mV vs. Ag/AgCl (Figure 7.2).

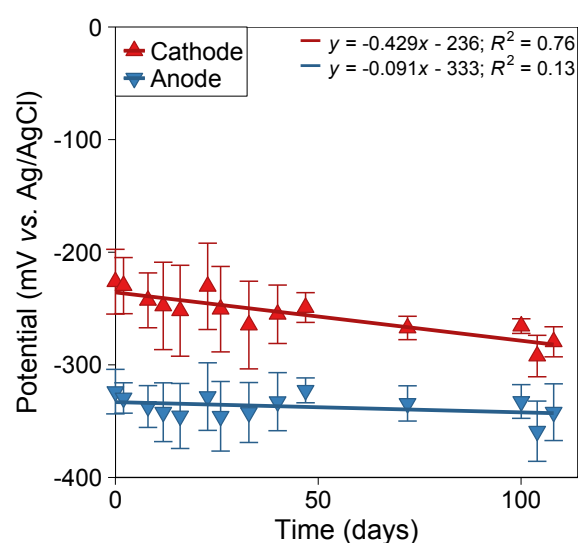


Figure 7.2: Average peak anode and cathode potential plotted against time showing cathode degradation (decrease in potential) for batch-mode cells C and D. Only GGA-based medium cycles above the saturation limit (approximately 270 mg/l O<sub>2</sub> BOD<sub>5</sub>) in Calibration 1 were included (t = 0 is start of Calibration 1). Error bars are the range from cells C and D.

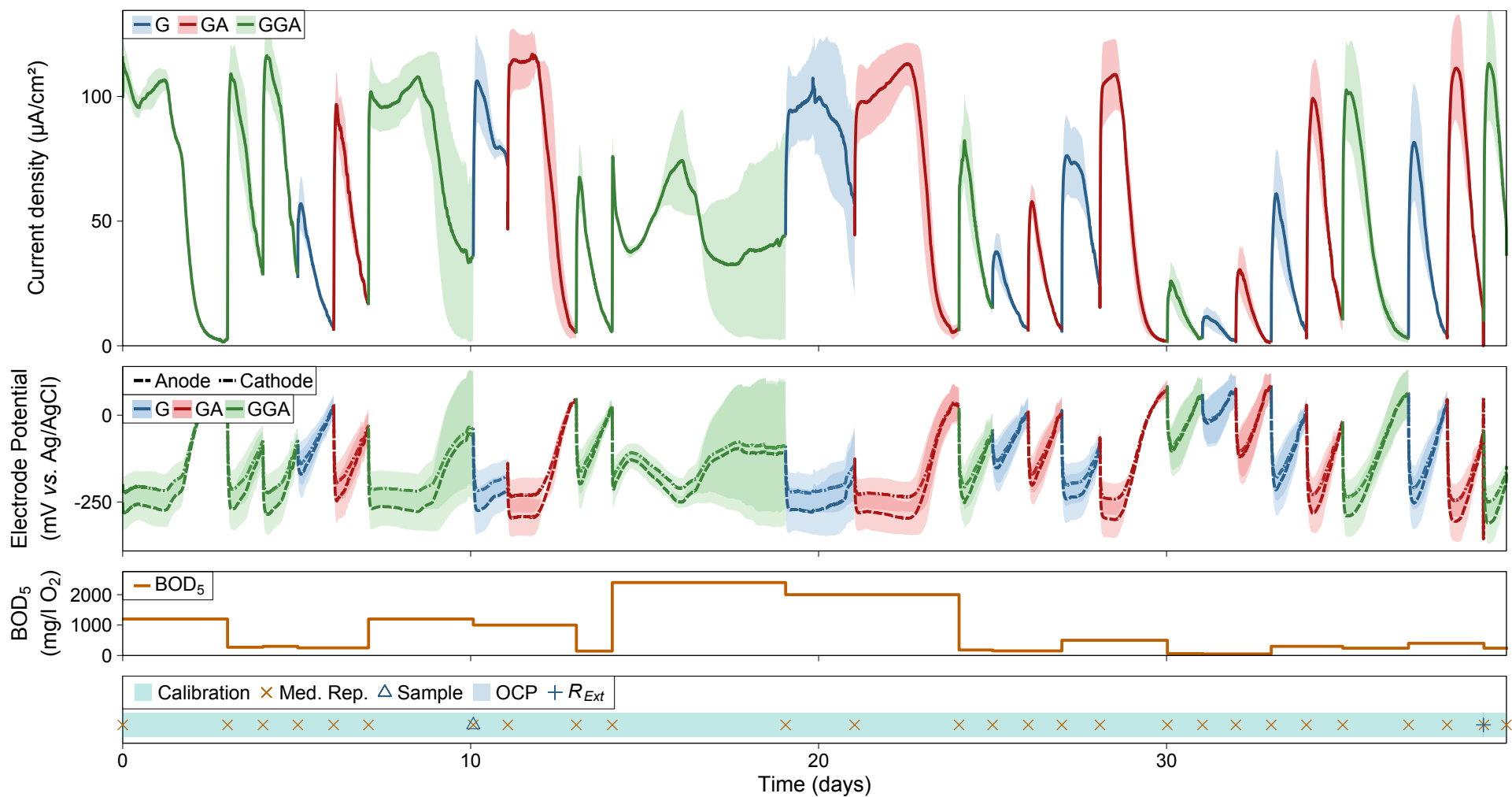


Figure 7.3: The average response of batch-mode MFCs A and B current density, anode and cathode potential to changes in BOD<sub>5</sub> (estimated from substrate concentration) with each medium replacement during Calibration 10. Coloured lines represent medium composition of glucose (G), glutamic acid (GA) and GGA.

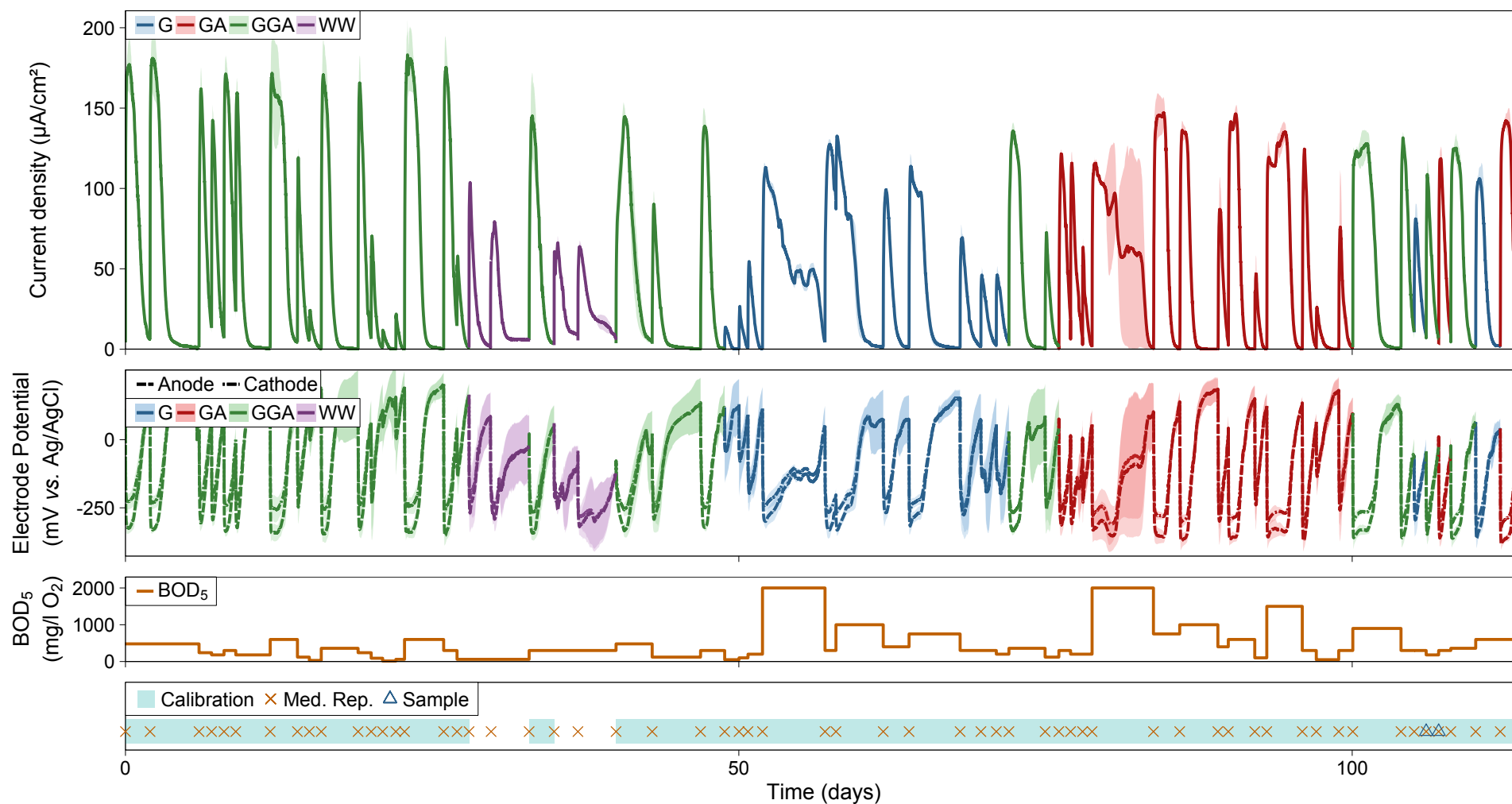


Figure 7.4: The average response of batch-mode MFCs C and D current density, anode and cathode potential to changes in  $BOD_5$  (estimated from substrate concentration) with each medium replacement during Calibration 1. Coloured lines represent medium composition of glucose (G), glutamic acid (GA), GGA and wastewater (WW).

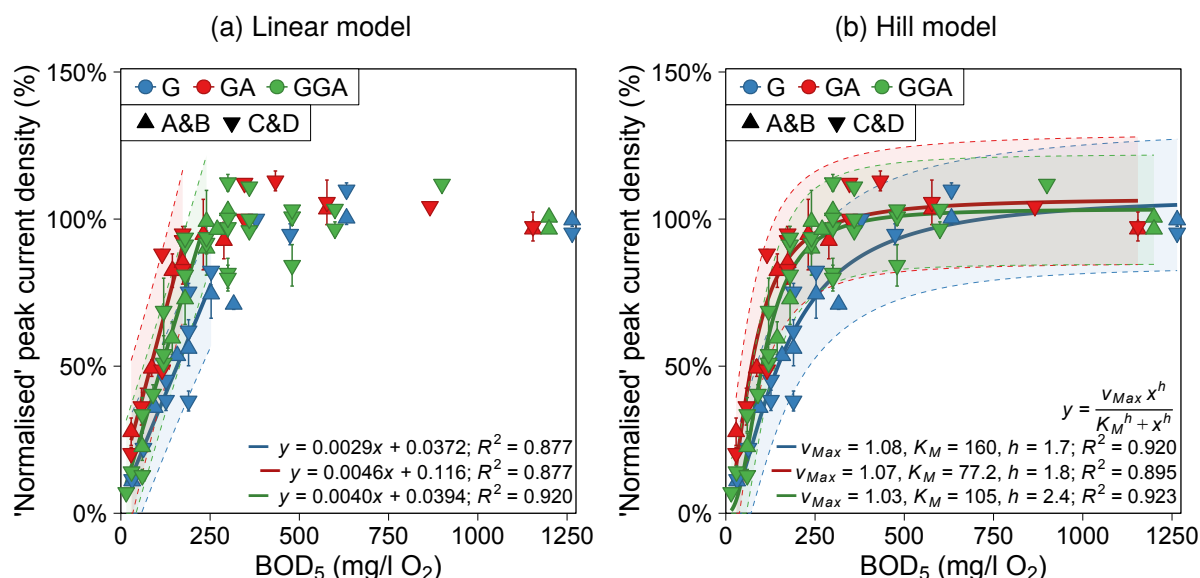


Figure 7.5: Calibration of batch-mode cells A, B, C and D with different concentrations of glucose (G), glutamic acid (GA) and GGA. Each averaged calibration is modelled by (a) linear regression model and (b) the Hill equation against BOD<sub>5</sub> (estimated from substrate concentration). Error bars are the range of values from duplicate cells (cell pair indicated by shape). Shaded bands represent the 95% prediction interval from model lines.

In order to compare calibrations, current densities were normalised to the maximum peak current density (at BOD<sub>5</sub> concentrations above the saturation limit; Figure 7.5). The calibration curves obtained exhibited a steeper response for increasing glutamic acid concentrations than for glucose or GGA. The GGA calibration was approximately the mean of the two single-substrate calibrations (as was observed for other parameters; Section 7.3.1). The half maximal concentrations ( $K_M$ ) from fitted Hill models were  $160 \pm 77$ ,  $77 \pm 39$  and  $105 \pm 38$  mg/l O<sub>2</sub> BOD<sub>5</sub> for glucose, glutamic acid and GGA respectively.

The  $p$ -value for ANOVA of linear regression using each substrate was  $1.24 \times 10^{-6}$  (with a null hypothesis that there was no difference from substrate). The  $p$ -values for Hill-modelled calibrations were 0.0643, 0.0773 and 0.0014 for glucose (df = 17), glutamic acid (df = 18) and GGA (df = 33) respectively. For glucose and glutamic acid, there was insufficient data to reject the null hypothesis (that each single-substrate Hill model was the same as the Hill model of the combined dataset for all substrates). However, the linear regression and GGA Hill model  $p$ -values indicated that the differences between linear calibrations with each substrate individually were statistically significantly different from the calibration with GGA. The implication is that the MFC sensor calibrated with a specific substrate could not be used to accurately predict BOD<sub>5</sub> values of analytes sufficiently different in composition.

The upper detection range limits using linear regression models were 253, 173 and 240 mg/l O<sub>2</sub> BOD<sub>5</sub> for G, GA and GGA respectively (Figure 7.5a). Less amino acid fermenting bacteria were found than sugar fermenting bacteria in the community analysis of cells A and B. Therefore there will have been less consumption of glutamic acid by competitive processes; thus greater coulombic efficiency was achieved and the MFC reached substrate saturation at lower

concentrations. This means that the sensor is capable of sensing higher concentrations of glucose than glutamic acid, or alternatively that the MFC was more mass-transfer limited with glucose-containing media.

Because the anode potential was measured against a Ag/AgCl reference electrode the value was not influenced by effects of cathode degradation and therefore the 'peak' potentials under saturating conditions (concentrations where the anode potential reached a lower limit) could be compared. Average anode potential minima for cells A, B, C and D were measured as  $-311 \pm 46$ ,  $-347 \pm 40$  and  $-336 \pm 25$  mV vs. Ag/AgCl for glucose, glutamic acid and GGA medium cycles respectively. The glutamic acid medium cycles exhibited the lowest anode potentials indicating that the overpotential was lowered or possibly the MFC bioanode was able to utilise a different metabolic pathway for GA oxidation to generate electricity.

At high concentrations ( $> 750$  mg/l  $O_2$  BOD<sub>5</sub>) of GGA, in some cases, a bimodal response was observed (*e.g.* Figure 7.6c and in Section 4.3.2), whereas at low concentrations only a single peak was observed after approximately 2 hours. Comparing medium cycles of 1000 mg/l glucose-only, glutamic acid-only and GGA compositions it is evident that the bimodal response could possibly be attributed to sequential glucose oxidation followed by glutamic acid oxidation (Figure 7.6).

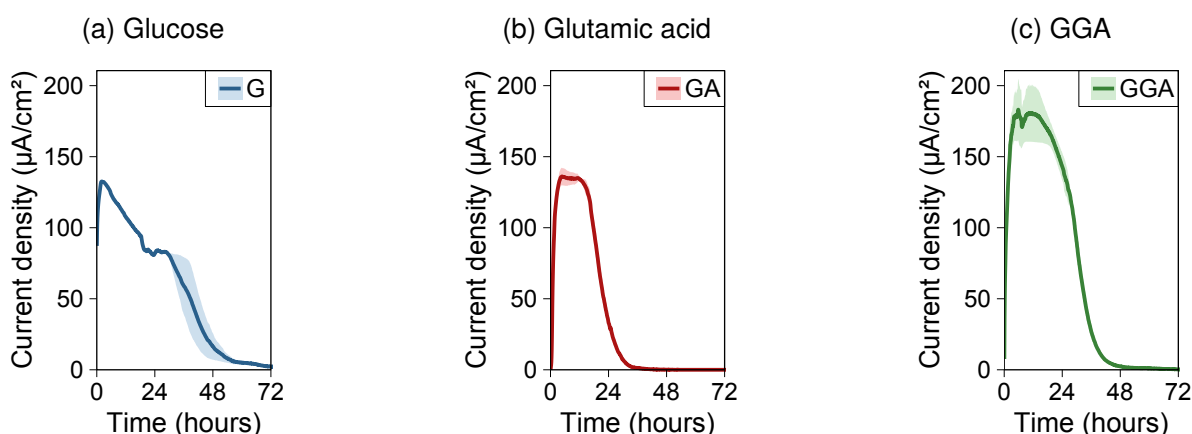


Figure 7.6: Average current density response for batch cycles in which 1000 mg/l (a) glucose, (b) glutamic acid and (c) GGA was fed to batch-mode MFCs C and D. Cycles were recorded on days 113, 141 and 67 of operation respectively during which time a fall in cathode potential was observed; therefore current densities should not be compared. Shaded bands are the range between cell C and D.

At high concentrations of glucose ( $> 450$  mg/l; Figure 7.6a), an immediate peak was observed within approximately 2 hours of medium replacement, followed by a steady decline as substrate depleted. During the steady decline an additional second peak was sometimes recorded, potentially associated with further utilisation of acetate generated from fermentation products (*e.g.* propionate). At high concentrations of glutamic acid (Figure 7.6b), a broad peak was observed which reached a maximum value after approximately 24 hours. In most of the high-concentration GGA medium cycles (1:1 glucose to glutamic acid) shown in Figure 7.3 and 7.4 the bimodal peaks occurred at 2h and 24h with the second peak usually at higher

current density. This result indicated that the response could be generated by sequential oxidation of glucose followed by glutamic acid. The trend in peak heights was concurrent with the results from Section 7.3.1; where higher current densities were observed for glutamic acid than for glucose at the same mass concentrations.

### 7.3.3 Response of MFC-based BOD Sensors to Raw Wastewater

On two occasions two 28 litre samples of real wastewater (WW1 and WW2) were collected from the WWTP raw influent (after grit filter). From each 28 litre sample the wastewater was divided into two sub-samples; 'A' a 10 l sample for immediate analysis and 'B' the remaining sample was stored at 4 °C for two days prior to analysis. With each sub-sample the pH, conductivity and MFC response was measured. With the first sub-sample the BOD<sub>5</sub>, COD, TOC and anion composition was also analysed (Table 7.3).

Table 7.3: Comparison of water quality parameters for a 300 mg/l GGA artificial wastewater (AWW) medium and two samples of real raw influent wastewater (WW1 and WW2) of which two sub-samples were taken (A and B). Water quality measurements were taken using the 'A' sub-sample on the day of wastewater collection.

Parameter	GGA AWW	WW1		WW2	
	300 mg/l	'A'	'B'	'A'	'B'
Volume prepared (l)	5.6	11.0	16.3	10.0	18.0
pH	6.96	7.04	6.73	7.30	7.26
Conductivity (mS/cm)	-	0.85	3.95	4.46	4.48
Adjusted conductivity (mS/cm) <sup>a</sup>	7.40	8.49	8.26	8.41	8.18
BOD <sub>5</sub> (mg/l O <sub>2</sub> )	179.9 ± 9.4	185.7 ± 8.7		168.1 ± 6.4	
COD (mg/l O <sub>2</sub> )	282.0 ± 4.1	450.5 ± 13.4		544 ± 2	
BOD <sub>5</sub> /COD ratio	0.607 ± 0.031	0.413 ± 0.032		0.309 ± 0.026	
DOC (mg/l C)	113.4 ± 1.2	82.5 ± 3.3		97.9 ± 3.8	
IC (mg/l C)	ND	53.8 ± 0.4		63.3 ± 1.3	
Fluoride (mg/l)	ND	6.5 ± 2.1		6.7 ± 2.2	
Chloride (mg/l)	63.7 ± 2.9	65.3 ± 0.5		193.8 ± 150.3	
Phosphate (mg/l)	1860.2 ± 210.3	24.5 ± 1.9		34.4 ± 14.9	
Sulphate (mg/l)	11.2 ± 1.8	65.1 ± 0.6		110.6 ± 42.5	

<sup>a</sup> Wastewater samples were adjusted by titrating an appropriate amount of 2 mol/dm<sup>3</sup> phosphate buffer to bring conductivity to approximately 8 mS/cm. <sup>b</sup> ND = Not detected.

All wastewater samples were approximately pH 7. With the WW1 sub-sample 'A' it appeared the bulk sample was not shaken well enough prior to sub-sampling as the non-adjusted conductivity was very low (0.85 mS/cm) compared to the remaining sub-sample 'B' (3.95 mS/cm). The average conductivity of WW2 was 4.47 ± 0.01 mS/cm. In all cases, prior to replacing the medium in the MFC, the wastewater conductivity was increased to approximately 8 mS/cm



by addition of an appropriate amount of 2 mol/dm<sup>3</sup> phosphate buffer solution (approximately 2.6 ml/l). The BOD<sub>5</sub> values of the real wastewater samples were similar to the 300 mg/l GGA standard medium, however BOD<sub>5</sub>/COD ratios and DOC values were less than the artificial wastewater. The COD was higher in real wastewater indicating the presence of non-biodegradable organic compounds. There was also fluoride and a higher concentration of sulphate ions present in the real wastewater compared to the AWW. The phosphate in the real wastewater was measured before conductivity adjustment and therefore in the MFC tests the level was closer to the AWW values (average addition of approximately 500 mg/l PO<sub>4</sub><sup>3-</sup>).

Batch-mode MFCs C & D were tested with the sub-samples of real wastewater (WW1 and 2) on days 28-33 and 35-40 of Calibration 1 (Figure 7.4). The three-stage, flow-mode MFCs (1D, 1E, 1F, 2D, 2E, 2F, 3D, 3E & 3F) were also tested with the same samples of wastewater. Average values from the continuous flow system were extracted and used for predictions (i) before sludge removal from the MFCs and (ii) afterwards. As the BOD<sub>5</sub> concentrations for the wastewater samples were known the response values could be positioned on the same plot as the calibration curves (Figure 7.7).

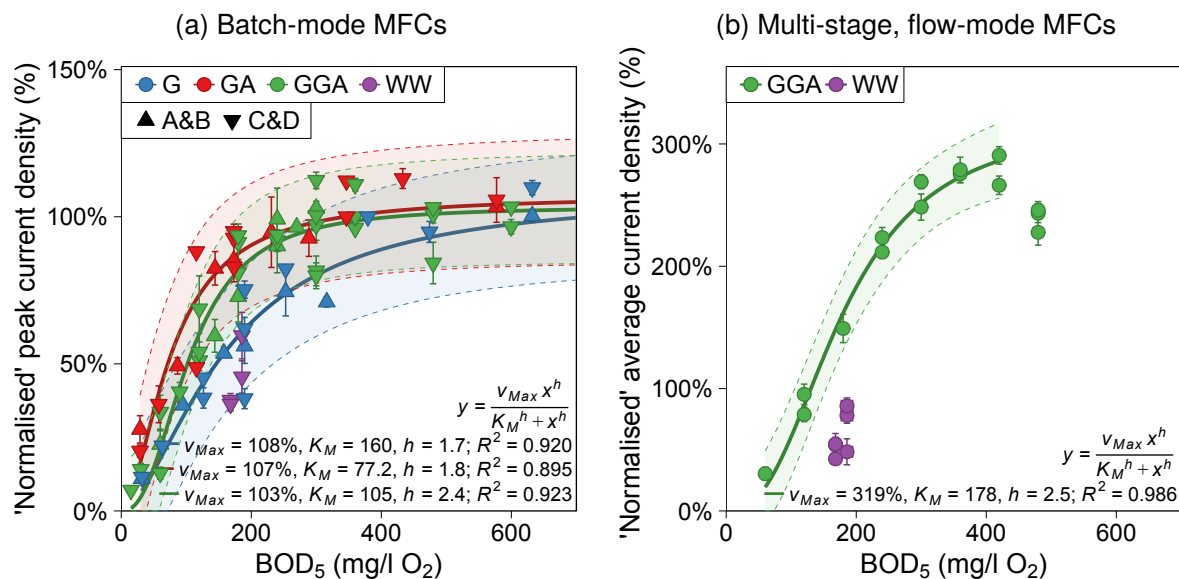


Figure 7.7: Average positioning of real wastewater samples (●) on Hill-modelled calibration curves of (a) 'normalised' peak current density from batch-mode cells A, B, C and D with different concentrations of glucose (G), glutamic acid (GA) and GGA and (b) 'normalised' average summed current density from multi-stage MFC cells in channels D, E and F against BOD<sub>5</sub> (estimated from substrate concentration). Error bars are the range of values from duplicate cells (cell pair indicated by shape) for batch-mode calibrations and  $\pm 1$  SD for triplicate flow-mode cells. The flow-mode data is normalised to 300% (sum of three MFC stages) to permit comparisons to non-normalised data for convenience. Shaded bands are the 95% prediction interval from model lines.

In the case of both the batch- and flow-mode MFCs, the wastewater samples did not fall on the GGA calibration curve and values were even below the batch-mode glucose calibration curve for samples of the same BOD<sub>5</sub> (Figure 7.7a). The BOD<sub>5</sub> values predicted by the linear



and Hill models were calculated for the four samples using the measured current densities (Figure 7.8, Table C.1 and D.3 in Appendices C and D). For the batch-mode sensor, in

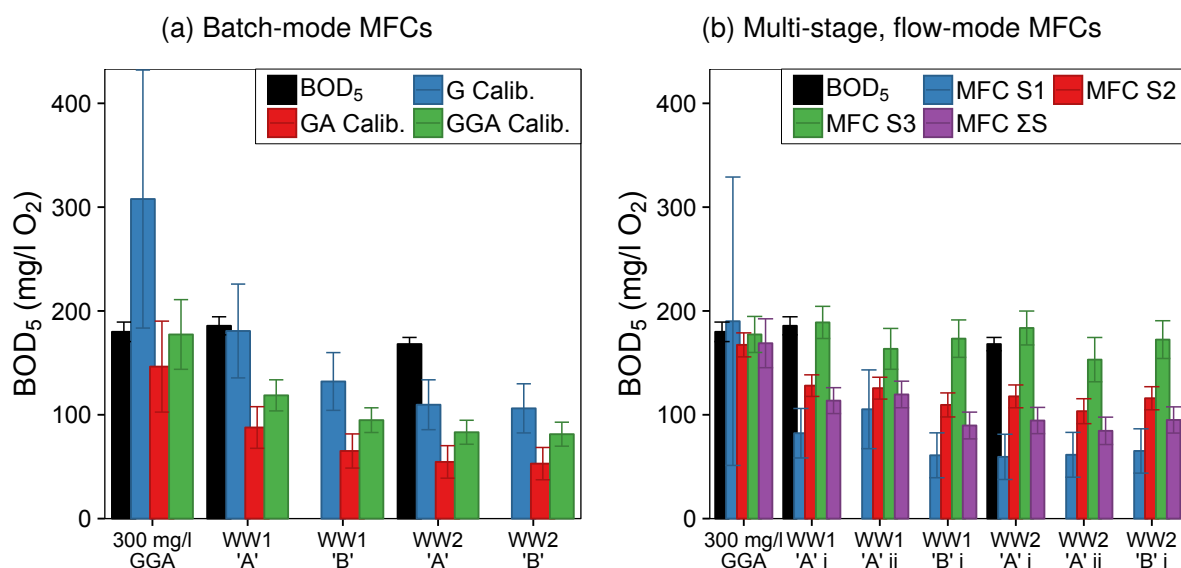


Figure 7.8: Evaluation of predicted  $BOD_5$  values for 300 mg/l GGA AWW and two samples of real wastewater using (a) the G, GA and GGA calibrated Hill models from the batch-mode MFCs and (b) the GGA calibrated Hill models for each stage (Stages 1-3 and the  $\Sigma$  of stages) from the multi-stage, flow-mode MFCs. Predictions were made (i) before and (ii) after sludge removal from the MFCs. Error bars for the  $BOD_5$  test are  $\pm 1SD$ , whereas for the predicted values they are the range of the 95% prediction interval for each model. Full corresponding data tables are Table C.1 and D.3 in Appendices C and D respectively.

all cases except one, the  $BOD_5$  value was under-estimated by 3 to 69 % (5 to 115 mg/l  $O_2$   $BOD_5$ ) in comparison to the actual  $BOD_5$  test determined value. Whereas, the flow-mode sensor under-estimated the actual  $BOD_5$  values more by 35 to 65 %. The batch-mode, glucose calibrated models were able to predict values closest to the true  $BOD_5$  values using batch-mode MFCs, perhaps indicating that, as the real wastewater was likely to contain more complex substrates, there were competing non-electrogenic processes occurring which resulted in reduced coulombic yield.

As Figure 7.8b shows, an ordered response was observed in the predicted  $BOD_5$  values with the multi-stage MFC sensor (e.g. for the WW1 'A' i sample with  $BOD_5 = 186 \pm 9$  mg/l  $O_2$  the predictions from stages 1, 2 and 3 were  $83 \pm 126$ ,  $116 \pm 65$  and  $185 \pm 44$  mg/l  $O_2$  respectively). As wastewater passed through the MFC hydraulic array from Stage 1 to Stage 3 the prediction accuracy increased. This response order was reminiscent of the behaviour observed with high concentrations of GGA medium which resulted in inhibition due to substrate excess (Section 6.3.1). In the AWW trials (Section 5.3.2 of Chapter 5), a decrease in coulombic efficiency was observed in the first stage MFCs which corresponded with the generation of a large amount of sludge dominated by a *Lactococcus* sp. This suggested that competitive anaerobic processes were occurring, which consumed the substrate through non-electrogenic pathways. With the real wastewater this response may also indicate that other

processes were occurring such as biomass production, degradation of complex substrates to intermediates which were subsequently consumed downstream in later stage MFCs or potentially the presence of toxic compounds.

Interestingly in each wastewater measurement the average predicted BOD<sub>5</sub> values by the third stage MFC were highly accurate (only 5 % below the actual value of WW1 and 4 % above the actual value of WW2). However, the accuracy of the predicted values could be a coincidental considering that the current density generated by the third stage MFCs during wastewater trials was only  $13.5 \pm 4.5$  and  $12.6 \pm 5.0 \mu\text{A}/\text{cm}^2$  (8 and 7 % of  $\bar{i}_{Max}$ ) using WW1 and WW2 respectively. Further trials including full scale, online wastewater monitoring would be required to determine whether the output of the later stage MFCs could be used for BOD determination during a current decrease event.

The 'B' sub-samples which had been stored for two days at 4 °C prior to MFC analysis both generated less electricity than the respective 'A' sub-samples which indicated that there had been some degradation during low-temperature storage. However with WW1 23 % less electricity was generated compared to 3 % for WW2, which may be due to the poor mixing of WW1 during preparation of the 'A' sub-sample as mentioned above. Potentially the less-settled fraction of the BOD present in WW1 sub-sample 'A' was more readily oxidised and therefore generated a higher electrical current.

The batch-mode linear regression models for glucose, glutamic acid and GGA had smaller mean percentage errors than the Hill equation models. The converse was true for the multi-stage flow-mode models where greater Hill coefficient ( $h$ ) values were calculated; indicating that a greater degree of co-operativity was occurring. Higher  $h$  values also meant that the proportion of the calibration curve which was linear decreased. Hill models are useful for describing the full calibration range including the non-linear asymptotes, however the linear model has been shown to have a higher resolving power (Section 5.3.3).

The MFC sensors in the present study were not able to accurately predict BOD<sub>5</sub> values for real wastewater samples (with the possible exception of the third stage of the flow-mode MFCs). The results indicated that the oxidation of GGA-based medium in the anaerobic, short-term MFC test did not resemble similar oxidation rates to that of the real municipal wastewater samples. Whilst the developed sensors had excellent sensing characteristics, for fixed medium compositions under well defined conditions, it is demonstrated here that such sensors should be enriched and calibrated with real wastewaters for real-world application.

#### **7.3.4 Critical Appraisal of Sensor Validation Methods Reported in the Literature for BES-based BOD Sensors**

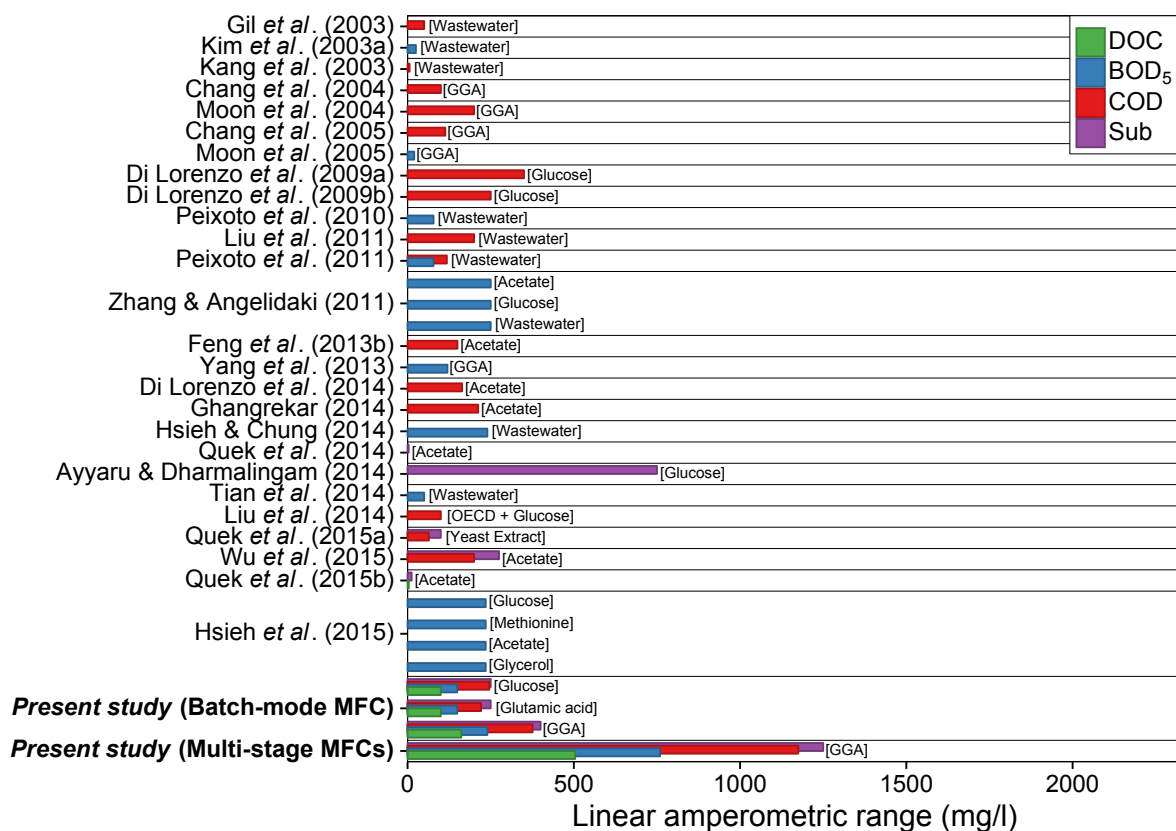
In order to confirm that a sensor can accurately measure BOD an external validation method must be used. In the literature review undertaken in the present study (Chapter 2), it was noted

that previous cross-study comparisons of BES-based BOD sensors have been conducted without consideration of the validation methods used. In recent MFC review articles the benefits of using the electrical response to monitor BOD have been detailed (Kim *et al.*, 2006b; Rabaey *et al.*, 2010), but the influence of the validation method used was not considered when comparing between different studies. Studies have been frequently evaluated in isolation using a variety of methods to give a measure of organic compounds present in the medium. It is evident that the BOD<sub>5</sub> test was used for the sensor validation in less than 50% of the sensor articles published. This was likely due to the time consuming nature of measuring samples; the very reason these sensors are being developed. Validation was also done by calibrating against the COD, dissolved/assimilable organic carbon (DOC/AOC) or substrate concentration; measurements which, to a varying degree dependent on substrate, did not provide an accurate representation of the BOD<sub>5</sub> value (Figure 7.9). This discrepancy is further complicated by authors using the term “*BOD concentration*” to reference substrate or COD concentrations interchangeably with BOD<sub>5</sub> values in unspecified units of mg/l.

Samudro and Mangkoedihardjo (2010) investigated typical BOD<sub>5</sub>/COD ratios for different wastewaters and found that a ratio greater than 0.5 was likely for domestic wastewaters and leachates, whereas much lower ratios could be found for industrial wastewaters and seawater due to the presence of high concentrations of non-readily biodegradable materials. Van Haandel and van der Lubbe (2007) found BOD<sub>5</sub>/COD ratios of 0.58 and 0.75 for glucose and acetate respectively. This is because the BOD<sub>5</sub> test, the standard industry measure, does not determine the ‘ultimate’ total BOD concentration over five days but only a fractional amount (*e.g.* 65% of the 300 mg/l GGA standard ThOD). For known organic substrates which are fully biodegradable, such as glucose and acetate, COD will be approximately equal to ThOD (Amarasinghe *et al.*, 1993) and the COD/TOC ratio is usually equivalent to the stoichiometric weight molar ratio of oxygen to carbon (Mara and Horan, 2003). A common misconception in the literature is that for fully biodegradable substrates COD = BOD<sub>5</sub> and therefore COD-validated sensors can be compared to BOD<sub>5</sub>-validated sensors. Importantly, this is an incorrect assertion as the chemical oxygen demand is only (approximately) equal to the ‘ultimate’ total BOD which no authors to date have determined as the test would take over 20 days to complete (*i.e.* COD  $\approx$  BOD  $\neq$  BOD<sub>5</sub>).

ThOD and COD values do not equate to BOD<sub>5</sub> values and the ratio relating them depends on the substrate employed. Thus, even for completely biodegradable substrates, validation other than by direct comparison with BOD<sub>5</sub> will over-estimate the dynamic range of a BOD sensor. For the studies where BOD<sub>5</sub> is not used it makes comparisons between the data difficult to ascertain. It is safe to assume that papers which use COD are likely to over-estimate by as much as double the BOD<sub>5</sub> value (based on assumed COD/BOD<sub>5</sub> ratio of 0.5 by Mara and Horan (2003)). When only the substrate concentration or DOC have been used the discrepancy could be larger (and the comparison is not meaningful as it is comparing mg/l O<sub>2</sub> to mg/l of substrate or C).

(a) Amperometric BES-based “BOD” sensors



(b) Coulometric BES-based “BOD” sensors

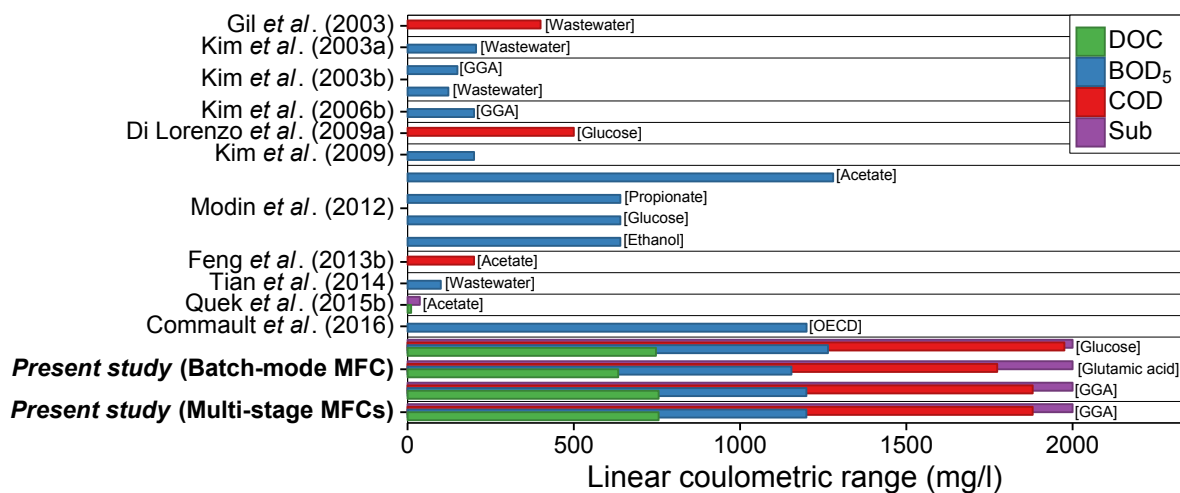


Figure 7.9: Comparison of linear ranges of (a) amperometric and (b) coulometric BES-based sensors reported in the literature (in units of mg/l of respective validation method (C for DOC, O<sub>2</sub> for BOD<sub>5</sub> and COD or Sub (substrate))). Bars for each study are coloured by the validation method(s) employed by each author. The carbon-containing substrate used for each sensor calibration is listed in square brackets at the end of each bar. Full corresponding data table is Table 2.2 in Chapter 2.

Figure 7.9 (and Table 2.2 in Chapter 2) allows comparisons between sensors to be drawn between the reported BES-based “BOD” sensors in the literature with due consideration of validation methods and substrate utilised. The only two BES-based BOD sensor articles omitted from the figures are by Kumlanghan *et al.* (2007) and Jia *et al.* (2016) which involved injection of sample into a large bioreactor (*e.g.* 10 litre scale). Subsequently, the reported detection ranges of 25 000 and 3000 mg/l O<sub>2</sub> respectively are not meaningful in comparison to other studies as the sample dilution was not taken into account. Studies such as those by Kumlanghan *et al.* (2007), Di Lorenzo *et al.* (2009a) and Modin and Wilén (2012) have frequently been cited by MFC review authors (Dai and Choi, 2013; Su *et al.*, 2011; Abrevaya *et al.*, 2015a) as achieving the highest MFC detection ranges. In the reviewed texts, the context of dilution, validation method and detection method (amperometric *vs.* coulometric) are not mentioned and the results are misreported as the undiluted, amperometric BOD<sub>5</sub> range (or simply unspecified). Additionally, it must be noted that not all authors set out to demonstrate their technology as a “BOD” sensor and therefore validate using alternative methods to suit their application (*e.g.* VFA sensor by Kaur *et al.* (2013) and AOC sensor by Quek *et al.* (2014)), however this is often not conveyed by reviewing authors.

Figure 7.9 shows that once the validation method is taken into account (*e.g.* BOD<sub>5</sub> ≈ ½ COD) a large number of studies with single-stage MFC sensors achieve approximately the same amperometric upper limit of around 250 mg/l O<sub>2</sub> BOD<sub>5</sub> and recent developments have done little to advance this. With coulometric sensors the range can be extended simply by increasing the incubation time (*e.g.* 20+ hours) and therefore is not really comparable to instantaneous amperometric sensors without contextual information. The multi-staged mode of operation developed in this study presents a clear progression of the technology to overcome the range limitations set by single-stage operation, without requiring sample modification or dilution and was extensively validated with multiple techniques to address comparison concerns. As has been highlighted in this chapter and by some other authors (Modin and Wilén, 2012; Hsieh *et al.*, 2015) there is a clear need for a standardised protocol for sensor calibration of predictive BOD sensors (especially in the BES literature).

To put the reported detection ranges in to perspective; Figure 7.10 shows the BOD<sub>5</sub>, COD and BOD<sub>5</sub>/COD ratios of a selection of various influent and process wastewaters from municipal and industrial treatment plants (as detailed in Table A.2; Henze and Comeau (2008); Lowe *et al.* (2007); Wang *et al.* (2006)). It is known that the BOD<sub>5</sub> test is incapable of measuring values above 7.09 mg/l O<sub>2</sub> at 20 °C (APHA, 1999b; YSI, 2013) and therefore all wastewaters currently require dilution in order to be analysed. The single-stage, batch-mode MFC sensor in the present study improves upon this situation by allowing values up to approximately 240 mg/l O<sub>2</sub> to be determined without sample dilution. This is applicable for certain lower strength wastewaters including livestock wastewaters, municipal wastewaters (raw and settled) and olive oil processing wastewaters (mill effluent).

The three-stage, flow-mode MFC sensor from the present study increases the range three fold

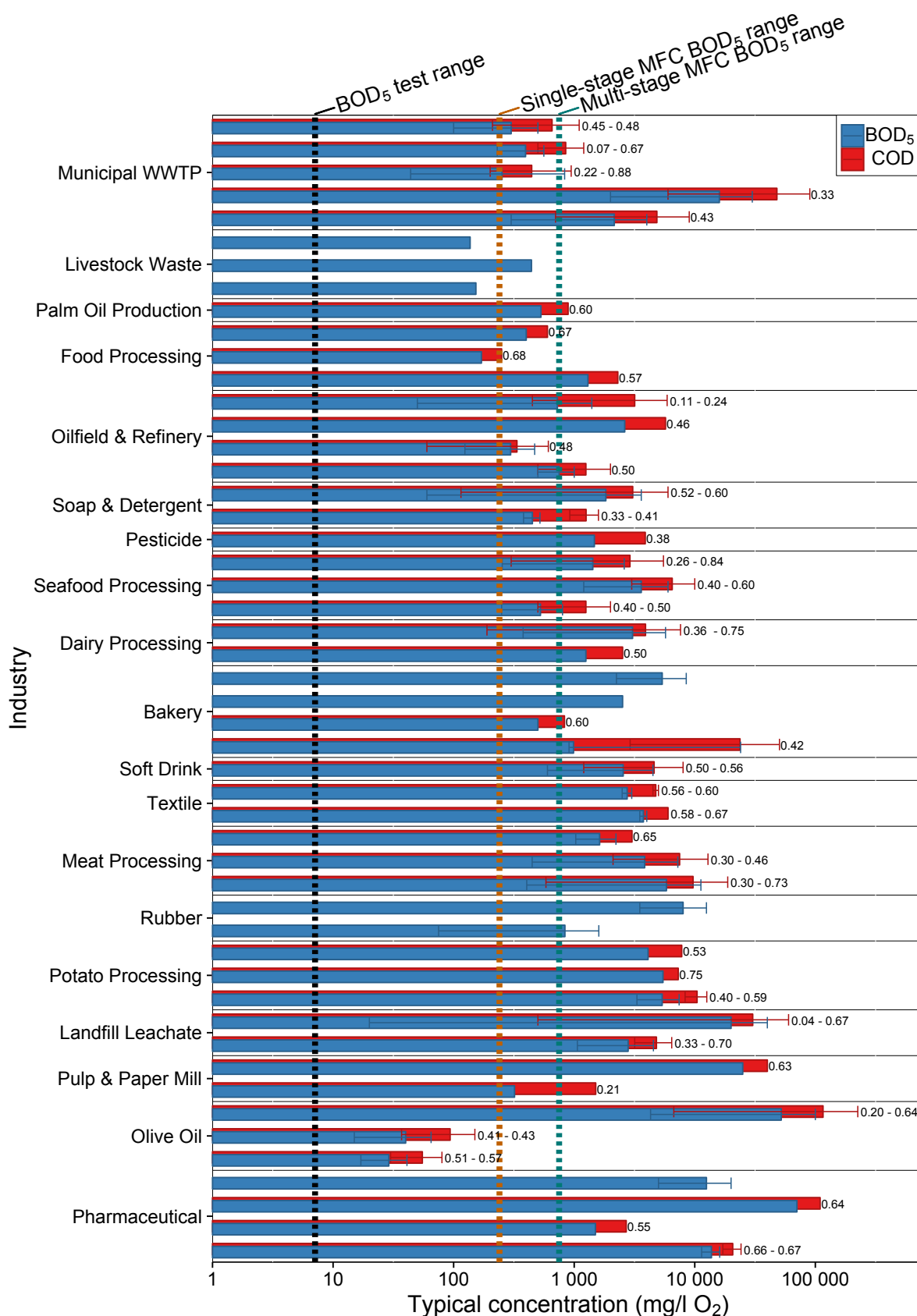


Figure 7.10: Comparison of typical BOD and COD values (on a logarithmic scale) for a selection of municipal wastewaters (Henze and Comeau (2008); Lowe *et al.* (2007)) and industrial wastewaters (compiled from Wang *et al.* (2006)). Linear detection range of BOD<sub>5</sub> test, amperometric batch-mode and multi-stage, flow-mode MFC sensors are shown by dashed lines. Error bars represent range and BOD<sub>5</sub>/COD ratio is given at the end of each bar (where data available). Full corresponding data table is Table A.2 in Appendix A.

and allows determinations up to 750 mg/l O<sub>2</sub> amperometrically. This advance broadens the scope to include urban wastewaters from municipal WWTPs, low strength anaerobic digester supernatant and industrial wastewaters including those associated with palm oil production, food processing, oilfield and refinery processing, and soap and detergent production. Indeed, already in the non-sensing BES literature, there are reports of authors successfully generating electricity using MFCs fed with industrial wastewaters associated with pulp and paper mills, dairy processing, bakery processing, brewing, agricultural waste, landfill leachate and food processing (Pant *et al.*, 2010b; Velasquez-Orta *et al.*, 2011). There is therefore a high likelihood that this technology could be applied for BOD monitoring purposes in these types of industrial treatment processes with bespoke calibrations. Certain industrial wastewaters may lend themselves better to accurate calibration given the concerns raised previously in this chapter because, for example, in bakery wastewaters the chemical composition of BOD-containing constituents is unlikely to vary significantly and therefore there would be no need to frequently recalibrate the sensor.

#### **7.4 Conclusions & Recommendations for Standardised Validation of BES-based BOD Sensors**

From the experiments conducted comparing different validation techniques and using different medium compositions in MFCs the following conclusions can be drawn:

- Oxygen demand values determined using traditional oxygen demand methods (BOD<sub>5</sub> and COD) were approximately 5% higher for glucose and 5% lower for glutamic acid than the corresponding GGA value for equal mass concentrations. The GGA value was approximately the mean of both G and GA values. The BOD<sub>5</sub>/COD ratios for glucose, glutamic acid and GGA respectively were 0.640, 0.584 and 0.607.
- The response outputs from MFCs ( $\hat{I}$ ,  $Q_{Cyc}$  and  $C_E$ ) did not exhibit the same oxidation trends; glucose values were 25% lower and glutamic acid 25% higher than the corresponding GGA values. The reason was likely due to competitive anaerobic processes (*e.g.* fermentation and methanogenesis) resulting in lower coulombic efficiencies, especially with readily fermented glucose.
- The lower coulombic efficiencies obtained using glucose as a substrate result in a greater BOD sensing range due to increased mass transfer limitations at the MFC biofilm (compared to glutamic acid).
- The bimodal response observed with high concentrations of GGA fed to a batch-mode MFC are likely due to sequential oxidation of glucose followed by glutamic acid, resulting in current density peaks at 2h and 24h in the batch medium cycle.
- Batch-mode and flow-mode MFC-based sensors in the present study were incapable

of predicting BOD<sub>5</sub> values for real samples of raw influent wastewater. The ordered inhibition response (1>2>3) was similar to previously observed inhibition due to substrate excess, indicating that biomass and/or metabolic intermediate production was likely occurring in the early stages of the hydraulic array of MFCs resulting in less electricity generation.

- The discrepancies in previous reviews of BES-based sensors were outlined and the detection ranges, taking into account validation method, were presented. There is a clear need to standardise BOD sensor calibration using BESs to allow sensors to be compared validly.

The data obtained in this chapter demonstrated that the current generation from a MFC is not proportional to BOD or BOD<sub>5</sub> (although it could be correlated for specific substrates). The result of calibrating with different substrates (glucose, glutamic acid and GGA) indicated that the current response was different depending on the medium composition. As indicated by the coulombic efficiencies, this was likely due to additional fermentation processes occurring which do not occur in the aerobic BOD<sub>5</sub> test. Accurate calibrations, correlated precisely with BOD<sub>5</sub>, can only be obtained with wastewater streams which do not vary significantly. This requirement drives the technology towards bespoke sensors which are calibrated to specific waste streams (*i.e.* certain industrial wastewater streams, including bakery and brewing, are unlikely to vary by composition).

The findings from this study limits the application of MFC-based BOD sensors from being used for wastewaters where the organic composition is highly variable. However, if the application requires only an early-warning system where identification rather than quantification is desirable the MFC sensor is still viable (as an estimation accurate to approximately  $\pm 200$  mg/l O<sub>2</sub> can be provided). Additionally, if operators are prepared to frequently calibrate the sensor (or if regulations require frequent standard BOD<sub>5</sub> samples must be taken anyway) the MFC-based sensor could still be used.

Recommendations for standardised calibration of BES-based BOD sensors have been derived from a thorough, systematic review of the available literature and extensive experimentation within this study:

- Validation should be performed using a method which is applicable to all calibrations which could be performed with a “BOD” sensor. Consequently, use of the substrate concentration should be avoided as the method is inapplicable to real-world wastewater samples where the identity and quantity of the substrate is not easily ascertained.
- There are currently no standardised anaerobic tests for determining biodegradable organic compounds/oxygen demand used by the wastewater industry. Therefore, the existing methods of COD and BOD<sub>5</sub> likely represent the techniques of interest as they are the regulated parameters WWTPs must adhere to. BOD<sub>5</sub> is the more relevant



determination of oxygen demand as it only contains the biodegradable portion of the carbonaceous organic compounds which can be utilised by the MFC and thus BOD<sub>5</sub> is the recommended method for validation.

- The substrate/medium composition used for calibration of the BES-based sensor should be stated as this influences the response and range achieved.
- For sensors which utilise injection of sample into a large-volume vessel the range should be reported as the values after dilution has been taken into account.
- The detection method(s) which were used for sensor calibration should be listed. For example, amperometric detection using peak current (batch-mode sensors) or average current (flow-mode sensors) and coulometric detection using the charge passed over a specified incubation time (also reported).
- Additional operational factors should be considered when performing cross-study comparisons. Flow rate and external resistance have been shown to alter the calibration detection range (Chapter 5, Section 5.3.4 and Chapter 4, Section 4.3.4 respectively) and thus should also be reported. It is best practice to optimise these factors so that the sensor reported is the optimised configuration.

Under these recommended practices the characteristics of the batch- and flow-mode sensors developed in the present study are listed in Table 7.4.

Table 7.4: Characteristics of MFC-based BOD sensors developed in the present study.

Configuration & Mode	Operational parameters	Calibrated substrate	Validation method	Linear range (dilution corrected)	
				Amperometric	Coulometric <sup>a</sup>
SCMFC (Batch)	44 Ω	Glucose	BOD <sub>5</sub>	253 mg/l O <sub>2</sub>	1264 mg/l O <sub>2</sub> (48h)
SCMFC (Batch)	44 Ω	Glutamic acid	BOD <sub>5</sub>	173 mg/l O <sub>2</sub>	1155 mg/l O <sub>2</sub> (72h)
SCMFC (Batch)	44 Ω	GGA	BOD <sub>5</sub>	240 mg/l O <sub>2</sub>	1199 mg/l O <sub>2</sub> (72h)
Multi-stage SCMFCs (Single-pass)	305 Ω, 0.51 ml/min	GGA	BOD <sub>5</sub>	750 mg/l O <sub>2</sub>	1199 mg/l O <sub>2</sub> (5h)

<sup>a</sup> Coulometric range with incubation period in brackets



## Chapter 8. Conclusions & Future Work

### 8.1 Conclusions

#### 8.1.1 Defining the Research Problem

The main aim of this thesis (as outlined in Chapter 1) was to enhance the BOD detection range and establish methods which could overcome the limitations associated with MFC-based BOD sensors. Namely, the first limitation to be addressed was that at high BOD concentrations the anodic biofilm saturated with substrate (maximum current density was achieved) and further increases in BOD were undetected. The second limitation was that it was not possible to differentiate between decreases in BOD, substrate excess nor toxicant presence; all of which resulted in current decreases. Over the course of experiments conducted in the present study, data was collected which has been used to illustrate the problems with single-stage MFC sensors (Figure 8.1).

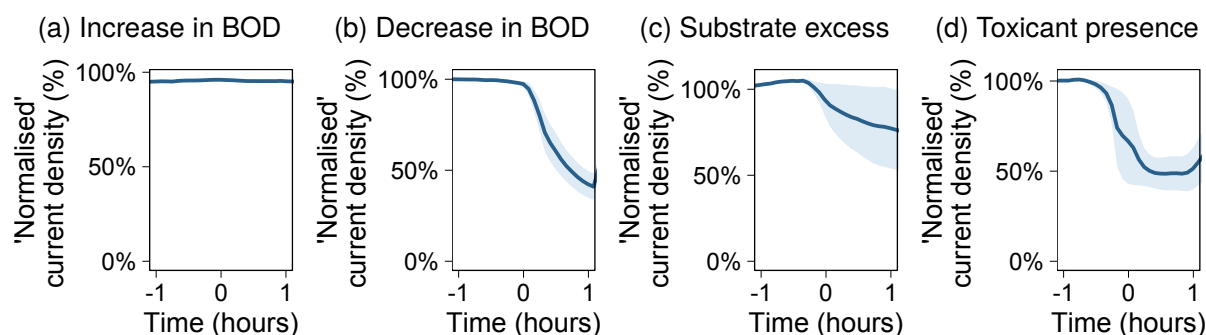


Figure 8.1: Representative examples of the limitations present with single-stage, flow-mode MFCs. (a) BOD increases cannot be detected when the normalised cell density is already at 100%. It is also not possible to distinguish between decreases in current density due to (b) BOD decrease, (c) substrate excess or (d) toxicant presence (4-NP). Average current density for triplicate first-stage MFCs is shown (shaded region is  $\pm$ SD).  $t = 0$  is the approximate point at which the change occurred.

Figure 8.1a demonstrates that, with single-stage MFC sensors, it was not possible to determine that BOD had increased with MFCs in which the current density had already reached maximum values (normalised to 100%). This demonstrates that the use of a single-stage, MFC-based BOD sensor with high-strength wastewaters would not be viable as pollution incidents could potentially be undetected.

It was also not possible to distinguish (using the current density alone) between the three causes of current decrease; decreases in BOD (Figure 8.1b), substrate excess (Figure 8.1c) nor toxicant presence (4-nitrophenol; Figure 8.1d). In each of the current decrease scenarios (Figure 8.1b–d), the current density was observed to decrease in response to each event with no distinguishing features.

### 8.1.2 Optimisation & Characterisation of MFCs

Batch- and flow-mode microbial fuel cells were successfully enriched and maintained over lengthy operational periods of up to 847 days. With batch-mode MFCs the effect of external resistance on BOD calibration was determined. It was observed that with decreasing external resistance ( $R_{Ext}$  from 5100 to 44  $\Omega$ ) the BOD linear detection range was increased. This may have occurred because the MFCs were less limited by the fuel cell and more by the anodic biofilm and mass transfer kinetics and thus the anode could operate at maximum capacity. The result was that the MFC current density plateaued at higher concentrations of substrate. This parameter has been assessed by other authors but here the effect on calibration was shown. This finding demonstrated that for BOD sensing a lower external resistance is desirable for enhanced detection range.

The effect of flow rate on BOD calibration was determined using the multi-stage, flow-mode MFCs. It was observed that as the flow rate was decreased from 1.24 to 0.52 ml/min the detection range of the flow-mode sensor was increased. Longer residence times inside the upstream MFCs corresponded to a greater degree of substrate utilisation. This resulted in the downstream MFCs not receiving substrate (or generating electricity) until the BOD<sub>5</sub> was increased further, thus extending the dynamic range. The flow rate could therefore be used innovatively to ‘tune’ operating conditions to meet requirements of individual wastewater streams and adapt sensors to the range required. Additionally, a maximum flow rate could be used to saturate MFCs with substrate and determine maximum current density values for normalisation.

Each MFC was assessed by electrochemical analysis techniques to assess the performance as a fuel cell. With batch-mode MFCs it was observed that the best-performing fuel cell (with highest current density, peak power density and lowest ohmic resistance) did not achieve the best BOD detection range. Increased mass transfer limitations may have increased the concentration at which point the anodic biofilm saturated with substrate. The highest power densities achieved with flow-mode MFCs were up to 27  $\mu\text{W}/\text{cm}^2$ . Redox peaks were identified in the cyclic voltammetry of MFC biofilms with a formal potential of approximately –357 mV vs. Ag/AgCl consistent with peaks observed with cytochromes of *Geobacter sulfurreducens* (Fricke *et al.*, 2008).

Bacterial community analysis was performed with samples from the batch- and flow-mode MFCs in comparison to sludge removed from the flow-mode system and electrodes which had

been incubated at OCP. The polarised electrodes clustered separately from non-polarised electrodes in principal co-ordinate analysis, indicating the community compositions were distinct. On the polarised electrodes *Geobacter* sp. unclassified *Porphyromonadaceae* and unclassified *Cryomorphaceae* were enriched in high relative abundance and had high (>99%) 16S rRNA gene sequence identity with bacteria previously found in BESs associated with electrogenic processes. The remaining bacterial community, which was also found in the sludge and OCP electrodes, comprised sugar fermenters (*Dysgonomonas* spp., *Lactococcus* spp. and *Enterobacteriaceae*) and amino acid fermenters (*Anaeromusa* spp., unclassified *Comamonadaceae* & *Tolomonas* spp.) which degraded the glucose and glutamic acid substrates to products such as acetate and propionate.

### 8.1.3 Calibration of MFC-based BOD Sensors

Independent BOD calibrations were performed with each series of MFCs by altering the concentration of GGA. Under optimised conditions the best amperometric calibrations achieved with batch-mode sensors were linear up to 240 mg/l O<sub>2</sub> BOD<sub>5</sub> (comparable with other single-stage MFCs reported in the literature). Coulometric calibrations were conducted with the batch-mode MFCs and linear detection ranges correlated with charge density up to 1199 mg/l O<sub>2</sub>. However, to achieve this range the incubation time ranged from 48–72 hours to obtain linearity by allowing medium cycles to run to completion. A novel 1-hour coulometric calibration was proposed which enabled the BOD<sub>5</sub> value to be estimated before peak current density had been reached within a medium cycle. The 1-hour calibration had a similar detection range to the amperometric calibration, albeit with reduced accuracy.

In this thesis multi-stage, flow-mode MFCs were calibrated with different BOD<sub>5</sub> concentrations for the first time. The configuration was tested extensively to determine the applicability for sensing. Predictable response from each stage of MFCs was observed, with cells generating current in order as BOD<sub>5</sub> was increased. An innovative calibration of the sum of the stable current densities from each MFC in the hydraulic array was proposed which was linear with BOD<sub>5</sub> up to 740 mg/l O<sub>2</sub> under optimised conditions. The calibrations were highly accurate and able to predict BOD<sub>5</sub> values with smaller standard deviation than the accepted variability in the standard BOD<sub>5</sub> test (*SD* < 9% vs. 15%). The enhanced detection range with the sum current was three-fold greater than that observed with the first stage of MFCs in the hydraulic array individually.

Kinetic models designed for simulating enzyme dose-response relationships were fitted to calibration data from the MFC-based BOD sensors in the present study. Michaelis-Menten (M-M) models did not fit the responses of the MFCs enriched with GGA. However, the Hill equation, which is a modified version of M-M, was used for the first time to model BOD<sub>5</sub> values with amperometric and coulometric responses from batch-mode MFCs and cells in each stage of the flow-mode array up to non-inhibiting concentrations. The Hill models

incorporated a co-operativity parameter (the Hill coefficient;  $h$ ), which indicated there was a positive co-operation effect with the MFCs calibrated with GGA. The models were also able to simulate the 'lag'-phase exhibited by downstream flow-mode MFCs which did not generate current until upstream MFCs had saturated with substrate. Three-parameter Hill models described calibrations accurately and were convenient for comparing between conditions, however the resolving power for BOD prediction was generally higher with linear regression models.

A key finding from operating MFCs over long experimental periods was that the biosensors did not require re-calibration. Once fully enriched, the linear detection range and minimum limiting anode potential of the MFC sensors did not drift and appeared to have been constrained by the operating conditions (*e.g.* cell architecture, external resistance, flow rate). In order to compare calibrations across time periods it was necessary to normalise data to the maximum current densities achieved during operation with a saturating level of substrate. Sensor calibrations were also reproducible across identical MFC configurations, with the variation between sensors no larger than the variation within independent calibrations. This has significant implications for the future application of MFC-based BOD sensors, as it means that the operational maintenance requirement is greatly reduced as only normalisation is required to be performed to account for degradation of cathodic performance.

Calibrations were conducted using glucose-only, glutamic acid-only and GGA as the carbon source in medium fed to batch-mode MFCs. For a true BOD sensor the current response of the MFC would be expected to be equal for equal BOD concentrations. However, it was determined that there was a difference between the current density achieved with each substrate at equimolar BOD<sub>5</sub> concentrations. This was an important issue uncovered with MFC-based BOD sensors. The outcome means that there can be no single "BOD" sensor and that each wastewater stream would require bespoke calibration with the composition of interest (*e.g.* for bakery or brewing wastewaters). This provides opportunities to tailor devices to specific industrial needs but raises potential problems with wastewaters which are not of fixed organic constituents (*e.g.* municipal wastewater). The MFC-based sensors could still be used as an early warning system in these applications but the quantification of the BOD<sub>5</sub> value could be inaccurate (*e.g.* by approximately  $\pm 200$  mg/l O<sub>2</sub> for broadly different organic compositions). Samples of real municipal wastewater were tested using the batch- and flow-mode MFC sensors and in both cases the BOD<sub>5</sub> values were under-predicted by the calibration models (by 3 to 69%).

#### **8.1.4 Overcoming Limitations of MFC-based BOD Sensors and Toxicity Detection**

The three-stage array of MFCs was successfully able to determine BOD<sub>5</sub> values above the saturation limit of the first stage MFCs. As a representative example, Figure 8.2a shows

that the first and second stage current densities remained constant (saturated at 100%) as the BOD<sub>5</sub> was increased from 480 to 540 mg/l O<sub>2</sub>. By considering the summed current from the first, second and third stages of MFCs, the change in BOD<sub>5</sub> can be detected by the multi-stage MFCs, as long as at least the final stage MFC is unsaturated with substrate.

Figure 8.2b–d shows how the detection of three types of current decrease were characterised by the three-stage MFCs which was not possible with single-stage MFCs (Figure 8.1).

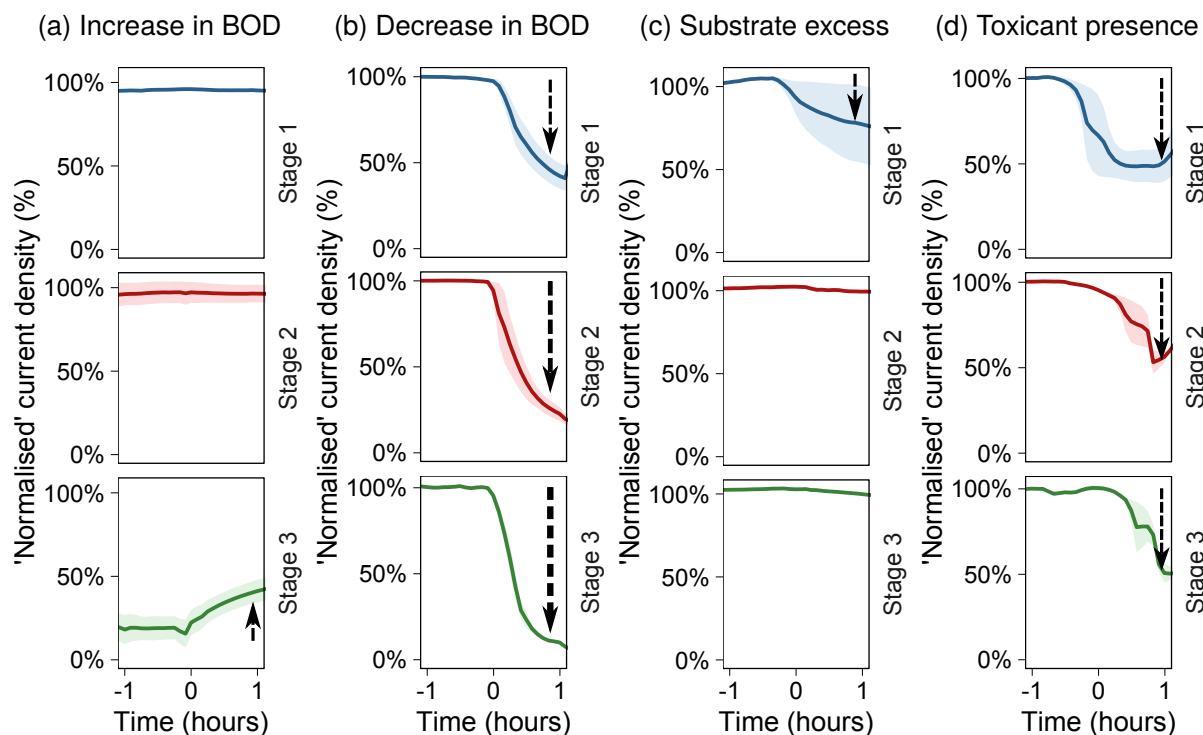


Figure 8.2: Representative examples of the average current densities (shaded region is  $\pm$ SD) obtained from multi-stage MFCs to scenarios which would not be distinguishable with single-stage MFCs. (a) BOD increase can be detected by response of third stage MFCs (which are not at 100% saturation). It is also possible to distinguish between decreases in current density due to (b) BOD decrease (current decreases in  $3 > 2 > 1$  order), (c) substrate excess (current decreases in  $1 > 2 > 3$  order) and (d) toxicant (4-NP) presence (equal current decreases in each stage).  $t = 0$  is the approximate point at which the change occurred. Arrows indicate relative change in current density from prior condition.

With decreases in BOD (Figure 8.2b), the third stage MFCs 'starved first' as their anodic biofilms received the least amount of substrate from the effluent of the upstream MFCs. The loss of current response was observed in the order  $3 > 2 > 1$  (agreeing with the hypothesis made in Chapter 1). The behaviour of the multi-staged MFCs experiencing substrate excess (at 1199 mg/l O<sub>2</sub> BOD<sub>5</sub>) was the same as would be expected for assimilable toxicants. As substrate was consumed by non-electrogenic processes in the first stage MFCs (sludge generation), the feed was depleted to non-inhibitory levels and the response of the second and third stage MFCs was consequently not reduced (order of  $1 > 2 > 3$ ). Toxicant presence was assessed using 4-nitrophenol in the three-stage MFCs and an approximately equal decreases in current density were observed in each MFC stage.

These findings from operation of multi-stage MFCs as BOD/toxicity sensors enabled current decrease events to be explicitly distinguished by the ordered response (or lack of) of the sequential MFCs connected hydraulically in series. Thus the main aims of the thesis were achieved and the developed multi-stage sensor was able to overcome the two major limitations observed with single-stage sensors.

## **8.2 Recommendations for Future Work**

The outcomes from this thesis provide a positive outlook for future development of MFC-based BOD and toxicity sensors. The proof-of-concept multi-stage configuration presented in this work has shown how existing limitations of MFC sensors can be overcome and laid the foundations for translating the technology from laboratory to field.

### **8.2.1 Development of a Optimised Cell & System Architecture**

The proof-of-concept sensor has proven how the sensing principle of using multiple MFCs hydraulically linked in series can enhance the detection range. However, the actual experimental set-up was prone to leakage, sludge build-up and was not practical for field testing in real-world wastewater applications.

There is therefore a need with future developments to focus on design of an optimised cell and system architecture which is robust and does not require frequent user interaction or maintenance. In the literature, MFCs used for electricity generation have been reported which possess optimised architectures which could readily be applied to MFC sensing applications (Kim *et al.*, 2011a; Winfield *et al.*, 2012). Multi-stage configurations lend themselves to the modular approach employed in the present thesis which would enable MFCs to be added or removed based on the range requirements of the wastewater in question.

As a direct consequence of the results from this PhD thesis, a new project on the development of an 'Online Microbial Fuel Cell Biofilm BOD Sensor' has begun at Newcastle University in collaboration with WH Partnership and University of South Wales (funded by InnovateUK/BBSRC; 1506\_FS\_EMTECH\_I\_BF). The project is combining the University of South Wales' expertise on design of optimised tubular MFCs (Figure 8.3) with WH Partnership's knowledge of industrialisation of biotechnological solutions. Together using the MFC-based biosensing techniques and principles developed in the present thesis at Newcastle University, the aim is to produce a 'prototype' device capable of being tested with real-world applications.



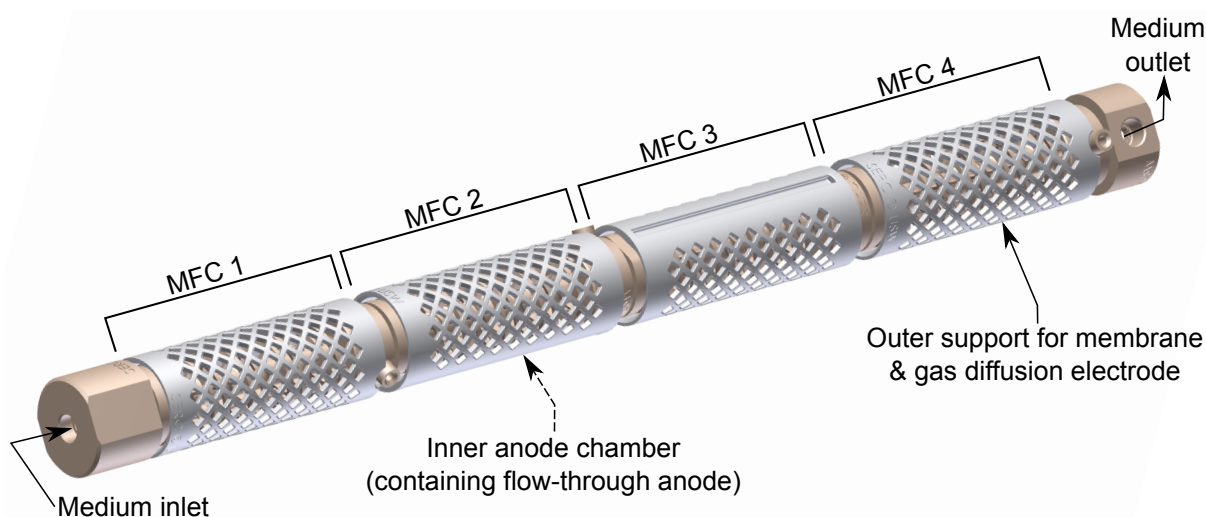


Figure 8.3: Optimised tubular, multi-staged MFC design with inner anodic flow chamber surrounded by membrane/gas diffusion electrode-lined walls. Image used with permission, the design of the University of South Wales, in the context of the InnovateUK/BBSRC 'Online Microbial Fuel Cell Biofilm BOD Sensor' project (1506\_FS\_EMTECH\_I\_BF).

### 8.2.2 Determination of Working Range & Correction Factors for Non-Target Variables

In the present thesis, BOD calibrations and toxicity exposure tests were conducted under precisely controlled environmental conditions. Ambient temperatures in the MFC enclosure were regulated at  $28 \pm 2$  °C, medium was buffered at neutral pH and highly conductive due to the presence of 50 mmol/dm<sup>3</sup> phosphate buffer and dissolved oxygen was purged from solution by nitrogen sparging. Each environmental variable was controlled because variations in these parameters can result in changes to the current generated by the MFCs. Whilst this strategy of controlling conditions works for laboratory-based testing, it is not practical for on-site measurements at a WWTP. Additionally, the economic and labour cost of maintaining a system with heating and chemical amendment is likely to make the sensor less feasible.

The present literature has only established optimum conditions for electricity generation and not BOD calibration. Future studies should look to establish the minimum working requirements for effective MFC-based sensing. Once established correction models could be applied to facilitate BOD and toxicity prediction under variable environmental conditions. Development of advanced kinetic models is required to take into account the various current generation variables (*i.e.* increased BOD, temperature, conductivity or optimum pH) and current decreasing variables (*i.e.* decreased BOD, substrate excess, non-/degradable toxicants presence, decrease in temperature, conductivity or non-optimal pH).

### **8.2.3 Application to Real-world Wastewater Treatment Plants and Beyond**

Only a small number of MFC-based sensors have been applied to real-world systems (Kim *et al.*, 2003b, 2007; Liu *et al.*, 2011). However, field testing is vital for determination of robustness, stability and reliability of the sensors in practice with variable environmental conditions. Once sensors have been proven in the field to provide reliable, real-time monitoring data, great improvements can be made in regard to process control, treatment efficiency, process knowledge and ultimately identification and prevention of environmentally hazardous pollution incidents.

Outside of wastewater treatment plants in the environment, there is a need to identify pollution incidents as soon as they occur. An interesting recent proposal coupled floating MFC-based sensors with energy-harvesting power management electronics to enable truly remote sensing (Schievano *et al.*, 2016). Potentially, electricity generated by the MFC sensor could be stored capacitively, until sufficient energy is recovered to send asynchronous data communications to a central mainframe for interpretation. By combining the bioreceptor, transducer and power source (from the MFC) with the data communication electronics in a remote device, there is a real possibility of producing sensors using MFC technology which are low-cost and can be used in any location. This development would be of great interest to regulatory bodies and water treatment organisations, and points towards a future where ubiquitous sensors could be deployed along water courses for monitoring purposes.

## **Appendix A. Literature Survey Data**

### **List of Tables**

A.1	Literature survey of BES-based BOD sensor materials & operating parameters. . . . .	214
A.2	Comparison of typical BOD and COD values for a selection of municipal wastewaters and industrial wastewaters taken from the literature. . . .	219

Table A.1: Literature survey of BES-based BOD sensor materials &amp; operating parameters.

<b>Reference</b>	<b>Anode material / area / volume</b>	<b>Cathode</b>	<b>Membrane</b>	<b>External Load</b>	<b>Inoculum</b>	<b>Flow rate</b>	<b>Temp.</b>
Gil <i>et al.</i> (2003)	Graphite felt / 25 cm <sup>2</sup> / 25 ml	Graphite felt	CEM	10 Ω	Starch WW, AS & ADS	N/A	37 °C
Kim <i>et al.</i> (2003a)	Graphite felt / 25 cm <sup>2</sup> / 25 ml	Graphite felt	CEM	10 Ω	Starch WW, AS & ADS	N/A	30 °C
Kang <i>et al.</i> (2003)	Graphite felt / 4 cm <sup>2</sup> / 20 ml	Pt-coated graphite felt	CEM	500 Ω	River sediment oligotrophs	0.15 ml/min	33 °C
Kim <i>et al.</i> (2003b)	Graphite felt / 26 cm <sup>2</sup> / 17 ml	Graphite felt	CEM	10 Ω	Domestic WW & AS	0.3 ml/min	30 °C
Chang <i>et al.</i> (2004)	Graphite felt / 24 cm <sup>2</sup> / 25 ml	Graphite felt	CEM	10 Ω	Activated sludge	0.35 ml/min	35 °C
Moon <i>et al.</i> (2004)	Graphite felt / 24 cm <sup>2</sup> / 5, 25 ml	Graphite felt	CEM	10 Ω	Activated sludge	0.35 ml/min	35 °C
Chang <i>et al.</i> (2005)	Graphite felt / 24 cm <sup>2</sup> / 25 ml	Graphite felt	CEM	10 Ω	Activated sludge	0.35 ml/min	35 °C

<sup>a</sup> CEM = Cation exchange membrane; PEM = Proton exchange membrane; AS = Activated sludge; ADS = Anaerobic Digester sludge; AnS = Anaerobic sludge; WW = Wastewater

Table A.1: continued...

<b>Reference</b>	<b>Anode material / area / volume</b>	<b>Cathode</b>	<b>Membrane</b>	<b>External Load</b>	<b>Inoculum</b>	<b>Flow rate</b>	<b>Temp.</b>
Moon <i>et al.</i> (2005)	Graphite felt / 4 cm <sup>2</sup> / 20 ml	Pt-coated graphite felt	CEM	10 Ω	Surface water oligotrophs	0.53 ml/min	33 °C
Kim <i>et al.</i> (2006b)	Unknown - details are not provided in report						35 °C
Kumlanghan <i>et al.</i> (2007)	Graphite rod / 134 cm <sup>2</sup> / 100 ml	Graphite roll	PEM	800 Ω	Anaerobic sludge	N/A	37 °C
Di Lorenzo <i>et al.</i> (2009a)	Carbon cloth / 12.5 cm <sup>2</sup> / 50 ml	Pt/C GDE	PEM	500 Ω	Anaerobic sludge	0.46 ml/min	RT; 21±2 °C
Di Lorenzo <i>et al.</i> (2009b)	Graphite granules / 496 cm <sup>2</sup> / 37.5 ml	Pt/C GDE	PEM	500 Ω	Anaerobic sludge	0.46 ml/min	RT; 21±2 °C
Kim <i>et al.</i> (2009)	Unknown	Pt-coated carbon cloth	CEM	Unknown	Unknown	N/A	Unknown
Peixoto <i>et al.</i> (2010)	Carbon paper / 9 cm <sup>2</sup> / 1000 ml	Pt/C GDE	PEM	1000 Ω	Domestic WW	N/A	RT; 22±2 °C
Liu <i>et al.</i> (2011)	Graphite roll / 6.28 cm <sup>2</sup> / 1.6 ml	Graphite roll	PEM	200 Ω	Anaerobic sludge	7.74 ml/min	36.5 °C (feed)

<sup>a</sup> CEM = Cation exchange membrane; PEM = Proton exchange membrane; AS = Activated sludge; ADS = Anaerobic Digester sludge; AnS = Anaerobic sludge; WW = Wastewater

Table A.1: continued...

<b>Reference</b>	<b>Anode material / area / volume</b>	<b>Cathode</b>	<b>Membrane</b>	<b>External Load</b>	<b>Inoculum</b>	<b>Flow rate</b>	<b>Temp.</b>
Peixoto <i>et al.</i> (2011)	Carbon paper / 9 cm <sup>2</sup> / 1000 ml	Pt/C GDE	PEM	1000 Ω	Domestic WW	N/A	33 °C
Zhang and Angelidaki (2011)	Carbon paper / 9 cm <sup>2</sup> / 1000 ml	Pt/C GDE	PEM	1000 Ω	Domestic WW	N/A	RT; 25 °C
Modin and Wilén (2012)	Graphite rod / 17.4 cm <sup>2</sup> / 11.8 ml	C nano- particles GDE	None; filter paper	+250 mV applied	AS & ADS	N/A	RT
Feng <i>et al.</i> (2013b)	Carbon fibre / 20 cm <sup>2</sup> / 20, 40 ml	Pt/C GDE	CEM	470 Ω	Activated sludge	N/A	23 °C
Yang <i>et al.</i> (2013)	PAN-carbon felt / 48 cm <sup>2</sup> / 75 ml	Pt/C GDE	Film ion exchange	1000 Ω	AS & AnS	Unknown	RT; 25±5 °C
Di Lorenzo <i>et al.</i> (2014)	Carbon cloth / 4 cm <sup>2</sup> / 2 ml	Carbon cloth	PEM	1000 Ω	MFC effluent	0.1 ml/min	RT; 20±3 °C
Ghangrekar (2014)	Carbon felt / 90 cm <sup>2</sup> / 40 ml	Carbon felt	Nafion; CWPEM	10 Ω	Septic tank sludge	N/A	20-25 °C

<sup>a</sup> CEM = Cation exchange membrane; PEM = Proton exchange membrane; AS = Activated sludge; ADS = Anaerobic Digester sludge; AnS = Anaerobic sludge; WW = Wastewater

Table A.1: continued...

<b>Reference</b>	<b>Anode material / area / volume</b>	<b>Cathode</b>	<b>Membrane</b>	<b>External Load</b>	<b>Inoculum</b>	<b>Flow rate</b>	<b>Temp.</b>
Hsieh and Chung (2014)	Unknown	Unknown	Unknown	500 $\Omega$	Known mixed cultures	N/A	35 °C
Quek <i>et al.</i> (2014)	Graphite granules / 54 cm <sup>2</sup> / 54 ml	Graphite granules	CEM	+/-250 mV vs. Ag/AgCl poised	Ocean sediment	Unknown	RT
Ayyaru and Dharmalingam (2014)	Wet-proof carbon cloth / 12.5 cm <sup>2</sup> / 50 ml	Pt/C GDE	SPEEK; Nafion PEM	500 $\Omega$	Anaerobic sludge	0.43 ml/min	RT; 30 °C
Tian <i>et al.</i> (2014)	Unknown	Unknown	Unknown	500 $\Omega$	Anaerobic sludge	N/A	Unknown
Liu <i>et al.</i> (2014)	Graphite rolls / 6.28 cm <sup>2</sup> / 1.6 ml	Graphite rolls	PEM	200 $\Omega$	MFC effluent	7.74 ml/min	36.5 °C (feed)
Quek <i>et al.</i> (2015a)	Graphite granules / 100 ml	Graphite granules	CEM	+250 mV vs. Ag/AgCl poised	Marine sediment	5 ml/min	RT
Wu <i>et al.</i> (2015a)	Granular carbon / 700 kg/m <sup>2</sup> / 100 ml	K <sub>3</sub> [Fe(CN) <sub>6</sub> ] + graphite felt	CEM	20-100 $\Omega$	MFC effluent	20 ml/min	RT; 25±1.5 °C

<sup>a</sup> CEM = Cation exchange membrane; PEM = Proton exchange membrane; AS = Activated sludge; ADS = Anaerobic Digester sludge; AnS = Anaerobic sludge; WW = Wastewater

Table A.1: continued...

<b>Reference</b>	<b>Anode material / area / volume</b>	<b>Cathode</b>	<b>Membrane</b>	<b>External Load</b>	<b>Inoculum</b>	<b>Flow rate</b>	<b>Temp.</b>
Quek <i>et al.</i> (2015b)	Graphite granules / 250 ml	K <sub>3</sub> [Fe(CN) <sub>6</sub> ] + graphite granules	CEM	56 Ω	Marine sediment & seawater	Unknown	RT
Hsieh <i>et al.</i> (2015)	Unknown / 98 cm <sup>2</sup>	Unknown	Unknown	5000 Ω	Known mixed cultures	0.27- 1.63 ml/min	35 °C
Jia <i>et al.</i> (2016)	Carbon felt / 64 cm <sup>2</sup> / 10000 ml	Pt/C GDE	None	1000 Ω	Anaerobic sludge	7-42 ml/min	25±2 °C
Commault <i>et al.</i> (2016)	Graphite rod / 5.81 cm <sup>2</sup> / c ml	Carbon cloth	CEM	-360 mV vs. Ag/AgCl poised	Water-saturated soil	N/A	21 °C

<sup>a</sup> CEM = Cation exchange membrane; PEM = Proton exchange membrane; AS = Activated sludge; ADS = Anaerobic Digester sludge; AnS = Anaerobic sludge; WW = Wastewater



Table A.2: Comparison of typical BOD and COD values for a selection of municipal wastewaters and industrial wastewaters taken from the literature. BOD<sub>5</sub> and COD values are in units of mg/l O<sub>2</sub>.

Industry	Description	BOD <sub>5</sub> (range)	BOD <sub>5</sub> (ave)	COD (range)	COD (ave)	BOD <sub>5</sub> /COD
Municipal WWTP	Urban wastewater <sup>a</sup>	100 - 500	300	210 - 1100	655	0.45 - 0.48
	Raw municipal WW including industrial WW <sup>a</sup>	230 - 560	395	500 - 1200	850	0.07 - 0.67
	Settled tank effluent <sup>b</sup>	44 - 833	252	201 - 944	444	0.22 - 0.88
	Septic sludge <sup>a</sup>	2000 - 30000	16000	6000 - 90000	48000	0.33
	Digester supernatant <sup>a</sup>	300 - 4000	2150	700 - 9000	4850	0.43
Livestock Waste <sup>c</sup>	Cattle		137			-
	Dairy		442			-
	Poultry		153			-
Palm Oil Production <sup>c</sup>	Physical refining & dry fractionation		530		890	0.60
Food Processing <sup>c</sup>	Meat processing WW		400		600	0.67
	Dairy products WW		170		250	0.68
	Starch and gluten WW		1300		2300	0.57

<sup>a</sup> Data from Henze and Comeau (2008)    <sup>b</sup> Data from Lowe *et al.* (2007)    <sup>c</sup> Data from Wang *et al.* (2006)

Table A.2: continued...

Industry	Description	BOD <sub>5</sub> (range)	BOD <sub>5</sub> (ave)	COD (range)	COD (ave)	BOD <sub>5</sub> /COD
Oilfield & Refinery <sup>c</sup>	Produced Water (brought to surface w/ oil)	50 - 1400	725	450 - 5900	3175	0.11 - 0.24
	Spent Drilling Mud		2625		5720	0.46
	Crude desalting (process WW)	124 - 470	297	60 - 610	335	0.48
	Sour condensates from distillation cracking (process WW)	500 - 1000	750	500 - 2000	1250	0.50
Soap & Detergent <sup>c</sup>	Fat splitting WW	60 - 3600	1830	115 - 6000	3057.5	0.52 - 0.60
	Air sulfation and sulfonation WW	380 - 520	450	920 - 1589	1254.5	0.33 - 0.41
Pesticide <sup>c</sup>	Raw waste load design levels (from USEPA survey)		1470		3886	0.38
Seafood Processing <sup>c</sup>	All salmon WW	253 - 2600	1426.5	300 - 5500	2900	0.26 - 0.84
	All herring WW	1200 - 6000	3600	3000 - 10000	6500	0.40 - 0.60
	All oysters WW	250 - 800	525	500 - 2000	1250	0.40 - 0.50
Dairy Processing <sup>c</sup>	Cheese/whey plant WW	377 - 5722	3050	189 - 7619	3904	0.36 - 0.75
	Butter/Comté cheese plant WW		1250		2520	0.50
Bakery <sup>c</sup>	Cake plant overall	2240 - 8500	5370			-

<sup>a</sup> Data from Henze and Comeau (2008)    <sup>b</sup> Data from Lowe *et al.* (2007)    <sup>c</sup> Data from Wang *et al.* (2006)

Table A.2: continued...

Industry	Description	BOD <sub>5</sub> (range)	BOD <sub>5</sub> (ave)	COD (range)	COD (ave)	BOD <sub>5</sub> /COD
Bakery <sup>c</sup>	Cake Plant: 1pm - 6pm		2520			-
	Influent WW (Keebler Co.)		500		830	0.60
	Bakery Raw Water	906 - 24000	987	2910 - 50400	23730	0.42
Soft Drink <sup>c</sup>	Soft drink plant WW	600 - 4500	2550	1200 - 8000	4600	0.50 - 0.56
Textile <sup>c</sup>	Starch desizing	2500 - 3000	2750	4500 - 5000	4750	0.56 - 0.60
	Protein desizing	3500 - 4000	3750		6000	0.58 - 0.67
Meat Processing <sup>c</sup>	Hog WW	1030 - 2220	1625		3015	0.65
	Cattle WW	448 - 7237	3842.5	2100 - 12873	7486.5	0.30 - 0.46
	Mixed meat WW	404 - 11244	5824	583 - 18768	9675.5	0.30 - 0.73
Rubber <sup>c</sup>	Reclaimed rubber manufacturing plant raw WW	3500 - 12500	8000			-
	Synthetic rubber manufacturing plant raw WW	75 - 1600	837.5			-
Potato Processing <sup>c</sup>	French fries & starch plant effluent		4100		7794	0.53
	Potato chips plant WW		5450		7293	0.75

<sup>a</sup> Data from Henze and Comeau (2008)    <sup>b</sup> Data from Lowe *et al.* (2007)    <sup>c</sup> Data from Wang *et al.* (2006)

Table A.2: continued...

Industry	Description	BOD <sub>5</sub> (range)	BOD <sub>5</sub> (ave)	COD (range)	COD (ave)	BOD <sub>5</sub> /COD
Potato Processing <sup>c</sup>	Potato flour raw WW	3314 - 7420	5367	8314 - 12582	10448	0.40 - 0.59
Landfill Leachate <sup>c</sup>	Raw landfill leachate	20 - 40000	20010	500 - 60000	30250	0.04 - 0.67
	Leachate treatment plant influent (Mechernich)	1062 - 4540	2801	3176 - 6440	4808	0.33 - 0.70
Pulp & Paper Mill <sup>c</sup>	Spent NSSC pulping liquor		25000		40000	0.63
	Sulfite mill aerated lagoon influent		320		1508	0.21
Olive Oil <sup>c</sup>	Olive Oil WW (Alpechin)	4300 - 100000	52150	6700 - 225000	115850	0.20 - 0.64
	Small mill WW	15 - 65	40	37 - 150	93.5	0.41 - 0.43
	Big mill WW	17 - 41	29	30 - 80	55	0.51 - 0.57
Pharmaceutical <sup>c</sup>	Typical spent fermentation broth	5000 - 20000	12500			-
	Synthetic organic chemical waste: composite		70365		109585	0.64
	Allopathic medicine production WW		1500		2700	0.55
	Liver & beef extract biological production WW	11400 - 16100	13750	17100 - 24200	20650	0.66 - 0.67

<sup>a</sup> Data from Henze and Comeau (2008)    <sup>b</sup> Data from Lowe *et al.* (2007)    <sup>c</sup> Data from Wang *et al.* (2006)

## Appendix B. Method Data

### List of Figures

B.1	Schematic diagram of detailed set-up for triplicate channels of three-stage SCMFCs and position of three-way valves including tubing sizing and type. . . . .	224
B.2	Chart showing removal of dissolved oxygen from 250 ml solution of GGA medium whilst sparging with N <sub>2</sub> . . . . .	224
B.3	Calibration of absorbances measured from (a) 10-150 mg/l O <sub>2</sub> and (b) 25-1500 mg/l O <sub>2</sub> photometric COD test kits with known solutions of GGA medium. . . . .	225
B.4	Charts showing ion chromatogram recorded for VFA standard solution and calibration of peak areas for known VFA concentrations. . . . .	225
B.5	Charts showing ion chromatogram and single-point calibration of peak areas for known anion concentrations. . . . .	226
B.6	Calibration of absorbances measured from D-glucose UV spectrophotometric assay with known solutions of GGA medium. . . . .	226
B.7	Calibration of absorbances measured from L-glutamic acid UV spectrophotometric assay with known solutions of GGA medium. . . . .	227
B.8	Calibration of absorbances measured from known solutions of toxicant-doped GGA medium containing 4-nitrophenol at 320 nm. . . . .	227
B.9	Microscope images of stage micrometer at 100× and 400× magnification	227
B.10	Typical images of (a) micrograph of SYBR® Gold-stained bacteria and (b) CellC automated counting result. . . . .	228
B.11	Calculation of the theoretical oxygen demand (ThOD) of (a) 150 mg/l glucose and (b) 150 mg/l glutamic acid. . . . .	229

### List of Tables

B.1	Hydraulic retention time of each component and total path of the flow-mode system at 0.52 & 1.24 ml/min. . . . .	230
-----	--	-----

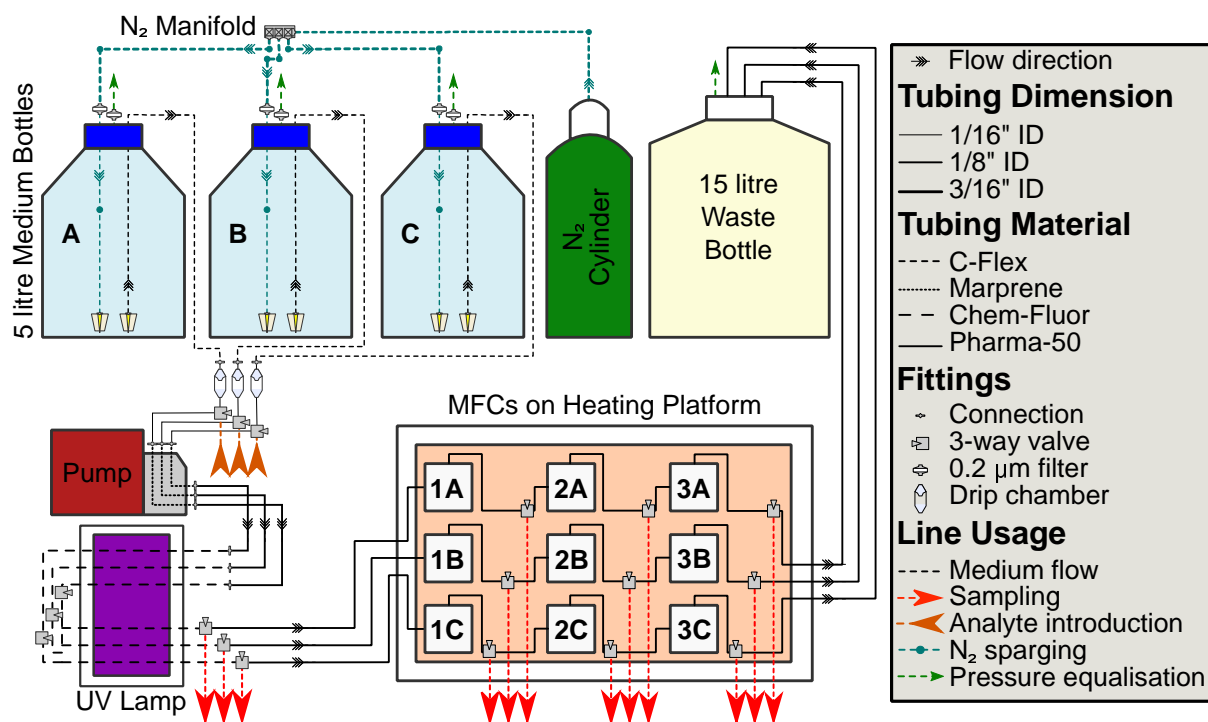


Figure B.1: Schematic diagram of detailed set-up for triplicate channels of three-stage SCMFCs and position of three-way valves including tubing sizing and type.

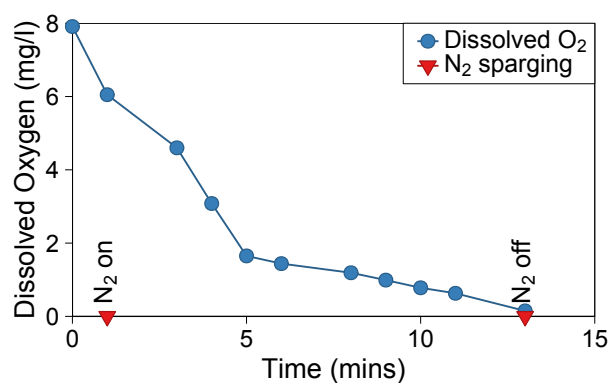


Figure B.2: Chart showing removal of dissolved oxygen from 250 ml solution of GGA medium whilst sparging with N<sub>2</sub>.

(a) 10-150 mg/l O<sub>2</sub> COD test kit calibration (absorbance of unconsumed Cr<sub>2</sub>O<sub>7</sub><sup>2-</sup> at 445 nm). (b) 25-1500 mg/l O<sub>2</sub> COD test kit calibration (absorbance of produced Cr<sup>3+</sup> at 605 nm).

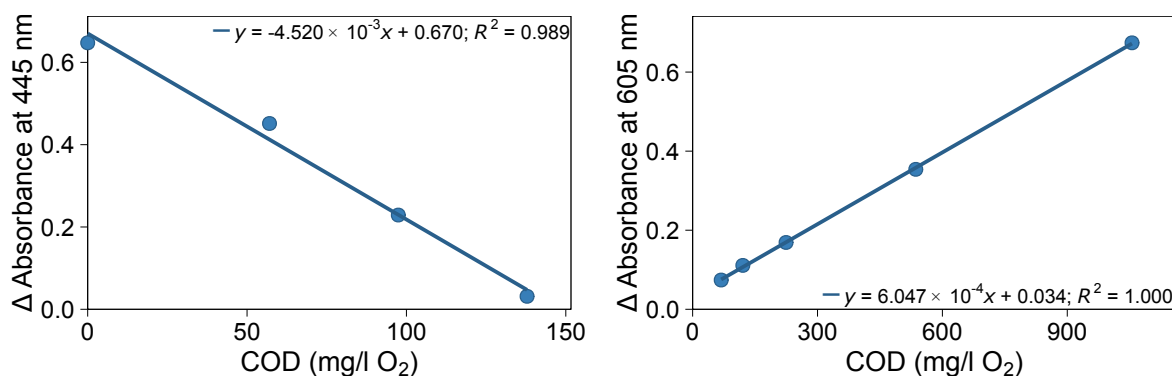
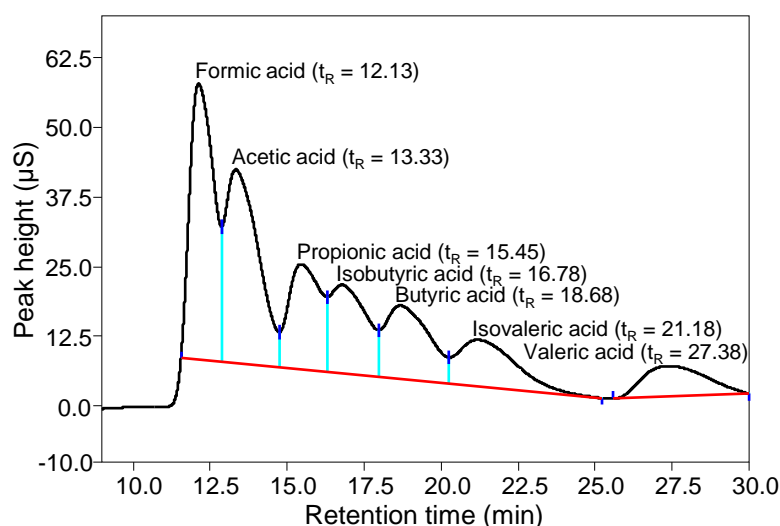


Figure B.3: Calibration of absorbances measured from (a) 10-150 mg/l O<sub>2</sub> and (b) 25-1500 mg/l O<sub>2</sub> photometric COD test kits with known solutions of GGA medium.

(a) Ion chromatogram showing 500 mg/l VFA retention times ( $t_R$ ).



(b) Calibration of known VFA concentrations.

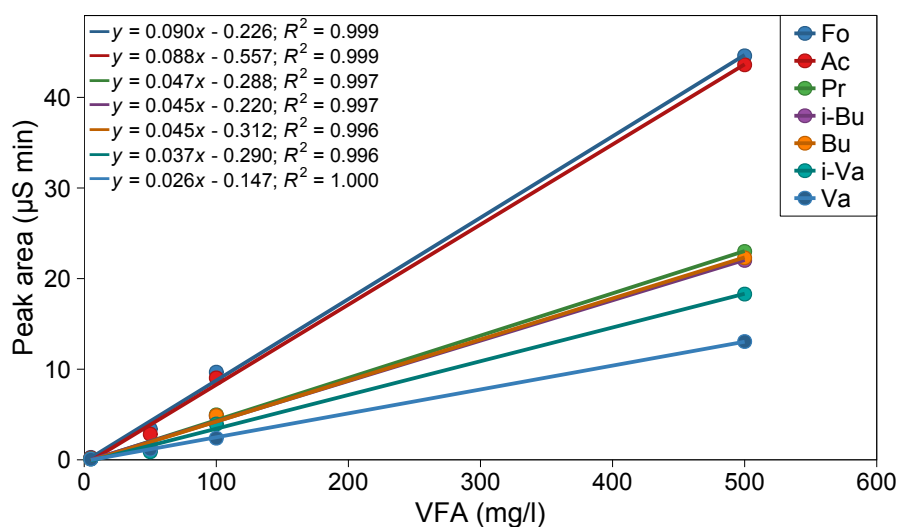


Figure B.4: Charts showing (a) ion chromatogram recorded for 500 mg/l VFA standard solution showing peak retention times and (b) calibration of peak areas for solutions of known VFA concentrations.

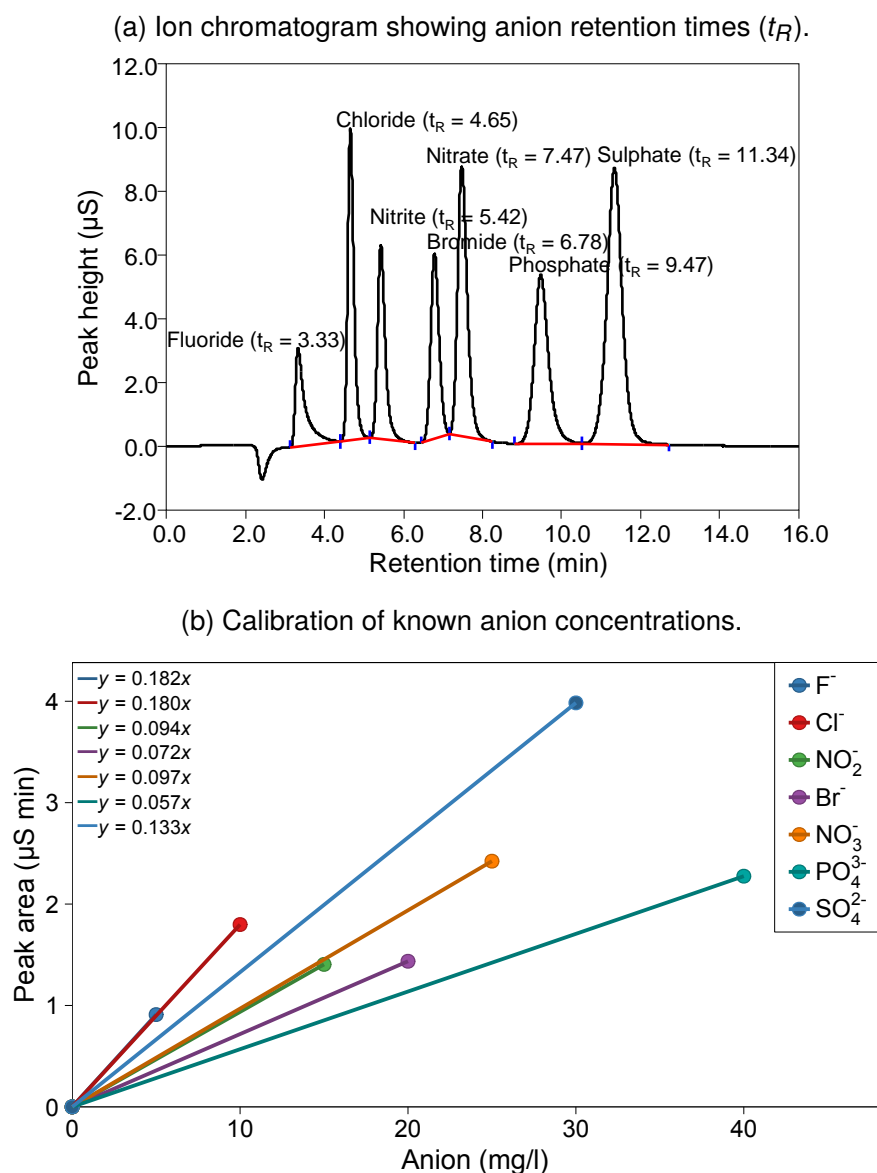


Figure B.5: Charts showing (a) ion chromatogram recorded for anion standard solution up to 40 mg/l showing peak retention times and (b) single-point calibration of peak areas for a solution of known anion concentrations.

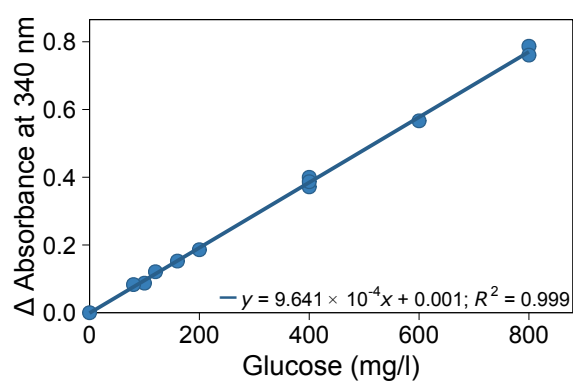


Figure B.6: Calibration of absorbances measured from D-glucose UV spectrophotometric assay with known solutions of GGA medium. Error bars represent range of duplicate measurement values.



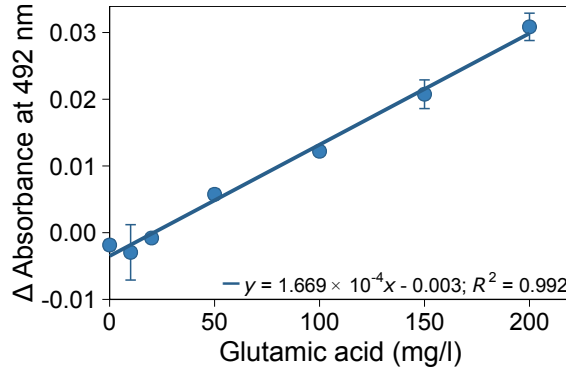


Figure B.7: Calibration of absorbances measured from L-glutamic acid UV spectrophotometric assay with known solutions of GGA medium. Error bars represent range of duplicate measurement values.

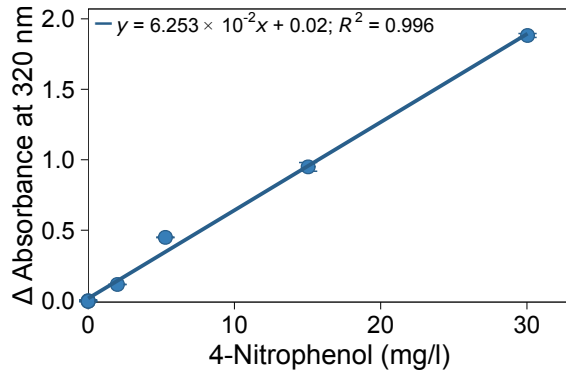
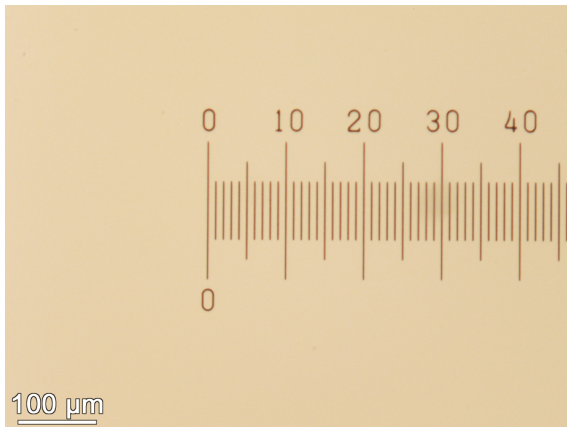


Figure B.8: Calibration of absorbances measured from known solutions of toxicant-doped GGA medium containing 4-nitrophenol with a UV spectrophotometer at 320 nm. Error bars represent range of duplicate measurement values.

(a) 100× magnification of stage micrometer (image dimensions = 729 × 546 μm).



(b) 400× magnification of stage micrometer (image dimensions = 182 × 136 μm).

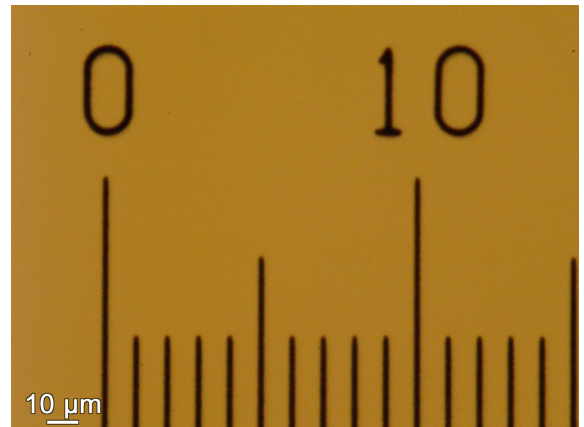
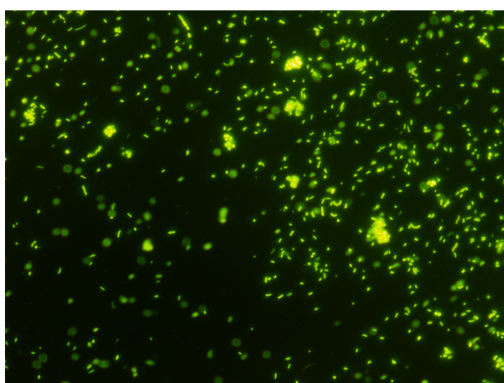


Figure B.9: Microscope images of stage micrometer at 100× and 400× magnification.

(a) Fluorescence image



(b) CellC result

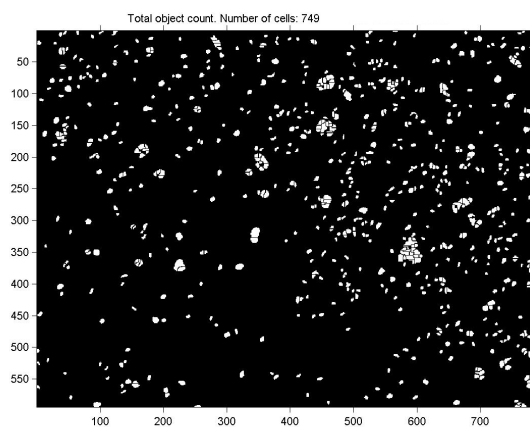
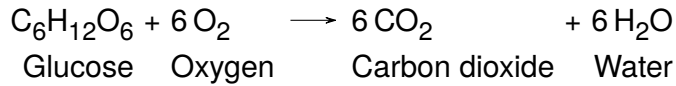


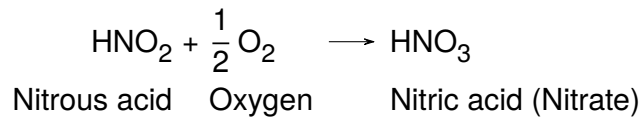
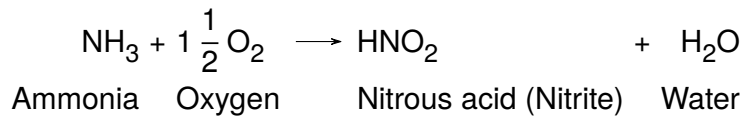
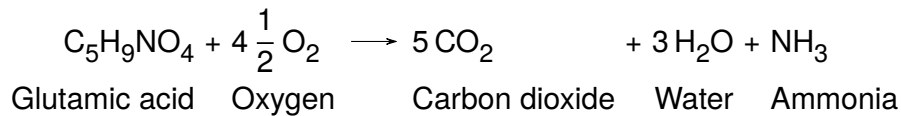
Figure B.10: Typical images of (a) micrograph of SYBR® Gold-stained bacteria and (b) CellC automated counting result.

(a) Stoichiometric calculation of ThOD for 150 mg/l glucose.



$$\begin{aligned} \text{ThOD, mg/l} &= \frac{6 \text{ mol O}_2}{\text{mol C}_6\text{H}_{12}\text{O}_6} \times \frac{32.00 \text{ g/mol O}_2}{180.16 \text{ g/mol C}_6\text{H}_{12}\text{O}_6} \times 150 \text{ mg/l C}_6\text{H}_{12}\text{O}_6 \\ &= 1.07 \text{ g(O}_2\text{)/g(C}_6\text{H}_{12}\text{O}_6) \times 150 \text{ mg/l C}_6\text{H}_{12}\text{O}_6 \\ &= 159.86 \text{ mg/l O}_2 \end{aligned}$$

(b) Stoichiometric calculation of ThOD for 150 mg/l glutamic acid.



$$\begin{aligned} \text{ThOD, mg/l} &= \frac{4.5 \text{ mol O}_2}{\text{mol C}_5\text{H}_9\text{NO}_4} \times \frac{32.00 \text{ g/mol O}_2}{147.13 \text{ g/mol C}_5\text{H}_9\text{NO}_4} \times 150 \text{ mg/l C}_5\text{H}_9\text{NO}_4 \\ &= 0.98 \text{ g(O}_2\text{)/g(C}_5\text{H}_9\text{NO}_4) \times 150 \text{ mg/l C}_5\text{H}_9\text{NO}_4 \\ &= 146.81 \text{ mg/l O}_2 \\ \text{Total ThOD, mg/l} &= \frac{6.5 \text{ mol O}_2}{\text{mol C}_5\text{H}_9\text{NO}_4} \times \frac{32.00 \text{ g/mol O}_2}{147.13 \text{ g/mol C}_5\text{H}_9\text{NO}_4} \times 150 \text{ mg/l C}_5\text{H}_9\text{NO}_4 \\ &= 1.41 \text{ g(O}_2\text{)/g(C}_5\text{H}_9\text{NO}_4) \times 150 \text{ mg/l C}_5\text{H}_9\text{NO}_4 \\ &= 212.06 \text{ mg/l O}_2 \end{aligned}$$

Figure B.11: Calculation of the theoretical oxygen demand (ThOD) of (a) 150 mg/l glucose and (b) 150 mg/l glutamic acid.

Table B.1: Hydraulic retention time of each component and total path of the flow-mode system at 0.52 &amp; 1.24 ml/min.

ID	Flow-mode system component	Volume (ml)		Hydraulic Retention Time (min)			
		Unit	Path	at 0.52 ml/min		at 1.24 ml/min	
				Unit	Path	Unit	Path
Line 1	Medium bottle to drip chamber inlet (1/16" ID C-Flex®)	1.8	1.8	3:28	3:28	1:23	1:23
Line 2	Inlet & outlet line from drip chamber to 3-way valve (1/8" ID Pharma-50)	1.58	3.38	3:03	6:31	1:13	2:36
3-W M	3-way valve for test analyte introduction	2.5	5.88	4:49	11:20	1:56	4:32
Line 3	Peristaltic pump tubing (2.79 mm ID Autoclavable Marprene®)	2.78	8.66	5:21	16:41	2:09	6:40
Line 4	Pump to UV inlet (1/8" ID Pharma-50)	0.79	9.45	1:31	18:12	0:37	7:17
Line 5	UV-transparent tubing to/from 3-way valve (1/16" ID ChemFluor® 367)	1.29	10.74	2:29	20:41	1:00	8:17
3-W L	3-way valve for in-line medium sampling	2.5	13.24	4:49	25:30	1:56	10:12
Line 6	Valve to Stage 1 SCMFC inlet (1/8" ID Pharma-50)	4.75	17.99	9:09	34:39	3:40	13:52
MFC 1	Stage 1 SCMFC	9.8	27.79	18:53	53:32	7:33	21:25
Line 7	Stage 1 SCMFC outlet to 3-way valve (1/8" ID Pharma-50)	4.35	32.14	8:23	61:55	3:21	24:46
3-W 1	3-way valve for in-line sampling after Stage 1 SCMFC	2.5	34.64	4:49	66:44	1:56	26:41
Line 8	Valve to Stage 2 SCMFC inlet (1/8" ID Pharma-50)	4.35	38.99	8:23	75:06	3:21	30:03
MFC 2	Stage 2 SCMFC	9.8	48.79	18:53	93:59	7:33	37:36
Line 9	Stage 2 SCMFC outlet to 3-way valve (1/8" ID Pharma-50)	4.35	53.14	8:23	102:22	3:21	40:57
3-W 2	3-way valve for in-line sampling after Stage 2 SCMFC	2.5	55.64	4:49	107:11	1:56	42:52
Line 10	Valve to Stage 3 SCMFC inlet (1/8" ID Pharma-50)	4.35	59.99	8:23	115:33	3:21	46:13
MFC 3	Stage 3 SCMFC	9.8	69.79	18:53	134:26	7:33	53:46
Line 11	Stage 3 SCMFC outlet to 3-way valve (1/8" ID Pharma-50)	4.35	74.14	8:23	142:49	3:21	57:08
3-W 3	3-way valve for in-line sampling after Stage 3 SCMFC	2.5	76.64	4:49	147:38	1:56	59:03
Line 12	Valve to waste bottle (1/8" ID Pharma-50 - 3/16" ID C-Flex®)	22.12	98.76	42:37	190:14	17:03	76:06

## **Appendix C. Batch Calibration Data**

### **List of Figures**

- C.1 Peak current density calibration curves fitted with Hill models for data obtained during calibrations of batch-mode MFCs. . . . . 232
- C.2 Cycle charge density calibration curves fitted with Hill models for data obtained during calibrations of batch-mode MFCs. . . . . 235
- C.3 Plots of average current density in Calibrations 1, 2, 5, 7, 8 and 9 for batch-mode MFCs A and B. . . . . 239
- C.4 Plots of average current density in Calibration 10 for batch-mode MFCs A and B and Calibration 1a for cells C and D. . . . . 240

### **List of Tables**

- C.1 Evaluation of predicted BOD<sub>5</sub> values using the calibrated linear and Hill models from the batch-mode MFCs for samples of real wastewater. 241

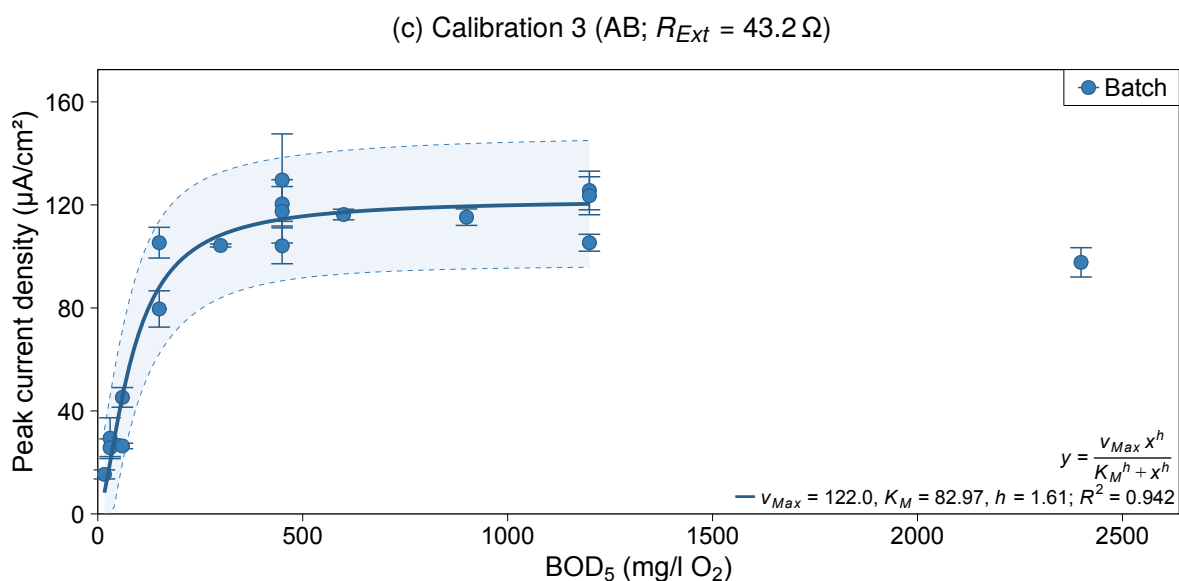
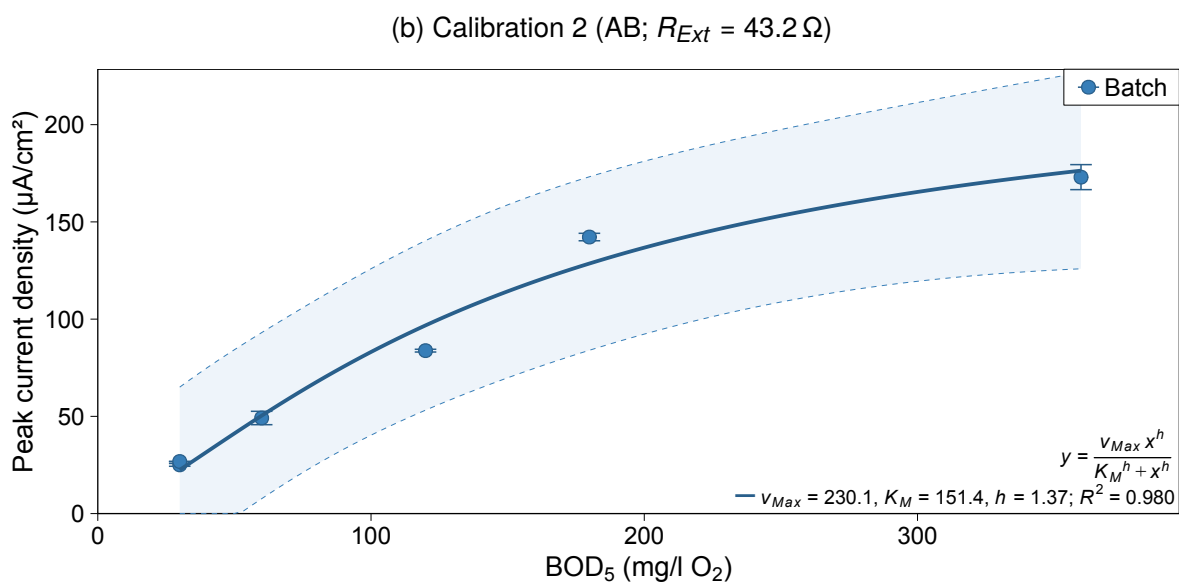
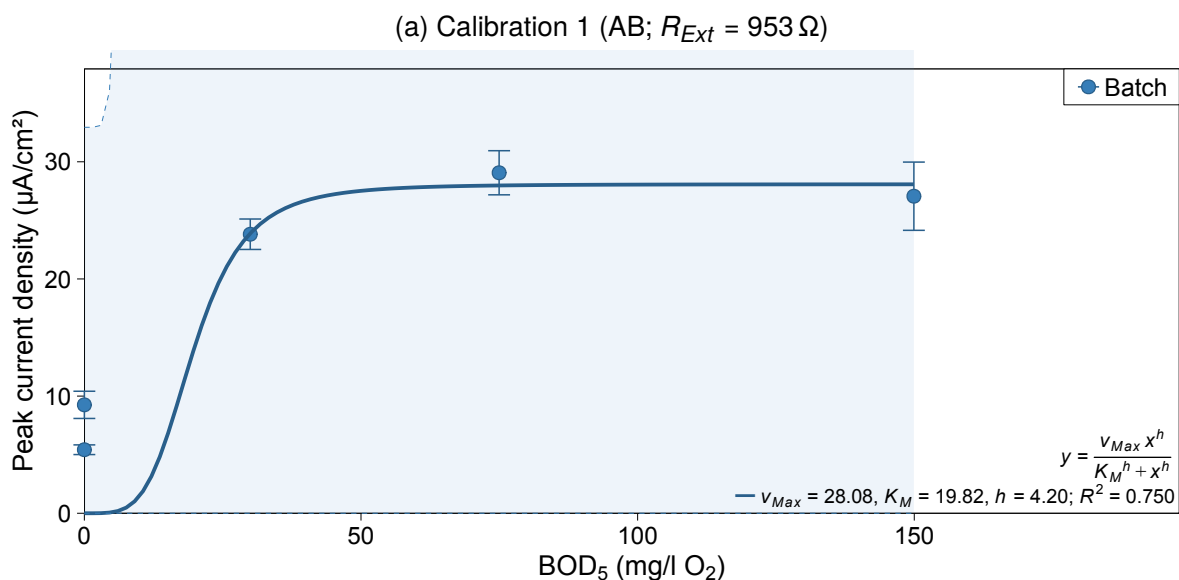
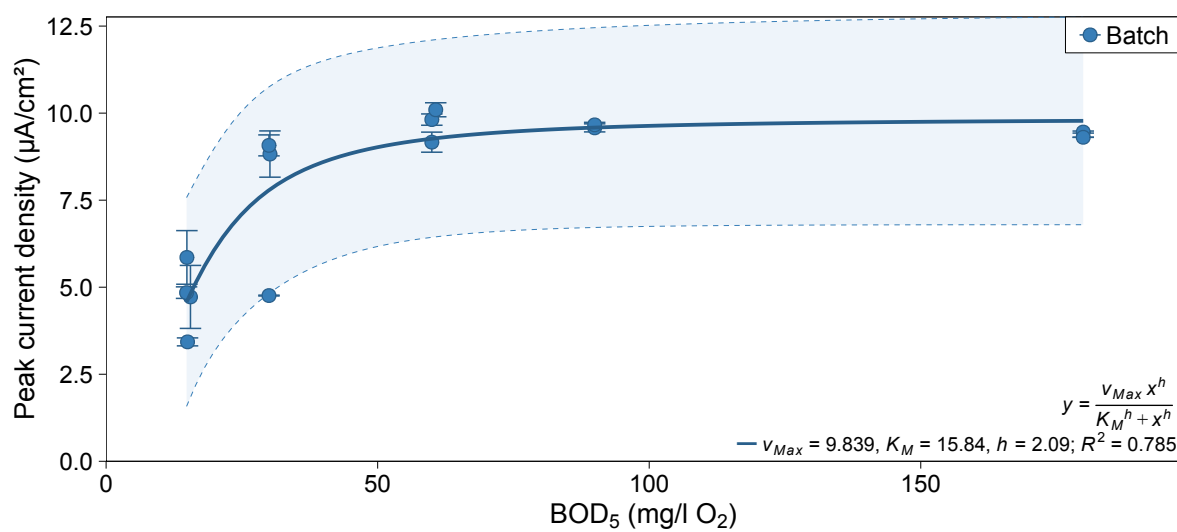
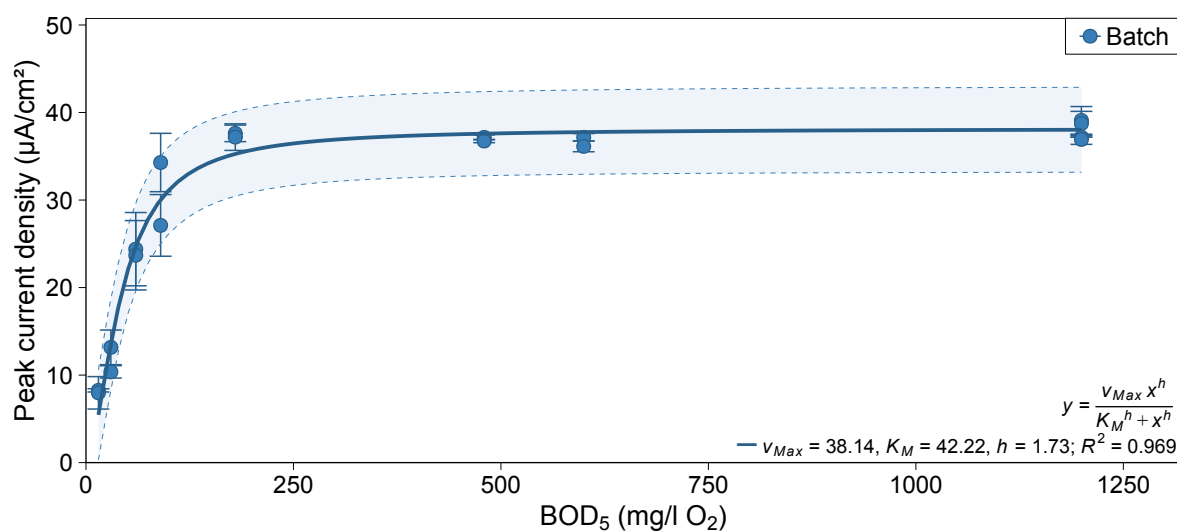


Figure C.1: Peak current density calibration curves fitted with Hill models against BOD<sub>5</sub> (estimated from GGA concentration) for data obtained during calibrations of batch-mode MFCs A & B and C & D. Shaded bands represent the 95% prediction interval from model lines and error bars are the range of values from duplicate cells.

(d) Calibration 5 (AB;  $R_{Ext} = 5100 \Omega$ )



(e) Calibration 6 (AB;  $R_{Ext} = 953 \Omega$ )



(f) Calibration 7 (AB;  $R_{Ext} = 305 \Omega$ )

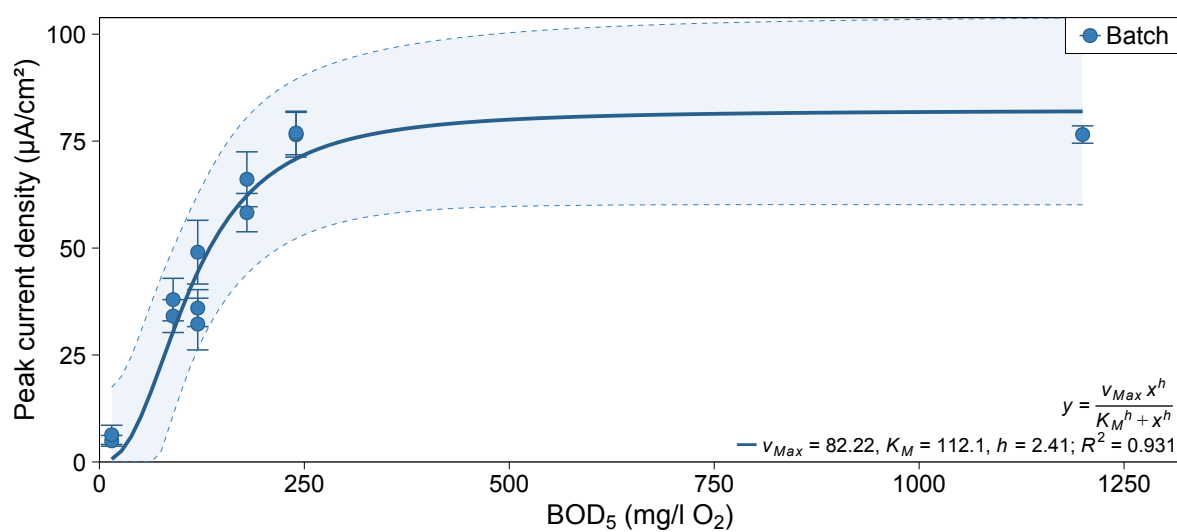
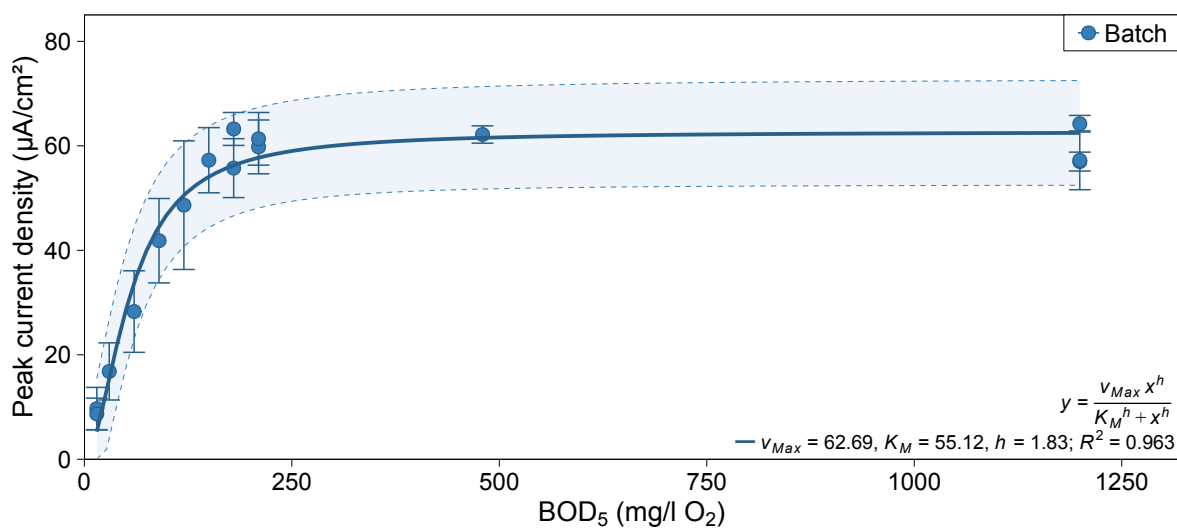
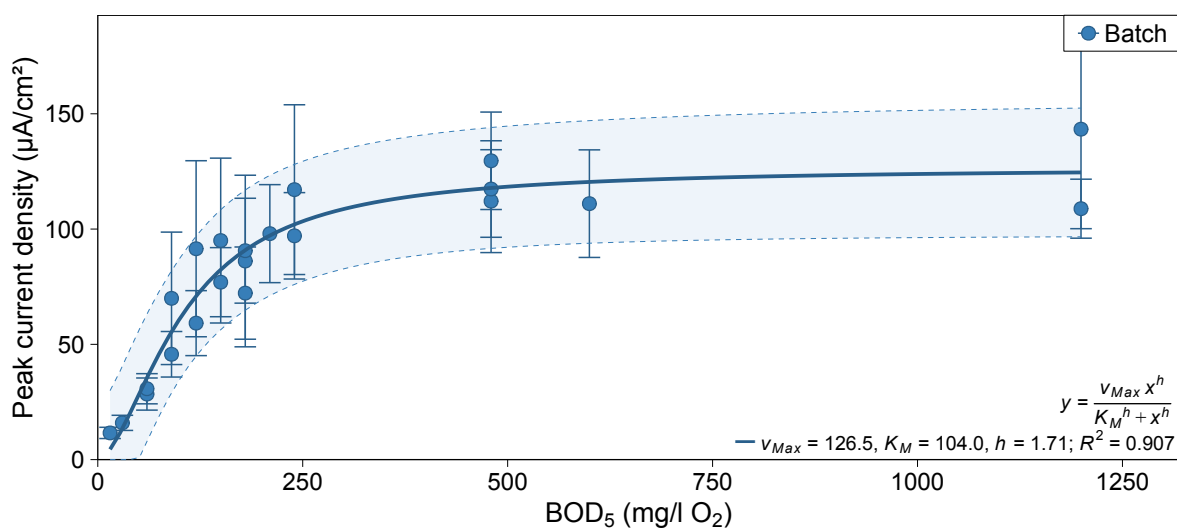


Figure C.1 (cont.): Peak current density calibration curves for batch-mode MFCs A and B.

(g) Calibration 8 (AB;  $R_{Ext} = 305 \Omega$ )



(h) Calibration 9 (AB;  $R_{Ext} = 43.2 \Omega$ )



(i) Calibration 10a (AB;  $R_{Ext} = 43.2 \Omega$ )

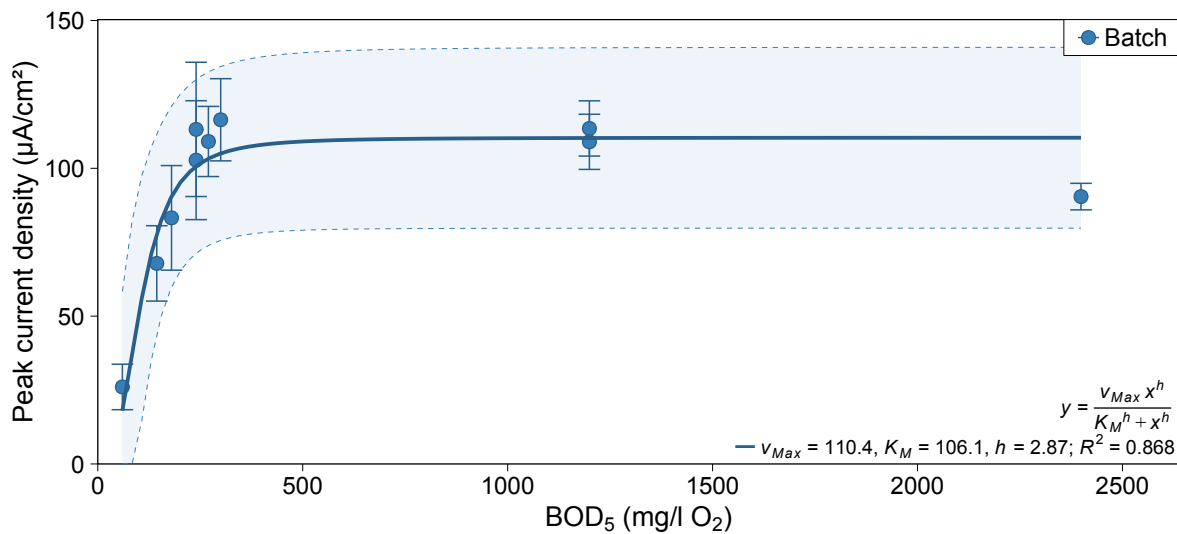


Figure C.1 (cont.): Peak current density calibration curves for batch-mode MFCs A and B.



(j) Calibration 1a (CD;  $R_{Ext} = 43.2 \Omega$ )

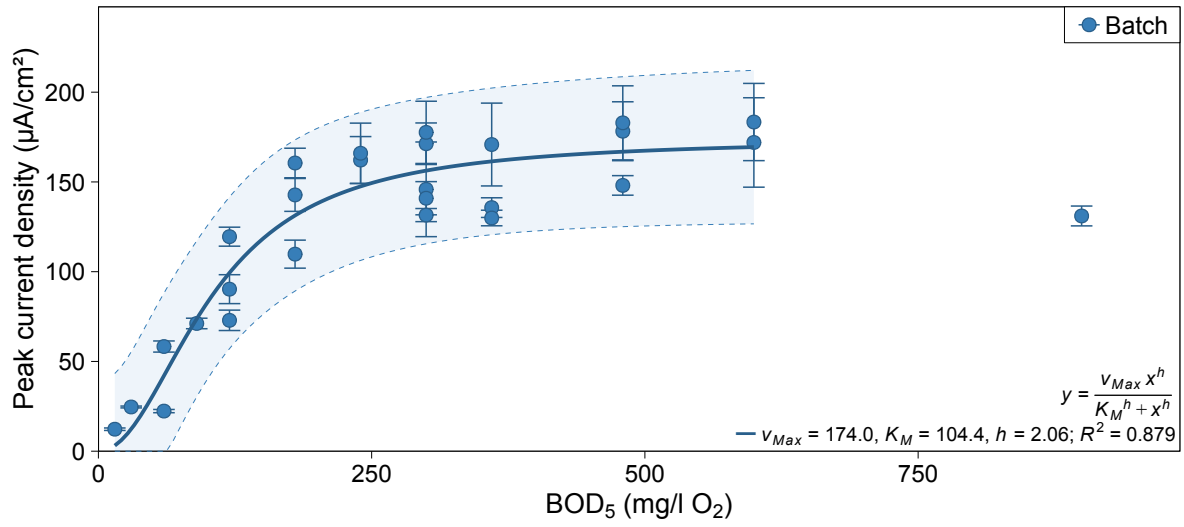


Figure C.1 (cont.): Peak current density calibration curves for batch-mode MFCs C and D.

(a) Calibration 1 (AB;  $R_{Ext} = 953 \Omega$ )

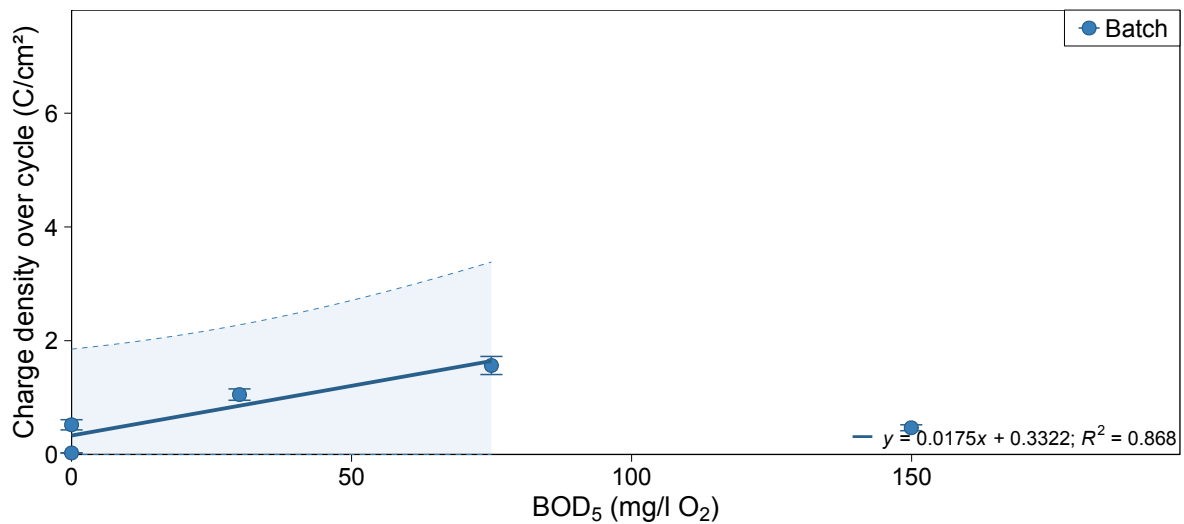
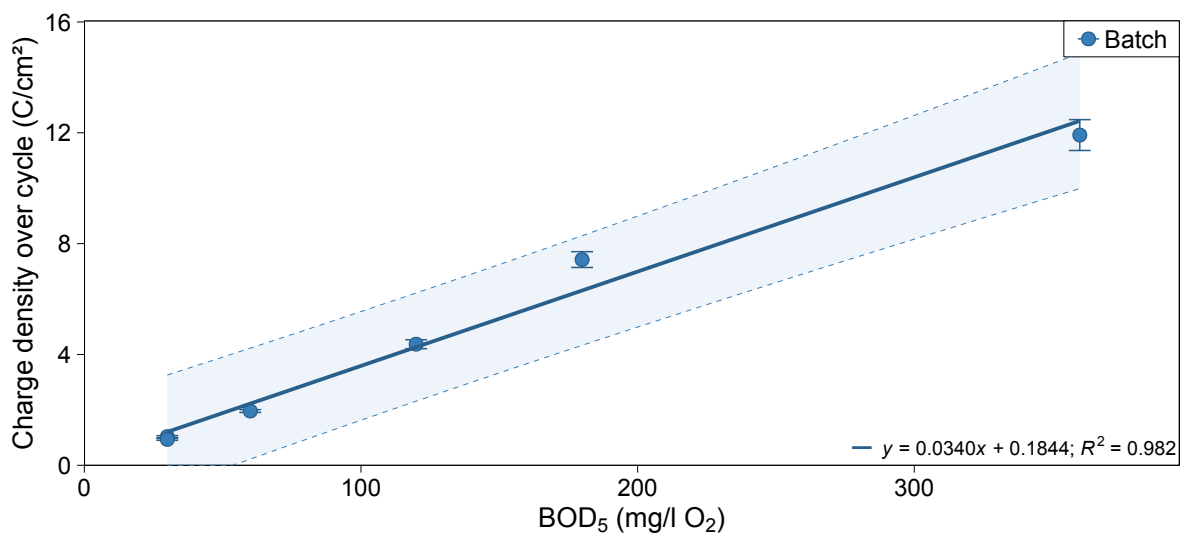
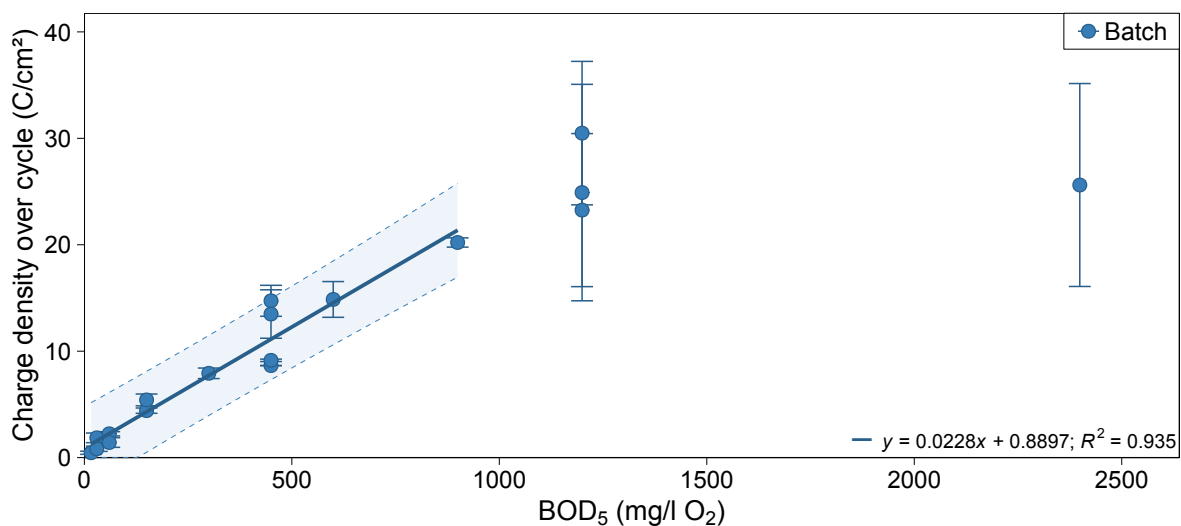


Figure C.2: Cycle charge density calibration curves fitted with Hill models against BOD<sub>5</sub> (estimated from GGA concentration) for data obtained during calibrations of batch-mode MFCs A & B and C & D. Shaded bands represent the 95% prediction interval from model lines and error bars are the range of values from duplicate cells.

(b) Calibration 2 (AB;  $R_{Ext} = 43.2 \Omega$ )



(c) Calibration 3 (AB;  $R_{Ext} = 43.2 \Omega$ )



(d) Calibration 5 (AB;  $R_{Ext} = 5100 \Omega$ )

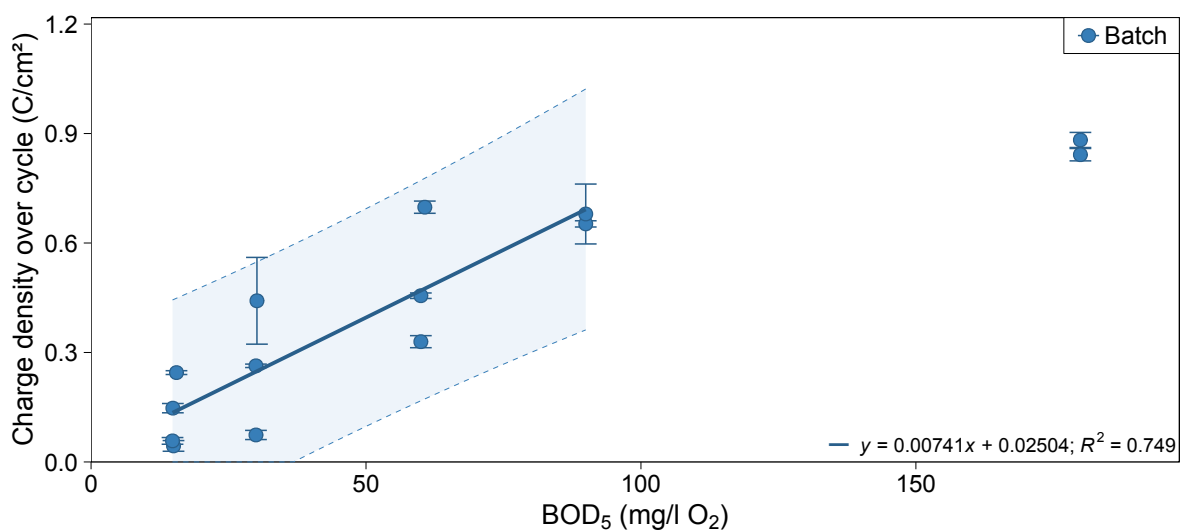
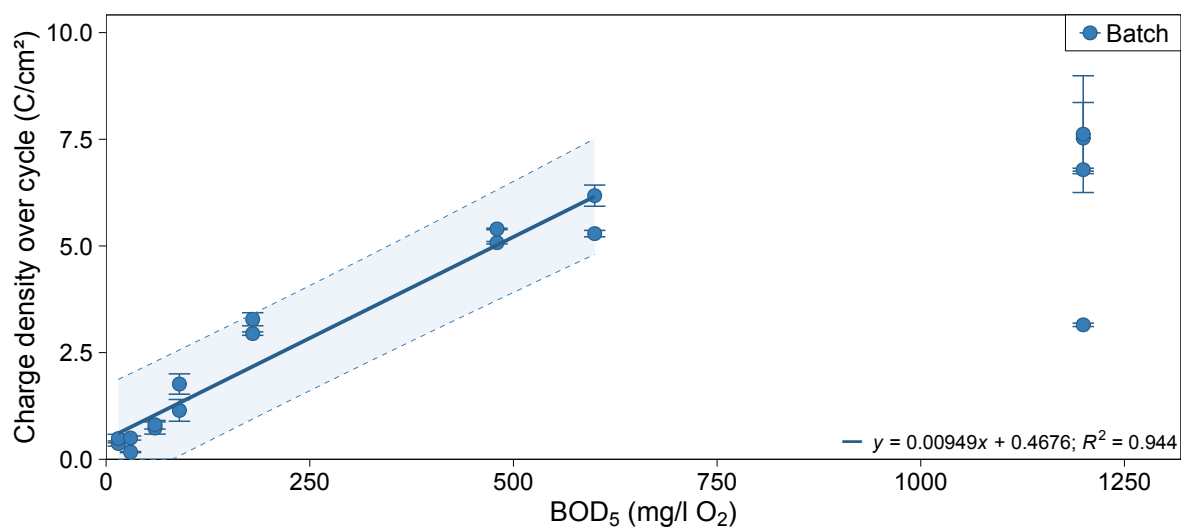
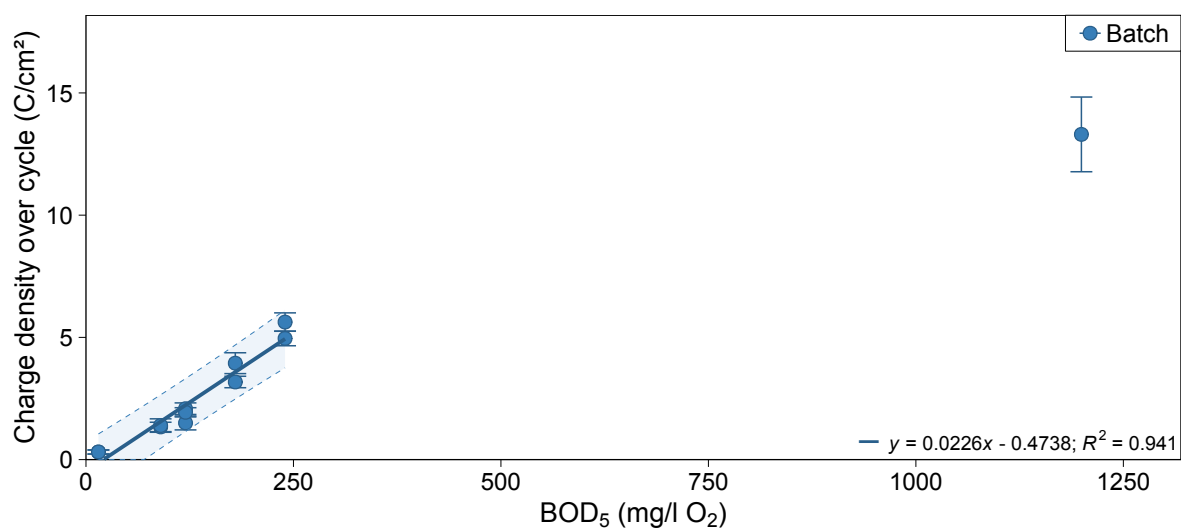


Figure C.2 (cont.): Cycle charge density calibration curves for batch-mode MFCs A and B.

(e) Calibration 6 (AB;  $R_{Ext} = 953 \Omega$ )



(f) Calibration 7 (AB;  $R_{Ext} = 305 \Omega$ )



(g) Calibration 8 (AB;  $R_{Ext} = 305 \Omega$ )

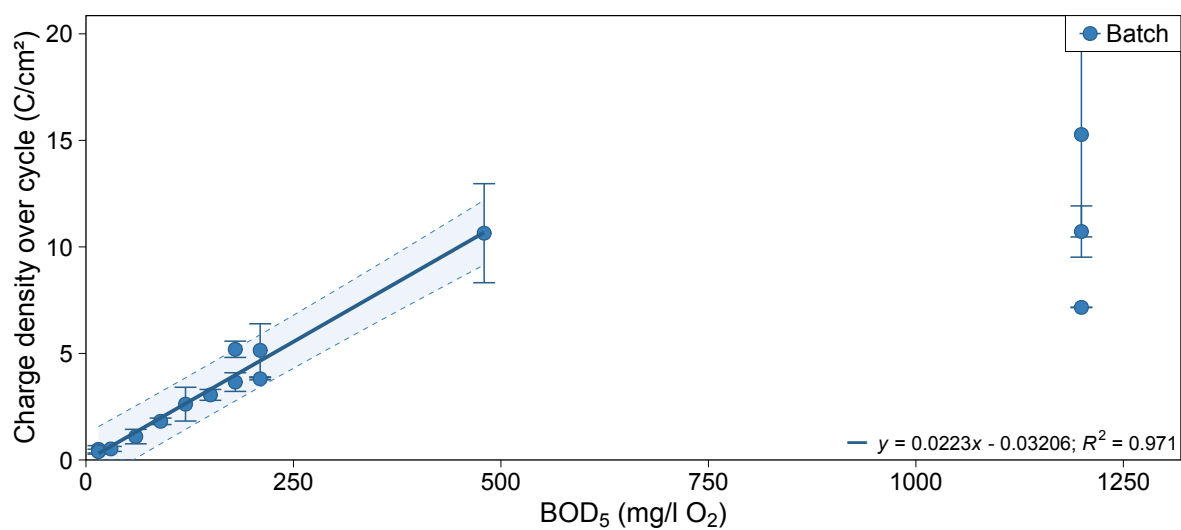
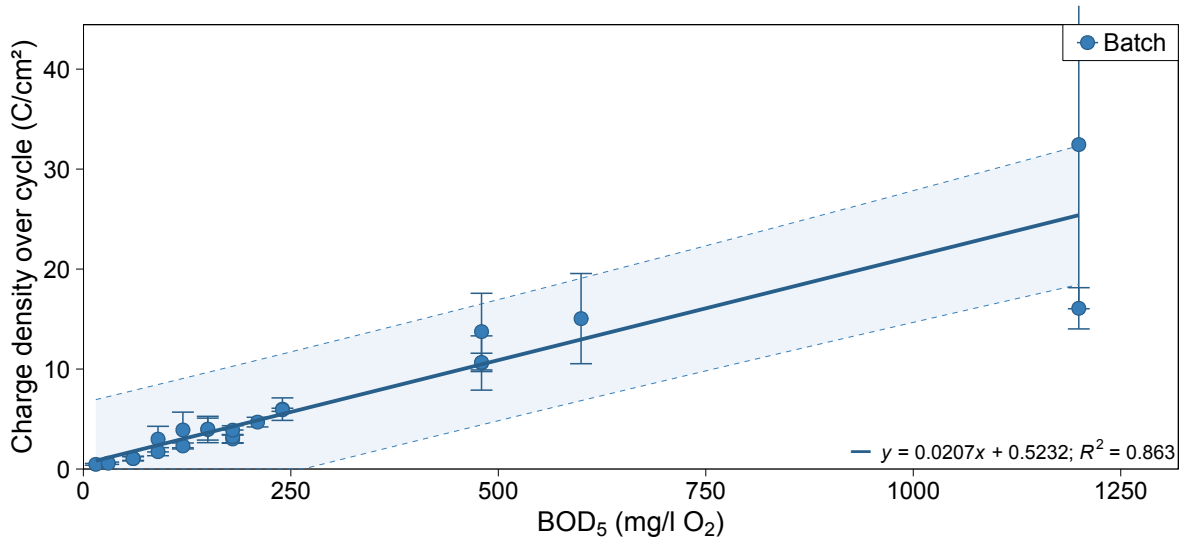
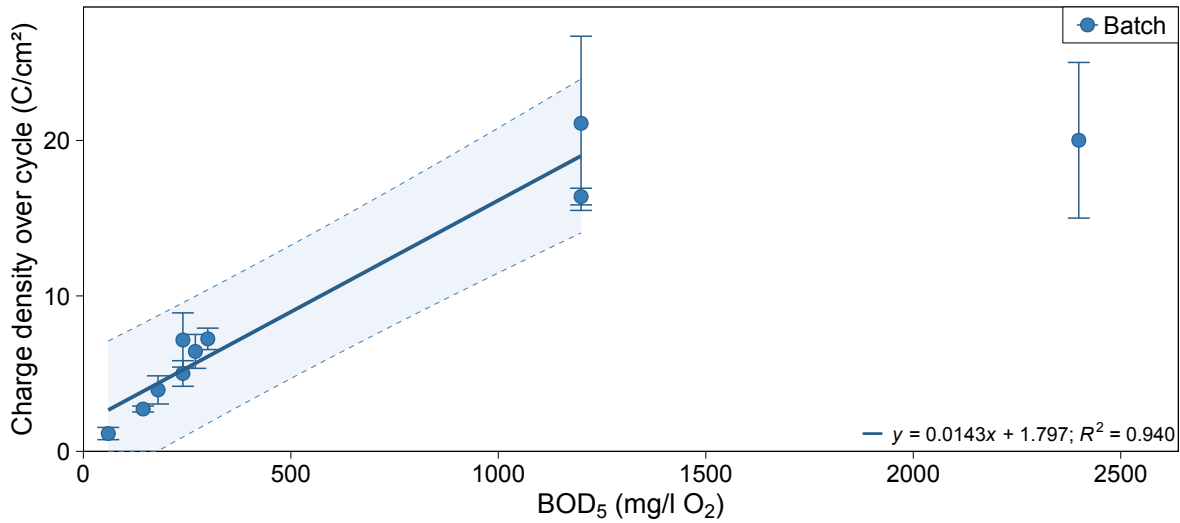


Figure C.2 (cont.): Cycle charge density calibration curves for batch-mode MFCs A and B.

(h) Calibration 9 (AB;  $R_{Ext} = 43.2 \Omega$ )



(i) Calibration 10a (AB;  $R_{Ext} = 43.2 \Omega$ )



(j) Calibration 1a (CD;  $R_{Ext} = 43.2 \Omega$ )

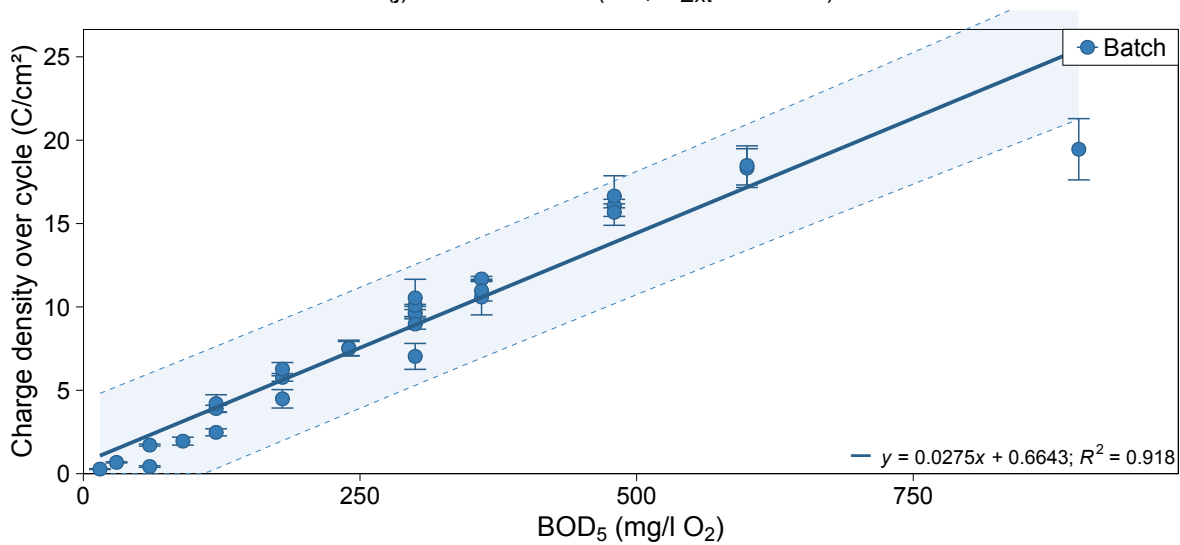


Figure C.2 (cont.): Cycle charge density calibration curves for batch-mode MFCs A & B and C & D.

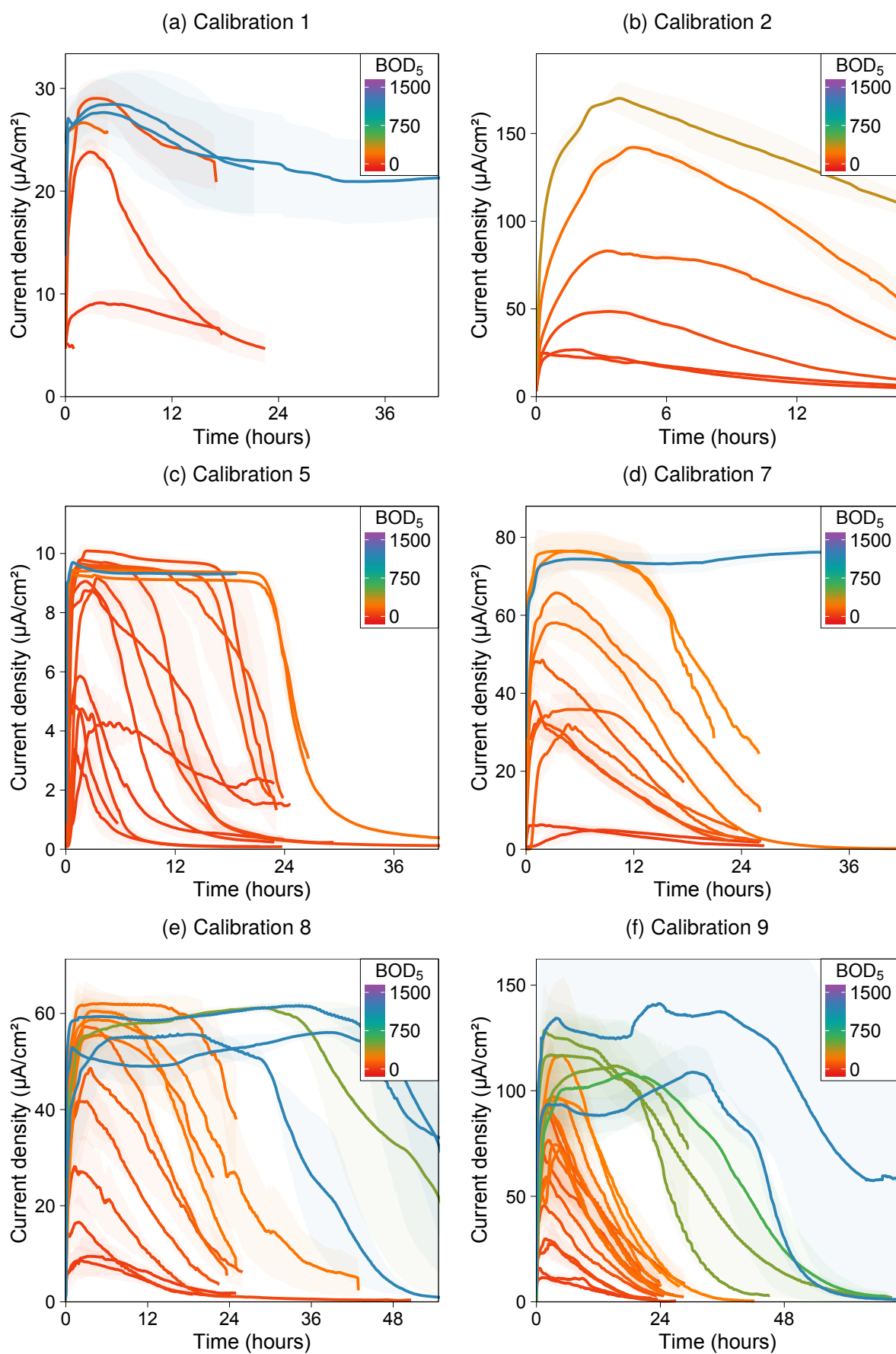


Figure C.3: Plots of average current density in Calibrations 1, 2, 5, 7, 8 and 9 for batch-mode MFCs A and B. Responses are coloured by  $\text{BOD}_5$  (estimated from GGA concentration). Shaded bands are the range between cell A and B.

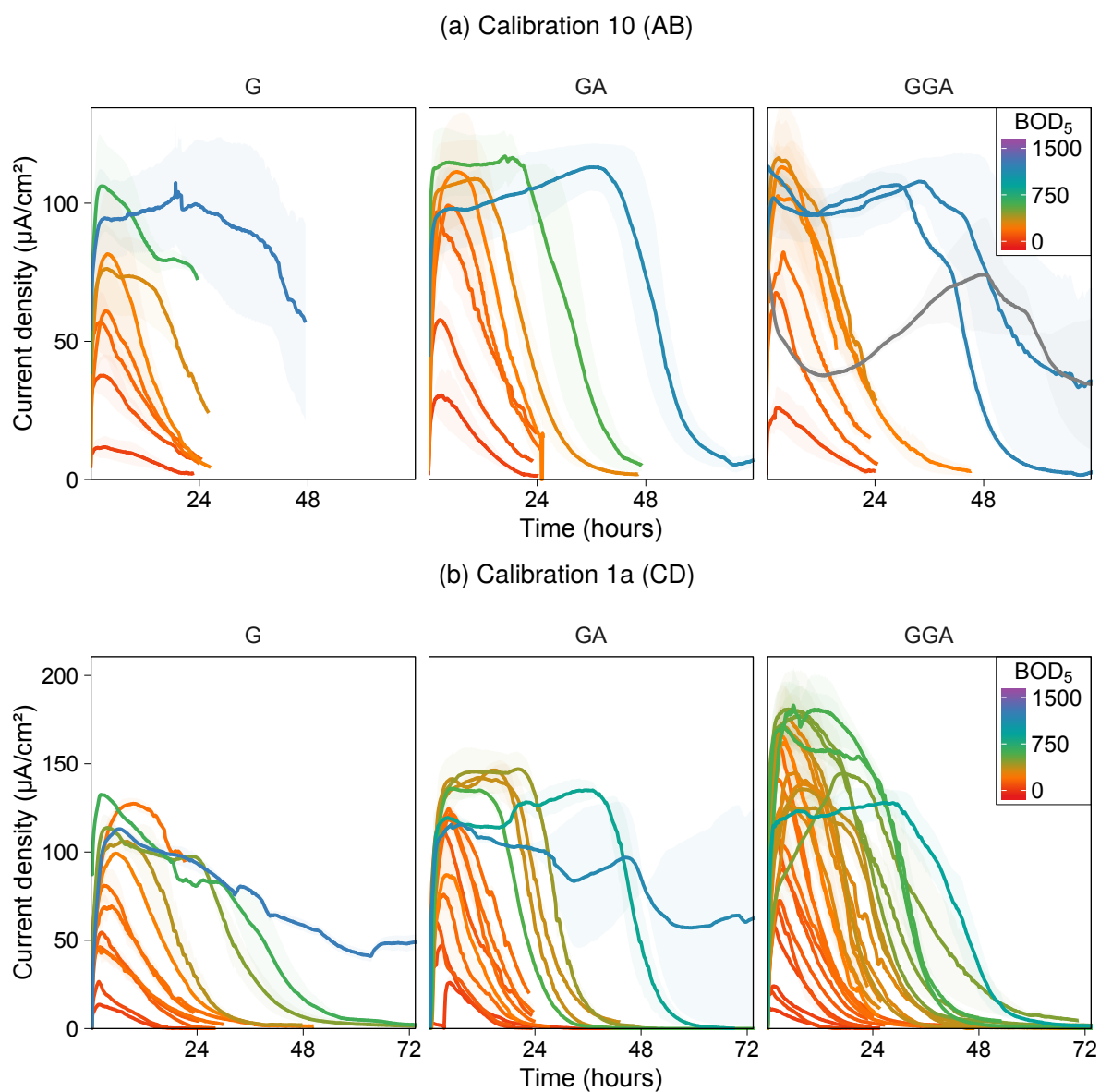


Figure C.4: Plots of average current density in Calibration 10 for batch-mode MFCs A and B and Calibration 1a for cells C and D with different medium compositions of glucose (G), glutamic acid (GA) and GGA. Responses are coloured by  $\text{BOD}_5$  (estimated from substrate concentration). Shaded bands are the range between respective duplicate cells.

Table C.1: Evaluation of predicted BOD<sub>5</sub> values using the G, GA and GGA calibrated linear and Hill models from the batch-mode MFCs for four samples of real wastewater. Mean percentage errors are given in relation to the actual BOD<sub>5</sub> value measured by the standardised test.

Sample	$\hat{i}$ ( $\mu\text{A}/\text{cm}^2$ )	BOD <sub>5</sub> (mg/l O <sub>2</sub> )	Model	Predicted BOD <sub>5</sub> (mg/l O <sub>2</sub> )					
				GGA		G		GA	
				Value	% error	Value	% error	Value	% error
300 mg/l GGA	160.6 ± 16.5	180 ± 9	Linear	191 ± 39	(6 ± 22%)	263 ± 30	(46 ± 17%)	152 ± 25	(-16 ± 14%)
			Hill	177 ± 34	(-1 ± 19%)	308 ± 124	(71 ± 69%)	146 ± 44	(-19 ± 24%)
WW1 'A'	104.1 ± 2.7	186 ± 9	Linear	138 ± 37	(-26 ± 20%)	190 ± 27	(2 ± 14%)	105 ± 23	(-44 ± 13%)
			Hill	119 ± 15	(-36 ± 8%)	181 ± 45	(-3 ± 24%)	65 ± 16	(-53 ± 11%)
WW1 'B'	79.7 ± 0.1	-	Linear	103 ± 36	(-44 ± 20%)	142 ± 26	(-23 ± 14%)	74 ± 24	(-60 ± 13%)
			Hill	95 ± 12	(-49 ± 6%)	132 ± 28	(-29 ± 15%)	65 ± 16	(-65 ± 9%)
WW2 'A'	66.3 ± 8.0	168 ± 6	Linear	84 ± 37	(-50 ± 22%)	115 ± 26	(-31 ± 15%)	57 ± 25	(-66 ± 15%)
			Hill	83 ± 12	(-51 ± 7%)	110 ± 24	(-35 ± 14%)	55 ± 16	(-68 ± 9%)
WW2 'B'	64.0 ± 7.1	-	Linear	80 ± 37	(-52 ± 22%)	111 ± 26	(-34 ± 15%)	54 ± 25	(-68 ± 15%)
			Hill	81 ± 12	(-52 ± 7%)	106 ± 24	(-37 ± 14%)	53 ± 16	(-69 ± 9%)

<sup>a</sup>  $\hat{i}$  = Average peak current density. <sup>b</sup> Mean percentage error is calculated from the difference between actual and fitted values as a percentage of the actual BOD<sub>5</sub>.

<sup>c</sup> Values are reported  $\pm 1/2 Rng$  from the 95% prediction interval. <sup>d</sup> The BOD<sub>5</sub> test was not repeated for 'B' samples which had been stored at 4 °C prior to MFC analysis.





## **Appendix D. Flow Calibration Data**

### **List of Figures**

D.1	Average current density calibration curves fitted with the Hill equation for the 'ABC' series of flow-mode MFCs. . . . .	245
D.2	Average current density calibration curves fitted with the linear model for Calibration 7 of the 'ABC' flow-mode MFCs. . . . .	247
D.3	Normalised average current density calibration curves fitted with the linear model for Calibration 7 (ABC) and 1 (DEF). . . . .	247
D.4	Average measured chemical parameters of samples obtained during Calibration 7 (ABC) of the flow-mode MFCs. . . . .	251

### **List of Tables**

D.1	Pt catalyst loadings on replacement GDEs used for operation of 'ABC' and 'DEF' flow-mode MFCs. . . . .	244
D.2	Evaluation of predicted BOD <sub>5</sub> values using the calibrated linear and Hill models from the flow-mode MFCs for 300 mg/l GGA. . . . .	248
D.3	Evaluation of predicted BOD <sub>5</sub> values using the GGA calibrated linear and Hill models from the flow-mode MFCs for real wastewater. . . . .	249

Table D.1: Pt catalyst loadings on replacement GDEs used for operation of 'ABC' flow-mode MFCs; 1A, 1B, 1C, 2A, 2B, 2C, 3A, 3B & 3C and the 'DEF' flow-mode MFCs; 1D, 1E, 1F, 2D, 2E, 2F, 3D, 3E & 3F. The number of days is given since inoculation of the cell and the start of the flow-mode series in brackets. The optimum (100%) loading was 0.5 mg/cm<sup>2</sup>.

Time (days)	1A	1B	1C
0 (0)	0.53 mg/cm <sup>2</sup> (106%)	0.50 mg/cm <sup>2</sup> (100%)	0.55 mg/cm <sup>2</sup> (109%)
258 (258)	0.47 mg/cm <sup>2</sup> (94%)	0.37 mg/cm <sup>2</sup> (74%)	0.40 mg/cm <sup>2</sup> (80%)
358 (358)	0.82 mg/cm <sup>2</sup> (163%)	0.58 mg/cm <sup>2</sup> (116%)	0.58 mg/cm <sup>2</sup> (116%)
396 (396)	0.53 mg/cm <sup>2</sup> (106%)	-	-
607 (607)	0.47 mg/cm <sup>2</sup> (94%)	0.46 mg/cm <sup>2</sup> (93%)	0.47 mg/cm <sup>2</sup> (95%)
	2A	2B	2C
0 (155)	0.28 mg/cm <sup>2</sup> (57%)	0.41 mg/cm <sup>2</sup> (81%)	0.56 mg/cm <sup>2</sup> (112%)
385 (540)	0.56 mg/cm <sup>2</sup> (111%)	-	0.48 mg/cm <sup>2</sup> (96%)
452 (607)	0.45 mg/cm <sup>2</sup> (91%)	0.43 mg/cm <sup>2</sup> (86%)	0.42 mg/cm <sup>2</sup> (83%)
	3A	3B	3C
0 (212)	0.41 mg/cm <sup>2</sup> (81%)	0.31 mg/cm <sup>2</sup> (61%)	0.31 mg/cm <sup>2</sup> (61%)
189 (401)	0.53 mg/cm <sup>2</sup> (105%)	-	-
269 (481)	0.54 mg/cm <sup>2</sup> (108%)	-	-
325 (537)	-	0.51 mg/cm <sup>2</sup> (103%)	-
395 (607)	0.28 mg/cm <sup>2</sup> (57%)	0.41 mg/cm <sup>2</sup> (81%)	0.56 mg/cm <sup>2</sup> (112%)
	1D	1E	1F
0 (0)	0.56 mg/cm <sup>2</sup> (111%)	0.62 mg/cm <sup>2</sup> (124%)	0.61 mg/cm <sup>2</sup> (123%)
	2D	2E	2F
0 (0)	0.61 mg/cm <sup>2</sup> (122%)	0.65 mg/cm <sup>2</sup> (131%)	0.66 mg/cm <sup>2</sup> (131%)
	3D	3E	3F
0 (0)	0.68 mg/cm <sup>2</sup> (135%)	0.67 mg/cm <sup>2</sup> (134%)	0.60 mg/cm <sup>2</sup> (119%)

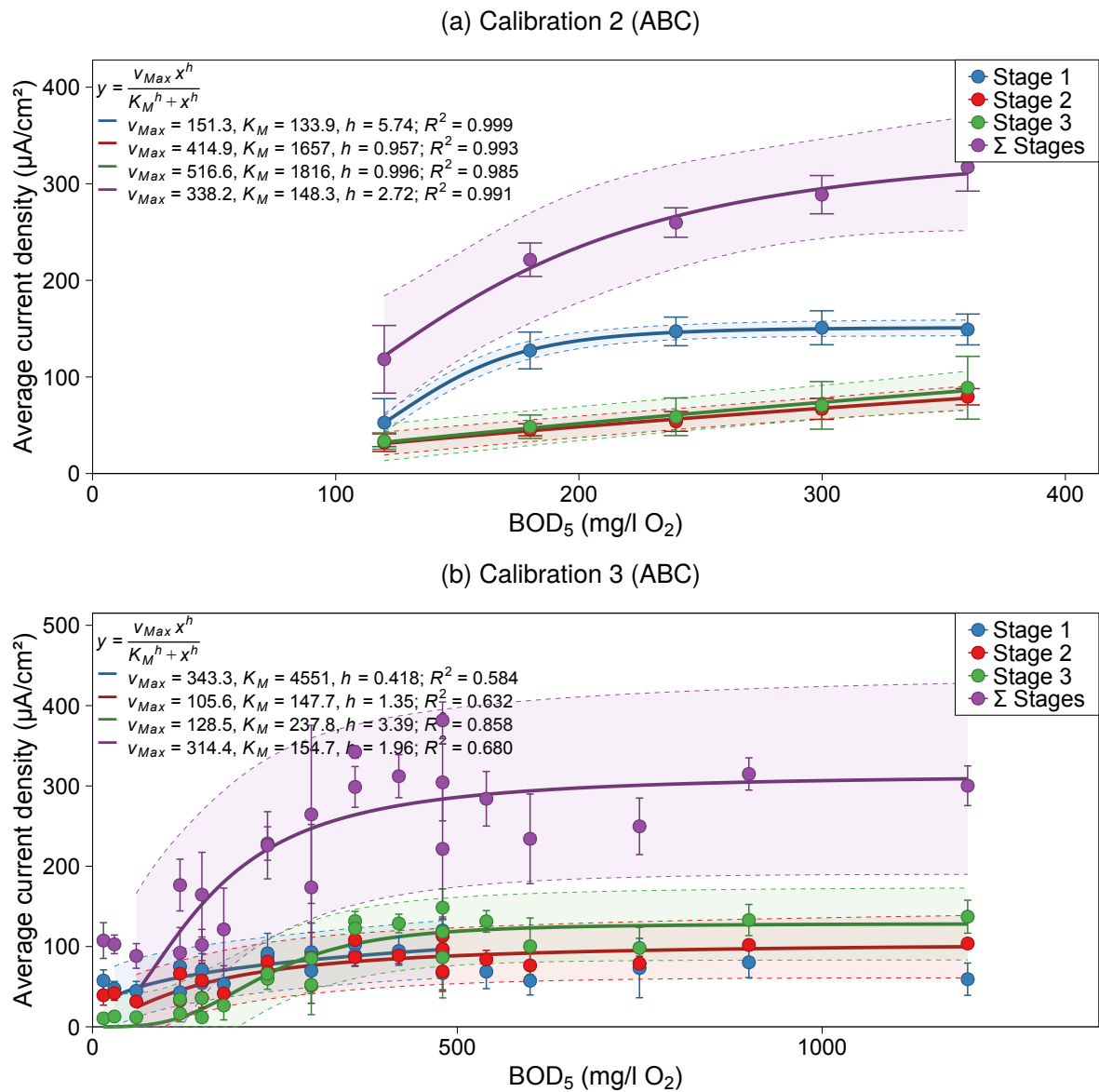
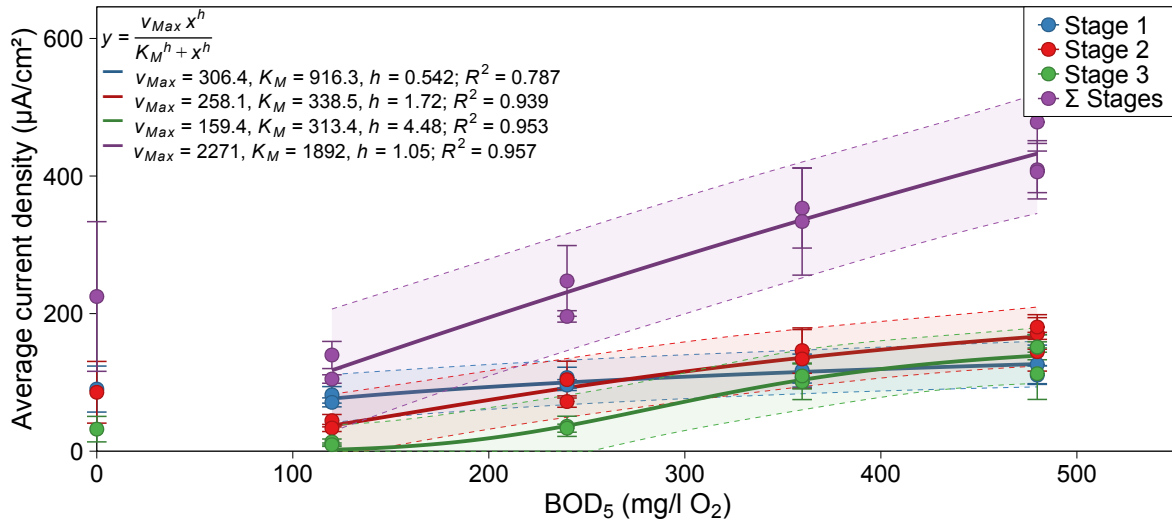


Figure D.1: Average current density calibration curves fitted with the Hill equation against  $\text{BOD}_5$  (estimated from GGA concentration) for data obtained during calibration of the 'ABC' series of flow-mode MFCs. Shaded bands represent the 95% prediction intervals from model lines and error bars are  $\pm\text{SD}$  from triplicate cells.

(c) Calibration 4 (ABC)



(d) Calibration 5 (ABC)

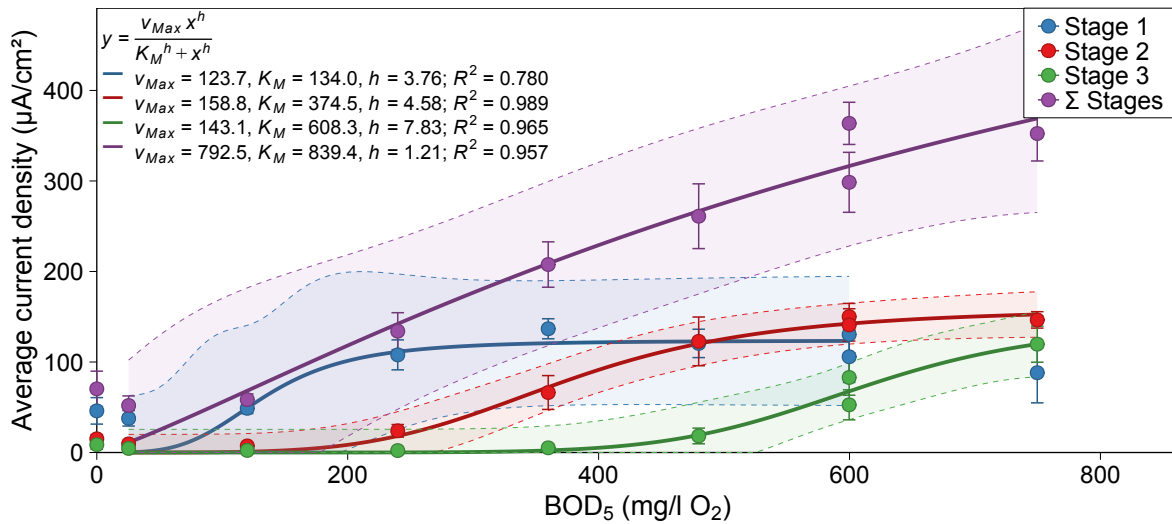


Figure D.1 (cont.): Average current density calibration curves fitted with the Hill equation for the 'ABC' series of flow-mode MFCs.

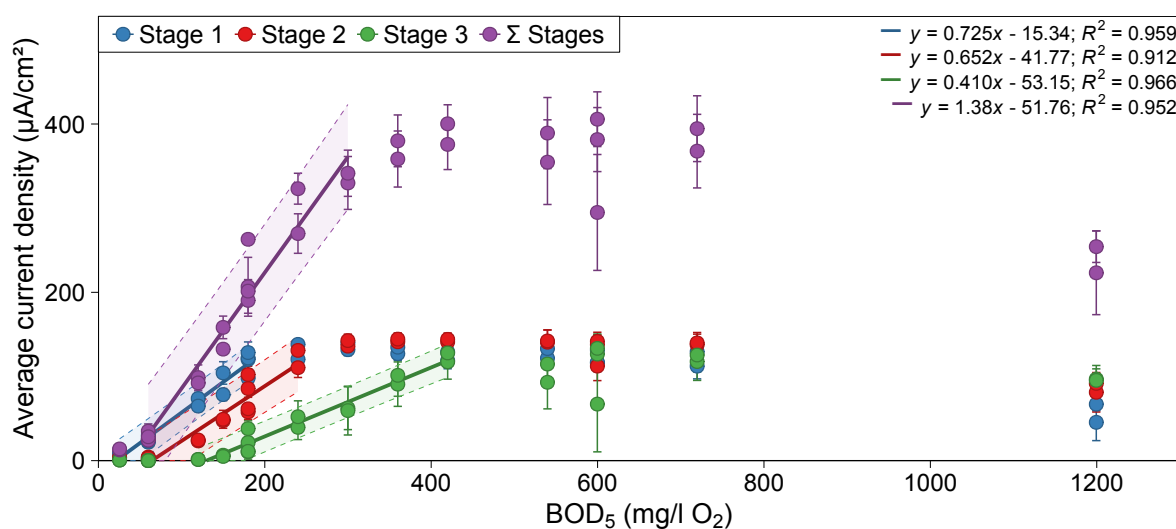


Figure D.2: Average current density calibration curves fitted with the linear model against  $BOD_5$  (estimated from GGA concentration) for data obtained during Calibration 7 of the 'ABC' series of flow-mode MFCs. Shaded bands represent the 95% prediction intervals from model lines and error bars are  $\pm$ SD from triplicate cells.

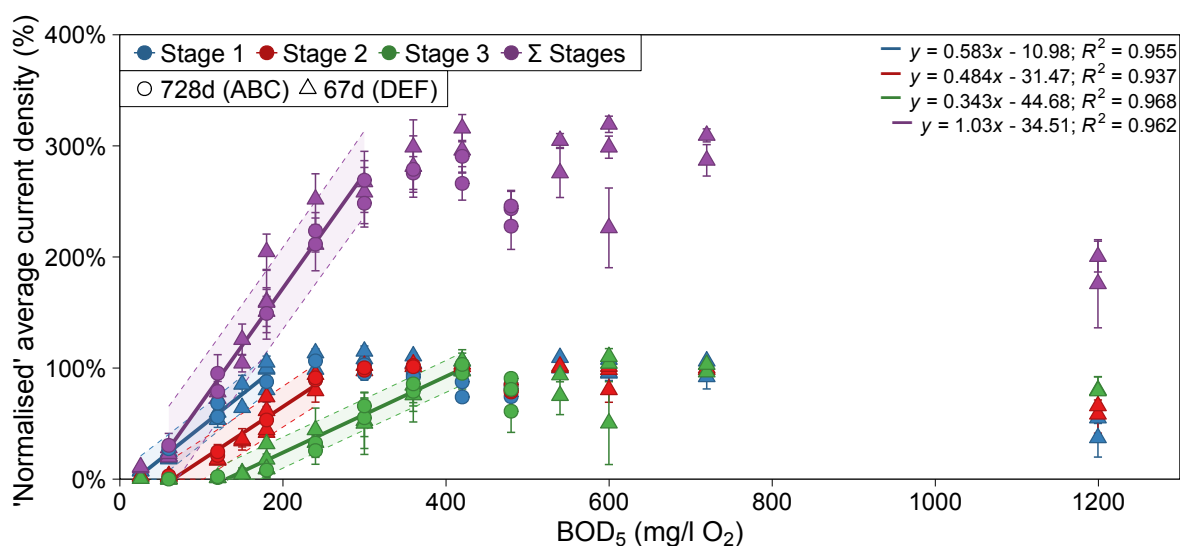


Figure D.3: Normalised average current density calibration curves fitted with the linear model against  $BOD_5$  (estimated from GGA concentration) for data obtained during Calibration 7 of the 'ABC' series (●) and Calibration 1 of the 'DEF' series (▲) of flow-mode MFCs. The Σ Stages data is normalised to 300% (sum of three MFC stages) to permit comparisons to non-normalised data for convenience. Shaded bands represent the 95% prediction intervals from model lines and error bars are  $\pm$ SD from triplicate cells.

Table D.2: Evaluation of predicted BOD<sub>5</sub> values using the calibrated linear and Hill models from the multi-stage, flow-mode MFCs for a 300 mg/l GGA medium sample (measured before (i) and after (ii) sludge removal). Mean percentage errors are given in brackets in relation to the actual BOD<sub>5</sub> value measured by the standardised test.

Setup	BOD <sub>5</sub> (mg/l O <sub>2</sub> )	Model	Stage 1		Stage 2		Stage 3		Σ Stages	
			$\bar{i}$ (μA/cm <sup>2</sup> )	Pred. BOD <sub>5</sub> (mg/l O <sub>2</sub> )	$\bar{i}$ (μA/cm <sup>2</sup> )	Pred. BOD <sub>5</sub> (mg/l O <sub>2</sub> )	$\bar{i}$ (μA/cm <sup>2</sup> )	Pred. BOD <sub>5</sub> (mg/l O <sub>2</sub> )	$\bar{i}$ (μA/cm <sup>2</sup> )	Pred. BOD <sub>5</sub> (mg/l O <sub>2</sub> )
'ABC' series 0.52 ml/min	180 ± 9	Lin	74.2 ±7.1	184 ± 85 (2 ± 45%)	8.5 ±2.4	267 ± 129 (48 ± 24%)	3.0 ±1.4	471 ± 167 (162 ± 69%)	85.9 ±9.7	186 ± 36 (3 ± 17%)
		Hill		166 ± 24 (-8 ± 21%)		285 ± 85 (59 ± 11%)		439 ± 60 (144 ± 110%)		194 ± 48 (8 ± 19%)

<sup>a</sup>  $\bar{i}$  = Average stable current density. <sup>b</sup> Mean percentage error is calculated from the difference between actual and fitted values as a percentage of the actual BOD<sub>5</sub>.

<sup>c</sup> Values are reported ±SD from the 95% prediction interval.

Table D.3: Evaluation of predicted BOD<sub>5</sub> values using the GGA calibrated linear and Hill models from the multi-stage, flow-mode MFCs for four samples of real wastewater (measured before (i) and after (ii) sludge removal). Mean percentage errors are given in brackets in relation to the actual BOD<sub>5</sub> value measured by the standardised test.

Sample	BOD <sub>5</sub> (mg/l O <sub>2</sub> )	Model	Stage 1		Stage 2		Stage 3		Σ Stages	
			$\bar{I}$ (μA/cm <sup>2</sup> )	Pred. BOD <sub>5</sub> (mg/l O <sub>2</sub> )	$\bar{I}$ (μA/cm <sup>2</sup> )	Pred. BOD <sub>5</sub> (mg/l O <sub>2</sub> )	$\bar{I}$ (μA/cm <sup>2</sup> )	Pred. BOD <sub>5</sub> (mg/l O <sub>2</sub> )	$\bar{I}$ (μA/cm <sup>2</sup> )	Pred. BOD <sub>5</sub> (mg/l O <sub>2</sub> )
300 mg/l GGA	180 ± 9	Linear	112.2	175 ± 137	82.5	179 ± 62	12.1	178 ± 45	206.5	185 ± 63
			±12.8	(-3 ± 76%)	±15.5	(0 ± 34%)	±9.9	(-1 ± 25%)	±16.2	(3 ± 35%)
		Hill		190 ± 139		167 ± 12		177 ± 17		169 ± 24
				(11 ± 147%)		(-13 ± 12%)		(-3 ± 18%)		(-12 ± 25%)
		Linear	52.9	83 ± 126	40.1	116 ± 65	16	185 ± 44	109.3	101 ± 67
			±7.3	(-55 ± 68%)	±7.8	(-38 ± 35%)	±4.4	(-1 ± 24%)	±13.8	(-46 ± 36%)
	186 ± 9	Hill		82 ± 24		128 ± 10		189 ± 15		114 ± 12
				(-56 ± 13%)		(-31 ± 6%)		(2 ± 8%)		(-39 ± 7%)
		Linear	71.5	113 ± 119	37.7	112 ± 65	8.3	171 ± 45	118	110 ± 66
			±8.4	(-39 ± 64%)	±7.9	(-40 ± 35%)	±1.8	(-8 ± 24%)	±14.5	(-41 ± 36%)
		Hill		105 ± 38		126 ± 11		163 ± 20		120 ± 13
				(-43 ± 20%)		(-32 ± 6%)		(-12 ± 11%)		(-36 ± 7%)
WW1 'A' ii	-	Linear	33.4	53 ± 142	22.7	91 ± 67	10.7	176 ± 45	66.7	66 ± 70
			±10.8	(-71 ± 77%)	±7.6	(-51 ± 36%)	±3.9	(-5 ± 24%)	±18.6	(-64 ± 38%)
		Hill		61 ± 22		109 ± 12		173 ± 18		90 ± 13
				(-67 ± 12%)		(-41 ± 6%)		(-7 ± 10%)		(-52 ± 7%)
		Linear								
WW1 'B' i	-	Linear								
		Hill								
		Linear								

<sup>a</sup>  $\bar{I}$  = Average stable current density. <sup>b</sup> Mean percentage error is calculated from the difference between actual and fitted values as a percentage of the actual BOD<sub>5</sub>.

<sup>c</sup> Values are reported ±SD from the 95% prediction interval. <sup>d</sup> The BOD<sub>5</sub> test was not repeated for 'B' samples which had been stored at 4 °C prior to MFC analysis.

Table D.3: continued...

Sample	BOD <sub>5</sub> (mg/l O <sub>2</sub> )	Model	Stage 1		Stage 2		Stage 3		$\Sigma$ Stages	
			$\bar{I}$ ( $\mu\text{A}/\text{cm}^2$ )	Pred. BOD <sub>5</sub> (mg/l O <sub>2</sub> )	$\bar{I}$ ( $\mu\text{A}/\text{cm}^2$ )	Pred. BOD <sub>5</sub> (mg/l O <sub>2</sub> )	$\bar{I}$ ( $\mu\text{A}/\text{cm}^2$ )	Pred. BOD <sub>5</sub> (mg/l O <sub>2</sub> )	$\bar{I}$ ( $\mu\text{A}/\text{cm}^2$ )	Pred. BOD <sub>5</sub> (mg/l O <sub>2</sub> )
WW2 'A' i	168 $\pm$ 6	Linear	32.3 $\pm 3$	51 $\pm$ 144 (-70 $\pm$ 86%)	29.5 $\pm 5.4$	101 $\pm$ 66 (-40 $\pm$ 39%)	14.2 $\pm 5.9$	181 $\pm$ 44 (8 $\pm$ 26%)	76.8 $\pm 13.4$	73 $\pm$ 70 (-57 $\pm$ 42%)
		Hill		59 $\pm$ 22 (-65 $\pm$ 13%)		118 $\pm$ 11 (-30 $\pm$ 7%)		184 $\pm$ 16 (9 $\pm$ 10%)		94 $\pm$ 13 (-44 $\pm$ 8%)
WW2 'A' ii	-	Linear	34 $\pm 2.7$	54 $\pm$ 142 (-68 $\pm$ 84%)	18.2 $\pm 2.2$	84 $\pm$ 68 (-50 $\pm$ 41%)	6.1 $\pm 3.6$	167 $\pm$ 46 (-1 $\pm$ 27%)	58.5 $\pm 8$	59 $\pm$ 71 (-65 $\pm$ 42%)
		Hill		61 $\pm$ 22 (-63 $\pm$ 13%)		103 $\pm$ 12 (-38 $\pm$ 7%)		153 $\pm$ 21 (-9 $\pm$ 13%)		85 $\pm$ 13 (-50 $\pm$ 8%)
WW2 'B'	-	Linear	37.3 $\pm 6.1$	59 $\pm$ 139 (-65 $\pm$ 82%)	27.9 $\pm 5.9$	98 $\pm$ 67 (-41 $\pm$ 40%)	10.6 $\pm 4.4$	175 $\pm$ 45 (4 $\pm$ 27%)	75.7 $\pm 14.7$	74 $\pm$ 70 (-56 $\pm$ 41%)
		Hill		65 $\pm$ 21 (-61 $\pm$ 13%)		116 $\pm$ 11 (-31 $\pm$ 7%)		172 $\pm$ 18 (3 $\pm$ 11%)		95 $\pm$ 13 (-43 $\pm$ 8%)

<sup>a</sup>  $\bar{I}$  = Average stable current density. <sup>b</sup> Mean percentage error is calculated from the difference between actual and fitted values as a percentage of the actual BOD<sub>5</sub>.

<sup>c</sup> Values are reported  $\pm$ SD from the 95% prediction interval. <sup>d</sup> The BOD<sub>5</sub> test was not repeated for 'B' samples which had been stored at 4 °C prior to MFC analysis.



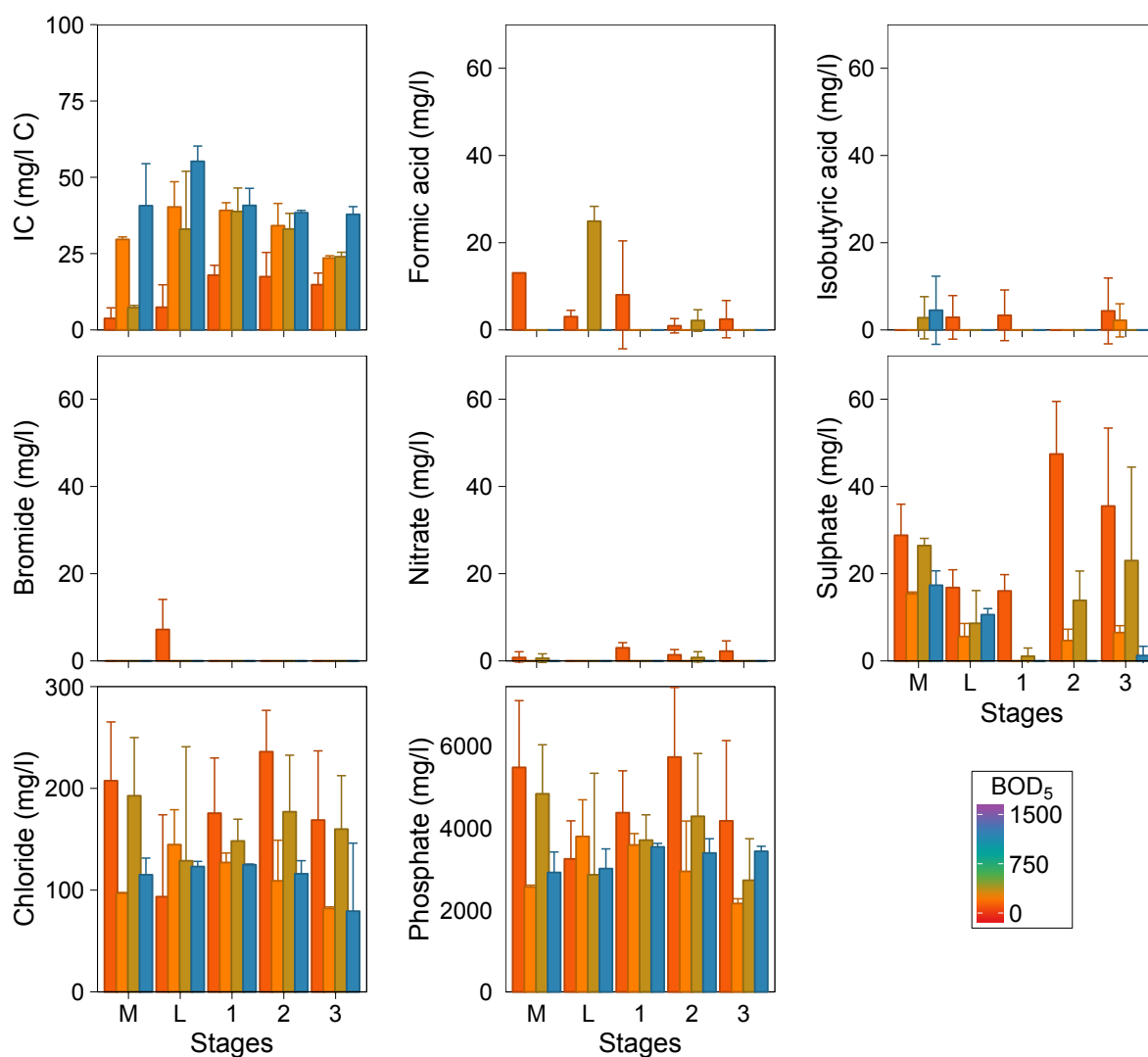


Figure D.4: Supplementary data for average measured chemical parameters of samples obtained during Calibration 7 (ABC) of the flow-mode MFCs. Bars are coloured according to the estimated BOD<sub>5</sub> of the as-prepared GGA medium. Number of bars indicates number of samples measured for each technique. Sampling was performed at the 3-W valves at medium bottle (M), feed line (L) and after each MFC (1, 2, 3). Error bars are  $\pm$ SD from triplicate cells. Main data in Figure 5.22.



## Appendix E. Electrochemical Analysis Data

### List of Figures

E.1	Linear sweep voltammetry measured over time at 1 mV/s under two different BOD <sub>5</sub> concentrations for batch-mode cells A and B. . . . .	254
E.2	Polarisation curves recorded on cells A & B over time. . . . .	255
E.3	Average ohmic resistance as measured by EIS and internal resistance estimated by PC gradient over time for cells A & B. . . . .	257
E.4	Charts showing effect of operational $R_{Ext}$ on average electrochemical performance parameters for batch-mode cells A and B. . . . .	258
E.5	Linear sweep voltammetry measured over time for flow-mode MFCs. .	258
E.6	1st derivative cyclic voltammograms measured over time at 5 mV/s for flow-mode MFCs in the (a) 'ABC' series and (b) 'DEF' series. . . . .	259

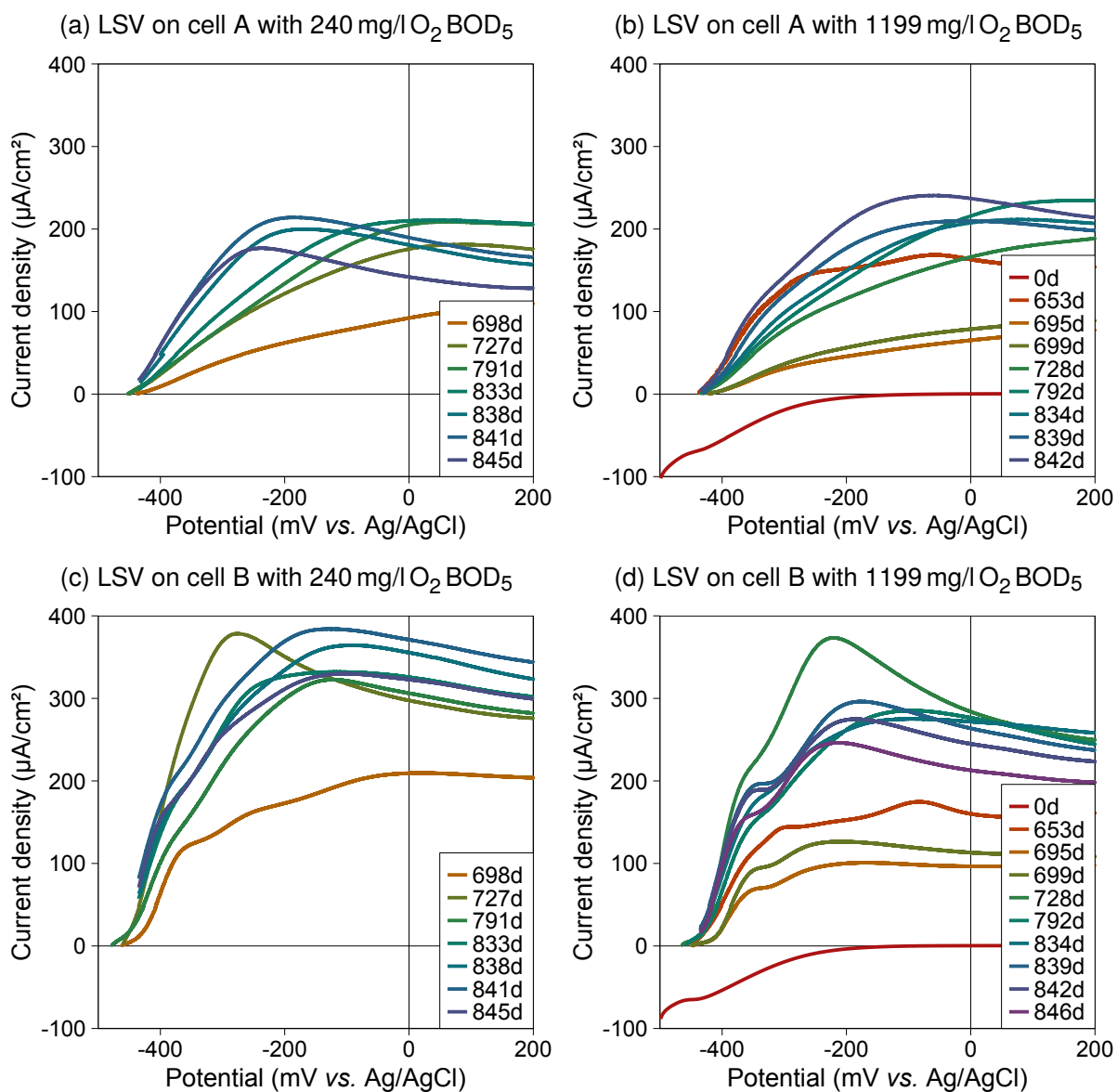


Figure E.1: Linear sweep voltammetry measured over time at 1 mV/s under two different BOD<sub>5</sub> concentrations for batch-mode cells A and B.

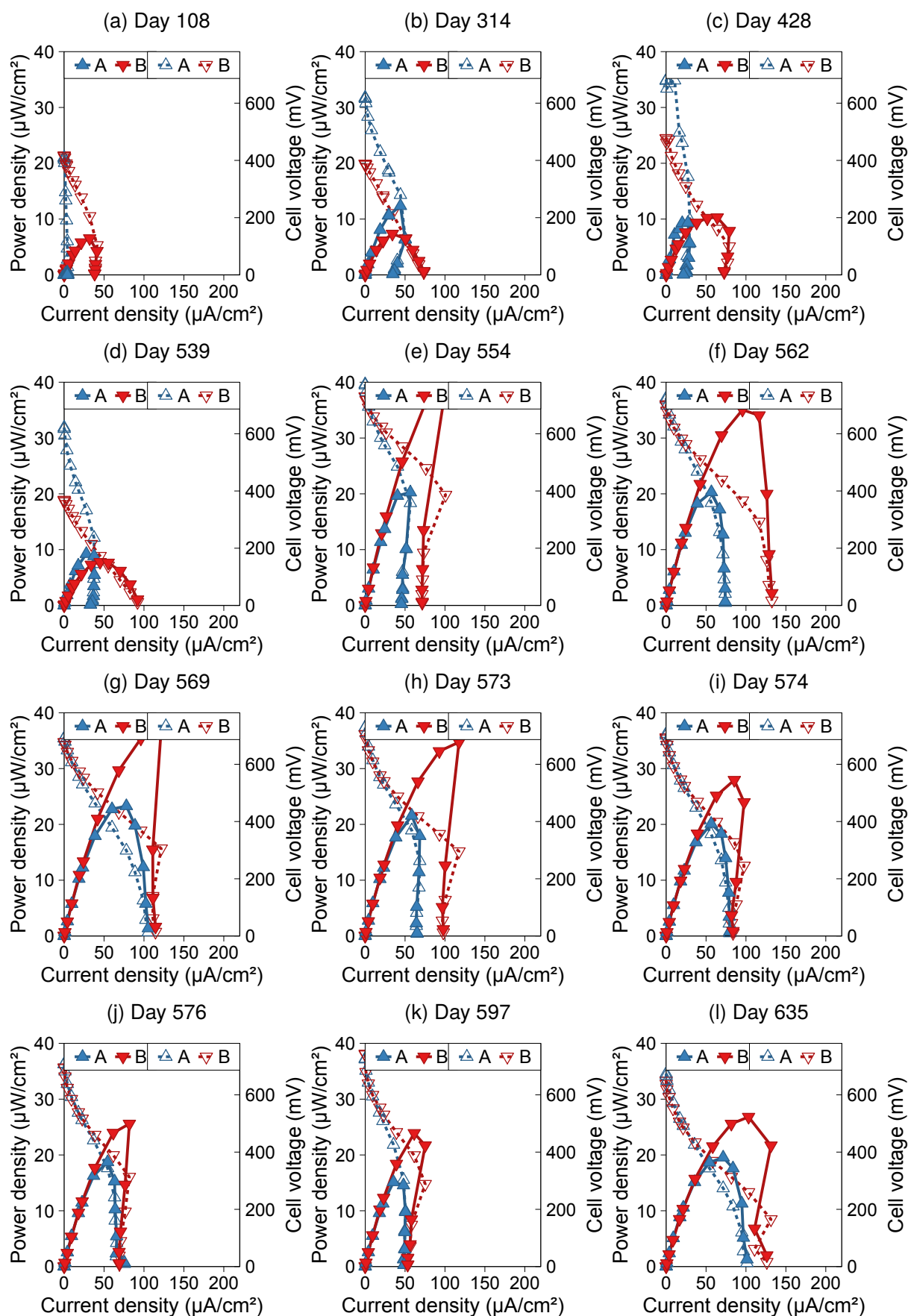


Figure E.2: Polarisation curves recorded on cells A & B over time.

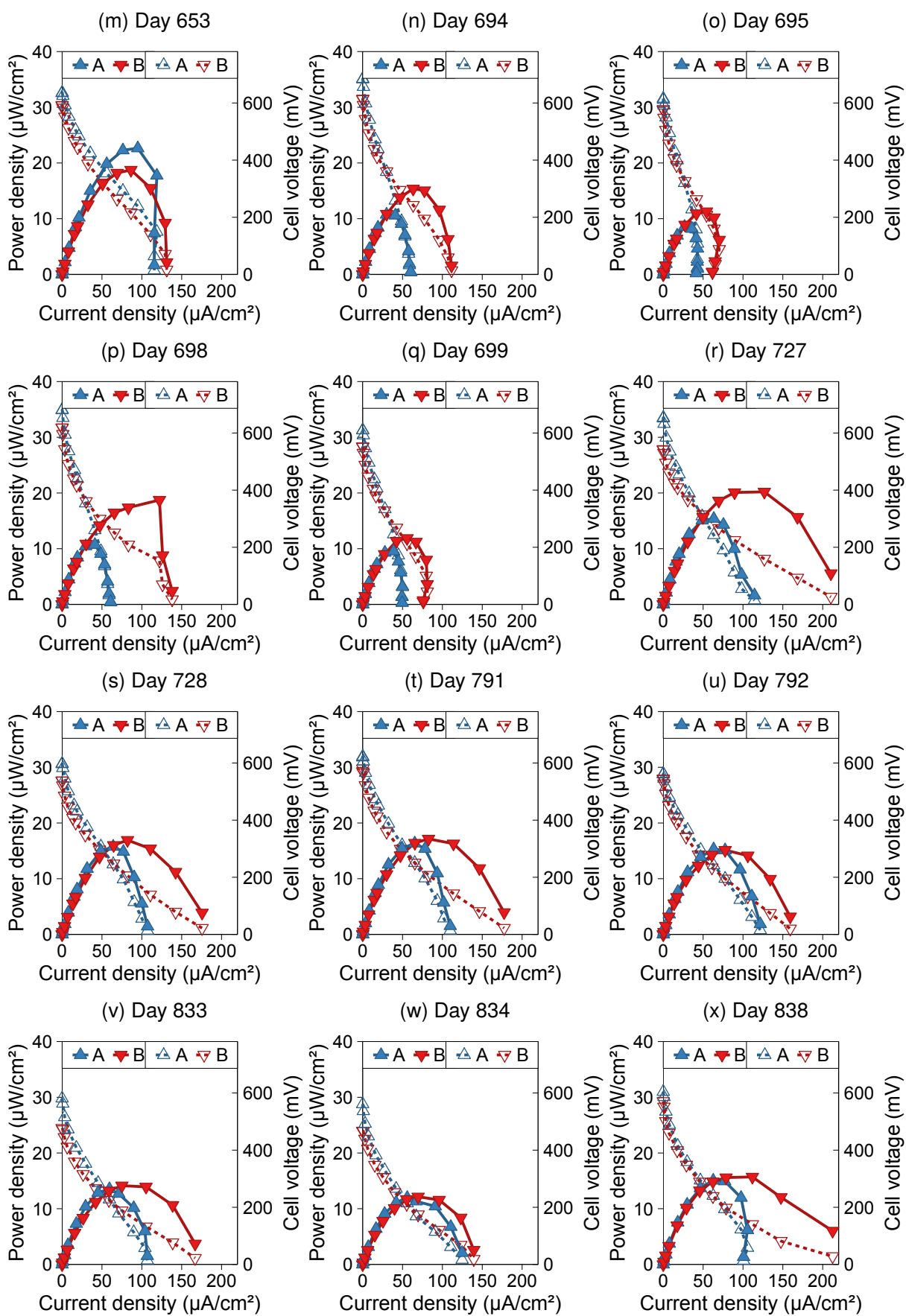


Figure E.2 (cont.): Polarisation curves recorded on cells A & B over time.

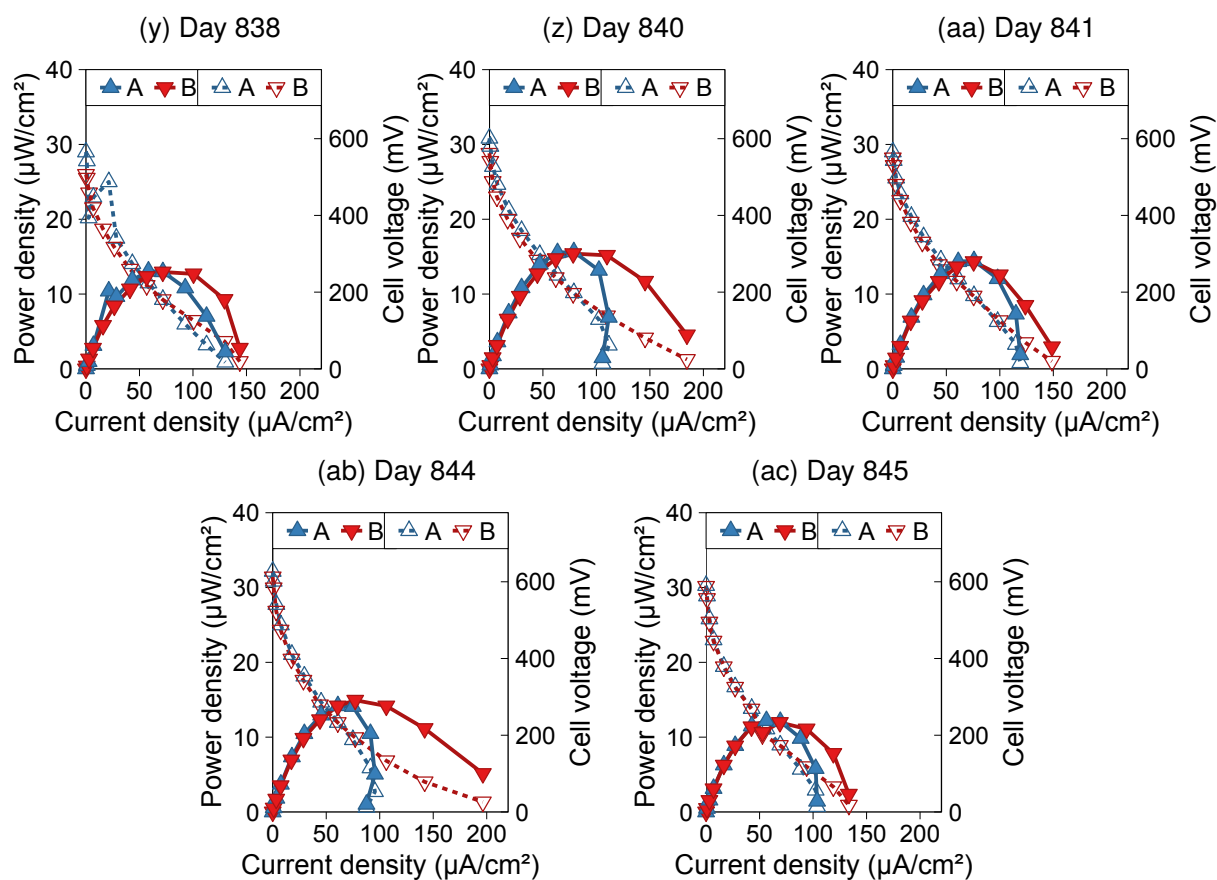


Figure E.2 (cont.): Polarisation curves recorded on cells A & B over time.

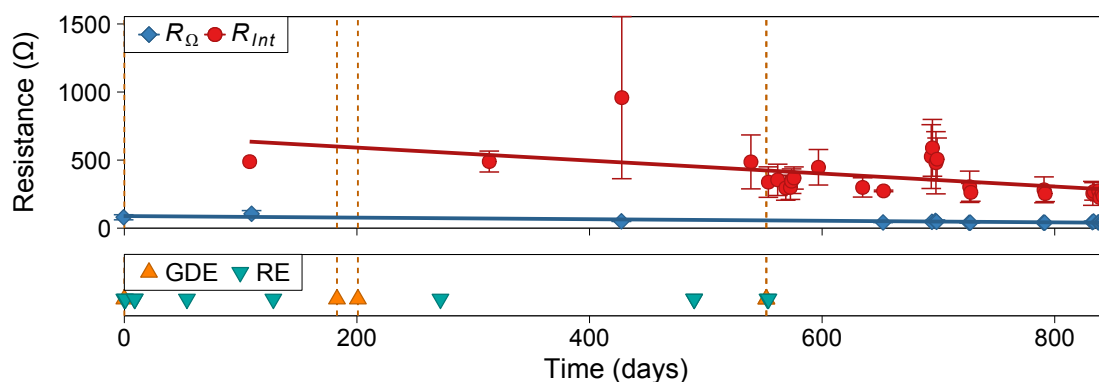


Figure E.3: Average ohmic resistance as measured by EIS and internal resistance estimated by PC gradient over time for cells A & B.

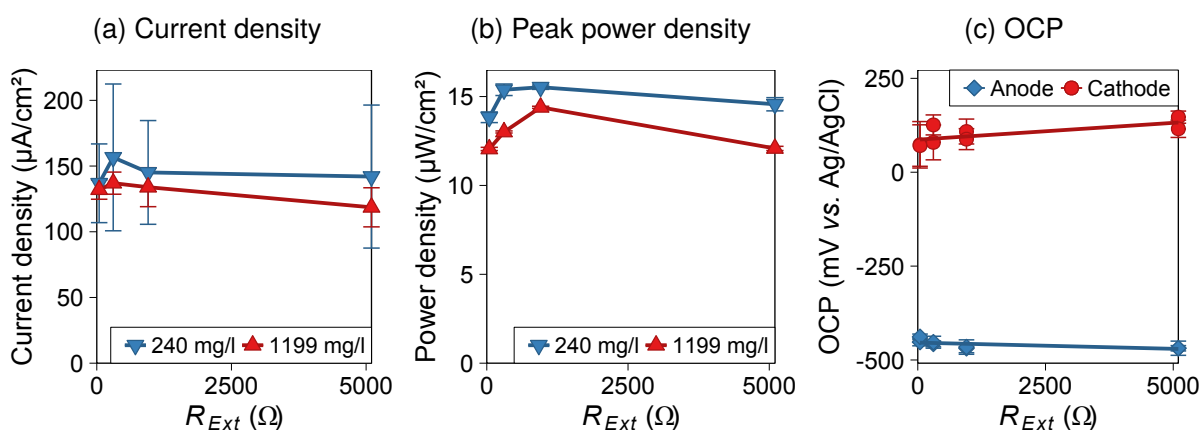


Figure E.4: Charts showing effect of operational  $R_{Ext}$  on average electrochemical performance parameters (a) maximum current density and (b) peak power density (coloured by medium BOD<sub>5</sub>); and (c) anode and cathode OCP, measured using polarisation curves for batch-mode cells A and B.

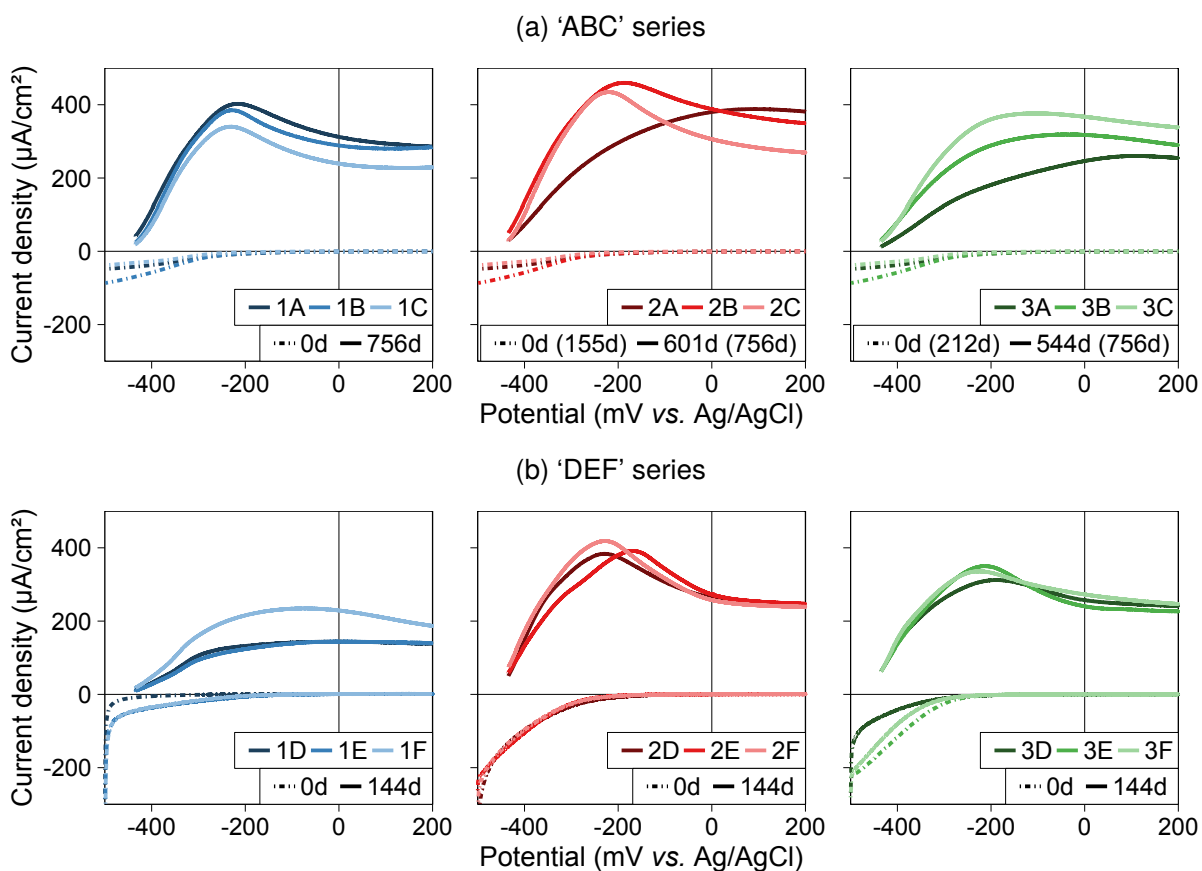


Figure E.5: Linear sweep voltammetry measured over time at 1 mV/s for flow-mode MFCs in the (a) 'ABC' series and (b) 'DEF' series.



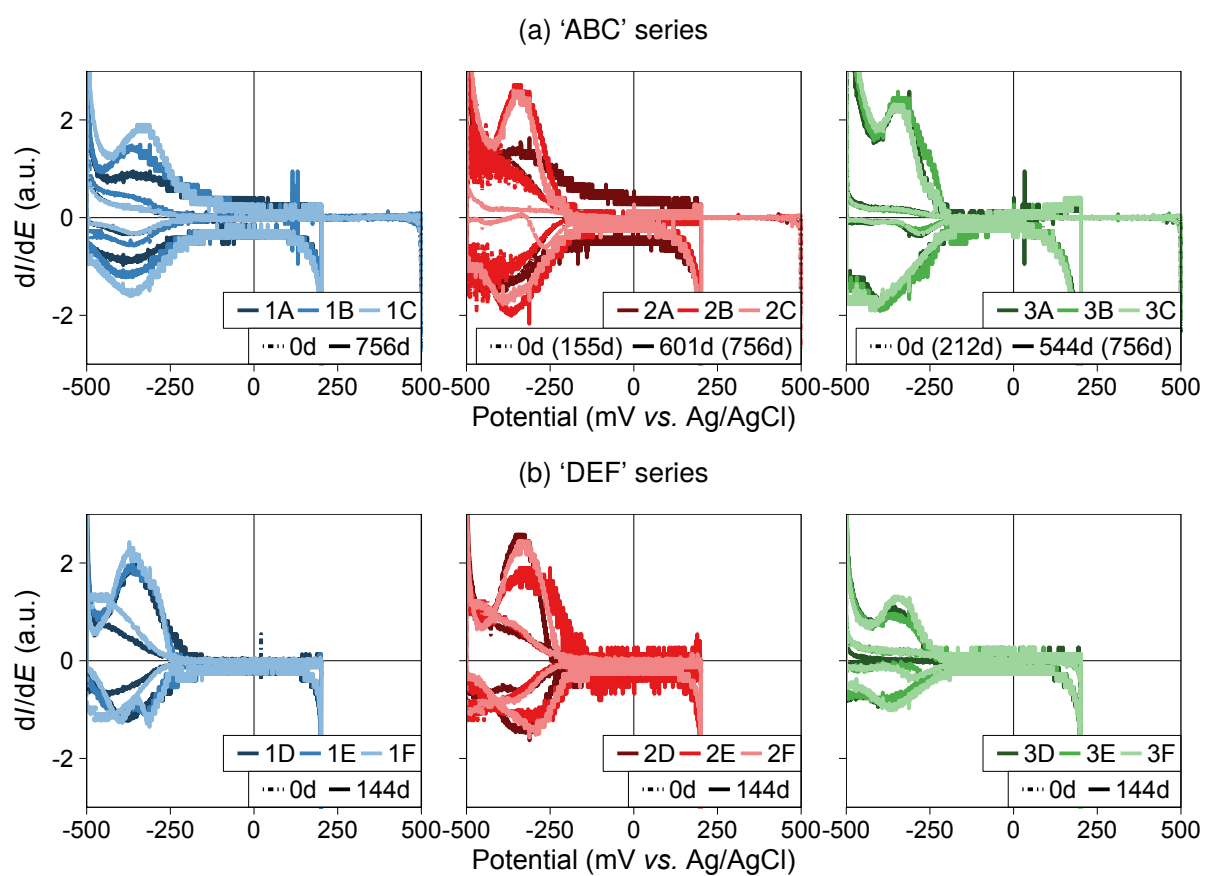


Figure E.6: 1st derivative cyclic voltammograms measured over time at 5 mV/s for flow-mode MFCs in the (a) 'ABC' series and (b) 'DEF' series.



## **Appendix F. Microbiological Analysis Data**

### **List of Figures**

- F.1 Photograph showing biofouled membranes and GDEs extracted from the 'ABC' series of flow-mode MFCs. . . . . 263
- F.2 Representative micrographs of SYBR® Gold-stained electrodes from 5000× diluted anode samples from flow-mode cells in the 'ABC' series. 265
- F.3 Electrophoresis gel plate images taken (a) after PCR and (b) after AMPure® purification showing a band between 400 and 500 base pairs (no band in controls). . . . . 266

### **List of Tables**

- F.1 Barcoded V4 forward (5'-adapter-barcode-primer-3') and V5 reverse (5'-adapter-primer-3') primers used in PCR amplification of 16S rRNA. 262
- F.2 DNA extraction quantification and quality scores. . . . . 264

Table F.1: Barcoded V4 forward (5'-adapter-barcode-primer-3') and V5 reverse (5'-adapter-primer-3') primers used in PCR amplification of 16S rRNA.

262

ID	Sample	A adaptor	Barcode	Spacer	Forward Primer
V4F BC38	Batch A	CCATCTCATCCCTGCGTGTCTCCGACTCAG	ACGGATCGTCAG	GAT	GTGNCAGCMGCCGCGGTAA
V4F BC39	Batch B	CCATCTCATCCCTGCGTGTCTCCGACTCAG	ACGGTGAGTGTC	GAT	GTGNCAGCMGCCGCGGTAA
V4F BC40	Flow 1A	CCATCTCATCCCTGCGTGTCTCCGACTCAG	ACGTACTCAGTG	GAT	GTGNCAGCMGCCGCGGTAA
V4F BC41	Flow 1B	CCATCTCATCCCTGCGTGTCTCCGACTCAG	ACGTCTGTAGCA	GAT	GTGNCAGCMGCCGCGGTAA
V4F BC42	Flow 1C	CCATCTCATCCCTGCGTGTCTCCGACTCAG	ACGTGAGAGAAT	GAT	GTGNCAGCMGCCGCGGTAA
V4F BC43	Flow 2A	CCATCTCATCCCTGCGTGTCTCCGACTCAG	ACGTGCCGTAGA	GAT	GTGNCAGCMGCCGCGGTAA
V4F BC44	Flow 2B	CCATCTCATCCCTGCGTGTCTCCGACTCAG	ACGTTAGCACAC	GAT	GTGNCAGCMGCCGCGGTAA
V4F BC45	Flow 2C	CCATCTCATCCCTGCGTGTCTCCGACTCAG	ACTACAGCCTAT	GAT	GTGNCAGCMGCCGCGGTAA
V4F BC46	Flow 3A	CCATCTCATCCCTGCGTGTCTCCGACTCAG	ACTACGTGTGGT	GAT	GTGNCAGCMGCCGCGGTAA
V4F BC47	Flow 3B	CCATCTCATCCCTGCGTGTCTCCGACTCAG	ACTAGCTCCATA	GAT	GTGNCAGCMGCCGCGGTAA
V4F BC48	Flow 3C	CCATCTCATCCCTGCGTGTCTCCGACTCAG	ACTATTGTCACG	GAT	GTGNCAGCMGCCGCGGTAA
V4F BC49	OCP A	CCATCTCATCCCTGCGTGTCTCCGACTCAG	ACTCACGGTATG	GAT	GTGNCAGCMGCCGCGGTAA
V4F BC50	OCP B	CCATCTCATCCCTGCGTGTCTCCGACTCAG	ACTCAGATACTC	GAT	GTGNCAGCMGCCGCGGTAA
V4F BC94	OCP C	CCATCTCATCCCTGCGTGTCTCCGACTCAG	AGTCCATAGCTG	GAT	GTGNCAGCMGCCGCGGTAA
V4F BC95	400S A	CCATCTCATCCCTGCGTGTCTCCGACTCAG	AGTCTACTCTGA	GAT	GTGNCAGCMGCCGCGGTAA
V4F BC96	400S B	CCATCTCATCCCTGCGTGTCTCCGACTCAG	AGTCTCGCATAT	GAT	GTGNCAGCMGCCGCGGTAA
V4F BC97	400S C	CCATCTCATCCCTGCGTGTCTCCGACTCAG	AGTGAGAGAAGC	GAT	GTGNCAGCMGCCGCGGTAA
V4F BC98	2000S A	CCATCTCATCCCTGCGTGTCTCCGACTCAG	AGTGCGATGCGT	GAT	GTGNCAGCMGCCGCGGTAA
V4F BC99	2000S B	CCATCTCATCCCTGCGTGTCTCCGACTCAG	AGTGGATGCTCT	GAT	GTGNCAGCMGCCGCGGTAA
V4F BC100	2000S C	CCATCTCATCCCTGCGTGTCTCCGACTCAG	AGTGTCACGGTG	GAT	GTGNCAGCMGCCGCGGTAA
ID	Sample	trP1 adaptor	Reverse Primer		
V5 R	All	CCTCTCTATGGGCAGTCGGTGAT	CCGYCAATTYMTTTRAGTTT		

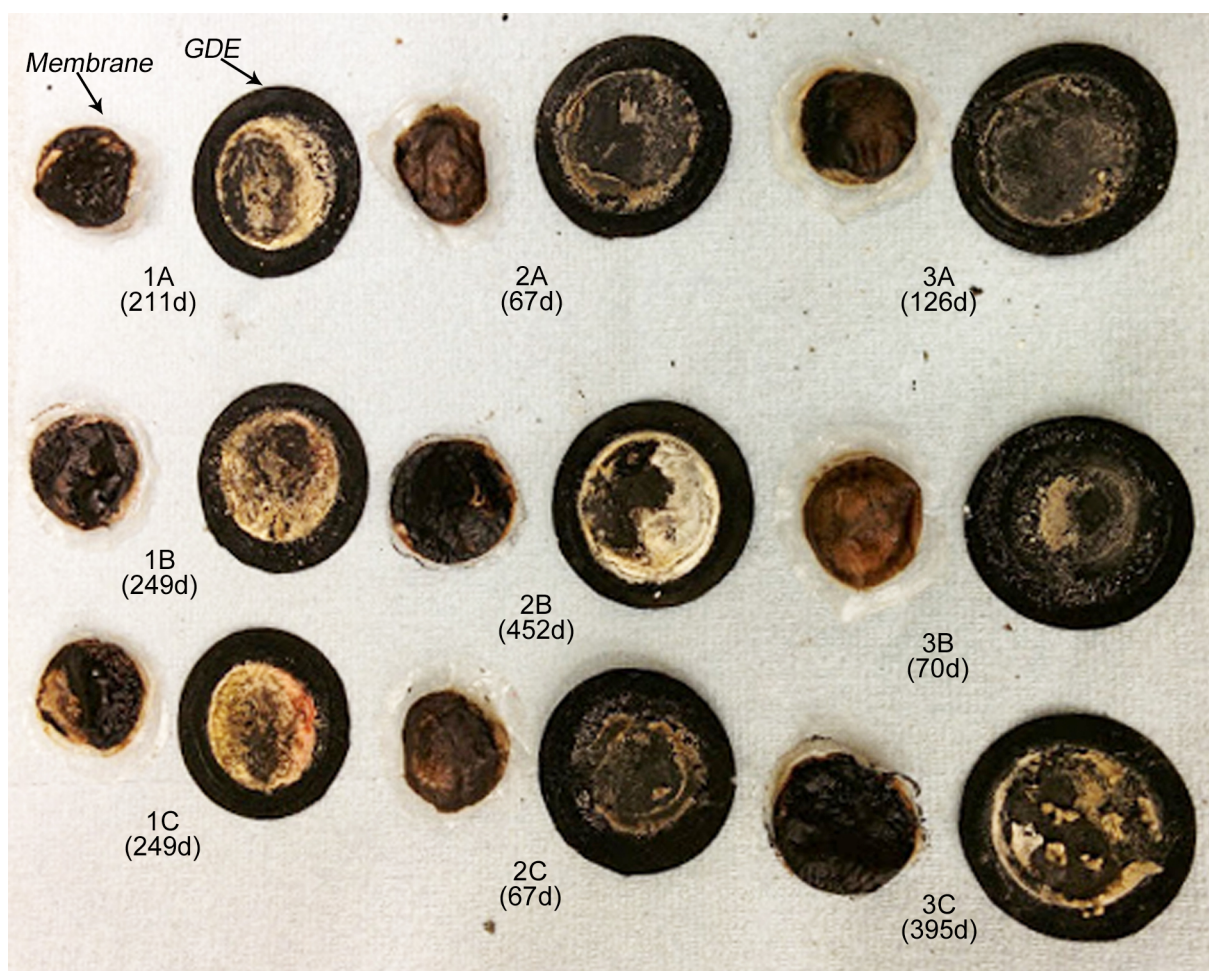


Figure F.1: Photograph showing biofouled membranes and GDEs extracted from the 'ABC' series of flow-mode MFCs on day 607 of operation (the age of each MEA is listed in brackets next to the electrode).

Table F.2: DNA extraction quantification and quality scores.

Sample	Replicate	DNA (ng/ul)	260/280 nm ratio <sup>a</sup>	260/230 nm ratio <sup>b</sup>
Batch	A	17.72 ± 0.11	1.85 ± 0.16	1.52 ± 0.06
	B	11.17 ± 0.30	1.73 ± 0.05	1.30 ± 0.01
Flow Stage 1	1A	23.49 ± 2.31	1.73 ± 0.12	1.23 ± 0.02
	1B	36.99 ± 1.09	1.82 ± 0.05	1.66 ± 0.16
	1C	19.19 ± 0.54	1.83 ± 0.08	1.10 ± 0.03
Flow Stage 2	2A	27.28 ± 0.37	1.83 ± 0.04	1.79 ± 0.02
	2B	22.32 ± 0.18	1.96 ± 0.03	1.45 ± 0.05
	2C	23.90 ± 0.07	1.82 ± 0.02	1.15 ± 0.02
Flow Stage 3	3A	28.40 ± 0.40	1.91 ± 0.02	1.37 ± 0.02
	3B	21.62 ± 0.36	1.82 ± 0.07	1.72 ± 0.02
	3C	21.89 ± 0.35	1.87 ± 0.08	1.65 ± 0.03
OCP	A	35.35 ± 0.48	1.81 ± 0.03	2.65 ± 0.11
	B	18.70 ± 0.16	1.91 ± 0.19	4.11 ± 0.57
	C	45.01 ± 1.10	1.84 ± 0.04	2.56 ± 0.03
Sld (400)	A	42.92 ± 0.13	1.90 ± 0.01	2.38 ± 0.03
	B	87.96 ± 0.90	1.85 ± 0.01	2.42 ± 0.04
	C	71.02 ± 2.14	1.88 ± 0.01	2.42 ± 0.04
Sld (2000)	A	23.19 ± 0.33	1.80 ± 0.03	1.90 ± 0.15
	B	47.99 ± 0.64	1.86 ± 0.03	2.14 ± 0.04
	C	35.38 ± 0.41	1.94 ± 0.07	2.44 ± 0.06
Supernatant	1A	12.99 ± 1.58	1.45 ± 0.10	1.14 ± 0.04
Blank	A	4.97 ± 1.24	2.34 ± 0.41	0.77 ± 0.09
	B	5.26 ± 1.34	1.87 ± 0.36	0.60 ± 0.01

<sup>a</sup> 260/280 nm ratio of 1.8 for 'pure' DNA. <sup>b</sup> 260/230 nm ratio of 2.0 to 2.2 for 'pure' nucleic acid.

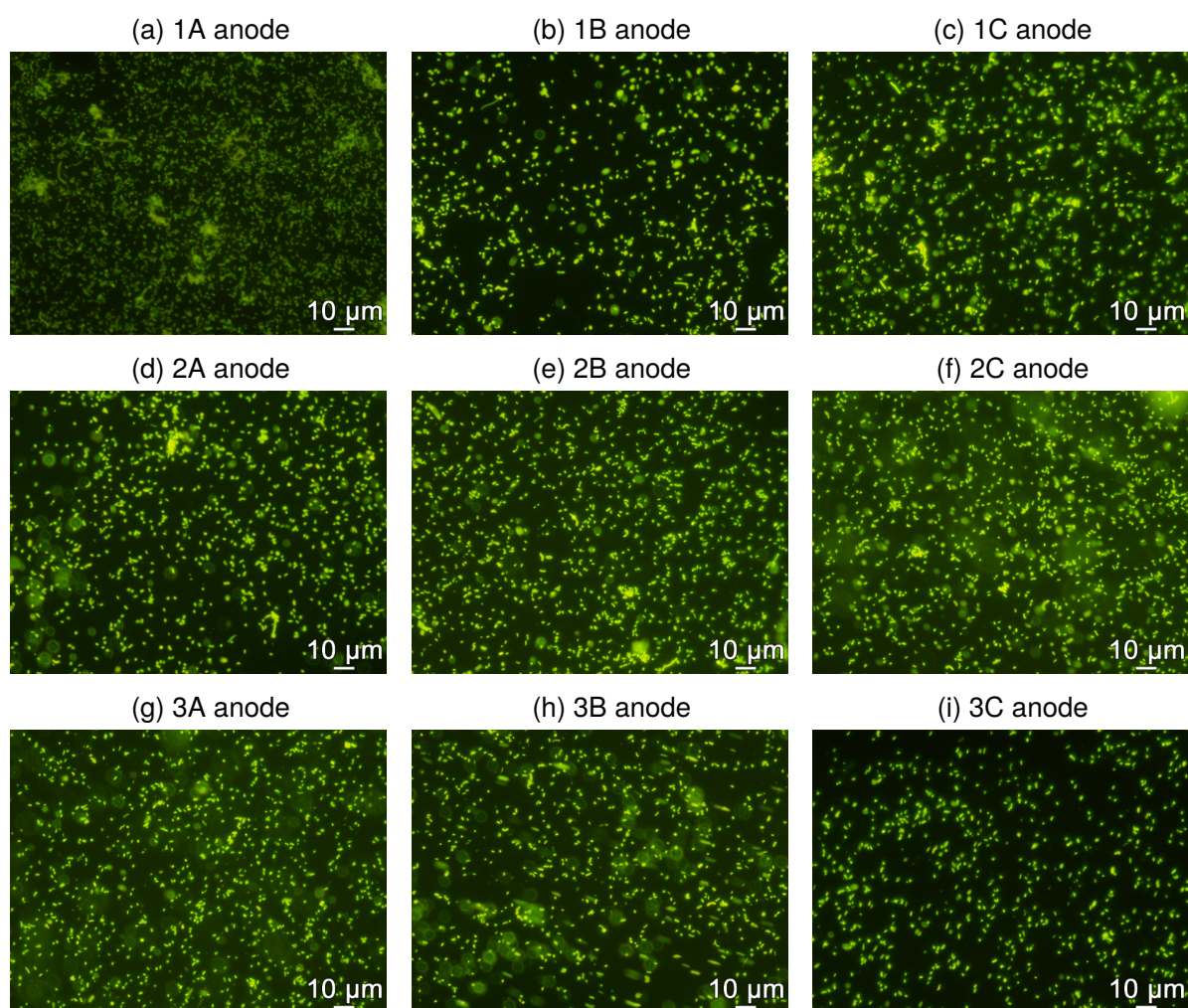


Figure F.2: Representative micrographs of SYBR® Gold-stained electrodes from 5000× diluted anode samples from flow-mode cells in the 'ABC' series.



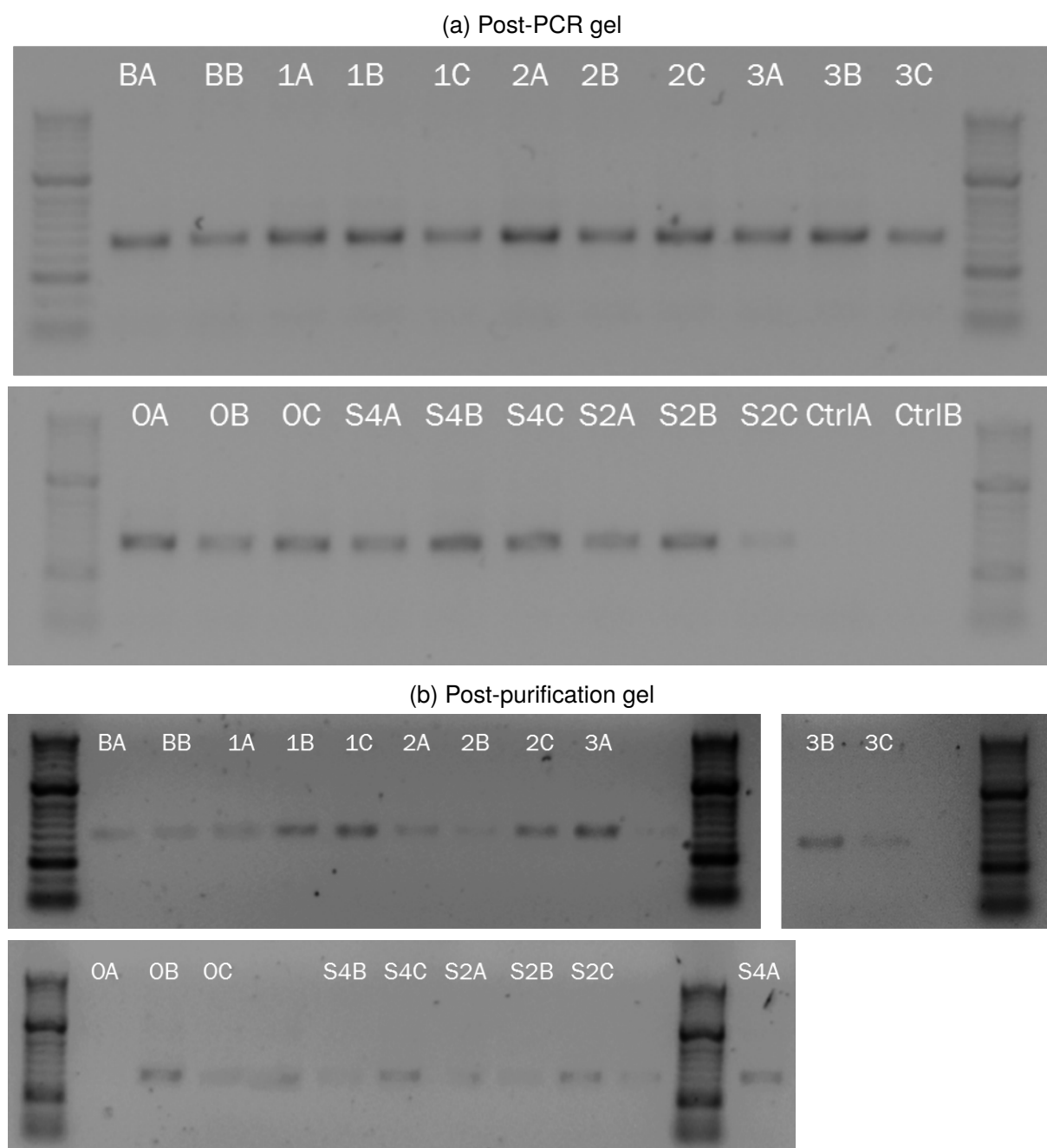


Figure F.3: Electrophoresis gel plate images taken (a) after PCR and (b) after AMPure® purification showing a band between 400 and 500 base pairs (no band in controls).

Batch-mode anodes = BA & BB; Flow Stage 1 anodes = 1A, 1B, 1C; Flow Stage 2 anodes = 2A, 2B & 2C; Flow Stage 3 = 3A, 3B & 3C; OCP electrodes = OA, OB & OC; Sludge (400 mg/l GGA) = S4A, S4B & S4C; Sludge (2000 mg/l GGA) = S2A, S2B & S2C; Ctrl = Sterile DI water control.



## References

- Abrevaya, X.C., Sacco, N.J., Bonetto, M.C., Hilding-Ohlsson, A. and Cortón, E., 2015a 'Analytical applications of microbial fuel cells. Part I: Biochemical oxygen demand.', *Biosensors and Bioelectronics*, 63C, pp. 580–590.
- Abrevaya, X.C., Sacco, N.J., Bonetto, M.C., Hilding-Ohlsson, A. and Cortón, E., 2015b 'Analytical applications of microbial fuel cells. part II: Toxicity, microbial activity and quantification, single analyte detection and other uses', *Biosensors and Bioelectronics*, 63C, pp. 591–601.
- Ahn, Y. and Logan, B.E., 2013 'Domestic wastewater treatment using multi-electrode continuous flow MFCs with a separator electrode assembly design', *Applied Microbiology and Biotechnology*, 97(1), pp. 409–416.
- Amarasinghe, H., Udeni, A., Gunawardena, H.D. and Jayatunga, Y.N.A., 1993 'Correlation between Biochemical Oxygen Demand (BOD) and Chemical Oxygen Demand (COD) for Different Industrial Wastewaters', *Journal of the National Science Council of Sri Lanka*, 21(2), pp. 259–266.
- APHA, 1999a 'Biochemical Oxygen Demand (BOD)', in: L.S. Clesceri, A.E. Greenberg and A.D. Eaton (Eds.), 'Standard Methods for the Examination of Water and Wastewater', American Public Health Association, Washington, DC, chap. 5, 20th edn., pp. 1–12.
- APHA, 1999b 'Chemical Oxygen Demand (COD)', in: L.S. Clesceri, A.E. Greenberg and A.D. Eaton (Eds.), 'Standard Methods for the Examination of Water and Wastewater', American Public Health Association, Washington, DC, 1, chap. 5, 20th edn., pp. 1–12.
- APHA, 2005 'Biochemical Oxygen Demand (BOD)', in: A.D. Eaton, L.S. Clesceri, E.W. Rice and A.E. Greenberg (Eds.), 'Standard Methods for the Examination of Water and Wastewater', American Public Health Association, Washington, DC, chap. 5, 21st edn., pp. 2–13.
- Ayyaru, S. and Dharmalingam, S., 2014 'Enhanced response of microbial fuel cell using sulphonated polyether ether ether ketone membrane as a biochemical oxygen demand sensor', *Analytica Chimica Acta*, pp. 7–11.

- Bactest, 2015 'Case Study – Evaluation of Shepherd Wastewater Management System - Site "A"', Tech. rep., Bactest, Cambridge, UK.
- Baena, S., Fardeau, M., Labat, M., Ollivier, B., Thomas, P., Garcia, J. and Patel, B.K.C., 1998 'Aminobacterium colombiense gen. nov. sp. nov., an Amino Acid-degrading Anaerobe Isolated from Anaerobic Sludge', *Anaerobe*, 4, pp. 241–250.
- Bard, A.J. and Faulkner, L.R., 2001 *Electrochemical Methods Fundamentals and Applications*, John Wiley & Sons, New York, NY, 2nd edn.
- Barron, J.J. and Ashton, C., 2007 'The Effect of Temperature on Conductivity Measurement', *Water*, pp. 1–5.
- BASi, 2016 'FAQ: EC Electrodes', [http://www.bioanalytical.com/products/ec/faqele.html#Ref\\_Type](http://www.bioanalytical.com/products/ec/faqele.html#Ref_Type), accessed: 2016-01-12.
- Beckman Coulter, 2013 'AMPure Beads Instructions For Use', Tech. Rep. B37419AA, Beckman Coulter.
- Biggs, A.I., 1954 'A spectrophotometric determination of the dissociation constants of p-nitrophenol and papaverine', *Transactions of the Faraday Society*, 50, p. 800.
- Bindslev, N., 2008 *Drug-Acceptor Interactions: Modeling Theoretical Tools to Test and Evaluate Experimental Equilibrium Effects*, Co-Action Publishing.
- Bitton, G., 2005 'Wastewater Microbiology', in: R. Mitchell (Ed.), 'Wiley Series in Ecological and Applied Microbiology', John Wiley & Sons, Hoboken, NJ, 3rd edn., p. 772.
- Bourgeois, W., Burgess, J.E. and Stuetz, R.M., 2001 'On-line monitoring of wastewater quality : a review', *Journal of Chemical Technology & Biotechnology*, 76, pp. 337–348.
- Bowman, J.P., Nichols, C.M. and Gibson, J.A.E., 2003 'Algoriphagus ratkowskyi gen. nov., sp. nov., Brumimicrobium glaciale gen. nov., sp. nov., Cryomorpha ignava gen. nov., sp. nov. and Crocinitomix catalasitica gen. nov., sp. nov., novel flavobacteria isolated from various polar habitats', *International Journal of Systematic and Evolutionary Microbiology*, 53(5), pp. 1343–1355.
- Brown, A., 2005 *An ecotoxicogenomic study in Escherichia coli K12-MG1655*, Ph.D. thesis, University of Newcastle upon Tyne.
- Buckel, W., 2001 'Unusual enzymes involved in five pathways of glutamate fermentation', *Applied Microbiology and Biotechnology*, 57(3), pp. 263–273.
- Caffoo, I., 2008 'Energy Efficient Water and Wastewater Treatment', Tech. rep., Environmental Knowledge Transfer Networks.
- Cao, X., Huang, X., Liang, P., Xiao, K., Zhou, Y., Zhang, X. and Logan, B.E., 2009 'A New

Method for Water Desalination Using Microbial Desalination Cells', *Environmental Science & Technology*, 43(18), pp. 7148–7152.

- Caporaso, J.G., Kuczynski, J., Stombaugh, J., Bittinger, K., Bushman, F.D., Costello, E.K., Fierer, N., Peña, A.G., Goodrich, J.K., Gordon, J.I., Huttley, G.A., Kelley, S.T., Knights, D., Koenig, J.E., Ley, R.E., Lozupone, C.A., McDonald, D., Muegge, B.D., Pirrung, M., Reeder, J., Sevinsky, J.R., Turnbaugh, P.J., Walters, W.A., Widmann, J., Yatsunenko, T., Zaneveld, J. and Knight, R., 2010 'QIIME allows analysis of high-throughput community sequencing data', *Nature Methods*, 7(5), pp. 335–336.
- Chang, I.S., Jang, J.K., Gil, G.C., Kim, M., Kim, H.J., Cho, B.W. and Kim, B.H., 2004 'Continuous determination of biochemical oxygen demand using microbial fuel cell type biosensor', *Biosensors and Bioelectronics*, 19(6), pp. 607–613.
- Chang, I.S., Moon, H., Jang, J.K. and Kim, B.H., 2005 'Improvement of a microbial fuel cell performance as a BOD sensor using respiratory inhibitors', *Biosensors and Bioelectronics*, 20(9), pp. 1856–1859.
- Chen, Z., Niu, Y., Zhao, S., Khan, A., Ling, Z., Chen, Y., Liu, P. and Li, X., 2016 'A novel biosensor for p-nitrophenol based on an aerobic anode microbial fuel cell', *Biosensors and Bioelectronics*, 85, pp. 860–868.
- Cheng, K.Y., Ho, G. and Cord-Ruwisch, R., 2008 'Affinity of microbial fuel cell biofilm for the anodic potential.', *Environmental science & technology*, 42(10), pp. 3828–34.
- Cheng, S., Liu, H. and Logan, B.E., 2006a 'Increased performance of single-chamber microbial fuel cells using an improved cathode structure', *Electrochemistry Communications*, 8(3), pp. 489–494.
- Cheng, S., Liu, H. and Logan, B.E., 2006b 'Power densities using different cathode catalysts (Pt and CoTMP) and polymer binders (Nafion and PTFE) in single chamber microbial fuel cells', *Environmental Science & Technology*, 40(1), pp. 364–369.
- Cheng, L., Quek, S.B. and Cord-Ruwisch, R., 2014 'Hexacyanoferrate-Adapted Biofilm Enables the Development of a Microbial Fuel Cell Biosensor to Detect Trace Levels of Assimilable Organic Carbon (AOC) in Oxygenated Seawater.', *Biotechnology and Bioengineering*, pp. 1–33.
- Chung, K. and Okabe, S., 2009 'Continuous power generation and microbial community structure of the anode biofilms in a three-stage microbial fuel cell system', *Applied Microbiology and Biotechnology*, 83(5), pp. 965–977.
- Commault, A.S., Lear, G., Bouvier, S., Feiler, L., Karacs, J. and Weld, R.J., 2016 'Geobacter-dominated biofilms used as amperometric BOD sensors', *Biochemical Engineering Journal*, 109, pp. 88–95.

- Commault, A.S., Lear, G. and Weld, R.J., 2015 'Maintenance of Geobacter-dominated biofilms in microbial fuel cells treating synthetic wastewater', *Bioelectrochemistry*, 106, pp. 150–158.
- CSH Protocols, 2006 'Preparation of 0.1 M Potassium Phosphate Buffer at 25C', *Cold Spring Harbor Protocols*, 2006(1).
- Cumming, G., Fidler, F. and Vaux, D.L., 2007 'Error bars in experimental biology.', *The Journal of cell biology*, 177(1), pp. 7–11.
- Dai, C. and Choi, S., 2013 'Technology and Applications of Microbial Biosensor', *Open Journal of Applied Biosensor*, 02(03), pp. 83–93.
- Davies, P.S., 2005 'The Biological Basis of Wastewater Treatment', *Strathkelvin Instruments Ltd.*
- Davila, D., Esquivel, J.P., Sabate, N., Mas, J., Dávila, D. and Sabaté, N., 2011 'Silicon-based microfabricated microbial fuel cell toxicity sensor.', *Biosensors and Bioelectronics*, 26(5), pp. 2426–2430.
- de los Ángeles Fernandez, M., de los Ángeles Sanromán, M., Marks, S., Makinia, J., Gonzalez del Campo, A., Rodrigo, M., Fernandez, F.J., Fernandez, M.d.I.Á., Sanromán, M.d.I.Á., Marks, S., Makinia, J., Gonzalez del Campo, A., Rodrigo, M. and Fernandez, F.J., 2016 'A grey box model of glucose fermentation and syntrophic oxidation in Microbial Fuel Cells', *Bioresource Technology*, 200, pp. 396–404.
- DEFRA, 2012 'Waste water treatment in the United Kingdom – 2012', Tech. rep., Department for Environment Food and Rural Affairs, London.
- Delzer, G.C. and McKenzie, S.W., 2003 'Five-Day Biochemical Oxygen Demand', in: 'USGS Techniques of Water-Resources Investigations, book 9', United States Geological Survey, vol. 7, chap. A7, 3rd edn., pp. 1–21.
- Di Lorenzo, M., 2015 'Use of microbial fuel cells in sensors', in: K. Scott and E.H. Yu (Eds.), 'Microbial Electrochemical and Fuel Cells', Woodhead Publishing, chap. 11, 1st edn., p. 410.
- Di Lorenzo, M., Curtis, T.P., Head, I.M. and Scott, K., 2009a 'A single-chamber microbial fuel cell as a biosensor for wastewaters', *Water Research*, 43(13), pp. 3145–3154.
- Di Lorenzo, M., Curtis, T.P., Head, I.M., Velasquez-Orta, S.B. and Scott, K., 2009b 'A single chamber packed bed microbial fuel cell biosensor for measuring organic content of wastewater', *Water Science & Technology*, 60(11), pp. 2879–2887.
- Di Lorenzo, M., Thomson, A.R., Schneider, K., Cameron, P.J. and Ieropoulos, I., 2014 'A

- small-scale air-cathode microbial fuel cell for on-line monitoring of water quality', *Biosensors and Bioelectronics*, 62, pp. 182–188.
- Dionex, 2012 'Methods development using Ion-Pair Chromatography with suppressed conductivity detection', Tech. rep., Thermo Scientific.
- Drancourt, M., Bollet, C., Carta, A. and Rousselier, P., 2001 'Phylogenetic analyses of Klebsiella species delineate Klebsiella and Raoultella gen. nov., with description of Raoultella ornithinolytica comb. nov., Raoultella terrigena comb. nov. and Raoultella planticola comb. nov.', *International Journal of Systematic and Evolutionary Microbiology*, 51(3), pp. 925–932.
- Du, Z., Li, H. and Gu, T., 2007 'A state of the art review on microbial fuel cells: A promising technology for wastewater treatment and bioenergy.', *Biotechnology Advances*, 25(5), pp. 464–482.
- Dworkin, M., Falkow, S., Rosenberg, E., Schleifer, K.H. and Stackebrandt, E., 2006 *The Prokaryotes: Vol. 4: Bacteria: Firmicutes, Cyanobacteria*, The Prokaryotes, Springer, New York, NY.
- Edgar, R.C., 2010 'Search and clustering orders of magnitude faster than BLAST', *Bioinformatics*, 26(19), pp. 2460–2461.
- Ercan, B., Duteanu, N.M., Ghangrekar, M.M., Dumas, C. and Scott, K., 2010 'Application of electro-active biofilms', *Biofouling: The Journal of Bioadhesion and Biofilm Research*, 26(1), pp. 57–71.
- Escobar, I.C. and Randall, a.a., 2001 'Assimilable organic carbon (AOC) and biodegradable dissolved organic carbon (BDOC): complementary measurements.', *Water research*, 35(18), pp. 4444–54.
- European Commission, 2000 'Directive 2000/60/EC of the European Parliament and of the Council of 23 October 2000 establishing a framework for Community action in the field of water policy', *Official Journal of the European Communities*, L327(1), pp. 1–82.
- Feng, Y., Barr, W. and Harper, W.F., 2013a 'Neural network processing of microbial fuel cell signals for the identification of chemicals present in water.', *Journal of Environmental Management*, 120C, pp. 84–92.
- Feng, Y., Kayode, O. and Harper, W.F., 2013b 'Using microbial fuel cell output metrics and nonlinear modeling techniques for smart biosensing', *The Science of the Total Environment*, 449C, pp. 223–228.
- Field, A., 2008 'One Way Independent ANOVA by Hand', Tech. rep., University of Sussex.
- Fricke, K., Harnisch, F. and Schröder, U., 2008 'On the use of cyclic voltammetry for the

- study of anodic electron transfer in microbial fuel cells', *Energy & Environmental Science*, 1(1), pp. 144–147.
- Fung, Y., Lee, J., Chang, I.N.S. and Kim, B.H., 2006 'Bacterial Communities in Microbial Fuel Cells Enriched with High Concentrations of Glucose and Glutamate', *J. Microbiol. Biotechnol.*, 16(9), pp. 1481–1484.
- Gadagkar, S.R. and Call, G.B., 2015 'Computational tools for fitting the Hill equation to dose-response curves', *Journal of Pharmacological and Toxicological Methods*, 71, pp. 68–76.
- Geveke, D.J., 2005 'UV Inactivation of Bacteria in Apple Cider', Tech. rep., U.S. Department of Agriculture, Wyndmoor, PA.
- Ghangrekar, M.M., 2014 'Development of microbial fuel cell as biosensor for detection of organic matter of wastewater', *Recent Research in Science and Technology*, 6(1), pp. 162–166.
- Gil, G.C., Chang, I.S., Kim, B.H., Kim, M., Jang, J.K., Park, H.S. and Kim, H.J., 2003 'Operational parameters affecting the performance of a mediator-less microbial fuel cell', *Biosensors and Bioelectronics*, 18(4), pp. 327–334.
- Górski, Ł., Trzebuniak, K.F. and Malinowska, E., 2012 'Low BOD Determination Methods: The State-of-the-art', *Chemical and Process Engineering*, 33(4), pp. 629–637.
- Goutelle, S., Maurin, M., Rougier, F., Barbaut, X., Bourguignon, L., Ducher, M. and Maire, P., 2008 'The Hill equation: A review of its capabilities in pharmacological modelling', *Fundamental and Clinical Pharmacology*, 22(6), pp. 633–648.
- Govindasamy, V., Senthilkumar, M., Gaikwad, K. and Annapurna, K., 2008 'Isolation and characterization of ACC deaminase gene from two plant growth-promoting rhizobacteria', *Current Microbiology*, 57(4), pp. 312–317.
- Grabowski, A., Tindall, B.J., Bardin, V., Blanchet, D. and Jeanthon, C., 2005 'Petrimonas sulfuriphila gen. nov., sp. nov., a mesophilic fermentative bacterium isolated from a biodegraded oil reservoir', *International Journal of Systematic and Evolutionary Microbiology*, 55(3), pp. 1113–1121.
- van Haandel, A. and van der Lubbe, J., 2007 *Handbook Biological Waste Water Treatment*, vol. 68, Quist Publishing, Leidschendam, The Netherlands.
- HACH, 2013 'Cuvette Test LCK 554 BOD5', Tech. rep., HACH Lange.
- Hamelers, H.V.M., Ter Heijne, A., Sleutels, T.H.J.A., Jeremiasse, A.W., Strik, D.P.B.T.B. and Buisman, C.J.N., 2010 'New applications and performance of bioelectrochemical systems', *Applied Microbiology and Biotechnology*, 85(6), pp. 1673–1685.

- Hammer Sr., M.J. and Hammer Jr., M.J., 2008 *Water and Wastewater Technology*, Prentice Hall, 6th edn.
- Haynes, W.M. (Ed.), 2010 *CRC Handbook of Chemistry and Physics*, CRC Press, 91st edn.
- He, Z. and Mansfeld, F., 2009 'Exploring the use of electrochemical impedance spectroscopy (EIS) in microbial fuel cell studies', *Energy & Environmental Science*, 2(2), pp. 215–219.
- Henze, M. and Comeau, Y., 2008 'Wastewater Characterization', *Biological Wastewater Treatment: Principles Modelling and Design.*, pp. 33–52.
- Heylen, K., Lebbe, L. and de Vos, P., 2008 'Acidovorax caeni sp. nov., a denitrifying species with genetically diverse isolates from activated sludge', *International Journal of Systematic and Evolutionary Microbiology*, 58(1), pp. 73–77.
- Hill, A.V., 1910 'The possible effects of the aggregation of the molecules of haemoglobin on its dissociation curves', *Proceedings of the Physiological Society*, 40, pp. iv–vii.
- Hill, A.V., 1913 'The Combinations of Haemoglobin with Oxygen and with Carbon Monoxide', *Biochemical Journal*, 7(1), pp. 471–480.
- Homann, T., Tag, C., Biebl, H., Deckwer, W.d., Schink, B., Biotechnologische, G.g., Weg, M., Braunschweig, D. and Republic, F., 1990 'Applied Microbiology Biotechnology Fermentation of glycerol to 1, 3-propanediol by Klebsiella and Citrobacter strains', *Applied and Microbiology Biotechnology*, 33(2), pp. 121–126.
- Hong, Y., Call, D.F., Werner, C.M. and Logan, B.E., 2011 'Adaptation to high current using low external resistances eliminates power overshoot in microbial fuel cells', *Biosensors and Bioelectronics*, 28(1), pp. 71–76.
- Hsieh, M.C., Cheng, C.Y., Liu, M.H. and Chung, Y.C., 2015 'Effects of Operating Parameters on Measurements of Biochemical Oxygen Demand Using a Mediatorless Microbial Fuel Cell Biosensor', *Sensors*, 16(1), p. 35.
- Hsieh, M.C. and Chung, Y.C., 2014 'Measurement of biochemical oxygen demand from different wastewater samples using a mediator-less microbial fuel cell biosensor', *Environmental Technology*, 35(17), pp. 1–8.
- Hudson, N., Baker, A., Ward, D., Reynolds, D.M., Brunsdon, C., Carliell-Marquet, C. and Browning, S., 2008 'Can fluorescence spectrometry be used as a surrogate for the Biochemical Oxygen Demand (BOD) test in water quality assessment? An example from South West England.', *Science of the Total Environment*, 391(1), pp. 149–158.
- Hui, Y.H. (Ed.), 2006 *Handbook of Food Science, Technology and Engineering*, CRC Press.
- Ieropoulos, I., Greenman, J. and Melhuish, C., 2008 'Microbial fuel cells based on carbon veil

- electrodes : Stack configuration and scalability', *International Journal of Energy Research*, 32(13), pp. 1228–1240.
- Ieropoulos, I., Winfield, J. and Greenman, J., 2010 'Effects of flow-rate, inoculum and time on the internal resistance of microbial fuel cells.', *Bioresource Technology*, 101(10), pp. 3520–5.
- Imperial, S. and Centelles, J.J., 2014 'Enzyme Kinetic Equations of Irreversible and Reversible Reactions in Metabolism', *J. Biosciences & Medicines*, 2(June), pp. 24–29.
- Indian Central Pollution Control Board, 2014 'Directions Under Section 18(1)(B) Of The Water (Prevention & Control Of Pollution) Act, 1974 And The Air (Prevention & Control Of Pollution) Act, 1981 In The Matter Of Pollution Control', B-29016/04/06/PCI-1/5401.
- Iranpour, R. and Zermeno, M., 2008 'Online Biochemical Oxygen Demand Monitoring for Wastewater Process Control - Full-Scale Studies at Los Angeles Glendale Wastewater Plant, California', *Water Environment Research*, 80(4), pp. 298–307.
- IUPAC, 1997 'Quantities related to the use of linear calibration functions', in: J. Inczédy, T. Lengyel and A.M. Ure (Eds.), 'Compendium of Analytical Nomenclature', Blackwell Science, Oxford, UK, 17, chap. 2.4, 3rd edn., pp. 1–7.
- IWA, 2016 'The 13th IWA Leading Edge Conference on Water and Wastewater Technologies Evaluating Impacts of Innovation Conference Programme', International Water Association, Jerez de la Frontera, Spain, June, p. 48.
- Jafary, T., Ghoreyshi, A.A., Najafpour, G.D., Fatemi, S. and Rahimnejad, M., 2013 'Investigation on performance of microbial fuel cells based on carbon sources and kinetic models', *International Journal of Energy Research*, 37(12), pp. 1539–1549.
- Jia, H., Yang, G., Wang, J., Ngo, H.H., Guo, W., Zhang, H. and Zhang, X., 2016 'Performance of a Microbial Fuel Cell - Based Biosensor for Online Monitoring in an Integrated System Combining Microbial Fuel Cell and Upflow Anaerobic Sludge Bed Reactor', *Bioresource Technology*, 218, pp. 286–293.
- Jiang, Y.B., Deng, H., Sun, D.M. and Zhong, W.H., 2015a 'Electrical signals generated by soil microorganisms in microbial fuel cells respond linearly to soil Cd<sup>2+</sup> pollution', *Geoderma*, 255-256, pp. 35–41.
- Jiang, Y., Liang, P., Liu, P., Bian, Y., Miao, B., Sun, X., Zhang, H. and Huang, X., 2016a 'Enhancing Signal Output and Avoiding BOD/Toxicity Combined Shock Interference by Operating a Microbial Fuel Cell Sensor with an Optimized Background Concentration of Organic Matter', *International Journal of Molecular Sciences*, 17(9), p. 1392.
- Jiang, Y., Liang, P., Zhang, C., Bian, Y., Yang, X., Huang, X. and Girguis, P.R., 2015b 'Enhancing the response of microbial fuel cell based toxicity sensors to Cu(II) with the applying of



- flow-through electrodes and controlled anode potentials', *Bioresource Technology*, 190, pp. 367–372.
- Jiang, X., Shen, J., Lou, S., Mu, Y., Wang, N., Han, W., Sun, X., Li, J. and Wang, L., 2016b 'Comprehensive comparison of bacterial communities in a membrane-free bioelectrochemical system for removing different mononitrophenols from wastewater', *Bioresource Technology*, 216, pp. 645–652.
- Jouanneau, S., Recoules, L., Durand, M.J., Boukabache, A., Picot, V., Primault, Y., Lakel, A., Sengelin, M., Barillon, B. and Thouand, G., 2013 'Methods for assessing biochemical oxygen demand (BOD): a review', *Water Research*, 49C, pp. 62–82.
- Kang, K.H., Jang, J.K., Pham, T.H., Moon, H., Chang, I.S. and Kim, B.H., 2003 'A microbial fuel cell with improved cathode reaction as a low biochemical oxygen demand sensor', *Biotechnology Letters*, 25(16), pp. 1357–1361.
- Kaur, A., Rae, J., Michie, I., Dinsdale, R.M., Guwy, A.J. and Premier, G.C., 2013 'Microbial fuel cell type biosensor for specific volatile fatty acids using acclimated bacterial communities', *Biosensors and Bioelectronics*, 47, pp. 50–55.
- Ketep, S.F., Fourest, E. and Bergel, A., 2013 'Experimental and theoretical characterization of microbial bioanodes formed in pulp and paper mill effluent in electrochemically controlled conditions.', *Bioresource Technology*, 149C, pp. 117–125.
- Kim, J.R., Beecroft, N.J., Varcoe, J.R., Dinsdale, R.M., Guwy, A.J., Slade, R.C.T., Thumser, A., Avignone-Rossa, C. and Premier, G.C., 2011a 'Spatiotemporal development of the bacterial community in a tubular longitudinal microbial fuel cell.', *Applied Microbiology and Biotechnology*, 90(3), pp. 1179–1191.
- Kim, K.Y., Chae, K.J., Choi, M.J., Ajayi, F.F., Jang, A., Kim, C.W. and Kim, I.S., 2011b 'Enhanced Coulombic efficiency in glucose-fed microbial fuel cells by reducing metabolite electron losses using dual-anode electrodes', *Bioresource Technology*, 102(5), pp. 4144–4149.
- Kim, B.H., Chang, I.S., Gil, G.C., Park, H.S. and Kim, H.J., 2003a 'Novel BOD (biological oxygen demand) sensor using mediator-less microbial fuel cell', *Biotechnology Letters*, 25(7), pp. 541–545.
- Kim, B.H., Chang, I.S. and Moon, H., 2006a 'Microbial Fuel Cell-Type Biochemical Oxygen Demand Sensor', in: C.A. Grimes, E.C. Dickey and M.V. Pishko (Eds.), 'Encyclopedia of Sensors', American Scientific Publishers, vol. 10, pp. 1–12.
- Kim, H.J., Hyun, M.S., Chang, I.S. and Kim, B.H., 1999 'A microbial fuel cell type lactate biosensor using a metal-reducing bacterium, *Shewanella putrefaciens*', *Journal of Microbiology and Biotechnology*, 9(3), pp. 365–367.

- Kim, M., Hyun, M.S., Gadd, G.M. and Kim, H.J., 2007 'A novel biomonitoring system using microbial fuel cells', *Journal of Environmental Monitoring*, 9(12), pp. 1323–1328.
- Kim, M., Hyun, M.S., Gadd, G.M., Kim, G.T., Lee, S.J. and Kim, H.J., 2009 'Membrane-electrode assembly enhances performance of a microbial fuel cell type biological oxygen demand sensor', *Environmental Technology*, 30(4), pp. 329–336.
- Kim, M., Park, H.S., Jin, G.J., Cho, W.H., Lee, D.K., Hyun, M.S., Choi, C.H. and Kim, H.J., 2006b 'A novel combined biomonitoring system for BOD measurement and toxicity detection using microbial fuel cells', in: '5th IEEE Conference on Sensors', IEEE, vol. 1-3, pp. 1251–1252.
- Kim, J.R., Rodríguez, J., Hawkes, F.R., Dinsdale, R.M., Guwy, A.J. and Premier, G.C., 2011c 'Increasing power recovery and organic removal efficiency using extended longitudinal tubular microbial fuel cell (MFC) reactors', *Energy & Environmental Science*, 4(2), pp. 459–465.
- Kim, J. R., Rodríguez, J., Hawkes, F. R., D.
- Kim, M., Youn, S.M., Shin, S.H., Jang, J.G., Han, S.H., Hyun, M.S., Gadd, G.M. and Kim, H.J., 2003b 'Practical field application of a novel BOD monitoring system', *Journal of Environmental Monitoring*, 5(4), pp. 640–643.
- Kimmel, D.W., LeBlanc, G., Meschievitz, M.E. and Cliffel, D.E., 2012 'Electrochemical sensors and biosensors.', *Analytical Chemistry*, 84(2), pp. 685–707.
- King, S.T., 2014 *Detecting Industrial Chemicals in water with Microbial Fuel Cells and Artificial Neural Networks*, Msc environmental engineering, Air Force Institute of Technology.
- Kodama, Y., Shimoyama, T. and Watanabe, K., 2012 'Dysgonomonas oryzae sp. nov., isolated from a microbial fuel cell', *International Journal of Systematic and Evolutionary Microbiology*, 62(12), pp. 3055–3059.
- Kompala, D.S., 2011 'Microbial Growth on Multiple Substrates', in: 'Bioprocess Engineering: Fundamentals and Applications', CRC Press, chap. 7.3, p. 750.
- Kong, Z., Vaerewijck, M. and Verstraete, W., 1996 'On-Line stBOD Measurement and Toxicity Control of Wastewaters with a Respirographic Biosensor', *Environmental Technology*, 14(4), pp. 399–406.
- Kumlanghan, A., Liu, J., Thavarungkul, P., Kanatharana, P. and Mattiasson, B., 2007 'Microbial fuel cell-based biosensor for fast analysis of biodegradable organic matter', *Biosensors and Bioelectronics*, 22(12), pp. 2939–2944.
- Kurganov, B.I., Lobanov, A.V., Borisov, I.A. and Reshetilov, A.N., 2001 'Criterion for Hill equation validity for description of biosensor calibration curves', *Analytica Chimica Acta*, 427(1), pp. 11–19.

- Kwak, J., Khang, B., Kim, E. and Kim, H., 2013 'Estimation of Biochemical Oxygen Demand Based on Dissolved Organic Carbon, UV Absorption, and Fluorescence Measurements', *Journal of Chemistry*, 2013, pp. 1–9.
- Ledezma, P., Greenman, J. and Ieropoulos, I., 2012 'Maximising electricity production by controlling the biofilm specific growth rate in microbial fuel cells.', *Bioresource Technology*, 118, pp. 615–8.
- Ledezma, P., Greenman, J. and Ieropoulos, I., 2013 'MFC-cascade stacks maximise COD reduction and avoid voltage reversal under adverse conditions.', *Bioresource Technology*, 134C, pp. 158–165.
- Lee, H., Yang, W., Wei, X., Fraiwan, A. and Choi, S., 2015 'A Microsized Microbial Fuel Cell Based Biosensor for Fast and Sensitive Detection of Toxic Substances in Water', in: 'MEMS 2015', IEEE, pp. 573–576.
- Life Technologies, 2011 'Ion Amplicon Library Preparation (Fusion Method)', Tech. Rep. 4468326, Life Technologies Corporation.
- Life Technologies, 2014 'Ion PGM Hi-Q Sequencing Kit-User Guide', Tech. rep., Thermo Fisher Scientific.
- Life Technologies, 2015 'Qubit dsDNA HS Assay Kits', Tech. rep., Thermo Fisher Scientific.
- Liu, H., Hu, T., Zeng, G., Yuan, X., Wu, J., Shen, Y. and Yin, L., 2013 'Electricity generation using p-nitrophenol as substrate in microbial fuel cell', *International Biodeterioration & Biodegradation*, 76, pp. 108–111.
- Liu, Z., Liu, J., Li, B., Zhang, Y. and Xing, X.H., 2014 'Focusing on the process diagnosis of anaerobic fermentation by a novel sensor system combining microbial fuel cell, gas flow meter and pH meter', *International Journal of Hydrogen Energy*, 39(25), pp. 1–7.
- Liu, Z., Liu, J., Zhang, S., Xing, X.H. and Su, Z., 2011 'Microbial fuel cell based biosensor for in situ monitoring of anaerobic digestion process', *Bioresource Technology*, 102(22), pp. 10,221–10,229.
- Liu, H. and Logan, B.E., 2004 'Electricity generation using an air-cathode single chamber microbial fuel cell in the presence and absence of a proton exchange membrane', *Environmental Science & Technology*, 38(14), pp. 4040–4046.
- Logan, B.E., 2008 *Microbial Fuel Cells*, John Wiley & Sons, Hoboken, NJ.
- Logan, B.E. and Rabaey, K., 2012 'Conversion of wastes into bioelectricity and chemicals by using microbial electrochemical technologies.', *Science*, 337(6095), pp. 686–690.
- Lohner, S., 2014 *Encyclopedia of Applied Electrochemistry*, Springer New York, New York, NY.

- Lovibond, 2008 'BOD-System OxiDirect® Instruction Manual', Tech. rep., Tintometer GmbH.
- Lowe, K., Rothe, N., Tomaras, J., DeJong, K., Tucholke, M., Drewes, J., McCray, J. and Munakata-Marr, J., 2007 *Influent Constituent Characteristics of the Modern Waste Stream from Single Sources : Literature Review*, Water Environment Research Foundation.
- Lynggaard-Jensen, A., 1999 'Trends in monitoring of waste water systems', *Talanta*, 50(4), pp. 707–716.
- Malina, J., 1992 *Design of Anaerobic Processes for Treatment of Industrial and Municipal Waste*, v. 7, Taylor & Francis.
- Manning, D.A.C. and Bewsher, A., 1997 'Determination of anions in landfill leachates by ion chromatography', *Journal of Chromatography A*, 770(1-2), pp. 203–210.
- Mara, D. and Horan, N. (Eds.), 2003 *Handbook of Water and Wastewater Microbiology*, Elsevier.
- Mathuriya, A.S. and Yakhmi, J.V., 2014 'Microbial fuel cells - Applications for generation of electrical power and beyond.', *Critical Reviews in Microbiology*, 7828(d), pp. 1–17.
- Merriman, B., Ion Torrent R&D Team and Rothberg, J.M., 2012 'Progress in Ion Torrent semiconductor chip based sequencing', *Electrophoresis*, 33(23), pp. 3397–3417.
- Metcalf & Eddy Inc, 2002 *Wastewater Engineering - Treatment and Reuse (Fourth Edition)*, McGraw-Hill, 4th edn.
- Mettler Toledo, 2012 'FiveEasyPlus Conductivity Meter FEP30', Tech. rep., Mettler-Toledo AG, Analytical.
- Milner, E.M., 2015 *Development of an Aerobic Biocathode for Microbial Fuel Cells*, Ph.D. thesis, Newcastle University.
- Mo Bio Laboratories, 2013 'PowerSoil DNA Isolation Kit', Tech. Rep. 12888, Mo Bio Laboratories.
- Modin, O. and Wilén, B.M., 2012 'A novel bioelectrochemical BOD sensor operating with voltage input', *Water Research*, 46(18), pp. 6113–6120.
- Moon, H., Chang, I.S., Jang, J.K., Kim, K.S., Lee, J., Lovitt, R.W. and Kim, B.H., 2005 'On-line monitoring of low biochemical oxygen demand through continuous operation of a mediator-less microbial fuel cell', *Journal of Microbiology and Biotechnology*, 15(1), pp. 192–196.
- Moon, H., Chang, I.S., Kang, K.H., Jang, J.K. and Kim, B.H., 2004 'Improving the dynamic response of a mediator-less microbial fuel cell as a biochemical oxygen demand (BOD) sensor', *Biotechnology Letters*, 26(22), pp. 1717–1721.

- Morozkina, E.V. and Zvyagil'skaya, R.A., 2007 'Nitrate Reductases: Structure, Functions, and Effect of Stress Factors', *Biochemistry (Moscow)*, 72(10), pp. 1151–1160.
- Moscoviz, R., Trably, E. and Bernet, N., 2016 'Consistent 1,3-propanediol production from glycerol in mixed culture fermentation over a wide range of pH', *Biotechnology for Biofuels*, 9(1), p. 32.
- Motulsky, H. and Christopoulos, A., 2004 *Fitting Models to Biological Data Using Linear and Nonlinear Regression: A Practical Guide to Curve Fitting*, Oxford University Press.
- Nakamura, H., Shimomura-Shimizu, M. and Karube, I., 2008 'Development of Microbial Sensors and Their Application', *Advances in Biochemical Engineering/Biotechnology*, 109, pp. 351–394.
- Namour, P. and Jaffrezic-Renault, N., 2010 'Sensors for measuring biodegradable and total organic matter in water', *Trends in Analytical Chemistry*, 29(8), pp. 848–857.
- Nogaj, T., Randall, A., Jimenez, J., Takacs, I., Bott, C., Miller, M., Murthy, S. and Wett, B., 2015 'Modeling of organic substrate transformation in the high-rate activated sludge process', *Water Science and Technology*, 71(7), pp. 971–979.
- Obst, M., Krug, A., Luftmann, H. and Steinbüchel, A., 2005 'Degradation of cyanophycin by *Sedimentibacter hongkongensis* strain KI and *Citrobacter amalonaticus* strain G isolated from an anaerobic bacterial consortium', *Applied and Environmental Microbiology*, 71(7), pp. 3642–3652.
- O'Connor, O.A. and Young, L.Y., 1989 'Toxicity and anaerobic biodegradability of substituted phenols under methanogenic conditions', *Environmental Toxicology and Chemistry*, 8(10), pp. 853–862.
- OECD, 2010 *Test No. 209: Activated Sludge, Respiration Inhibition Test, OECD Guidelines for the Testing of Chemicals, Section 2: Effects on Biotic Systems*, vol. 209, Organisation for Economic Co-operation and Development Publishing.
- Oliveira, V.B., Simoes, M., Melo, L.F. and Pinto, A.M.F.R., 2013 'Overview on the developments of microbial fuel cells', *Biochemical Engineering Journal*, 73, pp. 53–64.
- Ouattara, a.S., Traore, a.S. and Garcia, J.L., 1992 'Characterization of *Anaerovibrio burkinabensis* sp. nov., a Lactate Fermenting Bacterium Isolated from Rice Field Soils', *International Journal of Systematic Bacteriology*, 42(3), pp. 390–397.
- Page, D. and Dillon, P., 2007 'Measurement of the biodegradable fraction of dissolved organic matter relevant to water reclamation via aquifers', in: 'National Research Flagships', CSIRO, p. 33.
- Pant, D., Van Bogaert, G., De Smet, M., Diels, L. and Vanbroekhoven, K., 2010a 'Use of novel

- permeable membrane and air cathodes in acetate microbial fuel cells', *Electrochimica Acta*, 55(26), pp. 7710–7716.
- Pant, D., Van Bogaert, G., Diels, L. and Vanbroekhoven, K., 2010b 'A review of the substrates used in microbial fuel cells (MFCs) for sustainable energy production.', *Bioresource Technology*, 101(6), pp. 1533–1543.
- Parliamentary Office of Science and Technology, 2014 'Diffuse Pollution of Water by Agriculture', Tech. Rep. 478, POS&T, UK, London.
- Patil, S., Harnisch, F. and Schroder, U., 2010 'Toxicity response of electroactive microbial biofilms - a decisive feature for potential biosensor and power source applications', *ChemPhysChem*, 11(13), pp. 2834–2837.
- Peixoto, L., Min, B., Brito, A.G., Kroff, P., Parpot, P., Angelidaki, I. and Nogueira, R., 2010 'Submersible Microbial Fuel Cell-based Biosensor for in-situ BOD monitoring', in: 'Semana de Engenharia', University of Minho, pp. 1–2.
- Peixoto, L., Min, B., Martins, G., Brito, A.G., Kroff, P., Parpot, P., Angelidaki, I. and Nogueira, R., 2011 'In situ microbial fuel cell-based biosensor for organic carbon', *Bioelectrochemistry*, 81(2), pp. 99–103.
- Penn, M.R., Pauer, J.J. and Mihelcic, J.R., 2009 'Biochemical Oxygen Demand', in: A. Sabljic (Ed.), 'Environmental and Ecological Chemistry, Volume II', Encyclopedia of Life Support Systems, Oxford, UK, vol. II, pp. 278–297.
- Ponomareva, O.N., Arlyapov, V.A., Alferov, V.A. and Reshetilov, A.N., 2011 'Microbial biosensors for detection of biological oxygen demand (a Review)', *Applied Biochemistry and Microbiology*, 47(1), pp. 1–11.
- Prichard, L. and Barwick, V., 2003 'Preparation of Calibration Curves: A Guide to Best Practice', Tech. rep., LGC.
- Promega, 2010 'Plasmid and Protein Quantitation', Tech. rep., Promega.
- Quek, S.B., Cheng, L. and Cord-ruwisch, R., 2014 'Bio-Electrochemical Sensor for Fast Analysis of Assimilable Organic Carbon in Seawater', *Biosensors and Bioelectronics*, 5(2), pp. 2–5.
- Quek, S.B., Cheng, L. and Cord-Ruwisch, R., 2015a 'In-line deoxygenation for organic carbon detections in seawater using a marine microbial fuel cell-biosensor.', *Bioresource Technology*, 182C, pp. 34–40.
- Quek, S.B., Cheng, L. and Cord-Ruwisch, R., 2015b 'Microbial fuel cell biosensor for rapid assessment of assimilable organic carbon under marine conditions', *Water Research*, 77, pp. 64–71.

- Quevauviller, P., Thomas, O. and Van Der Beken, A., 2007 *Wastewater Quality Monitoring and Treatment, Water Quality Measurements*, vol. 13, Wiley.
- R Core Team, 2015 'R: A Language and Environment for Statistical Computing', Tech. rep., R Foundation for Statistical Computing, Vienna, Austria.
- Rabaey, K., Angenent, L.T., Schröder, U. and Keller, J. (Eds.), 2010 *Bioelectrochemical Systems: from extracellular electron transfer to biotechnological application*, IWA Publishing, London.
- Rabaey, K., Clauwaert, P., Aelterman, P. and Verstraete, W., 2005 'Tubular microbial fuel cells for efficient electricity generation', *Environmental Science & Technology*, 39(20), pp. 8077–8082.
- Ramalho, R., 1977 'Characterization of Domestic and Industrial Wastewaters', in: 'Introduction to Wastewater Treatment Processes', Academic Press, Quebec, Canada, chap. 2, pp. 26–69.
- Reguera, G., Nevin, K.P., Nicoll, J.S., Covalla, S.F., Woodard, T.L. and Lovley, D.R., 2006 'Biofilm and nanowire production leads to increased current in *Geobacter sulfurreducens* fuel cells.', *Applied and Environmental Microbiology*, 72(11), pp. 7345–7348.
- Reshetilov, A., Arlyapov, V., Alferov, V. and Reshetilova, T., 2013 'BOD Biosensors : Application of Novel Technologies and Prospects for the Development', in: T. Rinken (Ed.), 'State of the Art in Biosensors - Environmental and Medical Applications', InTech, chap. 3, pp. 57–77.
- Reshetilov, A.N., Iliasov, P.V. and Reshetilova, T.A., 2010 'The Microbial Cell Based Biosensors', in: V.S. Somerset (Ed.), 'Intelligent and Biosensors', InTech, Vukovar, Croatia, January, chap. 15, pp. 289–322.
- Richter, H., Nevin, K.P., Jia, H., Lowy, D.A., Lovley, R. and Tender, L.M., 2009 'Cyclic voltammetry of biofilms of wild type and mutant *Geobacter sulfurreducens* on fuel cell anodes indicates possible roles of OmcB , OmcZ , type IV pili , and protons in extracellular electron transfer', *Energy & Environmental Science*, 2, pp. 506–516.
- Riordan, F.O., 2003 'Trial of STIP Biox 1010 BOD Analyser', Tech. rep., Water Technology Ltd., Cork, Ireland.
- Rotaru, A.E., Woodard, T.L., Nevin, K.P. and Lovley, D.R., 2015 'Link between capacity for current production and syntrophic growth in *Geobacter* species', *Frontiers in Microbiology*, 6(JUL), pp. 1–8.
- RStudio Team, 2015 'RStudio: Integrated Development Environment for R', Tech. rep., RStudio, Inc., Boston, MA.

- Saint-Gobain, 2007 'CHEMFLUOR ® 367 Scientific Grade Tubing', Tech. rep., Saint-Gobain Performance Plastics.
- Sakaguchi, T., Morioka, Y., Yamasaki, M., Iwanaga, J., Beppu, K., Maeda, H., Morita, Y. and Tamiya, E., 2007 'Rapid and onsite BOD sensing system using luminous bacterial cells-immobilized chip', *Biosensors and Bioelectronics*, 22(7), pp. 1345–1350.
- Sambrook, J., Fritsch, E.F. and Maniatis, T., 1989 *Molecular Cloning: A Laboratory Manual (volume 3)*, Cold Spring Harbor Laboratory Press, New York, NY, 2nd edn.
- Samudro, G. and Mangkoedihardjo, S., 2010 'Review on BOD, COD and BOD/COD ratio: A triangle zone for toxic, biodegradable and stable levels', *International Journal of Academic Research*, 2(4), pp. 235–239.
- Samuel, M.S., Sivaramakrishna, A. and Mehta, A., 2014 'Bioremediation of p-Nitrophenol by *Pseudomonas putida* 1274 strain.', *Journal of Environmental Health Science & Engineering*, 12(1), p. 53.
- Sauro, H.M., 2012 'Basic Enzyme Kinetics', *Control Theory for Biologists And Bioengineers*, 2, pp. 55–84.
- Schievano, A., Pizza, F., Pino, C., Perrino, D., Colombo, A. and Cristiani, P., 2016 'Experiences of floating microbial fuel cells, supplying on-line sensors for water quality', in: 'Proceedings of the 13th IWA Leading Edge Conference on Water and Wastewater Technologies', International Water Association, vol. 1, pp. 1–4.
- Schneider, G., Kovács, T., Rákhely, G. and Czeller, M., 2016 'Biosensoric potential of microbial fuel cells', *Applied Microbiology and Biotechnology*.
- Scott, K. and Yu, E.H. (Eds.), 2015 *Microbial Electrochemical and Fuel Cells: Fundamentals and Applications*, Woodhead Publishing.
- Segel, I.H., 1976 *Biochemical Calculations: How to Solve Mathematical Problems in General Biochemistry*, Wiley.
- Selinummi, J., Seppälä, J., Yli-Harja, O. and Puhakka, J.A., 2005 'Software for quantification of labeled bacteria from digital microscope images by automated image analysis', *BioTechniques*, 39(6), pp. 859–862.
- Sharma, M., Bajracharya, S., Gildemyn, S., Patil, S.a., Alvarez-Gallego, Y., Pant, D., Rabaey, K. and Dominguez-Benetton, X., 2014 'A critical revisit of the key parameters used to describe microbial electrochemical systems', *Electrochimica Acta*, 140, pp. 191–208.
- Shen, Y.J., Lefebvre, O., Tan, Z. and Ng, H.Y., 2012 'Microbial fuel-cell-based toxicity sensor for fast monitoring of acidic toxicity.', *Water Science & Technology*, 65(7), pp. 1223–1228.



- Shen, Y., Wang, M., Chang, I.S. and Ng, H.Y., 2013 'Effect of shear rate on the response of microbial fuel cell toxicity sensor to Cu(II)', *Bioresource Technology*, 136, pp. 707–710.
- Showalter, A., 2013 'Micro-Scale Microbial Fuel Cell : Petroleum Biosensing', in: 'NNIN: 2013 Research Accomplishments', National Nanotechnology Infrastructure Network, Arizona, USA, pp. 44–45.
- Shrivastava, A. and Gupta, V., 2011 'Methods for the determination of limit of detection and limit of quantitation of the analytical methods', *Chronicles of Young Scientists*, 2(1), pp. 21–25.
- Sonnad, J.R. and Goudar, C.T., 2004 'Solution of the Haldane equation for substrate inhibition enzyme kinetics using the decomposition method', *Mathematical and Computer Modelling*, 40(5-6), pp. 573–582.
- de Souza, A.M. and Sutherland, I., 1994 'Exopolysaccharide and storage polymer production in *Enterobacter aerogenes* type 8 strains', *Journal of Applied Bacteriology*, 76(5), pp. 463–468.
- Stams, A. and Hansen, T., 1984 'Fermentation of glutamate and other compounds by *Acidaminobacter hydrogenofomans* gen. nov. sp. nov., an obligate anaerobe isolated from black mud. Studies', *Archives of microbiology*, 21, pp. 329–337.
- Stein, N.E., Hamelers, H.V.M. and Buisman, C.N.J., 2010 'Stabilizing the baseline current of a microbial fuel cell-based biosensor through overpotential control under non-toxic conditions', *Bioelectrochemistry*, 78(1), pp. 87–91.
- Stein, N.E., Hamelers, H.V.M. and Buisman, C.N.J., 2012a 'Influence of membrane type, current and potential on the response to chemical toxicants of a microbial fuel cell based biosensor', *Sensors and Actuators B: Chemical*, 163(1), pp. 1–7.
- Stein, N.E., Hamelers, H.V.M. and Buisman, C.N.J., 2012b 'The effect of different control mechanisms on the sensitivity and recovery time of a microbial fuel cell based biosensor', *Sensors and Actuators B: Chemical*, 171-172(1), pp. 816–821.
- Stein, N.E., Hamelers, H.V.M., van Straten, G. and Keesman, K.J., 2012c 'On-line detection of toxic components using a microbial fuel cell-based biosensor', *Journal of Process Control*, 22(9), pp. 1755–1761.
- Stein, N.E., Keesman, K.J., Hamelers, H.V.M. and van Straten, G., 2011 'Kinetic models for detection of toxicity in a microbial fuel cell based biosensor.', *Biosensors and Bioelectronics*, 26(7), pp. 3115–3120.
- Stoddard, S.F., Smith, B.J., Hein, R., Roller, B.R.K. and Schmidt, T.M., 2015 'rrnDB: Improved tools for interpreting rRNA gene abundance in bacteria and archaea and a new foundation for future development', *Nucleic Acids Research*, 43(D1), pp. D593–D598.

- Su, L., Jia, W., Hou, C. and Lei, Y., 2011 'Microbial biosensors: a review', *Biosensors and Bioelectronics*, 26(5), pp. 1788–1799.
- Sung, Y., Fletcher, K.E., Ritalahti, K.M., Apkarian, R.P., Ramos-Hernandez, N., Sanford, R.A., Mesbah, N.M. and Löffler, F.E., 2006 'Geobacter lovleyi sp. nov. Strain SZ, a Novel Metal-Reducing and Tetrachloroethene-Dechlorinating Bacterium', *Applied and Environmental Microbiology*, 72(4), pp. 2775–2782.
- Suzuki, K., Owen, R., MoK, J., Mochihara, H., Hosokawa, T., Kubota, H., Sakamoto, H., Matsuda, A., Tashiro, Y. and Futamata, H., 2016 'Comparison of electrochemical and microbiological characterization of microbial fuel cells equipped with SPEEK and Nafion membrane electrode assemblies', *Journal of Bioscience and Bioengineering*, 122(3), pp. 322–328.
- Tan, T.C., Li, F., Neoh, K.G. and Lee, Y.K., 1992 'Microbial Membrane-Modified Dissolved-Oxygen Probe for Rapid Biochemical Oxygen-Demand Measurement', *Sensors and Actuators B: Chemical*, 8(2), pp. 167–172.
- Ter Heijne, A., Hamelers, H.V., Saakes, M. and Buisman, C.J., 2008 'Performance of non-porous graphite and titanium-based anodes in microbial fuel cells', *Electrochimica Acta*, 53(18), pp. 5697–5703.
- Thermo Scientific, 2008 '260/280 and 260/230 Ratios', Tech. rep., Thermo Fisher Scientific.
- Tian, S., Zhang, P., Liang, Y., Zhang, D. and Wang, B., 2014 'Performances of double-chamber microbial fuel cell-based BOD sensor', *Chinese Journal of Environmental Engineering*, 8(6), pp. 2626–2632.
- Tindall, B.J., 1996 'Bacterium from Anoxic Sediments of a Freshwater Lake', *International Journal of Systematic Bacteriology*, 46(1), pp. 183–188.
- Torres, C.I., Kato Marcus, A. and Rittmann, B.E., 2007 'Kinetics of consumption of fermentation products by anode-respiring bacteria', *Applied Microbiology and Biotechnology*, 77(3), pp. 689–697.
- Tront, J.M., Fortner, J.D., Plötze, M., Hughes, J.B. and Puzrin, A.M., 2008 'Microbial fuel cell biosensor for in situ assessment of microbial activity', *Biosensors and Bioelectronics*, 24(4), pp. 586–590.
- Tuma, R.S., Beaudet, M.P., Jin, X., Jones, L.J., Cheung, C.Y., Yue, S. and Singer, V.L., 1999 'Characterization of SYBR Gold nucleic acid gel stain: a dye optimized for use with 300-nm ultraviolet transilluminators.', *Analytical Biochemistry*, 268(2), pp. 278–88.
- UK Statutory Instrument, 1994 'The Urban Waste Water Treatment (England and Wales) Regulations', 2841.

- UK Statutory Instrument, 2010 'The Environmental Permitting (England and Wales) Regulations 2010', 675.
- Underwood, S. and Avison, M.B., 2004 'Citrobacter koseri and Citrobacter amalonaticus isolates carry highly divergent  $\beta$ -lactamase genes despite having high levels of biochemical similarity and 16S rRNA sequence homology', *Journal of Antimicrobial Chemotherapy*, 53(6), pp. 1076–1080.
- US EPA, 2014 'Priority Pollutant List', 40 CFR Part 423, Appendix A.
- US PHS, 1992 'Toxicological profile for nitrophenols: 2-nitrophenol, 4-nitrophenol', Tech. Rep. Agency for Toxic Substances and Disease Registry, US Public Health Service.
- Van Eerten-Jansen, M.C.A.A., Veldhoen, A.B., Plugge, C.M., Stams, A.J.M., Buisman, C.J.N. and Ter Heijne, A., 2013 'Microbial community analysis of a methane-producing biocathode in a bioelectrochemical system', *Archaea*, 2013.
- Velasquez-Orta, S.B., Head, I.M., Curtis, T.P. and Scott, K., 2011 'Factors affecting current production in microbial fuel cells using different industrial wastewaters.', *Bioresource Technology*, 102(8), pp. 5105–5112.
- Verstraete, W. and Rabaey, K., 2006 'Critical Review Microbial Fuel Cells : Methodology and Technology', *Environmental Science & Technology*, 40(17), pp. 5181–5192.
- Wagner, D.D., Hug, L.a., Hatt, J.K., Spitzmiller, M.R., Padilla-Crespo, E., Ritalahti, K.M., Edwards, E.a., Konstantinidis, K.T. and Löffler, F.E., 2012 'Genomic determinants of organohalide-respiration in *Geobacter lovleyi*, an unusual member of the *Geobacteraceae*', *BMC Genomics*, 13(200), pp. 1–17.
- Wang, G.S., Chen, H.W. and Kang, S.F., 2001 'Catalyzed UV oxidation of organic pollutants in biologically treated wastewater effluents', *Science of the Total Environment*, 277(1-3), pp. 87–94.
- Wang, X., Gao, N. and Zhou, Q., 2012 'Concentration responses of toxicity sensor with *Shewanella oneidensis* MR-1 growing in bioelectrochemical systems.', *Biosensors and Bioelectronics*, 43(1), pp. 264–267.
- Wang, Q., Garrity, G.M., Tiedje, J.M. and Cole, J.R., 2007 'Naive Bayesian classifier for rapid assignment of rRNA sequences into the new bacterial taxonomy', *Applied and Environmental Microbiology*, 73(16), pp. 5261–5267.
- Wang, L.K., Hung, Y.T., Lo, H.L., Yapijakis, C. and Li, K.H. (Eds.), 2006 *Handbook of Industrial and Hazardous Wastes Treatment*, Marcel Dekker, New York, NY, 2nd edn.
- Wang, H. and Ren, Z.J., 2014 'Bioelectrochemical metal recovery from wastewater: a review.', *Water research*, 66, pp. 219–32.

- Wang, J., Zheng, Y., Jia, H. and Zhang, H., 2014 'Bioelectricity generation in an integrated system combining microbial fuel cell and tubular membrane reactor: Effects of operation parameters performing a microbial fuel cell-based biosensor for tubular membrane bioreactor', *Bioresource Technology*, 170, pp. 483–490.
- Wang, J., Zheng, T., Wang, Q., Xu, B. and Wang, L., 2015 'A bibliometric review of research trends on bioelectrochemical systems', *Current Science*, 109(12), pp. 2204–2211.
- Water Environment Federation, 2008 'Characterization and Sampling of Wastewater', *Operation of Municipal Wastewater Treatment Plants: MoP No.11*, pp. 1–24.
- Weiss, J.N., 1997 'The Hill equation revisited: uses and misuses', *The FASEB journal : official publication of the Federation of American Societies for Experimental Biology*, 11(11), pp. 835–841.
- Wett, B., Buchauer, K. and Fimml, C., 2007 'Energy self-sufficiency as a feasible concept for wastewater treatment systems', *Proceedings of the IWA Leading Edge Technology Conference (Singapore)*, pp. 21–24.
- Winfield, J., Ieropoulos, I. and Greenman, J., 2012 'Investigating a cascade of seven hydraulically connected microbial fuel cells', *Bioresource Technology*, 110, pp. 245–250.
- Wu, W., Gu, Z., Liu, X., Bai, L. and Tang, Z., 2014 'Nanograss Array Boron-Doped Diamond Electrode for Toxicity Sensor with *Shewanella loihica* PV-4 in Bioelectrochemical Systems', *Sensor Letters*, 12(1), pp. 191–196.
- Wu, S., Liang, P., Zhang, C., Li, H., Zuo, K. and Huang, X., 2015a 'Enhanced performance of microbial fuel cell at low substrate concentrations by adsorptive anode', *Electrochimica Acta*, 161, pp. 245–251.
- Wu, F., Liu, Z., Zhou, S.G., Wang, Y.Q. and Huang, S.H., 2009 'Development of a low-cost single chamber microbial fuel cell type BOD sensor', *Huan Jing Ke Xue*, 30(10), pp. 3099–3103.
- Wu, F., Liu, Z., Zhou, B., Zhou, S.G., Rao, L.Q. and Wang, Y.Q., 2010 '[Development of a low-cost single chamber microbial fuel cell type BOD sensor]', *Huan Jing Ke Xue*, 31(7), pp. 1596–600.
- Wu, X.Y., Tong, F., Song, T.S., Gao, X.Y., Xie, J.J., Zhou, C.C., Zhang, L.X. and Wei, P., 2015b 'Effect of zeolite-coated anode on the performance of microbial fuel cells', *Journal of Chemical Technology & Biotechnology*, 90(1), pp. 87–92.
- Xiao, Y., Araujo, C.D., Sze, C.C. and Stuckey, D.C., 2014 'Toxicity measurement in biological wastewater treatment processes: A review.', *Journal of hazardous materials*, 286C, pp. 15–29.

- Xu, Z., Liu, B., Dong, Q., Lei, Y., Li, Y., Ren, J., McCutcheon, J. and Li, B., 2015 'Flat microliter membrane-based microbial fuel cell as "on-line sticker sensor" for self-supported in situ monitoring of wastewater shocks', *Bioresource Technology*, 197, pp. 244–251.
- Xu, Z., Liu, Y., Williams, I., Qian, F., Li, Y., Zhang, H., Cai, D., Wang, L. and Li, B., 2016 'Disposable Self-support Paper-based Multi-anode Microbial Fuel Cell (PMMFC) Integrated with Power Management System (PMS) as the Real Time "Shock" Biosensor for Wastewater', *Biosensors and Bioelectronics*, 85, pp. 232–239.
- Yang, G.X., Sun, Y.m., Kong, X.Y., Zhen, F., Li, Y., Li, L.H., Lei, T.Z., Yuan, Z.H. and Chen, G.Y., 2013 'Factors affecting the performance of a single-chamber microbial fuel cell-type biological oxygen demand sensor', *Water Science & Technology*, 68(9), pp. 1914–1919.
- You, J., Walter, X.A., Greenman, J., Melhuish, C. and Ieropoulos, I., 2015 'Stability and reliability of anodic biofilms under different feedstock conditions: Towards microbial fuel cell sensors', *Sensing and Bio-Sensing Research*, 6, pp. 43–50.
- YSI, 2009 'The Dissolved Oxygen Handbook', Tech. rep., YSI.
- YSI, 2013 'Dissolved Oxygen and Pressure Tables', Tech. rep., YSI.
- Zellner, G., Messner, P., Kneifel, H. and Winter, J., 1989 'Desulfovibrio simplex spec. nov., a new sulfate-reducing bacterium from a sour whey digester', *Archives of Microbiology*, 152(4), pp. 329–334.
- Zhang, Y. and Angelidaki, I., 2011 'Submersible microbial fuel cell sensor for monitoring microbial activity and BOD in groundwater: Focusing on impact of anodic biofilm on sensor applicability', *Biotechnology and Bioengineering*, 108(10), pp. 2339–2347.
- Zhang, Y. and Angelidaki, I., 2012 'A simple and rapid method for monitoring dissolved oxygen in water with a submersible microbial fuel cell (SBMFC)', *Biosensors and Bioelectronics*, 38(1), pp. 189–194.
- Zhou, M., Wang, H., Hassett, D.J. and Gu, T., 2013 'Recent advances in microbial fuel cells (MFCs) and microbial electrolysis cells (MECs) for wastewater treatment, bioenergy and bioproducts', *Journal of Chemical Technology & Biotechnology*, 88(4), pp. 508–518.
- Zhuang, L., Yuan, Y., Wang, Y. and Zhou, S., 2012 'Long-term evaluation of a 10-liter serpentine-type microbial fuel cell stack treating brewery wastewater', *Bioresource Technology*, 123, pp. 406–412.